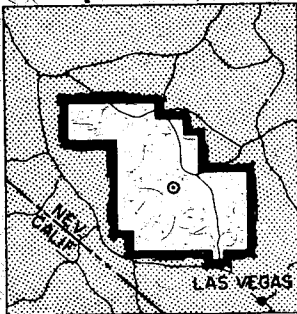


WT-1468

AEC Category: HEALTH AND SAFETY

Military Category: 12

OPERATION PLUMBBOB



NEVADA TEST SITE
MAY-OCTOBER 1957

Project 33.2

SECONDARY MISSILES GENERATED BY
NUCLEAR-PRODUCED BLAST WAVES

Issuance Date: Oct. 28, 1963



CIVIL EFFECTS TEST GROUP

DISCLAIMER

This report was prepared as an account of work sponsored by an agency of the United States Government. Neither the United States Government nor any agency Thereof, nor any of their employees, makes any warranty, express or implied, or assumes any legal liability or responsibility for the accuracy, completeness, or usefulness of any information, apparatus, product, or process disclosed, or represents that its use would not infringe privately owned rights. Reference herein to any specific commercial product, process, or service by trade name, trademark, manufacturer, or otherwise does not necessarily constitute or imply its endorsement, recommendation, or favoring by the United States Government or any agency thereof. The views and opinions of authors expressed herein do not necessarily state or reflect those of the United States Government or any agency thereof.

DISCLAIMER

Portions of this document may be illegible in electronic image products. Images are produced from the best available original document.

NOTICE

This report is published in the interest of providing information which may prove of value to the reader in his study of effects data derived principally from nuclear weapons tests.

This document is based on information available at the time of preparation which may have subsequently been expanded and re-evaluated. Also, in preparing this report for publication, some classified material may have been removed. Users are cautioned to avoid interpretations and conclusions based on unknown or incomplete data.

PRINTED IN USA

Price \$5.50. Available from the Office of
Technical Services, Department of Commerce,
Washington 25, D. C.

Report to the Test Director

SECONDARY MISSILES GENERATED BY NUCLEAR-PRODUCED BLAST WAVES

By

I. Gerald Bowen
Mary E. Franklin
E. Royce Fletcher
Ray W. Albright

Approved by: **CLAYTON S. WHITE**
Director
Program 33

Approved by: **L. J. DEAL**
Acting Chief
Civil Effects Branch

Lovelace Foundation for Medical Education and Research
Albuquerque, New Mexico
February 1962



ABSTRACT

The generation of secondary missiles by blast waves was investigated in Operation Plumb-bob for three nuclear detonations with estimated yields of 11, 38, and 44.5 kt. A trapping technique was used to determine the impact velocities for 17,524 missiles (stones, glass fragments, spheres, and military debris or steel fragments) which occurred in open areas, houses, and an underground shelter with an open entryway. The equivalent ideal-wave peak overpressures computed from measured blast data for the open-area stations varied from 3.8 to 21 psi. Two houses and an underground shelter were located where the overpressures were 3.8 and 65 psi, respectively. The effect of hill-and-dale terrain on the production of missiles was investigated on one of the shots. Precursor effects were noted on two of the shots at stations near Ground Zero (GZ).

Missile velocities measured at all stations except the underground shelter were compared with those computed by use of a model based on an ideal blast wave. An analytical procedure was presented by which translational velocities of man can be estimated using the measured velocities of spheres and stones.

Total distances of displacement were measured for 145 stones that weighed up to 20 kg and for 1528 fragments from a concrete-block wall.

ACKNOWLEDGMENTS

Recognition should be given to V. R. Clare and R. V. Taborelli who, as assistant project officers, shared responsibility for the completion of the field work at the Nevada Test Site (NTS). Mr. Clare's participation in the project was made possible by the interest and generosity of Chemical Warfare Laboratories, Edgewood, Md.

Weapons-test operations involve the coordinated efforts of many organizations. Some of those contributing directly to the execution of the secondary-missile project were Civil Effects Test Group (now Civil Effects Test Operations), Division of Biology and Medicine, Atomic Energy Commission

Armed Forces Special Weapons Project (now Defense Atomic Support Agency), Department of Defense

Federal Civil Defense Administration (now Office of Civil and Defense Mobilization)

Ballistic Research Laboratories

Sandia Corporation

Kirtland Air Force Base

Indian Springs Air Force Base

Holmes & Narver, Inc., Architectural Engineers

Reynolds Electrical and Engineering Co., Inc.

Acknowledgment is made of the efforts of the following personnel of the Lovelace Foundation who assisted not only in the field work, but also in the tedious and exacting procedures involved in the analysis of the data and preparation of the test report:

Members of the Physics Department who were involved in the field work, data analysis, and related activities are J. J. Anderson, J. M. Craig, A. W. Dennis, K. A. Doherty, J. Kleinfeld, J. D. McCurdy, M. A. Osoff, R. F. D. Perrett, and W. R. Roeder.

Members of the Department of Medical Illustration who were responsible for photographic work at the Test Site and for the preparation of illustrative material for the report are R. A. Smith, G. S. Bevil, Holly M. Ferguson, E. M. Johnson, and R. A. MacMahon.

The final manuscript was prepared by Isabell D. Benton, K. Maureen Gilmore, Ruth P. Lloyd, Vicki J. Newsom, and Helen T. Vatosow.

Mention should be made of Robert L. Corsbie, who was Director of the Civil Effects Test Group at the time of the field operations, and of Dr. C. S. White, Director of Research of the Lovelace Foundation. The secondary-missile studies were initiated through their leadership.

Operations at NTS were financed jointly by the U. S. Atomic Energy Commission, the Department of Defense, and the Federal Civil Defense Administration. Postoperation analytical work and related studies were supported by the USAEC.

LIST OF SYMBOLS

Symbol	Definition	Unit of measurement
A	Impact area	Sq in.
a,b,c	Regression coefficients	
Abs	Absorber	
Al	Aluminum sphere (fraction following type of sphere indicates diameter)	In.
α	Acceleration coefficient	Sq ft/lb
$\bar{\alpha}$	Acceleration coefficient for missiles of average mass M	Sq ft/lb
CB	Croquet ball	
c_0	Speed of sound in undisturbed air	Ft/sec
d	Distance traveled by missile	Ft
d_-	Minimum distance	Ft
d_+	Maximum distance	Ft
\bar{d}	Average distance	Ft
d_x	Distance traveled by missile parallel to direction of propagation of blast wave (downwind)	Ft
d_{x50}	Geometric mean of d_x	Ft
d_y	Distance traveled by missile perpendicular to direction of propagation of blast wave (crosswind)	Ft
\bar{D}_s	Average spatial density of missiles in trap	Missiles/sq ft
$\Delta V\%$	$(\bar{V} - V_{p50})/V_{p50}$	
E_{gm}	Geometric standard error of estimate in mass = antilog E_{lm}	
E_{gv}	Geometric standard error of estimate in velocity = antilog E_{lv}	
E_{lm}	Standard error of estimate of log mass	Log units
E_{lv}	Standard error of estimate of log velocity	Log units
$(E_{lv})\%$	Standard error of estimate of log velocity	% of velocity units
FPG	Plate glass, flat upon arrival at trap	
FWG	Window glass, flat upon arrival at trap	
G	Galileo	
G_l	Glass sphere, large (average mass = 72.6 mg)	
Gr	Gravel	
G_s	Glass sphere, small (average mass = 36.0 mg)	

Symbol	Definition	Unit of measurement
G_x	Glass sphere, extra large (average mass = 242.4 mg)	
GZ	Ground Zero, the point on the surface vertically below the center of the burst	
h_1	Height above ground at which spheres were placed	In.
\bar{h}_2	Average impact height above ground	In.
I_p	Overpressure impulse	Psi-sec
k	Constant, added to depth of penetration for velocity calibration	In.
kt	Kiloton (kt), energy of nuclear (or atomic) explosion which is equivalent to that produced by the explosion of 1 kt (1000 tons) of TNT	
m	Mass of missile	Mg, unless otherwise specified
M_-	Minimum m	Mg, unless otherwise specified
M_+	Maximum m	Mg, unless otherwise specified
\bar{M}	Mean or average mass	Mg, unless otherwise specified
M_{50}	Geometric mean mass	Mg, unless otherwise specified
MD	Military debris	
n	Number of missiles	
NS	Natural stones	
N_y	Nylon sphere (fraction following type of sphere indicates diameter)	In.
P	Priscilla	
p	Overpressure or pressure in excess of p_0	Psi
p_0	Pressure of undisturbed air or ambient pressure	Psi
p_s	Maximum overpressure or shock overpressure	Psi
PG	Plate glass	
q	Dynamic pressure	Psi
R	Range, distance of station from GZ	Ft
S	Smoky	
s	Depth of penetration of missile in absorber	In.
s_-	Minimum s	
s_+	Maximum s	
S_{dy}	Standard deviation of d_y	
S_{gm}	Standard geometric deviation of mass = antilog S_{lm}	
S_{gv}	Standard geometric deviation of velocity = antilog S_{lv}	
S_{ld_x}	Standard deviation of log d_x	Log units
S_{lm}	Standard deviation of log mass	Log units
S_{lv}	Standard deviation of log velocity	Log units
S_m	Standard deviation of m	
S_v	Standard deviation of v	
St	Steel sphere (fraction following type of sphere indicates diameter)	In.

Symbol	Definition	Unit of measurement
t	Time after arrival of blast wave	Sec
t_p^+	Duration of positive pressure phase of blast wave	Sec
v	Velocity	Ft/sec
V_-	Minimum v	Ft/sec
V_+	Maximum v	Ft/sec
\bar{V}	Mean or average velocity	Ft/sec
V_{50}	Geometric mean velocity	Ft/sec
V_{p50}	Predicted velocity for missiles of mass M_{50} (if M_{50} not listed, \bar{M})	Ft/sec
$(V_{p50})_{Gr}$	V_{p50} for gravel	
$(V_{p50})_R$	V_{p50} assuming reflected pressure	
WG	Window glass	
WGH	Window glass inside concrete house	

Roman numerals designate type of absorber identified in Table 2.1, page 30.



1

2



3

4

CONTENTS

ABSTRACT	5
ACKNOWLEDGMENTS	6
LIST OF SYMBOLS	7
CHAPTER 1 INTRODUCTION	25
1.1 Background	25
1.2 Categories of Biological Effects of Blast	26
1.3 Objectives	26
CHAPTER 2 MISSILE-ABSORBING TECHNIQUES AND METHODS OF ANALYSIS	29
2.1 Introduction	29
2.2 Missile Absorbers	29
2.3 Construction of Trap Housing and Anchors and Window Mounts	30
2.4 Calibration of Missile Absorbers	31
2.4.1 Experimental Procedure	31
2.4.2 Glass Fragments with Random Orientations	32
2.4.3 Glass Fragments with Flat Orientations	33
2.4.4 Gravel and Natural Stones	34
2.4.5 Spheres and Military Debris	34
2.4.6 Summary of Calibration Results	35
2.5 Threshold Velocities	35
2.6 Statistical Analysis of Field Data	38
CHAPTER 3 PREDICTION OF TRANSLATIONAL VELOCITIES BY USE OF MEASURED BLAST-WAVE AND MISSILE PARAMETERS	49
3.1 General	49
3.2 Prediction of Missile Velocities	49
3.3 Determination of the Ideal Blast Wave from the Field Data	50
3.4 Acceleration Coefficients for Small Nonspherical Missiles	50
3.5 Glass-fragment Studies	50
3.6 Natural-stone, Gravel, Military-debris, and Sphere Studies	51
CHAPTER 4 SHOT PRISCILLA, EXPERIMENTAL PROCEDURE AND RESULTS	52
4.1 Prospectus	52
4.2 Station 4P, 6120-ft Range	53
4.2.1 Experimental Plan	53
4.2.2 Blast Parameters	53

CONTENTS (Continued)

4.2.3	Window-glass Installation 4P1	54
4.2.4	Window-glass Trap 4P2b (Above Dog Trap 4P2A)	54
4.2.5	Plate-glass Trap 4P3b (Above Dog Trap 4P3A)	55
4.2.6	Military-debris and Gravel Installations 4P4 and 4P5	55
4.2.7	Gravel and Sphere Installations 4P6 and 4P7	55
4.2.8	Window-glass Installation 4P8	56
4.2.9	Window-glass Trap 4P9b (Above Pig Trap 4P9A)	56
4.2.10	Natural-stone Data from Station 4P Traps	56
4.3	Station 4PP (Pig Study), 6120-ft Range	56
4.4	Station 5P, 5320-ft Range	57
4.4.1	Experimental Plan and Blast Parameters	57
4.4.2	Window-glass Installation 5P1	57
4.4.3	Window-glass Trap 5P2b (Above Dog Trap 5P2A)	57
4.4.4	Plate-glass Trap 5P3b (Above Dog Trap 5P3A)	57
4.4.5	Military-debris and Gravel Installations 5P4, 5P5, and 5P6	57
4.4.6	Sphere Installation 5P7	59
4.4.7	Window-glass Installation 5P8	60
4.4.8	Window-glass Trap 5P9b (Above Pig Trap 5P9A)	60
4.5	Station 5PP (Pig Study), 5320-ft Range	60
4.6	Station 6P, 4770-ft Range	60
4.6.1	Experimental Plan and Blast Parameters	60
4.6.2	Window-glass Installation 6P1	61
4.6.3	Window-glass Trap 6P2b (Above Dog Trap 6P2A)	61
4.6.4	Plate-glass Installation 6P3	61
4.6.5	Military-debris and Gravel Installations 6P4 and 6P5	61
4.6.6	Sphere Installation 6P6 and Gravel Installation 6P7	63
4.6.7	Window-glass Installation 6P9	64
4.6.8	Window-glass Trap 6P10b (Above Pig Trap 6P10A)	64
4.6.9	Natural-stone Data from all Station 6P Traps.	65
4.7	Station 6PP (Pig Study), 4770-ft Range	65
4.8	Station 6.7PP (Pig Study), 4470-ft Range	65
4.9	Station 8P, 3930-ft Range	66
4.9.1	Experimental Plan and Blast Parameters	66
4.9.2	Window-glass Installation 8P1	66
4.9.3	Window-glass Trap 8P2b (Above Dog Trap 8P2A)	66
4.9.4	Plate-glass Installation 8P3	67
4.9.5	Military-debris and Gravel Installations 8P4 and 8P5	67
4.9.6	Sphere Installation 8P6 and Gravel Installation 8P7	69
4.9.7	Window-glass Installation 8P9	69
4.9.8	Window-glass Trap 8P10b (Above Pig Trap 8P10A)	70
4.9.9	Combined Analysis for Natural Stones and Gravel at Station 8P	70
4.10	Station 10P, 2730-ft Range.	71
4.10.1	Experimental Plan and Blast Parameters	71
4.10.2	Military-debris and Gravel Installation 10P1	71
4.10.3	Military-debris and Gravel Installation 10P2	72
4.10.4	Gravel Installation 10P3 and Sphere Installation 10P4	72
4.11	Station 15P, 2280-ft Range.	73
4.11.1	Experimental Plan and Blast Parameters	73
4.11.2	Military-debris and Gravel Installations 15P1 and 15P2	73
4.11.3	Gravel Installation 15P3 and Sphere Installation 15P4	73
4.12	Station 20P, 2030-ft Range.	74
4.12.1	Experimental Plan and Blast Parameters	74
4.12.2	Military-debris and Gravel Installations 20P1 and 20P2	74
4.12.3	Gravel Installation 20P3 and Sphere Installation 20P4	74

CONTENTS (Continued)

4.13	Underground Shelter with Open Entryway, Station OPS (UK 3.7)	75
4.13.1	Experimental Plan and Blast Parameters	75
4.13.2	Sphere Data	75
4.13.3	Molten-metal and Natural-stone Missiles	76
4.14	Underground Shelters with Closed Entryways	76
4.15	Large-stone, Concrete-block, and Brick Displacement	77
4.15.1	General	77
4.15.2	Large-stone Data	77
4.15.3	Concrete-block and Brick Data	79
4.15.4	Summary of Large-stone, Concrete-block, and Brick Data	79
4.16	Summary and Discussion, Shot Priscilla	79
4.16.1	Station Locations and Blast Parameters	79
4.16.2	Tabulated Results	79
4.16.3	Glass-fragment Missiles, Shot Priscilla	80
4.16.4	Marked-gravel and Natural-stone Missiles, Shot Priscilla	83
4.16.5	Sphere Data, Shot Priscilla	83
4.16.6	Military-debris Data, Shot Priscilla	84
4.16.7	Missiles in Shelters	84
4.16.8	Displacement of Large Stones, Concrete Blocks, and Bricks	84
CHAPTER 5 SHOT SMOKY, EXPERIMENTAL PROCEDURE AND RESULTS		246
5.1	General	246
5.2	Northeast Blast Line	247
5.2.1	Terrain Effects	247
5.2.2	Station 1S	249
5.2.3	Station 2S	249
5.2.4	Station 3S	250
5.2.5	Station 6S	250
5.2.6	Station 7S	251
5.2.7	Station 8S	251
5.3	South Blast Line	251
5.3.1	Station 4S	252
5.3.2	Station 9S	253
5.4	North Blast Line, Station 5S	253
5.5	Summary, Shot Smoky	253
CHAPTER 6 SHOT GALILEO, EXPERIMENTAL PROCEDURE AND RESULTS		339
6.1	General	339
6.2	Station 3G, 4700-ft Range	339
6.2.1	General Discussion and Blast Parameters	339
6.2.2	Concrete-slab Location, Installations 3G1 to 3G4	340
6.2.3	Open Area, Installations 3G5 to 3G9	341
6.2.4	Reinforced Concrete-block House, Traps 3G10a to 3G11e	342
6.2.5	Precast-concrete House, Traps 3G12a to 3G13e	343
6.2.6	Analysis of Combined Data Obtained in Houses	343
6.3	Station 4.3GTS, 3750-ft Range	344
6.3.1	General	344
6.3.2	Marked-gravel Data	344
6.3.3	Natural-stone Data	345
6.3.4	Sphere Data	345
6.4	Station 7GTS, 2750-ft Range	345
6.4.1	General	345
6.4.2	Marked-gravel Data	346

CONTENTS (Continued)

6.4.3	Natural-stone Data	346
6.4.4	Sphere Data	347
6.5	Station 7G, 2750-ft Range	347
6.5.1	General	347
6.5.2	Concrete-block Wall, Traps 7G1a to 7G3b	347
6.5.3	Spheres and Natural Stones, Traps 7G4a to 7G5b	349
6.5.4	Window-glass and Plate-glass Installations, Traps 7G6a to 7G9b	349
6.5.5	Marked-gravel and Natural-stone Installation 7G10	351
6.6	Analysis of Combined Data from Stations 7G and 7GTS	351
6.7	Summary and Discussion, Shot Galileo	351
6.7.1	Blast Parameters	351
6.7.2	Tabulated Results	352
6.7.3	Station 3G, 4700-ft Range	352
6.7.4	Station 4.3GTS, 3750-ft Range	352
6.7.5	Station 7GTS, 2750-ft Range	352
6.7.6	Station 7G, 2750-ft Range	355
CHAPTER 7 DISCUSSION AND SUMMARY		471
7.1	Missile Stations and Blast-wave Parameters	471
7.2	Summary of Traps and Missiles	472
7.3	Glass Fragments from Windows	473
7.4	Natural Stones and Gravel	474
7.5	Spheres	474
7.6	Military Debris	475
7.7	Spallation Missiles	475
7.8	Large Stones, Concrete Blocks, and Bricks	476
APPENDIX THE RELATION BETWEEN THE MEAN, THE GEOMETRIC MEAN, AND THE GEOMETRIC STANDARD DEVIATION FOR A LOG-NORMAL DISTRIBUTION.		479

ILLUSTRATIONS

CHAPTER 2 MISSILE-ABSORBING TECHNIQUES AND METHODS OF ANALYSIS

2.1	Construction Details of Trap Housing	40
2.2	Photograph Showing Trap Anchors, Aluminum Foil for Thermal Protection, and Added Thermal Shield 1 Ft in Front of the Trap	41
2.3	Window- and Plate-glass Mounts	42
2.4	Plot of Calibration Equations for Glass Missiles in Type II Absorber	43
2.5	Nomogram for Determining Velocities of Missiles Striking Type II Absorber Flat	44
2.6	Threshold Velocities for Glass Fragments	45
2.7	Threshold Velocities for Window and Plate Glass Striking Type II Absorber Flat	45
2.8	Threshold Velocities for Natural Stones and Gravel	46
2.9	Threshold Velocities for Nylon and Aluminum Spheres	46
2.10	Threshold Velocities for Steel Spheres	47
2.11	Threshold Velocities for Soda-glass Spheres	47
2.12	Relation Between the Ratio of the Mean to the Geometric Mean and the Standard Geometric Deviation (\bar{x}/x_{50} vs. S_{gx}) for Log-normal Distributions	48

ILLUSTRATIONS (Continued)

CHAPTER 4 SHOT PRISCILLA, EXPERIMENTAL PROCEDURE AND RESULTS

4.1	Station Locations for Shot Priscilla in Frenchman Flat, NTS	85
4.2	Station 4P Layout Chart	86
4.3	Dynamic Pressure vs. Time for Station 4P	87
4.4	Traps 4P1a (Bottom) and 4P1b (Top), Placed 7.8 Ft Behind Window, Postshot	88
4.5	Analysis of Window-glass Missiles from Trap 4P1a	89
4.6	Analysis of Window-glass Missiles from Trap 4P1b	90
4.7	Trap 4P2b, Placed Above Dog Trap (4P2A)	91
4.8	Analysis of Window-glass Missiles from Trap 4P2b	92
4.9	Installation 4P3 Looking Toward GZ, Preshot	93
4.10	Traps 4P4a and b Looking Toward GZ, Preshot	93
4.11	Front Surface of Traps 4P4a and b, Postshot	94
4.12	Installations 4P6 (Right) and 4P7 (Left), Preshot	95
4.13	Analysis of Gravel Missiles from Station 4P Traps, d = 10.9 Ft	96
4.14	Analysis of Gravel Missiles from Station 4P Traps, d = 28.0 Ft	97
4.15	Traps 4P8a and b, Placed 17.8 Ft Behind Window, Postshot	98
4.16	Analysis of Window-glass Missiles from Trap 4P8a	99
4.17	Analysis of Window-glass Missiles from Trap 4P8b	100
4.18	Trap 4P9b, Postshot	101
4.19	Analysis of Window-glass Missiles from Trap 4P9b	102
4.20	Analysis of Natural-stone Missiles from Station 4P Traps	103
4.21	Analysis of Window-glass Missiles from Trap 4PPa	104
4.22	Analysis of Window-glass Missiles from Trap 4PPb	105
4.23	Station 5P Layout Chart	106
4.24	Dynamic Pressure vs. Time for Station 5P	107
4.25	Traps 5P1a and b, Postshot	108
4.26	Analysis of Window-glass Missiles from Trap 5P1a	109
4.27	Analysis of Window-glass Missiles from Trap 5P1b	110
4.28	Analysis of Window-glass Missiles from Trap 5P2b	111
4.29	Trap 5P3b, Postshot	112
4.30	Analysis of Plate-glass Missiles from Trap 5P3b	113
4.31	Traps 5P6a and b, Preshot	114
4.32	Military-debris and Gravel Installation 5P4, Postshot	115
4.33	Analysis of Gravel Missiles from Traps 5P4b, 5P5b, and 5P6a and b	116
4.34	Analysis of Gravel Missiles from Station 5P Traps	117
4.35	Traps 5P7a and b, Postshot	118
4.36	Traps 5P8a and b, Postshot	118
4.37	Analysis of Window-glass Missiles from Trap 5P8a	119
4.38	Analysis of Window-glass Missiles from Trap 5P8b	120
4.39	Analysis of Window-glass Missiles from Trap 5P9b	121
4.40	Analysis of Window-glass Missiles from Trap 5PPa	122
4.41	Analysis of Window-glass Missiles from Trap 5PPb	123
4.42	Station 6P Layout Chart	124
4.43	Overpressure vs. Time at Station 6P	125
4.44	Dynamic Pressure vs. Time at Station 6P	126
4.45	Analysis of Window-glass Missiles from Trap 6P1a	127
4.46	Analysis of Window-glass Missiles from Trap 6P1b	128
4.47	Analysis of Natural-stone Missiles from Trap 6P1b	129
4.48	Analysis of Window-glass Missiles from Trap 6P2b	130
4.49	Analysis of Natural-stone Missiles from Trap 6P2b	131
4.50	Traps 6P3a and b, Postshot	132
4.51	Analysis of Plate-glass Missiles which Arrived Flat at Trap 6P3b	133

ILLUSTRATIONS (Continued)

4.52	Analysis of Plate-glass Missiles from Traps 6P3a and b.	134
4.53	Analysis of Natural-stone Missiles from Trap 6P3a	135
4.54	Analysis of Natural-stone Missiles from Trap 6P3b	136
4.55	Military-debris and Gravel Installation 6P4, Postshot	137
4.56	Analysis of Natural-stone Missiles from Trap 6P4b	138
4.57	Analysis of Natural-stone Missiles from Trap 6P5b	139
4.58	Traps 6P6a and b, 6P7a and b, and 6P8A (Right to Left), Preshot	140
4.59	Traps 6P6a and b, Postshot	141
4.60	Gravel Installation 6P7, Behind Asphalt Area, Postshot	141
4.61	Analysis of Natural-stone Missiles from Trap 6P6a	142
4.62	Analysis of Natural-stone Missiles from Trap 6P6b	143
4.63	Analysis of Gravel Missiles from Station 6P Traps, d = 14.0 Ft	144
4.64	Analysis of Gravel Missiles from Station 6P Traps, d = 36.0 Ft	145
4.65	Traps 6P9a and b, Postshot	146
4.66	Analysis of Window-glass Missiles from Trap 6P9a	147
4.67	Analysis of Window-glass Missiles from Trap 6P9b	148
4.68	Analysis of Natural-stone Missiles from Trap 6P9b	149
4.69	Trap 6P10b, Postshot	150
4.70	Analysis of Window-glass Missiles from Trap 6P10b	151
4.71	Analysis of Natural-stone Missiles from Trap 6P10b	152
4.72	Analysis of Window-glass Missiles from Trap 6PPa	153
4.73	Analysis of Window-glass Missiles from Trap 6PPb	154
4.74	Traps 6.7PPa and b, Postshot	155
4.75	Analysis of Window-glass Missiles from Trap 6.7PPa	156
4.76	Analysis of Window-glass Missiles from Trap 6.7PPb	157
4.77	Station 8P Layout Chart	158
4.78	Station 8P, Preshot	159
4.79	Overpressure vs. Time at Station 8P	160
4.80	Dynamic Pressure vs. Time at Station 8P	161
4.81	Traps 8P1a and b, Postshot	162
4.82	Analysis of Window-glass Missiles from Trap 8P1a	163
4.83	Analysis of Window-glass Missiles from Trap 8P1b	164
4.84	Analysis of Window-glass Missiles from Trap 8P2b	165
4.85	Analysis of Natural-stone Missiles from Trap 8P2b	166
4.86	Traps 8P3a and b, Postshot	167
4.87	Analysis of Plate-glass Missiles from Trap 8P3a	168
4.88	Analysis of Plate-glass Missiles from Trap 8P3b	169
4.89	Analysis of Plate-glass Missiles that Arrived Flat at Trap 8P3b	170
4.90	Traps 8P5a and b, Postshot	171
4.91	Analysis of Gravel Missiles from Trap 8P4a	172
4.92	Analysis of Gravel Missiles from Trap 8P4b	173
4.93	Analysis of Gravel Missiles from Trap 8P5a, d = 6.5 Ft	174
4.94	Analysis of Gravel Missiles from Trap 8P5b, d = 6.5 Ft	175
4.95	Analysis of Gravel Missiles from Trap 8P5a, d = 16.8 Ft	176
4.96	Analysis of Gravel Missiles from Trap 8P5b, d = 16.8 Ft	177
4.97	Analysis of Gravel Missiles from Trap 8P5b, d = 43.0 Ft	178
4.98	Sphere Installation 8P6, Postshot	179
4.99	Analysis of Natural-stone Missiles from Trap 8P6b	180
4.100	Analysis of Gravel Missiles from Trap 8P7a	181
4.101	Analysis of Gravel Missiles from Trap 8P7b, d = 16.8 Ft	182
4.102	Analysis of Gravel Missiles from Trap 8P7b, d = 43.0 Ft	183
4.103	Analysis of Window-glass Missiles from Trap 8P9a	184
4.104	Analysis of Window-glass Missiles from Trap 8P9b	185
4.105	Analysis of Window-glass Missiles from Trap 8P10b	186

ILLUSTRATIONS (Continued)

4.106	Analysis of Natural-stone Missiles from Trap 8P10b	187
4.107	Station 10P Layout Chart	188
4.108	Overpressure vs. Time at Station 10P	189
4.109	Dynamic Pressure vs. Time at Station 10P	190
4.110	Traps 10P1a and b, Postshot	191
4.111	Analysis of Gravel Missiles from Trap 10P1a, d = 19.1 Ft	192
4.112	Analysis of Gravel Missiles from Trap 10P1a, d = 49.0 Ft	193
4.113	Analysis of Natural-stone Missiles from Trap 10P1a	194
4.114	Installation 10P2, Postshot	195
4.115	Analysis of Gravel Missiles from Installation 10P2, d = 19.1 Ft	196
4.116	Analysis of Gravel Missiles from Installation 10P2, d = 49.0 Ft	197
4.117	Analysis of Natural-stone Missiles from Installation 10P2	198
4.118	Analysis of Military-debris Missiles from Trap 10P1a and Installation 10P2	199
4.119	Installation 10P3, Postshot	200
4.120	Installation 10P3 and Traps 10P4a and b, Postshot	201
4.121	Analysis of Gravel Missiles from Installation 10P3	202
4.122	Analysis of Natural-stone Missiles from Installation 10P3	203
4.123	Analysis of Gravel Missiles from Trap 10P4a	204
4.124	Analysis of Natural-stone Missiles from Trap 10P4a	205
4.125	Station 15P Layout Chart	206
4.126	Overpressure vs. Time at Station 15P	207
4.127	Dynamic Pressure vs. Time at Station 15P	208
4.128	Installations 15P1 (Left) and 15P2, Preshot	209
4.129	Installation 15P2, Postshot	210
4.130	Analysis of Gravel Missiles from Installation 15P2	211
4.131	Analysis of Military-debris Missiles from Installation 15P2	212
4.132	Analysis of Natural-stone Missiles from Installation 15P2	213
4.133	Stabilized Area at Station 15P	214
4.134	Installations 15P3 and 15P4, Preshot	215
4.135	Installation 15P3, Postshot	216
4.136	Installation 15P4, Postshot	216
4.137	Analysis of Gravel Missiles from Installation 15P4	217
4.138	Analysis of Natural-stone Missiles from Installation 15P4	218
4.139	Station 20P Layout Chart	219
4.140	Overpressure vs. Time at Station 20P	220
4.141	Dynamic Pressure vs. Time at Station 20P	221
4.142	Installations 20P1 and 20P2, Preshot, Looking Toward GZ	222
4.143	Destroyed Installation 20P1, Postshot	223
4.144	Destroyed Installation 20P2, Postshot	223
4.145	Station 20P, Preshot, Showing Stabilized Area and Installations 20P3 and 20P4 with Spheres and Gravel Set Out	224
4.146	Station 20P, Stabilized Area, Postshot	225
4.147	Installation 20P3, Postshot	225
4.148	Analysis of Natural-stone Missiles from Installation 20P3	226
4.149	Installation 20P4, Postshot	227
4.150	Station OPS Layout Chart	228
4.151	Station OPS, Preshot	229
4.152	Station OPS, Postshot	230
4.153	Drawing for Station OPS	231
4.154	Analysis of Natural-stone Missiles from Station OPS	232
4.155	Spatial Distribution of Natural-stone Missiles Recovered from Station OPS	233

ILLUSTRATIONS (Continued)

4.156	Spatial Distribution of the Average Masses (in mg) of Natural-stone Missiles Recovered from Station OPS	233
4.157	Spatial Distribution of the Average Velocities (in ft/sec) of Natural-stone Missiles Recovered from Station OPS	234
4.158	Typical Trap Installation in Arch Type Shelters	235
4.159	Typical Installation of Missile Absorber in Conduit Type Shelters	235
4.160	Station 4P and Large Stones, Preshot	236
4.161	Station 4P and Large Stones, Postshot	237
4.162	Mass vs. Distance for Large Stones Displaced at Station 4P	238
4.163	Mass vs. Distance for Large Stones Displaced at Station 5P	239
4.164	Mass vs. Distance for Large Stones Displaced at Station 6P	240
4.165	Mass vs. Distance for Large Stones Displaced at Station 8P	241
4.166	Mass vs. Distance for Large Stones Displaced at Station 10P	242
4.167	Mass vs. Distance for Large Stones Displaced at Station 15P	243
4.168	Mass vs. Distance for Large Stones Displaced at Station 20P	244
4.169	Displacement of Marked Large Stones for Seven Stations, Shot Priscilla	245

CHAPTER 5 SHOT SMOKY, EXPERIMENTAL PROCEDURE AND RESULTS

5.1	Station Locations for Shot Smoky in Area 2C, NTS	255
5.2	Typical Placement of Military Debris and Large Steel Spheres (on Trough-like Support)	256
5.3	Typical Trap Installation Showing Use of Extra Thermal Shield, which Consisted of Aluminum Foil Held in Frame Approximately 1 Ft in Front of Traps	256
5.4	Profile of Northeast Blast Line, Shot Smoky	257
5.5	Profile of Northeast Blast Line, Shot Smoky, Range: 2500 to 3600 Ft	258
5.6	Profile of Northeast Blast Line, Shot Smoky, Range: 3600 to 5100 Ft	259
5.7	Station 1S Layout Chart	260
5.8	Station 1S, Preshot	261
5.9	Overpressure vs. Time at Station 1S	262
5.10	Dynamic Pressure vs. Time at Station 1S	263
5.11	Traps 1S1a and b, Postshot	264
5.12	Installation 1S2, Postshot.	265
5.13	Analysis of Natural-stone Missiles from Trap 1S1a.	266
5.14	Analysis of Natural-stone Missiles from Trap 1S1b.	267
5.15	Analysis of Natural-stone Missiles from Trap 1S2	268
5.16	Station 2S Layout Chart	269
5.17	Station 2S, Preshot	270
5.18	Overpressure vs. Time at Station 2S	271
5.19	Dynamic Pressure vs. Time at Station 2S	272
5.20	Installation 2S1, Postshot.	273
5.21	Traps 2S2a and b, Postshot	274
5.22	Analysis of Natural-stone Missiles from Installation 2S1	275
5.23	Analysis of Natural-stone Missiles from Trap 2S2a.	276
5.24	Analysis of Natural-stone Missiles from Trap 2S2b.	277
5.25	Station 3S Layout Chart	278
5.26	Station 3S, Preshot	279
5.27	Overpressure vs. Time at Station 3S	280
5.28	Dynamic Pressure vs. Time at Station 3S	281
5.29	Traps 3S1a and b, Postshot	282
5.30	Installation 3S2, Postshot.	283
5.31	Analysis of Natural-stone Missiles from Trap 3S1a.	284
5.32	Analysis of Natural-stone Missiles from Trap 3S1b.	285

ILLUSTRATIONS (Continued)

5.33	Analysis of Natural-stone Missiles from Installation 3S2	286
5.34	Station 6S Layout Chart	287
5.35	Station 6S, Preshot	288
5.36	Overpressure vs. Time at Station 6S	289
5.37	Dynamic Pressure vs. Time at Station 6S	290
5.38	Traps 6S1a and b, Postshot	291
5.39	Installation 6S2, Postshot	292
5.40	Analysis of Natural-stone Missiles from Trap 6S1a	293
5.41	Analysis of Natural-stone Missiles from Trap 6S1b	294
5.42	Analysis of Natural-stone Missiles from Installation 6S2	295
5.43	Station 7S Layout Chart	296
5.44	Station 7S, Preshot	297
5.45	Overpressure vs. Time at Station 7S	298
5.46	Traps 7S1a and b, Postshot	299
5.47	Trap 7S2, Postshot	300
5.48	Analysis of Natural-stone Missiles from Trap 7S1a	301
5.49	Analysis of Natural-stone Missiles from Trap 7S1b	302
5.50	Analysis of Natural-stone Missiles from Trap 7S2	303
5.51	Station 8S Layout Chart	304
5.52	Installation 8S2 at Station 8S	305
5.53	Overpressure vs. Time at Station 8S	306
5.54	Dynamic Pressure vs. Time at Station 8S	307
5.55	Installation 8S1, Postshot	308
5.56	Traps 8S2a and b, Postshot	309
5.57	Analysis of Natural-stone Missiles from Installation 8S1	310
5.58	Analysis of Natural-stone Missiles from Trap 8S2a	311
5.59	Analysis of Natural-stone Missiles from Trap 8S2b	312
5.60	Profile of South Blast Line, Shot Smoky	313
5.61	Station 4S Layout Chart	314
5.62	Installation 4S2, Preshot	315
5.63	Overpressure vs. Time at Station 4S	316
5.64	Dynamic Pressure vs. Time at Station 4S	317
5.65	Installation 4S1, Postshot	318
5.66	Postshot View of Traps 4S2a and b	319
5.67	Analysis of Natural-stone Missiles from Installation 4S1	320
5.68	Analysis of Natural-stone Missiles from Trap 4S2a	321
5.69	Analysis of Natural-stone Missiles from Trap 4S2b	322
5.70	Station 9S Layout Chart	323
5.71	Traps 9S2a and b, Preshot	324
5.72	Overpressure vs. Time at Station 9S	325
5.73	Traps 9S2a and b, Postshot	326
5.74	Analysis of Natural-stone Missiles from Installation 9S1	327
5.75	Analysis of Natural-stone Missiles from Trap 9S2a	328
5.76	Analysis of Natural-stone Missiles from Trap 9S2b	329
5.77	Profile of North Blast Line, Shot Smoky	330
5.78	Station 5S Layout Chart	331
5.79	Station 5S, Preshot, Looking Toward GZ	332
5.80	Overpressure vs. Time at Station 5S	333
5.81	Traps 5S1a and b, Postshot	334
5.82	Installation 5S2, Postshot	335
5.83	Analysis of Natural-stone Missiles from Trap 5S1a	336
5.84	Analysis of Natural-stone Missiles from Trap 5S1b	337
5.85	Analysis of Natural-stone Missiles from Installation 5S2	338

ILLUSTRATIONS (Continued)

CHAPTER 6 SHOT GALILEO, EXPERIMENTAL PROCEDURE AND RESULTS

6.1	Station Locations for Shot Galileo in Area 1, NTS	356
6.2	Photograph of Galileo Installations Taken from the 500-ft Tower at GZ	357
6.3	Overpressure vs. Time at Station 3G	358
6.4	Layout Chart for Installations 3G1, 3G2, 3G3, and 3G4	359
6.5	Preshot View of Installations 3G1, 3G2, 3G3, and 3G4 (from Right to Left)	360
6.6	Missiles That Were Set Out 22.5 Ft in Front of Installations 3G2 and 3G3	361
6.7	Installation 3G3, Postshot	362
6.8	Layout Chart for Installations 3G5, 3G6, 3G7, 3G8b, and 3G9. Trap 3G8b is Stacked Above 3G8A	363
6.9	Preshot View of Installations 3G6, 3G7, 3G8b, and 3G9	364
6.10	Installation 3G6, Postshot	365
6.11	Installation 3G7, Postshot	366
6.12	Analysis of Window-glass Missiles from Installation 3G6	367
6.13	Analysis of Plate-glass Missiles from Installation 3G7	368
6.14	Analysis of Window-glass Missiles from Trap 3G8b	369
6.15	Analysis of Window-glass Missiles from Installation 3G9	370
6.16	Floor Plan of Reinforced Concrete-block House	371
6.17	Traps 3G10a, b, and c, Postshot	372
6.18	Spatial Distribution of Window-glass Missiles in Installation 3G10 Traps	373
6.19	Analysis of Window-glass Missiles from Trap 3G10a	374
6.20	Analysis of Window-glass Missiles from Trap 3G10b	375
6.21	Analysis of Window-glass Missiles from Trap 3G10c	376
6.22	Traps 3G11a, b, d, and e, Postshot	377
6.23	Spatial Distribution of Window-glass Missiles in Installation 3G11 Traps	378
6.24	Analysis of Window-glass Missiles from Trap 3G11a	379
6.25	Analysis of Window-glass Missiles from Trap 3G11b	380
6.26	Analysis of Window-glass Missiles from Trap 3G11d	381
6.27	Analyses of Window-glass Missiles from Trap 3G11e	382
6.28	Floor Plan of Precast-concrete House	383
6.29	Traps 3G12a, b, and c, Postshot	384
6.30	Spatial Distribution of Window-glass Missiles in Installation 3G12 Traps	385
6.31	Analysis of Window-glass Missiles from Trap 3G12a	386
6.32	Analysis of Window-glass Missiles from Trap 3G12b	387
6.33	Analysis of Window-glass Missiles from Trap 3G12c	388
6.34	Traps 3G13a, b, d, and e, Postshot	389
6.35	Postshot View of the Living Room of the Precast-concrete House where Traps 3G12a, b, d, and e were Located	390
6.36	Spatial Distribution of Window-glass Missiles in Installation 3G13 Traps	391
6.37	Analysis of Window-glass Missiles from Trap 3G13a	392
6.38	Analysis of Window-glass Missiles from Trap 3G13b	393
6.39	Analysis of Window-glass Missiles from Trap 3G13d	394
6.40	Analysis of Window-glass Missiles from Trap 3G13e	395
6.41	Analysis of Window-glass Missiles from 14 Traps (Stations 3G10, 3G11, 3G12, and 3G13)	396
6.42	Glass-fragment Data for 14 Traps in Houses Showing Per Cent of Total Missiles with Masses or Velocities Less Than a Given Value	397
6.43	Layout Chart for Station 4.3GTS	398

ILLUSTRATIONS (Continued)

6.44	Preshot Photograph of Station 4.3GTS Planted Missiles	399
6.45	Postshot Photograph of Station 4.3GTS Installation	400
6.46	Analysis of Gravel Missiles from Station 4.3GTS	401
6.47	Analysis of Gravel Missiles from Station 4.3GTS	402
6.48	Spatial Distribution of Gravel Missiles Recovered from Station 4.3GTS	403
6.49	Spatial Distribution of the Average Masses (in mg) of Gravel Missiles Recovered from Station 4.3GTS	404
6.50	Spatial Distribution of the Average Velocities (in ft/sec) of Gravel Missiles Recovered from Station 4.3GTS	405
6.51	Analysis of Natural-stone Missiles from Station 4.3GTS	406
6.52	Spatial Distribution of Natural-stone Missiles Recovered from Station 4.3GTS	407
6.53	Spatial Distribution of the Average Masses (in mg) of Natural-stone Missiles Recovered from Station 4.3GTS	408
6.54	Spatial Distribution of the Average Velocities (in ft/sec) of Natural-stone Missiles Recovered from Station 4.3GTS	409
6.55	Overpressure vs. Time for Stations 7GTS and 7G	410
6.56	Dynamic Pressure vs. Time for Stations 7GTS and 7G	411
6.57	Layout Chart for Station 7GTS	412
6.58	Station 7GTS, Postshot	413
6.59	Analysis of Gravel Missiles from Station 7GTS	414
6.60	Analysis of Gravel Missiles from Station 7GTS	415
6.61	Spatial Distribution of Gravel Missiles Recovered from Station 7GTS	416
6.62	Spatial Distribution of the Average Masses (in mg) of Gravel Missiles Recovered from Station 7GTS	417
6.63	Spatial Distribution of the Average Velocities (in ft/sec) of Gravel Missiles Recovered from Station 7GTS	418
6.64	Analysis of Natural-stone Missiles from Station 7GTS	419
6.65	Spatial Distribution of Natural-stone Missiles Recovered from Station 7GTS	420
6.66	Spatial Distribution of the Average Masses (in mg) of Natural-stone Missiles Recovered from Station 7GTS	421
6.67	Spatial Distribution of the Average Velocities (in ft/sec) of Natural-stone Missiles Recovered from Station 7GTS	422
6.68	Layout Chart for Station 7G	423
6.69	Concrete-block Wall (64 in. High, 40 ft Long, and 7.5 in. Thick) at Station 7G, Preshot	424
6.70	Photograph Illustrating the Scatter of Blocks from the Wall at Station 7G	425
6.71	Blocks from the Concrete-block Wall and Traps 7G1a and b, 7G2a and b, and 7G3b, Postshot	426
6.72	Traps 7G1a and b (Foreground) and 7G2a and b (Background)	427
6.73	Traps 7G2a and b, Postshot	428
6.74	Trap 7G3b	429
6.75	Final Positions of Whole, Half, and Joined Blocks from the Concrete-block Wall	430
6.76	Downwind Distribution of the Whole, Half, and Joined Blocks from the Concrete-block Wall	431
6.77	The Mass Distribution of all Fragments with Masses Over 0.1 Lb from the Concrete-block Wall	432
6.78	The Downwind Distribution of all Fragments with Masses Over 0.1 Lb from the Concrete-block Wall	433
6.79	Standard Deviation of Crosswind Displacement (S_{d_y}) vs. Downwind Displacement Squared ($d_x^2 \cdot d_x/ d_x $) for all Fragments with Masses Over 0.1 Lb from the Concrete-block Wall	434

ILLUSTRATIONS (Continued)

6.80	Spatial Distribution of all Fragments with Masses Over 0.1 Lb from the Concrete-block Wall	435
6.81	Analysis of Natural-stone Missiles from Trap 7G2a	436
6.82	Analysis of Natural-stone Missiles from Trap 7G2b	437
6.83	Analysis of Natural-stone Missiles from Trap 7G3b	438
6.84	Station 7G Installation from Traps 7G4a and b (in the Foreground on the Right) Through Traps 7G10a and b (in the Background), Preshot	439
6.85	Installation 7G4, Postshot, Showing Frame That Held Aluminum Foil for Extra Protection	440
6.86	Installation 7G5, Postshot, Showing Remains of Frame That Held Aluminum Foil for Extra Thermal Protection	441
6.87	Analysis of Natural-stone Missiles from Trap 7G4a	442
6.88	Analysis of Natural-stone Missiles from Trap 7G4b	443
6.89	Analysis of Natural-stone Missiles from Trap 7G5a	444
6.90	Analysis of Natural-stone Missiles from Trap 7G5b	445
6.91	Traps 7G6a and b, Postshot	446
6.92	Analysis of Window-glass Missiles from Trap 7G6a	447
6.93	Analysis of Window-glass Missiles from Trap 7G6b	448
6.94	Analysis of Window-glass Missiles That Arrived Flat at Traps 7G6a and 7G6b (Two from 7G6a and Two from 7G6b)	449
6.95	Analysis of Natural-stone Missiles from Trap 7G6a	450
6.96	Analysis of Natural-stone Missiles from Trap 7G6b	451
6.97	Trap 7G8b, Postshot	452
6.98	Analysis of Plate-glass Missiles from Trap 7G7b	453
6.99	Analysis of Plate-glass Missiles That Arrived Flat at Trap 7G7b	454
6.100	Analysis of Window-glass Missiles from Trap 7G8b	455
6.101	Analysis of Natural-stone Missiles from Trap 7G7b	456
6.102	Analysis of Natural-stone Missiles from Trap 7G8b	457
6.103	Installation 7G9, Preshot	458
6.104	Installation 7G9 Traps, Postshot	459
6.105	Analysis of Window-glass Missiles from Trap 7G9a	460
6.106	Analysis of Window-glass Missiles from Trap 7G9b	461
6.107	Analysis of Window-glass Missiles That Arrived Flat at Traps 7G9a and 7G9b (11 from 7G9a and 7 from 7G9b)	462
6.108	Analysis of Natural-stone Missiles from Trap 7G9a	463
6.109	Analysis of Natural-stone Missiles from Trap 7G9b	464
6.110	Installation 7G10 Traps, Postshot	465
6.111	Analysis of Gravel Missiles from Trap 7G10a	466
6.112	Analysis of Gravel Missiles from Trap 7G10b	467
6.113	Analysis of Gravel Missiles from Trap 7G10b	468
6.114	Analysis of Natural-stone Missiles from Trap 7G10a	469
6.115	Analysis of Natural-stone Missiles from Trap 7G10b	470

CHAPTER 7 DISCUSSION AND SUMMARY

7.1	Overpressure vs. Range Plots for Missile Stations on Shots Priscilla, Smoky, and Galileo	477
7.2	Theoretical Relations Between Maximum Velocities of Man and Stone Computed for each of the Missile Stations in Open Areas	478

TABLES

CHAPTER 2 MISSILE-ABSORBING TECHNIQUES AND METHODS OF ANALYSIS

2.1	Absorbers Used to Trap Missiles	30
2.2	Results of All Calibrations	36
2.3	Threshold Velocities for Spheres in Type II, III, IV, and V Absorbers	37

CHAPTER 4 SHOT PRISCILLA, EXPERIMENTAL PROCEDURE AND RESULTS

4.1	Partial Results for Spheres Recovered from Station 5P7	58
4.2	Partial Results for Spheres Recovered from Station 6P6	62
4.3	Partial Results for Spheres Recovered from Station 8P6	68
4.4	Masses and Distances Displaced for Large Stones, Blocks, and Bricks, Shot Priscilla	78
4.5	Blast Parameters, Shot Priscilla	80
4.6	Summary of Results, Shot Priscilla	81

CHAPTER 5 SHOT SMOKY, EXPERIMENTAL PROCEDURE AND RESULTS

5.1	Blast Parameters, Shot Smoky	247
5.2	Summary of Results, Shot Smoky	248

CHAPTER 6 SHOT GALILEO, EXPERIMENTAL PROCEDURE AND RESULTS

6.1	Blast Parameters, Shot Galileo	340
6.2	Summary of Results, Shot Galileo	353

CHAPTER 7 DISCUSSION AND SUMMARY

7.1	Summary of Traps	472
7.2	Summary of Objects Placed in Front of Traps	472
7.3	Number of Missiles for Which Velocities Were Determined	472



Chapter 1

INTRODUCTION

1.1 BACKGROUND

Experience with large-scale explosions, e.g., those of Hiroshima, Nagasaki,¹ and Texas City,^{2,3} has demonstrated that missiles resulting from blast effects are a significant cause of biological damage. These casualty-producing missiles were mostly fragments of glass from broken window panes, but they could have been any object not securely anchored which could be translated by the high winds accompanying a blast wave. Indeed, in many instances people themselves became missiles by virtue of their involuntary translation by the blast winds.

A systematic study⁴ of the translational velocities of window-glass fragments and stones was made during the 1955 weapons tests in Nevada (Operation Teapot). During the following Nevada test series in 1957 (Operation Plumbbob), translational effects were investigated by five separate projects: (1) Project 4.1, which used window-glass fragments as missiles and swine as targets;⁵ (2) Project 33.1, which used dogs in shelters as translational objects;⁶ (3) Project 33.3, which used anthropomorphic dummies in open areas as translational objects;⁷ (4) Project 33.4, which used window-glass fragments, gravel, and concrete blocks as missiles and dogs as targets;⁸ and (5) Project 33.2 whose studies are reported herein.

In addition to the field investigations noted above, a few laboratory type studies have been made which are pertinent to the evaluation of translational effects of blast waves. One study⁹ was aimed at establishing the penetrating potential of glass-fragment missiles into the abdominal cavity of dogs as a function of fragment mass and velocity at impact. Another study was concerned with the biological effects of direct impact of experimental subjects¹⁰ (mice, rats, guinea pigs, and rabbits) with a smooth hard surface, a situation similar to that which could occur as a result of translation by blast winds. A third study involved the use of a shock tube to accelerate goats and dummies;¹¹ these goats and dummies were then allowed to decelerate by tumbling over a flat grassy surface. It was concluded that the principal source of damage to the goats was the decelerative tumbling.

Two other studies of an analytical nature should be mentioned since they were motivated by the voluminous field data contained in this report. The first study resulted in a mathematical model¹² that allowed numerical computations of the velocity, displacement, and acceleration histories of arbitrary objects when exposed to classical blast waves such as those resulting from nuclear detonations. Before such a model could be used, it was necessary to determine certain aerodynamic parameters of the translated objects. Thus drop-test experiments¹³ were performed to permit the determination of acceleration coefficients for the experimental objects that were used in the present study (glass fragments, stones, etc.) as well as for mice, rats, guinea pigs, and rabbits. These efforts made it possible to present predicted velocities in this report for comparison with the ones determined experimentally.

1.2 CATEGORIES OF BIOLOGICAL EFFECTS OF BLAST

For purposes of orientation, the categories into which the biological effects of blast are usually divided are mentioned here briefly.¹⁴⁻¹⁷ These effects can be thought of as being of four distinct types: (1) primary; (2) secondary; (3) tertiary; and (4) miscellaneous.

The *primary* effects are those due to variations in environmental pressure caused by explosive events. As a general rule critical pathology is most marked in the air-containing organs (the lungs, gastrointestinal tract, ear, and paranasal sinuses) and at those locations where there is the greatest variation in tissue density.^{6,18-23}

Secondary blast effects are those due to missiles that are energized by the blast overpressures and winds or by ground shock and gravity.

Missiles may consist of fragments of window glass, stones, pieces of building debris, or any object other than man which is set in motion by the blast wave. Injury may result from penetration of the surface wall or organs of the body or from nonpenetrating impact of the missile.

If the biologic target is translated by the blast wave, ground shock, or gravity, the effect is called *tertiary*. Injury can occur during the accelerative phase of displacement; however, significant damage is more likely to occur during decelerative tumbling or upon impact with a stationary object.

The fourth category of blast damage consists of *miscellaneous* effects such as those due to blast-induced dust and fires as well as to gases, dust, or debris that have been heated aerodynamically or by direct thermal radiation.

1.3 OBJECTIVES

The purpose of the field tests reported herein was to produce information on blast-produced missiles which would be of value in assessing the secondary type blast injury described in the previous section. It will be apparent later that the results are also applicable to some extent to the evaluation of biological effects in the tertiary category.

Specifically, it was planned to determine individual translational velocities for various types of small objects (window-glass fragments, stones, spheres, etc.) by means of a trapping technique that was used first for this purpose during Operation Teapot.⁴ The technique used, described in Chap. 2, permitted the evaluation of velocities and masses for large samples of missiles that occurred near the location of the trap.

It was planned to obtain velocities, masses, and spatial distributions (where applicable) for the following types of missiles in the environments noted:

1. Window- and plate-glass fragments inside houses and in open areas where the windows were mounted without "benefit" of a house.
2. Natural (or native) stones in flat and hill-and-dale terrain.
3. Gravel that had been marked for identification and placed at various distances in front of traps in open areas.
4. Small metallic, nylon, and wooden spheres placed in front of traps in flat and hill-and-dale terrain and in a shelter with an open entryway.
5. "Military" debris (fragments of steel) placed in front of traps in flat and hill-and-dale terrain.

Since the size of objects that could be accommodated by a missile trap is limited, other studies were planned in which only the total displacement was to be determined. This included the displacement of large stones (up to about 20 kg) and of concrete blocks from a wall exposed to a blast wave.

The final and perhaps most significant objective was to compare missile velocities that were empirically determined with velocities that were computed* through use of the analytical work mentioned in the last paragraph of Sec. 1.1. From these comparisons it was hoped that

*The blast parameters used in these computations were determined from overpressure measurements made at each missile station by Ballistic Research Laboratories, Aberdeen, Md.

some degree of confidence could be established in the computational methods used. These methods could then be used to predict secondary-missile hazards for range-yield combinations different from those used in the test series.

REFERENCES

1. Samuel Glasstone (Ed.), "The Effects of Nuclear Weapons," Superintendent of Documents, U. S. Government Printing Office, Washington, D. C., June 1957.
2. George Armistead, Jr., The Ship Explosions at Texas City, Texas, on April 16 and 17, 1947, and Their Results, Engineering Consultants Report to John G. Simonds and Company, Inc., Oil Insurance Underwriters, New York City; Washington, D. C., June 1, 1947.
3. Virginia Blocker and T. G. Blocker, The Texas City Disaster — A Survey of 3000 Casualties, *Am. J. Surg.*, 78: 756-771(1949).
4. I. G. Bowen, A. F. Strehler, and M. B. Wetherbe, Distribution and Density of Missiles from Nuclear Explosions, Operation Teapot Report, WT-1168, December 1956.
5. G. M. McDonnell, H. A. Claypool, W. A. Moncrief, and J. D. Goldstein, Effects of Nuclear Weapons on a Large Biological Specimen (Swine), Project 4.1, Operation Plumbbob Report, ITR-1428, Nov. 5, 1957.
6. D. R. Richmond, R. V. Taborelli, I. G. Bowen, T. L. Chiffelle, F. G. Hirsch, B. B. Longwell, J. G. Riley, C. S. White, F. Sherping, V. C. Goldizen, J. D. Ward, M. B. Wetherbe, V. R. Clare, M. L. Kuhn, and R. T. Sanchez, Blast Biology — A Study of the Primary and Tertiary Effects of Blast in Open Underground Protective Shelters, Operation Plumbbob Report, WT-1467, June 30, 1959.
7. R. V. Taborelli, I. G. Bowen, and E. R. Fletcher, Tertiary Effects of Blast — Displacement, Operation Plumbbob Report, WT-1469, May 22, 1959.
8. V. C. Goldizen, D. R. Richmond, and T. L. Chiffelle, Missile Studies with a Biological Target, Operation Plumbbob Report, WT-1470, Jan. 23, 1961.
9. I. G. Bowen, D. R. Richmond, M. G. Wetherbe, and C. S. White, Biological Effects of Blast from Bombs: Glass Fragments as Penetrating Missiles and Some of the Biological Implications of Glass Fragmented by Atomic Explosions, USAEC Report AECU-3350, Lovelace Foundation for Medical Education and Research, June 18, 1956.
10. D. R. Richmond, I. G. Bowen, and C. S. White, Tertiary Blast Effects. 1. Effects of Impact on Mice, Rats, Guinea Pigs, and Rabbits, *Aerospace Med.*, 32: 789-805(September 1961).
11. R. S. Anderson, F. W. Stemler, and E. B. Rogers, Air Blast Studies with Animals, Part II, Report CRDLR-3049, Army Chemical Research and Development Laboratories, April 1961.
12. I. G. Bowen, R. W. Albright, E. R. Fletcher, and C. S. White, A Model Designed to Predict the Motion of Objects Translated by Classical Blast Waves, USAEC Report CEX-58.9, June 29, 1961.
13. E. R. Fletcher, R. W. Albright, V. C. Goldizen, and I. G. Bowen, Determinations of Aerodynamic-drag Parameters of Small Irregular Objects by Means of Drop Tests, USAEC Report CEX-59.14, October 1961.
14. C. S. White, I. G. Bowen, D. R. Richmond, and R. L. Corsbie, Comparative Nuclear Effects of Biomedical Interest, USAEC Report CEX-58.8, Jan. 12, 1961.
15. C. S. White, Biological Blast Effects, Hearings Before the Special Subcommittee on Radiation of the Joint Committee of Atomic Energy, Congress of the United States, Eighty-Sixth Congress, First Session on Biological and Environmental Effects of Nuclear War, Part 1, pp. 311-372, U. S. Government Printing Office, Washington, D. C., June 22-26, 1959.
16. C. S. White, Blast Biology — A Summary, a Contribution to the Holifield Subcommittee Hearings, May 1, 1958. Published in Report of Hearings Before a Subcommittee on Government Operations, House of Representatives, Part I — Atomic Shelter Tests, pp. 80-93, U. S. Government Printing Office, Washington, D. C., 1958.
17. C. S. White, Biological Blast Effects, USAEC Report TID-5564, Lovelace Foundation for Medical Education and Research, September 1959.
18. C. S. White, T. L. Chiffelle, D. R. Richmond, W. H. Lockyear, I. G. Bowen, V. C. Goldizen, H. W. Merideth, D. E. Kilgore, B. B. Longwell, J. T. Parker, F. Sherping, and M. E. Cribb, Biological Effects on Pressure Phenomena Occurring Inside Protective Shelters Following A Nuclear Detonation, Operation Teapot Report, WT-1179, Oct. 28, 1957.

19. D. R. Richmond, M. V. Wetherbe, R. V. Taborelli, T. L. Chiffelle, and C. S. White, The Biologic Response to Overpressure. I. Effects on Dogs of Five- to Ten-second Duration Overpressures Having Various Times of Pressure Rise, *J. Aviation Med.*, 28: 447-460 (1957).
20. D. R. Richmond, R. V. Taborelli, F. Sherping, M. B. Wetherbe, R. T. Sanchez, V. C. Goldizen, and C. S. White, Shock Tube Studies on the Effects of Sharp-rising, Long-duration Overpressures on Biological Systems, USAEC Report TID-6056, Lovelace Foundation for Medical Education and Research, Dec. 21, 1960.
21. C. S. White and D. R. Richmond, Blast Biology, USAEC Report TID-5764, Lovelace Foundation for Medical Education and Research, Sept. 18, 1959.
22. D. R. Richmond, V. R. Clare, V. C. Goldizen, D. E. Pratt, R. T. Sanchez, and C. S. White, Biological Effects of Overpressure. II. A Shock Tube Utilized to Produce Sharp-rising Overpressures of 400 Milliseconds Duration and Its Employment in Biomedical Experiments, *Aerospace Med.*, 32: 997-1008(1961).
23. D. R. Richmond, V. C. Goldizen, V. R. Clare, D. E. Pratt, F. Sherping, R. T. Sanchez, C. C. Fischer, and C. S. White, The Biologic Response to Overpressure. III. Mortality in Small Animals Exposed in a Shock Tube to Sharp-rising Overpressures of 3-4 Msec Duration, *Aerospace Med.*, 33: 1-27(1962).

Chapter 2

MISSILE-ABSORBING TECHNIQUES AND METHODS OF ANALYSIS

2.1 INTRODUCTION

It was possible to obtain impact velocities for large numbers of secondary missiles (objects translated by the blast wave) by techniques that required quite simple instrumentation. The field operation consisted of placing a suitable absorbing material downwind from the source of secondary missiles. Following the detonation the absorbing material was taken to the laboratory where each missile was extracted, and the depth of penetration and missile mass were measured. Impact velocity could then be determined by use of a calibration equation applicable to the type of absorber used and the type of missile caught.

This chapter will be concerned first with a description of the missile absorbers used and the methods of placing them in the field. Next will follow an account of the laboratory and analytical procedures used to arrive at calibration equations for each absorber and missile type combination. Finally, some of the statistical methods used to organize the large quantities of missile data obtained from the field tests will be reviewed.

2.2 MISSILE ABSORBERS

The missile-absorbing technique used in blast studies is characterized by the translated object's being accelerated by weak pressures applied over long distances in air and then being decelerated by stronger pressures over shorter distances in the absorber. This arrangement of pressure strengths is necessary so that the absorber will not be crushed by the dynamic pressure accelerating the missile as well as by the usually greater static pressure (or overpressure), especially if the latter is reflected at the surface of the absorber. Thus an absorber should be strong enough to withstand the pressures accompanying the blast wave yet weak enough to be penetrated by the missiles generated by the same wave. It should be noted that the blast wave does not decay appreciably between the time the missiles are generated and the time the wave reaches the absorbing material.

Mechanical properties other than compressive yield strength, described above, need to be considered in the choice of an absorber. It is important, for instance, that the shear strength be low so that each deformation be localized, i.e., the depth of penetration for each missile should not be influenced by the penetration of other missiles in the vicinity. Furthermore, it was found that the more nonresilient the material, the more reliably it could be calibrated. It is apparent that a material that would even partially return to its original shape after impact would be of little value in the measurement of impact velocities. In addition, obviously the material should be structurally uniform so that a velocity calibration obtained from using a sample of the absorber would apply to other material of the same type used in the field operation.

Another important consideration in the choice of an absorbing material is its resistance to heat. Even a temporary change in the mechanical properties of the absorber due to heating,

especially in the outer layer which is exposed to thermal radiation in most instances and to hot blast winds, could change the depth to which a missile would penetrate. Since the outer layer is most susceptible to thermal effects,* the errors introduced in the evaluation of missile velocities would be most significant for the objects with small depths of penetration.

The materials that were found to be suitable (with reservations) for the present study are listed in Table 2.1. Absorber types I, II, III, and IV are expanded polystyrenes.† Types V and VI are balsa wood, selected on the basis of density.

TABLE 2.1—ABSORBERS USED TO TRAP MISSILES*

Type	Description	Density, lb/cu ft	Compressive yield strength, psi	Shear strength, psi	Maximum temp. for continuous use, °F
I	Special order	1.54			
II	Styrofoam 22	1.6 to 2.0	16 to 32	27 to 36	175
III	Q-103.15	2.8 to 3.2	50 to 80	53 to 62	175
IV	Q-103.21	4.3 to 4.7	120 to 140	80 to 95	175
V	Balsa wood	7.85			
VI	Balsa wood	10.78			

* All absorbers except balsa wood were manufactured by Dow Chemical Co., Midland, Mich., using expanded polystyrene. Specifications for types II, III, and IV absorbers were supplied by the manufacturer. Balsa wood was used end-grain only.

Type I absorber was prepared on a special order,‡ but types II, III, and IV are stock items. These materials were tested in a shock tube for compressive yield strength under dynamic conditions. Samples that were 2 in. thick and 1 ft square were cemented to the closed end of the tube. For types II, III, and IV, it was found that the compressive yield strengths determined in the dynamic tests were approximately the same as those specified by the manufacturer for static loading (see the fourth column of Table 2.1). Thus these data served as a guide in the selection of the type of absorber to be used at various field installations.

The mechanical properties of the expanded polystyrene were found to be reasonably good. The principal difficulty encountered with the balsa wood was its nonuniformity. Homogeneity was improved by dividing pieces of wood into two groups according to density and making calibrations for each group separately. It was found that when the wood was used end-grain the deformations were localized to the areas of impact.

Since all types of absorbing material used were susceptible to modification by heat, it was necessary to provide thermal protection without appreciably changing the missile-catching properties of the absorber. In shot Priscilla this consisted in placing two 0.0007-in.-thick layers of aluminum foil over the exposed side of the absorber. This proved to be insufficient protection in some instances; therefore additional protection was arranged for some of the installations in later shots (see Sec. 2.3 and Fig. 2.2).

2.3 CONSTRUCTION OF TRAP HOUSING AND ANCHORS AND WINDOW MOUNTS

Construction details for the trap housing that was used at most installations are illustrated in Fig. 2.1. The housing was designed to hold absorbing material 36 in. wide, 12 in. high, and 11 in. deep. Types II, III, and IV absorbing material were placed in the housing in 1- and 2-in.

* The reasons for this are that (1) the times of exposure to thermal effects are relatively short and (2) the absorbing materials with the required mechanical properties are usually good thermal insulators (low conductance) with low heat capacities.

† Manufactured by Dow Chemical Co.

‡ This is the same material that was used by Project 33.4 during Operation Teapot.¹

layers by removing the back, which was secured with wood screws (see the $\frac{3}{4}$ -in. plywood member shown in Section B of Fig. 2.1). The $\frac{3}{8}$ -in. plywood lid was easily removed and was convenient for the protection of the absorber during shipment and during and after installation in the field. Except for the front and back, the housing was assembled with glue, screws, and bolts, countersunk where necessary.

The housing, illustrated in Fig. 2.1, was also used with balsa absorbers (types V and VI). Small blocks of balsa wood measuring about 4 in. along the grain were cemented end-grain to a sheet of $\frac{3}{4}$ -in. plywood that was 36 in. long and 12 in. wide. This assembly was then placed in the trap with the balsa surface against the flange that held the trap lid. The extra space between the balsa assembly and the back of the trap was filled with suitable structures made of $1\frac{1}{2}$ -in. plywood.

Type I absorber was procured in sheets about 2 ft wide, 2 ft high, and 1 in. thick. The housing used for this material accommodated an approximate 2-ft cube of absorber. A more complete description of this type housing as well as its anchor can be found in Ref. 1.

Another type trap was constructed in the field by cementing a 2-in. layer of absorber (type II, III, or IV) to the walls of a structure with ordinary linoleum cement (see Secs. 4.13, 6.3, and 6.4).

A typical trap installation using the housing illustrated in Fig. 2.1 is shown in Fig. 2.2. The trap was secured to the 4.5-ft-wide by 3.5-ft-long by 3-ft-deep concrete base by three 6-in. I-beams in the rear and four 1-in. rods holding a 12-in. channel on top of the trap. A wooden frame mounted about 1 ft in front of the trap held one layer of 0.0015-in.-thick aluminum foil. This foil protected the trap from the thermal pulse that occurred before the arrival of the blast wave. The blast wave then ruptured the foil before the arrival of secondary missiles. In some instances the wooden frame itself was blown away by the blast wave.

Figure 2.3 is a sketch of a window mount and a double-trap installation, one stacked above the other. The dashed lines on the drawing represent structures below ground level: two concrete slabs whose upper surfaces were at ground level and part of the timber framework holding the steel window. The only parts of the above-ground structures, other than the glass, which showed any permanent deformation due to the blast waves were the steel window frames, which were usually slightly bent in the direction away from GZ.

The steel frames (Fig. 2.3) were fitted with ordinary double-strength window glass* that had a nominal thickness of $\frac{1}{8}$ in. The frames were always oriented so that the putty holding the panes in place was toward GZ. At a few of the installations, a single piece of plate glass† ($\frac{1}{4}$ in. nominal thickness) was mounted using the timber structure illustrated but without the steel frame. The stronger side of the support was oriented away from GZ.

Window-glass missiles were also investigated in two houses on shot Galileo. The structural details of these experiments are described in Secs. 6.2.4 and 6.2.5.

2.4 CALIBRATION OF MISSILE ABSORBERS

2.4.1 Experimental Procedure

The air gun and the velocity-measuring device used in the calibration of absorbers are described in Ref. 1. Three sizes of gun barrels were used; the gun barrels were about 8 ft long and were 1, 2, and 3 in. in inside diameter. Sabots were made of various types of expanded polystyrene (see Table 2.1). The sabots consisted of cylindrical plugs with diameters somewhat smaller than, and lengths at least as large as, the diameter of the gun barrel to be used.

For the larger sized gun barrels it was not feasible to use a choke to stop the sabot, as described in Ref. 1. Instead, the following procedure was used: A hole about one-half as long as the sabot was drilled in one of its flat surfaces. The missile to be shot was placed at the bottom of the hole.‡ The rim of the cup-like sabot, which contacted the target first, served to

* Libby Owens Ford, B quality.

† Franklin Glass Corp.

‡ The fragment missiles could be given an impact orientation by lightly imbedding an edge of the fragment in the sabot.

decelerate the sabot before the impact of the missile. The advantage of this procedure was that the light beams that controlled the electronic timer were interrupted by a sabot of regular shape instead of by a missile of irregular shape followed by a sabot.

To serve as a check on the velocity determinations that were made with the gun, as well as to produce additional calibration data, free-fall experiments were performed in an elevator shaft where the usable free-fall distance was about 48 ft (with corresponding impact velocities up to approximately 55 ft/sec). In these experiments the absorbing material was placed at the bottom of the shaft, and the missiles ($\frac{1}{16}$ - to $\frac{15}{16}$ -in.-diameter steel spheres) were dropped from a measured distance. Results obtained from another study² were used to evaluate impact velocity. The penetration data obtained in this way were found to be comparable to those resulting from the air-gun experiments.

2.4.2 Glass Fragments with Random Orientations

Experimentation with the calibration of type II absorber with glass fragments showed that the depth of penetration was almost independent of impact orientation of the fragment provided the angle made by the flat side of the missile and the absorber was greater than about 15° . It was also found that the thickness of the glass from which the fragment was made was not significant in determining its depth of penetration. Two significant parameters, however, were missile mass and impact velocity. It was empirically determined that, for fragments of a given mass, the calibration data would fit an equation of the form

$$\log v = A + B \log s \quad (2.1)$$

where A and B are constants if the missile masses are constant, v is the impact velocity, and s is the depth of penetration.

Further investigation showed that A and B could be represented within wide ranges of mass by

$$A = a + c \log m \quad B = b + d \log m \quad (2.2)$$

where a, c, b, and d are constants and m is missile mass. Thus, when Eqs. 2.1 and 2.2 are combined, the resulting calibration equation is

$$\log v = a + c \log m + (b + d \log m) \log s \quad (2.3)$$

The experimental data for randomly oriented glass fragments in type II absorber consisted of values of impact velocity, mass, and depth of penetration for 258 shots. As an aid to the analysis of the data, the missiles were grouped according to mass; the range of masses within each group was ± 2.5 per cent of the average. The average masses of seven groups of fragments thus formed were from 0.0274 to 11.406 g.

It was necessary to determine two fits with Eq. 2.3: one for missiles of small mass and the other for missiles of large mass. The resulting equations, along with appropriate plots, are presented in Fig. 2.4.

An enlarged version of the chart in Fig. 2.4 was used to evaluate velocities* for glass fragments that were caught in the field operation by the type II absorber. The velocity vs. mass analysis for each sample of missiles caught (described and illustrated later in the report) demonstrated that log velocity was an approximately linear function of log mass. Thus for analytical purposes it was decided to group the field data into constant log-mass and log-velocity intervals. The log intervals used (based on common logarithms, \log_{10}) were 0.1 for mass and 0.05 for velocity. These intervals, labeled a through v for velocity and A through Z and AA through KK for mass, are plotted in Fig. 2.4. The appropriate group identifier was determined for each missile by means of simultaneous mass and depth-of-penetration entries on the chart.

*At the time this work was done an electronic computer was not available.

The standard error of estimate in log velocity obtained for the 258 data points using the least-squares analysis described above was 0.0485 log unit, or about 11 per cent. It is of interest to note that this value (0.0485) is only slightly smaller than the log-velocity intervals (0.05) plotted in Fig. 2.4. Also noteworthy is the observation that at high velocities the depth of penetration, percentagewise, is much less dependent on missile mass than at low velocities; e.g., at 398 ft/sec a fragment that weighs 10 g penetrates about three times as deep as one that weighs 0.1 g, whereas at 39.8 ft/sec the ratio between depths of penetration is approximately 30 for missiles of the same masses.

2.4.3 Glass Fragments With Flat Orientations

A few of the absorbers that were placed behind windows (especially those containing plate glass) received impressions that indicated that fragments had struck with a flat surface forward and that no appreciable change in orientation occurred during deceleration. In most cases the larger fragments impacting in this manner did not remain in the absorber but fell to the ground. However, the missile could be described even though it was not retrieved, since the thickness and density of the glass were known and the area of the fragment could be estimated from the impression in the absorber.

Calibration experiments were designed for the flat type impact with the assumption that the missile could be described by two parameters: (1) mass per unit impact area or area density (m/A) and (2) impact area (A). Average values of m/A corresponding to double-strength window glass and plate glass used in the field tests were 4.957 and 9.498 g/sq in. It was not feasible to shoot actual plates from the air gun; therefore plates were simulated by cementing 0.064- to 0.130-in.-thick Plexiglass disks to the end of balsa cylinders, and the total mass was adjusted to achieve the desired values of area density. These missiles, which were made to fit three sizes of gun barrels, had impact areas of 0.7466, 3.032, and 6.998 sq in. Three missiles were made with each of the above areas, but with different area densities, making a total of nine test objects.

Each of the nine test missiles was shot 10 times into type II absorber at velocities ranging from about 59 to 220 ft/sec; the depth of penetration was from 0.026 to 1.96 in. Data for each missile were fitted by the least-squares method to the following form, area density and impact area being constant:

$$\log v = C + 0.5 \log (s + k) \quad (2.4)$$

where v is the impact velocity, C and k are the regression coefficients, and s is the depth of penetration.

Further analysis showed that k was a function of area alone and could be represented by

$$\log k = -0.7099 + 0.3502 \log A \quad (2.5)$$

where A is in square inches and k , to be added to s , is in inches.

By use of data for missiles of the same area density, C in Eq. 2.4 could be represented by

$$C = c_1 + c_2 \log A \quad (2.6)$$

where c_1 and c_2 are regression coefficients but can be defined in terms of area density as

$$c_1 = d_1 + d_2 \left(\frac{m}{A}\right) + d_3 \left(\frac{m}{A}\right)^2 \quad (2.7)$$

and

$$c_2 = e_1 + e_2 \left(\frac{m}{A}\right) + e_3 \left(\frac{m}{A}\right)^2 \quad (2.8)$$

When Eqs. 2.4, 2.6, 2.7, and 2.8 are combined and values for the regression coefficients are substituted, the following calibration equation results:

$$\log v = 2.3472 + 0.00045 \left(\frac{m}{A} \right) - 0.002244 \left(\frac{m}{A} \right)^2 + \left[-0.01756 + 0.00009 \left(\frac{m}{A} \right) - 0.000439 \left(\frac{m}{A} \right)^2 \right] \log A + 0.5 \log (s + k) \quad (2.9)$$

where k is defined in Eq. 2.5 as a function of A , and the units are: for v , feet per second; m , grams; A , square inches; and s , inches. When only the data for test missiles with area densities that corresponded to double-strength window glass and plate glass were used, the standard error of estimate in log velocity was found to be 0.0122 log unit, or about 3 per cent.

An enlarged version of the nomogram in Fig. 2.5 was used to solve Eq. 2.9 for the purpose of evaluating velocities for the appropriate missiles caught in the field operation. Equation 2.5, which defines k in terms of impact area, was solved by a simple graph (which is not shown). Use of the nomogram is illustrated in the lower left portion of Fig. 2.5; the illustration involves one step where values of A and m/A are entered and another where $(s + k)$ is entered and velocity is read.

2.4.4 Gravel and Natural Stones

Calibration data for gravel and natural stones were not significantly different from each other and were therefore combined for analysis. The experimental and analytical procedures followed were essentially the same as those described in Sec. 2.4.2 for glass fragments with random orientations. In some instances it was necessary to divide the data into two or more parts, according to missile mass, and to apply a regression equation of the form of Eq. 2.3 to each part separately. Calibration data for the balsa absorbers showed much more variability than did those for the more structurally uniform plastic absorbers. Detailed information in regard to the resulting calibration equations as well as their limits of applicability will be presented in Sec. 2.4.6 and Table 2.2.

2.4.5 Spheres and Military Debris

With the exception of the soda-glass spheres, the mass for each type and diameter of sphere could be considered constant. Thus, for spheres of constant mass, the following simpler type of calibration equation was used:

$$\log v = a + b \log (s + k) \quad (2.10)$$

where v is impact velocity, a and b are regression coefficients, s is depth of penetration, and k is a correction term added to the total depth of penetration to yield the depth of a cylindrical deformation of the same diameter and volume as the one observed but with a flat bottom instead of the rounded one made by a sphere.

The correction k , defined above, was used only in instances where its application would reduce the standard error of estimate in log velocity. In some cases depths of penetration less than the sphere radius were of interest. For these shallow deformations the actual depth was used to compute an equivalent depth—the equivalent depth is defined as the depth of a flat-bottom cylindrical hole with the same diameter as the sphere and same volume as the actual deformation.

Soda-glass-sphere data for penetration in the plastic absorbers were analyzed in a manner similar to that used for glass fragments (Sec. 2.4.2). However, for the type V balsa absorber, the calibration equation used was similar to Eq. 2.10 with $k = 0$; the results are applicable to spheres with masses within specified limits.

Detailed information regarding the individual calibration equations is given in Table 2.2.

The military debris used in this study consisted mostly of steel fragments that were produced by the deformation of small steel-encased charges of high explosives.

The depths of penetration for steel fragments of constant mass and velocity were averaged for a number of randomly oriented impacts. It was found that steel spheres of the same mass

and impact velocity would penetrate to a depth not significantly different from that for the average value for the fragments. Thus the steel-sphere penetration data were used to estimate the impact velocities of military debris, using the calibration for the sphere whose mass was nearest the steel fragment of interest. The steel spheres varied from $\frac{1}{8}$ to $\frac{15}{16}$ in. in diameter and from 0.1308 to 54.95 g in mass (see Table 2.2).

2.4.6 Summary of Calibration Results

The results obtained from the calibration procedures discussed in the previous sections are listed in Table 2.2. The equations presented in tabular form are those which were used to determine impact velocity for missiles trapped in the various absorbers employed in the field operation. Other quantities are specified which make it possible to assess the limits of applicability of the calibration equations.

The numbers listed under a, b, c, and d are regression coefficients for the general calibration equation stated at the top of the table. The values given under k are corrections to be added to the depth of penetration, s. In some instances a different form of regression equation was used, in which case the appropriate equation is presented as a footnote to the table.

Maximum and minimum values of the following parameters used in the calibration procedures are designated by the subscripts + and -, respectively: M for missile mass, grams; s for depth of penetration, inches; and V for impact velocity, feet per second.

The numbers listed under n in the table designate the number of missile penetrations used to determine the calibration equations. E_{lv} is the standard error of estimate in log-velocity units and $(E_{lv})\%$ is the same quantity expressed in per-cent-of-velocity units.

2.5 THRESHOLD VELOCITIES

Threshold velocity, as used in this report, is the lowest velocity of impact that can be evaluated for a given missile-absorber combination. The importance of the concept in the design of secondary-missile experiments was implied in Sec. 2.2. The use of threshold velocities in the interpretation of field data will be discussed in the latter part of this section.

With the exception of glass fragments that impacted flat, the criterion for computing threshold velocity was that the depth of penetration be just sufficient for the missile to be retained in the absorber. In the case of spheres, the "sufficient" depth was assumed to be equal to the radius of the sphere. For stones the critical, or threshold, depth was taken to be the radius of a sphere with the same mass and density as that of the stone. A similar assumption was made for randomly oriented glass fragments,* except that both the radius and diameter of the "equivalent" sphere were used. This resulted in a band of threshold velocities, as illustrated in Fig. 2.6; the upper limit is for a penetration depth of one diameter of the equivalent sphere, and lower limit, one radius. The reason for the greater uncertainty of the threshold velocities for glass fragments is that retention is more dependent on orientation of impact for plate-like missiles than for objects that are usually more spherical, such as stones.

Since it was not necessary to recover the impacting glass fragment if its broad surface had the same orientation as the surface of the absorber (see Sec. 2.4.3), the requirement for velocity determination was simply that the impression made in the absorber be detectable. Figure 2.7 is a plot of threshold velocity as a function of missile mass for window and plate glass with flat orientations at impact. The data in this figure were computed on the assumption that a 0.05-in. deformation is detectable and measurable.

Threshold velocities for natural stone and gravel are shown in Fig. 2.8 as a function of missile mass for absorber types II, III, IV, V, and VI. A density of 2.72 g/cm^3 was used for both natural stones and gravel to make the necessary computations.

Figure 2.9 displays threshold velocities for $\frac{1}{8}$ -in.-diameter nylon spheres in absorber types II, III, and IV, and seven $\frac{1}{8}$ - to $\frac{15}{16}$ -in.-diameter aluminum spheres impacting in ab-

*The average density of window and plate glass was 2.42 g/cm^3 .

TABLE 2.2—RESULTS OF ALL CALIBRATIONS
(See List of Symbols)

$\log v = a + c \log m + (b + d \log m) \log (s + k)$ where v is in feet per second, m , grams; and a , inches; and a , b , c , and d are constants

Missile	Absorber Type	a	b	c	d	k	M ₁	M ₂	a ₁	a ₂	V ₁	V ₂	n	E _N ⁽¹⁾	(E _N) ⁽¹⁾			
WG; PG	I	2.1790	0.5	-0.01955	0	0	0.0164	4.990	0.385	7.230	123	344	96	0.0456	10.5			
	II(2)	2.2464	0.5641	-0.1525	0.1608	0	0.0274	0.3814	0.065	1.913	120	391	258	0.0485	11.2			
		2.2124	0.5389	-0.2704	0.1409	0	1.443	11.406	0.445	4.450	69.0	262						
FWG; FPG	II	See footnote 3										0.026	1.96	59.0	220	90	0.0122	2.8
NS; Gr	I	See footnote 4																
	II	2.2865	0.8126	-0.1477	0.1763	0	0.0353	0.145	0.143	0.939	105	287	240	0.0387	8.9			
		2.1756	0.8128	-0.2890	0.1783	0	0.145	0.402	0.148	1.367	190	251						
		2.2310	0.8126	-0.1399	0.1783	0	0.402	0.569	0.302	1.438	95.3	234						
		2.2125	0.8517	-0.2414	-0.1607	0	0.680	2.150	0.322	2.156	80.7	205						
		2.5050	0.5429	-0.1648	0.0233	0	0.011	0.0433	0.048	1.093	151	795	47	0.0548	12.5			
		See footnote 5																
	IV	2.4906	0.5790	-0.2273	0.0259	0	0.0311	3.291	0.089	7.765	145	1015	243	0.0348	8.0			
	V	2.7528	0.5294	-0.2398	-0.0604	0	0.251	10.610	0.072	4.860	108	849	81	0.0991	20.9			
	VI	2.8630	0.8142	-0.1442	0.1089	0	0.030	0.233	0.042	1.844	151	1015	65	0.0339	24.2			
		2.8134	0.6037	-0.2384	0.0535	0	0.233	7.950	0.080	3.100	93.4	1015	85	0.0962	22.3			
Ny 1/4	II	2.5389	1.9550	0	0	-0.021	0.01973		0.070	6.526	188	309	10	0.0206	4.8			
	III	2.7475	0.4057	0	0	0	0.01973		0.280	6.821	328	458	10	0.0096	2.2			
	IV	2.8478	0.3930	0	0	-0.021	0.01973		0.102	0.512	262	534	9	0.0107	2.5			
Al 1/4	II	2.4119	0.3794	0	0	0	0.04734		0.159	8.802	128	233	9	0.0083	1.9			
	III	2.5828	0.4272	0	0	0	0.04734		0.139	0.868	150	342	14	0.0123	2.8			
	IV	2.8697	0.3934	0	0	-0.021	0.04734		0.133	0.435	291	338	10	0.0073	1.7			
	V	3.0298	0.5845	0	0	0	0.04734		0.036	0.539	149	807	17	0.0526	12.1			
Al 1/8	II	2.3453	0.4112	0	0	0	0.1537		0.242	2.098	123	311	10	0.0155	3.6			
	III	2.4732	0.4350	0	0	0	0.1537		0.143	0.948	126	284	10	0.0105	2.4			
	IV	2.8008	0.4254	0	0	-0.031	0.1537		0.130	0.500	149	286	10	0.0091	2.1			
	V	2.8873	0.5717	0	0	0	0.1537		0.072	0.992	152	782	12	0.0555	12.1			
Al 1/4	II	2.2688	0.4326	0	0	0	0.3767		0.282	1.963	102	246	10	0.0120	2.8			
	III	2.3982	0.4828	0	0	0	0.3767		0.231	1.321	123	293	10	0.0056	1.3			
	IV	2.5408	0.4472	0	0	-0.042	0.3767		0.192	0.760	151	299	9	0.0092	2.2			
	V	2.8098	0.5814	0	0	0	0.3767		0.084	1.993	145	907	11	0.0289	6.8			
Al 1/8	II	2.1583	0.5019	0	0	0	1.2662		0.303	1.741	78.9	192	10	0.0026	0.6			
	III	2.3082	0.5342	0	0	0	1.2662		0.215	1.299	86.5	227	10	0.0092	2.1			
	IV	2.4823	0.4951	0	0	-0.062	1.2662		0.353	0.993	153	276	10	0.0092	2.2			
Al 1/2	II	2.0707	0.5115	0	0	0	2.9441		0.416	1.574	75.6	150	10	0.0090	2.1			
	III	2.2515	0.6286	0	0	0	2.9441		0.237	1.452	70.7	224	10	0.0077	1.8			
Al 1/4	II	1.9305	0.8199	0	0	0	10.172		0.393	1.735	47.8	117	10	0.0284	6.1			
	III	2.1347	0.6587	0	0	0	10.172		0.307	1.195	62.3	153	10	0.0038	0.9			
Al 1/16	II	1.8827	0.6125	0	0	0	19.828		0.677	1.900	59.8	110	10	0.0126	2.9			
	III	2.1116	0.6995	0	0	0	19.828		0.265	1.283	46.8	138	10	0.0066	1.5			
St 1/4	II	2.2178	0.3494	0	0	-0.021	0.13008		0.091	0.852	82.7	157	9	0.0153	3.2			
	III	2.3687	0.4530	0	0	0	0.13008		0.134	0.544	95.8	181	10	0.0112	2.6			
	IV	2.4859	0.4271	0	0	-0.021	0.13008		0.094	0.382	96.7	190	10	0.0071	1.7			
	V	2.6971	0.5195	0	0	0	0.13008		0.042	0.995	90.8	505	17	0.0514	10.7			
St 1/8	II	2.0408	0.4317	0	0	-0.042	1.0434		0.172	1.281	48.1	121	10	0.0029	0.7			
	III	2.2075	0.5219	0	0	0	1.0434		0.252	0.839	78.3	146	10	0.0072	1.6			
	IV	2.3582	0.4703	0	0	-0.042	1.0434		0.183	0.622	91.6	179	10	0.0079	2.0			
	V	2.5231	0.5636	0	0	0	1.0434		0.139	2.257	114	439	21	0.0562	11.8			
St 1/4	IV	2.2686	0.5225	0	0	0	3.5211		0.387	4.580	109	412	11	0.0060	1.4			
	St 1/16	II(6)	1.9471	0.4771	0	0	(7)	5.5971		0.175	0.427	29.6	53.3	24	0.0063	1.4		
	III(8)	2.0610	0.5991	0	0	0	5.5971		0.104	1.515	29.6	145	32	0.0061	1.4			
	IV	2.2208	0.5927	0	0	0	5.5971		0.419	4.658	168	360	12	0.0039	0.9			
St 1/2	II(9)	1.8639	0.3898	0	0	(10)	8.353		0.180	0.522	29.7	53.5	24	0.0037	0.9			
	III	2.0414	0.5188	0	0	(9)	8.353		0.192	1.655	35.7	139	10	0.0032	0.7			
	IV	2.1784	0.5351	0	0	0	8.353		0.494	4.232	101	324	12	0.0071	1.6			
	V	2.4118	0.5095	0	0	0	8.353		0.178	2.975	94.3	444	21	0.0590	13.6			
St 1/16	II	1.8577	0.5387	0	0	0	11.874		0.194	0.5732	29.7	53.6	24	0.0059	1.4			
	III	2.0192	0.5154	0	0	(10)	11.874		0.245	1.747	39.2	137	10	0.0032	0.7			
	IV	2.1344	0.5516	0	0	0	11.874		0.516	4.412	93.7	306	12	0.007	1.5			
St 1/8	IV	2.0862	0.5510	0	0	0	28.110		0.767	5.201	103	298	15	0.0160	3.7			
	St 1/16	JV	2.0258	0.5447	0	0	0	54.95		0.971	4.311	99.4	246	12	0.0125	2.9		
	V	2.2848	0.4842	0	0	0	54.95		0.142	3.375	70.4	326	8	0.0355	8.2			
Ge, G1, G2	II	2.1978	0.5235	-0.1661	0.0870	(11)	0.030	0.300	0.181	2.048	118	294	43	0.0145	3.4			
	III	2.2171	0.5635	-0.1842	0.0950	0	0.0378	0.248	0.110	1.455	114	391	50	0.0185	4.3			
	IV	2.4540	0.5358	-0.1834	0.720	0	0.0378	0.248	0.051	1.141	139	429	58	0.0109	2.5			
G3	V	2.9987	0.4019	0	0	0	0.0416	0.0439	0.060	0.577	159	785	10	0.0442	10.2			
	Q1	2.9280	0.5191	0	0	0	0.0891	0.0727	0.040	1.012	153	807	10	0.0385	8.4			
CB	IV(6)	1.8915	0.4946	0	0	0	355.0	357.5	0.124	0.427	30.0	48.2	16	0.0361	8.3			

(1) E_N is the standard error of estimate in log-velocity units, and $(E_N)^2$ is the standard error of estimate in per-cent-of-velocity units.

(2) Figure 2.4 is a plot of these equations.

(3) $\log v = 2.3472 + 0.00045 (m/A) - 0.002244 (m/A)^2 + [-0.01756 + 0.00009 (m/A) - 0.000439 (m/A)^2] \log A + 0.5 \log (s + k)$, where $\log k = -0.7099 + 0.3502 \log A$; A , square inches; m , grams; and $4.958 \pm (m/A) \pm 9.602$ (see Fig. 2.5).

(4) G. Bowen, A. F. Strehler, and M. B. Wetherby, Distribution and Density of Missiles from Nuclear Explosions, Operation Teapot Report, WT-1168, December 1956, p. 21.

(5) $\log v = \log [1000 / (1.8968 \log m + 4.4704)] + [0.5505 + 0.0388 \log m + 0.00982 (\log m)^2] \log s$.

(6) Calibration data obtained by drop method.

(7) For $s \geq 0.219$, $k = -0.073$; for $s < 0.219$, $(s + k) = 6.950 s^2 (0.657 - s)$.

(8) Combined data from air-gun and drop method.

(9) For $s \geq 0.250$, $k = -0.093$; for $s < 0.250$, $(s + k) = 5.333 s^2 (0.750 - s)$.

(10) For $s \geq 0.281$, $k = -0.094$; for $s < 0.281$, $(s + k) = 4.222 s^2 (0.843 - s)$.

(11) $0.02513 (m)^{-1/3}$.

sorber types II, III, IV, and V. Note that the nylon spheres, because of their lesser density, require considerably higher velocities to penetrate the depth of one radius than do aluminum spheres of the same size.

Threshold velocities shown in Fig. 2.10 are for steel spheres with diameters from $\frac{1}{8}$ to $\frac{9}{16}$ in. for absorber types II and III and from $\frac{1}{8}$ to $\frac{15}{16}$ in. for absorber types IV and V. It is interesting to note that, for the more dense absorbers (types IV and V), the threshold velocities are about the same for the small as for the large spheres. For the two less-dense absorbers (types II and III), however, threshold velocities decrease with sphere diameter up to about $\frac{1}{2}$ in. The data for the $\frac{9}{16}$ -in.-diameter sphere suggest that larger spheres would have higher threshold velocities.

TABLE 2.3— THRESHOLD VELOCITIES FOR SPHERES IN TYPES II, III, IV, AND V ABSORBERS

Spheres	Velocity, ft/sec				Mass, mg
	Type II	Type III	Type IV	Type V	
Ny $\frac{1}{8}$	186	181	202		19.7
Al $\frac{1}{8}$	90	112	134	206	47.3
Al $\frac{3}{16}$	83.5	105	123	199	154
Al $\frac{1}{4}$	75.5	90.1	114	193	377
Al $\frac{3}{8}$	62.3	83.1	104		1,266
Al $\frac{1}{2}$	58.1	74.7			2,944
Al $\frac{3}{4}$	46.1	70.5			10,172
Al $\frac{15}{16}$	48.0	76.2			19,828
St $\frac{1}{8}$	54.3	66.6	78.3	118	131
St $\frac{1}{4}$	37.3	54.5	77.9	117	1,043
St $\frac{3}{8}$			77.4		3,532
St $\frac{1}{2}$	35.3	46.3	77.4		5,597
St $\frac{3}{4}$	36.4	43.5	71.8	127	8,353
St $\frac{9}{16}$	41.0	44.1	67.7		11,870
St $\frac{3}{4}$			71.0		28,161
St $\frac{15}{16}$			70.2	134	54,950
G \bar{s}	117	113	150		40.0
G \bar{s}				182	42.7
G \bar{l}	102	103	139		72.6
G \bar{l}				222	70.9
G \bar{x}	80	89	125		242.4

Threshold velocities for soda-glass beads with an average density of 2.55 g/cm^3 are plotted in Fig. 2.11. Consistent with the calibration equations (see Table 2.2), threshold velocities are shown as functions of sphere mass for the plastic absorbers (types II, III, and IV) and for two sphere-mass values for the balsa absorber (type V) (see points labeled "Small Spheres" and "Large Spheres" in Fig. 2.11).

For the convenience of the reader, the sphere threshold velocities that are presented graphically in Figs. 2.9 to 2.11 are listed in Table 2.3. The nomenclature used in the first column to describe the spheres is given in the List of Symbols, pages 7 to 9.

Although the assumptions made in computing threshold velocities were somewhat arbitrary, the results showed a reasonable agreement with the field data. Very few missile velocities were evaluated which were below the computed threshold; however, this does not mean that every missile that struck the trap with above-threshold velocities was retained in the absorber. (Also, some of the missiles that were not firmly imbedded in the absorber were dislodged during transport of the traps from the field to the laboratory.) Actually, a definite threshold velocity cannot be established for any missile. A more realistic concept is that of a band, or range, of threshold velocities as a function of missile mass, such as is portrayed for glass fragments in Fig. 2.6.

In spite of the limitations noted above, the computed threshold velocities proved to be quite useful in the interpretation of the field data. For example, if the mean of measured velocities was near the threshold, it could be assumed that the sample was truncated at the lower end, and therefore the computed mean was too high. Other discrepancies may result when the actual missile velocities are lower than the threshold value or values. This situation could result in a few missiles being caught because of their shapes and orientations at impact, e.g., a sliver of glass impacting on a sharp point. This again would result in the mean of the measured velocities being too high since the calibration equations were obtained for missiles of random shapes and orientations at impact. Also to be considered is the circumstance where the velocities measured for a sample of uniform missiles are above the threshold value but the expected velocity (based on blast-wave parameters) is below the threshold. This, along with collaborating evidence, would lead one to suspect that the absorber had been softened by thermal radiation before the time of impact or that the missile itself was hot.

2.6 STATISTICAL ANALYSIS OF FIELD DATA

In the computation of statistical parameters describing the velocities and masses of non-spherical missiles from a given sample (trap or group of traps), it was assumed that the distributions were log normal. A graphical verification is presented in Sec. 6.2.6 of the normalcy of distributions of log mass and log velocity by making use of data for 2523 glass fragments that were trapped in two houses.

Another type of test was developed (see the Appendix) by establishing the following theoretical relation between the ordinary mean of a log-normal distribution and its geometric mean and standard geometric deviation:

$$\frac{\bar{x}}{x_{50}} = \exp \left[\frac{(\ln_e S_{gx})^2}{2} \right] \quad (2.11)$$

where $\bar{x} = (\sum x)/n$ (ordinary mean of variable x)
 $x_{50} = \text{antilog} [(\sum \log x)/n]$ (geometric mean)
 $S_{gx} = \text{antilog} \sqrt{[\sum (\log x - \log x_{50})^2]/(n-1)}$ (standard geometric deviation)
 $n = \text{number of } x \text{ values in the sample}$

The relation between \bar{x}/x_{50} and S_{gx} , expressed by Eq. 2.11, is plotted as a solid line in Fig. 2.12. Note that, as the dispersion of the distribution (indicated by S_{gx}) increases, the magnitude of the mean also increases relative to the geometric mean.*

The points plotted on the chart in Fig. 2.12 represent velocity and mass parameters that were obtained from 111 missile samples (presented in detail later in the report). Note that the missile-velocity points (in the lower-left portion of the chart) are uniformly scattered about the theoretical line, indicating general agreement with the log-normal assumption. The missile-mass points, however, have a slight tendency to fall more to the right than to the left of the theoretical line. This means that, in general, the samples contained too few small missiles to satisfy the log-normal assumption. The scarcity of missiles of low masses could have been due to one or more of the following:

1. Some of the smaller missiles, because of their size, may have been overlooked in the absorber at the time the missiles were extracted.
2. Limitations in the calibration procedure prohibited use of missiles that were extremely small.†

* The geometric mean and the median are identical for a log-normal distribution.

† Masses of the missiles used for the calibrations are listed in Table 2.2. Actually, the calibration equations were used to evaluate velocities for missiles somewhat smaller than those used in the calibrations; e.g., the smallest missiles used to calibrate type II absorber for glass fragments weighed 0.0274 g, but velocities were evaluated for fragments as small as 0.010 g.

3. The gravel used had been screened to remove both the small and the large stones, and this screening had resulted in truncated samples.

It is appropriate to discuss briefly the significance of the statistical parameters that were defined in Eq. 2.11. Consider, for example, the distribution of missiles according to mass, where \bar{M} is the mean, M_{50} is the geometric mean, and S_{gm} is the standard geometric deviation. It can be shown that 84.13 per cent of the missiles from a given log-normal sample have velocities less than $M_{50} \times S_{gm}$ and that 15.87 per cent have velocities less than M_{50}/S_{gm} . Thus 68.26 per cent of the missiles have masses greater than M_{50}/S_{gm} and less than $M_{50} \times S_{gm}$. In some instances it is of interest to know the total mass of a sample of n missiles where only the geometric mean and the geometric standard deviation are known. An estimate of the total mass can be obtained by using Eq. 2.11 to obtain the mean mass and then multiplying this quantity by n .

In general, the impact velocities measured for missiles of a given sample were not independent of their masses. It was found that the following relation satisfactorily expressed the dependence of impact velocity on missile mass:

$$\log v = a + b \log m \quad (2.12)$$

where v is impact velocity, m is missile mass, and a and b are regression coefficients.

Note that the log-normal distributions discussed above are recognized in Eq. 2.12 by the use of $\log v$ and $\log m$ as variables instead of v and m . The coefficients a and b were determined by the least-squares method for each missile sample with the substitution $y = \log v$ and $x = \log m$. The geometric standard error of estimate, E_{gv} , was also determined for each sample, considering $\log v$ to be the dependent variable. The significance of E_{gv} is the same as that of S_{gv} , except that the reference for E_{gv} is the "geometric mean" velocity as a function of mass found from Eq. 2.12 instead of simply the geometric mean of the sample. Thus, if the regression velocity is given by $\text{antilog}(a + b \log m)$, then 84.13 per cent of the missiles from a log-normal distribution would have velocities less than $[\text{antilog}(a + b \log m)] E_{gv}$, 15.87 per cent would have velocities less than $[\text{antilog}(a + b \log m)]/E_{gv}$, and 68.26 per cent would have velocities between the two limits. In general, E_{gv} for a given missile sample is less than S_{gv} . However, if missile velocities are independent of their masses, then E_{gv} has approximately the same value as S_{gv} , and Eq. 2.12 expresses the geometric mean velocity (V_{50}) for all values of mass.

The equation used to compute E_{gv} is

$$E_{gv} = \text{antilog} \sqrt{\frac{\sum_{i=1}^n (a + b \log m_i - \log v_i)^2}{(n-2)}}$$

where m_i and v_i are paired values of mass and velocity and a and b are regression coefficients.

REFERENCES

1. I. G. Bowen, A. F. Strehler, and M. B. Wetherbe, Distribution and Density of Missiles from Nuclear Explosions, Operation Teapot Report, WT-1168, Dec. 14, 1956.
2. E. R. Fletcher, R. W. Albright, V. C. Goldizen, and I. G. Bowen, Determinations of Aerodynamic-drag Parameters of Small Irregular Objects by Means of Drop Tests, USAEC Report CEX-59.14, October 1961.

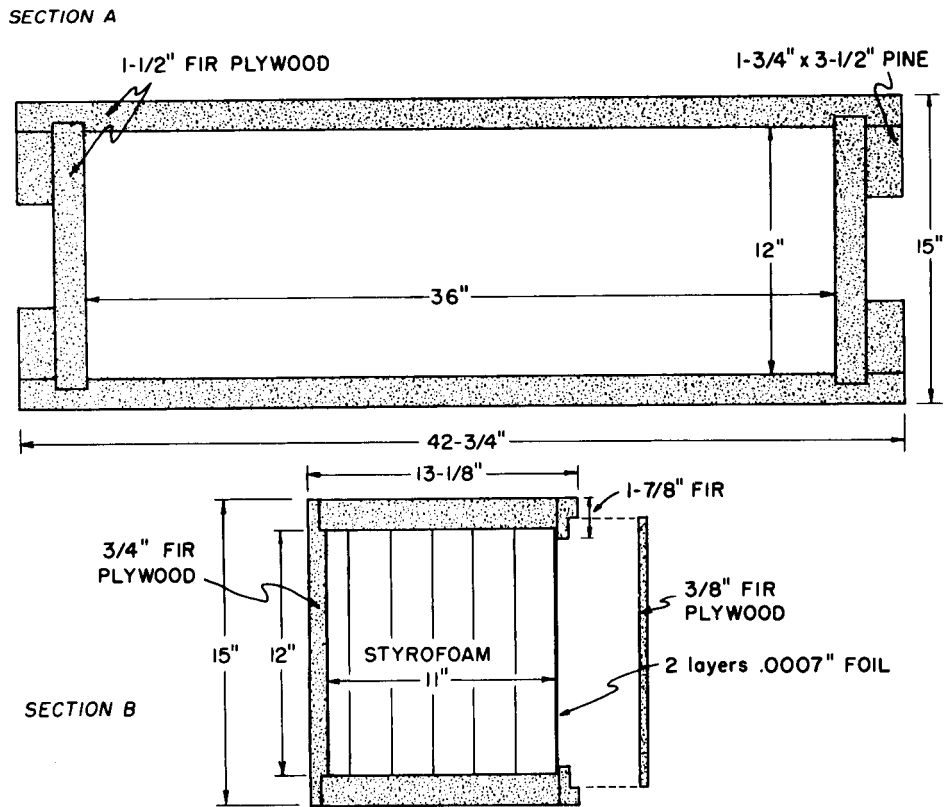
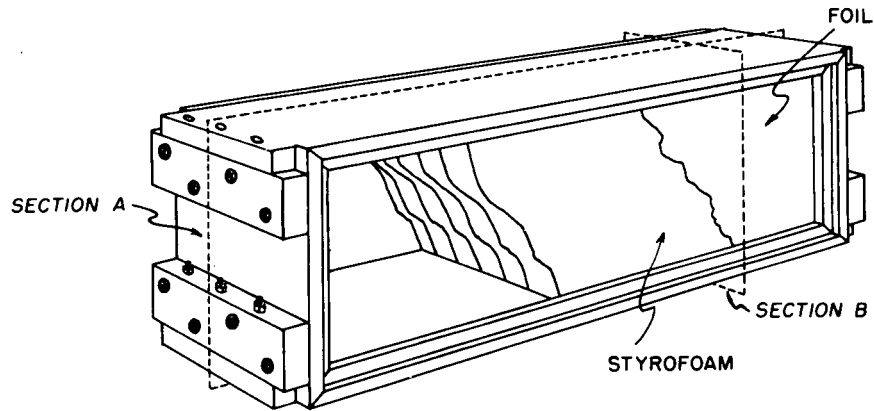


Fig. 2.1—Construction details of trap housing.

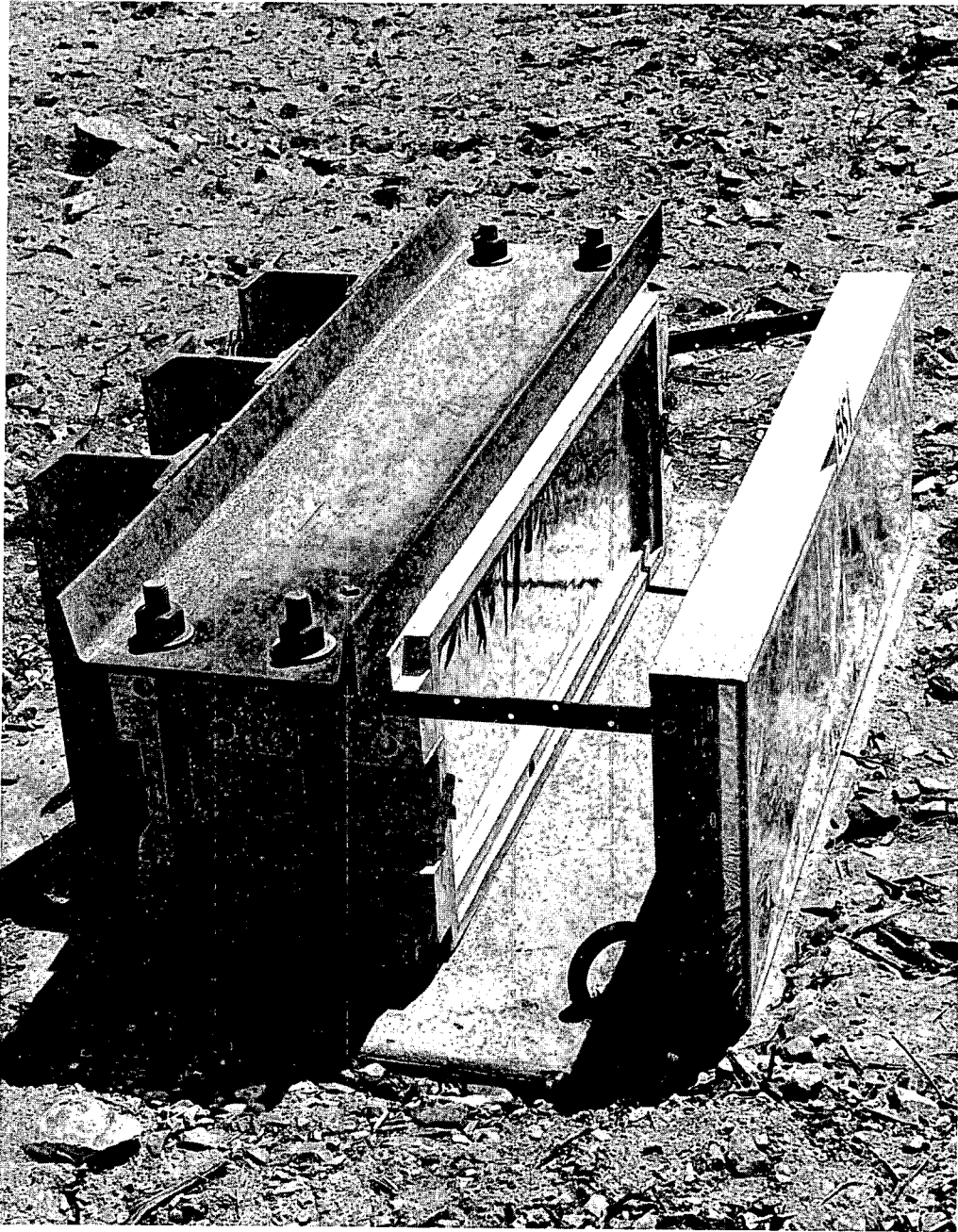


Fig. 2.2— Photograph showing trap anchors, aluminum foil for thermal protection, and added thermal shield 1 ft in front of the trap.

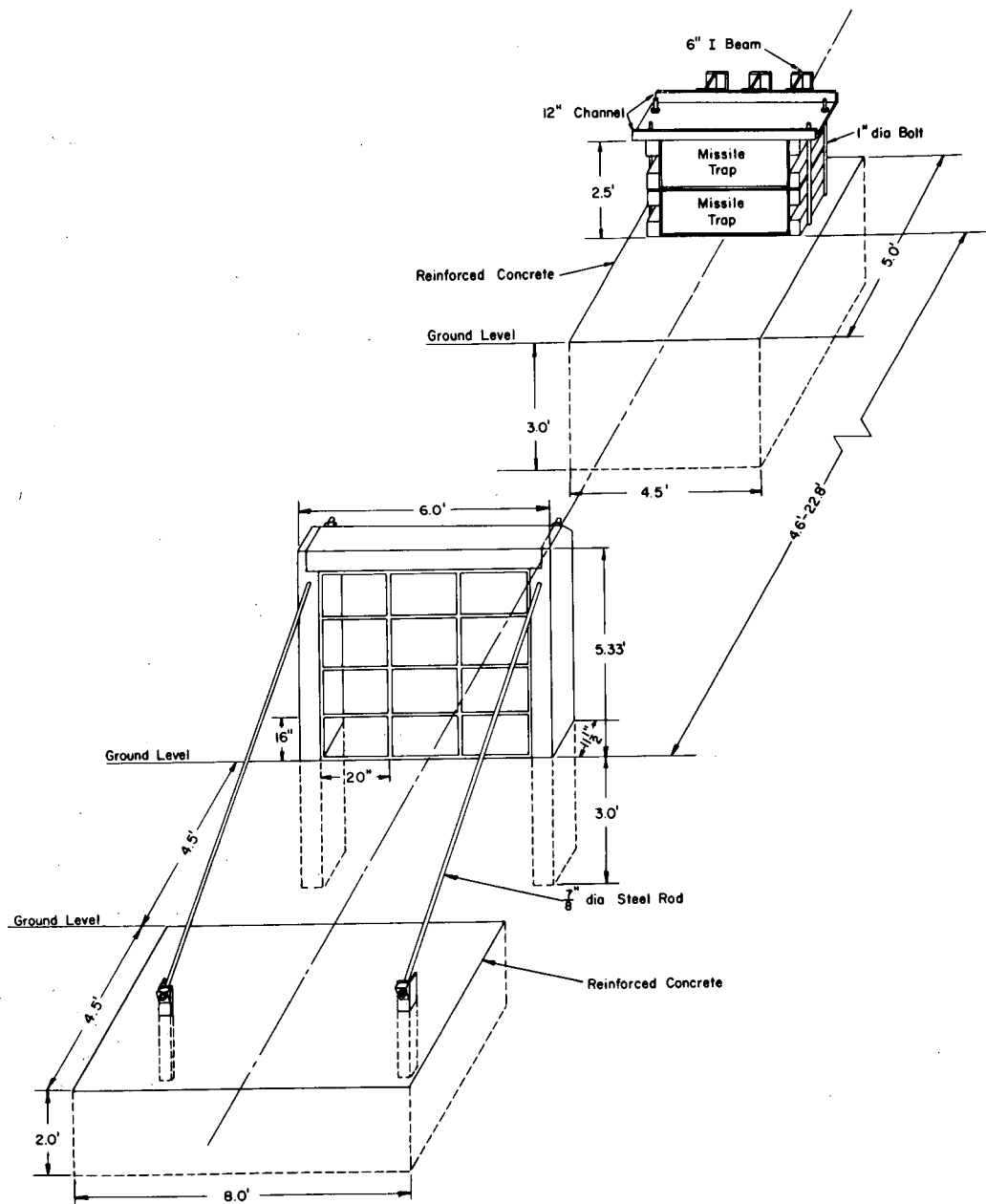


Fig. 2.3—Window- and plate-glass mounts. The window glass was 0.125 in. thick, and the plate glass was 0.25 in. thick.

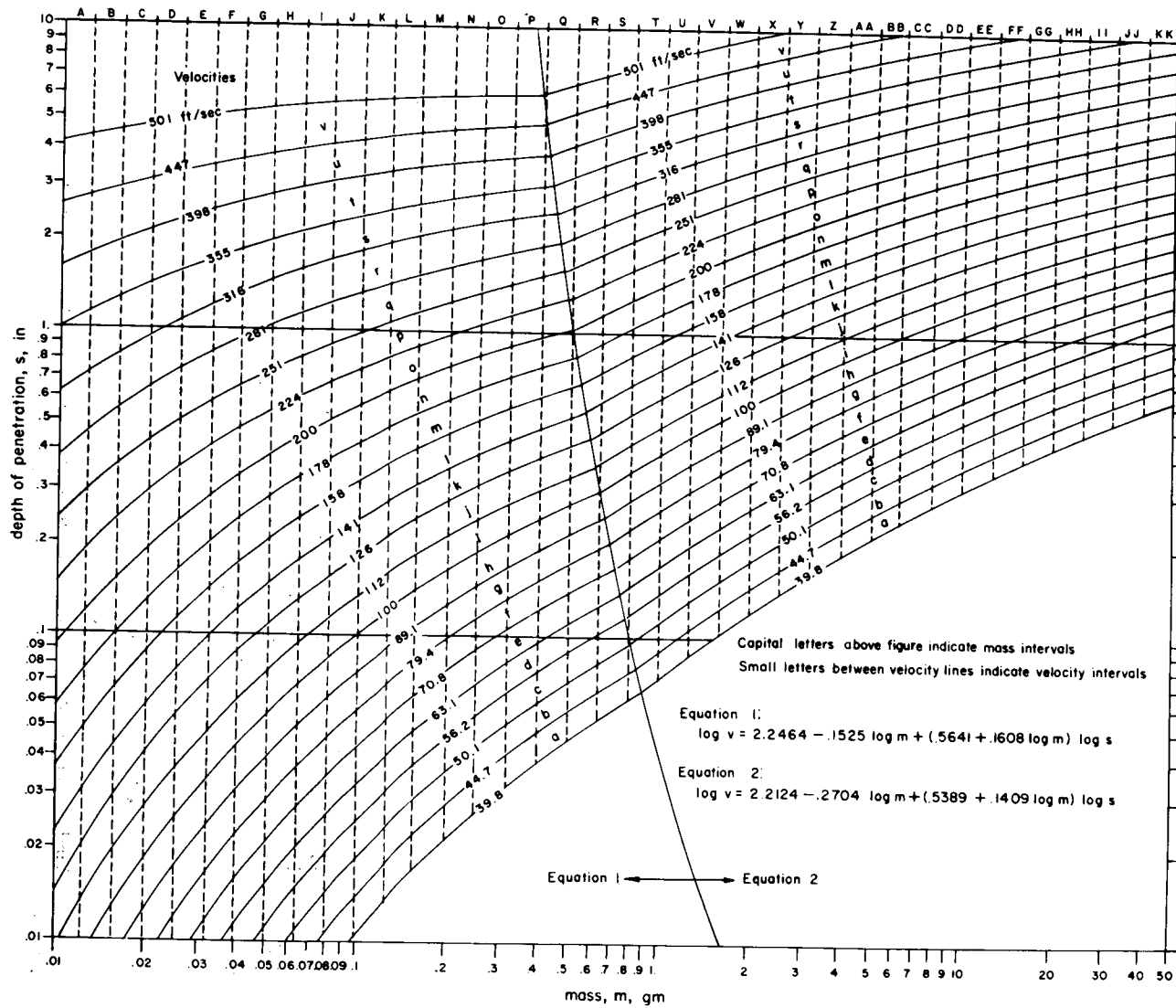


Fig. 2.4—Plot of calibration equations for glass missiles in type II absorber.

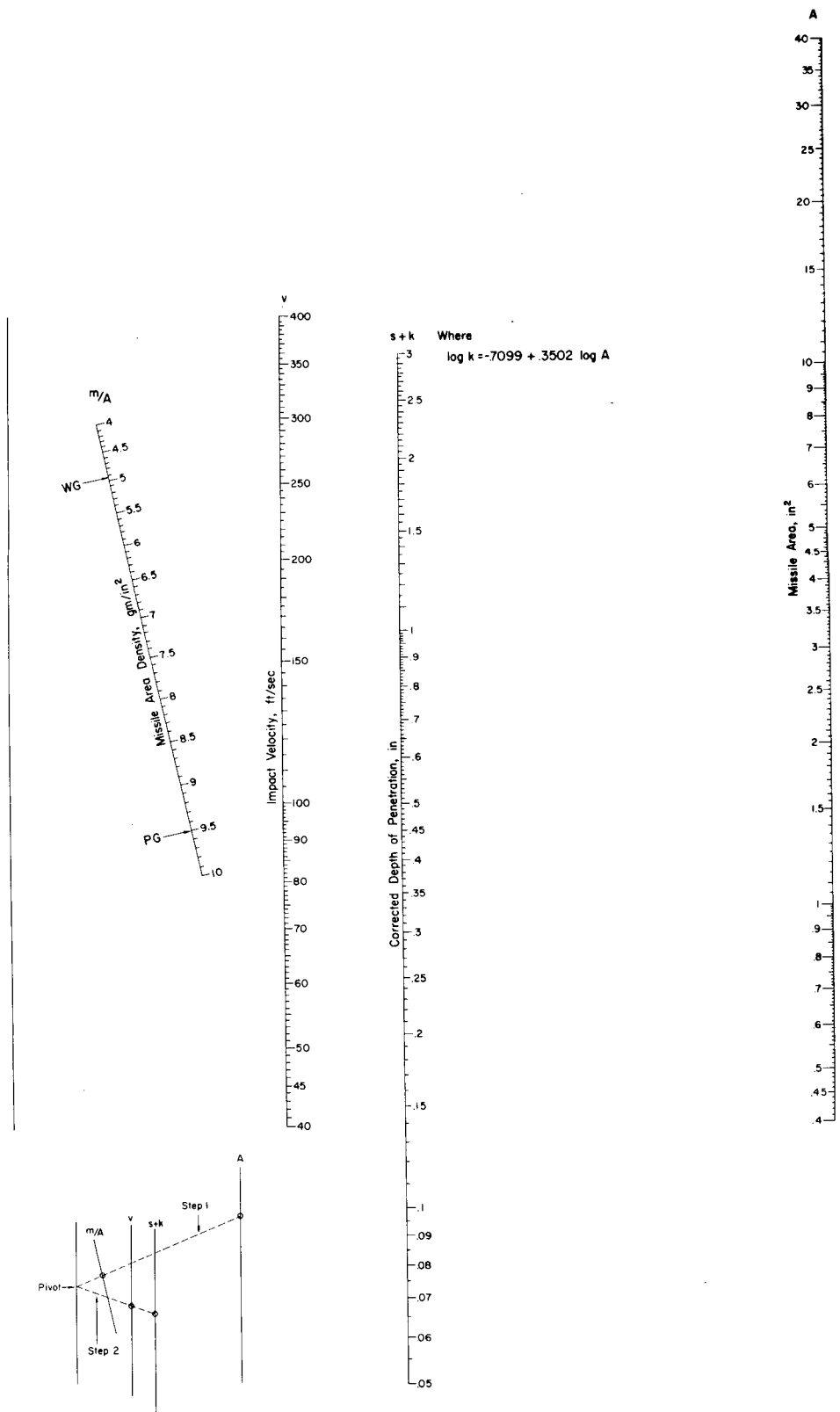


Fig. 2.5—Nomogram for determining velocities of missiles striking type II absorber flat. Diagram in lower-left corner indicates steps necessary.

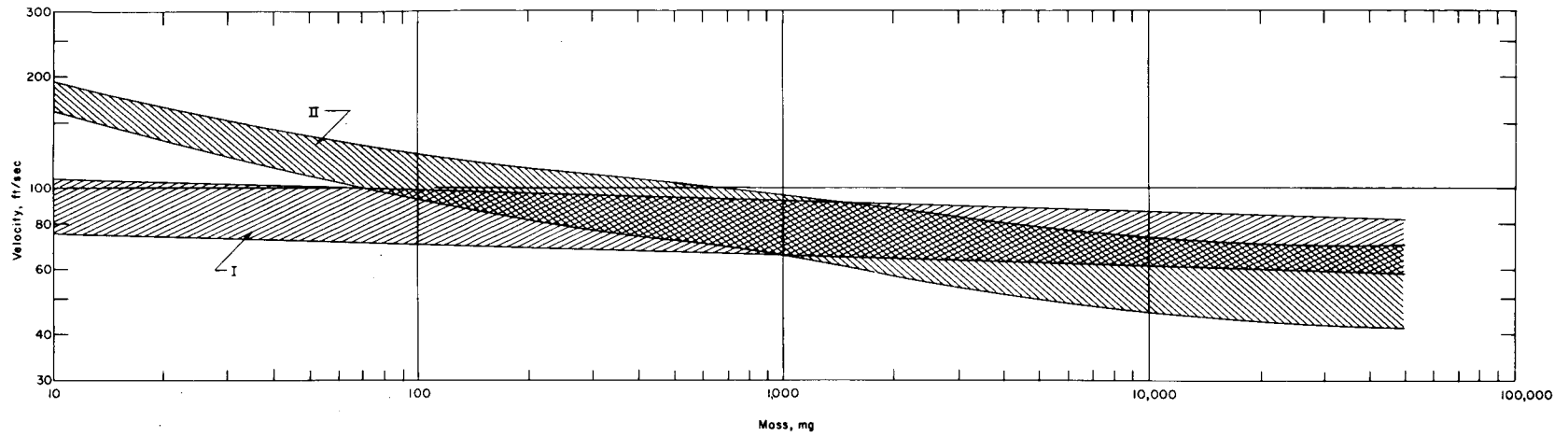


Fig. 2.6—Threshold velocities for glass fragments. Roman numerals designate type of absorber.

45

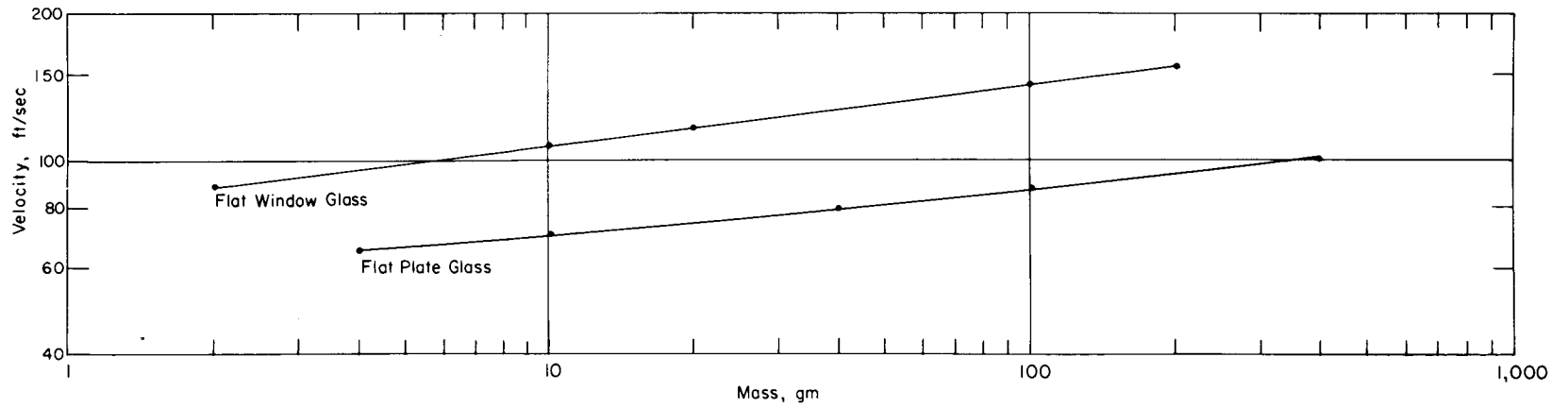


Fig. 2.7—Threshold velocities for window and plate glass striking type II absorber flat (assuming $s = 0.05$ in.).

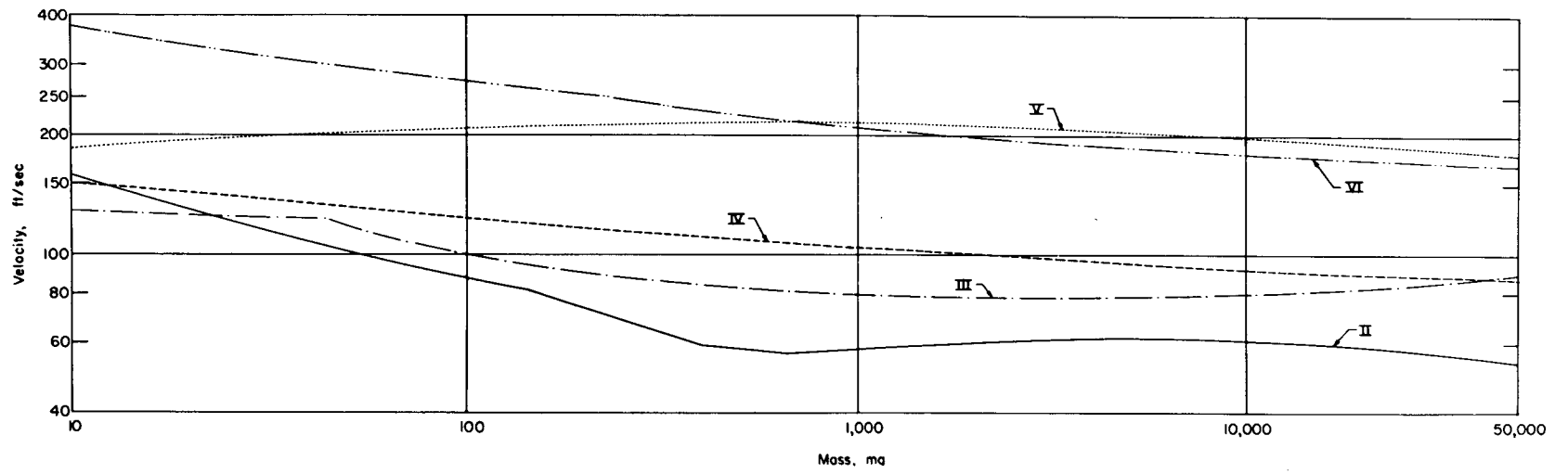


Fig. 2.8—Threshold velocities for natural stones and gravel. Roman numerals designate type of absorber.

46

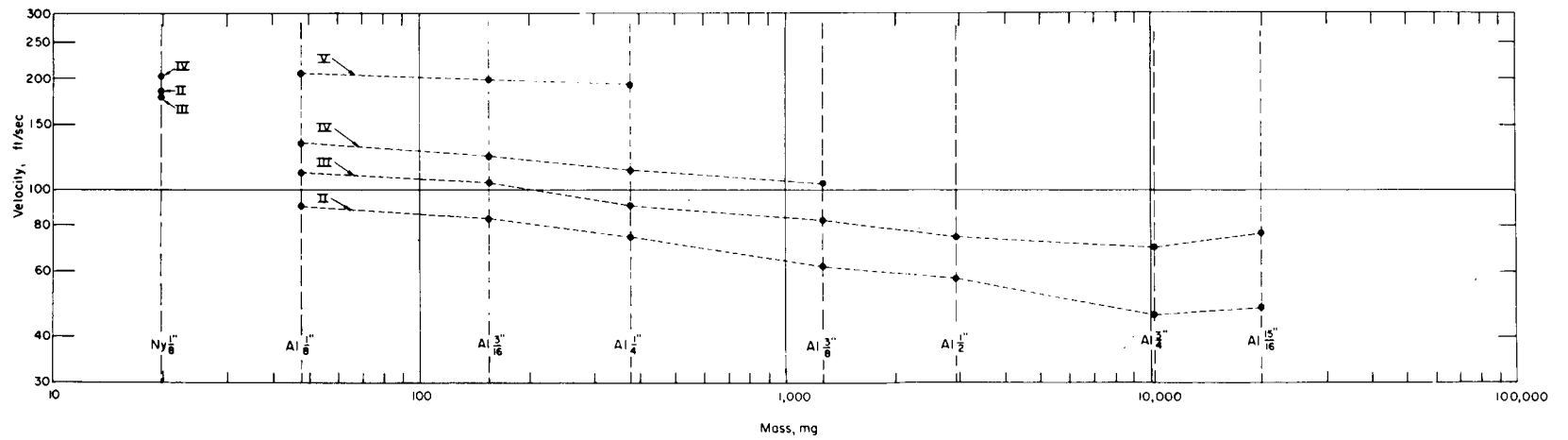


Fig. 2.9—Threshold velocities for nylon and aluminum spheres. Roman numerals designate type of absorber.

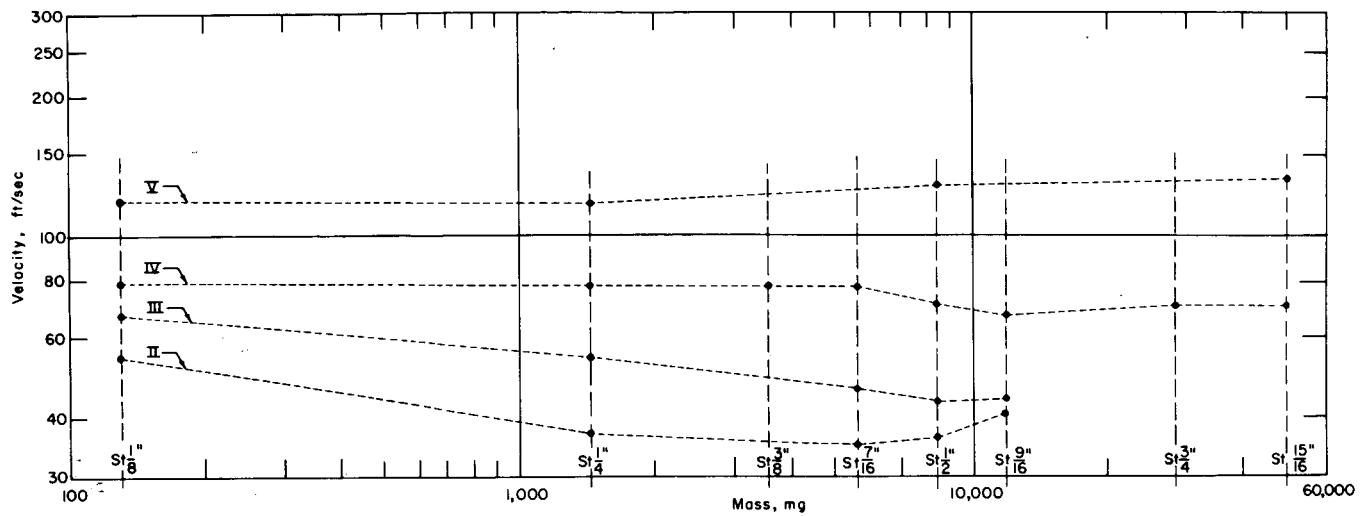


Fig. 2.10—Threshold velocities for steel spheres. Roman numerals designate type of absorber.

47

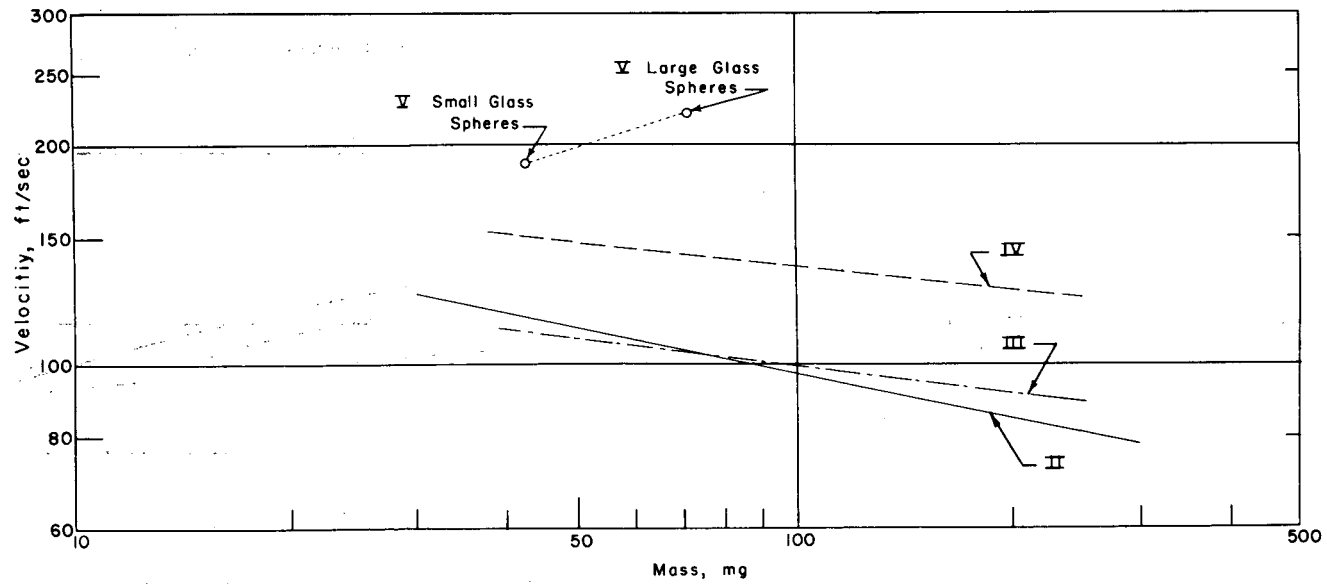


Fig. 2.11—Threshold velocities for soda-glass spheres. Roman numerals designate type of absorber.

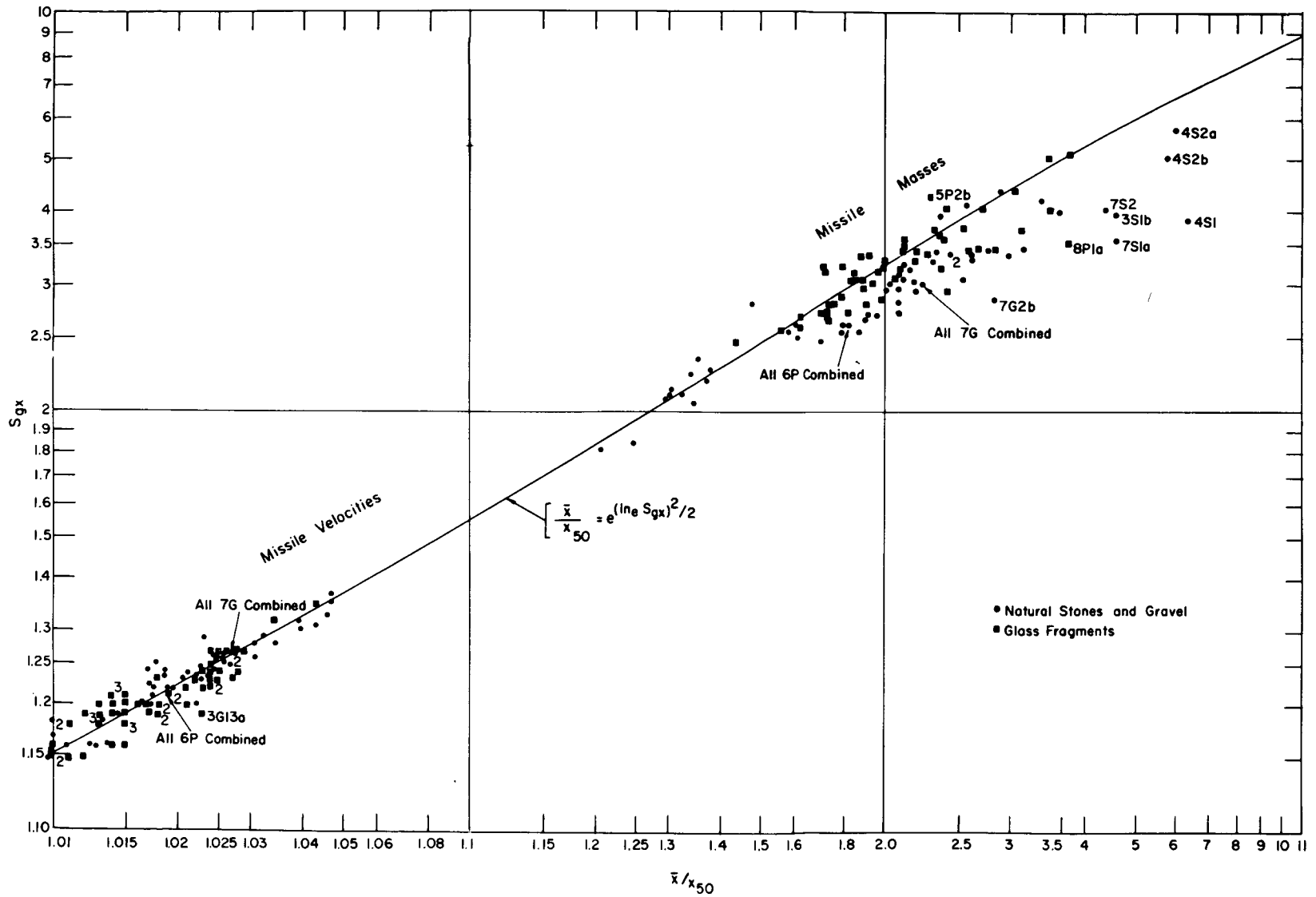


Fig. 2.12—Relation between the ratio of the mean to the geometric mean and the standard geometric deviation (\bar{x}/x_{50} vs. S_{gx}) for log-normal distributions. Data points are for missile samples which are presented later in the report. Points marked by trap numbers are those with large deviations from the theoretical line.

Chapter 3

PREDICTION OF TRANSLATIONAL VELOCITIES BY USE OF MEASURED BLAST-WAVE AND MISSILE PARAMETERS

3.1 GENERAL

One of the more important objectives (see Sec. 1.3) of the secondary-missile study was to compare the velocities measured for various secondary missiles with those which could be computed (or predicted) by use of appropriate values of the blast-wave and missile parameters. Two auxiliary studies had to be carried out before this objective could be reached. They are reported elsewhere.^{1,2} The first of these involved the solution of a mathematical model designed to simulate the salient phenomena of missile production by ideal or classical blast waves. The second was concerned with the measurement of appropriate aerodynamic parameters for irregular objects such as those used in the field operation. Through use of the blast-wave data measured by the Ballistics Research Laboratories,³ the computations were made specific for field situations.

This chapter describes briefly the work previously reported and discusses its application to the present study.

3.2 PREDICTION OF MISSILE VELOCITIES

For the sake of simplicity, it was assumed that the only force acting on the missile was due to the difference in the missile and wind velocities. The field experience indicated that objects being translated by blast winds tend to be lofted; thus the effects of surface (or ground) friction are minimized. The lofting effect, however, would be dependent on the strength and nature of the blast winds as well as on the physical characteristics of the displaced object.

The blast wave was assumed to be the ideal, or classical, type, unaffected by precursor or hill-and-dale effects. Winds and dynamic pressures associated with the ideal wave of given shock strength and duration were evaluated by use of the relations derived from numerical studies made by H. L. Brode of Rand Corporation.

No allowance was made in the secondary-missile model for the decay of the blast wave during the time (or distance) required for the missile to reach maximum velocity. This simplification would be justified at large ranges from GZ where both distance of missile travel and the decay rate of blast wave are small. At the smaller ranges, however, the blast wave experiences more significant attenuation over the distance required to accelerate a missile to maximum velocity. This effect could not be evaluated from the field experience since the blast waves at the shorter ranges were significantly modified by precursor effects.

The analytical procedure used in the missile model identified a missile by one parameter—the acceleration coefficient (α), defined as the product of the area presented to the wind and the drag coefficient divided by the mass ($\alpha = AC_D/m$) and assumed to be constant for a given missile. Two objects of vastly different shapes, sizes, and weights could have the same accelera-

tion coefficient and thus experience similar velocity vs. time histories when exposed to any particular blast wave. Use was made of this concept to investigate the displacement velocities for man by trapping objects smaller than man but possessing approximately equivalent acceleration coefficients, namely, $\frac{1}{16}$ -, $\frac{1}{2}$ -, and $\frac{9}{16}$ -in.-diameter steel spheres (see Ref. 1).

3.3 DETERMINATION OF THE IDEAL BLAST WAVE FROM THE FIELD DATA

Overpressure and dynamic pressure were measured as functions of time at most of the missile stations by Ballistic Research Laboratories (BRL) mechanical type gauges.³ Since the velocity-prediction model was solved for the ideal blast wave, it was desirable to determine the equivalent ideal wave for each of the measured blast waves. This was done in the case of the overpressure pulse by finding the ideal wave with the same impulse and duration as those measured by the gauges. The overpressures of the ideal wave as a function of time were then evaluated* and plotted for comparison on the graph showing the measured values of overpressure as a function of time.

Dynamic pressure as a function of time was determined for the ideal wave by making use of the maximum overpressure of the ideal wave and the measured duration of the positive overpressure. The relation between the ratio of durations of the positive dynamic pressure and the positive overpressure as a function of maximum overpressure is set forth in Sec. 2.3.4 of Ref. 1.

Section 2.3.2 of Ref. 1 describes the expression used for dynamic pressure vs. time for blast waves specified by maximum overpressure and duration.

3.4 ACCELERATION COEFFICIENTS FOR SMALL NONSPHERICAL MISSILES

Acceleration coefficients, defined in Sec. 3.2, could be determined for spheres of known presented area and mass by use of a drag coefficient of 0.47.† Acceleration coefficients for irregular objects such as stones and glass fragments were not so readily determined. Experiments were performed in which the test objects were dropped a known distance (about 48 ft) in a measured time. Acceleration coefficients could then be determined by comparing the measured drop times with the time required for the object to fall the same distance without air drag.² It should be pointed out that in these experiments the velocities encountered were relatively low and the compressibility effects of the air were small.

3.5 GLASS-FRAGMENT STUDIES

The drop-test studies reported in Ref. 2 indicated that orientation of the missile with respect to the wind was not important in determining acceleration coefficients for double-strength window fragments with masses less than 0.220 g and for plate-glass fragments with masses less than 0.860 g. As the fragment masses increased from these lower limits, their orientation became more important; e.g., 2-g window-glass fragments have acceleration coefficients for the edgewise orientation which are about 40 per cent lower than those obtained when the maximum areas are presented to the wind. The scatter in the velocity data obtained for a typical window-glass sample was too large to be explained by the orientation effect (see Fig. 6.19).

Velocities predicted for glass fragments on the basis of a free-field blast wave ignored any possible modification of the wave by the window installations in open areas or by the structure containing the window in the case of the house installations. In some instances, particularly for the houses, the modification noted (as signified by missile velocities) was great enough to suggest that velocities also be computed for a blast wave with a duration the same as that for the free-field wave and with a maximum overpressure equal to the reflected overpressure assuming normal incidence of the free-field blast wave. Although this procedure

* The techniques used are described in Sec. 2.3.3 of Ref. 1.

† This drag coefficient for spheres is valid within large ranges of Reynolds numbers if the flow can be considered to be incompressible.

cannot be rigorously defended by theory, its usefulness as an empirical guide in the prediction of missile velocities is apparent, provided, of course, that it conforms with the experimental evidence available.

3.6 NATURAL-STONE, GRAVEL, MILITARY-DEBRIS, AND SPHERE STUDIES

The point of origin and the distance of travel of the natural (or native) stones that were caught in the traps were unknown. Predicted velocities were computed by making the assumption that the displacement of the missile before striking the trap was that distance required by each missile to reach maximum velocity. Thus natural stones displaced distances other than the optimum would have velocities lower than the predicted values.

At the missile stations in open areas on shots Priscilla and Galileo, screened gravel, which had been dipped in paint for identification, was placed in front of traps at two or three distances. The greatest distance used at each station* was estimated to be that which would be necessary for a typical stone (about 0.1 g) to attain 98 per cent of its maximum velocity. The shorter distances were about 39 and about 15 per cent of the greatest distance. This procedure allowed a comparison of predicted and measured velocities for various known distances of travel.

Military debris was marked with paint and placed in the same manner as the gravel (see Chaps. 4 and 5). Spheres of various sizes, some marked with paint or dye, were also placed at the distances used for gravel. The sphere samples were placed at ground level and at various distances above the ground on appropriately designed supports.

REFERENCES

1. I. G. Bowen, R. W. Albright, E. R. Fletcher, and C. S. White, A Model Designed to Predict the Motion of Objects Translated by Classical Blast Waves, USAEC Report CEX-58.9, June 29, 1961.
2. E. R. Fletcher, R. W. Albright, V. C. Goldizen, and I. G. Bowen, Determinations of Aerodynamic-drag Parameters of Small Irregular Objects by Means of Drop Tests, USAEC Report CEX-59.14, October 1961.
3. J. J. Meszaros and J. H. Keefer, Blast Measurements for CETG Projects, Operation Plumb-bob Report, ITR-1501, June 6, 1958. (Classified).

* This distance increases with overpressure, i.e., small at low pressures and large at high pressures.

Chapter 4

SHOT PRISCILLA, EXPERIMENTAL PROCEDURE AND RESULTS

4.1 PROSPECTUS

Before the detonation of shot Priscilla (estimated yield, 38 kt) in Frenchman Flat, plans were made to investigate the production of secondary missiles at 19 locations (see area map, Fig. 4.1). Eleven of the stations were in open areas at ranges of 6120 to 2030 ft, seven were in closed shelters at ranges of 1360 to 860 ft, and one was in a shelter with open entryway at a range of 900 ft.

The number appearing in the designators for the stations in the open areas indicates the expected value of maximum overpressure; e.g., at 10P, 10 psi was the anticipated maximum overpressure. The letter "P" in the designators represents shot Priscilla, and "PP" represents the trap installations associated with a study¹ of biological damage caused by glass fragments using swine as targets.*

At stations 4P, 5P, 6P, and 8P, experiments were designed to study the translation of (1) fragments from windows mounted in open areas; (2) marked gravel and military debris; (3) marked spheres of various types; (4) natural stones; and (5) large stones, blocks, and bricks marked for identification. Similar experiments were conducted at stations 10P, 15P, and 20P except that the glass-fragment studies were omitted. Velocities were obtained for all missile types except the large marked stones, blocks, and bricks; the total distance of translation was measured for these missiles.

The experiment inside the open shelter, OPS, was concerned with the translational velocities of "human-equivalent" spheres.† Incidental to this experiment, velocity data were obtained for a number of small stones of unknown source.

The experiments inside the closed shelters were designed to measure the velocity of particles that might spall from the walls of the shelter owing to earth shock. Postshot examinations showed no evidence of significant spalling.‡

The material in this chapter is presented by station, starting with the one most remote from GZ. The only exception to this procedure was made for the large-stone study; the displacement data for this study (obtained at seven stations) are discussed in Sec. 4.15. Most of the results, because of their voluminous nature, are presented graphically along with pertinent statistical parameters. For purposes of comparison, predicted or computed missile velocities are shown on the data graphs. Two summary tables—one for the blast-wave parameters (Table 4.5) and the other for statistical parameters (Table 4.6)—describe missile data.

*Glass-fragment data were also collected at stations 4P, 5P, 6P, and 8P for the swine study (Project 4.1) and for Project 33.4 which conducted a similar study² but used dogs as targets.

†Spheres of such a size and weight that they acquire approximately the same velocity as would a human being under the same circumstances.

‡The closed shelters were tested by Projects 3.1 and 3.2. Details relevant to the performance of these shelters may be found in Refs. 3 and 4.

4.2 STATION 4P, 6120-FT RANGE

4.2.1 Experimental Plan

The experimental plan* for station 4P is illustrated in Fig. 4.2. Three of the five window installations provided for the exposure of animals to glass-fragment missiles. Dogs were used for the study² made by Project 33.4 and pigs were used for the study¹ made by Project 4.1.

Military debris, mostly steel fragments resulting from explosions, was painted for identification and was placed in front of installations 4P4 and 4P5 at 4.5, 10.9, and 28 ft,† a different color being used at each location. About 275 pieces of debris varying in mass from 1 to 2220 g were used at each distance.

Gravel was also painted for identification and placed in front of installations 4P4, 4P5, and 4P6 at the same distances as the military debris (see Fig. 4.2). (Note that an area in front of installations 4P6 and 4P7 was stabilized with asphalt to provide a more ideal surface over which gravel and spheres were to be translated.)

Painted spheres were placed in front of installation 4P7 at the same three distances used for military debris and gravel. The smaller spheres were packaged in tissue-paper containers, some placed on the asphalt surface and others suspended above the ground by wire frames (see Fig. 4.12). The heights above ground level, in inches, at which the spheres were placed are recorded in Table 4.6 for the spheres that were caught in traps. The larger steel spheres ($\frac{1}{2}$ and $\frac{9}{16}$ in. in diameter) were hung on wire frames and held in aluminum-foil containers that were constructed and mounted in such a way that the blast winds would rip them open and release the spheres.

The sphere samples, described in the following paragraphs, for this station were also used at stations 5P, 6P, 8P, 10P, 15P, and 20P. The distances of placement from the traps varied from station to station, but the samples exposed consisted of the same amounts.

At the shortest distance 10 steel spheres $\frac{7}{16}$ in. in diameter were placed on the asphalt surface and 10 steel spheres $\frac{9}{16}$ in. in diameter were hung from the wire frame.

At the intermediate distance, 10 steel spheres $\frac{1}{2}$ in. in diameter were suspended from the wire frame, but none were placed at ground level.

For each of the three distances, 2110 small spheres were placed at ground level and 1055 were suspended from the wire frame. All samples contained the spheres listed below in the indicated proportions:

$\frac{1}{8}$ -in.-diameter nylon (Ny $\frac{1}{8}$)	5.2%
$\frac{1}{8}$ -in.-diameter aluminum (Al $\frac{1}{8}$)	10.4%
$\frac{3}{16}$ -in.-diameter aluminum (Al $\frac{3}{16}$)	5.2%
$\frac{1}{4}$ -in.-diameter aluminum (Al $\frac{1}{4}$)	0.7%
$\frac{3}{8}$ -in.-diameter aluminum (Al $\frac{3}{8}$)	0.1%
$\frac{1}{8}$ -in.-diameter steel (St $\frac{1}{8}$)	10.4%
$\frac{1}{4}$ -in.-diameter steel (St $\frac{1}{4}$)	1.4%
36.0 mg (av.) soda glass (G _S)	53.5%
72.6 mg (av.) soda glass (G _L)	13.1%

A summary of the results at station 4P for window glass, plate glass, natural stones, gravel, and spheres appears in Table 4.6.

Displacement data obtained for the large stones, building blocks, and bricks are presented in Sec. 4.15 and Table 4.4.

4.2.2 Blast Parameters

A method was discussed in Sec. 3.3 for obtaining the peak overpressure of an ideal blast wave whose overpressure impulse and duration are the same as those measured in the field. This procedure was found to be necessary in order to arrive at predicted velocities for various missiles by use of a mathematical model⁵ based on the ideal blast wave. The computed as

*Missile traps, trap anchors, and window mounts are described in Chap. 2.

†The method used to determine the distance that missiles were placed in front of the traps is discussed in Chap. 3.

well as the measured blast parameters obtained for the various stations are summarized in Table 4.5. Unfortunately, gauge failure prohibited the measurement of overpressure vs. time at stations 4P and 5P. Therefore values of overpressure were determined for these stations by means of a regression equation based on the computed overpressures at five stations where records were obtained. (Refer to footnote ** in Table 4.5.) A similar procedure was followed to estimate the duration of the blast wave. Thus the overpressure and duration used to make velocity predictions at station 4P were 4.54 psi and 1.027 sec, respectively. These values were used to compute the dynamic pressure vs. time curve for an ideal wave which is shown in Fig. 4.3 as a dashed line. Illustrated as a solid line in the same chart is the dynamic pressure (q) measured by the BRL gauge. The measured q record appears erratic and indicates pressures generally lower than those computed for the ideal wave.

4.2.3 Window-glass Installation 4P1

Installation 4P1 consisted of two traps: 4P1b stacked above 4P1a. This installation was placed 7.8 ft behind a window of $\frac{1}{8}$ -in.-thick double-strength glass. Figure 4.4 is a postshot view of the two traps. Note that the aluminum foil used for thermal protection was ruptured by the glass fragments and torn in some places by blast winds.

The velocity and mass of individual fragments are plotted in Fig. 4.5 for trap 4P1a and in Fig. 4.6 for trap 4P1b. The numbers appearing with some of the points indicate the number of missiles in the velocity and mass intervals represented by those points. The points without numbers represent only one missile. (For a summary of results see Table 4.6.)

Note that for both traps most of the missiles had velocities that were greater than those predicted on the basis of the incident maximum overpressure (lower line of predicted velocities). The prediction line appearing in the upper part of each chart was made for the assumption that the blast wave had a maximum overpressure equal to the reflected (normal) value for the incident wave,* i.e., 10.34 psi instead of the incident maximum overpressure of 4.54 psi.

The slopes of the regression equations describing the data in Figs. 4.5 and 4.6 are -0.0924 and -0.0838 , respectively, whereas the average slopes of the prediction lines are much closer to zero. A partial explanation of this discrepancy is that small fragments require higher impact velocities in order to be retained by the absorber (type II) than do large fragments. This is illustrated by the threshold-velocity chart, Fig. 2.6.

4.2.4 Window-glass Trap 4P2b (Above Dog Trap 4P2A)

Installation 4P2 was located 12.8 ft behind a window. It consisted of a single missile trap, 4P2b, placed above a dog trap,² 4P2A, which was 31.5 in. high. Figure 4.7 is a postshot view of the installation taken after the dog had been removed.

The glass in each outside window installation extended from ground level to a height of 64 in. (see Fig. 2.3). The upper edge of the absorber in the trap at this location was 55 in. above ground level and the lower edge was 33 in. above ground level. Thus the upper edge of the absorber was only 9 in. lower than the top of the window. Unless a lofting effect compensated for the effect of gravity, the spatial density of missiles would be expected to decrease with increasing height above the ground. A comparison of the total missiles caught in trap 4P2b with those caught by other traps at this station is difficult because similar window installations were placed at different distances from the traps. For installation 4P1, placed nearer the window (7.8 ft compared with 12.8 ft for installation 4P2), the ground-level trap caught 68 missiles and the one placed 15 in. above the ground caught 58 missiles. Although the number of missiles (68 and 58) caught by installation 4P1 traps was greater than that (48) caught by trap 4P2b, their average masses were smaller. It is interesting to note that the trap placed highest above the ground (4P2b, 31.5 in. above the ground) caught the largest total mass† of glass, 148.8 g com-

*This concept is discussed in more detail in Chap. 3.

†The total mass of missiles caught can be obtained by multiplying the average mass, \bar{M} , by the number of missiles, n (both obtained from Table 4.6).

pared with 144.0 g for trap 4P1a and 64.7 g for trap 4P1b. Figure 4.8 and Table 4.6 present data for missiles recovered from trap 4P2b.

4.2.5 Plate-glass Trap 4P3b (Above Dog Trap 4P3A)

The experiment at installation 4P3 was the same as the one at 4P2, except that the window mount in front of 4P3 contained one large piece of plate glass that was $\frac{1}{4}$ in. thick, 64 in. high, and 60 in. wide. Figure 4.9 is a preshot view of this installation looking toward GZ. Segments of the plate glass were painted different colors for purposes of identification.

Only one fragment was recovered from trap 4P3b. This fragment had a mass of 60.3 g and an impact velocity of 47 ft/sec. Evidence obtained from the dog trap (4P3A) indicates that the spatial density of missiles at the lower height was considerably greater.² From this it may be concluded that the effect of gravity on the missiles was greater than that of lofting.

4.2.6 Military-debris and Gravel Installations 4P4 and 4P5

The placement of military debris and gravel at installations 4P4 and 4P5 was described in the second paragraph of Sec. 4.2.1 and illustrated in Fig. 4.2. Figure 4.10 is a preshot view of installation 4P4 (similar to installation 4P5); piles of gravel and debris are shown.

The postshot condition of both installations is illustrated in Fig. 4.11. The slightly dark areas on the surface of the absorber are thermal effects.

No military debris was caught in any of the four traps. A total of 17 pieces of gravel was recovered: 0 from trap 4P4b, 9 from trap 4P5a, and 4 from trap 4P5b. All gravel caught originated from the 10.9- and 28.0-ft distances (none from 4.5 ft). Two to six natural stones (total 14) were caught in each of the four traps. Because the sample sizes were small, the data for both natural stones and gravel were combined with similar data obtained at other traps at station 4P. Analysis of the gravel data is discussed in the next section and that for the natural stones is discussed in Sec. 4.2.10 (see also Table 4.6).

4.2.7 Gravel and Sphere Installations 4P6 and 4P7

(a) *General.* One-third cubic foot of painted gravel was placed at each of three distances (4.5, 10.9, and 28 ft) in front of installation 4P6 (see Fig. 4.2). Spheres were placed at the same distances in front of installation 4P7. (For description of spheres, see Sec. 4.2.1.) Figure 4.12 is a preshot view of the asphalt area; both the gravel and the spheres are shown. Note that the protective covers for the traps were in place when the photograph was taken.

(b) *Traps 4P6a and 4P6b.* At installation 4P6, 8 pieces of gravel were recovered from the lower trap and 10 from the upper trap. Only one gravel missile was caught which originated from the pile at the 4.5-ft distance. For purposes of analysis, the data for these missiles were combined with those obtained from installations 4P4 and 4P5. Velocity vs. mass is plotted in Fig. 4.13 for 14 gravel missiles whose translation distance was 10.9 ft. Similar data are shown in Fig. 4.14 for 20 missiles that traveled 28.0 ft before impact. Both plots indicate that the individual velocities were generally higher than those predicted. Other missiles undoubtedly impacted with the absorber but were not caught because of insufficient velocity or disadvantageous orientation at impact (see Sec. 2.5).

Two natural-stone missiles were caught in trap 4P6b. The data for these missiles were combined for analysis with those for natural stones caught in other station 4P traps (see Sec. 4.2.10 and Table 4.6).

(c) *Traps 4P7a and 4P7b.* Results obtained for 15 spheres caught by these traps are presented in Table 4.6. The largest sample obtained consisted of 11 small glass spheres whose average velocity was 135 ft/sec—39.2 per cent higher than the predicted velocity of 97 ft/sec. Deviations from the predicted velocity for the smaller samples were as much as 76.4 per cent higher. These discrepancies probably reflect the inaccuracies inherent in the trapping technique when the depths of penetration are small; i.e., impact velocities were near the threshold for retention of the missile in the trap.

Data for two natural stones caught at this installation, combined with others at this station, are presented in Sec. 4.2.10 and Table 4.6.

4.2.8 Window-glass Installation 4P8

This installation was similar to installation 4P1 (Sec. 4.2.3) except that the window was placed 17.8 ft from installation 4P8 traps (compared with a 7.8-ft separation for installation 4P1). Figure 4.15 is a postshot view of installation 4P8; fragments of glass imbedded in the absorber are shown.

Velocity vs. mass is plotted in Fig. 4.16 for 41 missiles recovered from trap 4P8a, and a similar analysis is portrayed in Fig. 4.17 for 54 missiles from trap 4P8b (upper trap). Only a small difference is observed between the data obtained at this installation (see Table 4.6) and those obtained from installation 4P1 where the window was considerably nearer the trap. In the instance of the greater translational distance, 25 per cent fewer missiles were caught and their masses were somewhat smaller, but the fragment velocities measured under the two conditions were not significantly different.

4.2.9 Window-glass Trap 4P9b (Above Pig Trap 4P9A)

At this installation a pig¹ was exposed in a box somewhat smaller than that used for dogs (see Fig. 4.18). The missile trap, 4P9b, placed above the pig installation, was 27 in. above ground level.

Data obtained for 62 fragments are plotted in Fig. 4.19. There appears to be little difference between these data and those obtained from other window installations at this station (see Table 4.6) even though the translational distances and the trap heights were different. As in the previous cases, a large portion of the fragments had velocities that were higher than those predicted on the basis of the incident peak overpressure but lower than those predicted for the "reflected" condition (see Sec. 3.5).

4.2.10 Natural-stone Data from Station 4P Traps

Velocity and mass data obtained for 18 natural stones caught in six traps* are plotted in Fig. 4.20, and the results are given in Table 4.6. Similar to the gravel trapped at station 4P, the velocities tend to be higher than predicted—particularly for the missiles of low mass (see Sec. 2.5).

4.3 STATION 4PP (PIG STUDY), 6120-FT RANGE

This station consisted of a double-trap installation inside an enclosure containing 70 pigs. The primary aim of the pig study¹ (Project 4.1) was to determine damaging effects of glass-fragment missiles. The 80-ft-long 13-ft-wide enclosure was orientated so that a long side faced GZ. The pen was made of 5- by 5-in.-mesh hog wire, except for the side toward the approaching blast wave; this side consisted of a 4.2-ft-high wall of double-strength glass.† Panes of glass 32 in. wide and 20 in. high were mounted in a 2- by 4-in.-lumber framework. The trap installation was placed 8.8 ft behind the central section of the glass wall. The pigs were restrained, preshot, in smaller pens made of electric fences. These enclosures were located at the same average distance from the glass wall as the traps. Thus shielding of the traps by the pigs was prevented.

Analyses for 81 missiles caught in the lower trap, 4PPa, and 68 caught in the upper trap, 4PPb, are presented graphically in Figs. 4.21 and 4.22, respectively, and are also given in Table 4.6 with station 4P window-glass data. A few more missiles were caught in these traps than at window-glass installations at station 4P; however, their masses and velocities were about the same. [Note that stations 4P and 4PP had the same range from GZ although they were at different locations (see Fig. 4.1).]

*Note that none of the six traps listed in Fig. 4.20 were behind windows.

†To prevent the pigs from escaping after the arrival of the blast wave, hog wire was also placed 18 in. in front of the glass wall.

4.4 STATION 5P, 5320-FT RANGE

4.4.1 Experimental Plan and Blast Parameters

The experimental plan for this station, illustrated in Fig. 4.23, was almost identical to that described in Sec. 4.2.1 for station 4P. A notable difference was that at station 5P the gravel and sphere installations were placed on opposite edges of an area that was stabilized with concrete; this area was used by another project studying the displacement of anthropomorphic dummies⁶ (see Fig. 4.23). The window installations were the same type as those at station 4P, but the gravel, military-debris, and sphere studies differed in that the placement distances were somewhat greater at station 5P.

Failure of the ground-baffle gauge prohibited the measurement of overpressure vs. time at this station. The methods used to estimate the peak overpressure and duration of the positive-pressure phase of the blast wave are discussed in Sec. 4.2.2. For station 5P the estimated values used to compute predicted missile velocities were 5.51 psi and 0.964 sec, respectively.

The dynamic pressure (q) measured as a function of time is plotted in Fig. 4.24 and, for comparison, the q values associated with an ideal blast wave (dashed line) are also shown. This "ideal" curve represents the q values actually used in the mathematical model⁵ to arrive at predicted values of missile velocity. Lack of consistency in the measured values of dynamic pressure is demonstrated by a comparison of this q record (Fig. 4.24) with the one obtained for station 6P (Fig. 4.44). Even though station 6P was 550 ft nearer GZ, the measured dynamic pressures were generally lower than at station 5P.

Station 5P summary of results for window glass, plate glass, natural stones, gravel, and spheres is given in Table 4.6, and displacement data for large stones, building blocks, and bricks are given in Table 4.4 (see also Sec. 4.15).

4.4.2 Window-glass Installation 5P1

Installation 5P1 was located 7.8 ft behind a window of double-strength glass. (See Fig. 4.25 for postshot view of this installation.) Velocity and mass data for 48 fragments recovered from the lower trap are plotted in Fig. 4.26, and similar data are plotted in Fig. 4.27 for 32 missiles from the upper trap. It is of interest to note that in each chart the geometric mean velocity is approximately equal to the average of the predicted velocities (see also Table 4.6).

4.4.3 Window-glass Trap 5P2b (Above Dog Trap 5P2A)

Trap 5P2b, which was anchored above a dog trap (31.5 in. high), was located 12.5 ft behind a standard window (see Fig. 4.23). A relatively large number (88) of fragments was recovered; however, the data for trap 5P2b in Fig. 4.28 demonstrate that the velocities measured were lower in relation to the predicted values than was evident at installation 5P1 (see Table 4.6) where the missiles were caught at lower heights above ground level.

4.4.4 Plate-glass Trap 5P3b (Above Dog Trap 5P3A)

Trap 5P3b, which was situated above a dog trap, was located 12.8 ft behind a plate-glass window. Figure 4.29 is an enlarged postshot view of the absorber surface. Although this photograph presents evidence that several large fragments struck the trap, the geometric mean mass for the nine missiles that were recovered was only 877 mg. Velocities measured for these fragments (Fig. 4.30) were generally a little higher than predicted (see also Table 4.6).

4.4.5 Military-debris and Gravel Installations 5P4, 5P5, and 5P6

Gravel mixed with military debris was placed at three distances in front of installations 5P4 and 5P5. These materials were placed directly on the surface of the dry lake bed (Frenchman Flat). Installation 5P6, however, was located behind the large concreted area, and two of the three piles of gravel for this installation were on the concrete (see Figs. 4.23 and 4.31).

Figure 4.32 is a postshot view of installation 5P4. Note that both the upper and lower traps were slightly damaged by thermal radiation.

TABLE 4.1 — PARTIAL RESULTS FOR SPHERES RECOVERED FROM STATION 5P7
(Samples of less than five not included; complete data in Table 4.6.)

Spheres*	Distance translated, ft	No. of missiles	Height above ground, in.		Velocity, ft/sec			% Deviation†	
			Placed	In trap, av.	Threshold	Measured, av.	Predicted	100% (M-P)/P	100% (P-T)/T
G _l (71.8)	12.5	9	0	16.8	102	124	102	21.6	0
St 1/8	12.5	6	0	17.0	54.3	82	67	22.4	23.4
G _s (36.8)	12.5	18	0	17.6	118	138	111	24.3	-5.9
Al 3/16	12.5	5	0	22.0	83.5	126	82	53.7	-1.8
Al 3/16	32.0	6	0	8.7	83.5	116	105	10.2	25.7
G _s (41.6)	32.0	7	29	11.1	117	138	126	9.5	7.7
G _s (37.0)	32.0	33	0	12.9	118	141	128	10.2	8.5
G _l (70.8)	32.0	9	0	14.4	102	133	117	13.7	14.7

*Numbers after Al (aluminum) and St (steel) are diameters (in in.). G_s and G_l represent two sizes of soda-glass spheres whose average masses (in mg) are indicated in parentheses.

†100% (M-P)/P is the per cent deviation of average measured velocity from predicted velocity; 100% (P-T)/T is the per cent deviation of predicted velocity from threshold velocity.

No military debris was trapped at station 5P. The gravel missiles that were caught were distributed in the following way:

Trap	Distance		
	4.8 ft	12.5 ft	32.0 ft
5P4a	1	0	1
5P4b	0	1	5
5P5a	0	0	0
5P5b	0	1	3
5P6a	0	6	13
5P6b	0	30	67
Total	1	38	89

It is apparent from the above tabulation that the upper traps (with "b" suffix) at each installation generally caught more missiles than the corresponding lower ones and that more gravel was trapped from the greater than from the lesser distances of placement. The gravel translated only a short distance before impact probably lacked sufficient velocity to cause the necessary penetration for trapping the missile. The most interesting thing to be noted, however, is that ten times as many gravel missiles were caught at station 5P6, which was behind the concrete area, as were caught at both stations 5P4 and 5P5, even though only twice as much gravel was placed before station 5P6 as in front of stations 5P4 and 5P5 (see Fig. 4.23).

Figures 4.33 and 4.34 represent analyses of the combined gravel data from these traps for translational distances of 12.5 and 32.0 ft, respectively. The gravel translated 32.0 ft was somewhat heavier and had slightly higher velocities than that translated 12.5 ft. Both sets of data are in good agreement with the predicted results (see Table 4.6).

4.4.6 Sphere Installation 5P7

Installation 5P7 was located on the right side (looking toward GZ) of the concrete area opposite installation 5P6 (see Fig. 4.23). Spheres were placed in front of installation 5P7 in the same manner as described in Sec. 4.2.1 and illustrated in Fig. 4.12.

It is interesting to note that the thermal radiation incident on this installation apparently increased with height above ground (see Fig. 4.35). This could have been caused by several different effects. However, the most plausible reason that the lower trap received less heating is that it was partially protected by a layer of dust generated close to the concrete surface in front of the installation by action of the thermal pulse itself. The formation of such a dust layer was documented by the motion pictures that were made by Project 33.3 to study the translation of anthropomorphic dummies due to blast winds.⁶ The differential-heating effect observed at this installation was present but to a lesser degree at installation 5P6, which was also behind the concrete slab. At installations 5P4 and 5P5, where there was no stabilization of the native soil, there was no noticeable difference in the thermal effects on the upper and lower traps (see Fig. 4.32).

Data for 120 spheres caught at installation 5P7 are summarized in Table 4.6. For comparison, some of these data were organized in a different fashion and are presented in Table 4.1. It is noteworthy that, of the spheres caught, those originating from 12.5 ft had higher average striking heights than those translated 32.0 ft. An explanation of this is that the missiles translated 12.5 ft had insufficient velocities to penetrate the lower trap (compare in Table 4.1 the threshold velocities with those predicted) but could penetrate the upper one whose absorber surface had been softened temporarily by heating. Thus the velocities determined for the spheres translated 12.5 ft were too high—from 21.6 to 53.7 per cent greater than predicted (see Table 4.1). The fact that the spheres translated 32.0 ft had average velocities only 9.5 to 13.7 per cent greater than predicted may be explained by (1) their average height at impact being lower (i.e., more of them struck the lower trap, which was relatively undamaged by thermal) and (2)

they struck the traps after the spheres translated 12.5 ft, allowing the absorber more time to cool by action of the blast winds, thereby restoring its natural resistance to missile penetration. Attention is called to the last column in Table 4.1 which gives the per cent deviation of the predicted from the threshold velocities. For the spheres translated 12.5 ft, three of the four samples had predicted velocities that were the same as or less than the threshold. The predicted velocities for the spheres translated 32.0 ft, on the other hand, were 7.7 to 25.7 per cent higher than for threshold values.

Data for two natural stones caught in trap 5P7b are recorded in the summary table (Table 4.6).

4.4.7 Window-glass Installation 5P8

Installation 5P8 was located 17.8 ft behind a window (see Fig. 4.36 for postshot view of this installation). The amount of protection afforded the trap installation from thermal radiation is apparent by comparing this photograph with the one depicting the sphere traps after the detonation (Fig. 4.35). A factor that enhanced the thermal protection by windows was the color coding of the glass (see Fig. 4.9).

The glass-fragment data obtained from the 5P8 traps (Figs. 4.37 and 4.38 and Table 4.6) are not significantly different from the data obtained from similar 5P installations, even though the distance between trap and window was considerably greater in the present instance.

4.4.8 Window-glass Trap 5P9b (Above Pig Trap 5P9A)

Trap 5P9b was placed above a pig trap in a manner similar to that illustrated in Fig. 4.18 for trap 4P9b. The distance from the traps to the window was also the same as for installation 4P9 (12.8 ft).

A comparison of the data obtained at the two installations (Figs. 4.19 and 4.39 and Table 4.6) indicates that the one nearest to GZ (5P9b) collected 16 per cent fewer fragments whose geometric mean mass was 28 per cent smaller but whose mean velocity was 8 per cent higher. In both instances the geometric mean velocities were approximately the same as the predicted ones.

4.5 STATION 5PP (PIG STUDY),¹ 5320-FT RANGE

The experiment at this station was the same as that at station 4PP (Sec. 4.3) except that the distance from the glass wall to the traps was 11.7 ft instead of 8.8 ft and the total length of the wall was 120 ft instead of 80 ft.

The data from these two traps (Figs. 4.40 and 4.41) are fairly representative of those obtained from the window installations at station 5P, the principal difference being that more fragments were caught at station 5PP and their masses were slightly lower.

Data for three natural stones caught at this station are presented in Table 4.6.

4.6 STATION 6P, 4770-FT RANGE

4.6.1 Experimental Plan and Blast Parameters

The experimental design for this station was essentially the same as at station 4P (Sec. 4.2.1) except in the placement of the dogs² by Project 33.4. Instead of locating a dog behind the plate-glass window, one was housed at a separate installation (6P8A) and marked gravel was placed at three distances in front of the installation. This installation is shown in the layout chart (Fig. 4.42) on the right side of the stabilized area.

Figure 4.43 contains a plot of overpressure vs. time measured at this station. Shown on the same chart, as a dashed line, is overpressure vs. time computed for an ideal blast wave whose overpressure impulse and duration are the same as those measured (see Sec. 3.3). Except for small deviations, the measured overpressure curve is in good agreement with the curve for the ideal wave.

The measured dynamic pressures, which are plotted in Fig. 4.44 as a function of time, are somewhat erratic and, in general, are lower than those computed for an ideal wave.

The data for large stones, building blocks, and bricks displaced at station 6P are presented in Sec. 4.15. Station 6P results for window glass, plate glass, natural stones, gravel, military debris, and spheres are summarized in Table 4.6.

4.6.2 Window-glass Installation 6P1

Installation 6P1, which consisted of two traps, was located 7.8 ft behind a standard window. Velocity data for 67 fragments from the lower trap (Fig. 4.45) and 41 fragments from the upper trap (Fig. 4.46) are evenly distributed about the lines of predicted velocity.

Data for ten natural stones caught in trap 6P1b are plotted in Fig. 4.47. Velocities for two of the stones were almost identical to the predicted ones. Velocities lower than predicted were measured for the remaining eight stones. This result is not surprising since the prediction assumed that the distance of translation, which was unknown, was the one necessary to attain maximum velocity. The natural-stone data are also presented, combined with others at station 6P, in Sec. 4.6.9.

Table 4.6 summarizes results at this installation.

4.6.3 Window-glass Trap 6P2b (Above Dog Trap 6P2A)

Trap 6P2b, which was located above a dog trap (31.5 in. high), was located 12.8 ft behind a standard window. Results obtained from this trap (Fig. 4.48) are similar to those from the corresponding installation at station 5P (refer to Sec. 4.4.3 and Table 4.6); i.e., a relatively large number of fragments were caught but their velocities were generally lower in relation to those predicted than at other glass installations at station 6P where the traps were located at a lower level above ground.

Twenty natural stones whose masses ranged from 0.014 to 1.62 g were recovered from trap 6P2b (Fig. 4.49). Measured velocities are generally equal to or lower than those predicted. The natural-stone data are also combined with others at station 6P for analysis in Sec. 4.6.9 and Table 4.6.

4.6.4 Plate-glass Installation 6P3

Installation 6P3 was located 12.8 ft behind a plate-glass window (see Fig. 4.50 for post-shot view of this installation). (A similar window is depicted preshot in Fig. 4.9.) Note the impressions made by large fragments that impacted flat. There was no evidence of thermal damage to the absorber at this installation or any installation behind a window.

Data were obtained from trap 6P3b for five large fragments, ranging in mass from 140 to 391 g, which impacted flat (Fig. 4.51). The scatter in velocity was quite low ($S_{gv} = 1.02$), and the geometric mean velocity (120 ft/sec) was only about 8 per cent lower than predicted (130 ft/sec).

Eight fragments with random impact orientations were caught in the two traps. The measured velocities were about equally distributed about the predicted velocity line (Fig. 4.52).

Data for natural stones recovered from traps 6P3a and 6P3b are plotted in Figs. 4.53 and 4.54, respectively. The upper trap (6P3b) caught more stones (49 vs. 19) whose velocities were generally higher than the lower one. Natural-stone data from these traps are combined with others at station 6P for analysis (see Sec. 4.6.9 and Table 4.6).

4.6.5 Military-debris and Gravel Installations 6P4 and 6P5

The military debris that was placed 5.5, 14.0, and 36.0 ft in front of these installations was similar to that described in Sec. 4.2.1. In addition to the military debris, $\frac{1}{6}$ cu ft of marked gravel was placed at each of the three distances (see layout chart, Fig. 4.42).

Both lower and upper traps at these installations were slightly damaged by thermal radiation (see Fig. 4.55 for postshot view of installation 6P4).

TABLE 4.2—PARTIAL RESULTS FOR SPHERES RECOVERED FROM STATION 6P6
(Samples of less than five not included; complete data in Table 4.6.)

Spheres*	Distance translated, ft	No. of missiles	Height above ground, in.		Velocity, ft/sec			% Deviation†	
			Placed	In trap, av.	Threshold	Measured, av.	Predicted	100% (M-P)/P	100% (P-T)/T
G ₁ (72.6)	5.5	5	13	7.1	102	147	97	51.5	-4.9
G _S (39.0)	5.5	6	13	9.0	117	157	106	48.1	-9.4
G _S (38.4)	5.5	7	0	10.8	117	153	107	43.0	-8.5
St 1/8	5.5	10	0	18.4	54.3	91.6	62	47.7	14.2
G _S (39.4)	14.0	18	18	13.3	117	158	132	19.7	12.8
Al 1/8	14.0	11	0	14.8	90.0	129	127	1.6	41.1
St 1/8	14.0	7	0	15.5	54.3	87.3	80	9.1	47.3
G ₁ (72.9)	14.0	21	0	17.6	102	136	122	11.5	19.6
G _S (47.0)	14.0	36	0	18.8	113	149	130	14.6	15.0
Al 3/16	14.0	10	0	22.1	83.5	128	108	18.5	29.3
St 1/8	36.0	7	0	12.6	54.3	91.6	93	-1.5	71.3
Al 1/8	36.0	10	0	12.7	90.0	137	146	-6.2	62.2
Al 3/16	36.0	6	0	12.7	83.5	122	125	-2.4	49.7
G _S (47.1)	36.0	10	30	12.8	113	147	149	-1.3	31.9
G ₁ (71.3)	36.0	12	0	14.3	102	135	142	-4.9	39.2
G _S (37.2)	36.0	43	0	14.8	118	156	155	0.6	31.3

*Numbers after Al (aluminum) and St (steel) are diameters (in in.). G_S and G₁ represent two sizes of soda-glass spheres whose average masses (in mg) are indicated in parentheses.

†100% (M-P)/P is the per cent deviation of average measured velocity from predicted velocity; 100% (P-T)/T is the per cent deviation of predicted velocity from threshold velocity.

The 55 missiles that were caught by the traps at installations 6P4 and 6P5 were distributed in the following way:

Trap	Natural stones	Military debris	Gravel		
			At 5.5 ft	At 14.0 ft	At 36.0 ft
6P4a	0	0	0	0	0
6P4b	14	0	1	4	0
6P5a	4	0	0	1	0
6P5b	25	1	0	3	2

The upper traps caught more missiles than the lower ones, a result similar to that at the corresponding 5P installations. Note that trap 6P4a caught no missiles.

The only missile type caught in sufficient numbers to merit plotting was natural stones at 6P4b (Fig. 4.56) and 6P5b (Fig. 4.57). In both cases the measured velocities were about the same as, or lower than, those predicted.* The data for these natural stones, combined with others at station 6P, are also discussed in Sec. 4.6.9 (see Table 4.6 for results).

The data for gravel caught from the two larger distances were combined with similar data from installation 6P7 and are presented in Sec. 4.6.6.

The one piece of military debris caught in trap 6P5b had a mass of 5.53 g and a measured impact velocity of 74 ft/sec, which is 32 per cent higher than the predicted velocity of 56 ft/sec (see Table 4.6).

4.6.6 Sphere Installation 6P6 and Gravel Installation 6P7

(a) *General.* These installations, along with trap 6P8A, were located behind an area that was stabilized with asphalt. Figure 4.58 is a preshot view of the area looking away from GZ. The BRL pressure instrumentation can be seen on the right side of the photograph. The packets held by wire frames, as well as those on the surface below the frames, contained an assortment of spheres (see Sec. 4.2.1 for description). Marked gravel was located at three distances in front of the other two installations, 6P7 and 6P8A. Note that the protective covers had not been removed from the missile traps and that the dog trap was empty at the time the photograph was taken.

Figures 4.59 and 4.60 are postshot views of these installations. Although the lower trap at the sphere installation (Fig. 4.59) appears to have been less affected by thermal radiation than the upper one, the damage incurred was noticeably greater than that for the lower trap at the corresponding sphere installation at station 5P (see Fig. 4.35). The photograph of the gravel traps (Fig. 4.60) shows no apparent difference in the thermal radiation incident on the lower and upper traps.

(b) *Data from Installation 6P6.* A total of 251 spheres was caught at installation 6P6 (134 by the lower trap and 117 by the upper trap). Complete data for these spheres are listed in Table 4.6; however, for purposes of discussion, certain data were abstracted and presented in Table 4.2 in a form similar to that used for installation 5P spheres (see Table 4.1 and Sec. 4.4.6). Inspection of Table 4.2 reveals that the spheres originating 5.5 ft from the traps had average measured velocities 43.0 to 51.5 per cent higher than those predicted. The velocities for the spheres translated 14.0 ft were 1.6 to 19.7 per cent higher than predicted and those for the spheres translated 36.0 ft ranged from 6.2 per cent lower to 0.6 per cent higher than predicted. These observations are in general agreement with the hypothesis presented in Sec. 4.4.6 for installation 5P spheres; viz., the spheres placed at the smaller distances arrived at the trap while the absorber was still soft due to thermal action, whereas those arriving later from the

*Refer to Sec. 3.6 for a discussion of measured velocities of natural stones in relation to those predicted.

greater distances found the absorber restored to its natural hardness due to the cooling action of the blast winds. It is of interest to note that this effect was absent at the 7G4 sphere installation (shot Galileo, Chap. 6) where the maximum overpressure was 8.38 psi* but where the traps were given extra thermal protection (see Fig. 6.84 and Table 6.2).

Since both traps at installation 6P6 were appreciably affected by thermal radiation, the spheres from the small distance, whose velocities are presumed to have been relatively small, penetrated both traps. Thus the average striking heights (see column 5 in Table 4.2) for the spheres translated 5.5 ft were small in comparison with those for corresponding spheres at station 5P where the lower trap was relatively free of thermal damage.

Information in the last column of Table 4.2 indicates that three of the four types of spheres that were translated 5.5 ft had predicted velocities lower than the threshold. This would indicate that such sphere types were caught only because the absorber had been modified through thermal action.

Data for 31 natural stones obtained from trap 6P6a and for 58 from trap 6P6b are plotted in Figs. 4.61 and 4.62, respectively. Both samples indicate that the smaller stones had high velocities and the larger ones had low velocities relative to the predicted ones. Table 4.6 gives the results of the analysis of natural stones at installation 6P6 as well as their data combined with data for all natural stones at station 6P (see also Sec. 4.6.9).

(c) *Data from Installation 6P7.* The lower trap at this installation (6P7a) caught two pieces of gravel originating from 36.0 ft and one natural stone. The upper trap (6P7b) caught 7 natural stones, 1 gravel missile from 5.5 ft, 12 from 14.0 ft, and 5 from 36.0 ft. Data for the natural-stone missiles were combined for analysis with similar data obtained from other station 6P traps (see Sec. 4.6.9 and Table 4.6). The data for the one gravel missile translated 5.5 ft were combined with similar data for one from trap 6P4b but were not plotted. Data obtained from traps 6P4b, 6P5a, 6P5b, and 6P7b for 20 gravel missiles translated 14.0 ft are plotted in Fig. 4.63. Data for nine gravel missiles translated 36.0 ft from traps 6P5b, 6P7a, and 6P7b are plotted in Fig. 4.64. Velocities for the gravel translated 14.0 ft are in good agreement with those predicted, the predicted velocity line being between the regression line and the upper standard-error-of-estimate line (see Fig. 4.63). Velocities for the larger gravel missiles translated 36.0 ft are considerably lower than those predicted (see Fig. 4.64). Table 4.6 gives a summary of the results of the analysis of the combined data for the gravel at each distance.

4.6.7 Window-glass Installation 6P9

This installation was located 22.8 ft behind a standard window. Slight scorching of the wood in the upper trap is indicated by the postshot photograph (Fig. 4.65), although the absorber was found to be free from thermal damage. Similar scorching did not occur at other glass installations (see Fig. 4.50) at this station where the windows were placed nearer the traps.

Glass-fragment missile data obtained from traps 6P9a and 6P9b are plotted in Figs. 4.66 and 4.67, respectively. In both instances only a few missiles had measured velocities exceeding those predicted.

Data for 39 natural stones caught in the upper trap are displayed in Fig. 4.68 and are given in Table 4.6. Data for five natural stones caught in the lower trap as well as the 39 from the upper trap were combined with similar data obtained at other station 6P traps (see Sec. 4.6.9 and Table 4.6). The line of predicted maximum velocity satisfactorily explains the higher velocities measured.

4.6.8 Window-glass Trap 6P10b (Above Pig Trap 6P10A)

Installation 6P10 was located 12.8 ft behind a standard window (see Fig. 4.69 for postshot view of this installation). There is evidence in this photograph that several large fragments of glass struck the absorber but were not caught. Data for 32 fragments that were retained by the

*Maximum overpressure at station 6P was 6.38 psi.

absorber are presented graphically in Fig. 4.70. Only two missiles had velocities above those predicted.

Data for 10 natural stones caught by this trap are plotted in Fig. 4.71. All velocities measured were somewhat lower than the predicted maximum velocities. The natural-stone data are discussed, combined with others at station 6P, in Sec. 4.6.9 (see Table 4.6 also).

4.6.9 Natural-stone Data from all Station 6P* Traps

Results of the analysis of all natural stones caught at stations 6P and 6PP are set forth in Table 4.6. A total of 305 stones was caught; these stones had a combined mass of 33.55 g. The predicted maximum velocity for a stone with a mass equal to the geometric mean of the sample (60 mg) is 188 ft/sec. The geometric mean of measured velocities being 157 ft/sec (16.5 per cent less than the predicted maximum) is a reasonable result since all the stones caught probably were not translated the proper distance to acquire maximum velocity. †

4.7 STATION 6PP (PIG STUDY),¹ 4770-FT RANGE

The experiment at this station was similar to the ones at stations 4PP, 5PP, and 6.7PP. ‡ This station had a 160-ft-long glass wall; the traps were located near its center and 16.0 ft downwind. Since this station was at the same range as station 6P, the same blast parameters were used to compute predicted missile velocities (see Table 4.5).

Results obtained at station 6PP are displayed graphically in Figs. 4.72 and 4.73 for the lower and upper traps, respectively. Data for the lower trap are quite similar to those obtained at installation 6P9 (see Figs. 4.66, 4.67, and 4.72), which was at the same range but was 22.8 ft from a standard window. However, data from the upper trap (6PPb) indicates that a greater number of fragments were caught and that their masses were smaller and their velocities higher. It is of interest to note that the total mass§ of the 390 fragments from the upper trap was 310 g, which is only 5 g greater than the total mass of 170 fragments from the lower trap.

One natural stone was caught in trap 6PPa and eight were caught in trap 6PPb. Data for these missiles were combined with similar data from the station 6P traps, which were also at 4770-ft range. Results obtained from the combined data were discussed in Sec. 4.6.9 and are given in Table 4.6 with station 6P data.

4.8 STATION 6.7PP (PIG STUDY),¹ 4470-FT RANGE

The experimental plan for this station was the same as for station 6PP (discussed in Sec. 4.7) except that station 6.7PP was 300 ft nearer GZ and the traps for station 6PP were 18.0 ft behind the glass wall. Since blast-wave measurements for station 6.7PP were not available, values of peak overpressure and duration of the positive pressure were obtained from regression equations derived from measurements made at other Priscilla stations. ¶ These quantities, 6.99 psi for peak overpressure and 0.891 sec for duration, were used to compute predicted missile velocities.

The postshot photograph of station 6.7PP (Fig. 4.74) provides evidence of some scorching of the exposed wood surfaces of the trap housings. The absorber, however, was found to be undamaged by heating effects. This, in contrast to the observation of thermal damage to station 6P absorbers not behind windows, serves to illustrate the thermal protection provided by ordi-

*The analysis includes data for nine natural stones caught at station 6PP, which was at the same range as station 6P.

†This topic was discussed in Sec. 3.6.

‡Studies at these stations were made in cooperation with Project 4.1 (see Sec. 4.3).

§Total mass can be obtained by multiplying the number of missiles, n , by the average mass, \bar{M} , found in Table 4.6.

¶The procedure for computing the regression equations is outlined in Table 4.5.

nary double-strength window glass. It should be pointed out that the glass used in the pig studies (stations 4PP, 5PP, 6PP, and 6.7PP) was unpainted, whereas that in the standard windows (stations 4P, 5P, 6P, and 8P) was painted for the purpose of color coding.

The glass-fragment data obtained by station 6.7PP traps (Figs. 4.75 and 4.76) are related to the predicted velocities in a manner similar to that observed for station 6PP data. However, fewer total missiles were recovered at station 6.7PP than at 6PP. This discrepancy is evidently attributable to the fact that more diligence was exercised in one instance than in the other in recovery from the absorber of small fragments that were difficult to find.

Four natural stones having an average velocity of 140 ft/sec were recovered from trap 6.7PPa. Additional data for these missiles are listed in Table 4.6.

4.9 STATION 8P, 3930-FT RANGE

4.9.1 Experimental Plan and Blast Parameters

The chart in Fig. 4.77 illustrates the experimental plan for station 8P. The principal difference between the plan for this station and the one for station 6P is that the gravel, military debris, and spheres were placed at greater distances from the traps at station 8P since a somewhat stronger blast wave was expected at this station (see Sec. 3.6). Another notable difference is that a more rugged absorber (type III) was used in all station 8P traps except those behind windows for which the windows themselves provided adequate protection against thermal radiation.

Figure 4.78 is an interesting preshot photograph of the 8P station taken at a height of about 15 ft above ground level. Installation 8P1 is in the background and 8P10 is in the foreground. Note the sandbags placed on the lee side of the installations prepared for the exposure of animals. Displacement results obtained for the large stones and building blocks, to be seen in a line in the foreground in Fig. 4.78, are reported in Sec. 4.15.

Overpressure measured as a function of time at this station is shown graphically in Fig. 4.79. The dashed curve on this chart depicts the overpressure vs. time relation for an ideal blast wave whose impulse and duration are the same as those measured* (2.574 psi-sec and 0.823 sec, respectively). The maximum overpressure of the ideal blast wave that was used in the prediction of missile velocities was found by computation to be 8.60 psi. This value is somewhat lower than the gauge maximum of 9.20 psi shown on the chart as a spike. However, the overall agreement between the measured and computed curves is good.

Dynamic pressure vs. time measured at this station is shown in Fig. 4.80. The dashed line represents the dynamic pressure computed for the ideal blast wave whose parameters were discussed in the preceding paragraph. Although there are large fluctuations in the measured curve, the average values are in reasonable agreement with the computed ones up to about 0.055 sec. After that time the measured curve is consistently lower than the computed one.

4.9.2 Window-glass Installation 8P1

Installation 8P1 was located 7.8 ft behind a standard window (see Fig. 4.81 for preshot view of this installation). The dark appearance of the absorber was due to dust discoloration rather than thermal effects.

Data for 103 fragments caught in the lower trap (8P1a) and 100 from the upper trap are plotted in Figs. 4.82 and 4.83, respectively. With a few exceptions the predicted-velocity lines form upper limits of the measured missile velocities.

Data for six natural stones caught by trap 8P1a are presented in Sec. 4.9.9 in combination with similar data from other station 8P traps.

4.9.3 Window-glass Trap 8P2b (Above Dog Trap 8P2A)

Trap 8P2b, which was placed above a dog trap, was 31.5 in. high. The installation was 12.8 ft behind a standard window.

*See Sec. 3.3.

Data for 497 fragments recovered from this trap (plotted in Fig. 4.84) indicate that most of the velocities measured were less than the predicted values. A relatively large number of missiles were recovered from this trap. At least part of the increase may be accounted for by the abundance of small fragments recovered.

Velocity and mass data for 25 natural stones from trap 8P2b are presented graphically in Fig. 4.85. The velocities measured were considerably lower than those predicted for stones that had traveled the optimum distance to maximize velocity.

4.9.4 Plate-glass Installation 8P3

At this location a standard plate-glass installation was placed 12.8 ft from the traps. The postshot photograph (Fig. 4.86) is remarkable in that it shows large depressed areas in the absorber caused by fragments of plate glass striking flat. In this photograph the absorber, which was originally white, appears gray due to the fine dust deposited by action of the blast wave.

Data for 25 fragments caught in the lower trap are shown in Fig. 4.87. The measured velocities were significantly lower than those predicted, especially for the larger missiles. This may have been caused by the fact that the orientations of the larger fragments were not truly random, as assumed in the calibration procedures for all fragments except those striking flat. An inspection of the lower trap in Fig. 4.86 indicates that the larger fragments appear to have struck almost flat, whereas none of them were judged to have struck in this orientation when the absorber was examined in the laboratory.

The upper trap (8P3b) caught 33 fragments whose orientations at impact were not flat (Fig. 4.88) and 7 whose orientations were flat (Fig. 4.89). The 33 fragments with non-flat orientations show velocity vs. mass relations similar to those noted for the lower trap. The "flat" fragments, however, were much larger and had measured velocities only slightly lower than those predicted. In agreement with theory, the larger of the flat fragments had somewhat higher average velocities than the smaller ones.

4.9.5 Military-debris and Gravel Installations 8P4 and 8P5

The chart in Fig. 4.77 illustrates the method of placement of military debris and gravel, color-coded for each of three distances, in front of installations 8P4 and 8P5. The postshot photograph (Fig. 4.90) indicates that the surface of the absorber at installation 8P5 was somewhat damaged by thermal radiation (note beaded appearance). The condition of installation 8P4 traps was about the same as that of 8P5 traps (Fig. 4.90).

No military debris was recovered from any of the four traps. The distribution, by trap and by displacement, of 214 gravel and natural-stone missiles caught is as follows:

Trap	Natural stones	Gravel			Total gravel
		At 6.5 ft	At 16.8 ft	At 43.0 ft	
8P4a	0	5	23	3	31
8P4b	6	5	103	3	111
8P5a	2	8	8	2	18
8P5b	0	20	10	16	46
Total	8	38	144	24	206

Data for the eight natural stones were combined for purposes of analysis with natural-stone data obtained from other traps at station 8P. The results are presented in Table 4.6. A similar procedure was followed for the gravel missiles where the sample size was less than eight.

The results obtained for the larger samples of gravel are plotted by trap and by displacement distance in Figs. 4.91 and 4.97. It is noteworthy that the upper traps caught more missiles than the lower ones and also that the two largest samples originated from the 16.8-ft distance.

TABLE 4.3—PARTIAL RESULTS FOR SPHERES RECOVERED FROM STATION 8P6
(Samples of less than five not included; complete data in Table 4.6.)

Spheres*	Distance translated, ft	No. of missiles	Height above ground, in.		Velocity, ft/sec			% Deviation†	
			Placed	In trap, av.	Threshold	Measured, av.	Predicted	100% (M-P)/P	100% (P-T)/T
G _s (47.6)	16.8	7	0	14.0	109	173	181	-4.4	66.1
G _s (37.5)	16.8	5	18.5	17.4	113	191	187	2.1	65.5
St ¹ / ₈	43.0	14	0	10.9	66.6	118	133	-11.3	99.7
G _l (71.9)	43.0	9	0	19.5	104	191	196	-2.6	88.5
G _s (37.9)	43.0	28	0	19.8	113	204	212	-3.8	87.6

*St ¹/₈: Steel spheres, ¹/₈ in. in diameter.

G_s: Small soda-glass spheres, average mass (mg) in parentheses.

G_l: Large soda-glass spheres, average mass (mg) in parentheses.

†100% (M-P)/P is the per cent deviation of average measured velocity from predicted velocity; 100% (P-T)/T is the per cent deviation of predicted velocity from threshold velocity.

Although there was little difference in the velocities of missiles caught in the upper and lower traps, provided the displacement distance was the same, there is to be noted an increase in velocity with increased distance of displacement. The regression lines describing the measured median velocities are in good agreement with the predicted velocities for the gravel displaced 16.8 and 43.0 ft (Figs. 4.91, 4.92, 4.95 to 4.97); however, the measured velocities for the missiles displaced 6.5 ft were appreciably higher than those predicted (Figs. 4.93 and 4.94).

Similar anomalies, probably due to the same causes, were noted in the sphere data at stations 5P and 6P, and were discussed in Secs. 4.4.6 and 4.6.6.

4.9.6 Sphere Installation 8P6 and Gravel Installation 8P7

A comparison of the layout chart in Fig. 4.77 with that in Fig. 4.42 shows that installations 8P6 and 8P7 were arranged in a manner very similar to that for installations 6P6 and 6P7 (see also Sec. 4.6.6). A notable difference between the installations of these stations was that a more dense absorber (type III) was used at station 8P than at station 6P (type II). As a result, the thermal damage observed at station 8P was somewhat less than at station 6P, even though the former was closer to GZ. This fact is made evident by comparing the postshot photograph (Fig. 4.98) with Figs. 4.59 and 4.60.

A total of 123 spheres was recovered from the two traps at installation 8P6. Complete results are recorded in Table 4.6; however, for the sake of discussion, certain data for the larger samples of missiles were extracted and are presented in Table 4.3. The average measured velocities varied from 118 ft/sec for $\frac{1}{8}$ -in.-diameter steel spheres to 204 ft/sec for the glass spheres whose average mass was 37.9 mg. The deviations of the measured velocities from those predicted were relatively low (compared with those in Table 4.2), varying from 2.1 per cent higher to 11.3 per cent lower than predicted. The probable reason for these low deviations is that the measured velocities were considerably higher than those just sufficient for penetration (threshold). This would tend to minimize the errors in measured velocity due to softening of a thin layer of the absorber near the exposed surface due to thermal radiation (see Secs. 4.4.6 and 4.6.6).

Although the lower trap (8P6a) caught no natural stones, the upper one (8P6b) caught 10 stones whose geometric mean mass and velocity were 40.9 mg and 254 ft/sec, respectively. The data for these missiles, plotted in Fig. 4.99, show good agreement between measured and predicted maximum velocities.

Colored gravel was placed at three distances (see Fig. 4.77) in front of installation 8P7. The distribution of gravel and natural stones found in the traps was as follows:

Trap	Gravel			Natural stones
	At 6.5 ft	At 16.8 ft	At 43.0 ft	
8P7a	0	7	2	2
8P7b	0	60	14	4

No gravel was caught from the 6.5-ft distance, although some was caught from this distance at installation 8P5 (see Figs. 4.93 and 4.94). Graphical data for the three largest samples listed above are presented in Figs. 4.100 to 4.102. In each instance the predicted velocities were only slightly higher than the median represented by the regression line.

Data for the three smaller samples listed above were combined for purposes of analysis with similar data obtained at station 8P and are presented in Table 4.6.

4.9.7 Window-glass Installation 8P9

This installation, which was located 22.8 ft behind a standard window, was similar to installation 6P9 (described in Sec. 4.6.7).

The following data are useful in comparing the results from the two installations:

Trap	No. of missiles	Geometric mean mass, mg	Geometric mean velocity, ft/sec
6P9a	178	419	123
6P9b	161	541	132
8P9a	180	318	154
8P9b	129	403	161

There is no apparent reason why only 129 fragments were recovered from trap 8P9b in comparison to 178, 161, and 180 from the other traps. It should be pointed out that the number of missiles recovered—especially small ones—is dependent to some extent on the diligence of search by the technician extracting the fragments from the absorber. Other significant patterns, however, may be noted in the above tabulation of results. The data for the higher overpressure (8P) indicate smaller missiles and higher velocities than the data for the lower overpressure. In contrast, the upper (b) traps in comparison to the lower (a) ones at the same station yielded both larger missiles and higher velocities.

Glass-fragment missile data for traps 8P9a and 8P9b are plotted in Figs. 4.103 and 4.104, respectively. Both sets of data show that the predicted maximum velocity defines an upper limit for the measured velocities.

4.9.8 Window-glass Trap 8P10b (Above Pig Trap 8P10A)

This installation, which was located 12.8 ft behind a standard window, was similar to the installation at station 6P (described in Sec. 4.6.8). (Figure 4.69 is a postshot view of this installation.) Results obtained are shown graphically in Fig. 4.105 for trap 8P10b and in Fig. 4.70 for trap 6P10b. The following summarizes the data obtained at the two installations:

Trap	No. of missiles	Geometric mean mass, mg	Geometric mean velocity, ft/sec
6P10b	32	1010	110
8P10b	204	302	160

The reason for the large difference in geometric mean mass of the missiles caught in the two traps is made apparent by examination of the plotted data in Figs. 4.70 and 4.105. At least as many large missiles were caught in trap 8P10b as in trap 6P10b, but many more smaller ones were recovered from trap 8P10b. The difference in geometric mean velocity between the two traps is undoubtedly significant and indicates that higher missile velocities are produced at higher overpressures.

Data for 20 natural stones caught in trap 8P10b are plotted in Fig. 4.106. The fact that the measured velocities are considerably lower than those predicted is not significant—especially considering the small sample caught—since the points of origin of the natural stones are not known.

4.9.9 Combined Analysis for Natural Stones and Gravel at Station 8P

In previous sections missile data have been presented for each trap. In this section all data for natural stones caught in various traps at station 8P have been combined, as well as the data for gravel missiles translated equal distances. The results of these analysis are recorded in Table 4.6; however, for purposes of discussion, the following data were extracted:

	Natural stones	Gravel		
		At 6.5 ft	At 16.8 ft	At 43.0 ft
Number	85	38	211	41
Geometric mean mass, mg	80.9	175	178	232
Geometric mean velocity, ft/sec	181	180	183	193
Predicted geometric mean velocity, ft/sec	246	155	197	214
Deviation of measured from predicted velocity, %	-26	16	-7.1	-9.8

The predicted velocity of 246 ft/sec for natural stones with a mass of 80.9 mg was computed for the displacement which would maximize velocity for stones of this size. Thus it is not surprising that the geometric mean of measured velocities is 26 per cent lower than the predicted velocity, since the source of the stones is unknown. The probable reason that velocities measured for the gravel displaced 6.5 ft were higher than predicted is discussed in Sec. 4.4.6.

The velocities measured for the gravel placed at 16.8 and 43.0 ft are in reasonable agreement with theory.

4.10 STATION 10P, 2730-FT RANGE

4.10.1 Experimental Plan and Blast Parameters

The experimental plan for station 10P, depicted in Fig. 4.107, is similar to those previously discussed except that window and plate glass were not used at station 10P. Note that two of the installations, 10P2 and 10P3, contained only one trap. All installations except 10P1 were reinforced by sandbags placed on the lee side of the traps. Types III, IV, and V absorbers (see Chap. 2) were used at this station.

Overpressure vs. time measured at this station is plotted in Fig. 4.108. The deviations of the measured from the ideal overpressures are quite significant, the measured curve being characterized by a long rise time and an irregular, but relatively flat, peak. The dynamic pressure record obtained at this station, Fig. 4.109, shows even greater deviations from the ideal than the overpressure record. It is significant to the interpretation of the missile data obtained at this station that the dynamic pressure reached relatively high values, but was slow in development. Thus translational velocities attained after short displacements could be expected to be inordinately low compared to those later attained after greater displacements.

The displacement data for large stones, building blocks, and bricks at station 10P are presented in Sec. 4.15.

4.10.2 Military-debris and Gravel Installation 10P1

Figure 4.110 is a postshot view of installation 10P1. No data were obtained from the upper trap, which contained type III absorber, because of excessive erosion. Gravel and natural-stone data from the lower trap are plotted in Figs. 4.111 to 4.113. Velocities of the gravel measured after 19.1 ft of travel were low relative to those predicted on the basis of the ideal blast wave defined in Figs. 4.108 and 4.109 (see discussion in Sec. 4.10.1). The velocities for the gravel translated 49 ft (Fig. 4.112) were about the same as those predicted, whereas the velocities of the natural stones (Fig. 4.113) measured at various stages during the displacement cycle ranged up to 400 ft/sec higher than those predicted.

Thirteen pieces of military debris were caught in trap 10P1a. Nine of these originated from the 49-ft distance and were combined for analysis with similar data obtained from installation 10P2 (see Sec. 4.10.3). Four of the 13 pieces caught were displaced only 7.4 ft. The data for these missiles are recorded in Table 4.6. It is sufficient to say here that their masses ranged from 12 to 271 g and their velocities from 110 to 203 ft/sec.

4.10.3 Military-debris and Gravel Installation 10P2

Figure 4.114 is a postshot view of installation 10P2. Note the damaged sandbags behind the installation and dry lake silt deposited in front of the trap.

Data for 31 pieces of gravel translated 19.1 ft before being caught are plotted in Fig. 4.115. The velocities shown in this figure are significantly higher than those in Fig. 4.111 for a similar type of experiment. A difference between the two situations, however, was that the trap absorber yielding the lower missile velocities (10P1a) was Styrofoam (type IV), whereas the other was balsa wood (type V). The balsa absorber was much less uniform than the Styrofoam and therefore yielded a less reliable velocity calibration. On the other hand, the balsa absorber was more resistant to the erosion effects due to the severe exposure conditions at this location. One circumstance that would tend to discredit the balsa data at installation 10P2 is that velocities of about the same magnitude were measured for the stones translated 19.1 ft (Fig. 4.115) as for those translated 49 ft before striking the trap (Fig. 4.116). In the Styrofoam trap, however, the gravel traveling the greater distance had higher velocities (see Figs. 4.111 and 4.112).

Data for 186 natural stones obtained from installation 10P2 are plotted in Fig. 4.117. The velocities are generally significantly higher than those to be expected from an ideal or classical blast wave whose overpressure impulse and duration are the same as those measured (3.329 psi-sec and 0.737 sec, respectively). It is also noteworthy that the velocities of the larger stones were only slightly lower than those for the smaller stones.

Six pieces of military debris that had traveled 19.1 ft were caught in installation 10P2 (see Table 4.6). These missiles had masses that ranged from 14 to 144 g and velocities that ranged from 165 to 310 ft/sec.

Data for three military-debris missiles displaced 49 ft were combined for analysis with similar data from trap 10P1a. Graphical data from both traps are shown in Fig. 4.118. Note that one missile penetrated through the balsa absorber to the plywood support to which the balsa was cemented. Data for this missile were not included in the analysis. The data for military debris from these two traps seem to be in agreement in contrast to the data for gravel, as noted above.

4.10.4 Gravel Installation 10P3 and Sphere Installation 10P4

The postshot condition of installation 10P3, depicted in Fig. 4.119, was similar to that of installation 10P2 (Fig. 4.114) except that installation 10P3 had accumulated a larger pile of native silt in front of it. Figure 4.120 shows installation 10P3 on the right and installation 10P4 on the left. Note that the dry lake bed, which had been smooth, suffered violent upheavals due to the shot. Although it is not evident from this photograph, the area in front of these installations had been paved with asphalt (see Fig. 4.107). The upper trap (10P4b) at the installation, shown on the left in Fig. 4.120, was found to be unusable for missile evaluation because of excessive erosion. This trap contained the same absorber (type IV) as the lower trap at installation 10P1, which did survive the traumatic environment produced by the explosion.

The only gravel caught in installation 10P3 which could be positively identified was that originating from the sample placed 49 ft from the trap. Velocities for the 78 gravel missiles caught in this installation (Fig. 4.121) are consistent with data for similar missiles obtained from installation 10P2 (Fig. 4.116). However, these velocities measured using the balsa absorber were significantly higher than those determined using type IV Styrofoam (Fig. 4.112).

Gravel missiles whose identification was doubtful were included with the natural-stone sample (Fig. 4.122). The velocities determined for this mixed sample were generally higher than those predicted.

Velocities for 66 gravel missiles (Fig. 4.123) and 96 natural stones (Fig. 4.124) caught in trap 10P4a are in general agreement with similar data from traps with balsa absorbers at this station.

Although 165 spheres were caught in trap 10P4a, the point of origin generally could not be determined. The thin coat of paint that the spheres had been given for identification purposes was destroyed by action of erosion and thermal radiation. However, two 1/2-in.-diameter steel spheres that were caught were identified since those spheres had been placed only at the 19.1-

ft distance from the trap. The impact velocities determined for these missiles were 197 and 198 ft/sec, 146 per cent higher than the predicted velocity of 81 ft/sec. Complete data for these two and the other 163 spheres that were caught are recorded in Table 4.6. The column listing the predicted velocities, V_{p50} , contains two velocities for each type of missile if the translational distance is unknown—the lower value corresponding to a displacement of 7.4 ft and the higher value to a displacement of 49 ft. The column in Table 4.6 containing deviations of measured from predicted velocities, $\Delta V\%$, lists two figures for most types of missiles for the same reason stated above. Measured velocities were higher than those predicted on the assumption of a 49-ft displacement—and even for a 7.4-ft displacement.

The velocities ranged from 0.5 to 143 per cent higher than predicted.

4.11 STATION 15P, 2280-FT RANGE

4.11.1 Experimental Plan and Blast Parameters

The experiment at this station (see Fig. 4.125) was similar to the one at station 10P. All installations at station 15P, however, contained single traps, and the marked missiles were placed at somewhat greater distances from the traps than at station 10P.

The overpressure measured at station 15P (Fig. 4.126) indicates similar anomalies as noted at station 10P (Fig. 4.108). At the nearer range, compared with the greater one, the overpressure duration decreased from 0.737 to 0.661 sec and the overpressure impulse increased from 3.329 to 3.829 psi-sec. Even though the blast waves of these stations were definitely not of the ideal or classical type, the changes noted above are in the proper direction for such a wave.

The dynamic pressure measured at station 15P, recorded in Fig. 4.127, indicates even greater variability in pressure than the corresponding station 10P record (Fig. 4.109).

Section 4.15 includes the displacement data for large stones, building blocks, and bricks at station 15P.

4.11.2 Military-debris and Gravel Installations 15P1 and 15P2

Figure 4.128 is a preshot photograph of installations 15P1 (left) and 15P2 (right), looking toward GZ. In the installation 15P1 trap, the blast and thermal effects destroyed the type IV Styrofoam absorber; however, the trap housing remained intact but eroded along the leading edges.

The postshot view of installation 15P2 (Fig. 4.129) indicates that this installation stopped a considerable amount of soil and rocks. However, only 16 stones whose origin could be determined were caught in the trap. The data for these missiles, which were displaced 9.4 ft, are plotted in Fig. 4.130. These data indicate that relatively high velocities were attained in a short distance and that there was little dependence of velocity on missile mass.

Ten military-debris missiles were caught in installation 15P2—two translated 9.4 ft; three, 24.2 ft; and five, 62.0 ft. Data for these missiles are plotted in Fig. 4.131, with individual coding for distance of translation. It is interesting that distance of translation made little difference in the measured impact velocities.

Data for 274 natural stones recovered from installation 15P2 are set forth in Fig. 4.132. Note that data for two missiles with velocities greater than 800 ft/sec are plotted above the upper edge of the chart. Data are given in the figure caption for two large stones that penetrated the entire thickness of the balsa absorber. The fact that the line indicating predicted velocities goes through the center of the data does not indicate agreement between measured and predicted velocities. The velocity predictions were made on the assumption of maximum velocity resulting from optimum distance of travel; therefore the line of predicted velocities should describe the higher missile velocities measured which presumably resulted from optimum displacement.

4.11.3 Gravel Installation 15P3 and Sphere Installation 15P4

Figure 4.133 depicts the arrangement of traps and missiles, "planted" preshot, for installations 15P3 (right) and 15P4. Figure 4.134 is another preshot view of these installations (15P3 at the upper left) illustrating the placement of sandbags behind the traps.

Figure 4.135 is a postshot view of installation 15P3. Note that the balsa absorber was completely removed from the trap housing by action of the blast wave and that the housing itself was left partly filled with native soil.

The postshot view of installation 15P4 (Fig. 4.136) shows that the balsa stayed in place but was severely eroded. Note that surprisingly little material accumulated in front of the trap.

Data for 20 identifiable gravel missiles caught in installation 15P4 are plotted in Fig. 4.137. These missiles, after traveling 62.0 ft, had velocities remarkably near those predicted on the assumption of an ideal blast wave. Data for 232 natural-stone missiles caught in this trap (Fig. 4.138) also conform fairly well to the maximum velocities predicted.

Twenty-eight spheres, none of which could be identified by the color code, were caught in installation 15P4. Complete data for these missiles are recorded in Table 4.6. Because the distances of translation were unknown, predicted velocities were computed for the shortest and the greatest distance. These are recorded in the column marked V_{p50} . The next column indicates that the average measured velocities varied from 26 per cent lower than predicted to 43.6 per cent higher.

4.12 STATION 20P, 2030-FT RANGE

4.12.1 Experimental Plan and Blast Parameters

The experimental plan for station 20P, similar to that for station 15P, is illustrated by the layout chart in Fig. 4.139. All four traps at this station had balsa absorbers; however, only one of them (20P3) was found to be usable for evaluation of missiles.

The overpressure and dynamic pressure records (Figs. 4.140 and 4.141) obtained at this station are very similar in type to those already discussed for stations 10P and 15P (see Secs. 4.10.1 and 4.11.1).

The displacement data for large stones, building blocks, and bricks at station 20P are presented in Sec. 4.15.

4.12.2 Military-debris and Gravel Installations 20P1 and 20P2

Figure 4.142 is a preshot view of installations 20P1 (left) and 20P2. The balloon in the background is at the approximate location of GZ. Figures 4.143 and 4.144 are postshot views of installations 20P1 and 20P2, respectively. At installation 20P1 the balsa absorber was completely removed by the blast wave; at installation 20P2 it was only partly removed. That part which remained, however, yielded no usable missile data.

4.12.3 Gravel Installation 20P3 and Sphere Installation 20P4

Figure 4.145 is a preshot view of installations 20P3 (right) and 20P4. Note the gravel placed in front of installation 20P3 and the spheres in packets on wire supports in front of installation 20P4.

Figure 4.146 is a postshot photograph depicting a localized disruption of the dry lake bed on and near the area stabilized with asphalt (see Fig. 4.139). This upheaval was typical of others that were observed after the detonation at various spots in the regions close to GZ.

Figure 4.147 is a postshot view of installation 20P3 indicating the poor condition of the balsa absorber owing to the abrasive action of high-velocity silt and stones. Velocities were obtained for 88 stones recovered from this trap. Minimal velocities were evaluated for 11 additional stones that penetrated the entire thickness of the balsa and were found imbedded in the plywood support. Data for these 11 missiles are indicated as triangles on the plot in Fig. 4.148. From the data shown in this figure, it is evident that there were many missiles that had velocities considerably in excess of those to be expected from an ideal blast wave whose overpressure impulse is the same as that measured at this station (4.211 psi-sec) (see Fig. 4.140). Although the samples of spheres were placed in front of installation 20P4, one $\frac{1}{8}$ -in.-diameter aluminum sphere, which had a velocity at impact of 357 ft/sec, was retrieved from installation 20P3 (see Table 4.6).

Figure 4.149 is a postshot view of trap 20P4, which was judged to be unsuitable for the evaluation of missile velocities due to excessive erosion.

4.13 UNDERGROUND SHELTER WITH OPEN ENTRYWAY, OPS (UK 3.7)

4.13.1 Experimental Plan and Blast Parameters

An underground shelter constructed and tested during Operation Upshot-Knothole was made available to this project (33.2) for the study of translation effects due to winds associated with the blast wave. The shelter was located 900 ft from GZ (see station-location chart, Fig. 4.1). The plan view of the OPS shelter (Fig. 4.150) illustrates the construction of the structure as well as the experimental arrangement used in the present study. Note that the stairway is orientated toward GZ and that it connects to the shelter itself by means of an open, although somewhat tortuous, passageway.

The pressure instrumentation placed in the shelter entrance (see Figs. 4.150 and 4.151) failed to function. However, a pressure gauge placed at ground level near the shelter measured 65.4 psi maximum overpressure.

To make the experimental results more meaningful, test objects were chosen whose acceleration coefficients closely approximated those of man;⁵⁻⁷ i.e., had people occupied the shelter, their impact velocities would have been approximately the same as those measured for the test objects. The devices used were steel spheres with $\frac{1}{16}$ -, $\frac{1}{2}$ -, and $\frac{9}{16}$ -in. diameters similar to those used at the surface stations. In addition, three croquet balls were used whose masses had been increased with brass plugs so that an acceleration coefficient of 0.035 sq ft/lb was obtained.

The placement positions of the spheres are indicated on the shelter drawing (Fig. 4.150); e.g., 20 steel spheres $\frac{1}{2}$ in. in diameter were suspended 5.4 ft above the floor and 14.8 ft from the wall to which the type IV absorbing material was cemented. Figure 4.151 is a photograph taken near the missile-absorbing wall, looking toward the open entryway. The spheres were held in aluminum-foil bags so constructed and suspended that the spheres were readily released by action of the blast winds. The bags were taped to transverse wires of about the same strength as ordinary clothesline.

4.13.2 Sphere Data

Figure 4.152 is a postshot view of the absorbing wall. Aluminum foil similar to that used in the above-ground traps for thermal protection for the absorbers was partly blown away. Before the photograph shown in Fig. 4.152 was taken, the remaining foil had been removed and the impact points of the sphere were marked with a felt pen. The absorbing material (type IV) was found to be in good condition; no effects of thermal radiation, abrasion, or overpressure were shown.*

Impact points labeled 1 through 6 (Figs. 4.152 and 4.153) are for $\frac{1}{2}$ -in.-diameter steel spheres that were placed 5.4 ft above the floor and 14.8 ft from the absorber. Three of these spheres struck the absorber at heights greater than the placement height, the average impact height being only 0.2 ft lower than that of placement. Thus lofting due to nonhorizontal winds is indicated. The average velocity of the $\frac{1}{2}$ -in.-diameter spheres was 129 ft/sec (see Table 4.6). Velocities ranged from 99.1 to 159 ft/sec, the higher values tending to be associated with missiles striking the upper-right portion of the absorber shown in Fig. 4.153.

Points labeled *b* and *c* in Figs. 4.152 and 4.153 mark the impact location of $\frac{9}{16}$ -in.-diameter steel spheres that, because of their impact location, probably originated from the group 9.8 ft from the absorber and 4.4 ft above the floor. Their average impact height was 4.6 ft above the floor. The average impact velocity (52.9 ft/sec) was considerably lower than that for the $\frac{1}{2}$ -in. spheres (129 ft/sec), both because of a lower acceleration coefficient and a shorter distance of translation.

*For testing purposes, a 1-ft-square 2-in.-thick piece of type III absorber was cemented to an unused portion of the shelter wall near the installation of type IV absorber. The exact position is indicated in Fig. 4.152 by the black cement visible on the wall on the left side in the photograph. After the shot and test material was found on the floor of the shelter. Even though the sample was protected with aluminum foil, there were signs of heat distortion and compression. This result may have been due in part to the fact that the material was blown from its original position on the wall.

The croquet-ball imprint labeled "A" was probably made by the ball originally placed 9.8 ft away and 4.4 ft above the floor (see position marked with a large triangle and letter A in Fig. 4.153). It is to be noted that the points of impact of all spheres tended to be to the right of their original positions (see Fig. 4.152). Since croquet-ball A impacted to the left of its original position, one might speculate that it may have struck the right wall at a grazing angle before impacting with the absorber.

Of the 63 spheres used at this installation, only 9 struck the absorber with sufficient velocity to be captured or to make an impression sufficiently deep to allow identification of the missile and evaluation of velocity. A few impressions were noted which did not meet the above requirements. With one exception, the missiles that made sufficiently deep impressions did so in the upper-right quadrant of the absorbing wall (see Figs. 4.152 and 4.153). This would suggest that the blast or pressure wave did not fill the chamber uniformly but had a swirling motion, both horizontally and vertically, which allowed higher winds to develop on the upper-right side than on the lower-left side (looking toward the absorbing wall). Another effect that might account for relatively few spheres striking the absorber is that the ground shock, which arrived before the blast wave, may have prematurely released some of the spheres from their aluminum-foil containers.

4.13.3 Molten-metal and Natural-stone Missiles

Sixty-nine missiles that were retrieved from the absorber were apparently formed from molten metal. They were almost spherical in shape, with masses that varied from 1 to 71 mg, similar to the beads that are commonly produced by welding operations. No attempt was made to estimate the impact velocity of these missiles since the holes they made in the Styrofoam indicated that they were hot at the time of impact; i.e., penetration was enhanced by melting the Styrofoam.

Data were obtained for 194 stone-like missiles whose origin was unknown. Many of these objects had the appearance of concrete chips. For want of a better title, they were called natural-stone missiles. The velocity vs. mass data, plotted in Fig. 4.154, indicate that their masses were small compared to those of the natural stones caught at the above-ground stations. Owing to calibration limitations, stones with masses less than 10 mg were omitted from the analysis. Measured velocities varied from 164 to 755 ft/sec (see Table 4.6), the smaller stones tending to have slightly higher velocities.

In order to better understand the production of the natural-stone missiles in this shelter, spatial-distribution charts were prepared which show as a function of location of impact the number of missiles per square foot (Fig. 4.155), the average masses (Fig. 4.156), and the average velocities (Fig. 4.157). The distribution chart in Fig. 4.155 indicates that most of the missiles impacted on the right side of the trap—a result similar to that obtained for the spheres evident in Figs. 4.152 and 4.153. The data in Fig. 4.156 indicate that the variation in the mass averages for various area segments was small (20.9 to 41.4 mg). However, the velocity data plotted in Fig. 4.157 show a significant tendency for missiles striking in the upper right region (looking toward the absorber) to have higher velocities than those impacting in the remaining area. This result is consistent with the velocity data obtained for the 1/2-in.-diameter spheres shown in Fig. 4.153.

4.14 UNDERGROUND SHELTERS WITH CLOSED ENTRYWAYS

The purpose of this study was to investigate a possible missile hazard within closed shelters due to spalling of concrete from the walls. In the seven shelters investigated, no missiles were caught, and there was no evidence of appreciable spalling. Pertinent blast parameters and details of shelter construction may be found in Refs. 3 and 4. The locations of these structures are indicated on the station-location chart (Fig. 4.1) at ranges from 860 to 1360 ft from GZ. Four of the shelters were of the arch type construction,³ and three were made with 8-ft-diameter concrete conduits.⁴

A single trap containing type II absorber was placed, face up, near the center of each of the arch type shelters. As illustrated in Fig. 4.158, each trap was secured to the floor with chain and stud bolts. This anchor was not disturbed in any case by ground shock.

The trap arrangement was somewhat different in the three conduit type shelters. In order to increase the missile-collecting area, 16 strips of 2- by 6- by 36-in. Styrofoam were cemented to the surface of the shelter (see Fig. 4.159).

4.15 LARGE-STONE, CONCRETE-BLOCK, AND BRICK DISPLACEMENT

4.15.1 General

This phase of the secondary-missile project involved measurement of the total displacement experienced by various test objects due to action of the blast wave. Additional studies would be required, making use of the experimental data reported here, in order to obtain estimates of the velocities attained by the displaced objects.

Twenty-five stones, two concrete blocks, and two ordinary bricks were placed near each of the seven above-ground missile stations already described. The placement positions are marked on the layout charts in Figs. 4.2, 4.23, 4.42, 4.77, 4.107, 4.125, and 4.139 for stations 4P, 5P, 6P, 8P, 10P, 15P, and 20P, respectively. The stones contained in each group, whose individual masses varied from about 150 g to 20 kg, were painted a distinctive color for later identification.

Figure 4.160 depicts a typical placement of large missiles at station 4P. The postshot photograph of the same installation (Fig. 4.161) shows that all displacements were relatively small but that the small stones traveled farther than the large ones. Note also that the concrete block or brick which initially presented the greater area to the wind (see Fig. 4.160) was displaced farther than its mate which presented a smaller area.

4.15.2 Large-stone Data

The relation between mass and distance displaced for the stones is shown graphically in Figs. 4.162 to 4.168 for each of the seven stations. After trying various types of plots, it was found that log mass vs. distance made the data as linear as any other and also had certain advantages; viz., zero distance could be plotted, and the points were separated into approximately equal mass intervals. In computing regression lines, either log mass or distance could be considered to be the dependent variable since scatter in the data was undoubtedly due to factors other than the measurement of mass or distance, e.g., variability in shape of the stones, non-homogeneous blast wave, etc. It was decided to compute the regression lines by minimizing the square of the deviations in log mass since this procedure produced much more stable results (or regression lines) for the data from the precursor region (see Figs. 4.166 to 4.168) than that which minimized the square of the distance deviations.

Results of the statistical analyses described above are listed in the captions of the figures presenting the displacement data for the individual stations* (Figs. 4.162 to 4.168). The units of mass and distance used in the regression equations are the same as those used in plotting the data, viz., kilograms and feet. The geometric standard error of estimate in mass, E_{gm} , is a measure of the scatter of the mass points about the regression line. The quantity M_{50} is the geometric mean mass of the stone sample. The average displacement of the stones at each station is indicated (in feet) by the quantity \bar{d} .

The average displacements of stones for the three stations most distant from GZ varied from 2.29 ft at station 4P (Fig. 4.162) to 1.15 ft at station 6P (Fig. 4.164). It is probably not significant, in view of the variability of the data, that the stones at the most distant of these three stations had the highest average displacement. The stones at the station next closest to GZ (station 8P at 3930-ft range) had a somewhat higher average displacement (7.50 ft) (see Fig. 4.165).

Station 10P, at the 2730-ft range, was 1200 ft closer to GZ than station 8P. The stones at station 10P, which had an average displacement of 739 ft, almost spanned this separation in station locations. Only 16 of the 25 stones placed at station 10P were recovered after the detonation. Some of these were smaller than they were originally due to splitting or chipping

*A more complete listing of statistical parameters can be found in Table 4.6.

TABLE 4.4—MASSES AND DISTANCES DISPLACED FOR LARGE STONES, BLOCKS, AND BRICKS, SHOT PRISCILLA

	Station 4P		Station 5P		Station 6P		Station 8P		Station 10P		Station 15P		Station 20P	
	m*	d*	m*	d*	m*	d*	m*	d*	m*	d*	m*	d*	m*	d*
Large stones	0.287	6.5	0.235	0.8	0.206	5.1	0.227	15.2	0.308	249	0.620	1217	0.152	1617
	0.332	5.5	0.277	0.1	0.256	0	0.254	19.2	0.665	1071	3.318	1237	0.384	872
	0.391	4.9	0.317	3.4	0.357	2.3	0.366	5.4	0.724	772	5.283	1814	0.384	1375
	0.551	4.5	0.485	0.1	0.461	0	0.419	0	0.886	868	8.296	1039	0.394	910
	0.641	4.1	0.528	2.9	0.514	3.6	0.528	14.5	0.998	943	12.975	1150	0.941	235
	0.740	3.8	0.577	2.9	0.575	1.1	0.614	6.5	2.332	396	18.855	1745	1.027	1600
	0.986	3.6	0.815	4.3	0.832	3.4	0.796	7.0	2.942	945			1.329	1190
	1.015	1.8	0.895	2.3	0.972	0	0.971	24.0	3.278	713			1.858	899
	1.159	3.4	1.053	0.6	1.250	0.5	1.061	13.0	3.787	1141			1.905	931
	1.476	3.2	1.071	0.2	1.503	1.8	1.310	8.5	5.175	826			1.952	573
	1.979	3.1	1.295	1.8	1.589	4.3	1.500	10.6	5.821	647			2.347	356
	2.365	1.2	1.671	1.1	1.980	0.1	1.933	12.6	6.777	800			3.215	1258
	2.862	1.5	2.261	0.7	2.120	1.0	2.189	6.9	9.734	608			3.249	881
	3.233	0.9	2.643	2.0	2.579	0	2.711	6.7	12.653	333			3.252	1683
	3.555	2.3	3.089	0.1	3.042	0.3	3.064	4.5	14.119	742			3.955	1190
	4.702	0.7	3.324	2.9	3.300	1.0	3.325	13.0	18.844	772			3.969	1361
	5.104	0.3	4.547	1.8	4.580	1.0	4.533	6.0					4.296	1525
	6.069	1.1	5.980	0.6	5.407	0.3	5.732	2.7					4.564	871
	7.083	0	6.837	0	6.100	0.3	7.028	2.5					5.895	1461
	9.073	0.1	8.685	0	8.796	1.8	8.278	0.8					6.022	1004
10.606	0	9.215	1.3	9.310	0	9.243	1.8					6.089	1199	
13.381	0.3	10.484	0.7	10.472	0	10.477	1.9					9.652	1356	
14.980	2.0	12.419	0	10.816	0	12.532	2.4					10.377	845	
16.946	0	16.195	0	16.509	0.8	16.027	0.3					10.766	1069	
		17.273	0	18.680	0.2	17.754	1.5							
Concrete blocks	15.491	2.5	14.014	1.0	14.293	12.8	15.239	40.5						
	15.695	0.3	14.090	4.8	15.670	0.3	15.367	3.6						
Bricks	2.507	6.7	3.373	2.9	2.636	5.5	2.525	10.4						
	1.957	4.0	2.530	1.7	1.961	0	1.910	14.1						

Note: Blank space indicates that object was not recovered after the shot.

*Mass (m), in kilograms; distance (d), in feet.

during translation. (Similar observations were made for stones placed at stations 15P and 20P.) The data presented in Fig. 4.166 for station 10P show that the distance translated had no significant dependence on stone mass.

Stone-translation data for stations 15P (2280-ft range) and 20P (2030-ft range) are plotted in Figs. 4.167 and 4.168, respectively. Only six of the stones at station 15P were recovered, and these had an average displacement of 1367 ft. The fact that the regression line in Fig. 4.167 suggests a larger displacement for the larger stones may be due to an inadequate sample. The data for 24 stones recovered from station 20P (Fig. 4.168) do not indicate a dependence of total distance of translation on stone mass (compare with Fig. 4.166 for station 10P).

4.15.3 Concrete-block and Brick Data

Probably owing to breakage, none of the concrete blocks or bricks that had been placed at the precursor stations (10P, 15P, and 20P) were recovered. Masses and displacements that were measured for the two concrete blocks and two bricks placed at each of the other stations are presented at the bottom of Table 4.4. The fact that one of each pair of blocks, or bricks, usually was displaced significantly farther than the other was due to their initial orientations, viz., one with maximum area presented to the wind, and one with minimum (see Fig. 4.160).

4.15.4 Summary of Large-stone, Concrete-block, and Brick Data

The mass and measured displacements for each test object that was recovered after the detonation are listed in Table 4.4. The large-stone data that were tabulated are presented graphically in Fig. 4.169. In this presentation the range of each station is plotted along the abscissa as a vertical line. Each stone recovered was located along the appropriate vertical line according to the logarithm of its mass (in kilograms). The distance of translation for each stone was represented as a dashed or dotted line for large distances or by points for small ones. The number appearing to the right of each dot or horizontal line is the measured displacement (in feet). Upon examination of this chart, it is somewhat surprising to note that two stones originally placed at station 15P came to rest downwind of station 8P, where the stones had experienced comparatively small displacements. The difference in the translational effects between the precursor and nonprecursor regions is quite evident.

4.16 SUMMARY AND DISCUSSION, SHOT PRISCILLA

4.16.1 Station Locations and Blast Parameters

The production of secondary missiles was investigated at 19 locations on shot Priscilla in Frenchman Flat (see Fig. 4.1). Eleven of these locations were in open areas at distances of 2030 to 6120 ft from GZ. A summary of the blast parameters determined for these stations is listed in Table 4.5. The column labeled $(I_p)_m$ contains the overpressure-impulse values for each station where records were obtained. Gauge failures at two stations made it necessary to determine extrapolated values of overpressure impulse. (Other parameters in the table which are designated with a subscript "r" were also extrapolated.) The extrapolation methods used are outlined in the footnotes contained in the table. The quantities t_p^+ and p_s represent the duration of the positive overpressure and its maximum value, respectively. The quantity $(p_s)_c$ is the peak, or shock, overpressure computed for an ideal blast wave using measured or extrapolated values of impulse and duration (see Chap. 3).

One secondary missile station was located inside a shelter with an open entryway that was 900 ft from GZ (see Sec. 4.13). The pressure instrumentation inside the shelter failed to function; however, the maximum overpressure measured at ground level near the shelter was 65.4 psi (see entry at bottom of Table 4.5). Missile traps were placed inside seven shelters with closed entryways^{3,4} at distances of 1360 to 860 ft from GZ.

4.16.2 Tabulated Results

A summary of all results obtained for shot Priscilla is given in Table 4.6. The data in each of three major divisions of Table 4.6 are listed by trap, or combination of traps at a particular station, in the order of decreasing range from GZ.

TABLE 4.5—BLAST PARAMETERS, SHOT PRISCILLA
(See List of Symbols.)

$p_0 = 13.3$ psi $c_0 = 1120$ ft/sec (17.0°C) Estimated yield: 38 kt* Terrain, dry lake bed (Frenchman Flat)

Station	Range, ft	Blast line	$(I_p)_m$, † psi-sec	$(I_p)_r$, ‡ psi-sec	$(t_p^+)_m$, † sec	$(t_p^+)_r$, § sec	$(p_s)_m$, † psi	$(p_s)_c$, ¶ psi	$(p_s)_r$, ** psi
4P	6120	33.2		1.832		1.027		(4.64)	4.54
4PP	6120	Main							
5P	5320	33.2		2.035		0.964		(5.59)	5.51
5PP	5320	Main							
6P	4770	33.2	2.202	2.208	0.920	0.917	6.6	6.38	6.40
6PP	4770	Main							
6,7PP	4470	Main				0.891			6.99
8P	3930	33.2	2.574	2.553	0.823	0.841	9.2	8.60	8.34
10P	2730	33.2	3.329	3.354	0.737	0.713	9.3	13.0	13.7
15P	2280	33.2	3.829	3.838	0.661	0.658	15.2	17.3	17.5
20P	2030	33.2	4.211	4.187	0.610	0.624	15.2	21.4	20.6
OPS	900						65.4		62.4

*Estimation made by comparing the overpressure-impulse data measured for stations 6P and 8P with data for a surface burst as described in *The Effects of Nuclear Weapons*.

†Determined from BRL mechanical-gauge records. (Gauges failed at stations 4P and 5P.)

‡Overpressure impulse computed by regression equation derived from $(I_p)_m$ values

$$\log (I_p)_r = 3.0982 - 0.7487 \log R$$

§Overpressure duration computed by regression equation derived from $(t_p^+)_m$ values

$$\log (t_p^+)_r = -1.6972 + 0.4512 \log R$$

¶Peak overpressure computed for a classical blast wave of impulse $(I_p)_m$ and of duration $(t_p^+)_m$. Measured values of impulse and duration were not obtained at 4P and 5P, therefore regression values, $(I_p)_r$ and $(t_p^+)_r$, were used.

**Peak overpressure computed by regression equation derived from $(p_s)_c$ values

$$\log (p_s)_r = 5.8300 - 1.3657 \log R$$

A summary of the large-stone displacement data is presented at the bottom of Table 4.6. The regression coefficients e and f are explained in the table. It should be noted that the symbol d is used here to designate the total distance of translation, whereas in other parts of the table it represents the distance traveled by the missile before striking the trap. The symbol \bar{d} designates the average distance of translation. Minimum and maximum distances are represented by d_- and d_+ , respectively.

4.16.3 Glass-fragment Missiles, Shot Priscilla

Impact velocities were evaluated for 3728 window-glass fragments caught in 32 traps placed at 6120- to 3930-ft ranges. At the greater ranges, compared to the smaller ones, fewer missiles were caught, and their masses were larger and their velocities smaller.

The predicted velocities for the fragments caught in the lower overpressure region (4.5 to 5.5 psi) were generally near the geometric mean of the measured velocities. This is in contrast to the predicted velocities applicable to the higher overpressure regions (6.4 to 8.6 psi), which were generally near the highest values of the measured velocities. At stations 4P and 5P, windows were placed 7.8, 12.8, and 17.8 ft from the traps. At stations 6P and 8P the distances were 7.8, 12.8, and 22.8 ft from the traps. In no instance was there a significant difference in missile velocity due to distance of translation. Thus the velocities of window-glass fragments were found to be (1) less dependent on the blast-wave parameters than specified by

TABLE 4.6 — SUMMARY OF RESULTS, SHOT PRISCILLA
(See List of Symbols.)

Regression Equation: $\log v = a + b \log m$

Missile	Trap	Absorber type	d	n	\bar{D}_s	a	b	E_{gv}	V_{p50}	$(V_{p50})_R$	V_{50}	\bar{V}	S_{gv}	V_-	V_+	M_{50}	\bar{M}	S_{gm}	M_-	M_+
WG	4P1a	II	7.8	68	24.7	2.3099	-0.0924	1.24	90	206	106	109	1.27	59.6	168	1230	2118	3.16	35.5	14130
WG	4P1b	II	7.8	58	21.1	2.2937	-0.0838	1.23	90	206	109	112	1.25	59.5	188	1150	2101	3.06	89.1	14130
WG	4PPa	II	8.8	81	29.4	2.3067	-0.0779	1.29	93	216	118	122	1.32	42.2	211	1070	3255	4.39	14.1	28180
WG	4PPb	II	8.8	68	24.7	2.3964	-0.1250	1.20	93	216	106	109	1.27	53.1	188	960	2172	3.37	89.1	17780
WG	4P2b	II	12.8	48	17.4	2.2928	-0.0836	1.23	104	247	107	110	1.27	75.0	188	1470	3100	3.56	28.2	28180
WG	4P9b	II	12.8	62	22.5	2.3052	-0.0854	1.24	101	237	110	113	1.27	66.8	168	1240	2969	4.08	35.5	28180
WG	4P8a	II	17.8	41	14.9	2.3025	-0.0864	1.20	107	260	114	117	1.23	53.1	168	677	1424	3.46	89.1	8913
WG	4P8b	II	17.8	54	19.6	2.1823	-0.0526	1.34	107	259	106	111	1.35	59.6	168	1040	1990	3.37	44.7	17780
PG	4P3b	II	12.8	1	0.4				88	214		47					60309			
NS	Comb ⁽¹⁾ 4P			18	1.1	2.5098	-0.2019	1.07	142		164	167	1.23	113	219	28.9	46.8	2.60	9.6	141
Gr	4P6a	II	4.5	1	0.4				70			136					246			
Gr	Comb ⁽²⁾ 4P		10.9	14	1.0	2.5462	-0.2183	1.13	93		112	117	1.33	72.2	202	186	291	3.28	14.0	662
Gr	Comb ⁽³⁾ 4P		28.0	20	1.4	2.6592	-0.2785	1.13	116		127	132	1.31	80.0	241	98	136	2.44	10.4	412
WG	5P1a	II	7.8	48	17.4	2.3506	-0.0948	1.19	110	254	114	116	1.23	75.0	188	1301	2338	3.23	89.1	11200
WG	5P1b	II	7.8	32	11.6	2.3596	-0.1031	1.21	110	254	116	119	1.27	53.1	168	734	1717	3.78	70.8	8910
WG	5PPa	II	11.7	123	44.7	2.2919	-0.0772	1.19	119	286	119	122	1.22	66.8	188	609	1550	3.75	22.4	35480
WG	5PPb	II	11.7	158	57.4	2.2809	-0.0781	1.22	119	286	116	119	1.24	59.6	188	588	1244	3.54	14.1	14130
WG	5P2b	II	12.8	88	32.0	2.2671	-0.0829	1.18	121	291	104	106	1.23	59.6	168	1000	2277	4.26	28.2	17800
WG	5P9b	II	12.8	52	18.9	2.3511	-0.0935	1.23	121	291	119	122	1.27	42.2	188	895	1531	3.21	44.7	8910
WG	5P8a	II	17.8	40	14.5	2.2142	-0.0450	1.23	130	311	120	122	1.23	53.1	211	1011	1779	2.81	112	8910
WG	5P8b	II	17.8	43	15.6	2.0389	0.0012	1.23	130	312	110	113	1.23	66.8	168	881	1370	2.58	112	7080
PG	5P3b	II	12.8	9	3.3	2.0396	0.0140	1.22	104	253	121	122	1.18	94.4	150	877	1331	2.51	140	5150
NS	5P7b	II		2	0.7				153			166		164	167		100		87.9	112
NS	5PPb	II		3	1.1				150			128		92.0	161		115		23.8	509
Gr	5P4a	II	4.8	1	0.4				92			130					169			
Gr	Comb ⁽⁴⁾ 5P		12.5	38	13.8	2.5578	-0.2123	1.10	116		120	122	1.19	90.1	173	180	221	1.96	33.2	723
Gr	Comb ⁽⁵⁾ 5P		32.0	89	32.3	2.6168	-0.2240	1.10	129		123	125	1.21	81.6	191	228	293	2.06	40.5	973
WG	6P1a	II	7.8	67	24.3	2.1924	-0.0294	1.15	126	129	130	1.15	94.4	188	594	1124	3.37	28.2	7079	
WG	6P1b	II	7.8	41	14.9	2.2258	-0.0447	1.21	125	124	126	1.21	59.6	168	981	1587	2.69	178	5623	
WG	6P2b	II	12.8	105	38.1	2.2484	-0.0762	1.18	145	108	110	1.21	66.8	168	651	1196	3.15	44.7	14130	
WG	6P10b	II	12.8	32	11.6	2.1360	-0.0310	1.21	144	110	112	1.22	59.6	168	1010	1635	2.60	178	5623	
WG	6PPa	II	16.0	170	61.7	2.2534	-0.0534	1.22	153	129	132	1.24	66.8	237	478	1795	5.14	11.2	28180	
WG	6PPb	II	16.0	390	141.6	2.3090	-0.0678	1.21	154	138	141	1.24	59.6	266	292	794	4.08	11.2	17780	
WG	6P9a	II	22.8	178	64.6	2.2053	-0.0446	1.19	161	123	124	1.19	53.1	188	419	768	2.69	56.2	11220	
WG	6P9b	II	22.8	161	58.5	2.2215	-0.0368	1.15	160	132	134	1.15	85.1	211	541	1024	2.98	56.2	11220	
PG	6P3a and b	II	12.8	8	1.4	2.1563	-0.0148	1.19	125	128	129	1.16	106	168	2347	8053	6.53	112	29368	
FPG	6P3b	II	12.8	5	1.8	1.8697	0.0390	1.01	130	120	120	1.02	117	123	223000	240600	1.47	140000	391000	
NS	6P1b	II		10	3.6	2.5835	-0.2181	1.13	178	144	145	1.16	115	200	89.8	98.4	1.56	35.8	164	
NS	6P2b	II		20	7.2	2.3675	-0.1110	1.15	184	146	148	1.19	108	207	68.6	175	3.26	13.6	1620	
NS	6P3a	II		19	6.8	2.3752	-0.1219	1.11	188	144	146	1.16	94.9	177	59.8	97.6	2.54	16.8	526	
NS	6P3b	II		49	17.8	2.4344	-0.1336	1.12	190	162	164	1.19	93.9	205	47.7	111	2.68	10.9	1779	
NS	6P4b	II		14	4.4	2.5749	-0.2138	1.19	172	134	138	1.28	71.7	186	123	172	2.39	26.0	438	
NS	6P5b	II		25	8.4	2.5385	-0.1744	1.13	184	166	169	1.23	95.5	266	67.4	108	2.58	12.1	554	
NS	6P6a	II		31	11.3	2.5957	-0.2306	1.10	194	169	172	1.18	120	247	39.0	48.1	1.84	14.0	239	
NS	6P6b	II		58	21.1	2.5897	-0.2192	1.10	190	166	170	1.26	95.4	262	49.0	86.1	2.60	12.5	756	
NS	6P9b	II		39	14.2	2.4510	-0.1338	1.09	187	163	164	1.14	118	199	62.1	82.5	2.10	17.2	270	
NS	6P10b	II		10	3.6	2.4627	-0.1615	1.11	174	135	137	1.19	97.8	181	117	181	2.48	32.8	550	
NS	Comb ⁽⁶⁾ 6P			305	6.5	2.4859	-0.1629	1.13	188	157	160	1.22	94.9	266	60.0	110	2.62	10.9	1779	
Gr	6P4b and 7b	II	5.5	2	0.4						124		111	138		40.2		23.9	56.5	
Gr	Comb ⁽⁷⁾ 6P		14.0	20	1.8	2.4110	-0.1257	1.11	145	138	139	1.15	102	188	147	212	2.30	23.2	1105	
Gr	Comb ⁽⁸⁾ 6P		36.0	9	1.1	2.6117	-0.2311	1.10	183	154	161	1.36	80.0	246	67.7	155	3.56	12.2	789	
MD	6P5b	II	14.0	1	0.4				56		74					5530				
WG	6.7PPa	II	18.0	112	40.7	2.1445	-0.0086	1.16	157	132	134	1.16	94.4	237	430	1334	3.73	44.7	22390	
WG	6.7PPb	II	18.0	194	70.4	2.2698	-0.0281	1.19	158	142	145	1.19	75.0	237	344	790	3.21	28.2	22390	
NS	6.7PPa	II		4	1.4				195	139	140		119	161	146	165		93.9	308	
WG	8P1a	II	7.8	103	37.4	2.2463	-0.0410	1.18	172	141	143	1.19	66.8	266	245	921	3.52	17.8	44670	
WG	8P1b	II	7.8	100	36.3	2.2032	-0.0276	1.19	171	135	137	1.19	75.0	211	415	827	2.86	35.5	7079	
WG	8P2b	II	12.8	497	180	2.2647	-0.0443	1.18	193	145	147	1.19	84.1	237	229	792	4.05	14.1	35480	
WG	8P10b	II	12.8	204	74.1	2.3216	-0.0470	1.20	192	160	163	1.21	75.0	237	302	853	3.46	22.4	35480	
WG	8P9a	II	22.8	180	65.4	2.2339	-0.0191	1.19	215	154	156	1.20	75.0	237	318	747	3.64	35.5	11220	
WG	8P9b	II	22.8	129	46.8	2.2433	-0.0143	1.16	214	161	162	1.16	106	211	403	886	3.41	32.8	11220	
FWG	8P10b	II	12.8	1	0.4				207		193					13775				
PG	8P3a	II	12.8	25	9.1	2.3450	-0.0954	1.13	165	108	110	1.19	75.0	150	1778	4253	3.56	178	35480	
PG	8P3b	II	12.8	33	12.0	2.2992	-0.0694	1.16	163	126	128	1.20	66.8	168	723	1711	3.96	56.2	14130	
FPG	8P3b	II	12.8	7	2.5	1.9018	0.056	1.06	172	155	155	1.05	146	167	123000	132800	1.48	69300	262600	
NS	8P2b	II		25	9.1	2.4717	-0.1466	1.11	258	170	173	1.22	104	217	43.6	159	3.13	13.1	2632	
NS	8P6b	III		10	3.6	2.6403	-0.1456	1.07	262	254	256	1.14	180	296	40.9	67.6	2.24	17.4	370	
NS	8P10b	II		20	7.3	2.4586	-0.1099	1.10	246	178	180	1.15	146	254	79.1	164	2.80	15.2	1371	
NS	Comb ⁽⁹⁾ 8P			85	3.1	2.5055	-0.1295	1.21	246	181	187	1.28	97.9	346	80.9	226	3.51	13.1	2632	
Gr	8P5a	III	6.5	8	2.9	2.5909	-0.1466	1.10	154	180	181	1.13	147	217	183	216	1.83	59.1	451	
Gr	8P5b	III																		

Missile	Trap	Absorber type	d	n	h ₁	h ₂	V _{p50}	ΔV%	V̄	S _v	V ₋	V ₊	M̄	S _m	M ₋	M ₊	ᾱ
Ny 1/8	4P7a	II	28.0	1	30	2.5	135	40.0	189				19.73				0.9210
Al 1/8	4P7b	II	28.0	1	30	19.0	99	34.3	133				47.34				0.3839
St 1/8	4P7b	II	4.5	2	0	22.1	50 ⁽²¹⁾	76.4	88.2	4.7	85.0	91.5	130.8				0.1389
			28.0														
G _S	4P7a and b	II	1, 4.5 ⁽²²⁾	11	22 ⁽²³⁾	17.9	97 ⁽²¹⁾	39.2	135	30.8	52.0	182	39.1	6.06	31.0	51.2	0.438
			3, 10.9														
			7, 28.0														
Ny 1/8	5P7b	II	32.0	1	0	24.2	166	29.5	215				19.73				0.9210
Al 1/8	5P7a and b	II	12.5	3	0	16.4	106	15.1	122	15.2	108	138	47.34				0.3839
			32.0	3	0	6.8	124	0	124	6.2	117	129	47.34				0.3839
			32.0	4	29	18.8	124	21.0	150	22.6	134	182	47.34				0.3839
Al 3/16	5P7a and b	II	4.9	1	14	4.1	69	82.6	126				153.7				0.2660
			12.5	5	0	22.0	82	53.7	126	19.9	110	153	153.7				0.2660
			12.5	1	19	25.6	82	68.3	138				153.7				0.2660
			32.0	6	0	8.7	105	10.2	116	7.7	107	125	153.7				0.2660
St 1/8	5P7a and b	II	12.5	6	0	17.0	67	22.4	82	8.7	67	92	130.8				0.1389
			12.5	1	19	27.8	67	32.8	89				130.8				0.1389
			32.0	4	0	8.0	76	23.7	94	10.8	86	110	130.8				0.1389
St 1/4	5P7a	II	4.9	1	14	4.4	37	43.2	53				1043				0.0697
G _S	5P7a and b	II	4.9	1	0	9.9	85	55.3	132				39.0				0.438
			12.5	18	0	17.6	111	24.3	138	13.5	122	176	36.8	3.63	31.0	42.8	0.446
			12.5	2	19	18.8	103	50.5	155	26.9	136	174	42.7	5.73	38.6	46.7	0.424
			32.0	33	0	12.9	128	10.2	141	17.3	113	170	37.0	3.01	32.6	43.4	0.444
			32.0	7	29	11.1	126	9.5	138	13.8	116	151	41.6	4.30	33.9	46.3	0.428
G _I	5P7a and b	II	4.9	1	0	11.0	78	44.9	113				67.4				0.363
			12.5	9	0	16.8	102	21.6	124	15.0	110	160	71.8	2.60	67.6	75.4	0.356
			12.5	1	19	7.4	102	14.7	117				70.7				0.358
			32.0	9	0	14.4	117	13.7	133	11.6	115	152	70.8	4.08	62.2	76.2	0.358
			32.0	3	29	13.0	117	10.3	129	15.9	111	139	70.7	2.55	68.5	73.5	0.358
Ny 1/8	6P6a and b	II	14.0	2	0	21.0	173	28.9	223	2.6	221	225	19.73				0.9210
			14.0	2	18	24.4	173	22.0	211	18.8	198	224	19.73				0.9210
			36.0	3	30	9.6	191	22.5	234	15.5	218	249	19.73				0.9210
Al 1/8	6P6a and b	II	5.5	2	0	8.9	100	35.0	135	25.0	117	152	47.34				0.3839
			5.5	2	13	5.5	100	54.0	154	12.3	146	163	47.34				0.3839
			14.0	11	0	14.8	127	1.6	129	6.8	117	143	47.34				0.3839
			36.0	10	0	12.7	146	-6.2	137	6.4	132	151	47.34				0.3839
			36.0	1	30	9.4	146	-4.1	140				47.34				0.3839
Al 3/16	6P6a and b	II	14.0	10	0	22.1	108	18.5	128	7.4	114	136	153.7				0.2660
			14.0	1	18	20.5	108	20.4	130				153.7				0.2660
			36.0	6	0	12.7	125	-2.4	122	5.0	115	128	153.7				0.2660
			36.0	1	30	21.7	125	-8.0	115				153.7				0.2660
Al 3/8	6P6a	II	*	1	*	10.2	58; 90	27.9; -17.6	74.2				376.7				0.1292
St 1/8	6P6a and b	II	5.5	10	0	18.4	62	47.7	91.6	16.2	78	124	130.8				0.1389
			5.5	4	13	11.2	62	59.7	99.0	13.7	85	117	130.8				0.1389
			14.0	7	0	15.5	80	9.1	87.3	6.3	80	97	130.8				0.1389
			36.0	7	0	12.6	93	-1.5	91.6	8.8	79	105	130.8				0.1389
			36.0	2	30	8.4	93	-7.8	85.7	11.2	78	94	130.8				0.1389
St 1/4	6P6a and b	II	5.5	1	13	4.6	46	104.3	94				1043				0.0697
			14.0	2	0	5.8	58	5.2	61	1.1	60	62	1043				0.0697
G _S	6P6a and b	II	5.5	7	0	10.8	107	43.0	153	8.9	143	168	38.4	3.71	31.6	42.6	0.443
			5.5	6	13	9.0	106	48.1	157	15.2	141	178	39.0	3.68	33.5	43.0	0.438
			14.0	36	0	18.8	130	14.6	149	9.0	130	178	47.0	3.14	40.9	52.9	0.406
			14.0	18	18	13.3	132	19.7	158	15.4	134	192	39.4	4.35	33.8	50.5	0.436
			36.0	43	0	14.8	155	0.6	156	10.6	134	188	37.2	3.25	32.3	44.9	0.444
			36.0	10	30	12.8	149	-1.3	147	5.1	136	154	47.1	3.08	42.5	52.4	0.405
G _I	6P6a and b	II	5.5	3	0	4.8	97	36.1	132	3.9	129	136	71.6	1.49	69.9	72.8	0.355
			5.5	5	13	7.1	97	51.5	147	9.7	134	157	72.6	2.34	70.0	75.1	0.354
			14.0	21	0	17.6	122	11.5	136	9.5	115	157	72.9	2.84	65.7	77.8	0.353
			14.0	1	18	19.3	122	15.6	141				76.0				0.351
			36.0	12	0	14.3	142	-4.9	135	10.7	119	152	71.3	2.75	65.1	75.2	0.355
			36.0	4	30	7.2	141	-7.1	131	9.7	123	145	73.5	1.50	71.5	75.1	0.352
Ny 1/8	8P6a and b	III	43.0	1	0	5.9	258	17.8	304				19.73				0.9210
			*	2	*	12.7	189; 258	29.6; -5.0	245	5.9	240	249	19.73				0.9210
Al 1/8	8P6a and b	III	16.8	1	18.5	22.8	177	14.1	202				47.34				0.3839
			43.0	4	0	19.7	302	-38.4	186	8.2	178	197	47.34				0.3839
			43.0	3	29.5	16.9	302	-38.4	186	16.8	167	201	47.34				0.3839
			*	1	*	19.9	138; 302	45.7; -33.4	201				47.34				0.3839
Al 3/16	8P6a and b	III	6.5	1	0	25.6	118	26.3	149				153.7				0.2660
			16.8	3	0	19.6	154	7.1	165	5.5	159	170	153.7				0.2660
			16.8	1	18.5	12.9	154	-12.3	135				153.7				0.2660
			43.0	4	0	15.5	176	-3.4	170	18.0	145	185	153.7				0.2660
			43.0	1	29.5	11.2	176	-22.7;	136				153.7				0.2660
St 1/8	8P6a and b	III	6.5	4	0	10.1	88	15.9	102	7.2	95	112	130.8				0.1389
			16.8	2	0	23.2	115	-1.7	113	6.9	109	118	130.8				0.1389
			16.8	3	18.5	6.4	115	16.5	134	13.7	126	150	130.8				0.1389
			43.0	14	0	10.9	133	-11.3	118	11.0	99	137	130.8				0.1389
			43.0	4	29.5	6.3	133	-23.3	102	3.5	99	107	130.8				0.1389
			*	4	*	16.7	88; 133	22.7; -18.8	108	13.0	95	123	130.8				0.1389
St 1/4	8P6a and b	III	6.5	1	0	10.4	63	28.6	81				1043				0.0697
			16.8	2	18.5	13.6	80	18.8	95	18.7	82	109	1043				0.0697
			43.0														

the model⁵ used to make predicted velocities and (2) independent of the distance of translation within the limits investigated.

From the above observations it must be assumed that certain phenomena which are not accounted for in the model have a noticeable influence on the velocity attained by glass fragments under the conditions of the experiments reported. Part of this extraneous influence on missile velocity may be due to the mechanism of breakage of glass panes. If a pane supported along its edges is bent, a certain amount of potential and kinetic energy is stored in the pane before actual breakage occurs. Fragments near the center of the pane possessing the greater part of this energy would "pop out" at higher velocities than those near the perimeter. It should be pointed out that the energy thus temporarily stored in each pane is not necessarily derived from the blast winds but is due principally to the sudden increase in pressure existing at the leading edge of a classical blast wave. The diffractive loading effect described above would be enhanced by the process of reflection but would be mitigated provided the blast wave arrived on the lee side of the pane before it shattered. Also, if shattering occurred before appreciable bending had taken place, as might be the case for a relatively strong blast wave, then the diffractive effect would be minimal since the pressure difference between the front and rear of the pane would quickly vanish when the glass is broken.

The effects postulated in the preceding paragraph would tend to equalize fragment velocities produced by blast waves of different strengths and also for different distances of translation. The different distances of translation follow from the assumption that the velocities are imparted to a fragment by diffractive loading in a very short time during which the missile travels a short distance.

The dispersion of fragment velocities, which was noted in all the experimental data except for the fragments striking flatwise, is a reasonable result of the method of mounting the glass panes. Since the edges of the panes were restrained, fragments arising near the perimeter of the pane would be expected to have lower velocities (and more tumbling) than those arising near the center.

Six traps placed behind plate-glass installations caught a total of 88 fragments. Velocities evaluated for 12 large fragments striking the trap flat were much more uniform than the velocities for the fragments striking in random orientation. Velocities for the flat missiles were only slightly lower than those predicted.

4.16.4 Marked-gravel and Natural-stone Missiles, Shot Priscilla

Velocities were determined for 799 gravel missiles with masses between 10 mg and 1.3 g which had been color coded and placed at measured distances from the traps. For samples greater than five which were caught at nonprecursor stations (4P, 5P, 6P, and 8P), the geometric mean velocities were generally in good agreement with the predicted ones. The least satisfactory agreement was obtained for 14 gravel missiles caught at station 4P after a displacement of 10.9 ft. In this instance the geometric mean of the measured velocities was 112 ft/sec, 20 per cent higher than the predicted value of 93 ft/sec. This deviation may have been partly due to the lower-velocity missiles' having insufficient penetration for retention in the absorber.

The geometric means of measured velocities for gravel placed at stations 10P and 15P in the precursor region were as much as 39 per cent higher than the values predicted assuming an ideal blast wave with the same overpressure impulse as that measured.

Velocities were evaluated for a total of 1756 natural-stone missiles, including 194 stone-like objects caught in the OPS shelter with open entryway. Because predicted velocities were based on the assumption of optimum distance of travel for maximum velocity, the values tended to be higher than those measured.

4.16.5 Sphere Data, Shot Priscilla

Of a total of approximately 67,000 spheres placed in front of traps, impact velocities were obtained for 712. The predicted and measured velocities were generally in agreement. In instances where agreement was not good, the deviations were probably due to (1) inaccuracies in the trapping technique for small depths of penetration and (2) softening of the outer layer of absorbing material due to action of the thermal pulse.

4.16.6 Military-debris Data, Shot Priscilla

Velocities were estimated for 32 military-debris missiles whose masses ranged from 4.5 to 289 g. Only one piece of debris was caught at a nonprecursor station, 6P, where the maximum overpressure was 6.4 psi. Velocities for the military-debris missiles caught in the precursor region varied from 110 to 373 ft/sec.

4.16.7 Missiles in Shelters

Missile studies were conducted in eight underground shelters that were located 860 to 1360 ft from GZ. Seven of the eight shelters had closed entryways. Missile traps were placed in these shelters in order to determine the velocity of any particles that might spall from the concrete walls. There was no evidence of appreciable spallation.

Missile-absorbing material was cemented to a wall of a shelter with open entryway in such a way that velocities could be determined for experimental spheres. The aerodynamic properties of the spheres used were such that their impact velocities would be approximately the same as for man. Velocities evaluated for nine such spheres ranged from 45 to 159 ft/sec for situations where the distances of translation were 9.8 and 14.8 ft. Velocities (165 to 755 ft/sec) were also obtained for 194 stone-like objects whose masses varied from 10 to 618 mg.

4.16.8 Displacement of Large Stones, Concrete Blocks, and Bricks

Twenty-five stones, two concrete blocks, and two ordinary bricks were placed near each of the seven above-ground stations 2030 to 6120 ft from GZ. The stones in each group of 25 had masses ranging from about 150 g to 20 kg. The purpose of the experiment was to obtain only the total displacement since the large sizes of the missiles prohibited measurement of velocity by the trapping technique. The greatest displacement experienced by any of the objects placed at the nonprecursor stations (4P, 5P, 6P, and 8P) was 24 ft; some of the experimental objects were not moved. Of the 46 stones recovered, which had been placed at the precursor stations (10P, 15P, and 20P), the greatest total distance of displacement measured was 1814 ft and the least was 249 ft. Thus this experiment demonstrated the great difference in translational capability between the precursor and nonprecursor blast waves.

REFERENCES

1. G. M. McDonnel, H. A. Claypool, W. A. Moncrief, and J. D. Goldstein, Effects of Nuclear Weapons on a Large Biological Specimen (Swine), Project 4.1, Operation Plumbbob Report, ITR-1428, Nov. 5, 1957.
2. V. C. Goldizen, D. R. Richmond, and T. L. Chiffelle, Missile Studies with a Biological Target, Operation Plumbbob Report, WT-1470, Jan. 23, 1961.
3. W. J. Flatau, R. A. Brechenridge, and C. K. Wiehle, Blast Loading and Response of Underground Concrete-Arch Protective Structures (U), Project 3.1, Operation Plumbbob Report, WT-1420. (Classified)
4. G. H. Albright, J. C. Ledoux, and R. A. Mitchell, Evaluation of Buried Conduits as Personnel Shelters, Project 3.2, Operation Plumbbob Report, WT-1421.
5. I. G. Bowen, R. W. Albright, E. R. Fletcher, and C. S. White, A Model Designed to Predict the Motion of Objects Translated by Classical Blast Waves, USAEC Report CEX-58.9, June 29, 1961.
6. R. V. Taborelli, I. G. Bowen, and E. R. Fletcher, Tertiary Effects of Blast—Displacement, Operation Plumbbob Report, WT-1469, May 22, 1959.
7. E. R. Fletcher, R. W. Albright, V. C. Goldizen, and I. G. Bowen, Determination of Aerodynamic Drag Parameters of Small Irregular Objects by Means of Drop Tests, USAEC Report CEX-59.14, October 1961.

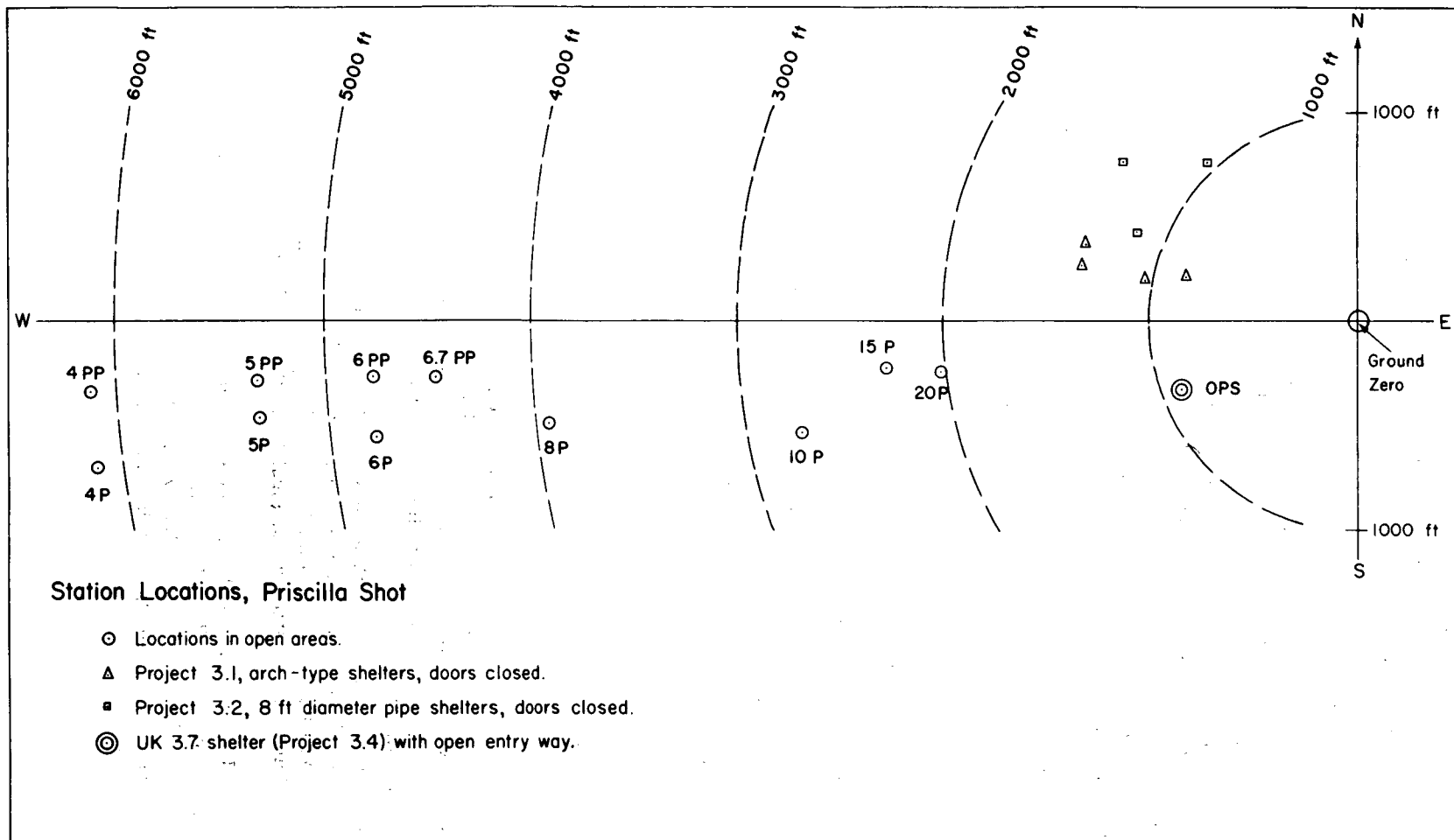


Fig. 4.1—Station locations for shot Priscilla in Frenchman Flat, NTS.

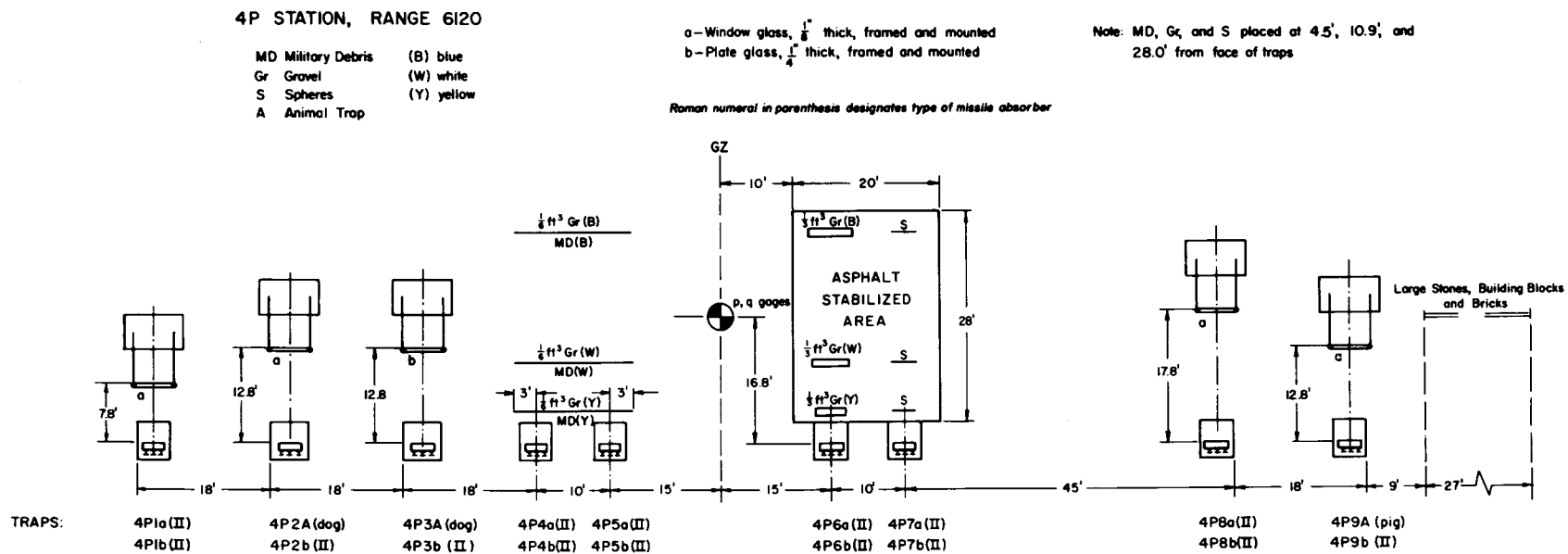


Fig. 4.2—Station 4P layout chart. Trap designators for shot Priscilla were identified by a number that indicated anticipated pressure, the letter P (for Priscilla), a number for the trap, and a small letter: "a" for a ground-level trap and "b" for a trap stacked above another.

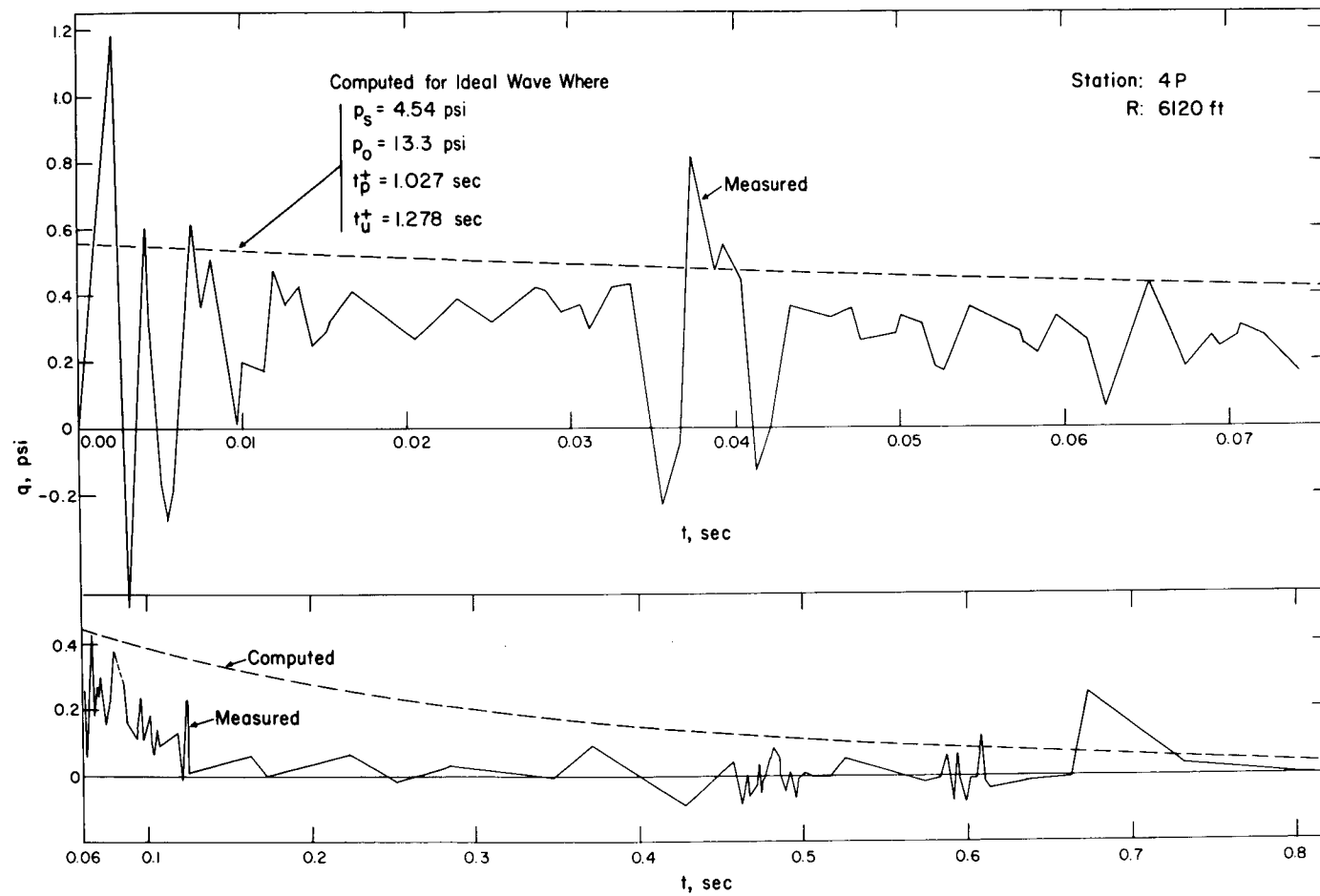


Fig. 4.3—Dynamic pressure vs. time for station 4P. (Gauge measuring overpressure vs. time failed at this station.)

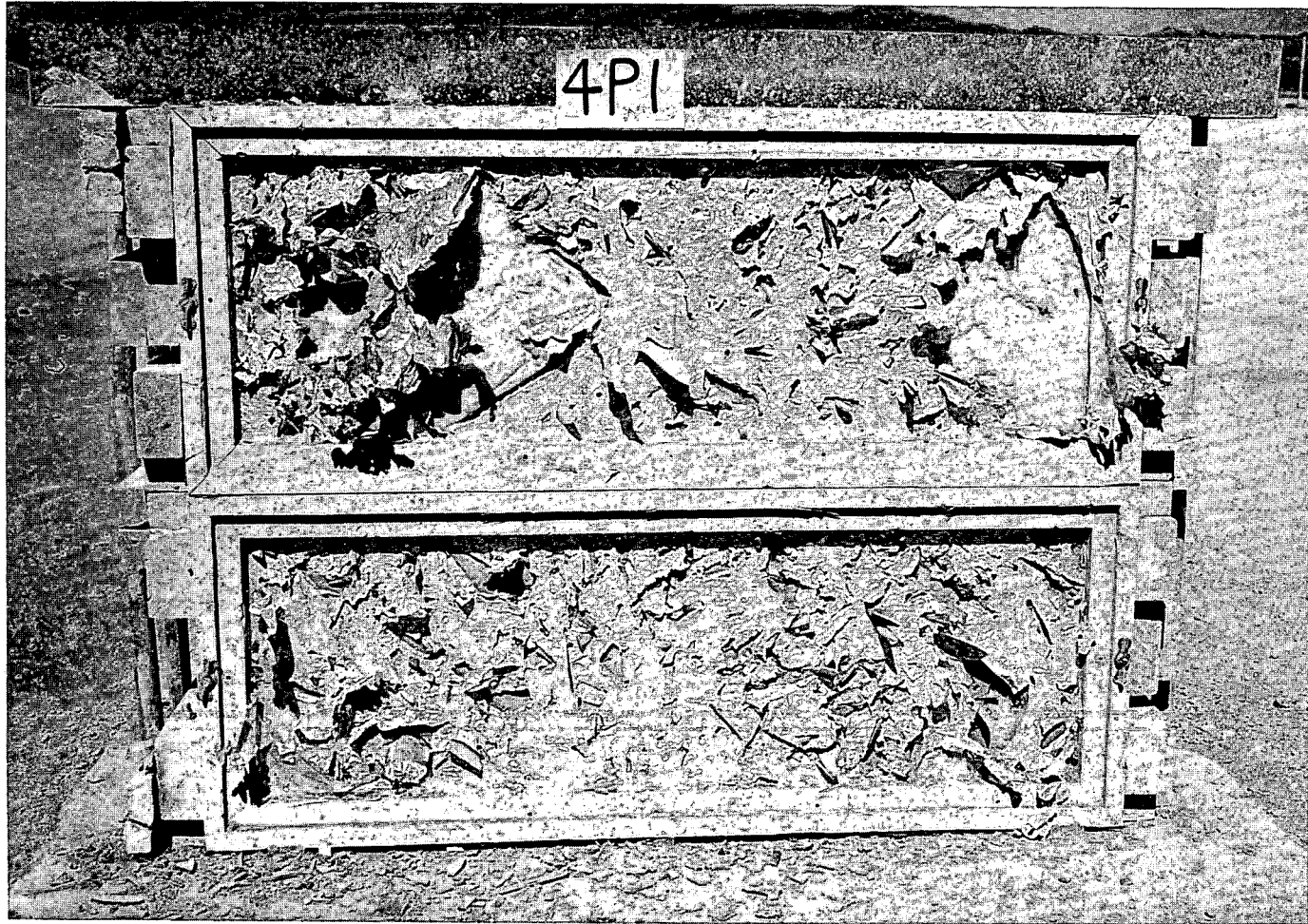


Fig. 4.4— Traps 4P1a (bottom) and 4P1b (top), placed 7.8 ft behind window, postshot.

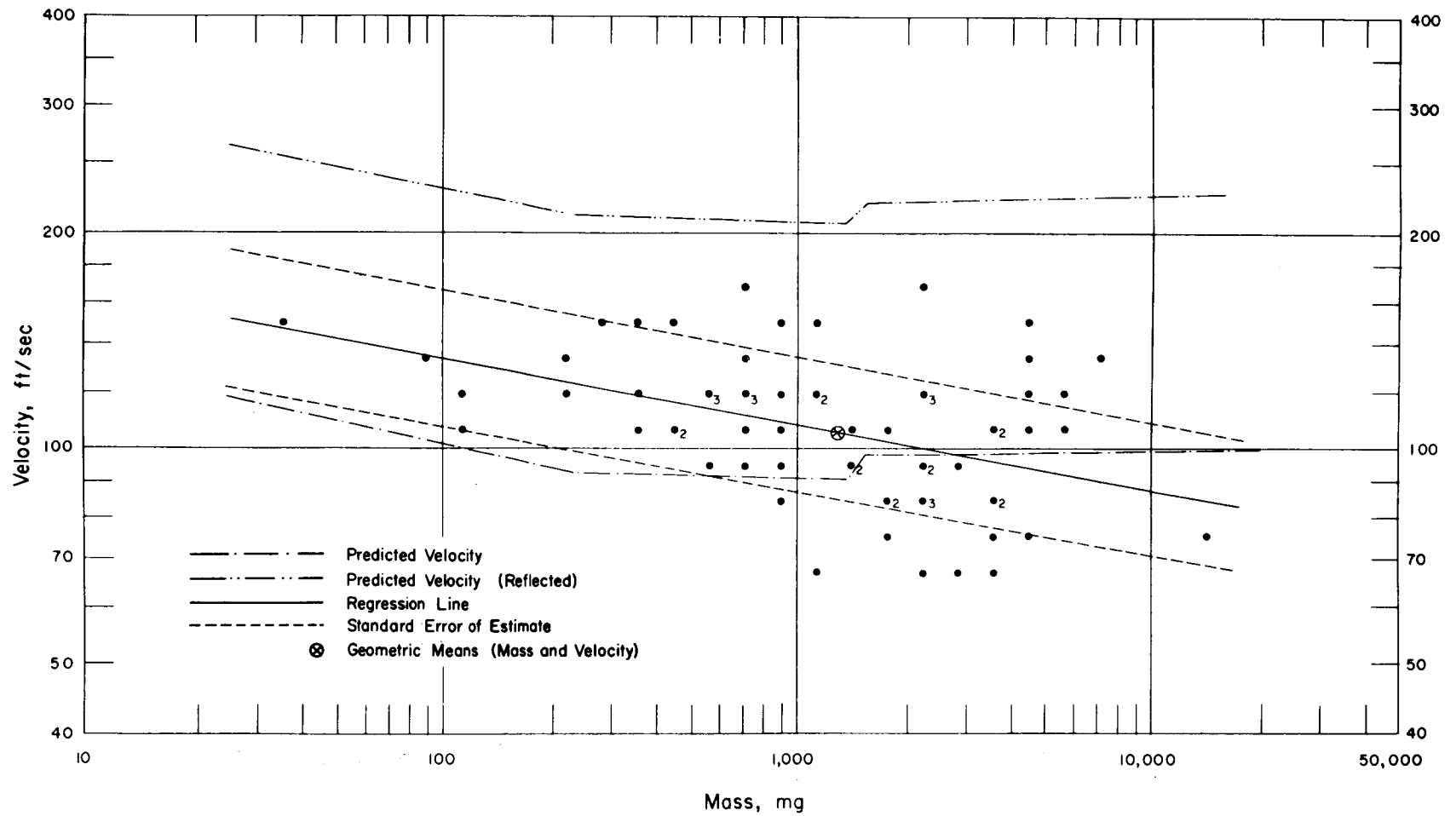


Fig. 4.5—Analysis of window-glass missiles from trap 4P1a: $d = 7.8$ ft; $n = 68$; $\log v = 2.3099 - 0.0924 \log m$; $E_{gv} = 1.24$; $M_{50} = 1230$ mg; $V_{50} = 106$ ft/sec.

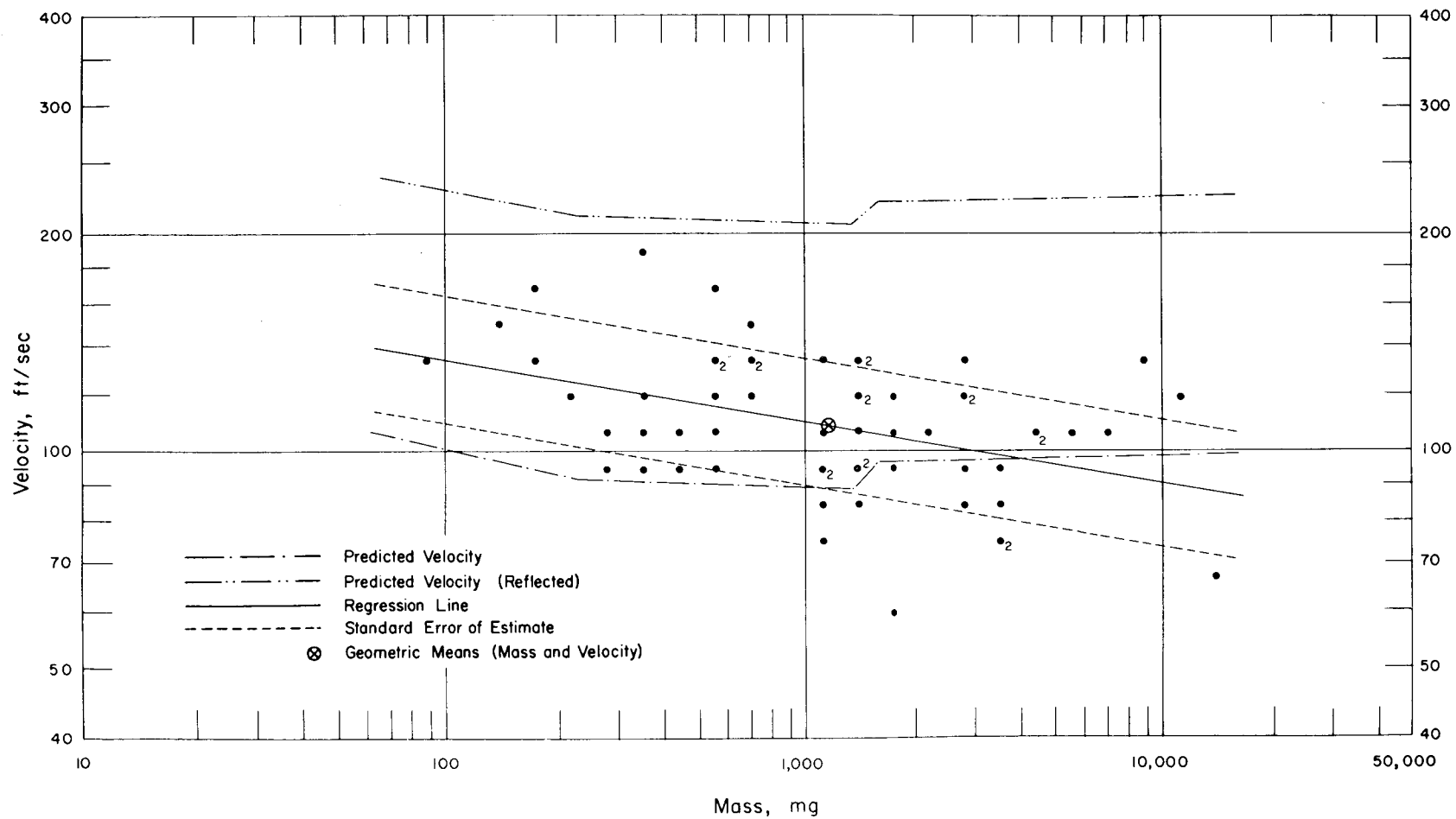


Fig. 4.6—Analysis of window-glass missiles from trap 4P1b: $d = 7.8$ ft; $n = 58$; $\log v = 2.2937 - 0.0838 \log m$; $E_{gV} = 1.23$; $M_{50} = 1150$ mg; $V_{50} = 109$ ft/sec.



Fig. 4.7— Trap 4P2b, placed above dog trap (4P2A). Distance to window installation was 12.8 ft. Bottom of missile trap was 31.5 in. above ground level.

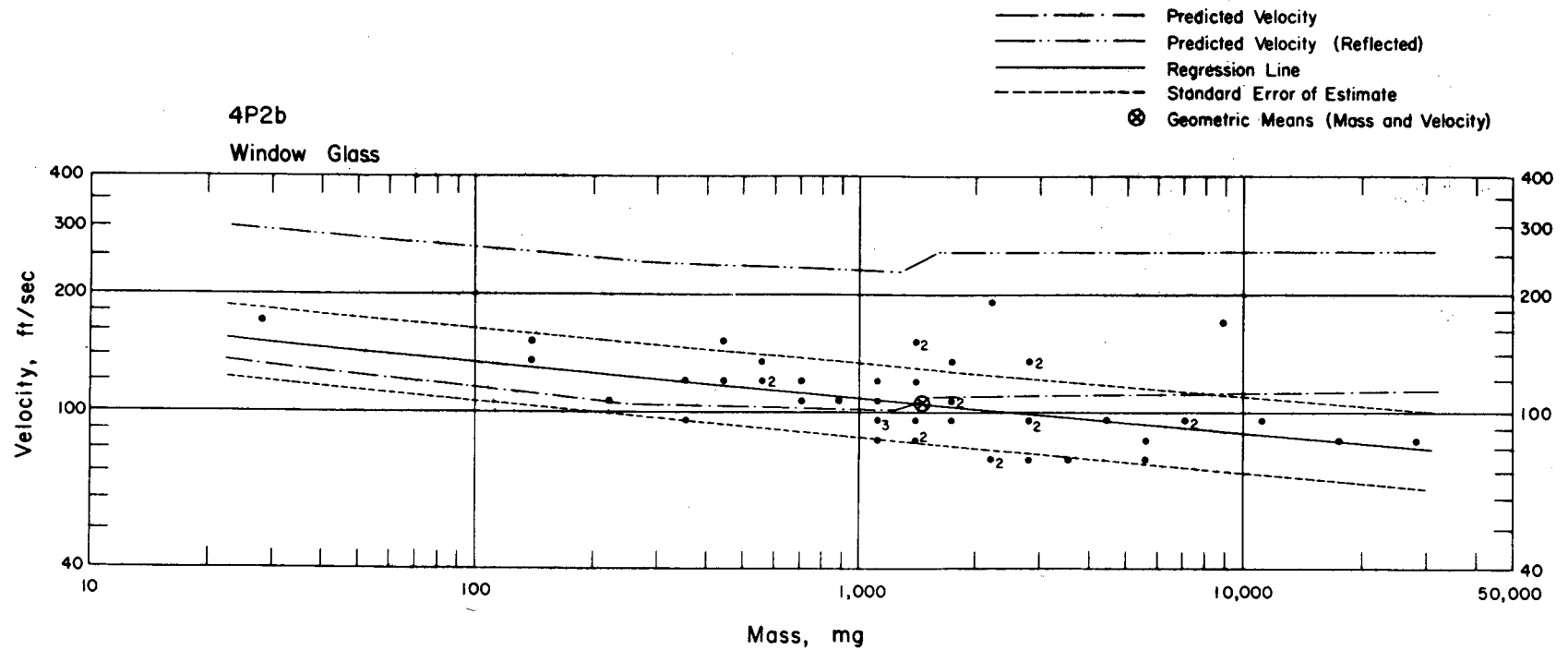


Fig. 4.8—Analysis of window-glass missiles from trap 4P2b: $d = 12.8$ ft; $n = 48$; $\log v = 2.2928 - 0.0836 \log m$; $E_{GV} = 1.23$; $M_{50} = 1470$ mg; $V_{50} = 107$ ft/sec.

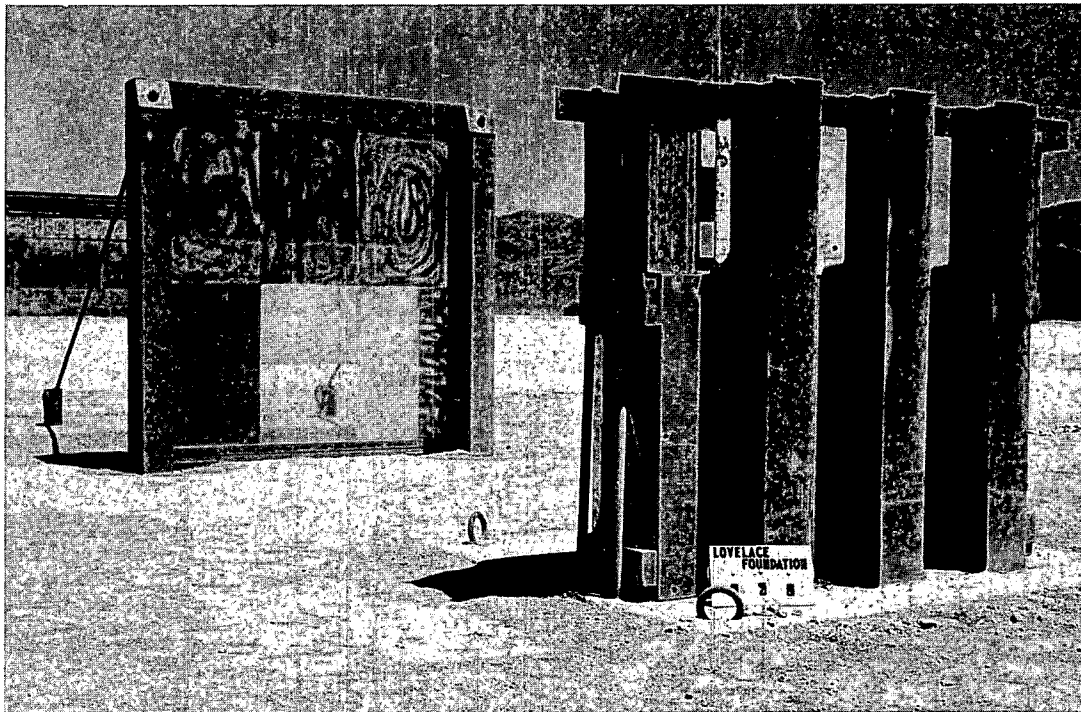


Fig. 4.9—Installation 4P3 looking toward GZ, preshot. Trap was above a dog trap, 31.5 in. above ground level and 12.8 ft from the plate-glass installation.

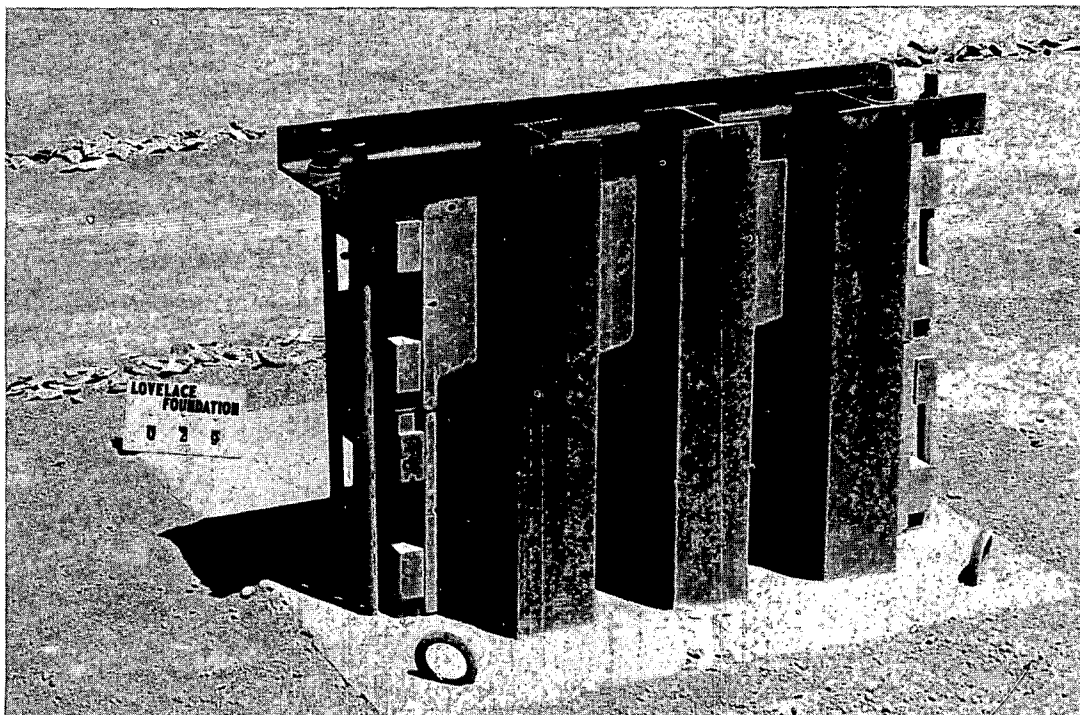


Fig. 4.10—Traps 4P4a and b looking toward GZ, preshot. Note piles of military debris mixed with marked gravel 4.5 and 10.9 ft in front of the traps. Piles on the right side of the picture were placed in front of traps 4P5a and b.

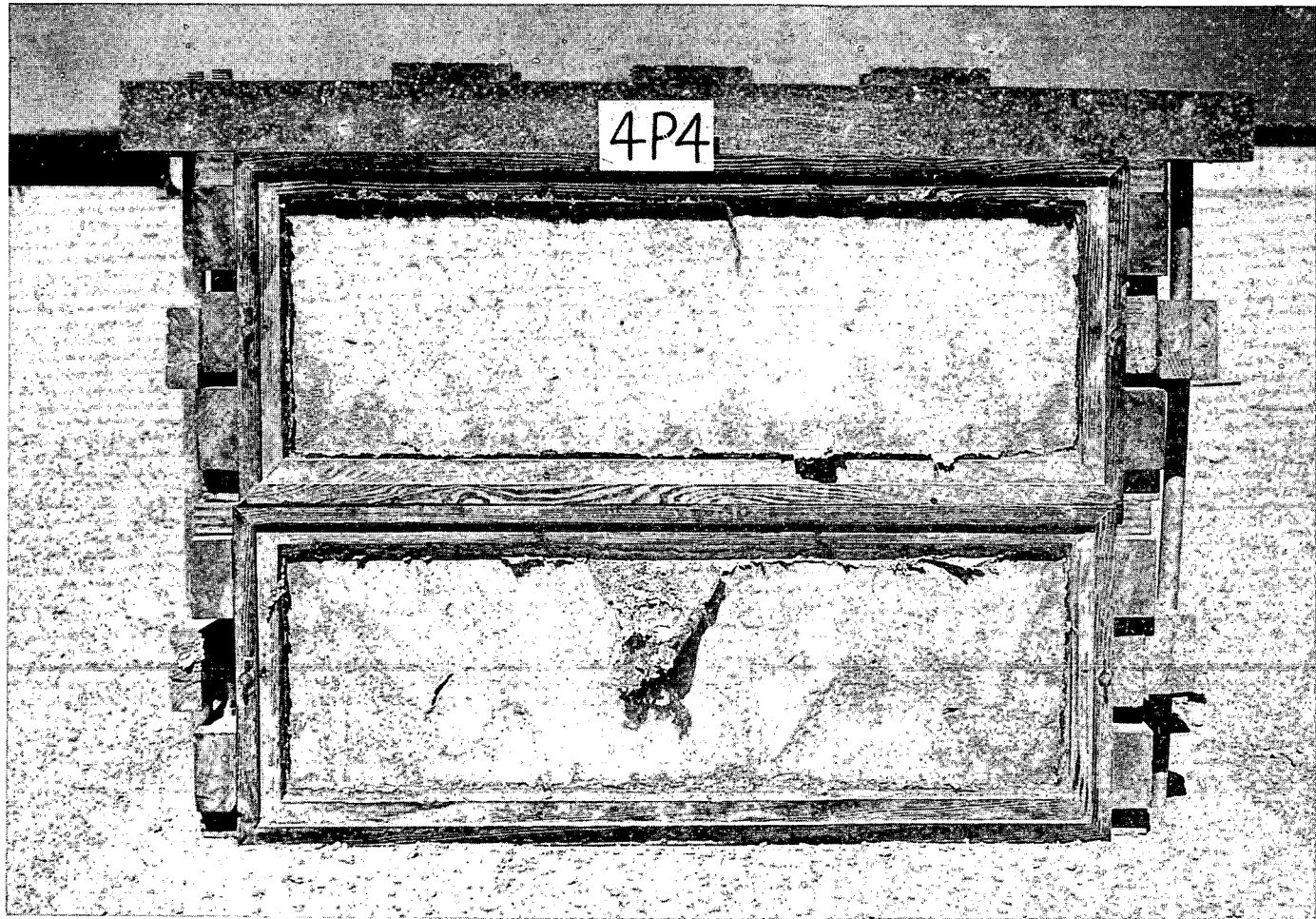


Fig. 4.11 — Front surface of traps 4P4a and b, postshot. Slight thermal damage to the absorber was noted.

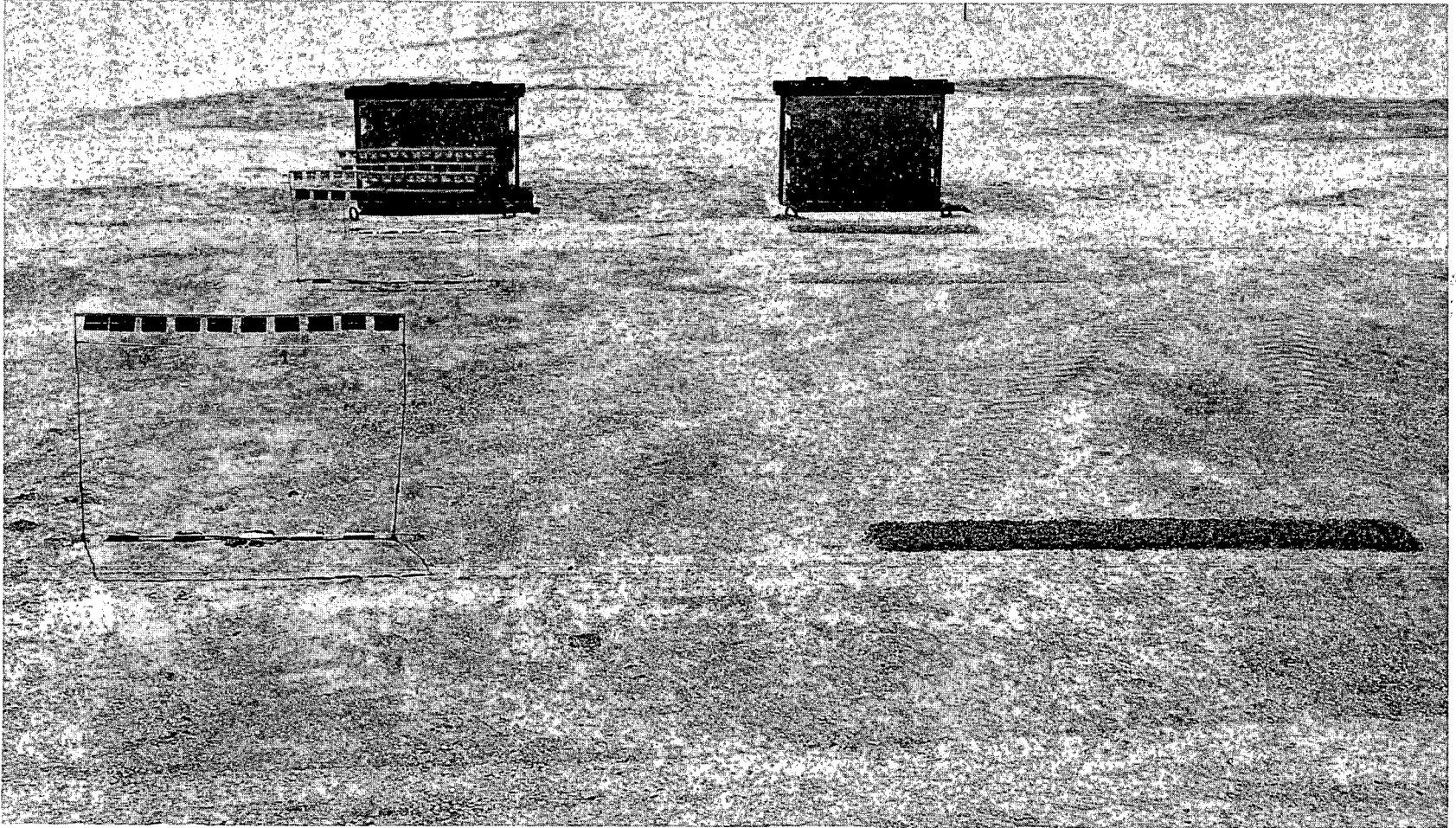


Fig. 4.12—Installations 4P6 (right) and 4P7 (left), preshot. Note packets of spheres on wire supports as well as on the ground. Piles of marked gravel can be seen on the right in front of installation 4P6 traps.

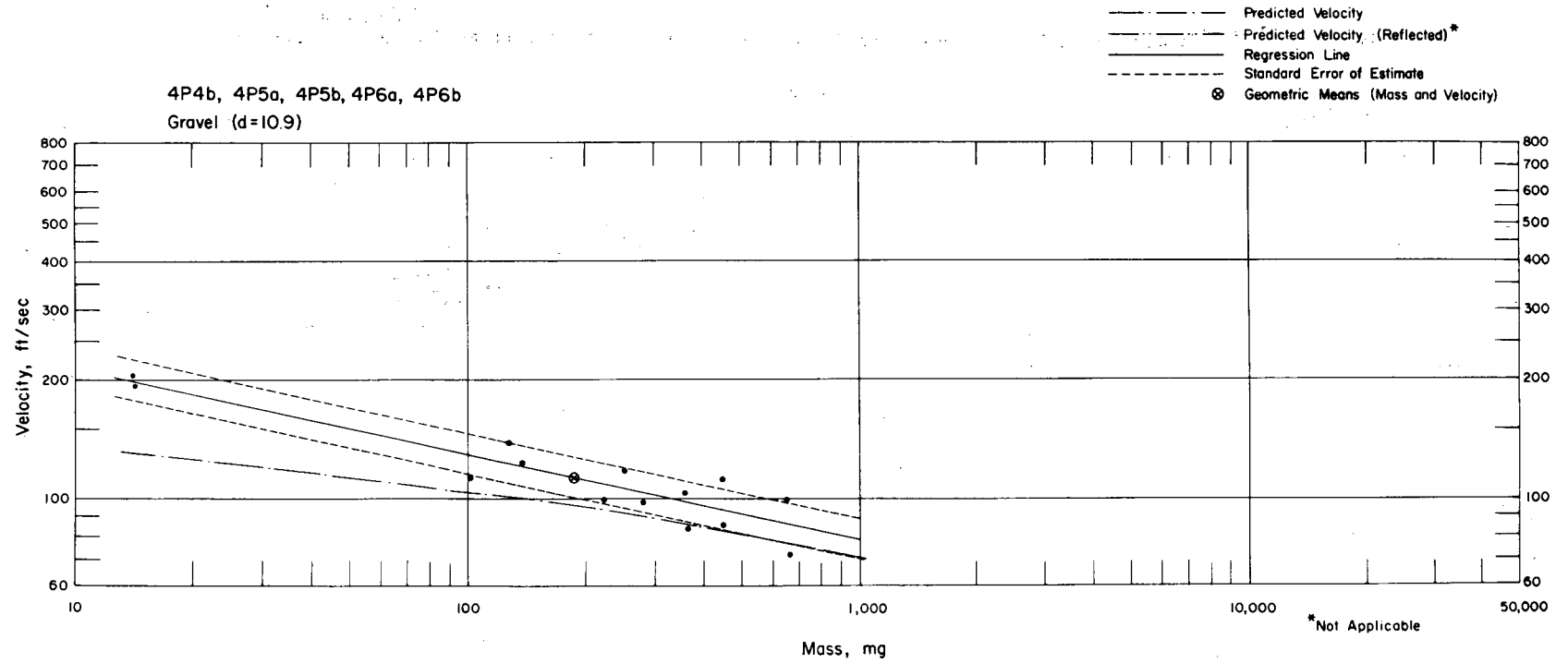


Fig. 4.13—Analysis of gravel missiles from station 4P traps: $d = 10.9$ ft; $n = 14$; $\log v = 2.5462 - 0.2183 \log m$; $E_{gv} = 1.13$; $M_{50} = 186$ mg; $V_{50} = 112$ ft/sec.

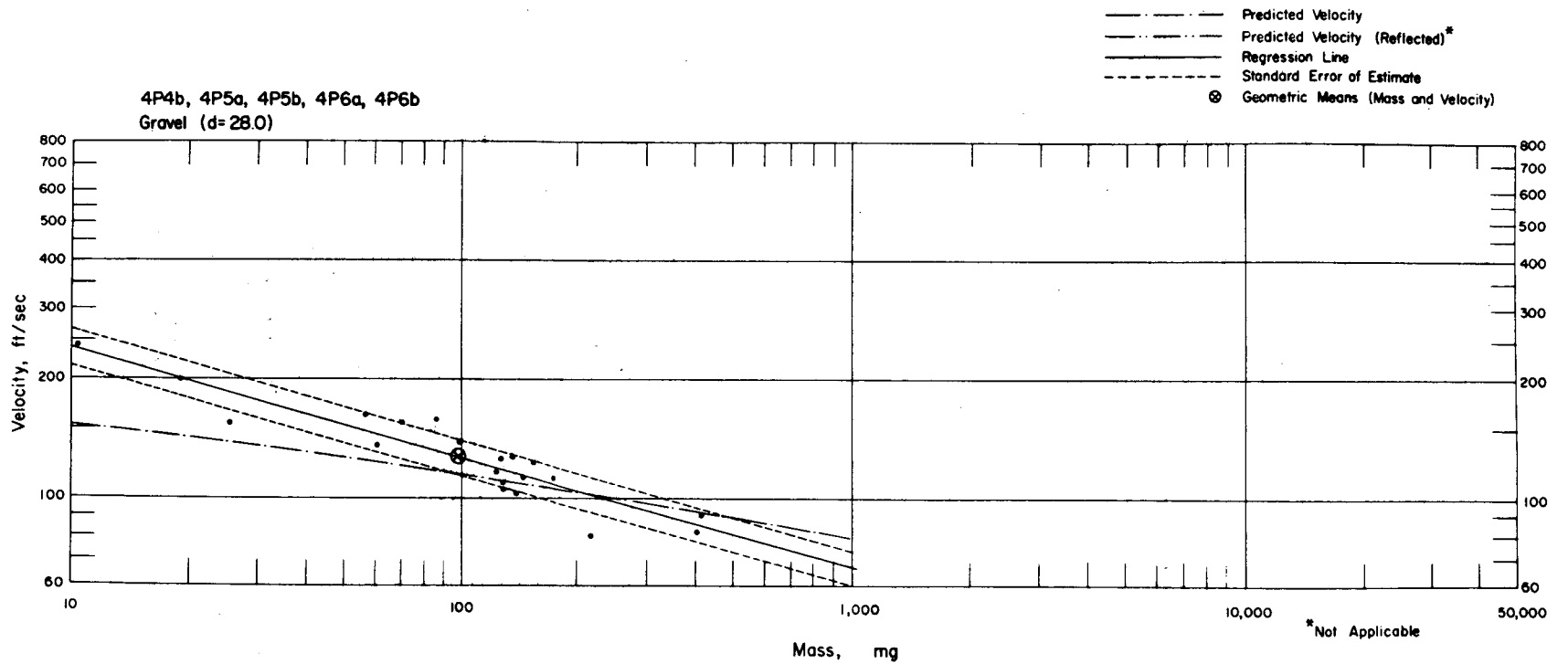


Fig. 4.14—Analysis of gravel missiles from station 4P traps: $d = 28.0$ ft; $n = 20$; $\log v = 2.6592 - 0.2785 \log m$; $E_{GV} = 1.13$; $M_{50} = 98$ mg; $V_{50} = 127$ ft/sec.

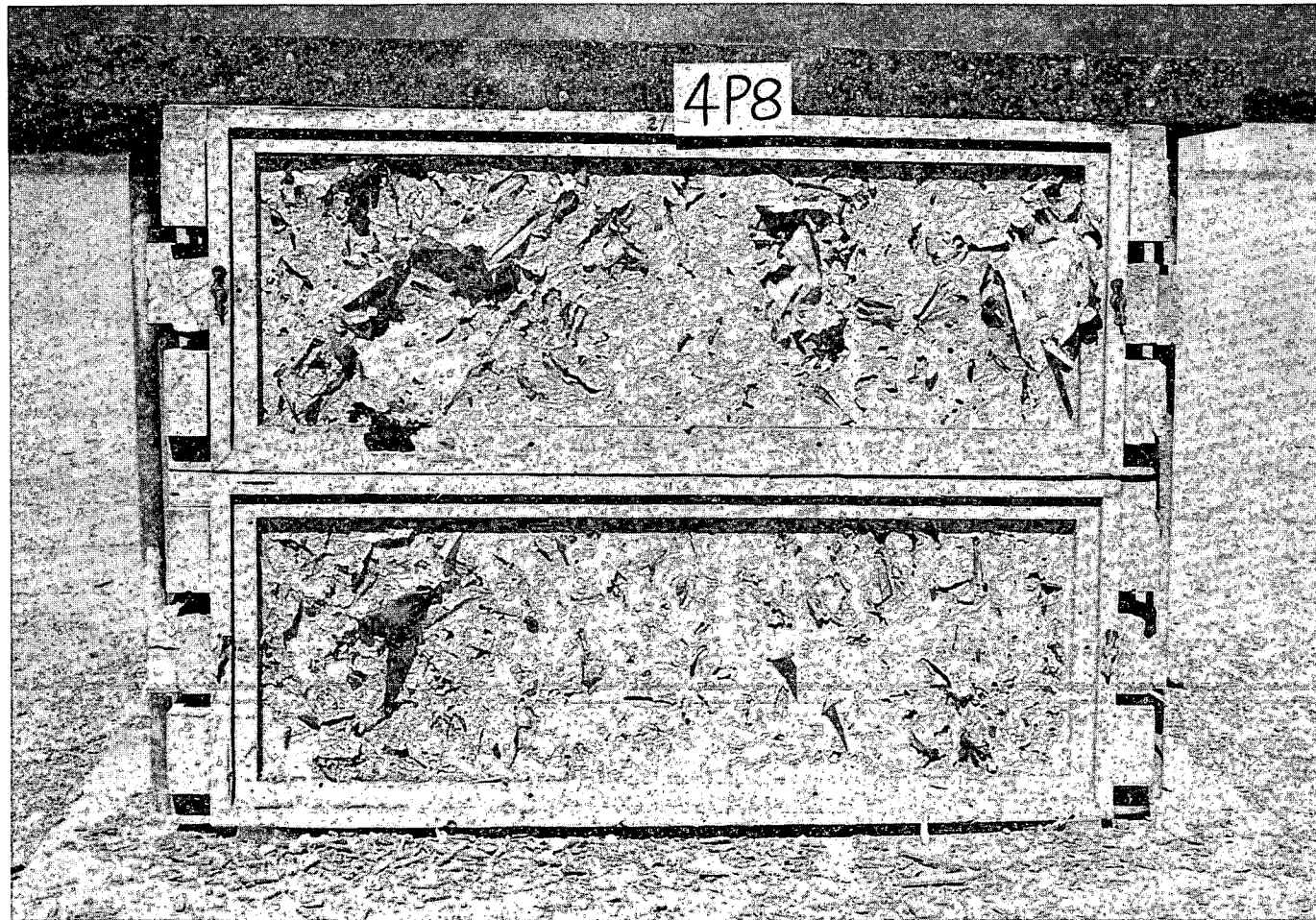


Fig. 4.15 — Traps 4P8a and b, placed 17.8 ft behind window, postshot.

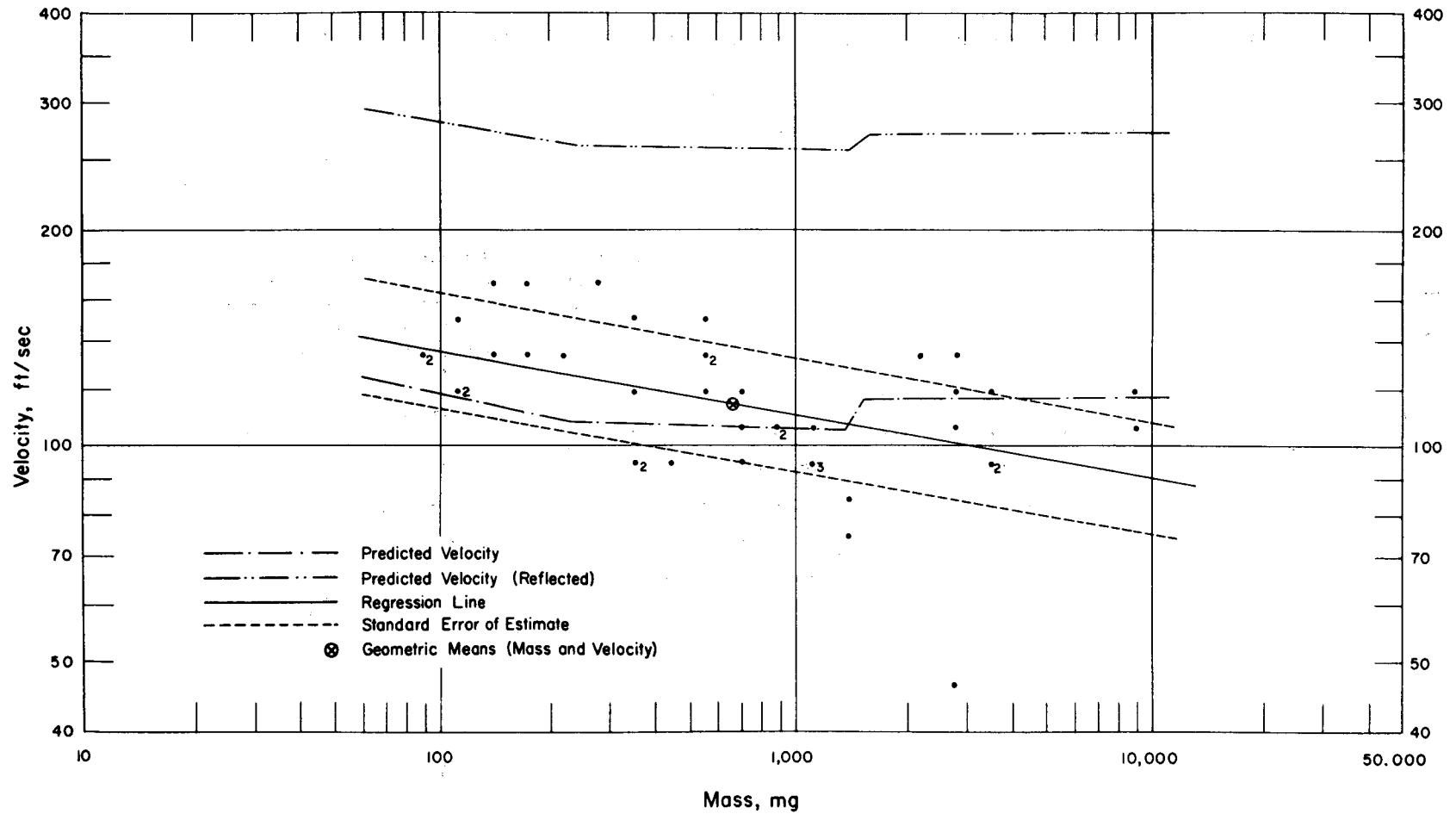


Fig. 4.16—Analysis of window-glass missiles from trap 4P8a: $d = 17.8$ ft; $n = 41$; $\log v = 2.3025 - 0.0864 \log m$; $E_{gv} = 1.20$; $M_{50} = 677$ mg; $V_{50} = 114$ ft/sec.

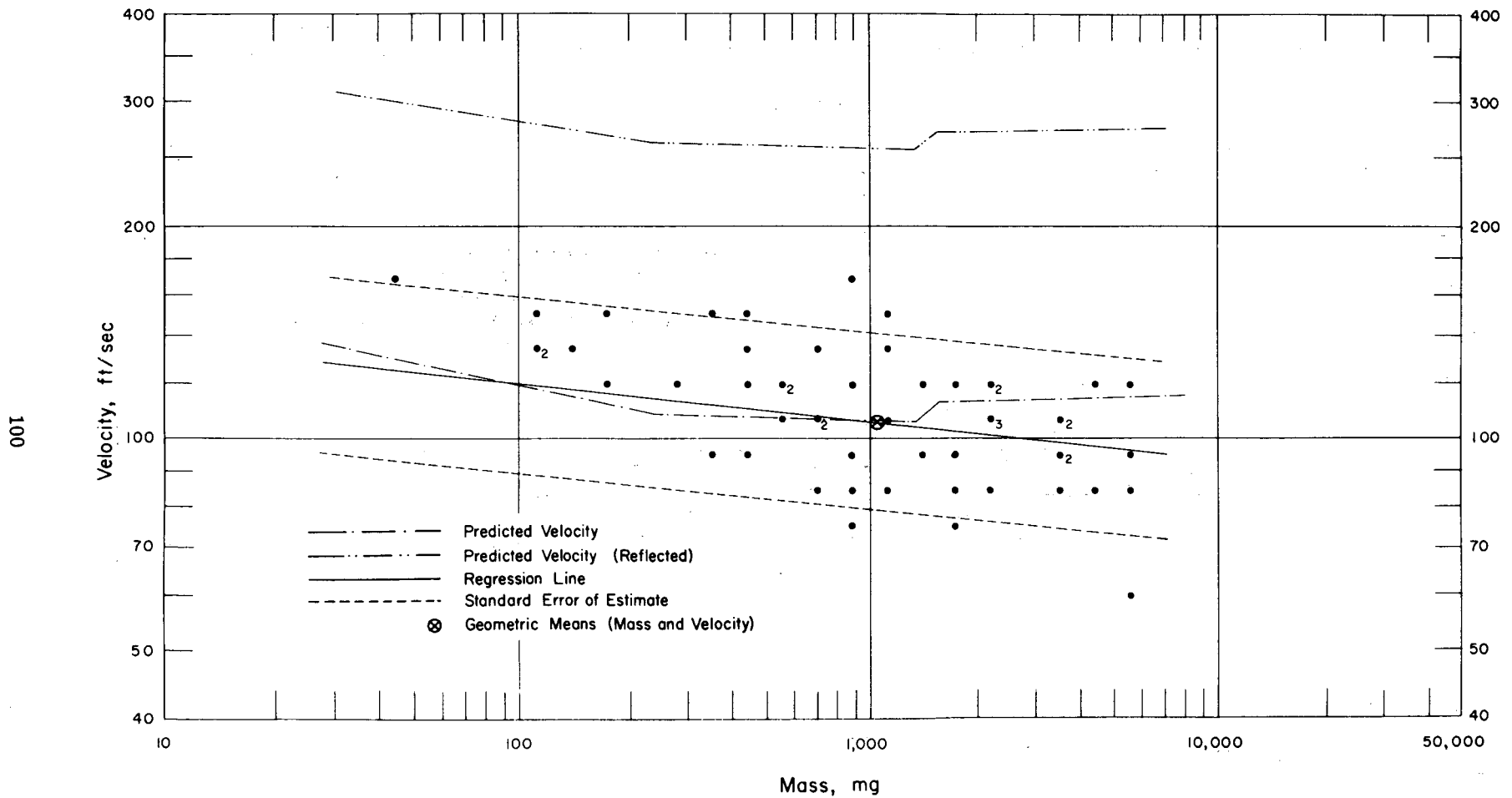


Fig. 4.17—Analysis of window-glass missiles from trap 4P8b: $d = 17.8$ ft; $n = 54$; $\log v = 2.1823 - 0.0526 \log m$; $E_{gv} = 1.34$; $M_{50} = 1040$ mg; $V_{50} = 106$ ft/sec.

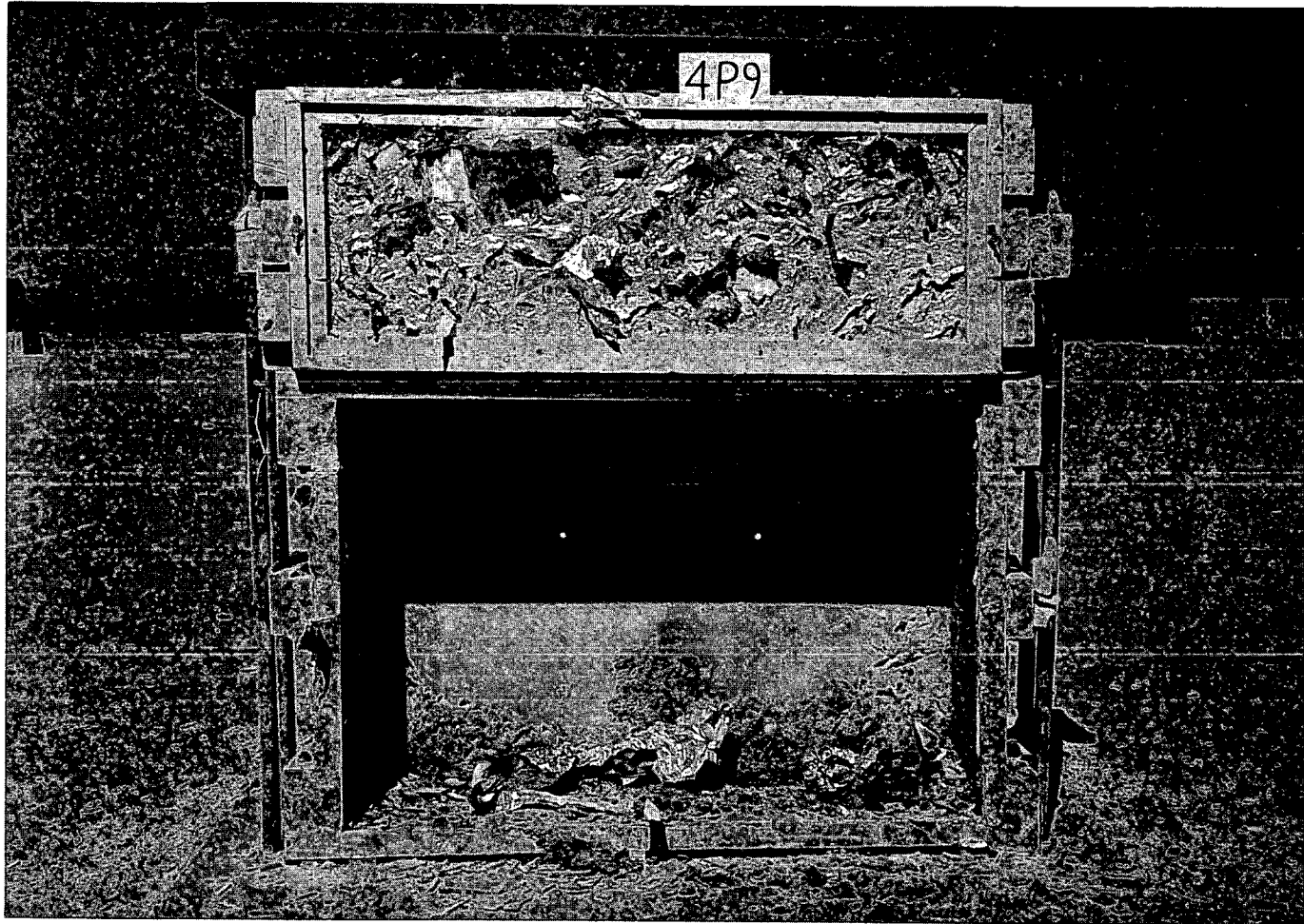


Fig. 4.18— Trap 4P9b, postshot, placed 12.8 ft from mounted window and above a 27-in.-high pig trap.

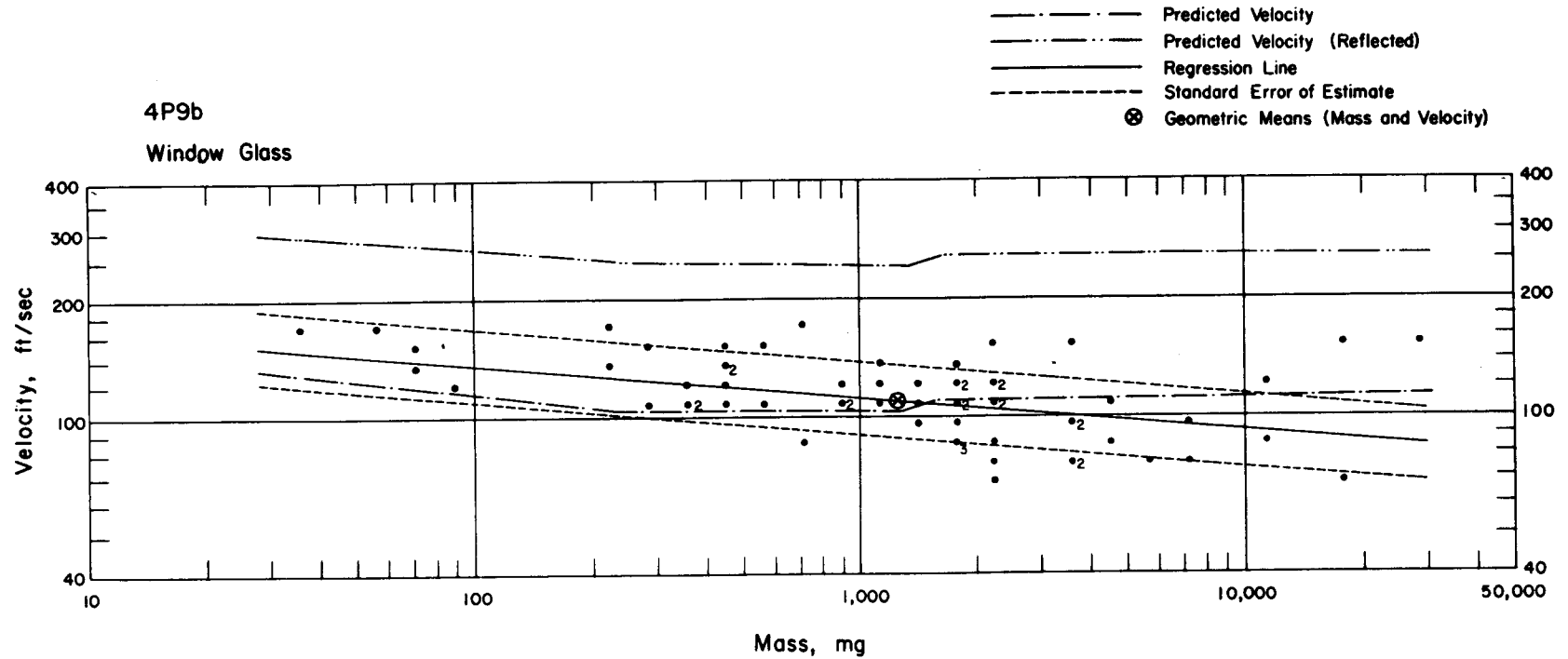


Fig. 4.19—Analysis of window-glass missiles from trap 4P9b: $d = 12.8$ ft; $n = 62$; $\log v = 2.3052 - 0.0854 \log m$; $E_{GV} = 1.24$; $M_{50} = 1240$ mg; $V_{50} = 110$ ft/sec.

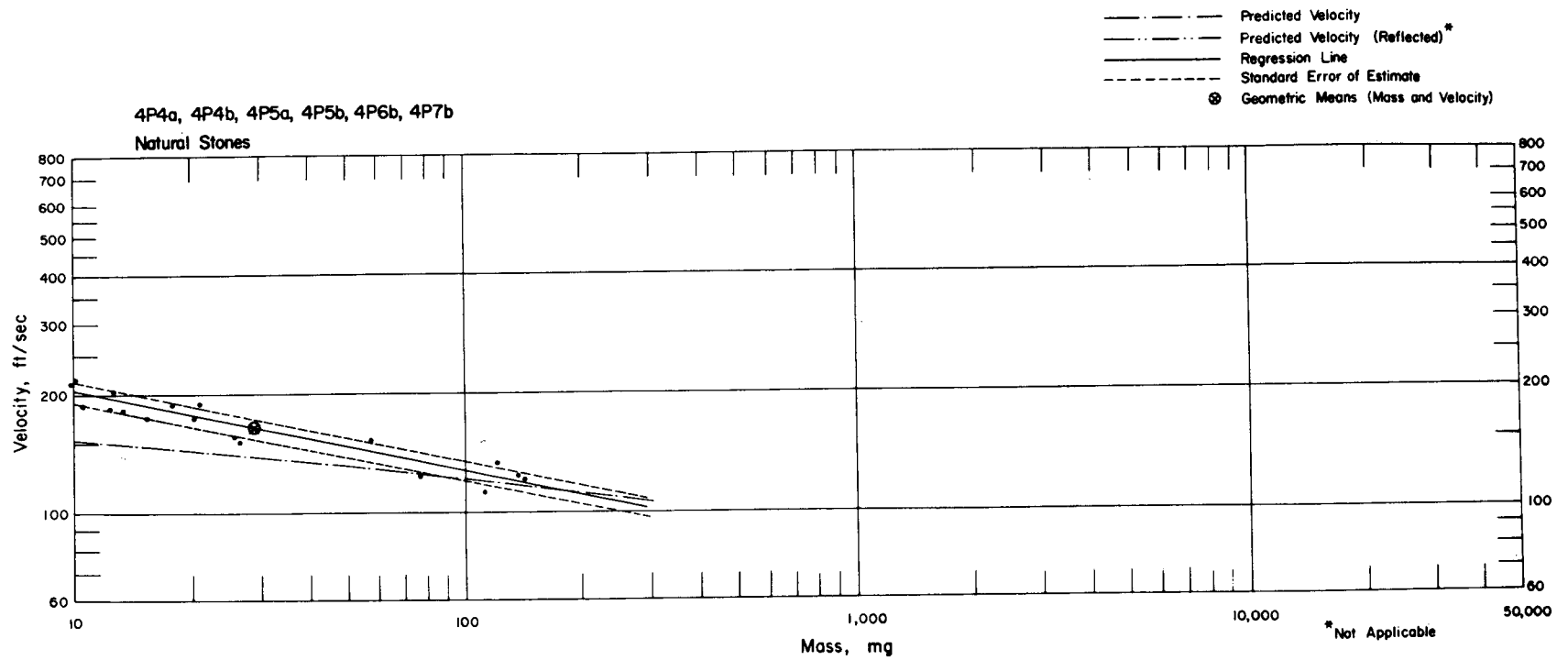


Fig. 4.20—Analysis of natural-stone missiles from station 4P traps: $n = 18$; $\log v = 2.5098 - 0.2019 \log m$; $E_{gv} = 1.07$; $M_{50} = 28.9$ mg;
 $V_{50} = 164$ ft/sec.

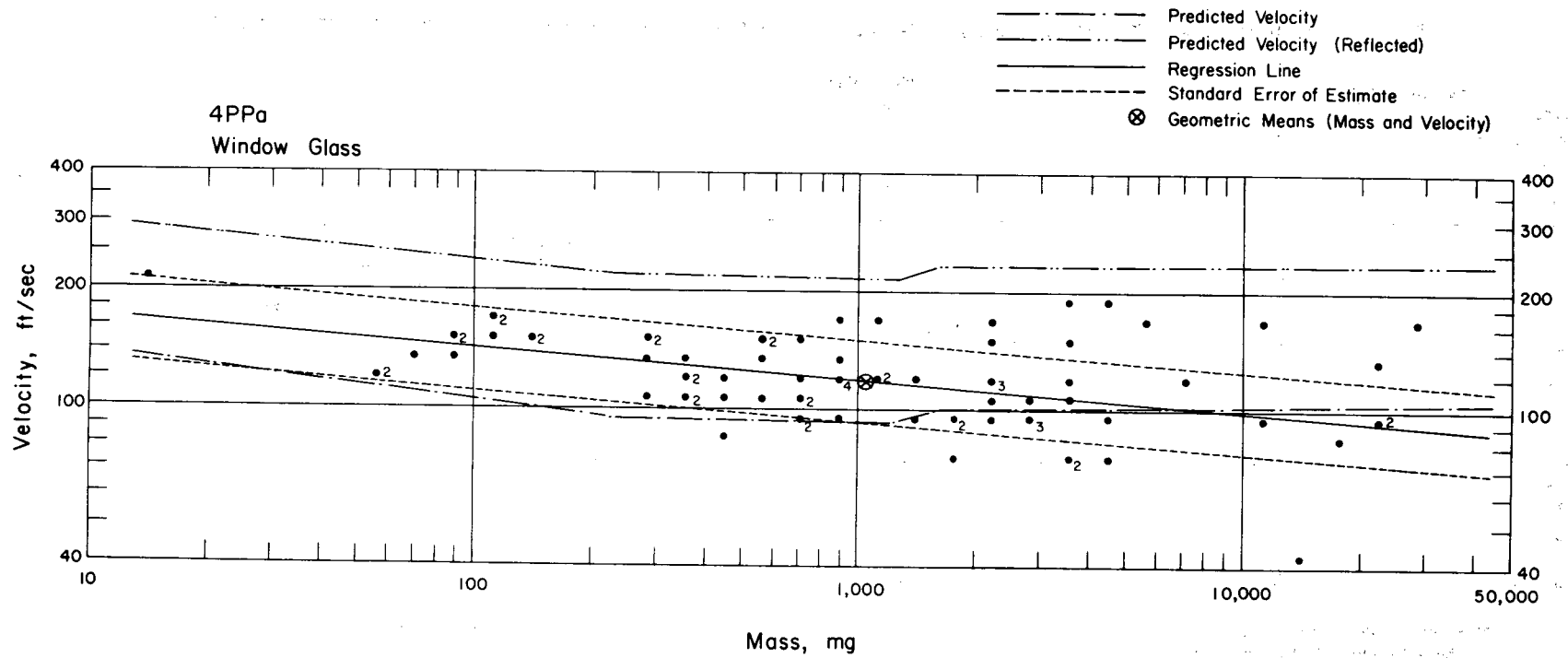


Fig. 4.21—Analysis of window-glass missiles from trap 4PPa: $d = 8.8$ ft; $n = 81$; $\log v = 2.3067 - 0.0779 \log m$; $E_{gv} = 1.29$; $M_{50} = 1070$ mg; $V_{50} = 118$ ft/sec.

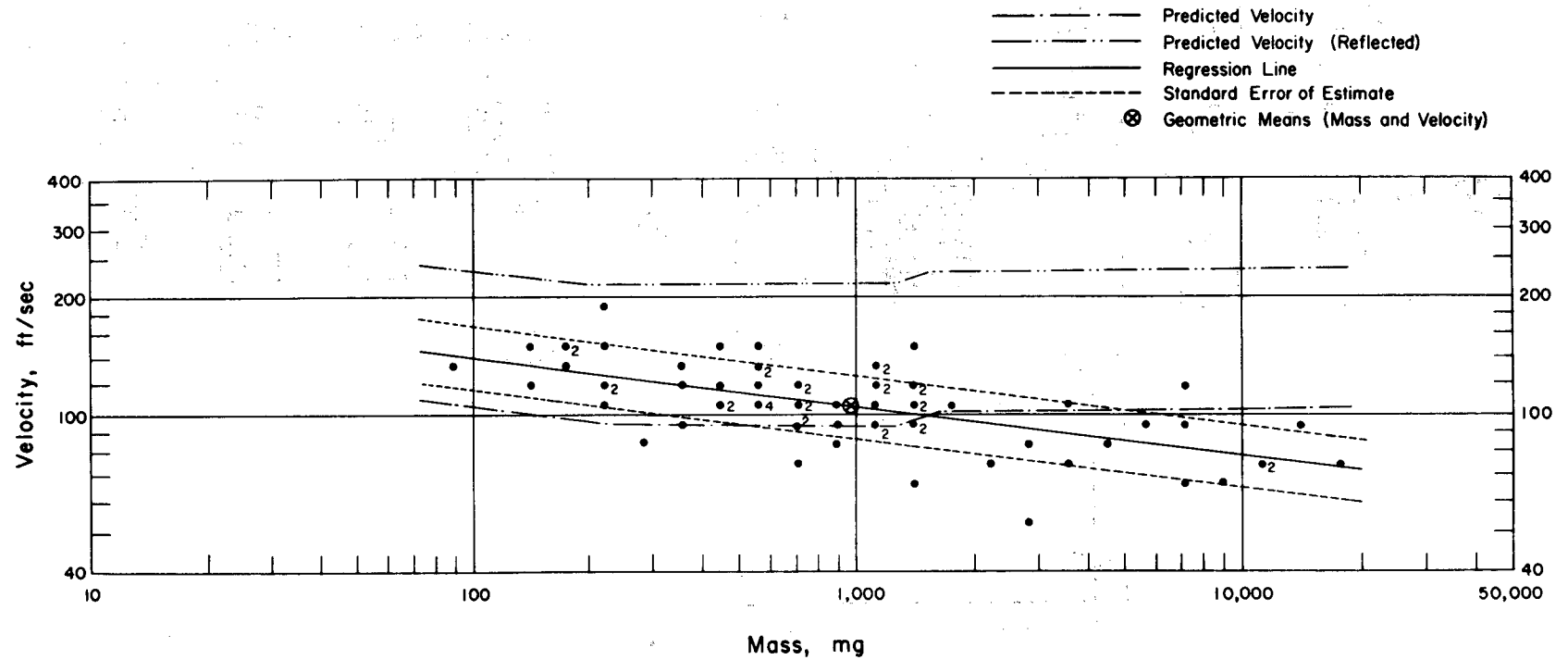


Fig. 4.22—Analysis of window-glass missiles from trap 4PPb: $d = 8.8$ ft; $n = 68$; $\log v = 2.3964 - 0.1250 \log m$; $E_{GV} = 1.20$; $M_{50} = 960$ mg; $V_{50} = 106$ ft/sec.

5P STATION, RANGE 5320

- MD Military Debris (B) blue
- Gr Gravel (W) white
- S Spheres (Y) yellow
- A Animal Trap

- a - Window glass, $\frac{1}{8}$ " thick, framed and mounted
- b - Plate glass, $\frac{1}{4}$ " thick, framed and mounted

Note: MD, Gr, and S placed at 4.8', 12.5', and 32.0' from face of traps

Roman numeral in parenthesis designates type of missile absorber

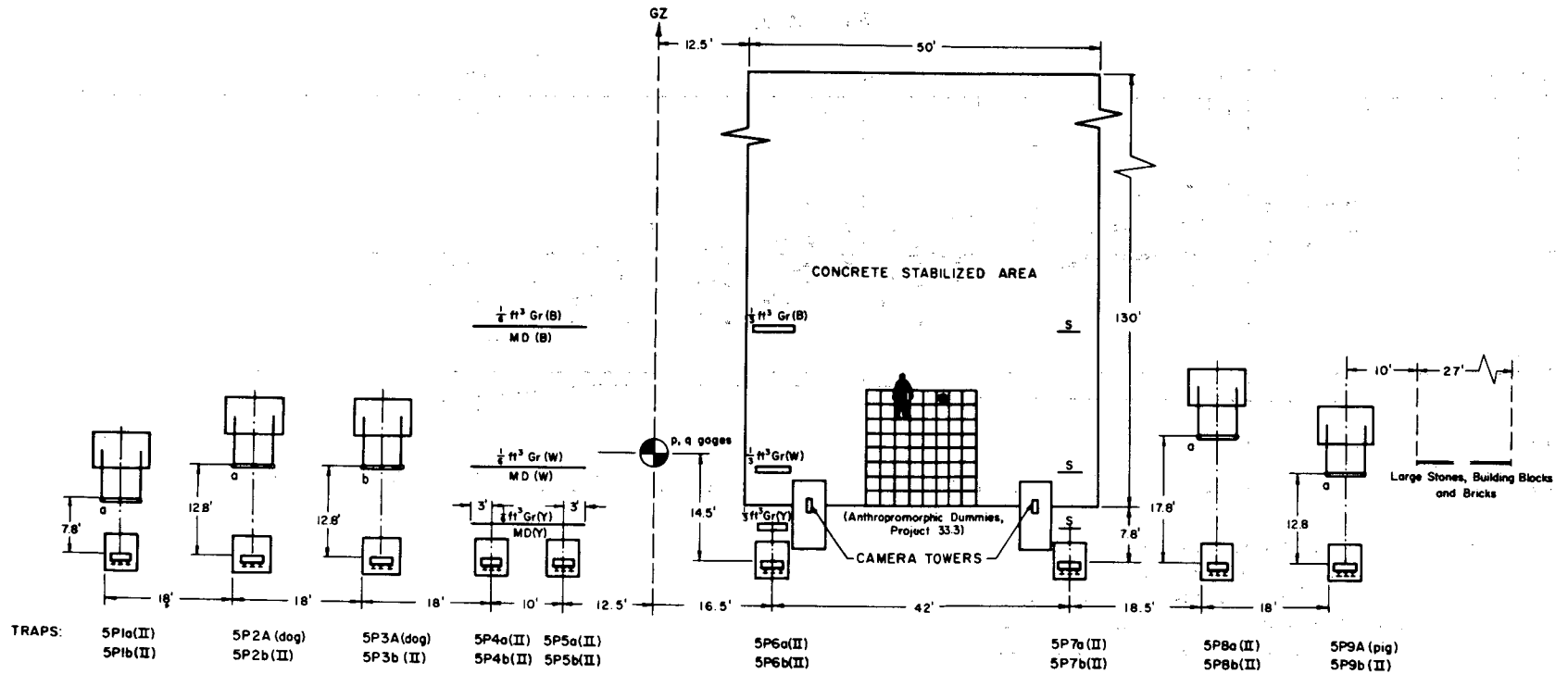


Fig. 4.23—Station 5P layout chart.

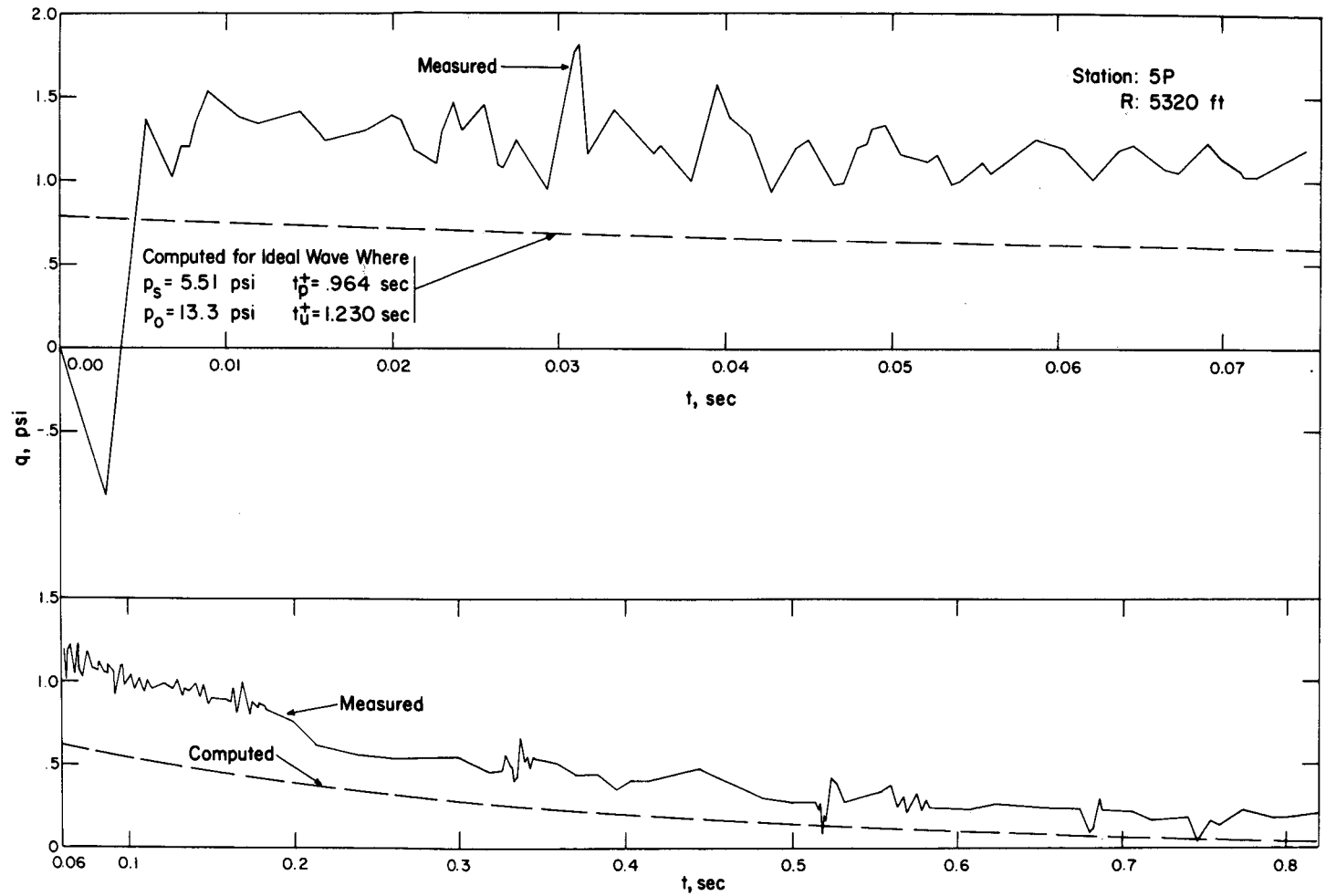


Fig. 4.24—Dynamic pressure vs. time for station 5P.

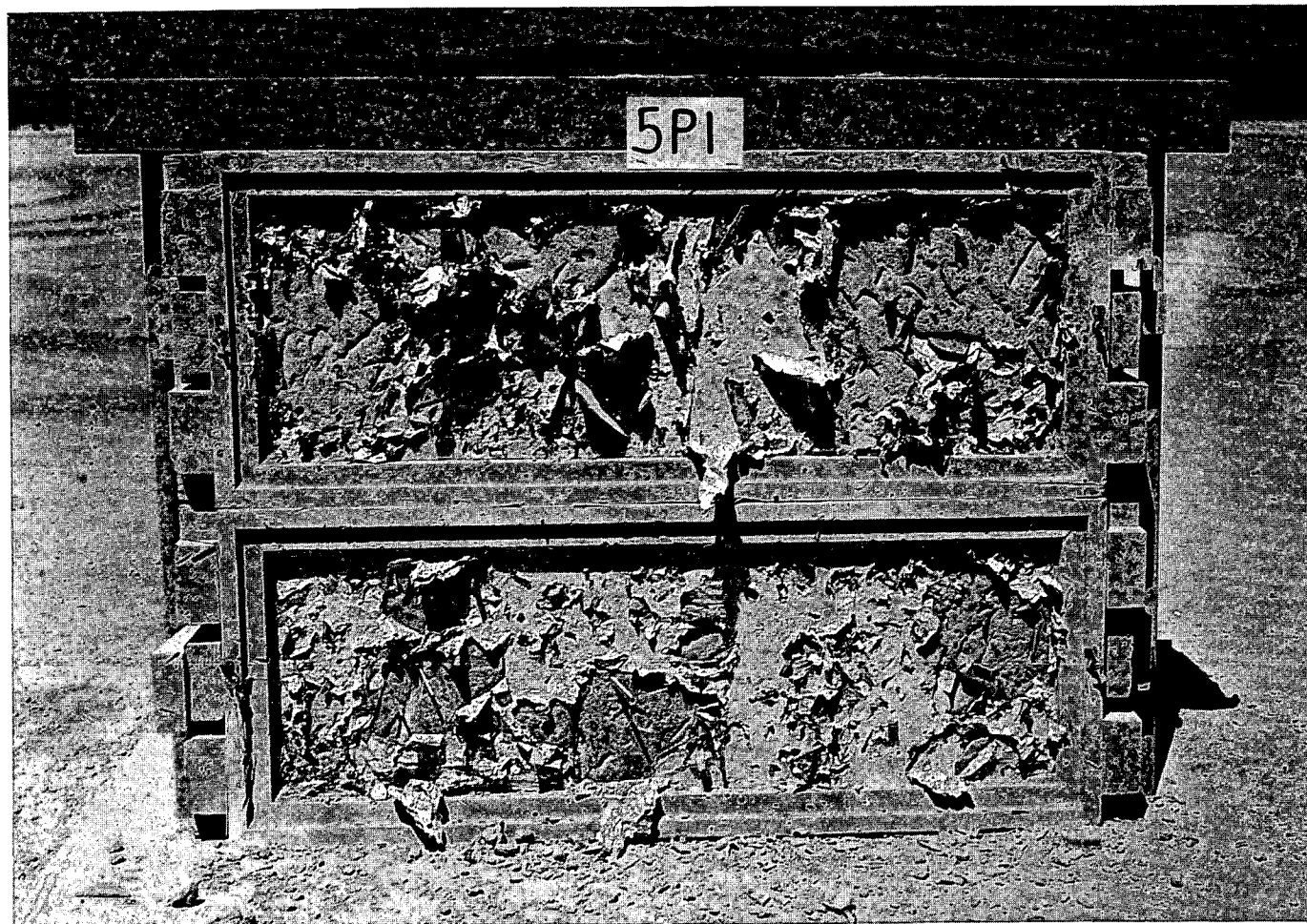


Fig. 4.25—Traps 5P1a and b, postshot.

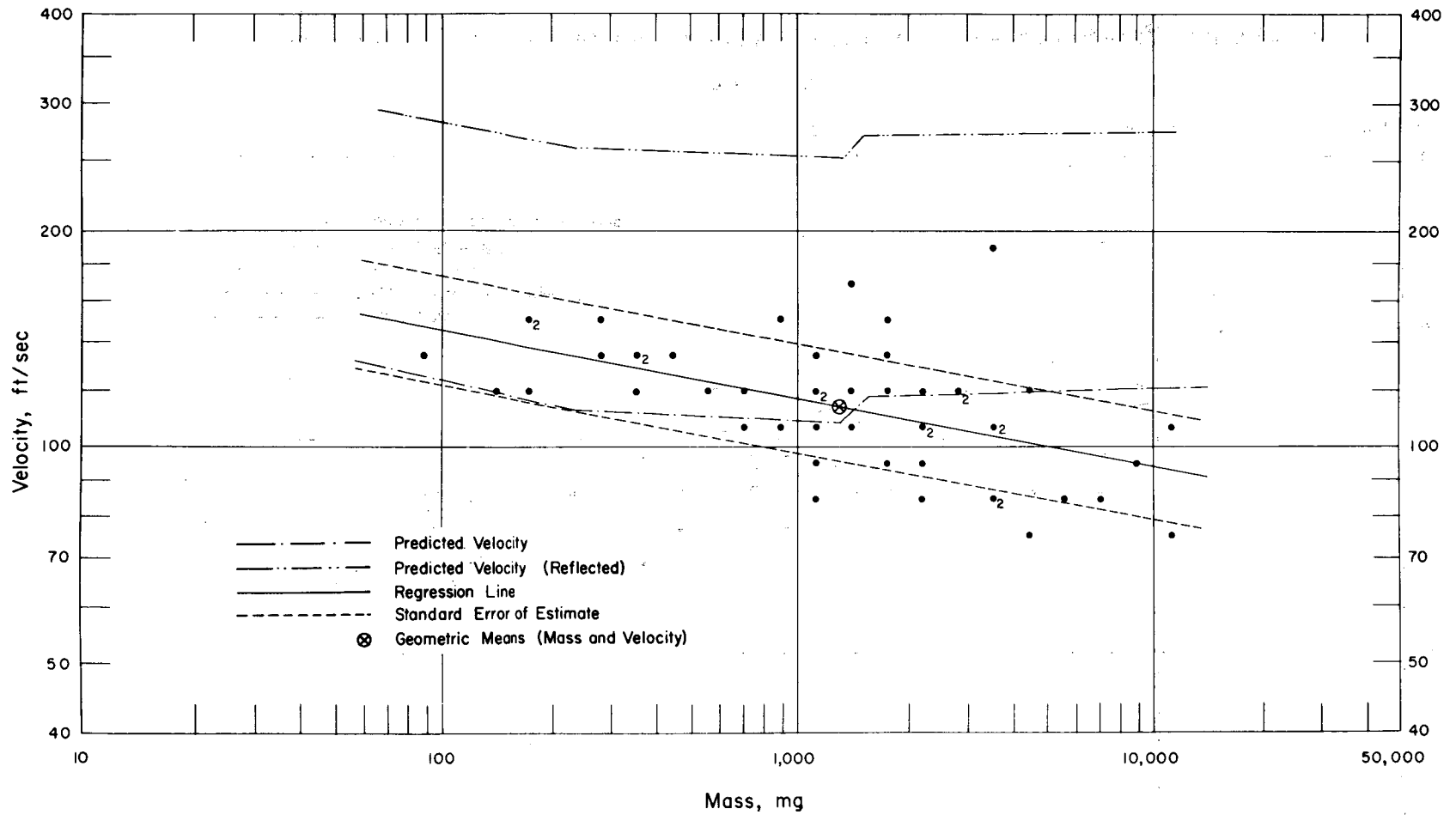


Fig. 4.26—Analysis of window-glass missiles from trap 5P1a: $d = 7.8$ ft; $n = 48$; $\log v = 2.3506 - 0.0948 \log m$; $E_{gv} = 1.19$; $M_{50} = 1301$ mg; $V_{50} = 114$ ft/sec.

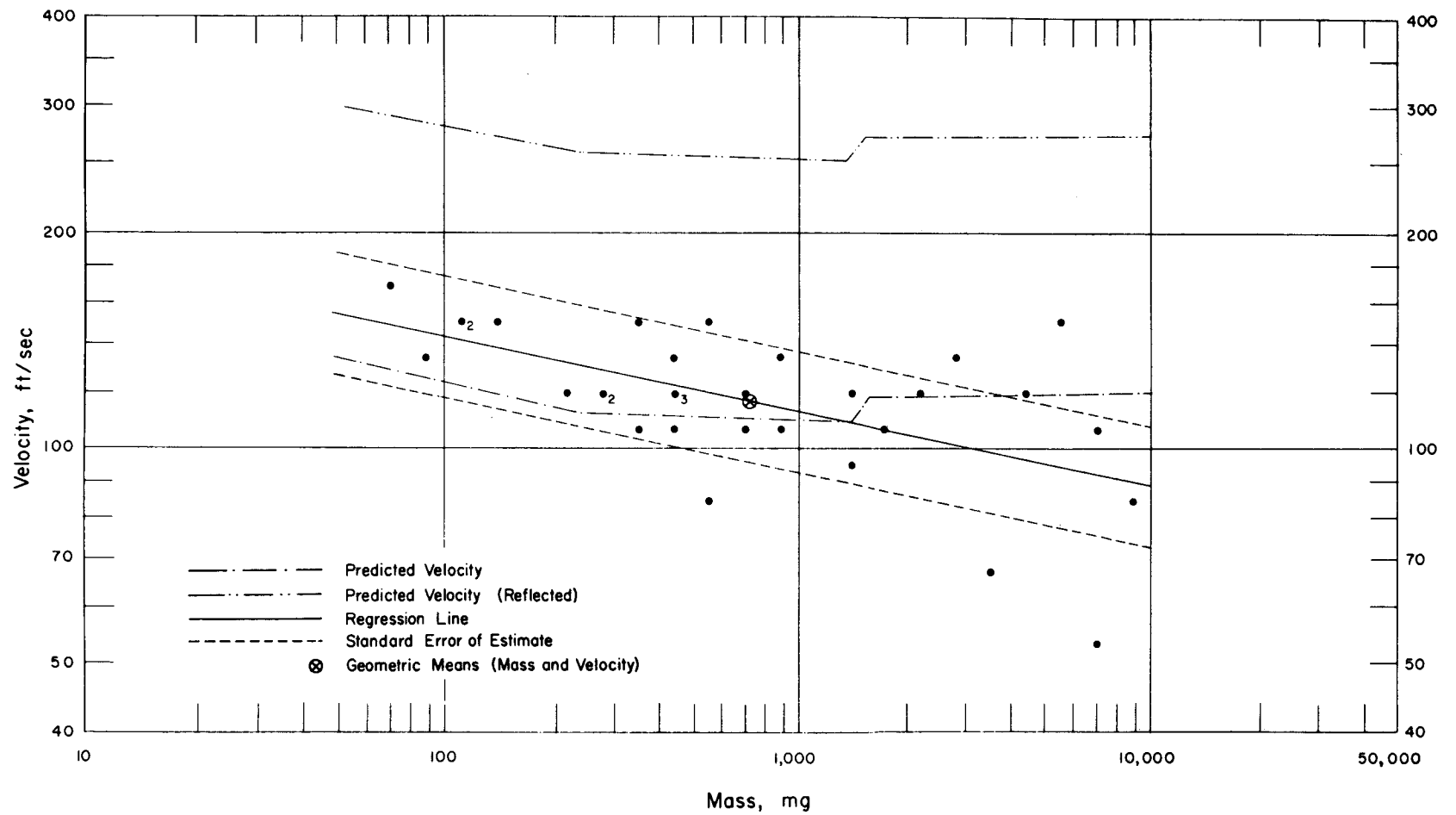


Fig. 4.27—Analysis of window-glass missiles from trap 5P1b: $d = 7.8$ ft; $n = 32$; $\log v = 2.3596 - 0.1031 \log m$; $E_{gv} = 1.21$; $M_{50} = 734$ mg; $V_{50} = 116$ ft/sec.

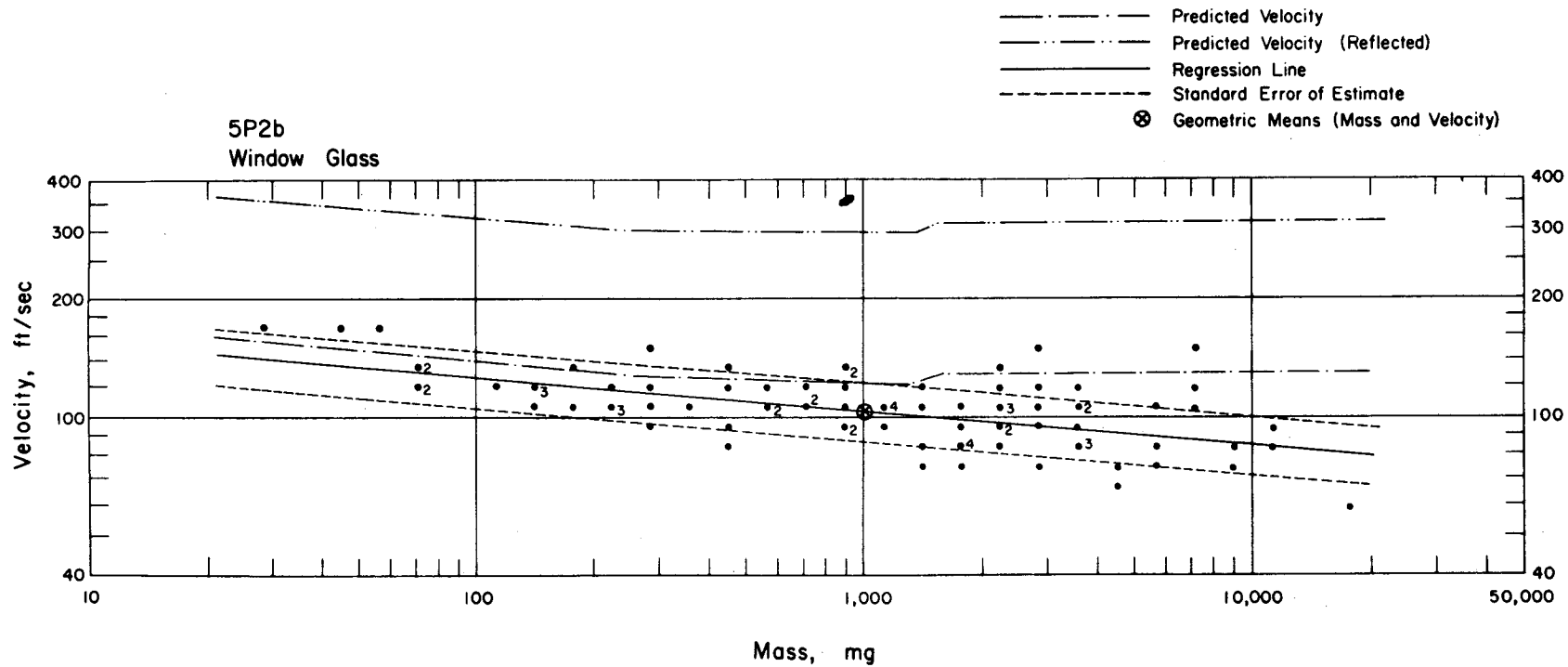


Fig. 4.28—Analysis of window-glass missiles from trap 5P2b: $d = 12.8$ ft; $n = 88$; $\log v = 2.2671 - 0.0829 \log m$; $E_{gv} = 1.18$; $M_{50} = 1000$ mg; $V_{50} = 104$ ft/sec.

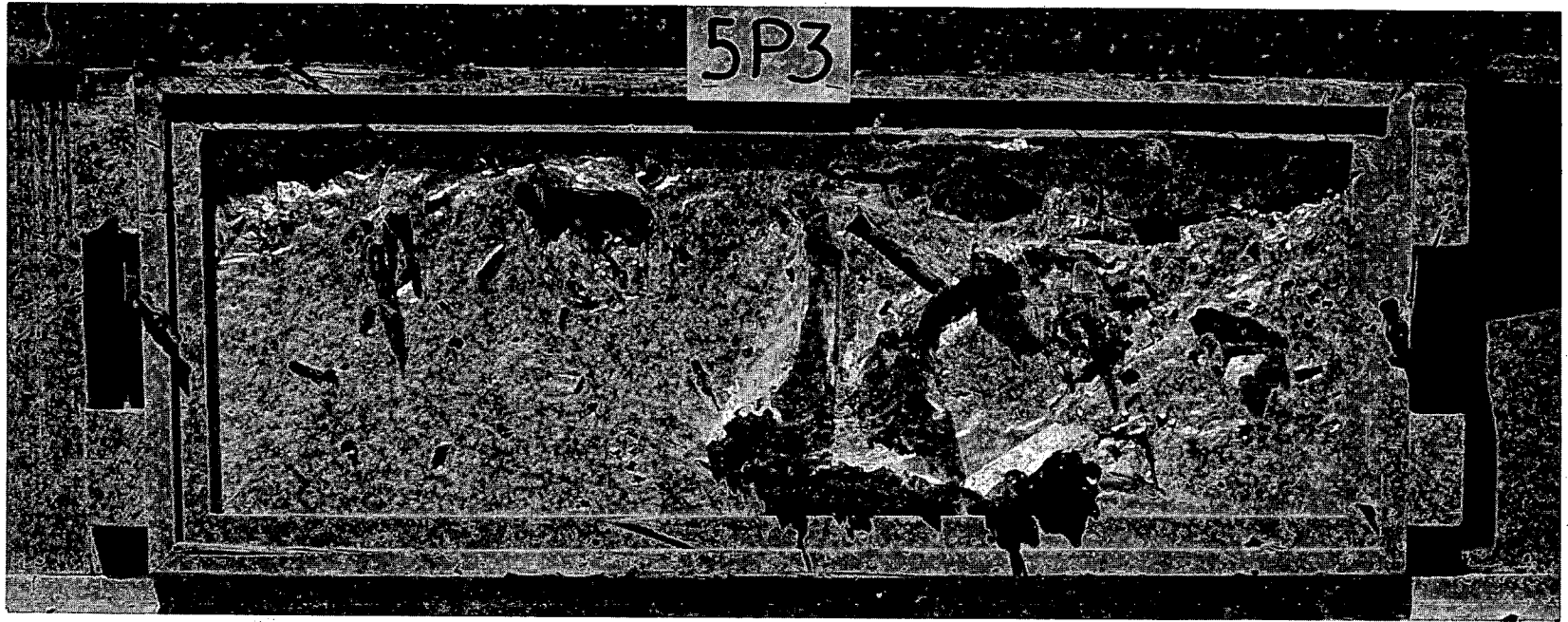


Fig. 4.29—Trap 5P3b, postshot.

5P3b
Trap 5P3b, postshot
5P3b
Trap 5P3b, postshot
5P3b
Trap 5P3b, postshot
5P3b
Trap 5P3b, postshot

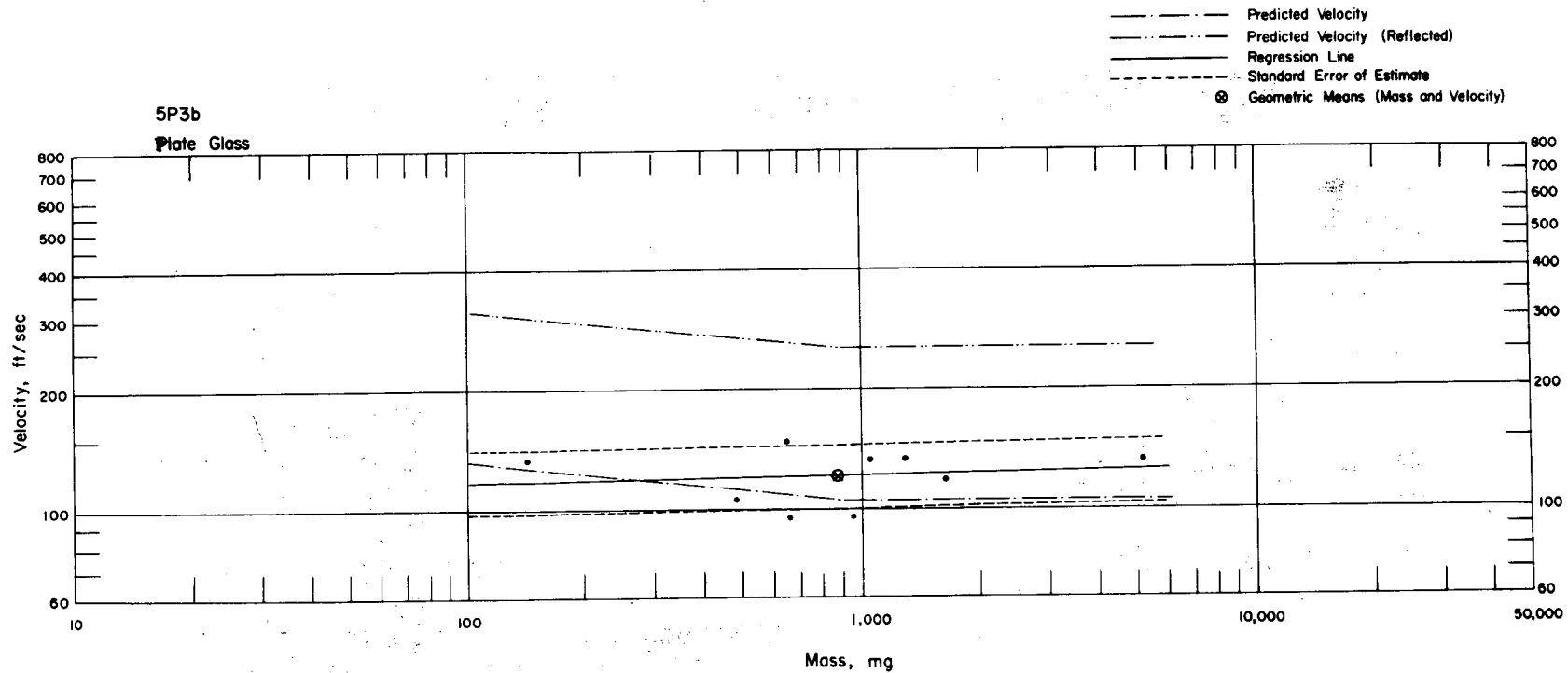


Fig. 4.30—Analysis of plate-glass missiles from trap 5P3b: $d = 12.8$ ft; $n = 9$; $\log v = 2.0396 + 0.0140 \log m$; $E_{gv} = 1.22$; $M_{50} = 877$ mg; $V_{50} = 121$ ft/sec.

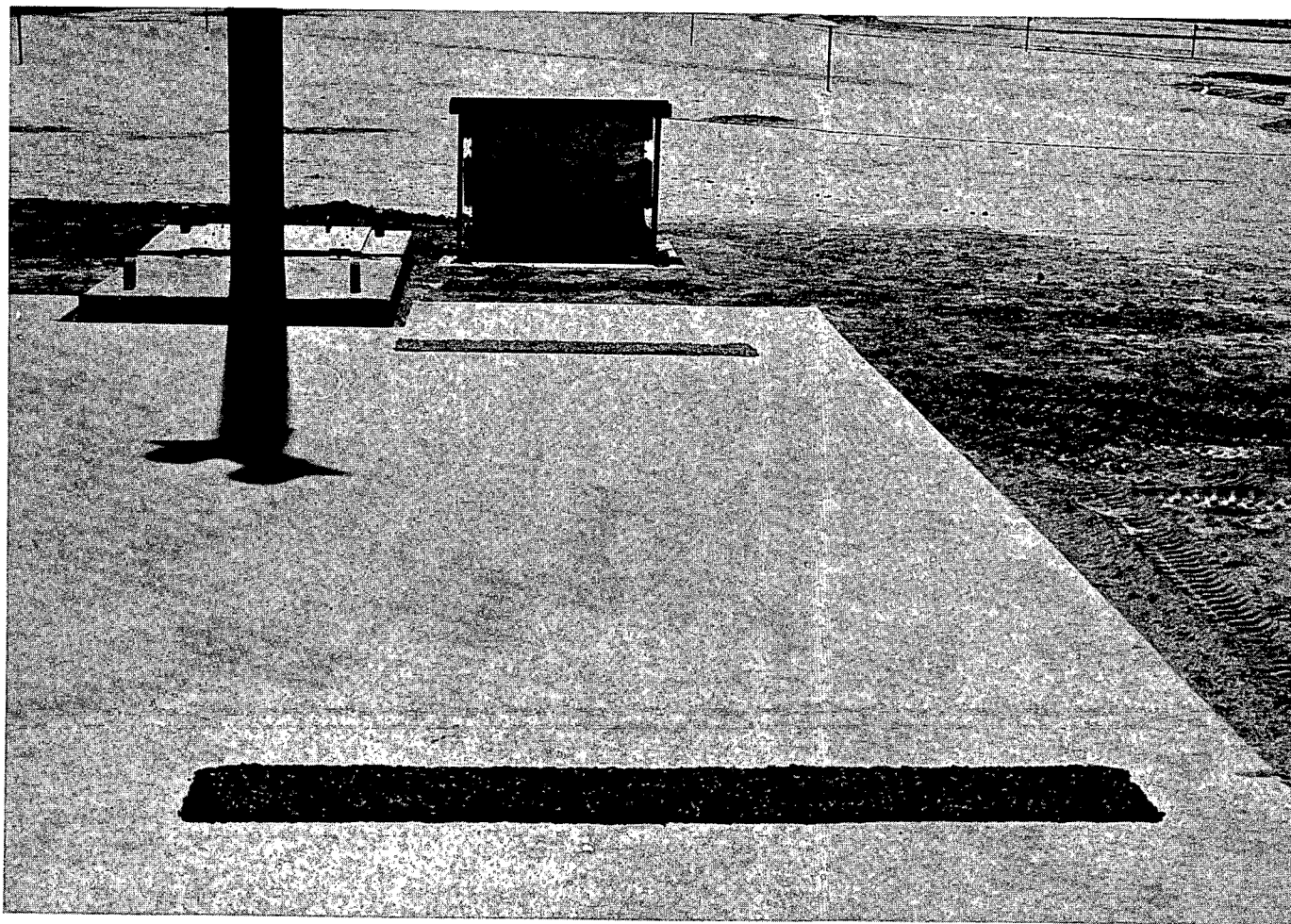


Fig. 4.31—Traps 5P6a and b, preshot. Note the piles of gravel (two on the concrete pad 32.0 and 12.5 ft from the traps and one on the ground 4.8 ft from the trap, between the pad and traps).

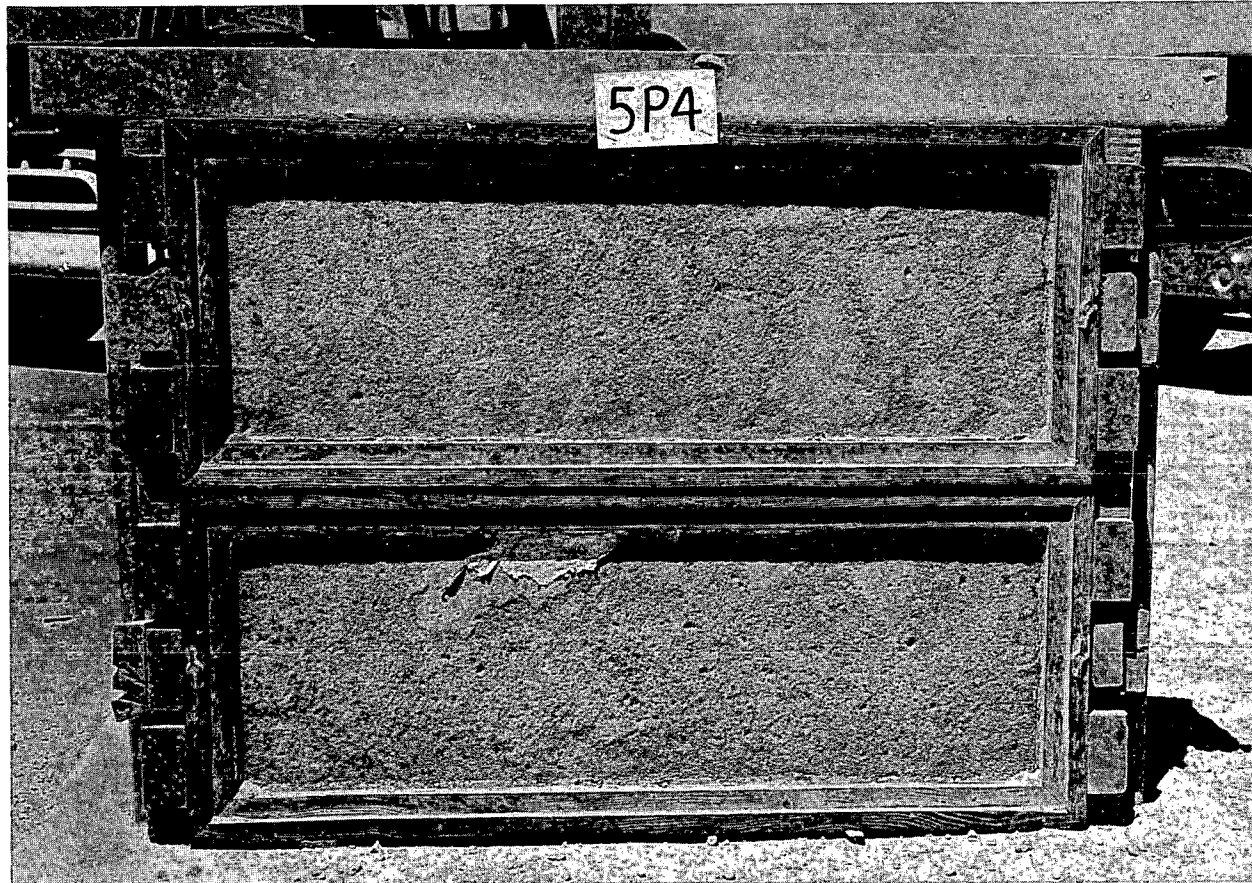


Fig. 4.32— Military-debris and gravel installation 5P4, postshot.

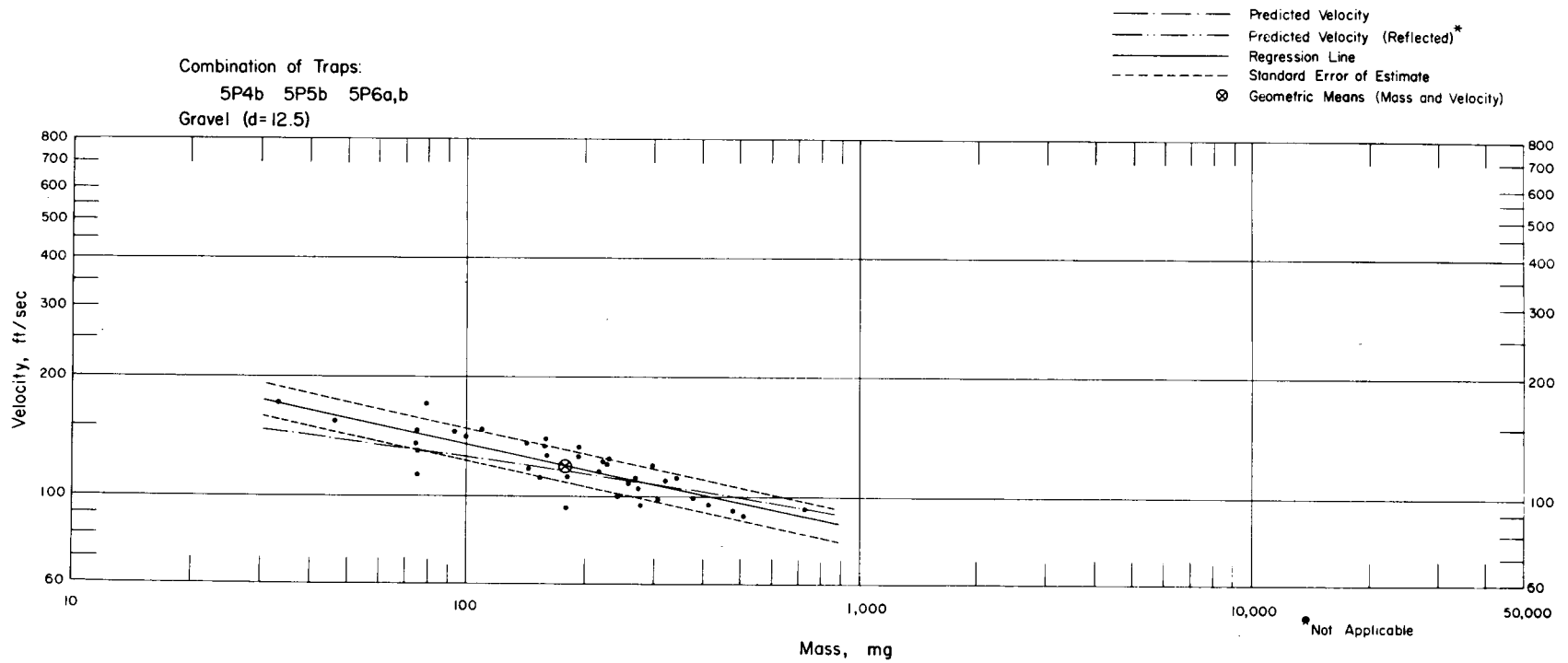


Fig. 4.33—Analysis of gravel missiles from traps 5P4b, 5P5b, and 5P6a and b: $d = 12.5$ ft; $n = 38$; $\log v = 2.5578 - 0.2123 \log m$; $E_{gv} = 1.10$; $M_{50} = 180$ mg; $V_{50} = 120$ ft/sec.

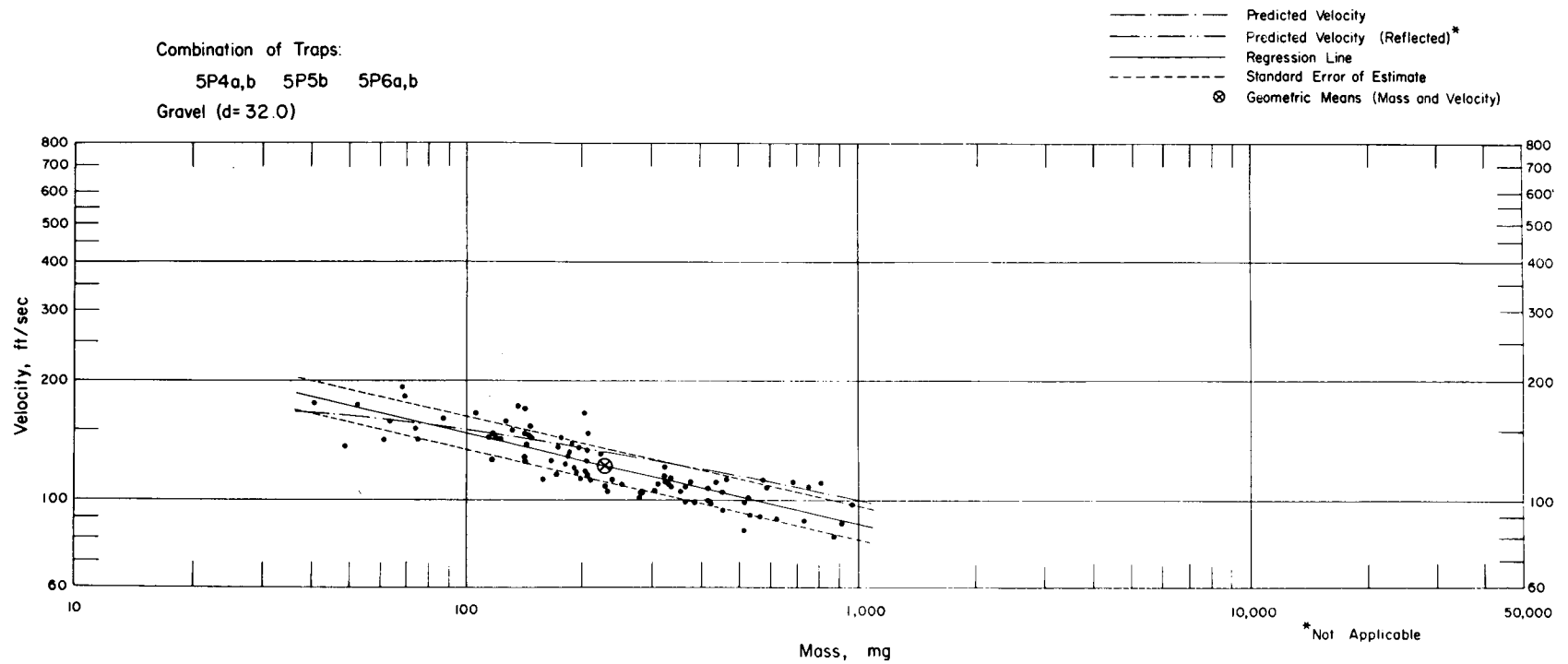


Fig. 4.34— Analysis of gravel missiles from station 5P traps: $d = 32.0$ ft; $n = 89$; $\log v = 2.6168 - 0.2240 \log m$; $E_{gv} = 1.10$; $M_{50} = 228$ mg; $V_{50} = 123$ ft/sec.

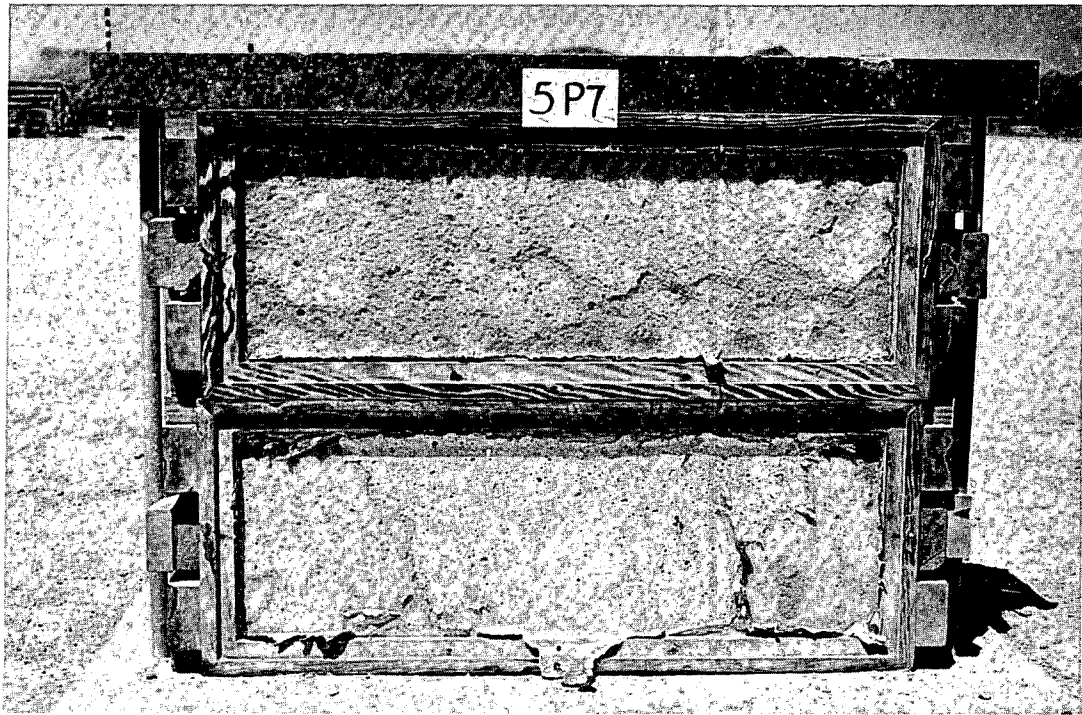


Fig. 4.35 — Traps 5P7a and b, postshot. Note that the thermal damage is greater in the upper trap.

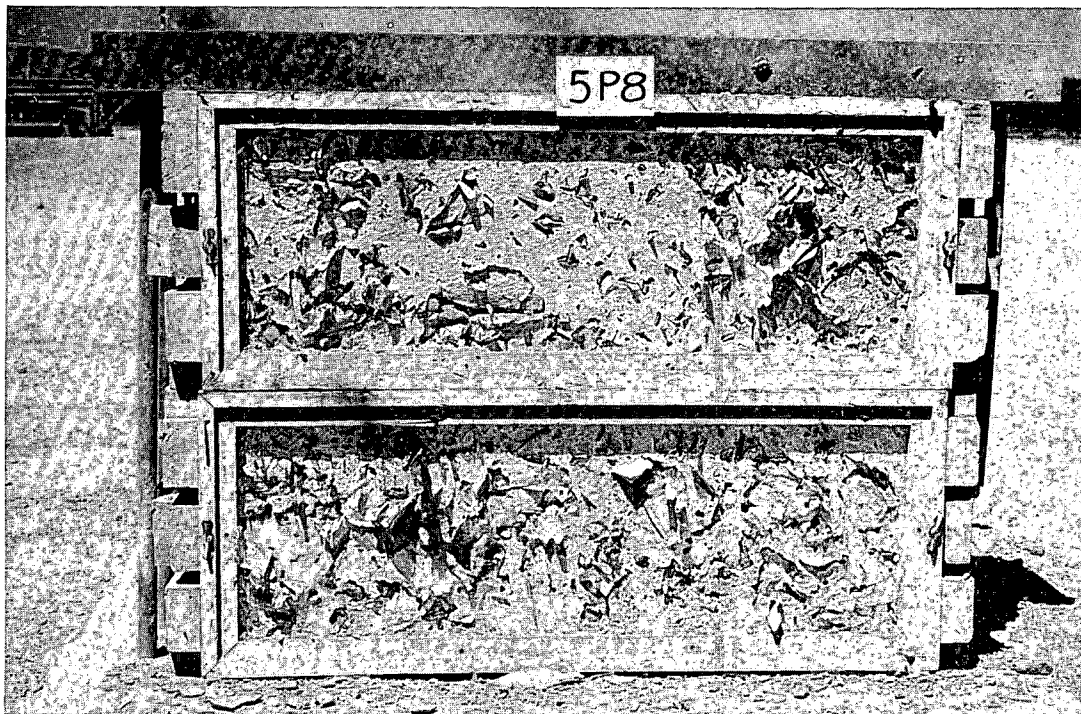


Fig. 4.36 — Traps 5P8a and b, postshot.

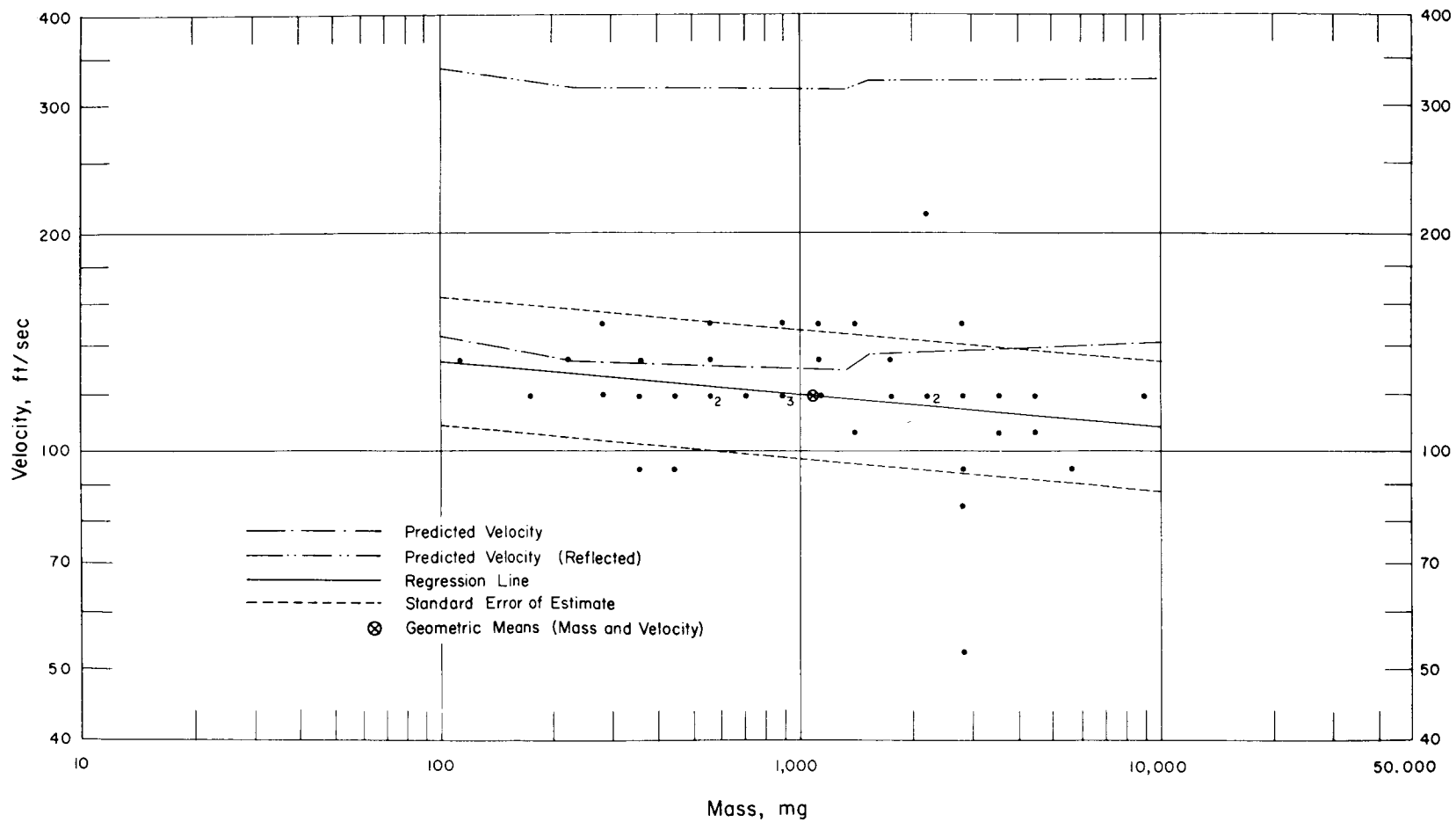


Fig. 4.37—Analysis of window-glass missiles from trap 5P8a: $d = 17.8$ ft; $n = 40$; $\log v = 2.2142 - 0.0450 \log m$; $E_{GV} = 1.23$; $M_{50} = 1011$ mg; $V_{50} = 120$ ft/sec.

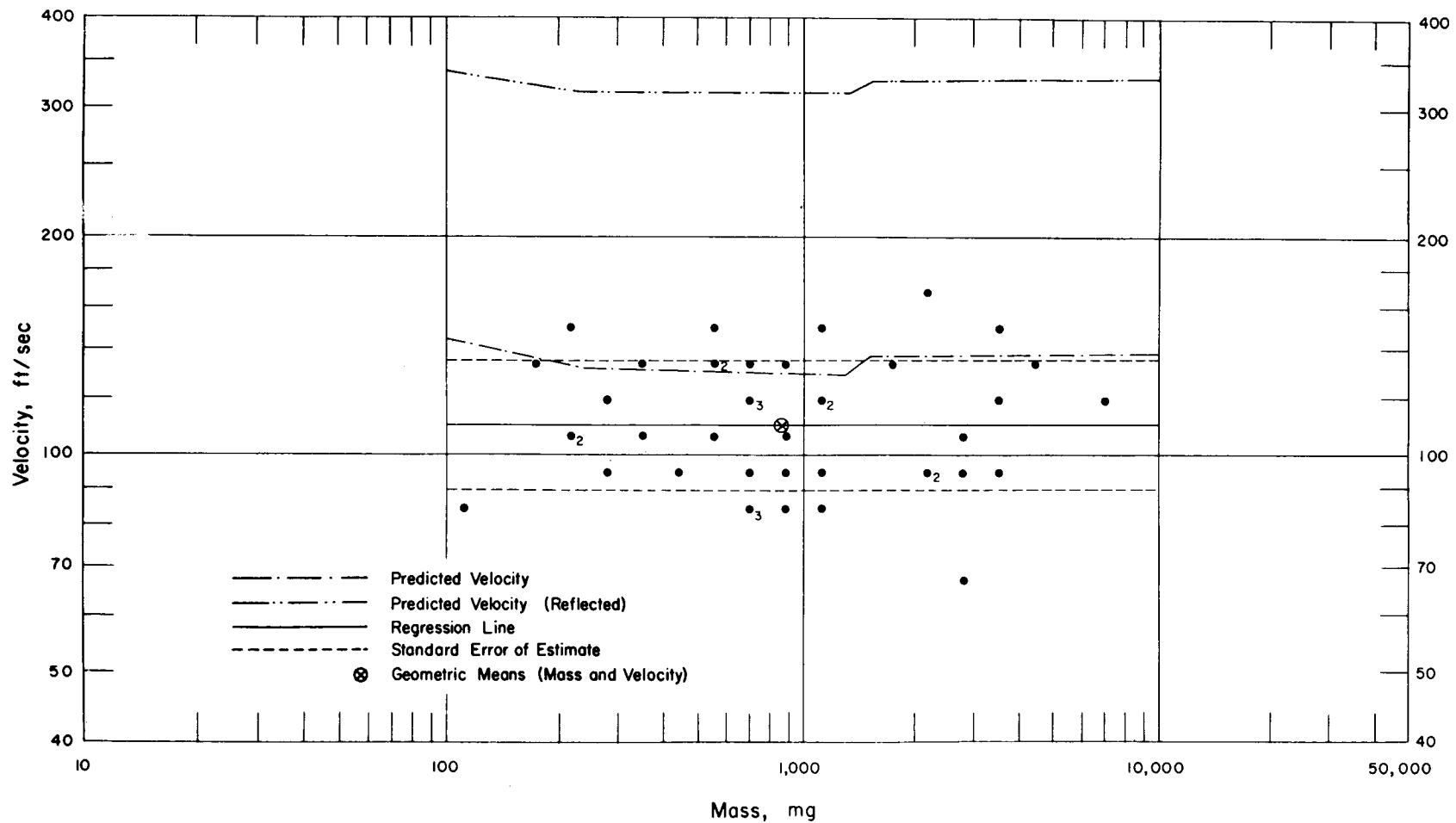


Fig. 4.38—Analysis of window-glass missiles from trap 5P8b: $d = 17.8$ ft; $n = 43$; $\log v = 2.0389 + 0.0012 \log m$; $E_{gv} = 1.23$; $M_{50} = 881$ mg; $V_{50} = 110$ ft/sec.

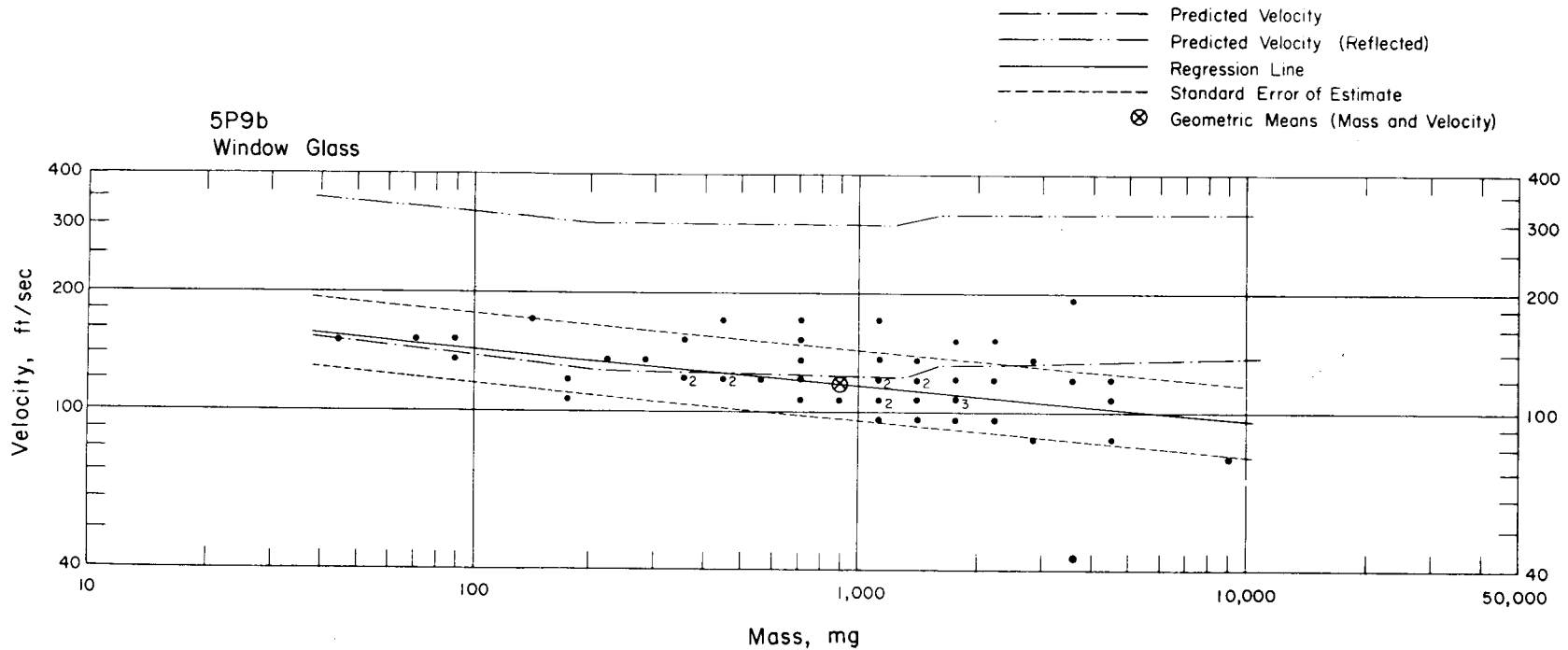


Fig. 4.39—Analysis of window-glass missiles from trap 5P9b: $d = 12.8$ ft; $n = 52$; $\log v = 2.3511 - 0.0935 \log m$; $E_{gv} = 1.23$; $M_{50} = 895$ mg; $V_{50} = 119$ ft/sec.

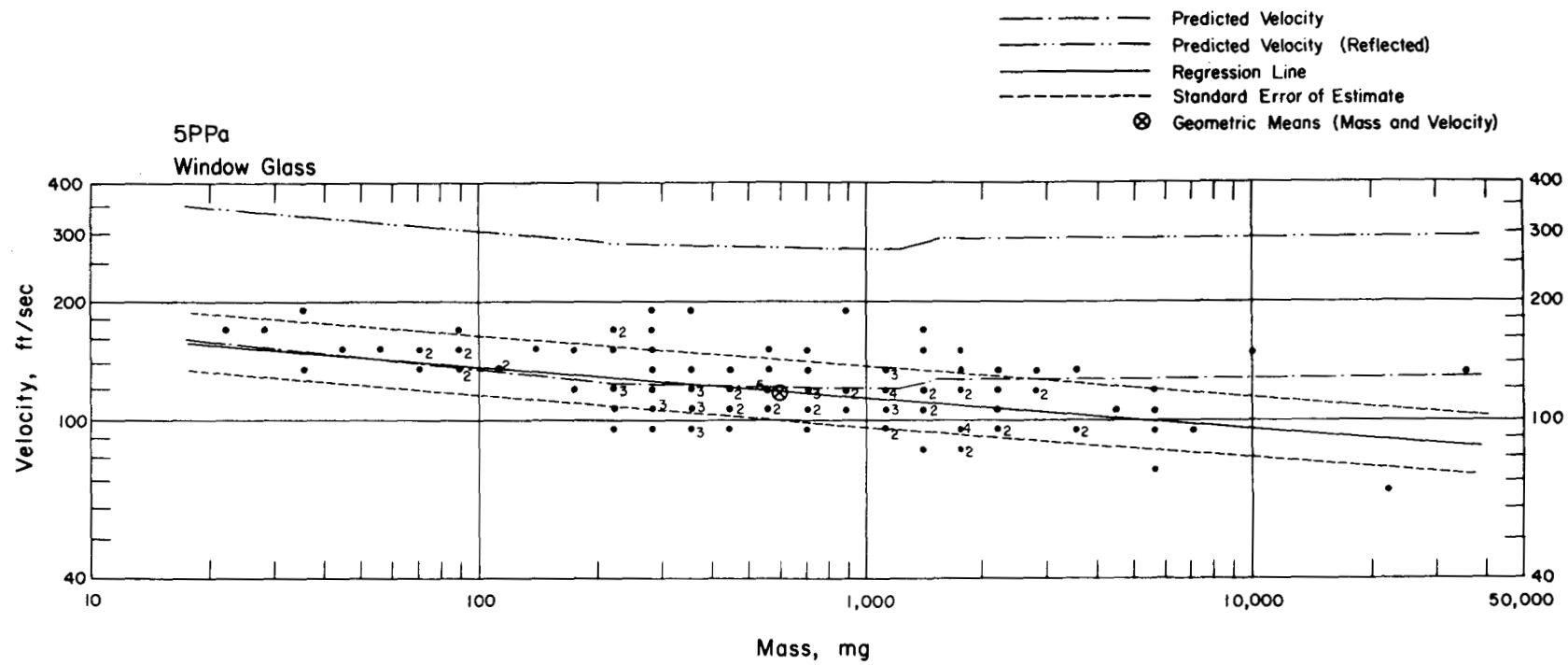


Fig. 4.40—Analysis of window-glass missiles from trap 5PPa: $d = 11.7$ ft; $n = 123$; $\log v = 2.2919 - 0.0772 \log m$; $E_{gv} = 1.19$; $M_{50} = 609$ mg; $V_{50} = 119$ ft/sec.

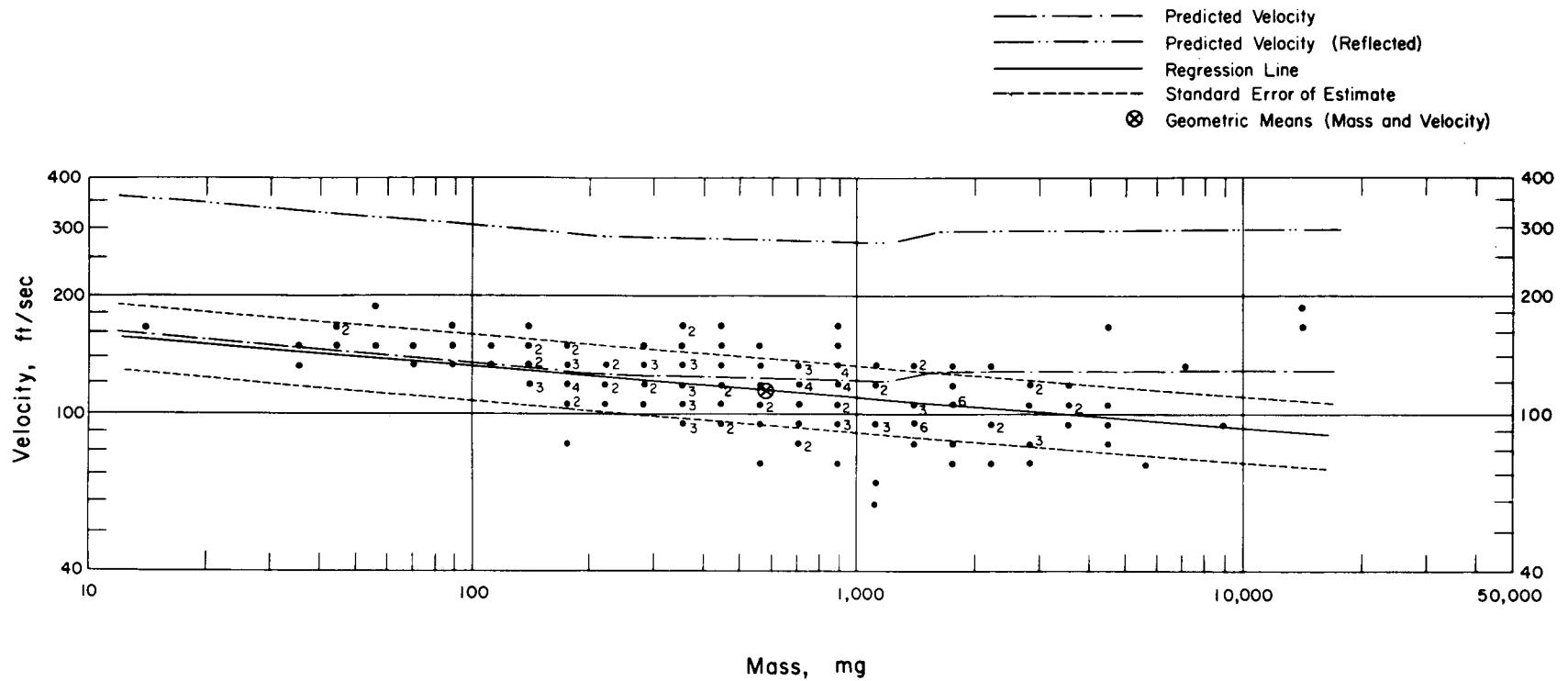


Fig. 4.41—Analysis of window-glass missiles from trap 5PPb: $d = 11.7$ ft; $n = 158$; $\log v = 2.2809 - 0.0781 \log m$; $E_{GV} = 1.22$; $M_{50} = 588$ mg; $V_{50} = 116$ ft/sec.

6P STATION, RANGE 4770

- MD Military Debris (B) blue
- Gr Gravel (W) white
- S Spheres (Y) yellow
- A Animal Trap

- a— Window glass, $\frac{1}{8}$ " thick, framed and mounted
- b— Plate glass, $\frac{1}{4}$ " thick, framed and mounted

Note: MD, Gr, and S placed at 5.5', 14.0', and 36.0' from face of traps

Roman numeral in parenthesis designates type of missile absorber

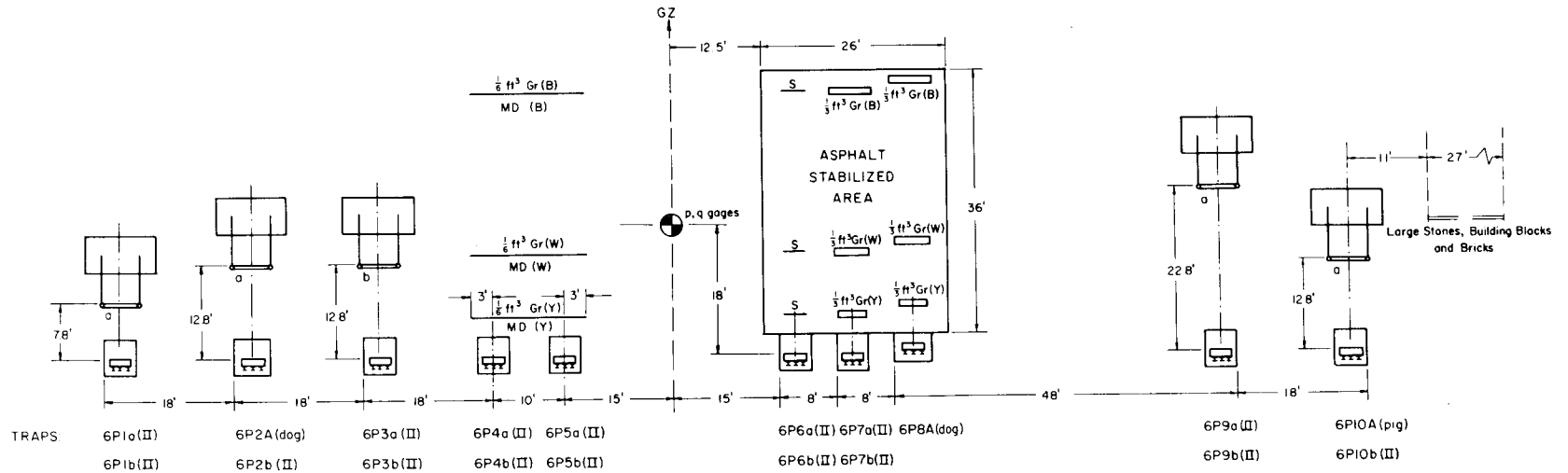


Fig. 4.42—Station 6P layout chart.

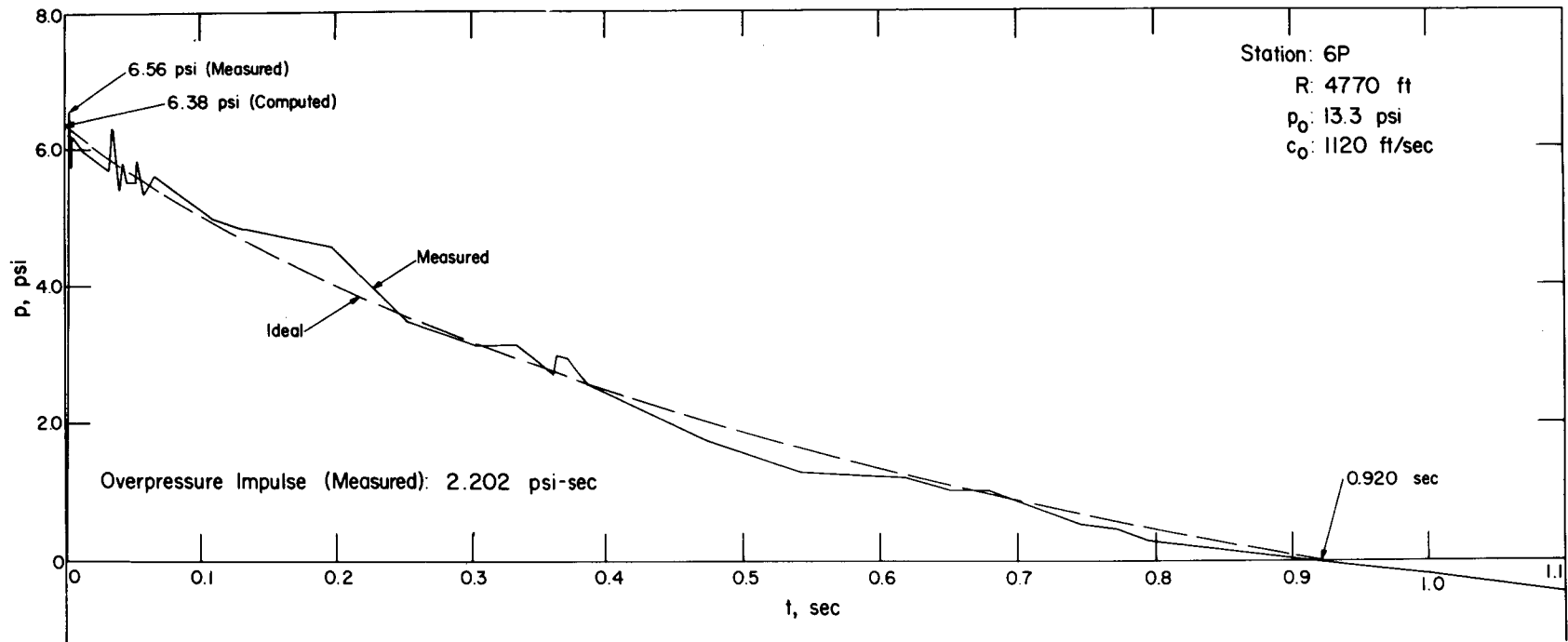


Fig. 4.43—Overpressure vs. time at station 6P.

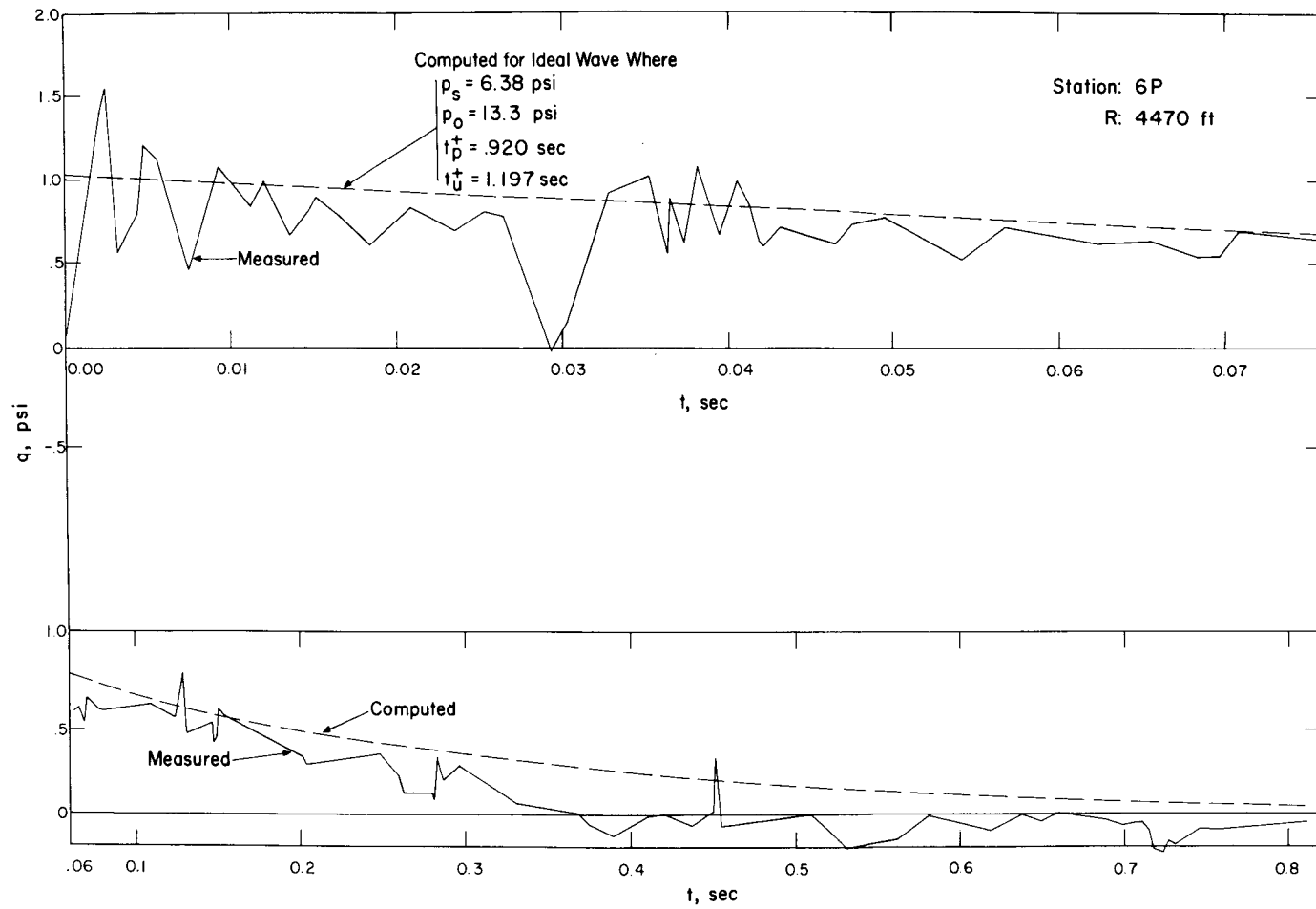


Fig. 4.44—Dynamic pressure vs. time at station 6P.

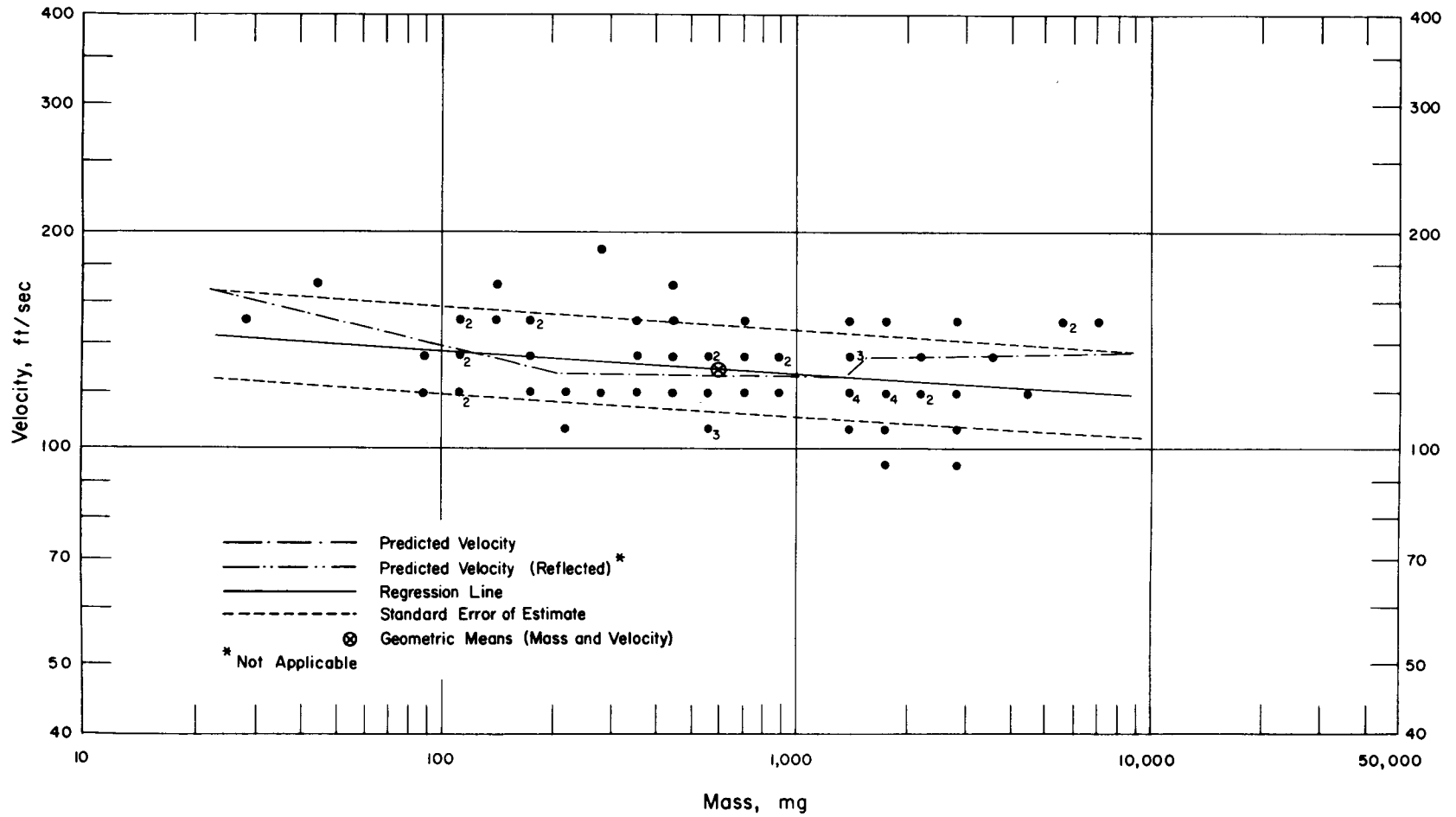


Fig. 4.45—Analysis of window-glass missiles from trap 6P1a: $d = 7.8$ ft; $n = 67$; $\log v = 2.1924 - 0.0294 \log m$; $E_{gv} = 1.15$; $M_{50} = 594$ mg; $V_{50} = 129$ ft/sec.

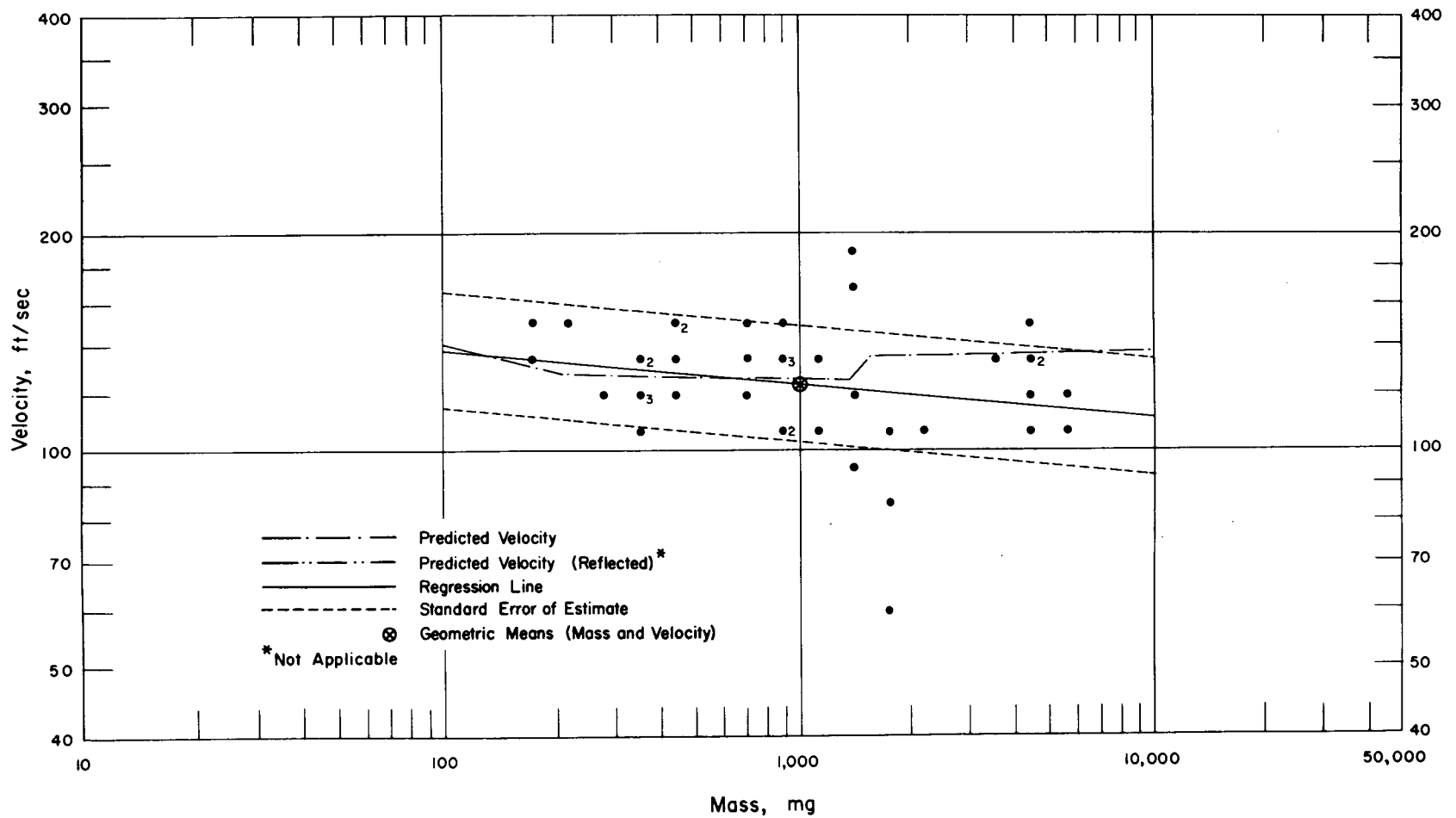


Fig. 4.46—Analysis of window-glass missiles from trap 6P1b: $d = 7.8$ ft; $n = 41$; $\log v = 2.2258 - 0.0447 \log m$; $E_{gv} = 1.21$; $M_{50} = 981$ mg; $V_{50} = 124$ ft/sec.

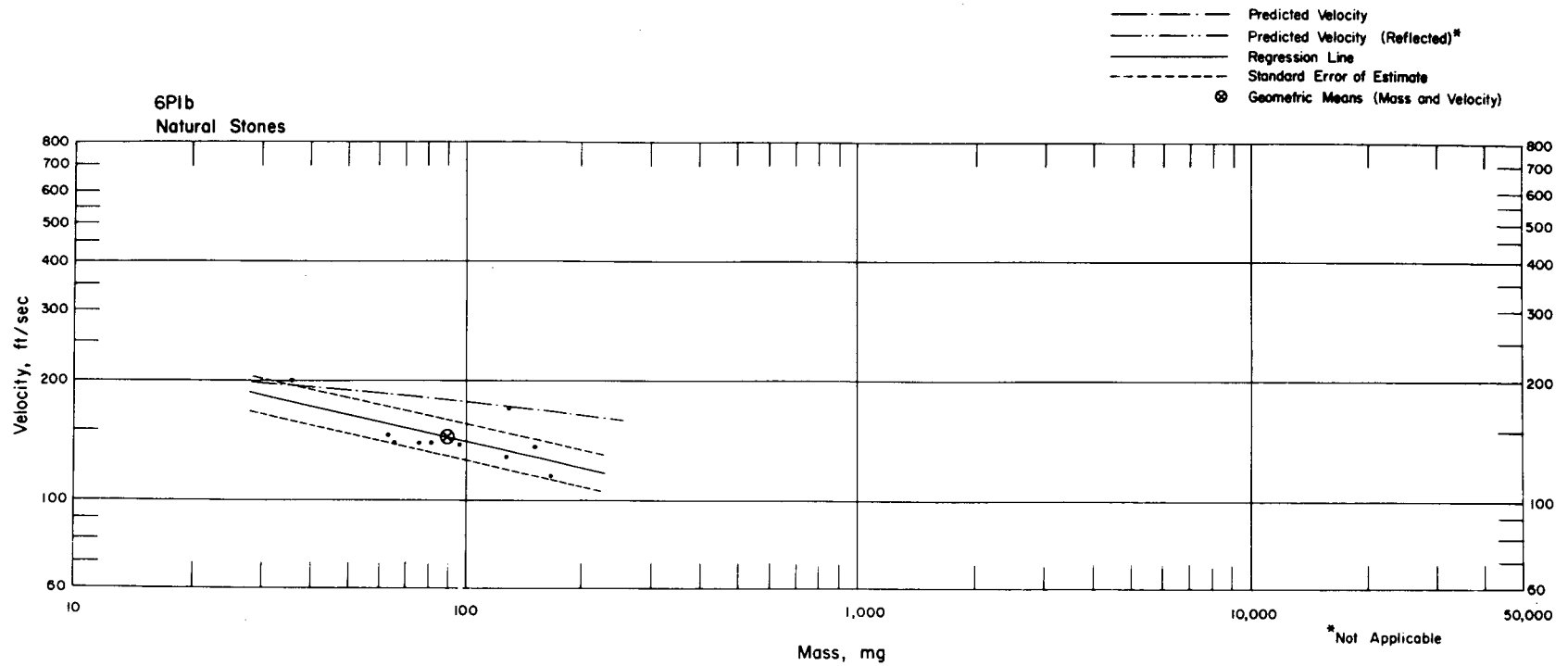


Fig. 4.47—Analysis of natural-stone missiles from trap 6P1b: $n = 10$; $\log v = 2.5835 - 0.2181 \log m$; $E_{gV} = 1.13$; $M_{50} = 89.8$ mg; $V_{50} = 144$ ft/sec.

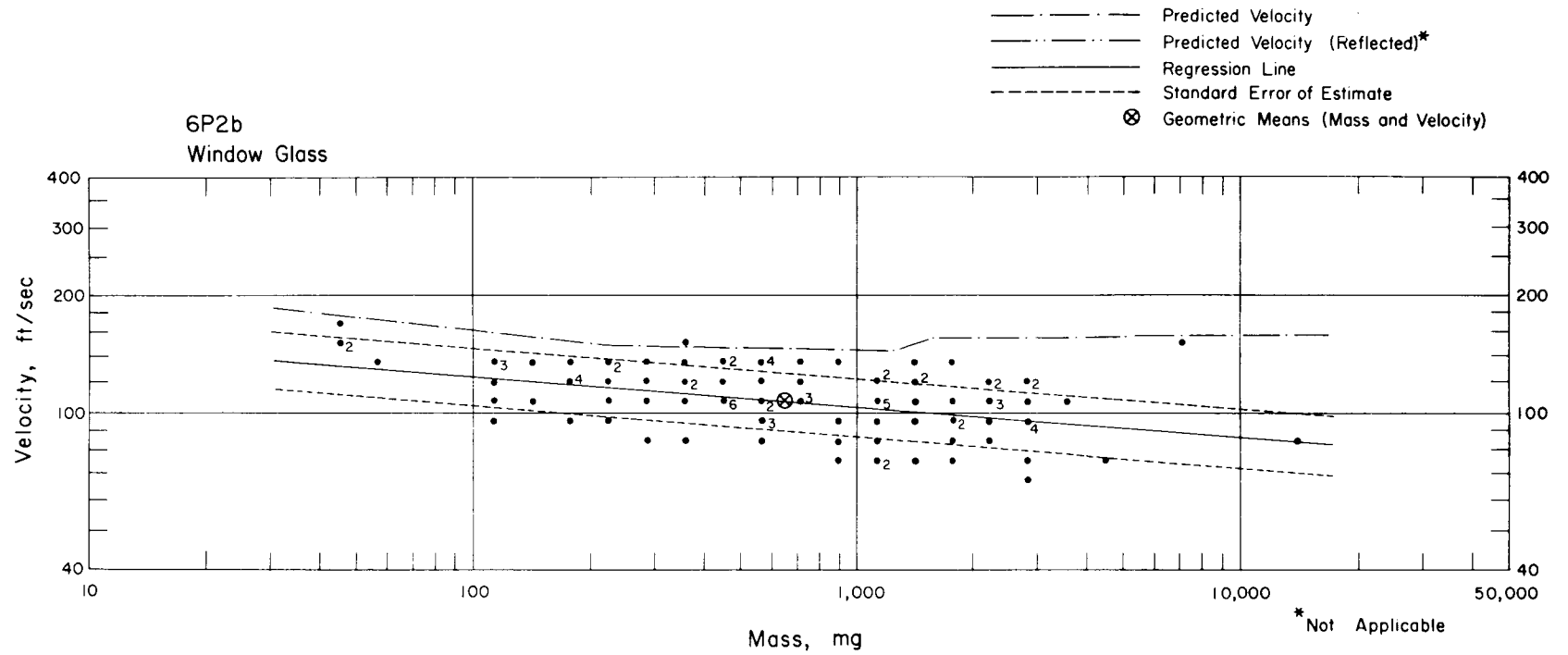


Fig. 4.48—Analysis of window-glass missiles from trap 6P2b: $d = 12.8$ ft; $n = 105$; $\log v = 2.2484 - 0.0762 \log m$; $E_{gv} = 1.18$; $M_{50} = 651$ mg; $V_{50} = 108$ ft/sec.

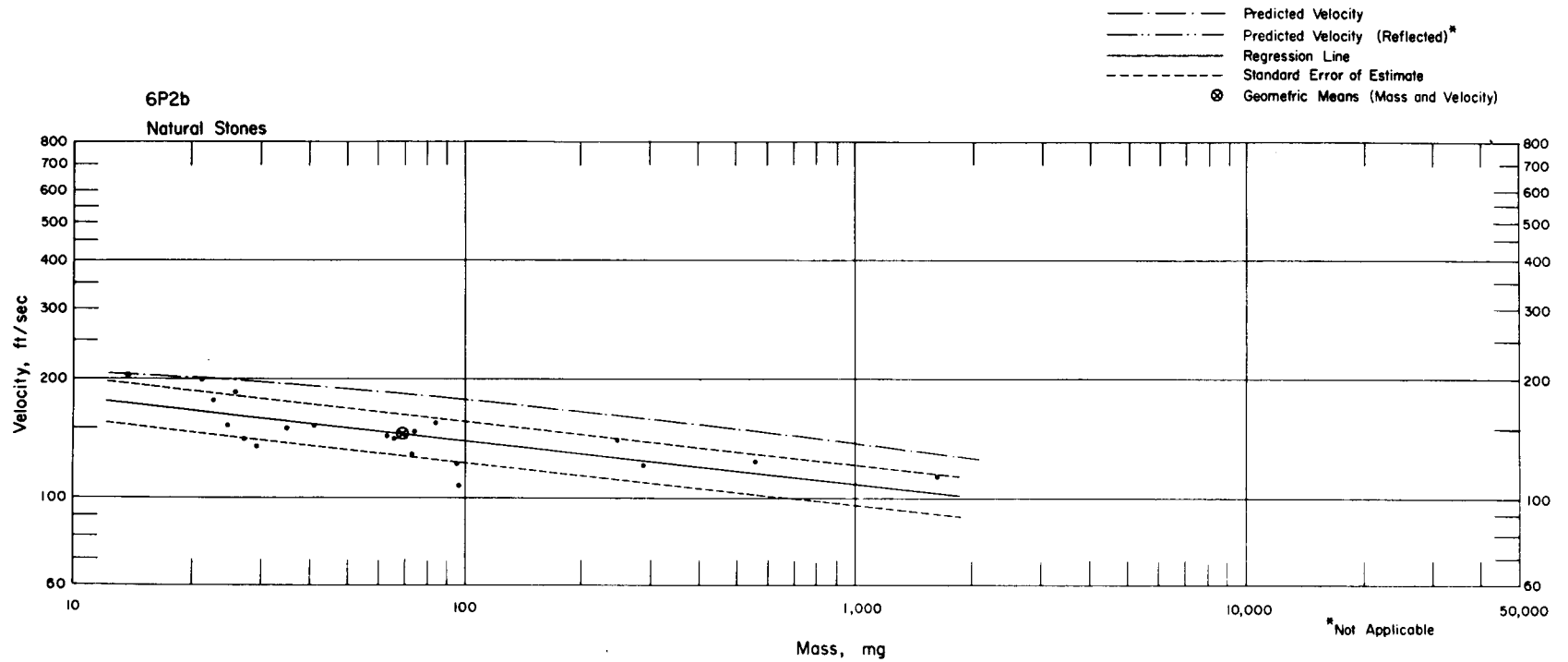


Fig. 4.49—Analysis of natural-stone missiles from trap 6P2b: $n = 20$; $\log v = 2.3675 - 0.1110 \log m$; $E_{gv} = 1.15$; $M_{50} = 68.6$ mg; $V_{50} = 146$ ft/sec.

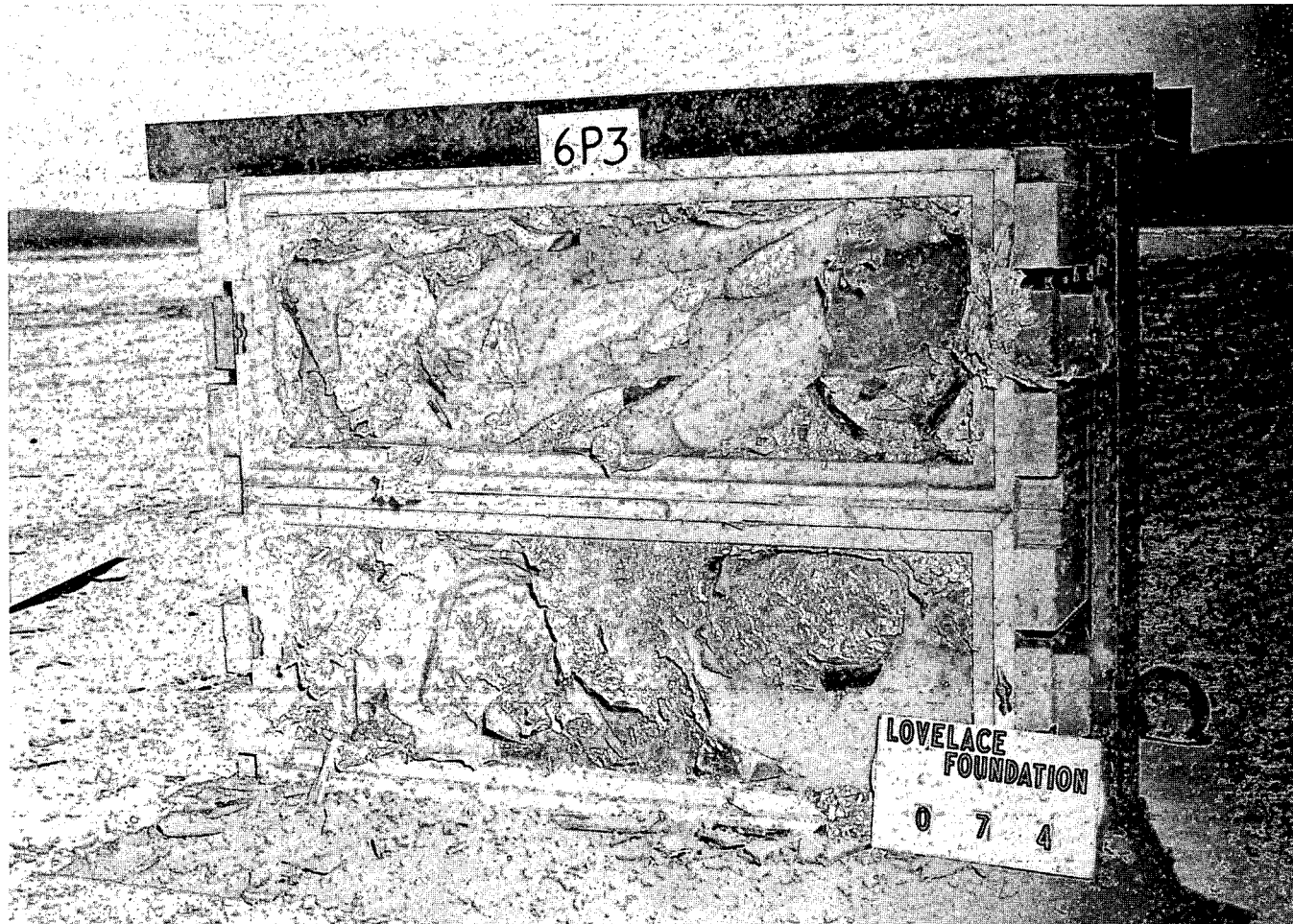


Fig. 4.50—Traps 6P3a and b, postshot, 12.8 ft behind plate-glass installation. Note large indentations made in upper trap by pieces of glass which were flat upon arrival at trap.

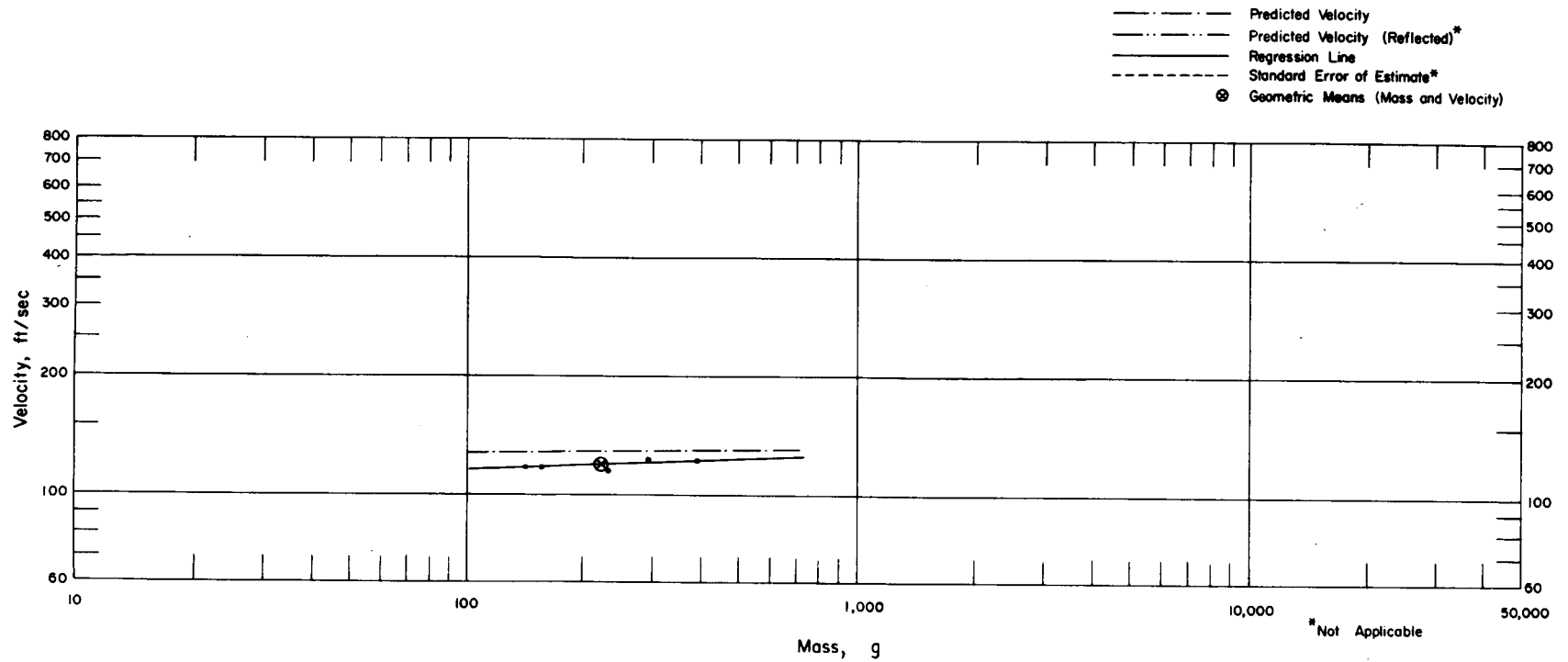


Fig. 4.51—Analysis of plate-glass missiles which arrived flat at trap 6P3b: $d = 12.8$ ft; $n = 5$; $\log v = 1.8697 + 0.0390 \log m$ (mg); $E_{gv} = 1.01$ (thus standard-error-of-estimate lines are almost identical to regression line); $M_{50} = 223,000$ mg; $V_{50} = 120$ ft/sec.

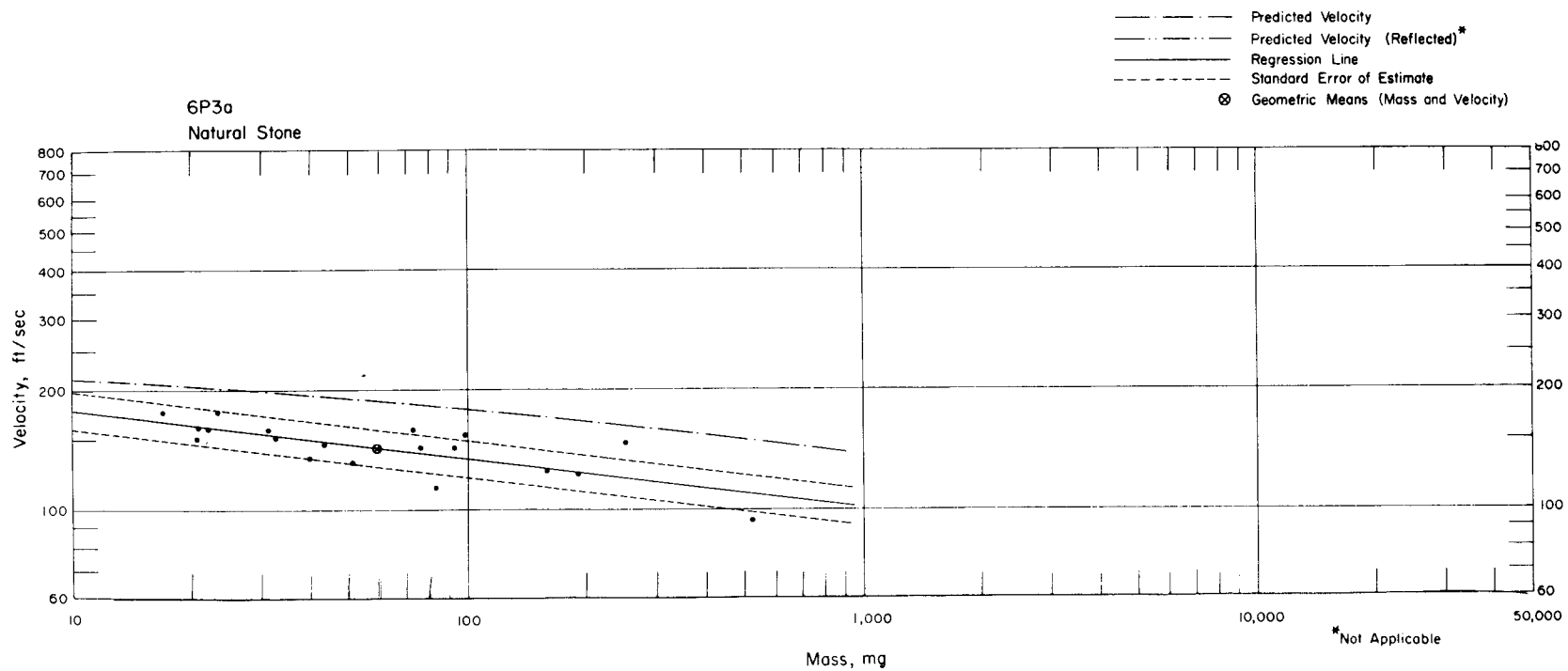


Fig. 4.53—Analysis of natural-stone missiles from trap 6P3a: $n = 19$; $\log v = 2.3752 - 0.1219 \log m$; $E_{gv} = 1.11$; $M_{50} = 59.8$ mg; $V_{50} = 144$ ft/sec.

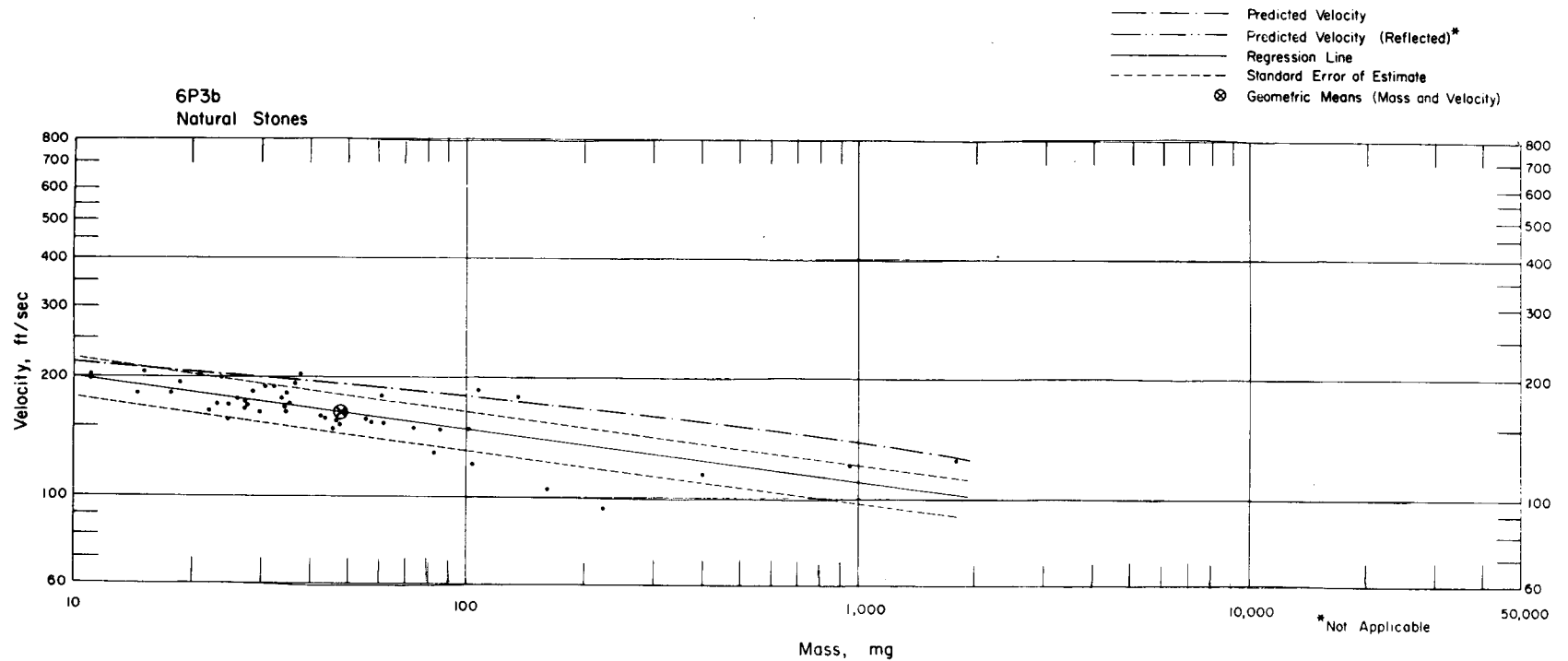


Fig. 4.54—Analysis of natural-stone missiles from trap 6P3b: $n = 49$; $\log v = 2.4344 - 0.1336 \log m$; $E_{gv} = 1.12$; $M_{50} = 47.7$ mg; $V_{50} = 162$ ft/sec.

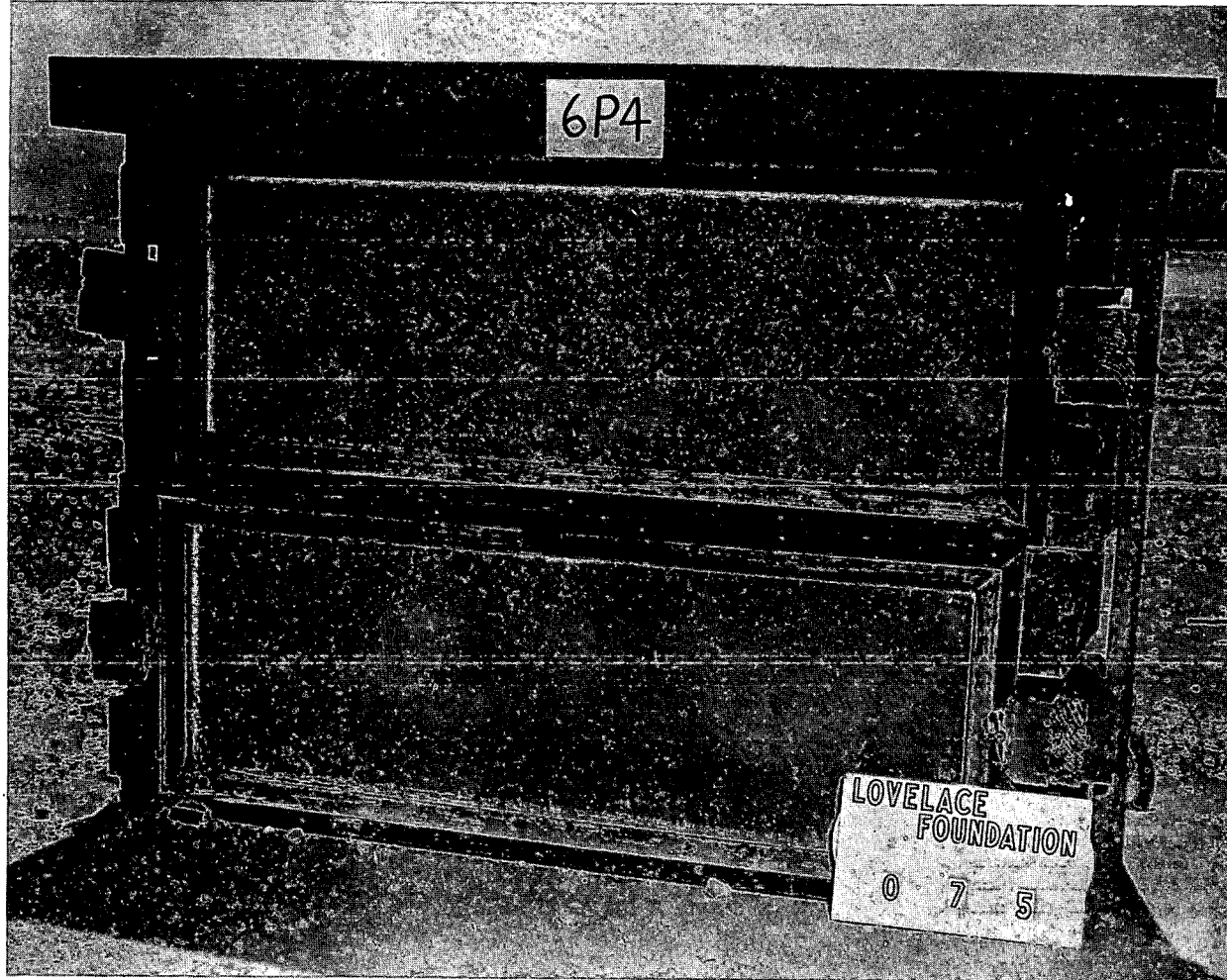


Fig. 4.55 — Military-debris and gravel installation 6P4, postshot.

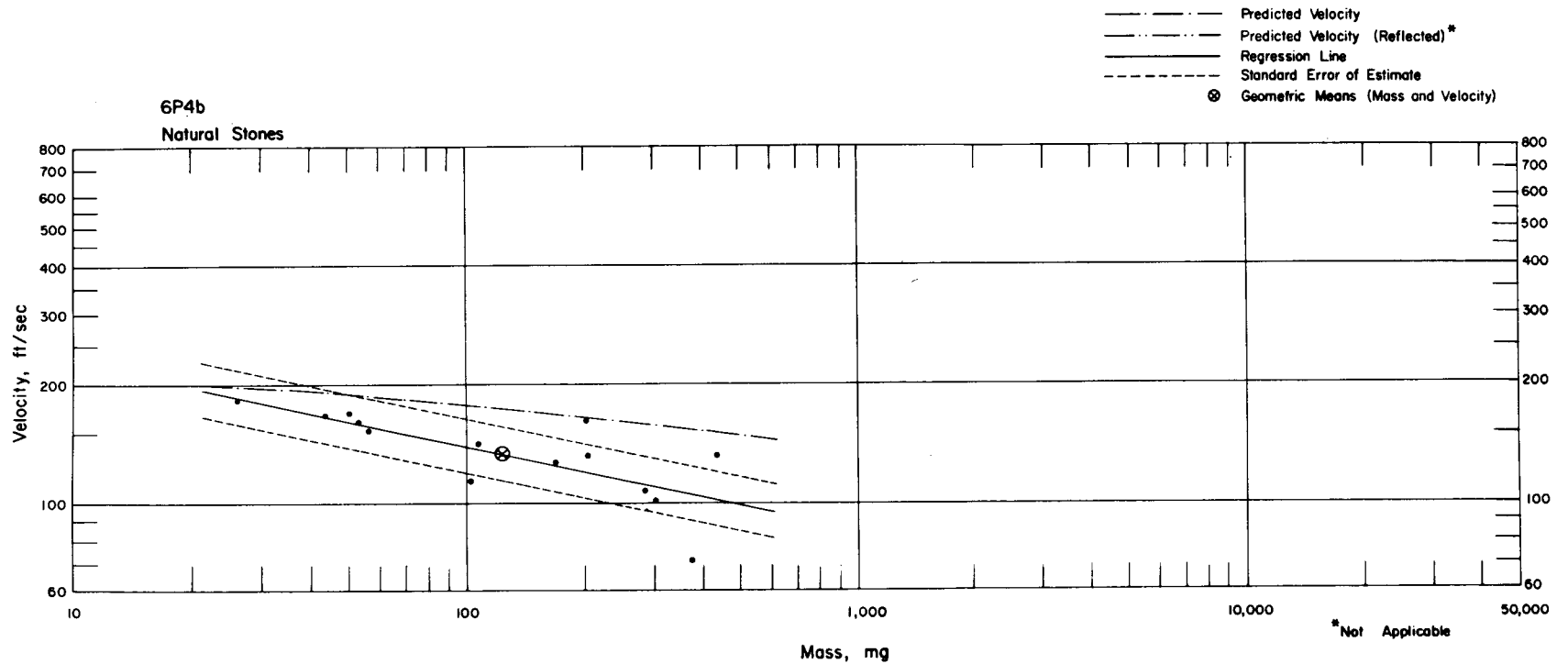


Fig. 4.56—Analysis of natural-stone missiles from trap 6P4b: $n = 14$; $\log v = 2.5749 - 0.2138 \log m$; $E_{gv} = 1.19$; $M_{50} = 123$ mg; $V_{50} = 134$ ft/sec.

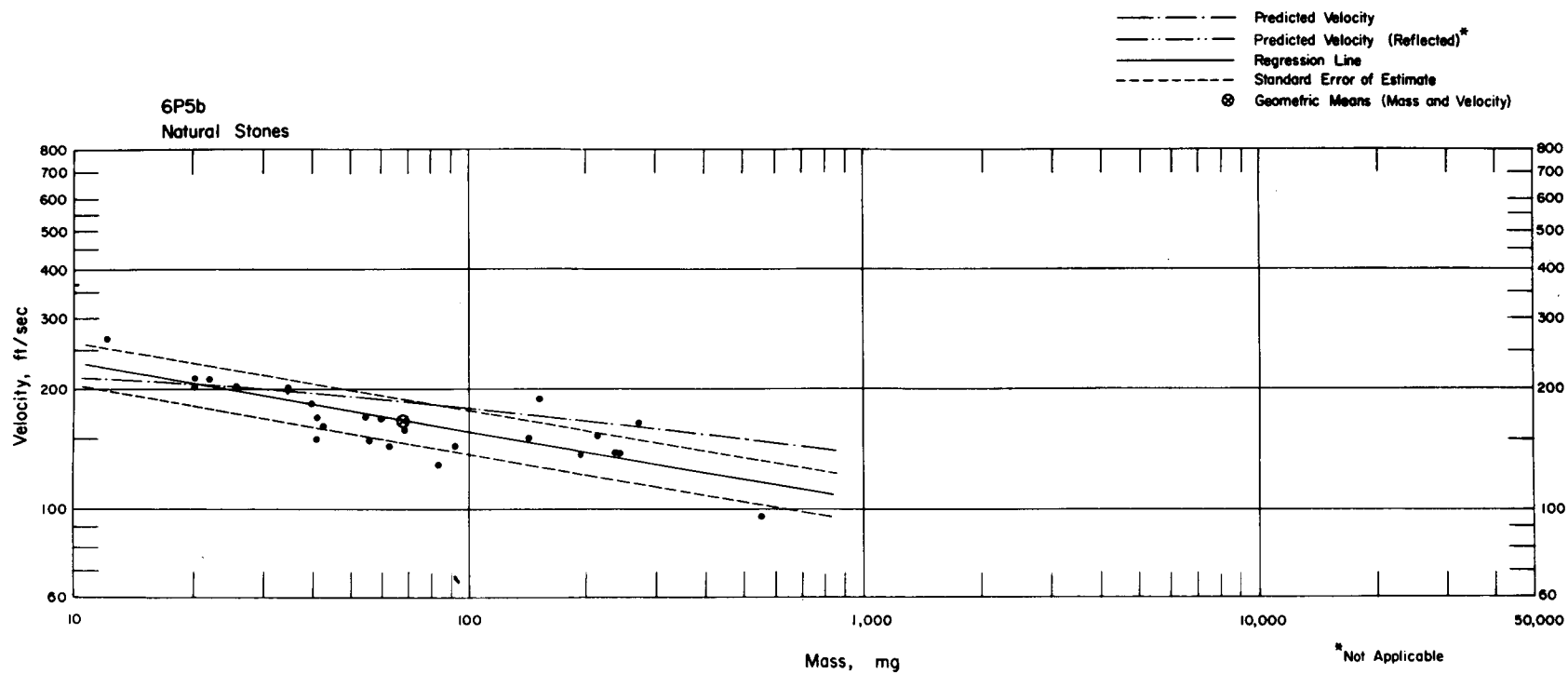


Fig. 4.57—Analysis of natural-stone missiles from trap 6P5b: $n = 25$; $\log v = 2.5385 - 0.1744 \log m$; $E_{gV} = 1.13$; $M_{50} = 67.4$ mg; $V_{50} = 166$ ft/sec.

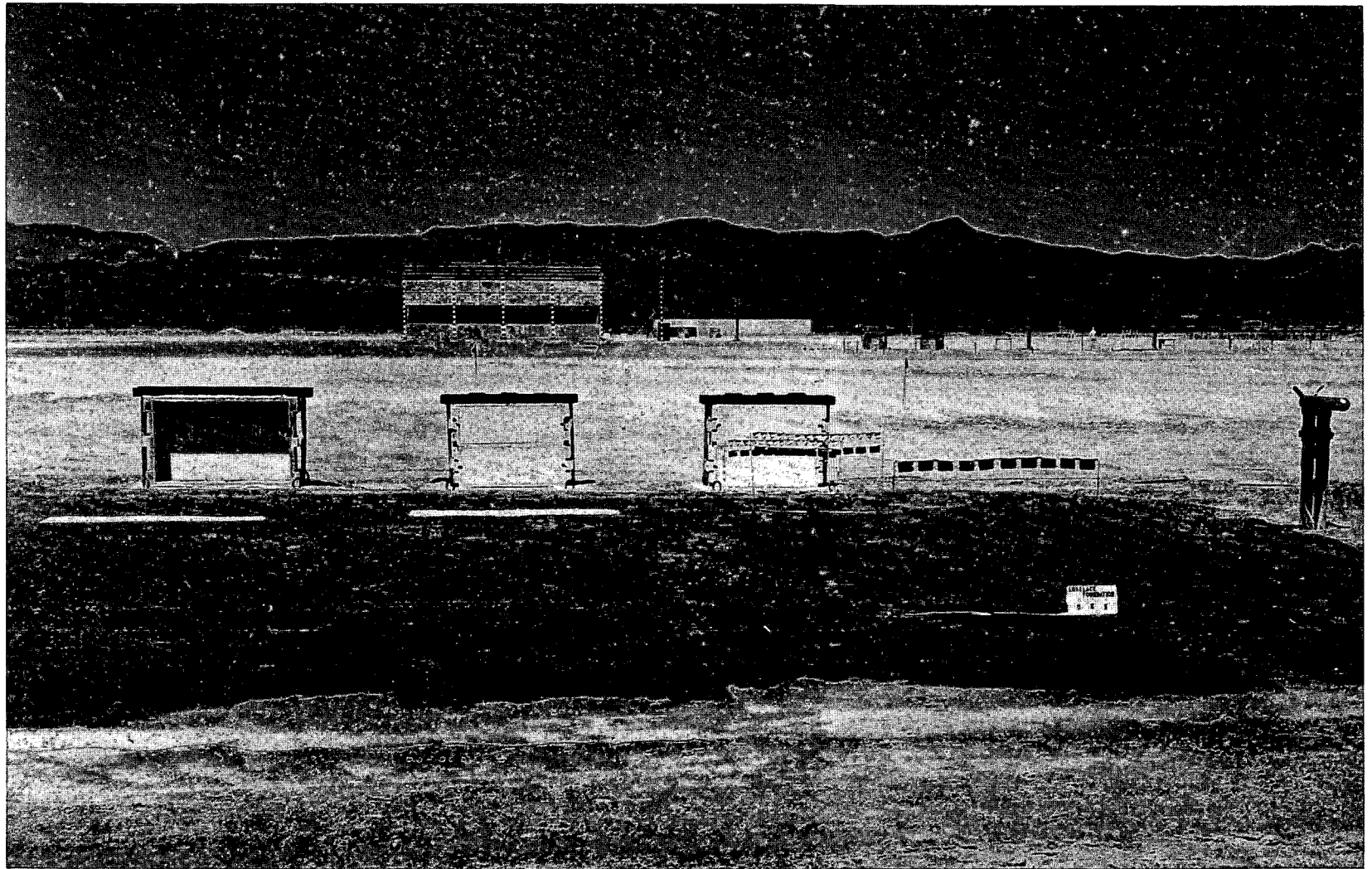


Fig. 4.58—Traps 6P6a and b, 6P7a and b, and 6P8A (right to left), preshot. Spheres on the ground and on wire mounts are on the asphalt pad in front of traps 6P6a and b. Piles of gravel are set out in front of other traps. A BRL gauge is shown at the right side of pad.

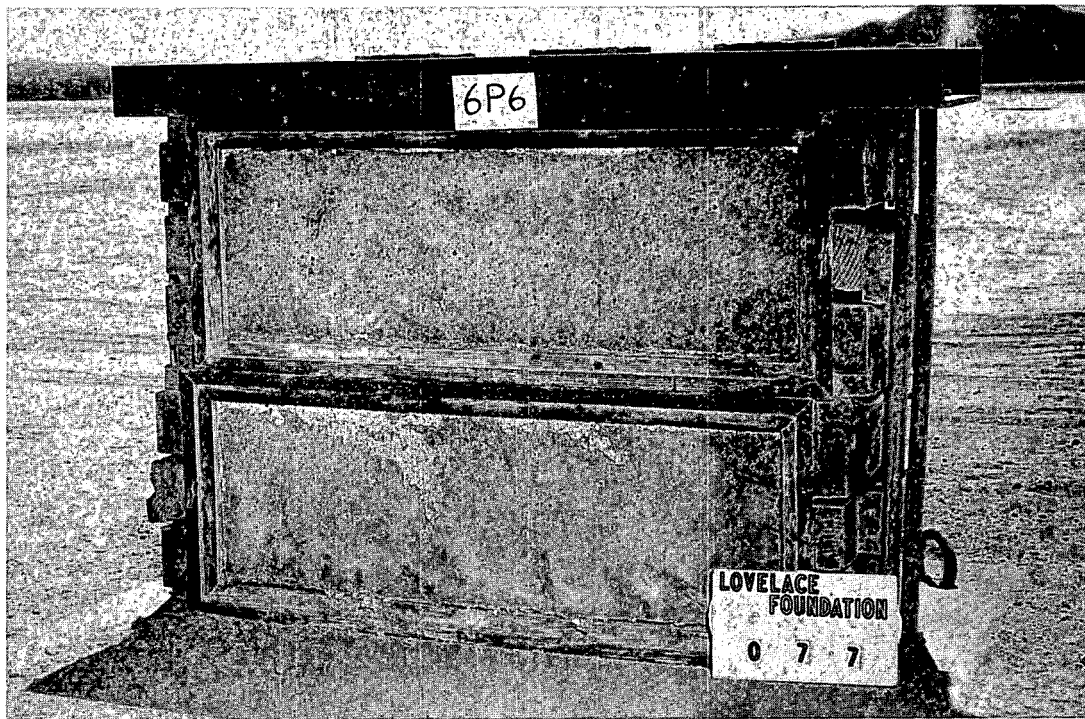


Fig. 4.59—Traps 6P6a and b, postshot.

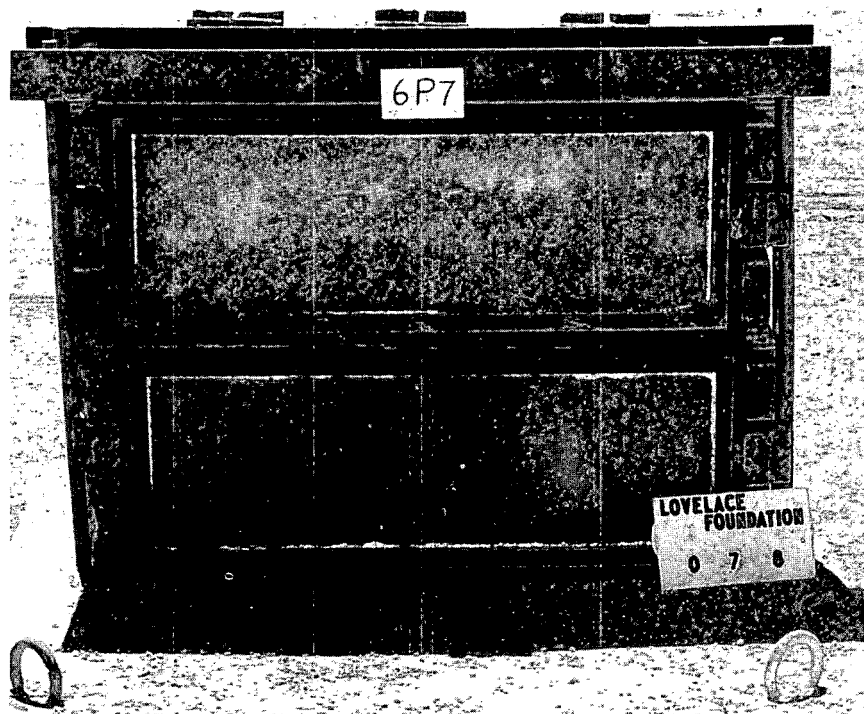


Fig. 4.60—Gravel installation 6P7, behind asphalt area, postshot.

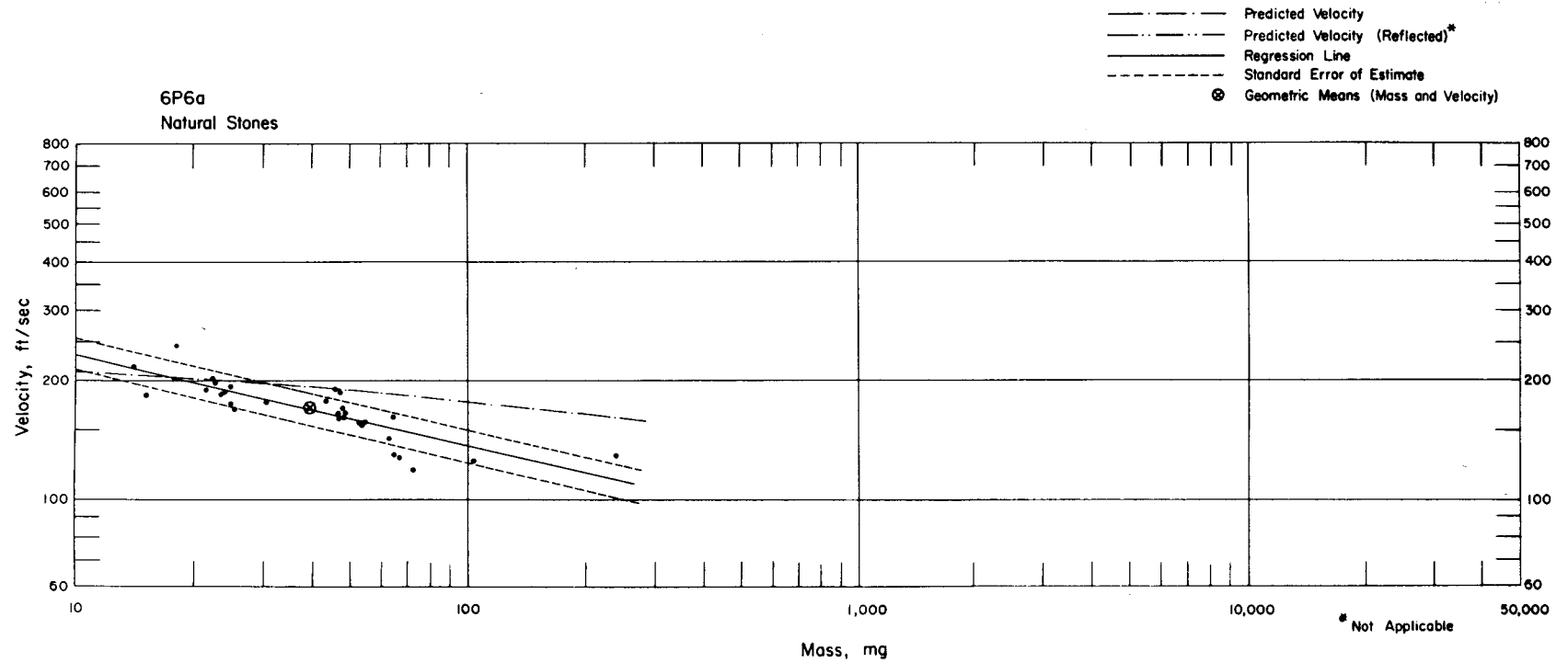


Fig. 4.61—Analysis of natural-stone missiles from trap 6P6a: $n = 31$; $\log v = 2.5957 - 0.2306 \log m$; $E_{gv} = 1.10$; $M_{50} = 39.0$ mg;
 $V_{50} = 169$ ft/sec.

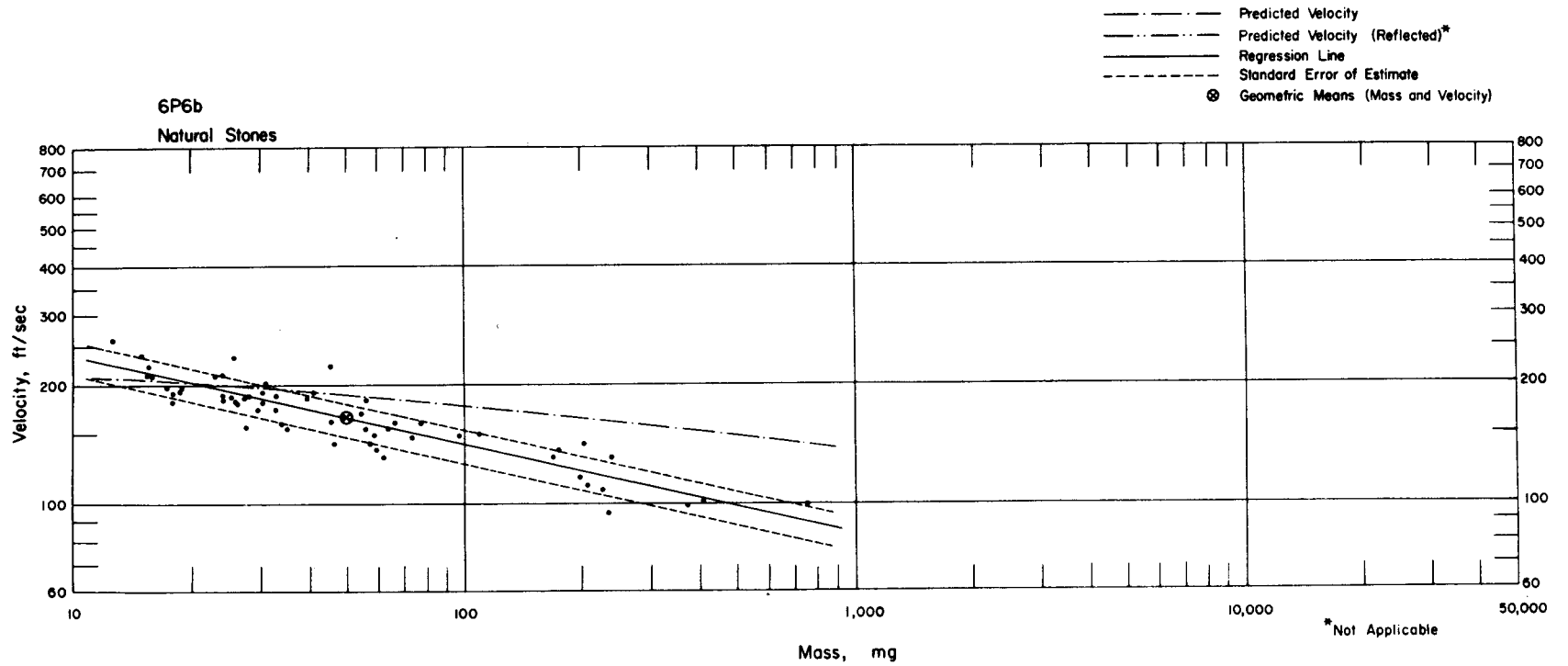


Fig. 4.62—Analysis of natural-stone missiles from trap 6P6b: $n = 58$; $\log v = 2.5897 - 0.2192 \log m$; $E_{gv} = 1.10$; $M_{50} = 49.0$ mg; $V_{50} = 166$ ft/sec.

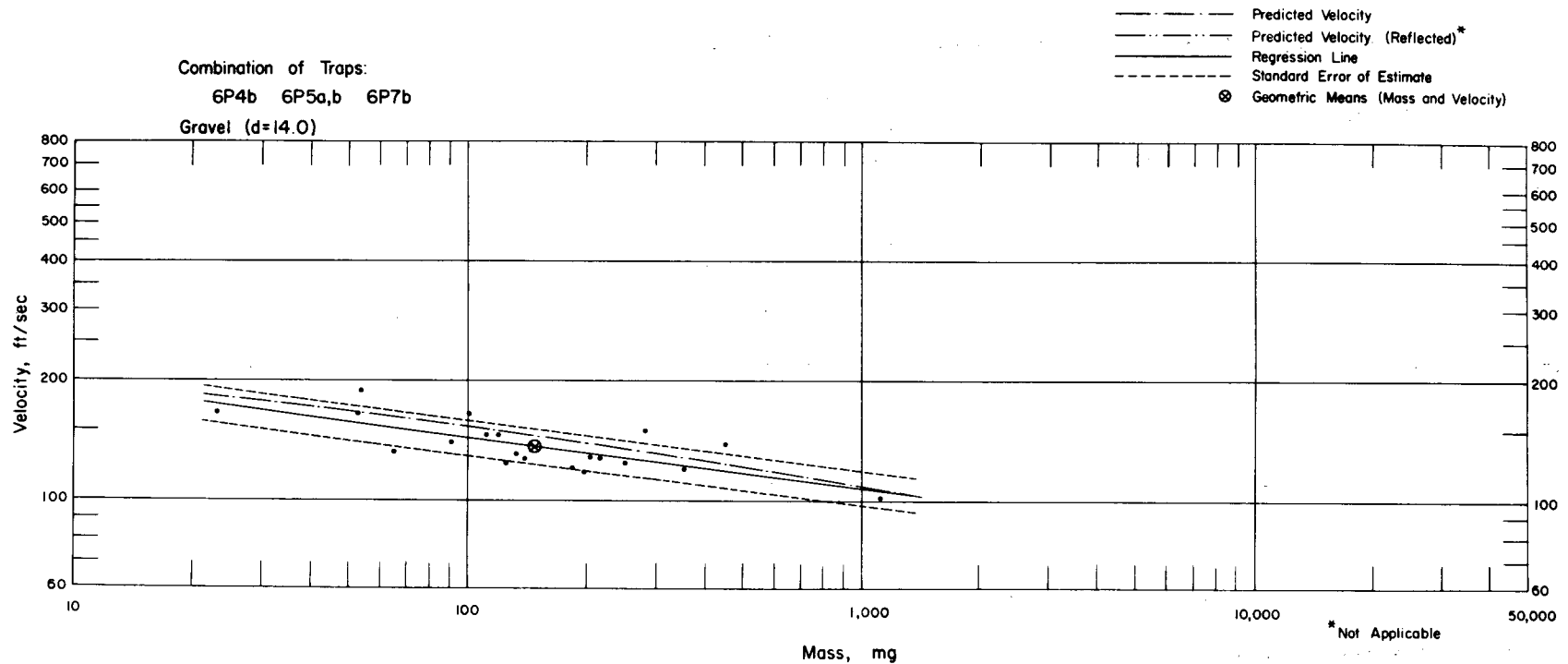


Fig. 4.63—Analysis of gravel missiles from station 6P traps: $d = 14.0$ ft; $n = 20$; $\log v = 2.4110 - 0.1257 \log m$; $E_{GV} = 1.11$; $M_{50} = 147$ mg; $V_{50} = 138$ ft/sec.

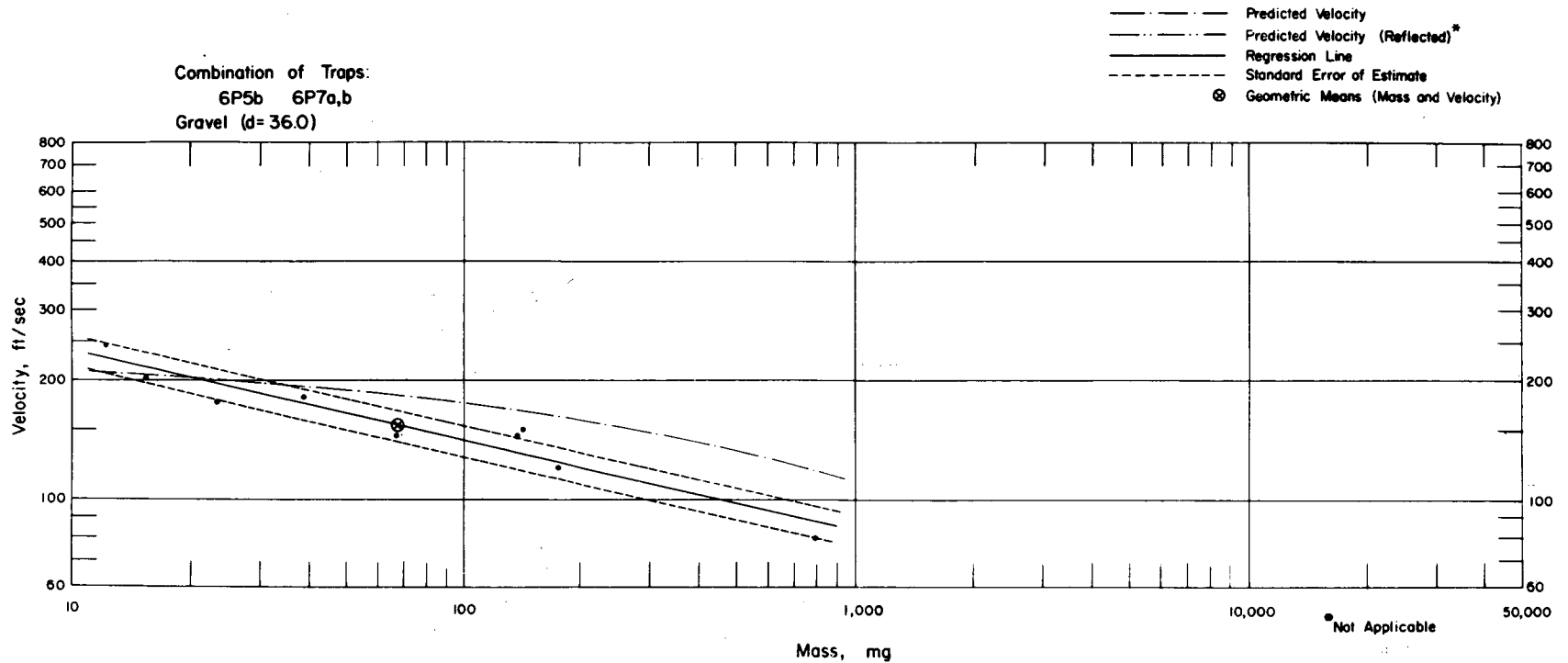


Fig. 4.64—Analysis of gravel missiles from station 6P traps: $d = 36.0$ ft; $n = 9$; $\log v = 2.6117 - 0.2311 \log m$; $E_{gv} = 1.10$; $M_{50} = 67.7$ mg; $V_{50} = 154$ ft/sec.

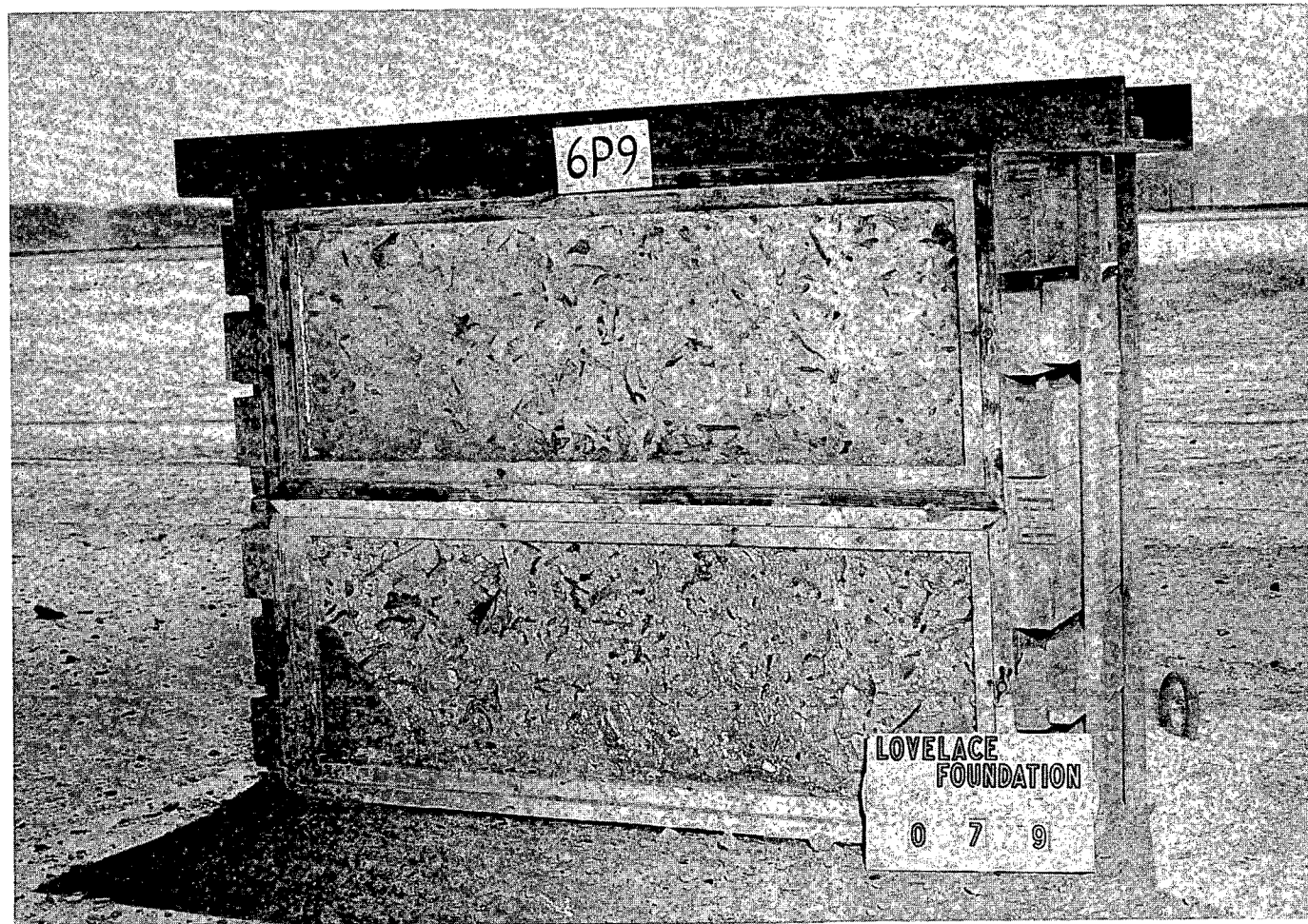


Fig. 4.65 — Traps 6P9a and b, postshot, 22.8 ft behind window-glass mount.

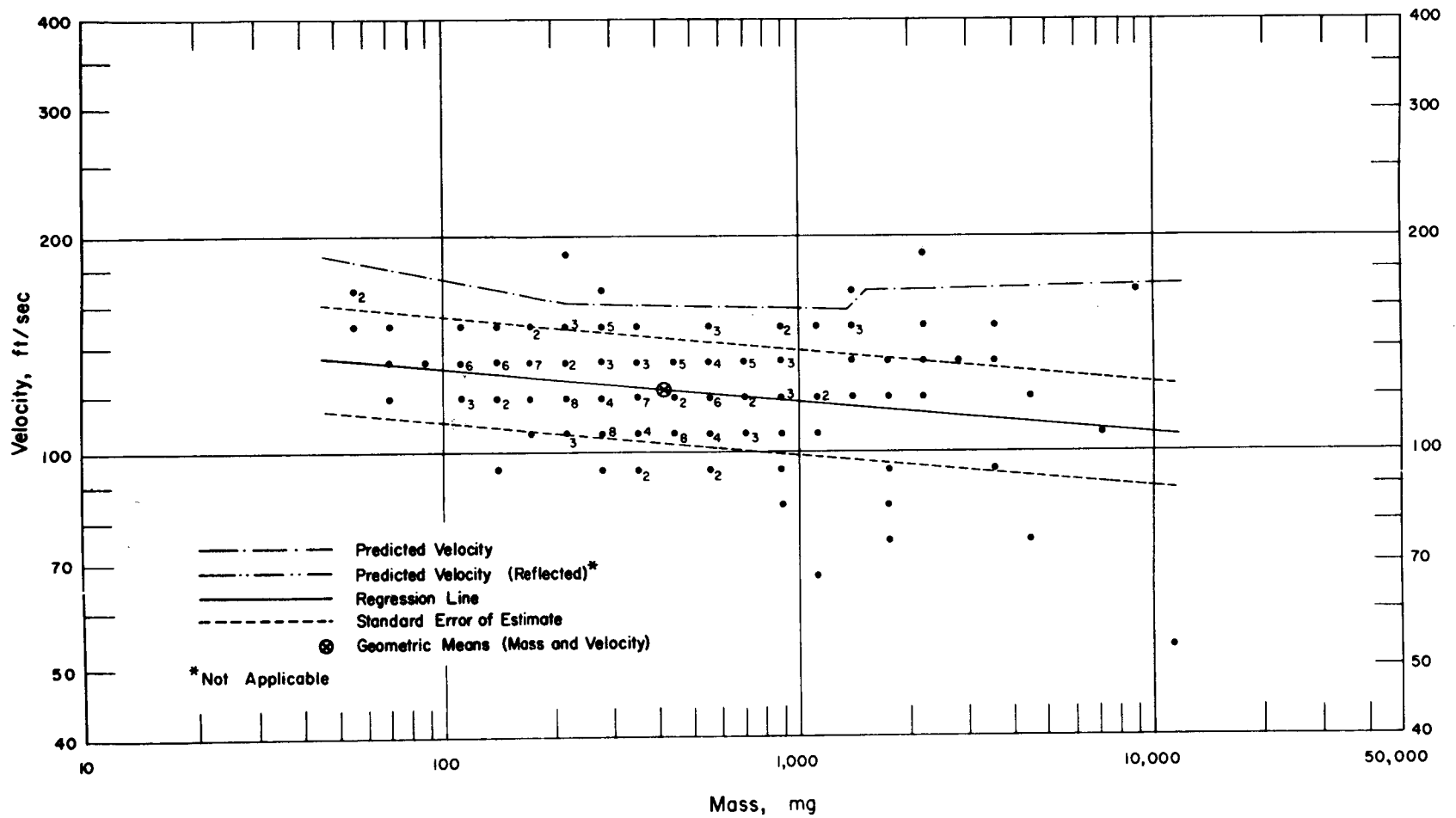


Fig. 4.66—Analysis of window-glass missiles from trap 6P9a: $d = 22.8$ ft; $n = 178$; $\log v = 2.2053 - 0.0446 \log m$; $E_{gv} = 1.19$; $M_{50} = 419$ mg; $V_{50} = 123$ ft/sec.

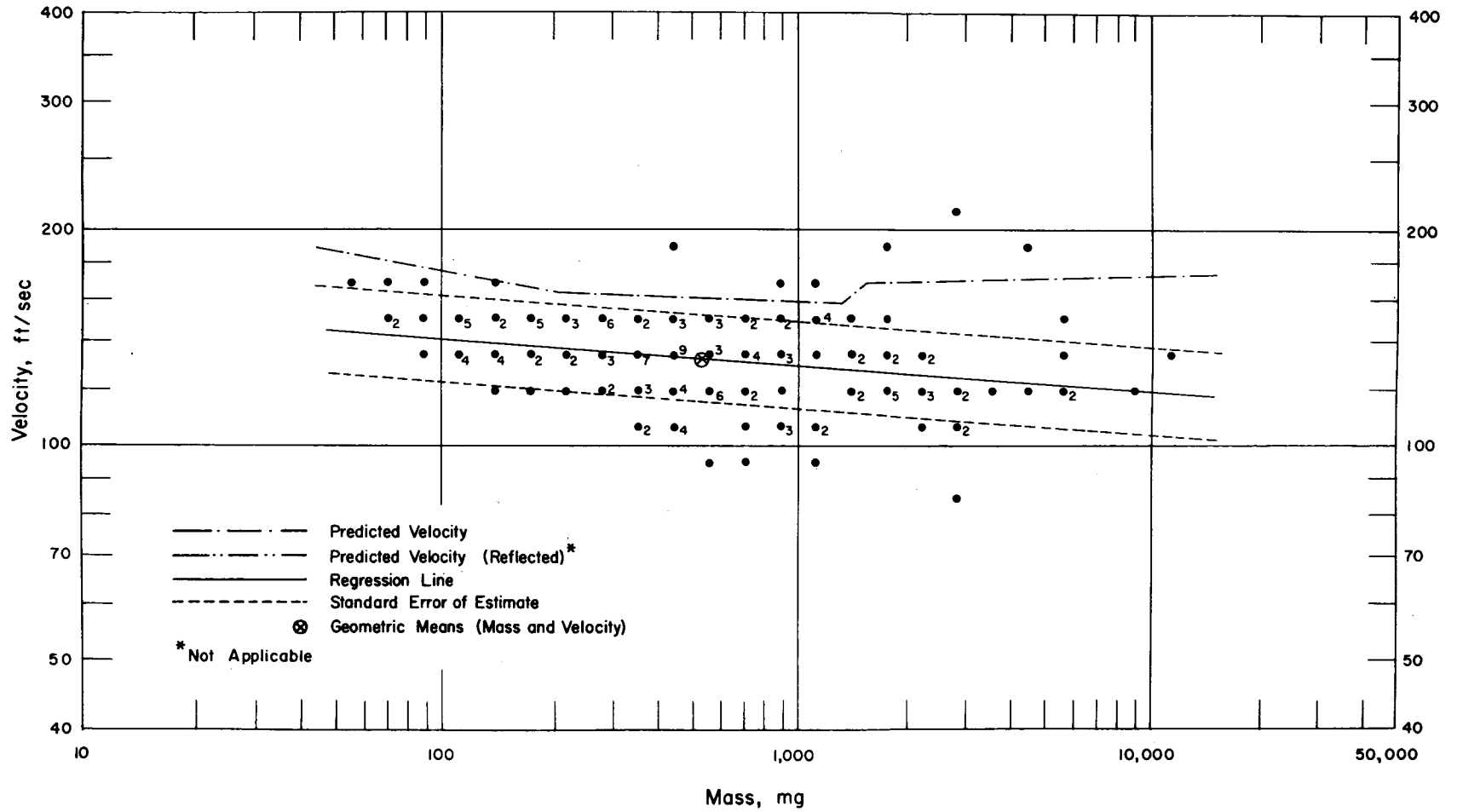


Fig. 4.67—Analysis of window-glass missiles from trap 6P9b: $d = 22.8$ ft; $n = 161$; $\log v = 2.2215 - 0.0368 \log m$; $E_{gv} = 1.15$; $M_{50} = 541$ mg; $V_{50} = 132$ ft/sec.

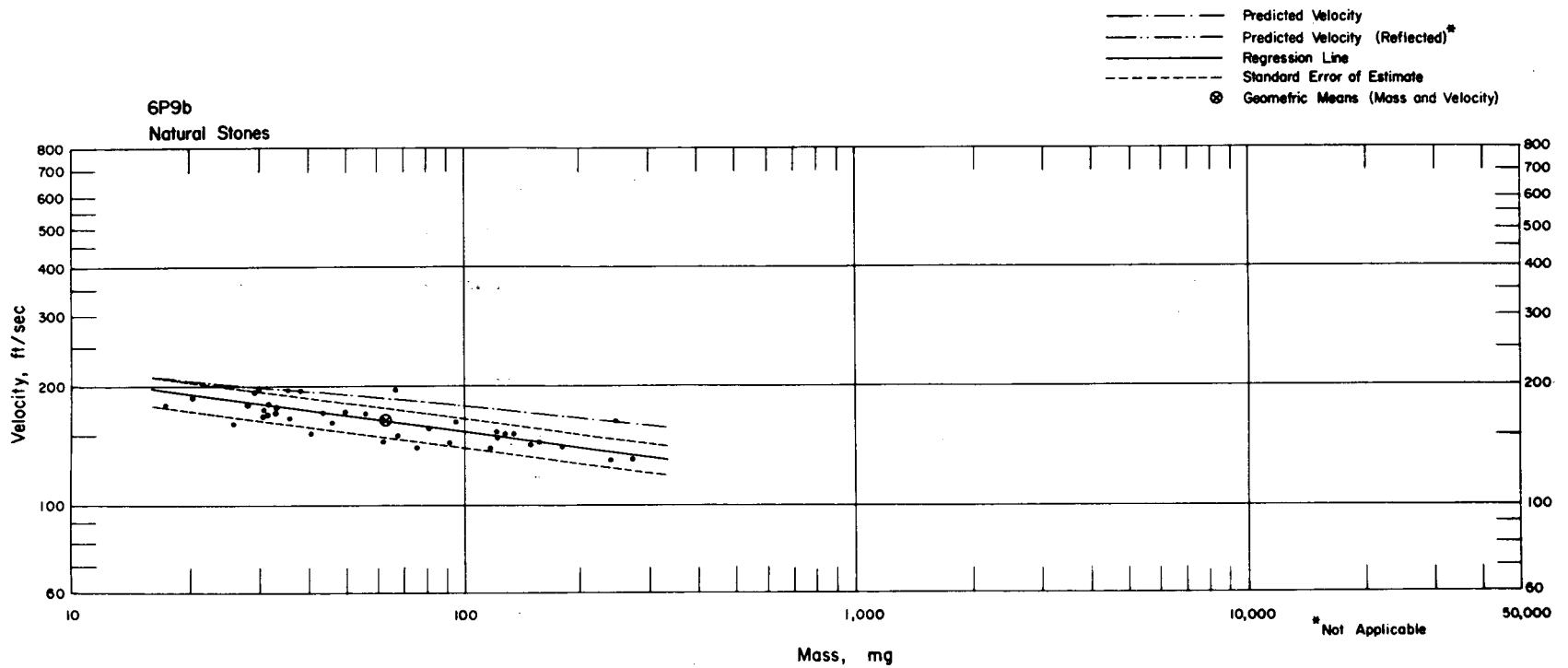


Fig. 4.68—Analysis of natural-stone missiles from trap 6P9b: $n = 39$; $\log v = 2.4510 - 0.1338 \log m$; $E_{gv} = 1.09$; $M_{50} = 62.1$ mg; $V_{50} = 163$ ft/sec.

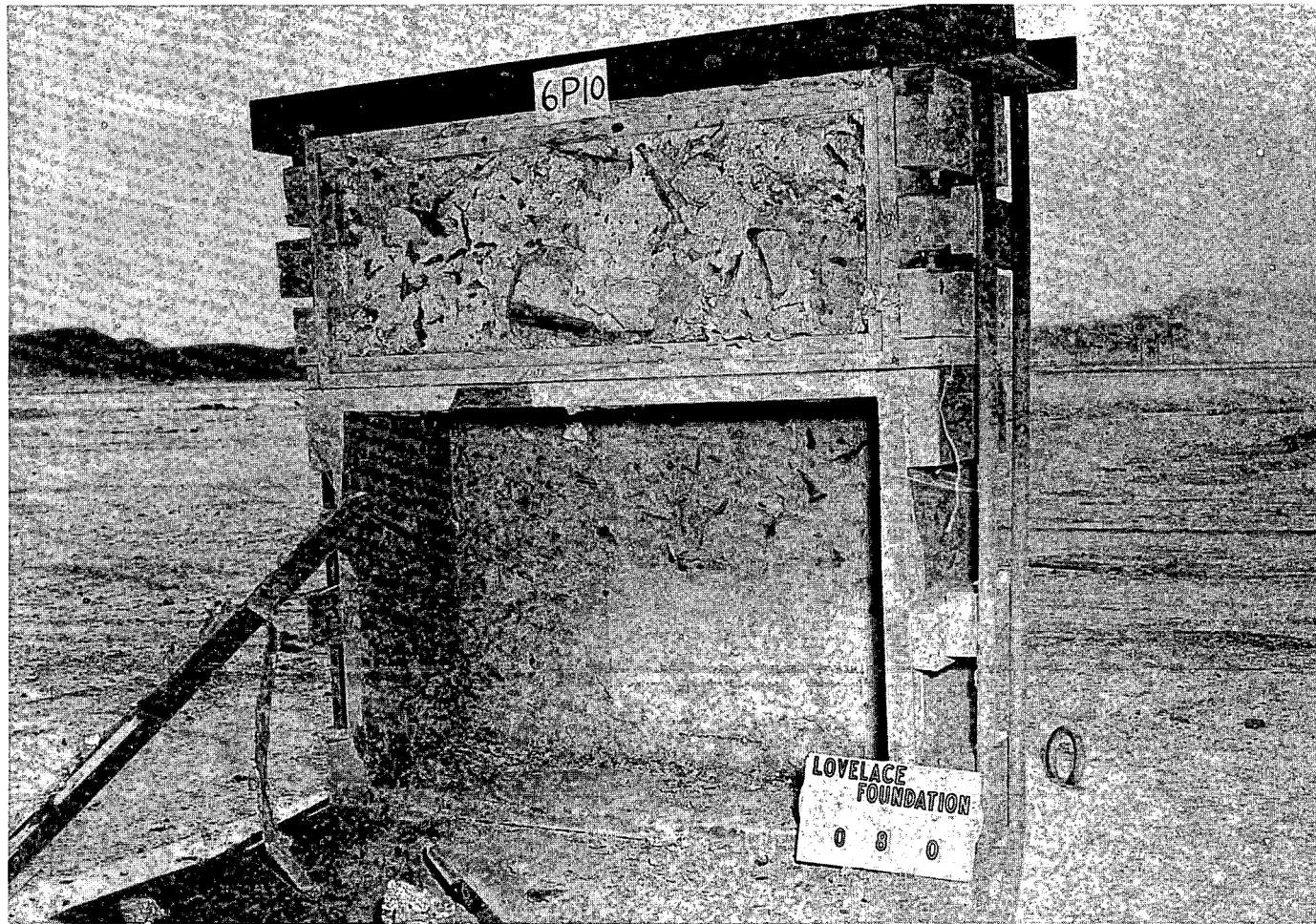


Fig. 4.69— Trap 6P10b, postshot, 12.8 ft behind window-glass mount and above a 27-in.-high pig trap. Outline of pig is visible in lower trap.

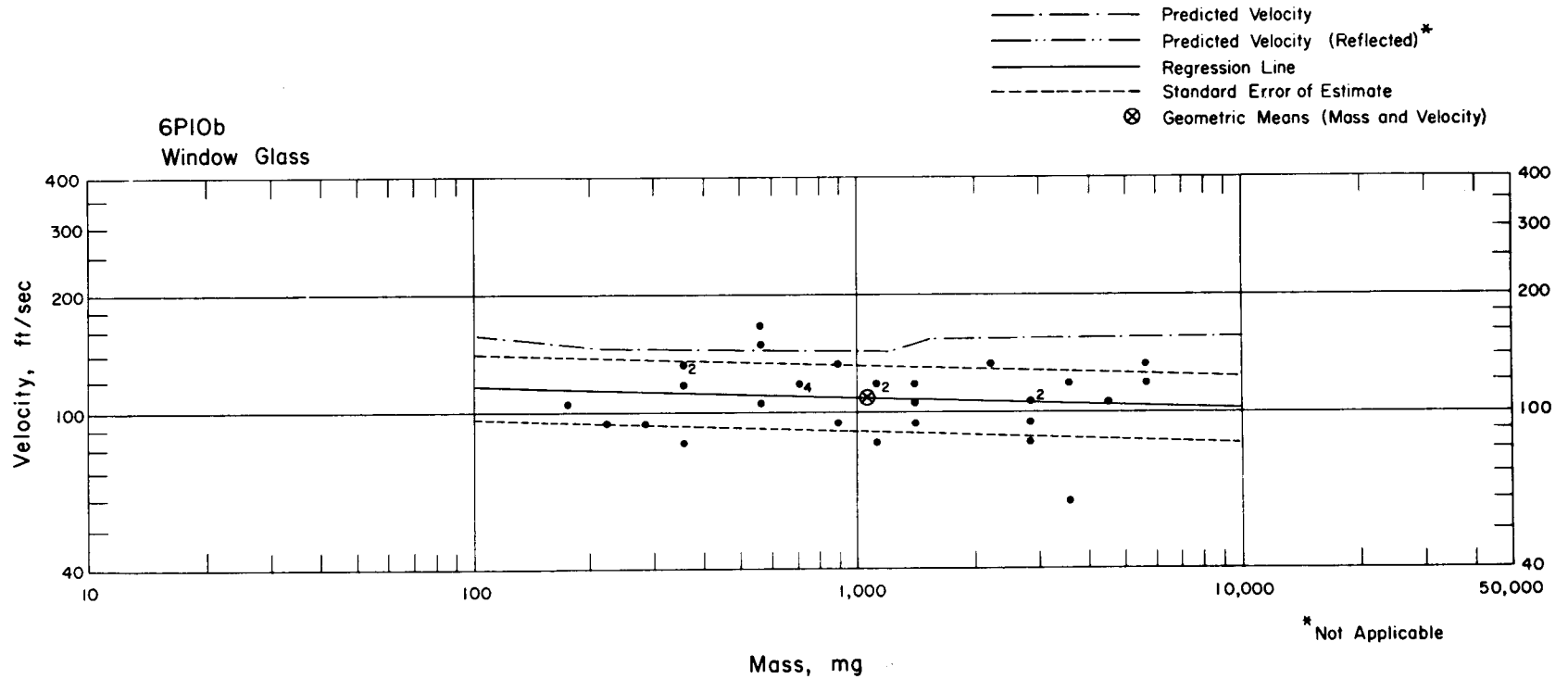


Fig. 4.70—Analysis of window-glass missiles from trap 6P10b: $d = 12.8$ ft; $n = 32$; $\log v = 2.1360 - 0.0310 \log m$; $E_{gv} = 1.21$; $M_{50} = 1010$ mg; $V_{50} = 110$ ft/sec.

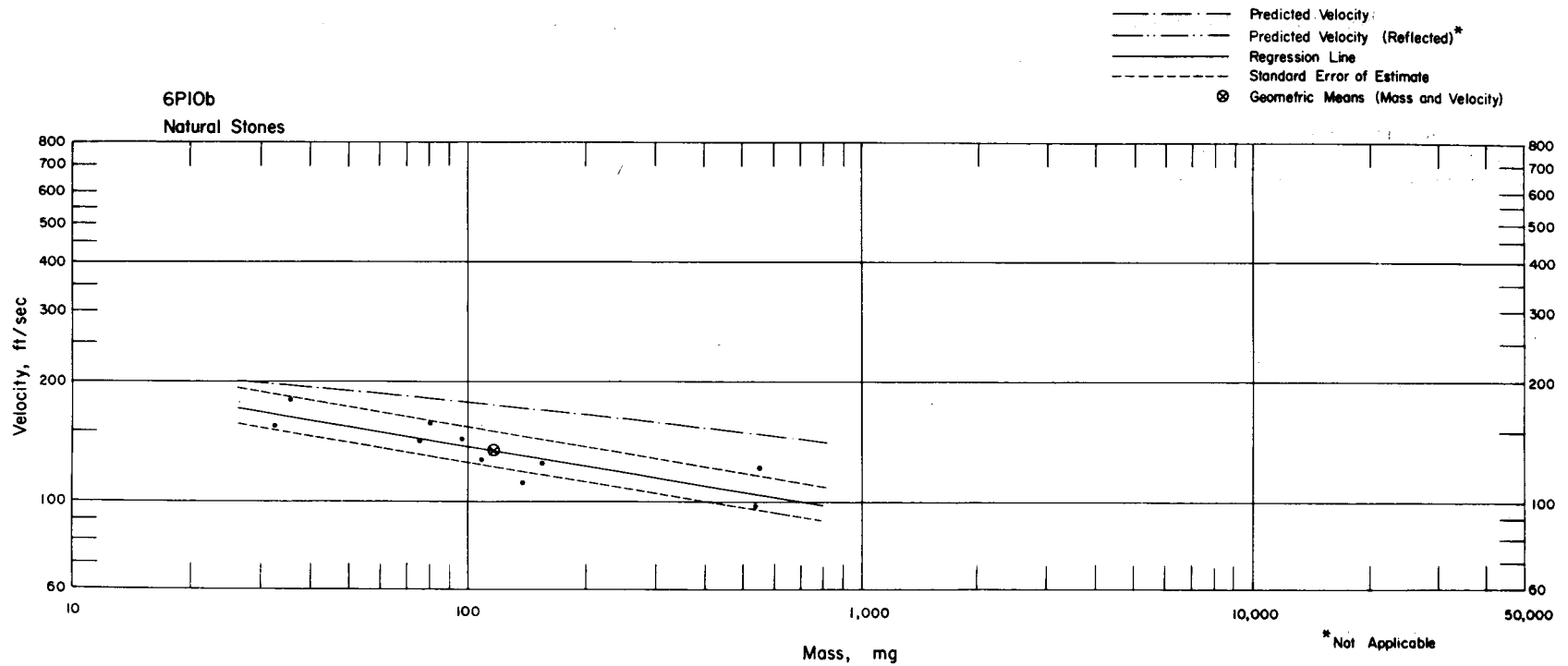


Fig. 4.71—Analysis of natural-stone missiles from trap 6P10b: $n = 10$; $\log v = 2.4627 - 0.1615 \log m$; $E_{gv} = 1.11$; $M_{50} = 117$ mg; $V_{50} = 135$ ft/sec.

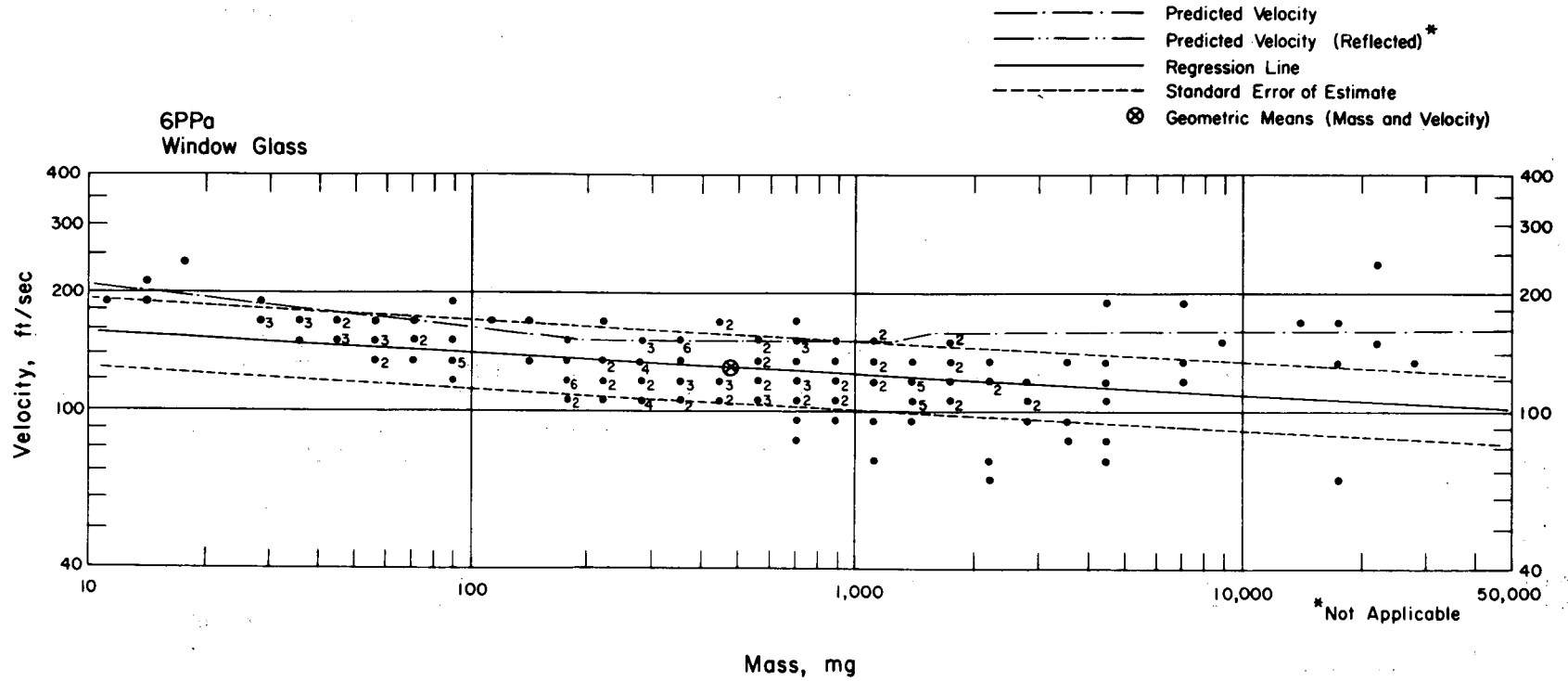


Fig. 4.72—Analysis of window-glass missiles from trap 6PPa: $d = 16.0$ ft; $n = 170$; $\log v = 2.2534 - 0.0534 \log m$; $E_{gv} = 1.22$; $M_{50} = 478$ mg; $V_{50} = 129$ ft/sec.

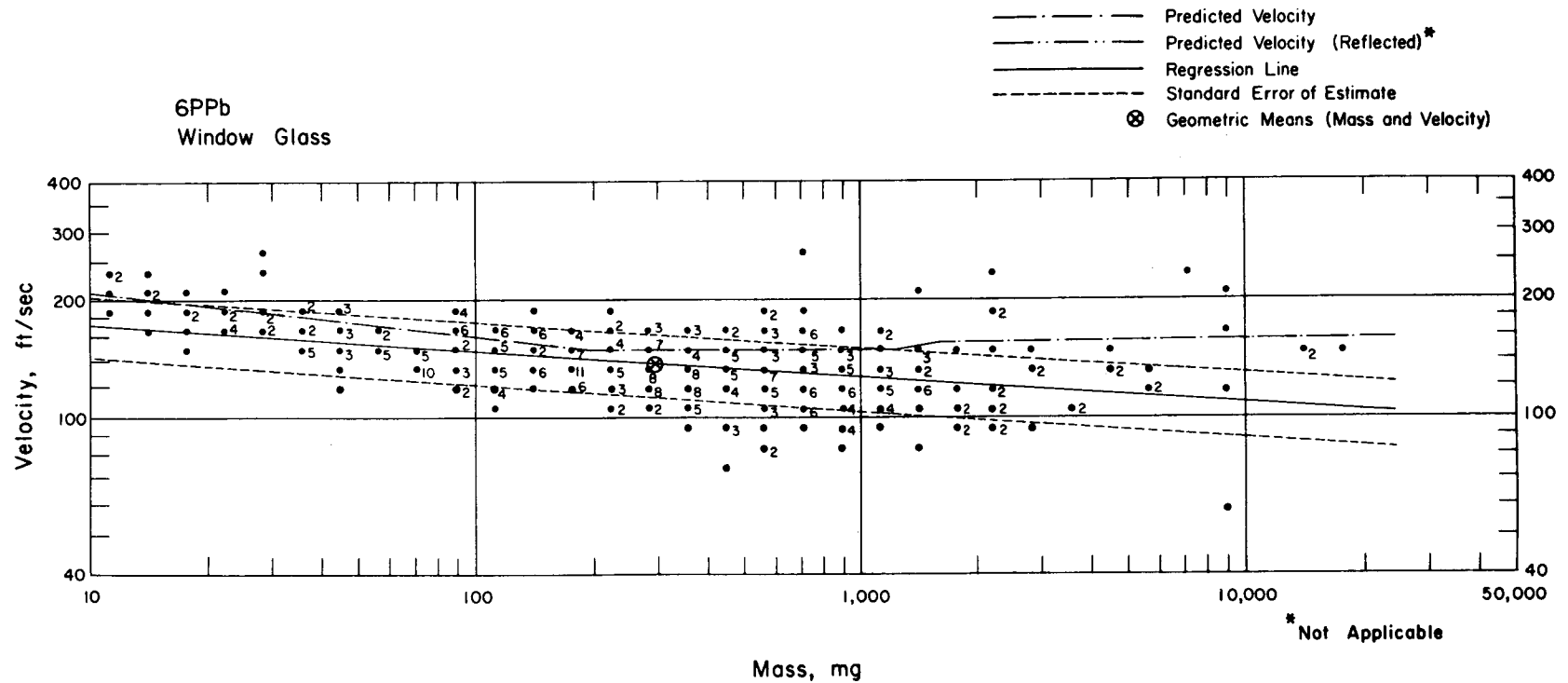


Fig. 4.73—Analysis of window-glass missiles from trap 6PPb: $d = 16.0$ ft; $n = 390$; $\log v = 2.3090 - 0.0678 \log m$; $E_{gv} = 1.21$; $M_{50} = 292$ mg; $V_{50} = 138$ ft/sec.

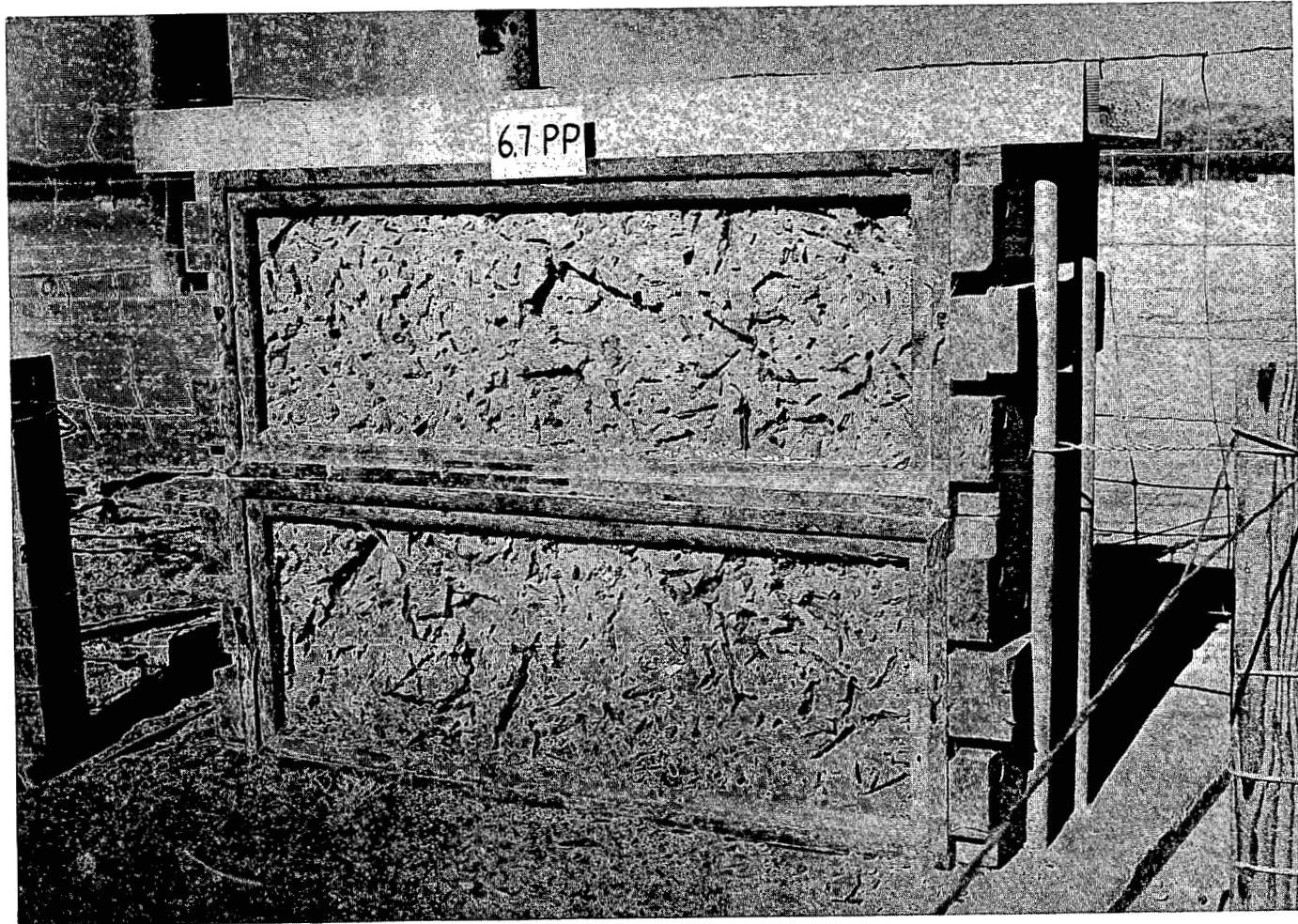


Fig. 4.74—Traps 6.7PPa and b, postshot.

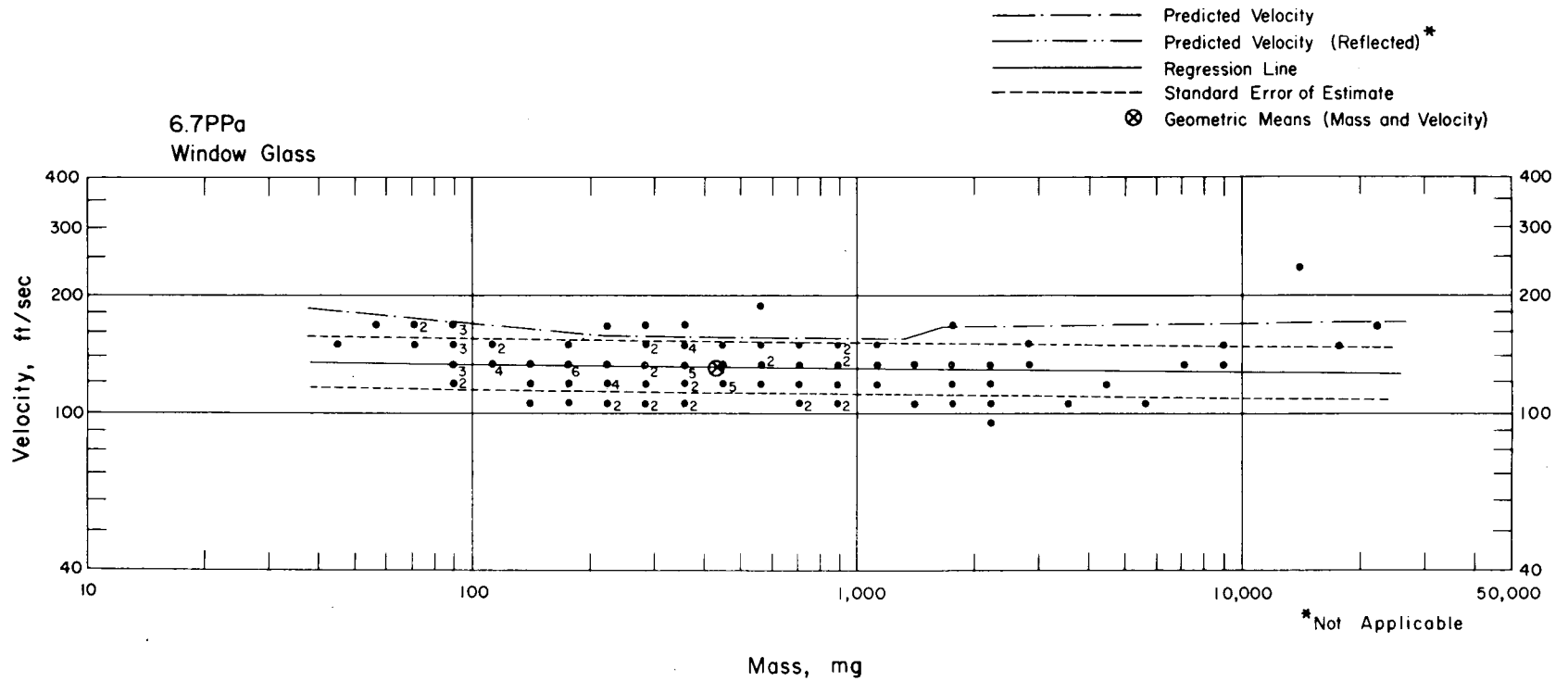


Fig. 4.75—Analysis of window-glass missiles from trap 6.7PPa: $d = 18.0$ ft; $n = 112$; $\log v = 2.1445 - 0.0086 \log m$; $E_{GV} = 1.16$; $M_{50} = 430$ mg; $V_{50} = 132$ ft/sec.

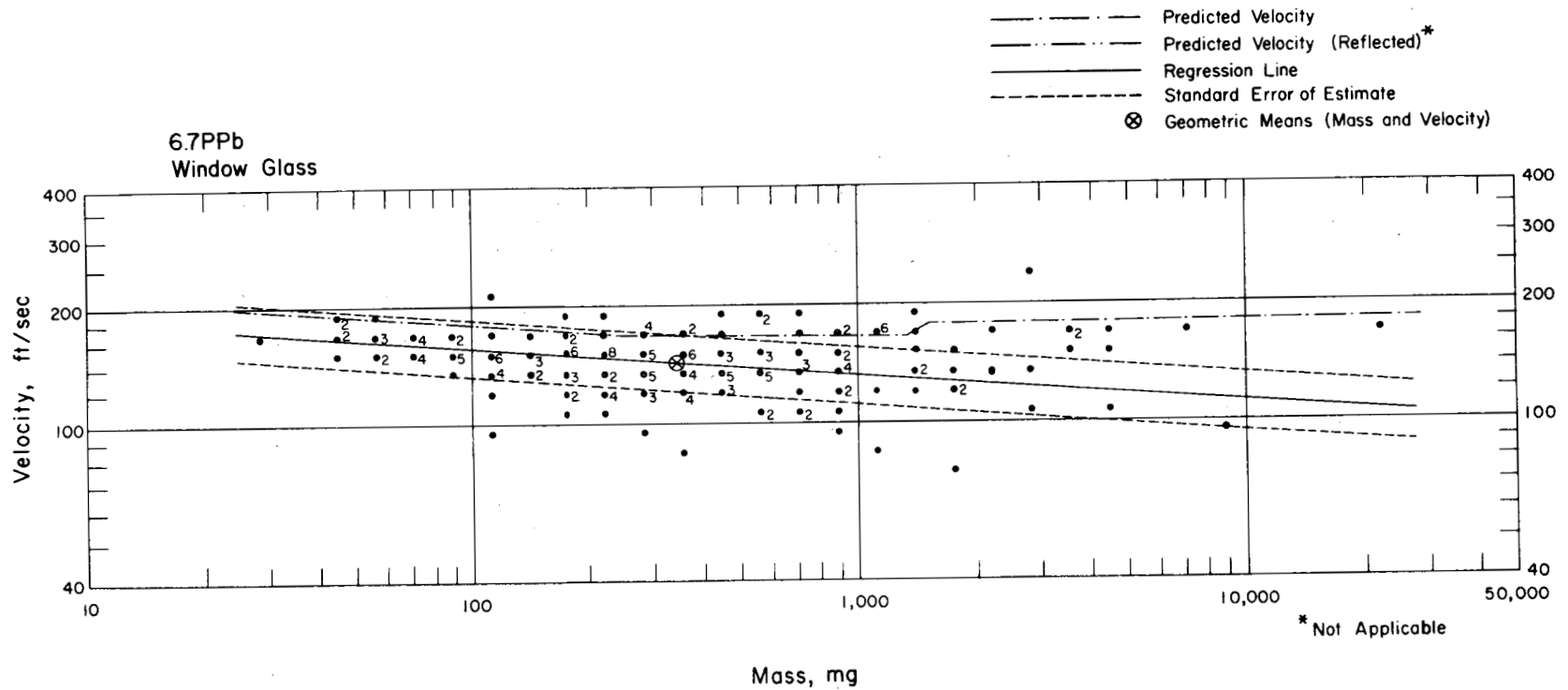


Fig. 4.76—Analysis of window-glass missiles from trap 6.7PPb: $d = 18.0$ ft; $n = 194$; $\log v = 2.2698 - 0.0281 \log mg$; $E_{gv} = 1.19$;
 $M_{50} = 344$ mg; $V_{50} = 142$ ft/sec.

8P STATION, RANGE 3930

MD Military Debris (B) blue
 Gr Gravel (W) white
 S Spheres (Y) yellow
 A Animal Trap

a—Window glass, $\frac{1}{8}$ " thick, framed and mounted
 b—Plate glass, $\frac{1}{4}$ " thick, framed and mounted

Note: MD, Gr, and S placed at 6.5', 16.8', and 43.0' from face of traps

Roman numeral in parenthesis designates type of missile absorber

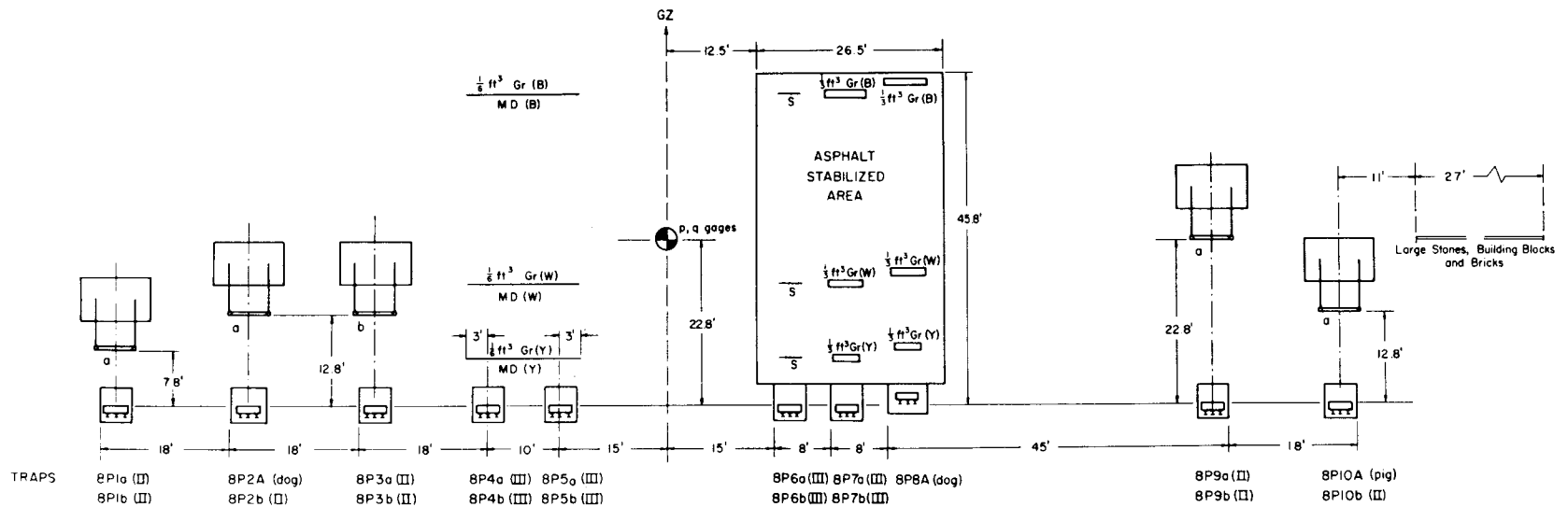


Fig. 4.77—Station 8P layout chart.

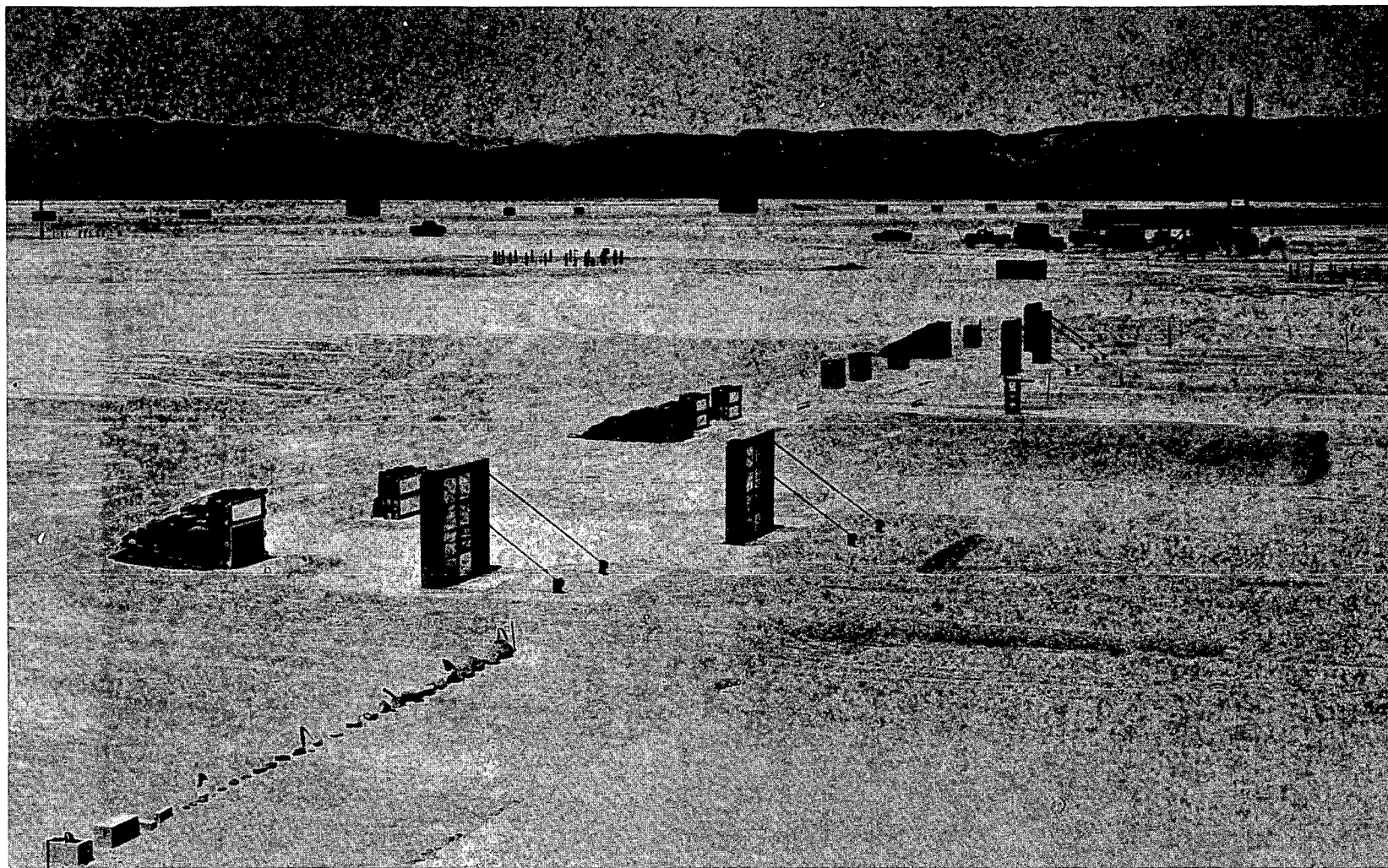


Fig. 4.78—Station 8P, preshot.

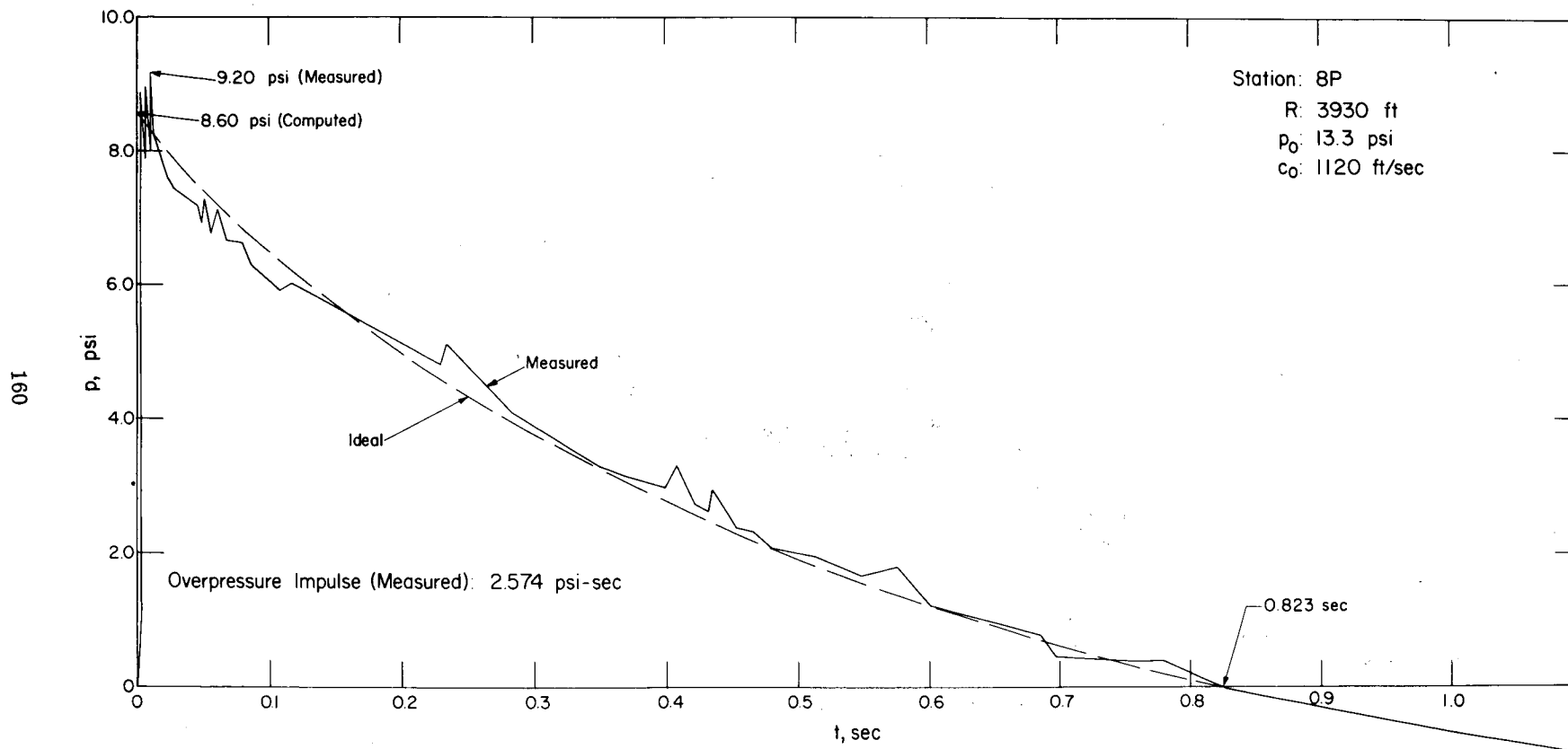


Fig. 4.79—Overpressure vs. time at station 8P.

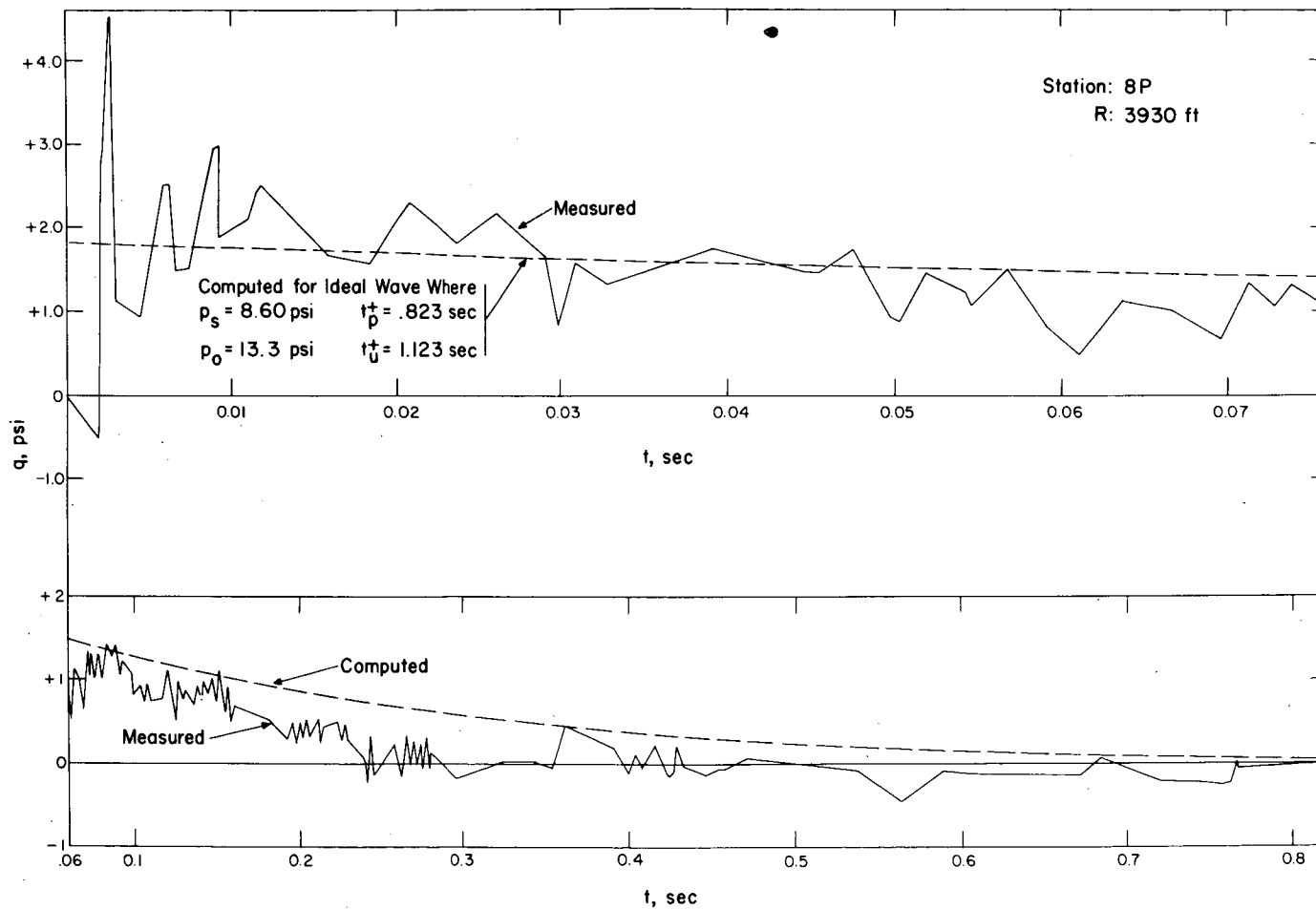


Fig. 4.80—Dynamic pressure vs. time at station 8P.

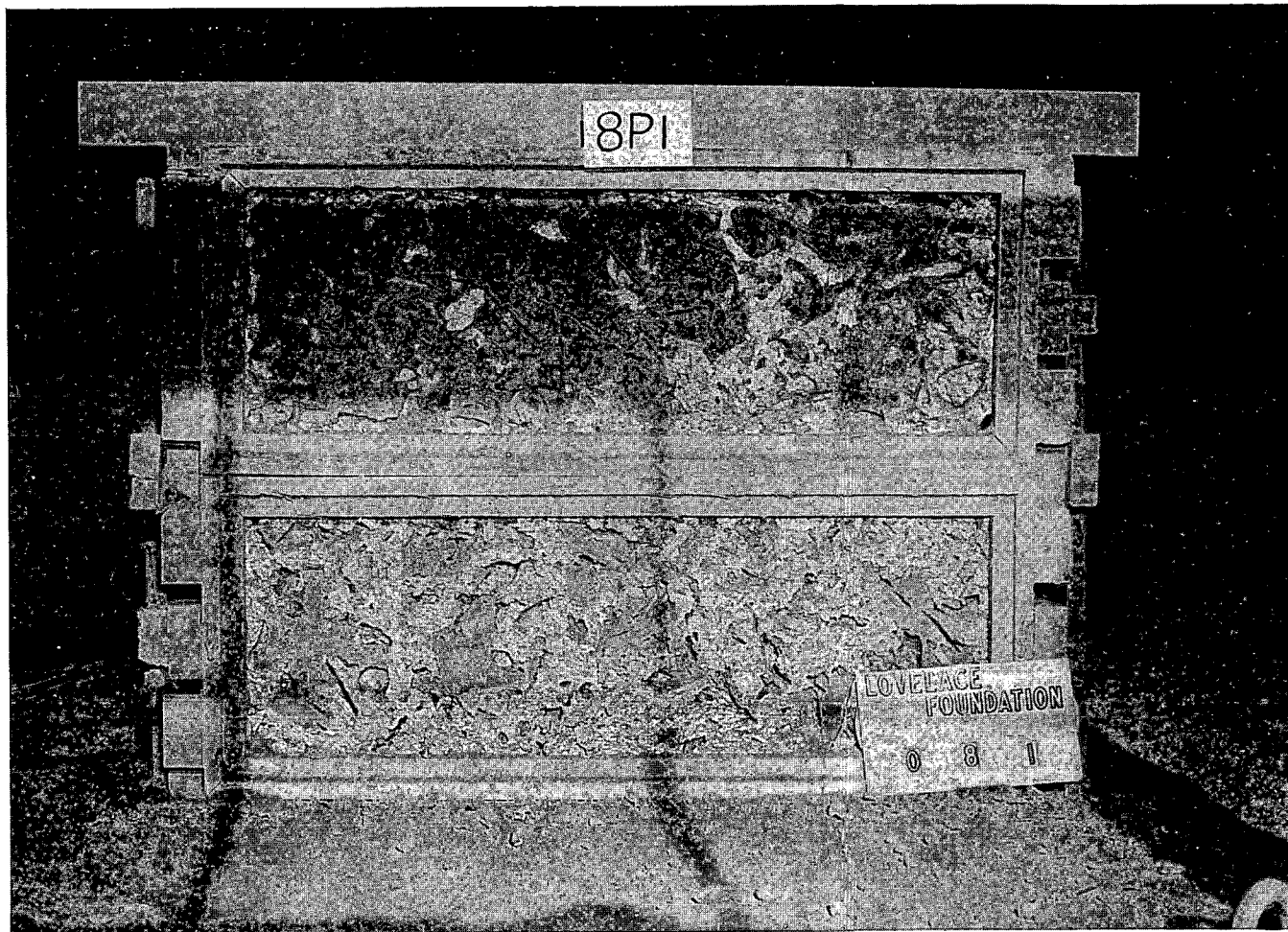


Fig. 4.81— Traps 8P1a and b, postshot.

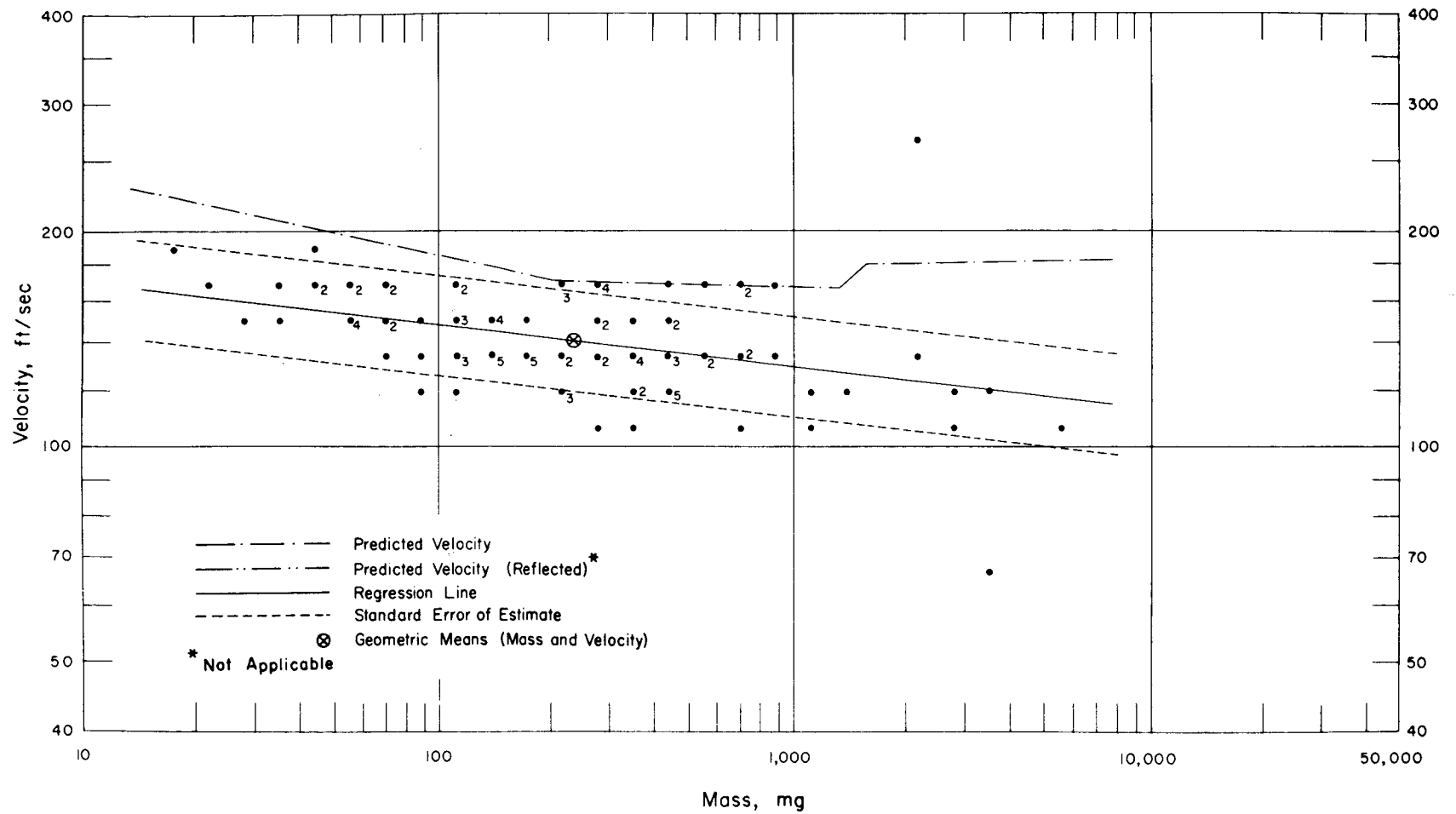


Fig. 4.82—Analysis of window-glass missiles from trap 8P1a: $d = 7.8$ ft; $n = 103$; $\log v = 2.2463 - 0.0410 \log m$; $E_{gv} = 1.18$; $M_{50} = 245$ mg; $V_{50} = 141$ ft/sec.

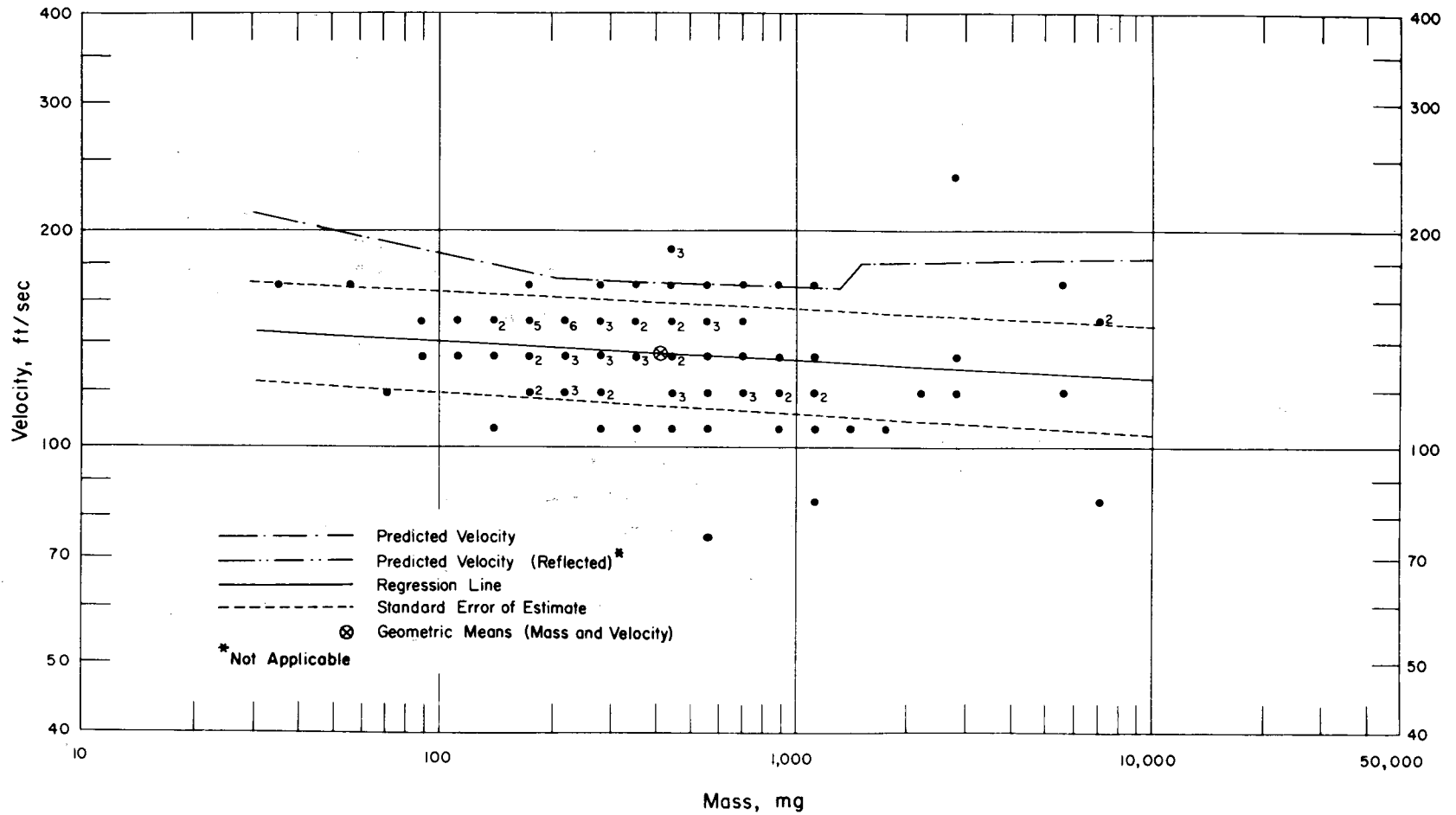


Fig. 4.83—Analysis of window-glass missiles from trap 8P1b: $d = 7.8$ ft; $n = 100$; $\log v = 2.2032 - 0.0276 \log m$; $E_{gv} = 1.19$; $M_{50} = 415$ mg; $V_{50} = 135$ ft/sec.

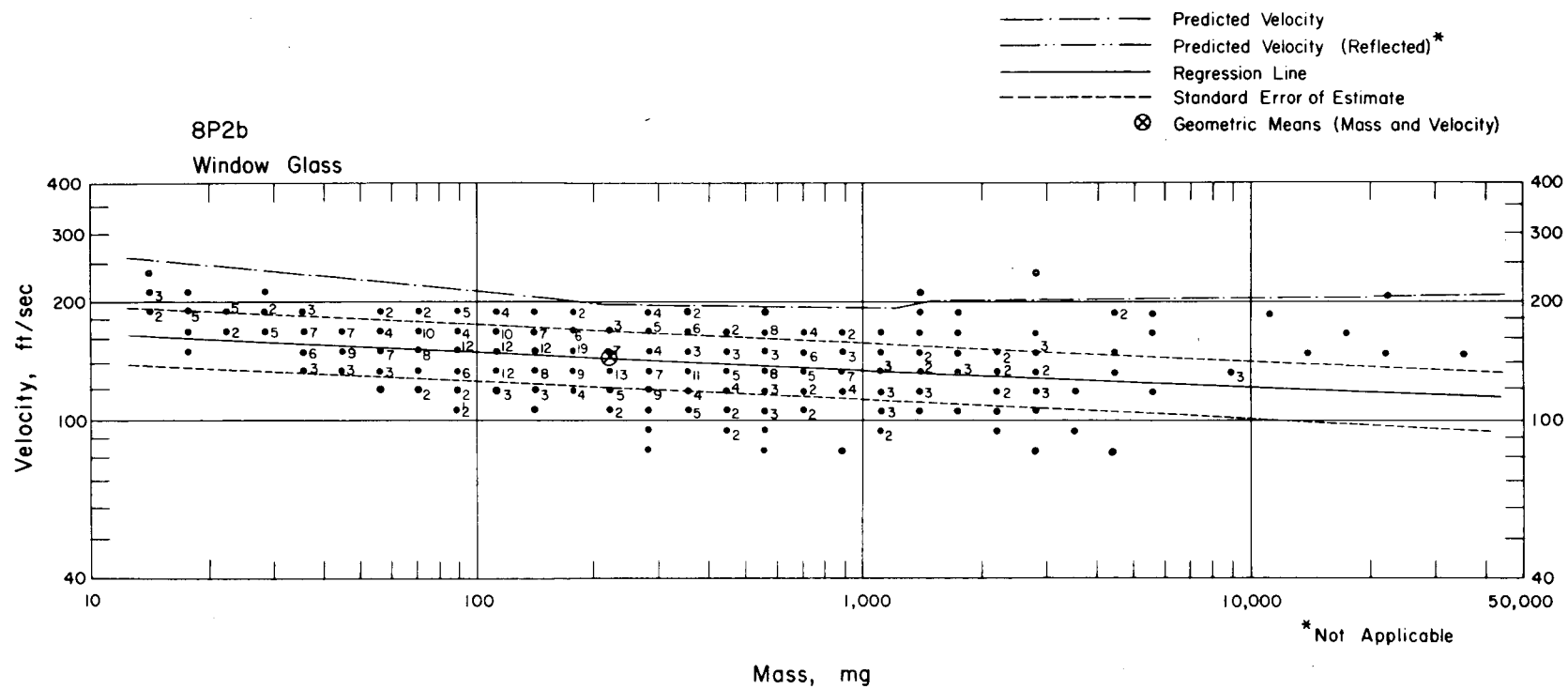


Fig. 4.84—Analysis of window-glass missiles from trap 8P2b: $d = 12.8$ ft; $n = 497$; $\log v = 2.2647 - 0.0443 \log m$; $E_{GV} = 1.18$; $M_{50} = 229$ mg; $V_{50} = 145$ ft/sec.

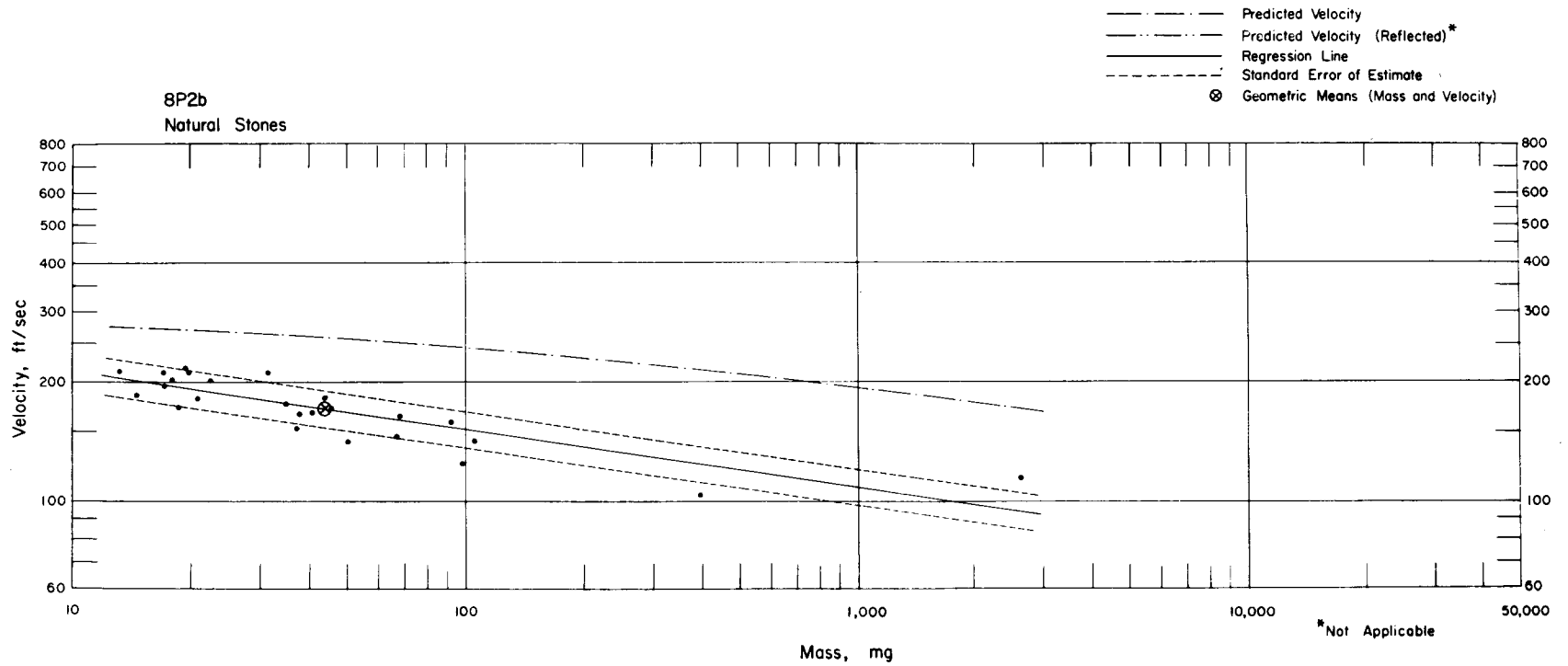


Fig. 4.85—Analysis of natural-stone missiles from trap 8P2b: $n = 25$; $\log v = 2.4717 - 0.1466 \log m$; $E_{gV} = 1.11$; $M_{50} = 43.6$ mg; $V_{50} = 170$ ft/sec.



Fig. 4.86—Traps 8P3a and b, postshot. Shadow of plate-glass frame, 12.8 ft from trap, can be seen. Note large indentations made in the absorber by glass that arrived flat and the dust and dirt on surface of white absorber.

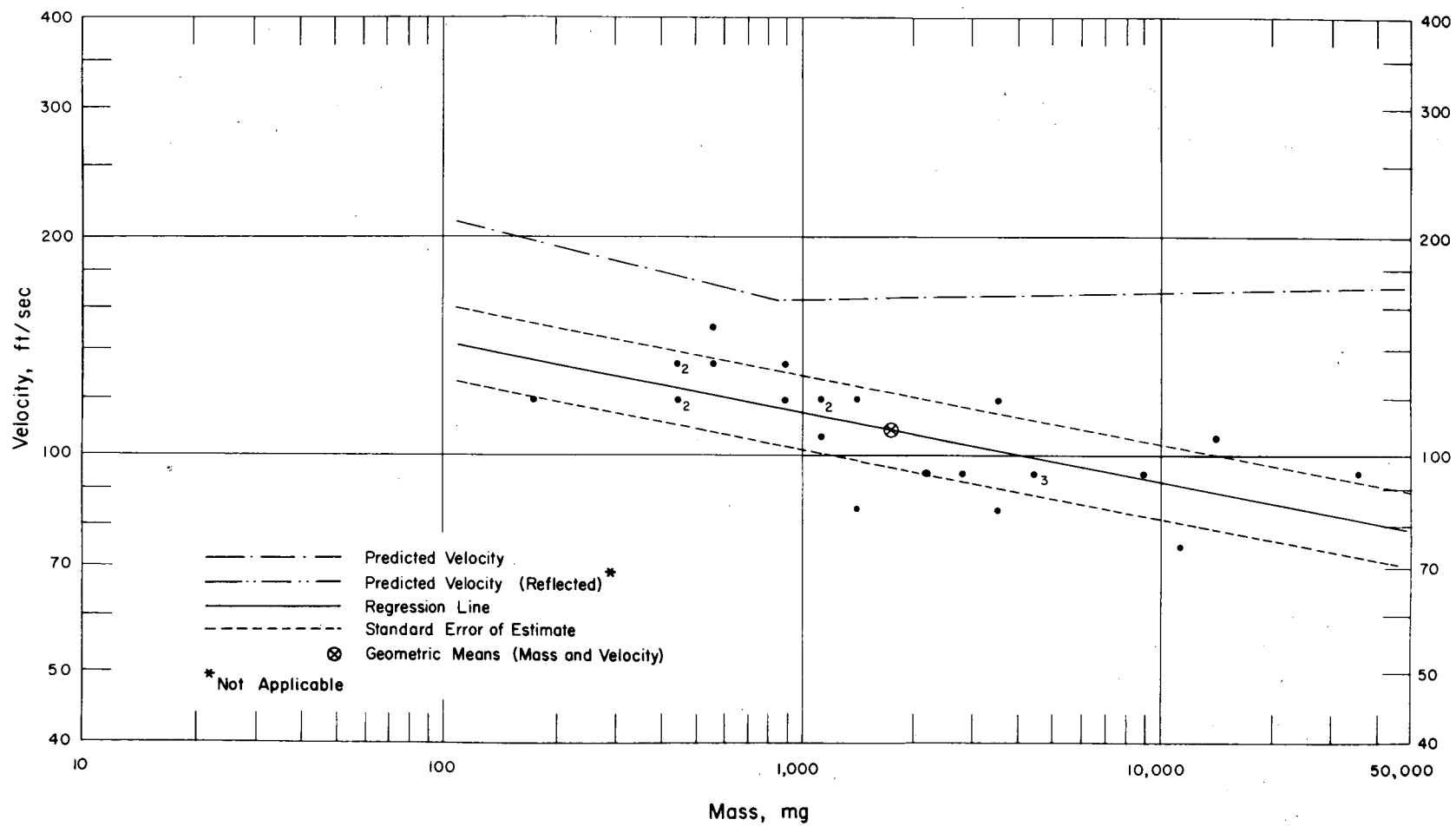


Fig. 4.87—Analysis of plate-glass missiles from trap 8P3a: $d = 12.8$ ft; $n = 25$; $\log v = 2.3450 - 0.0954 \log m$; $E_{gv} = 1.13$; $M_{50} = 1778$ mg; $V_{50} = 108$ ft/sec.

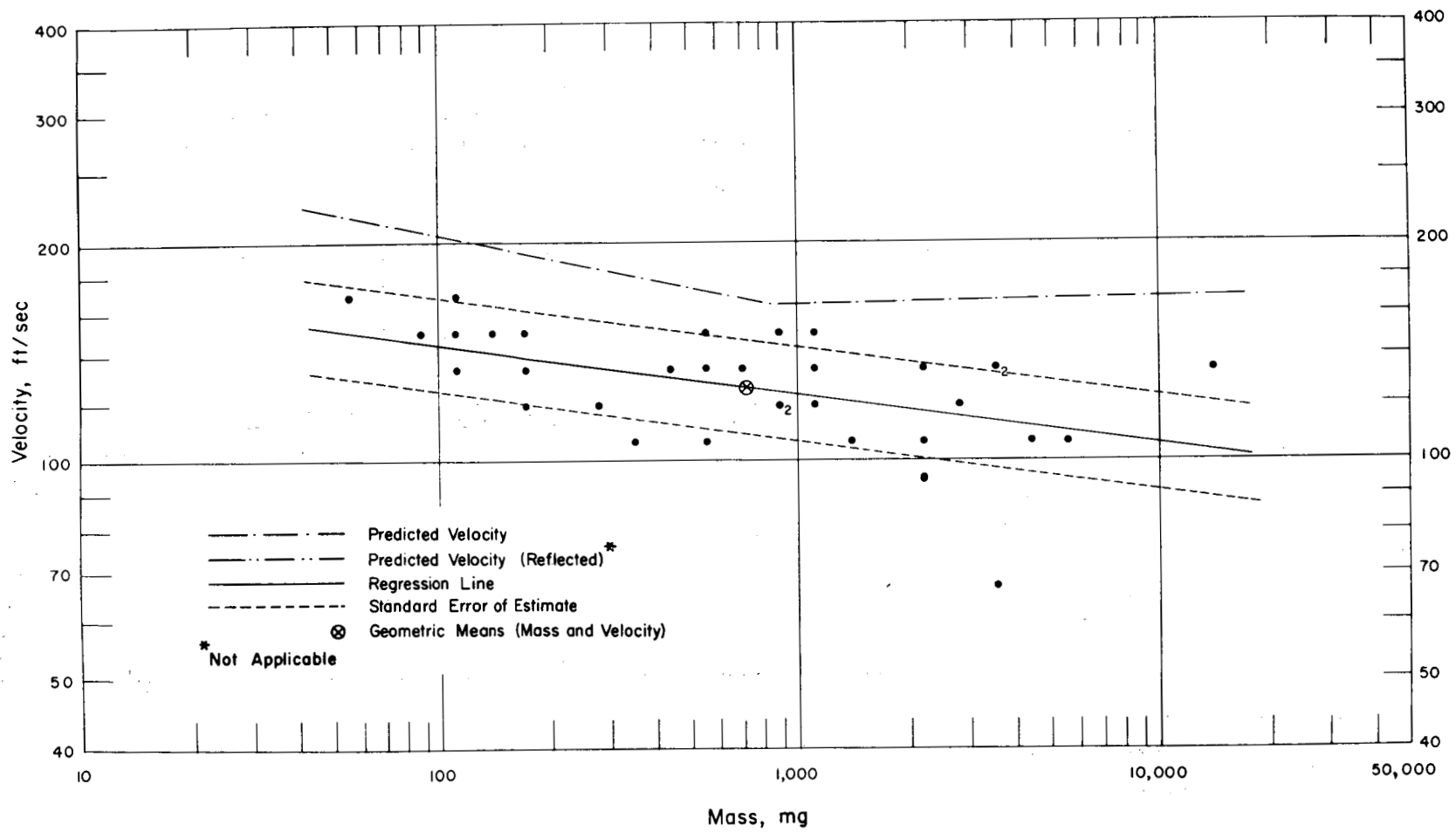


Fig. 4.88—Analysis of plate-glass missiles from trap 8P3b: $d = 12.8$ ft; $n = 33$; $\log v = 2.2992 - 0.0694 \log m$; $E_{gv} = 1.16$; $M_{50} = 723$ mg; $V_{50} = 126$ ft/sec.

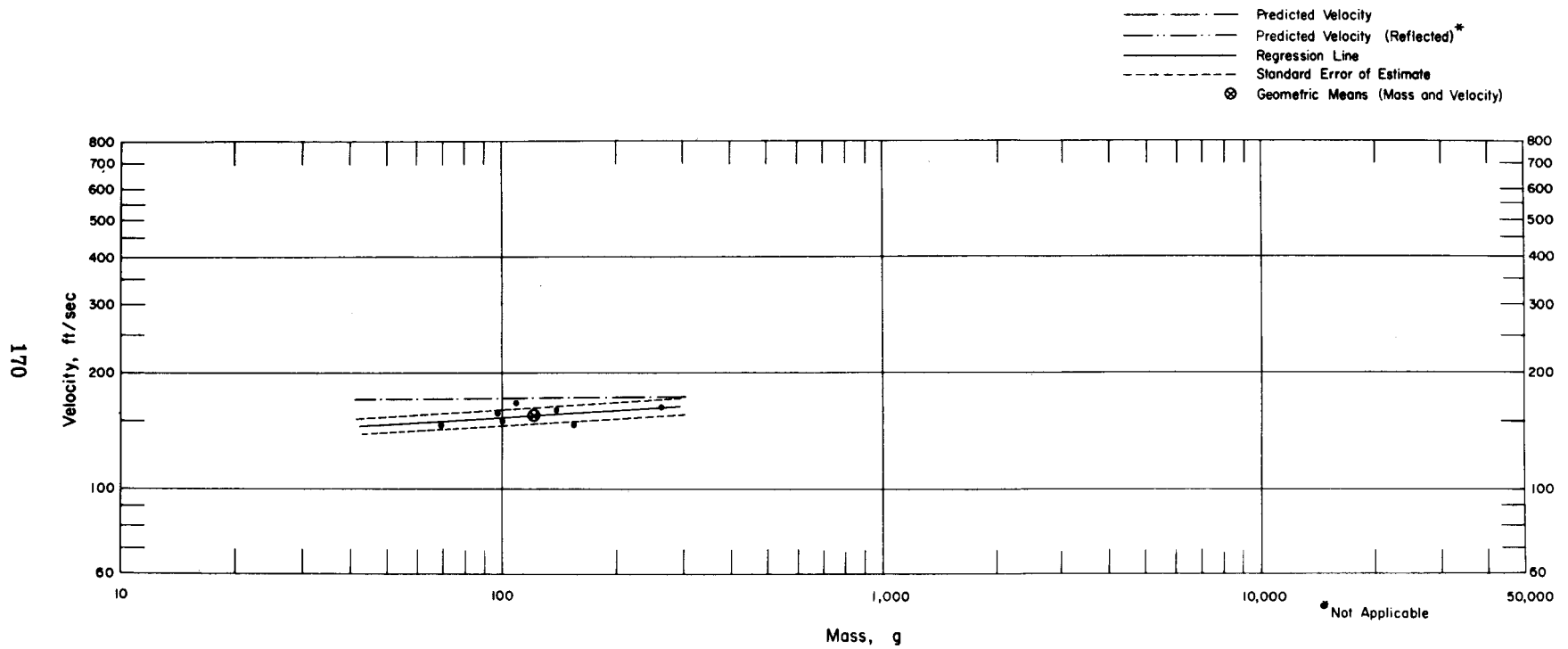


Fig. 4.89—Analysis of plate-glass missiles that arrived flat at trap 8P3b: $d = 12.8$ ft; $n = 7$; $\log v = 1.0918 + 0.0568 \log m$ (mg); $E_{gv} = 1.06$; $M_{50} = 123,000$ mg; $V_{50} = 155$ ft/sec.

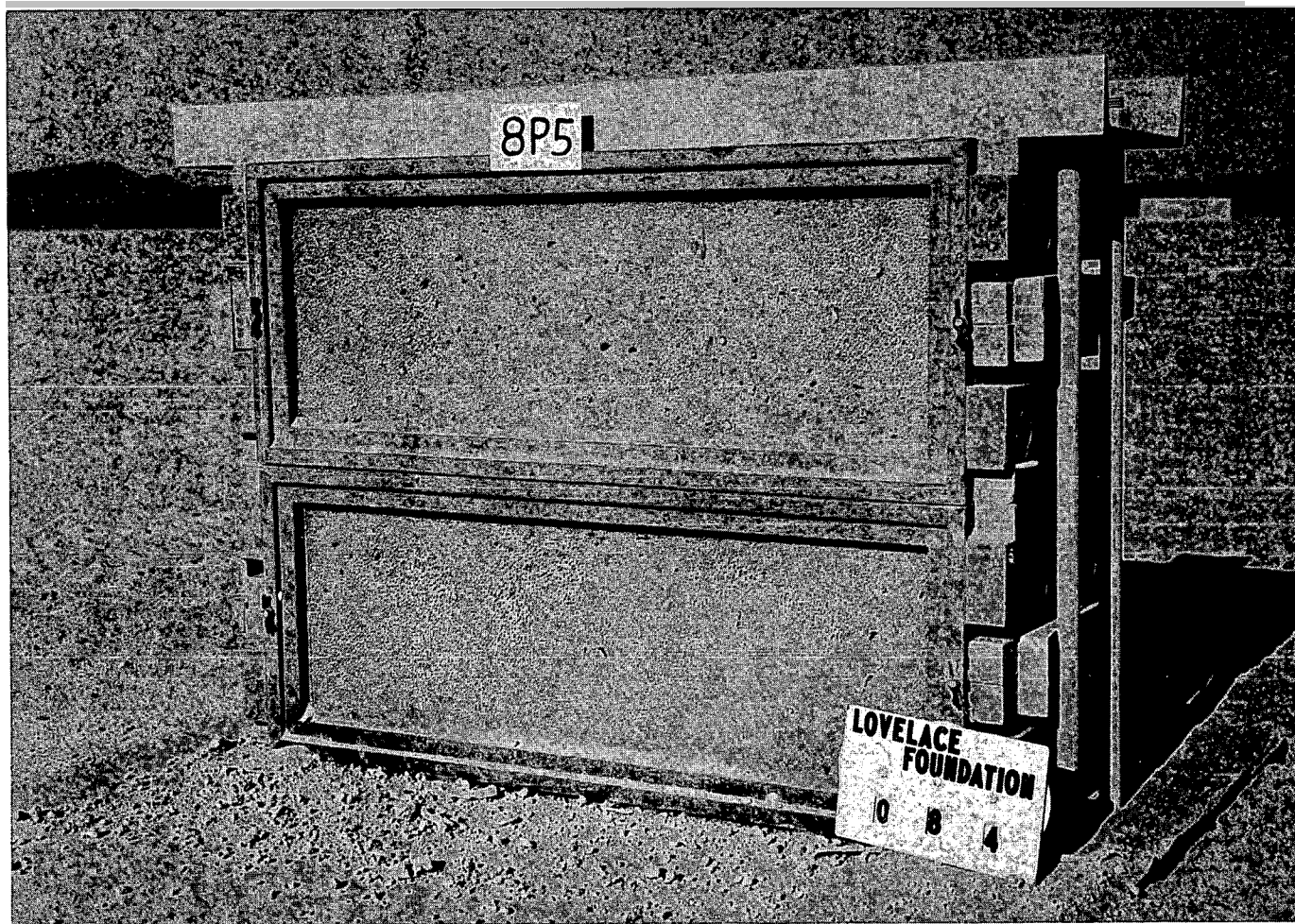


Fig. 4.90—Traps 8P5a and b, postshot. Gravel and military debris were set out in front of the traps at three locations. Surface of absorber was somewhat damaged by thermal energy from the bomb.

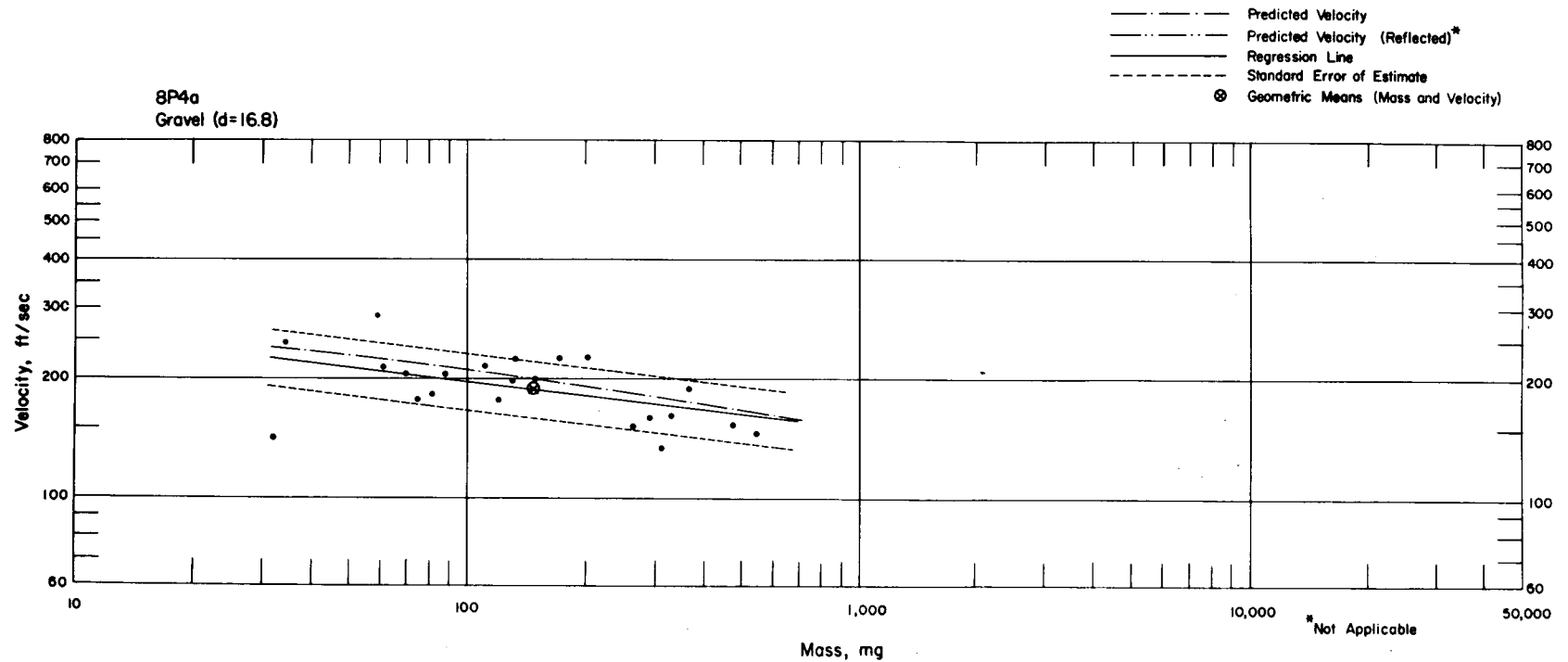


Fig. 4.91—Analysis of gravel missiles from trap 8P4a: $d = 16.8$ ft; $n = 23$; $\log v = 2.5226 - 0.1159 \log m$; $E_{gy} = 1.19$; $M_{50} = 146$ mg; $V_{50} = 187$ ft/sec.

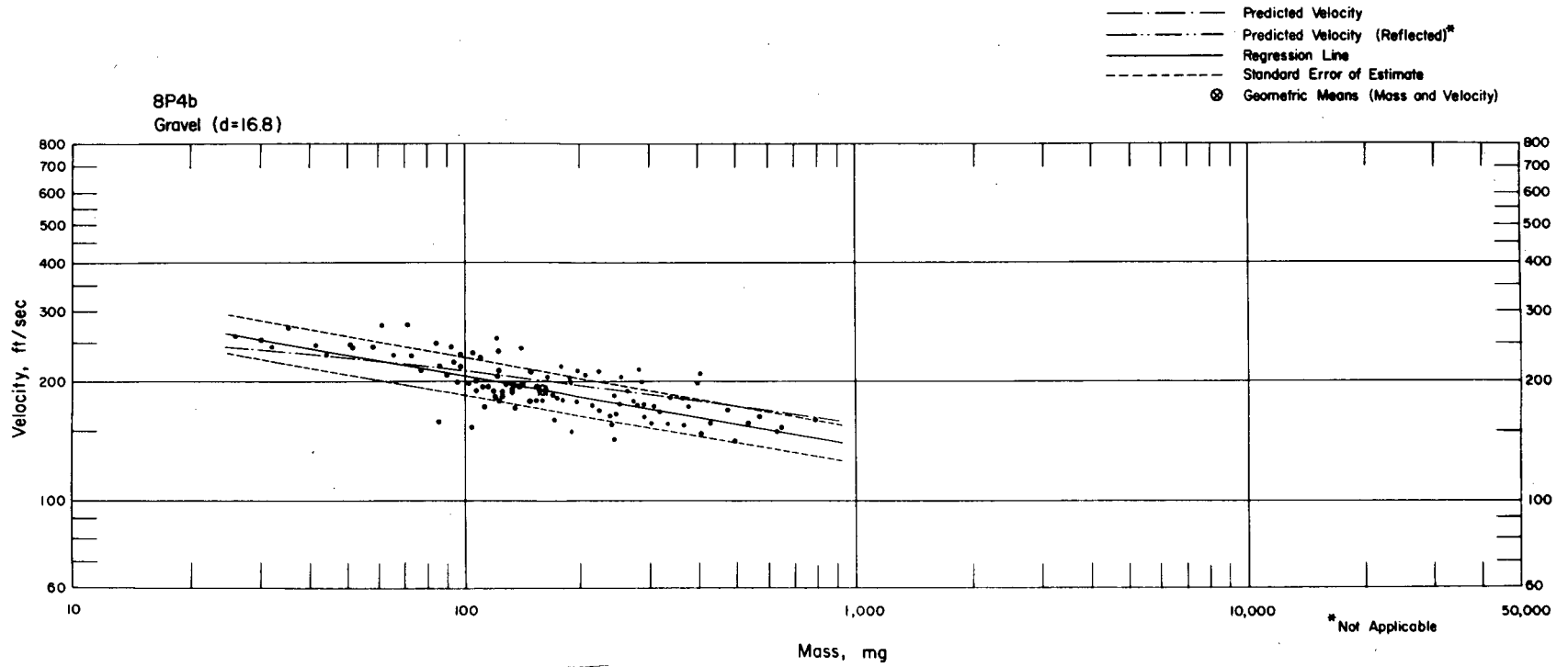


Fig. 4.92—Analysis of gravel missiles from trap 8P4b: $d = 16.8$ ft; $n = 103$; $\log v = 2.6573 - 0.1701 \log m$; $E_{gv} = 1.11$; $M_{50} = 157$ mg; $V_{50} = 192$ ft/sec.

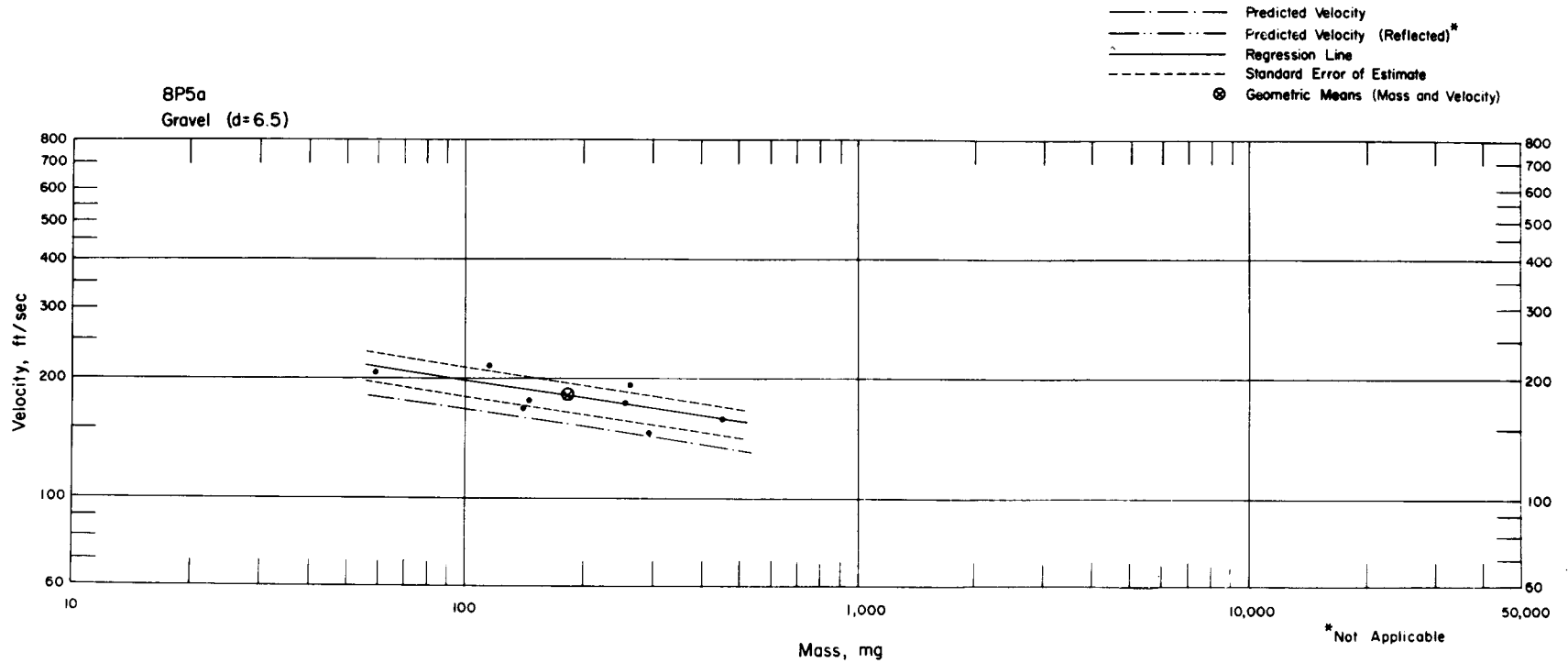


Fig. 4.93—Analysis of gravel missiles from trap 8P5a: $d = 6.5$ ft; $n = 8$; $\log v = 2.5909 - 0.1486 \log m$; $E_{gv} = 1.10$; $M_{50} = 183$ mg; $V_{50} = 180$ ft/sec.

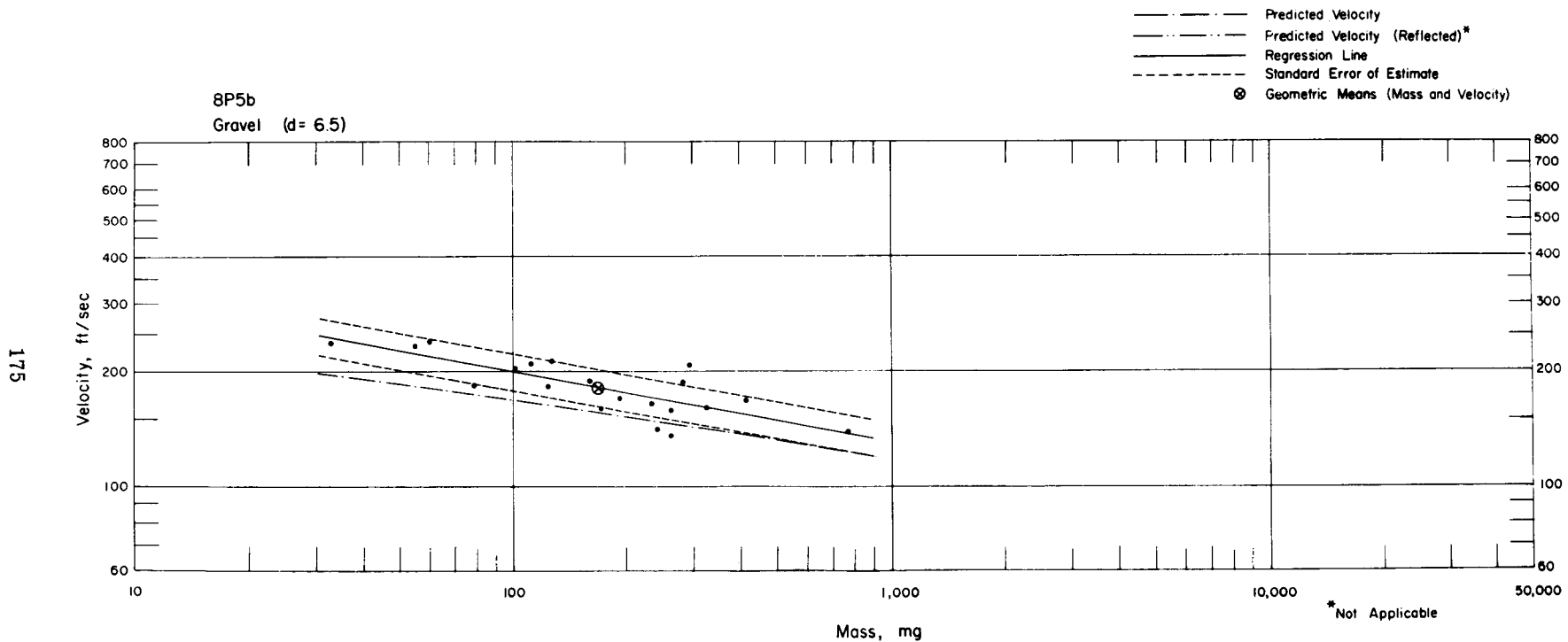


Fig. 4.94—Analysis of gravel missiles from trap 8P5b: $d = 6.5$ ft; $n = 20$; $\log v = 2.6573 - 0.1801 \log m$; $E_{GV} = 1.12$; $M_{50} = 165$ mg; $V_{50} = 181$ ft/sec.

5

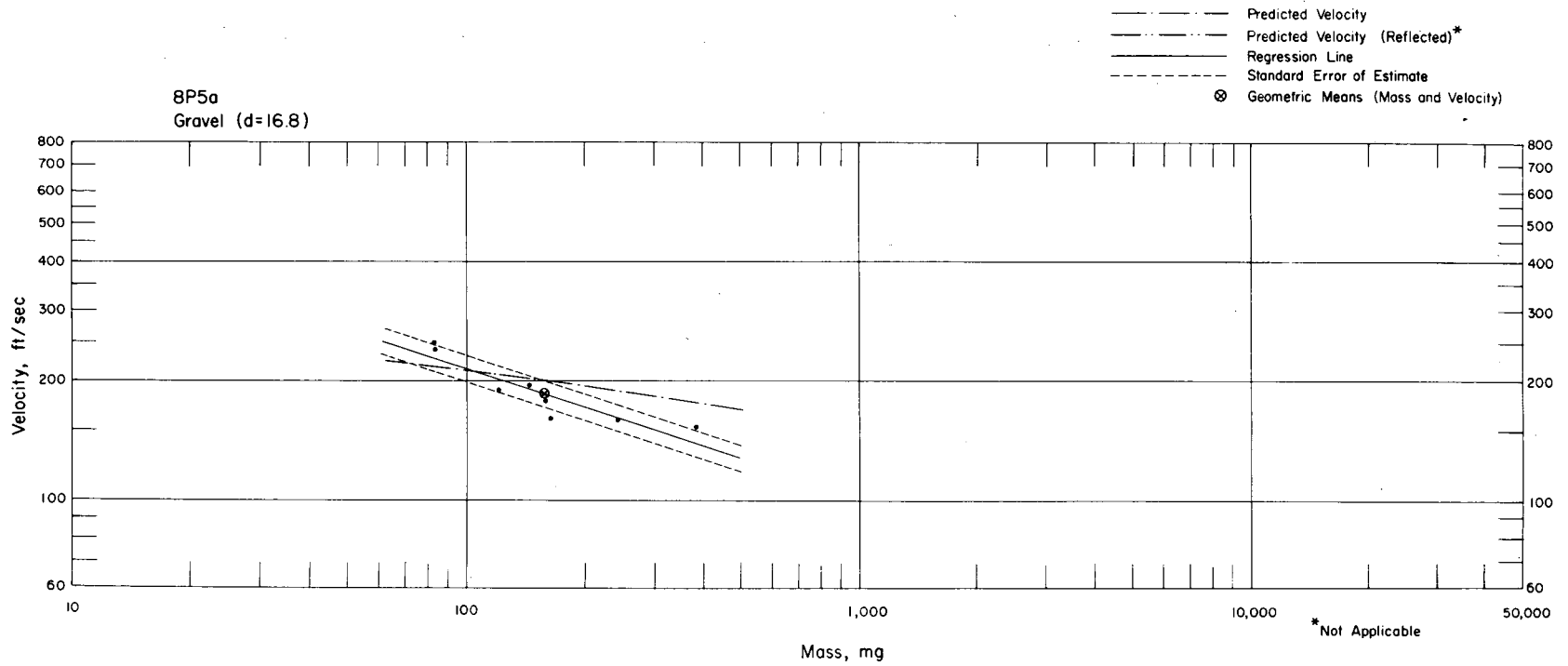


Fig. 4.95—Analysis of gravel missiles from trap 8P5a: $d = 16.8$ ft; $n = 8$; $\log v = 2.9724 - 0.3212 \log m$; $E_{gv} = 1.09$; $M_{50} = 152$ mg; $V_{50} = 187$ ft/sec.

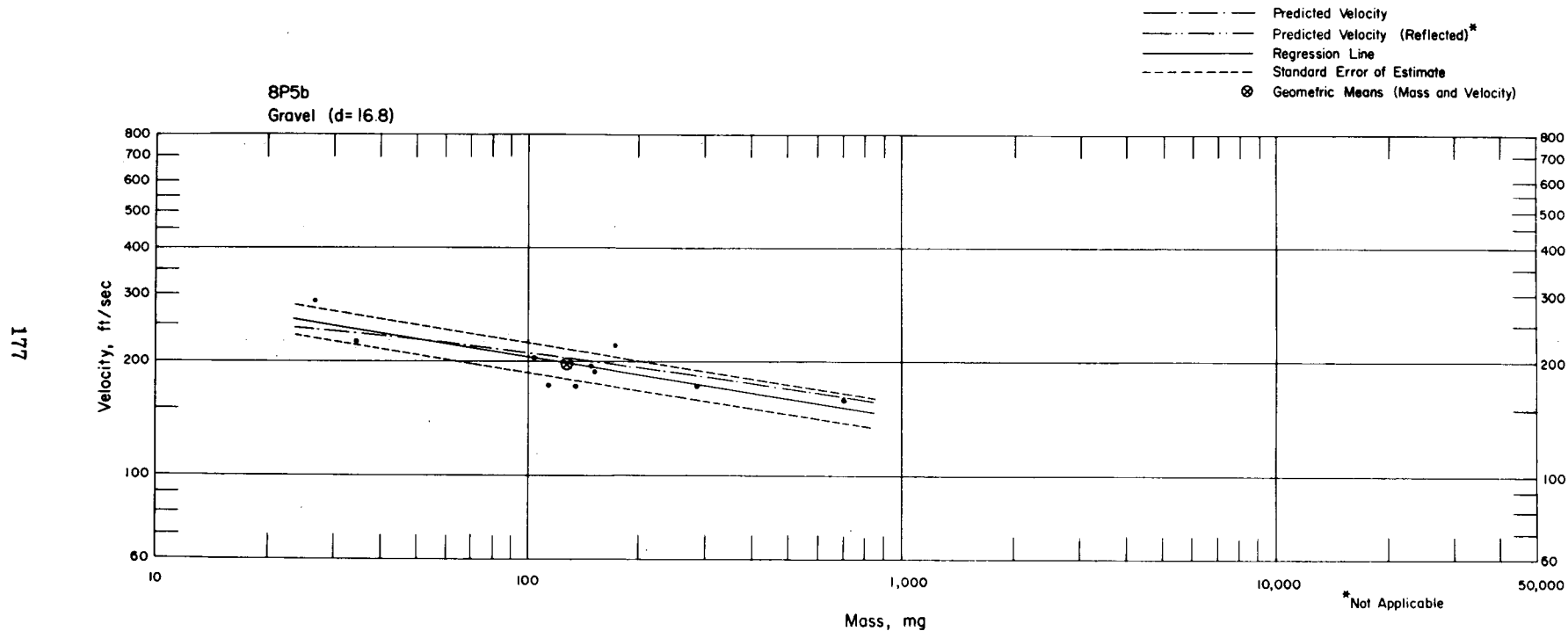


Fig. 4.96—Analysis of gravel missiles from trap 8P5b: $d = 16.8$ ft; $n = 10$; $\log v = 2.6275 - 0.1571 \log m$; $E_{gv} = 1.11$; $M_{50} = 128$ mg; $V_{50} = 198$ ft/sec.

178

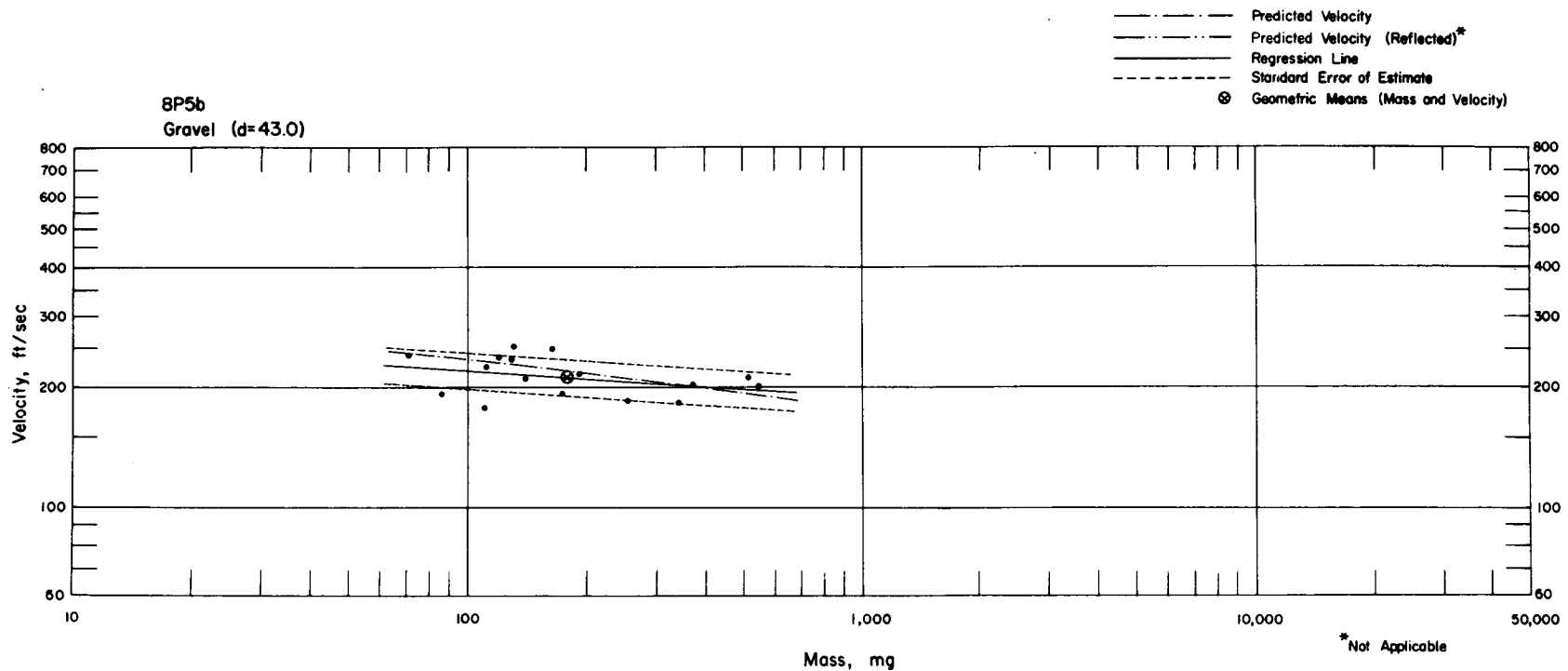


Fig. 4.97—Analysis of gravel missiles from trap 8P5b: $d = 43.0$ ft, $n = 16$; $\log v = 2.4748 - 0.0661 \log m$; $E_{gv} = 1.12$; $M_{50} = 178$ mg; $V_{50} = 212$ ft/sec.

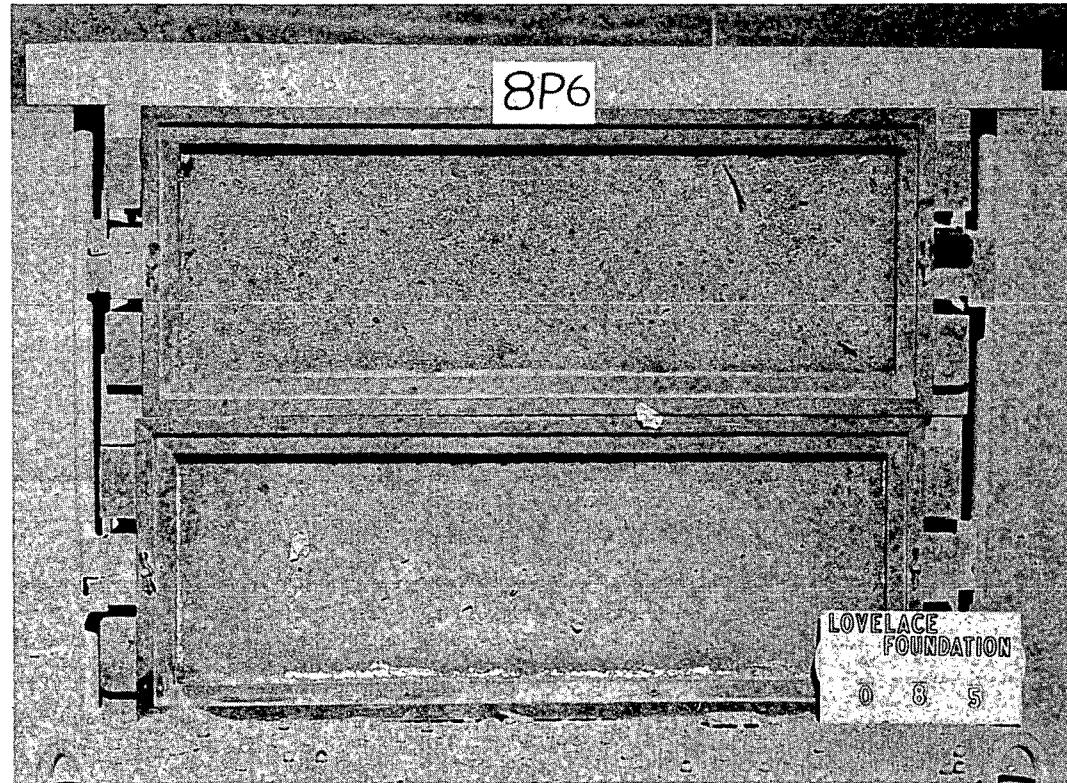


Fig. 4.98—Sphere installation 8P6, postshot. (Behind asphalt area.)

180

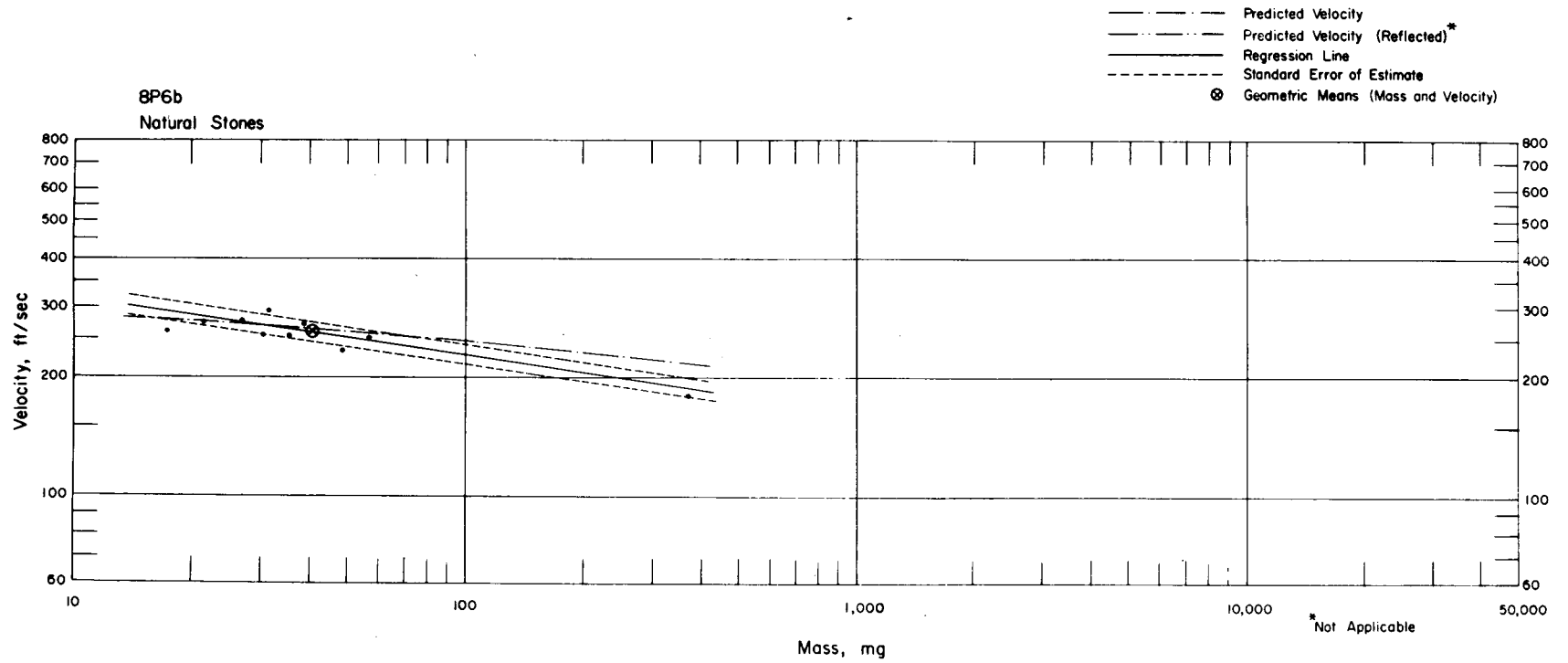


Fig. 4.99—Analysis of natural-stone missiles from trap 8P6b: $n = 10$; $\log v = 2.6403 - 0.1456 \log m$; $E_{gv} = 1.07$; $M_{50} = 40.9$ mg; $V_{50} = 254$ ft/sec.

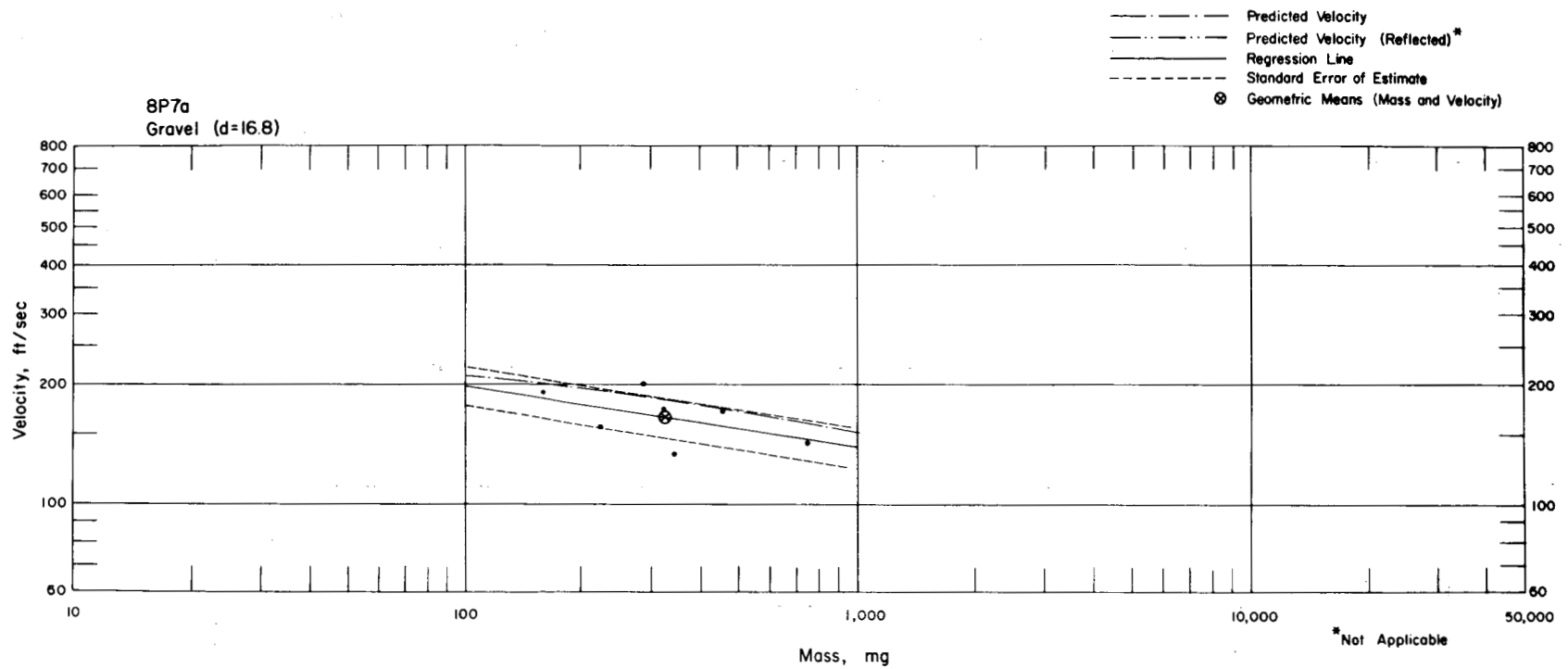


Fig. 4.100—Analysis of gravel missiles from trap 8P7a: $d = 16.8$ ft; $n = 7$; $\log v = 2.6117 - 0.1564 \log m$; $E_{gv} = 1.15$; $M_{50} = 324$ mg; $V_{50} = 166$ ft/sec.

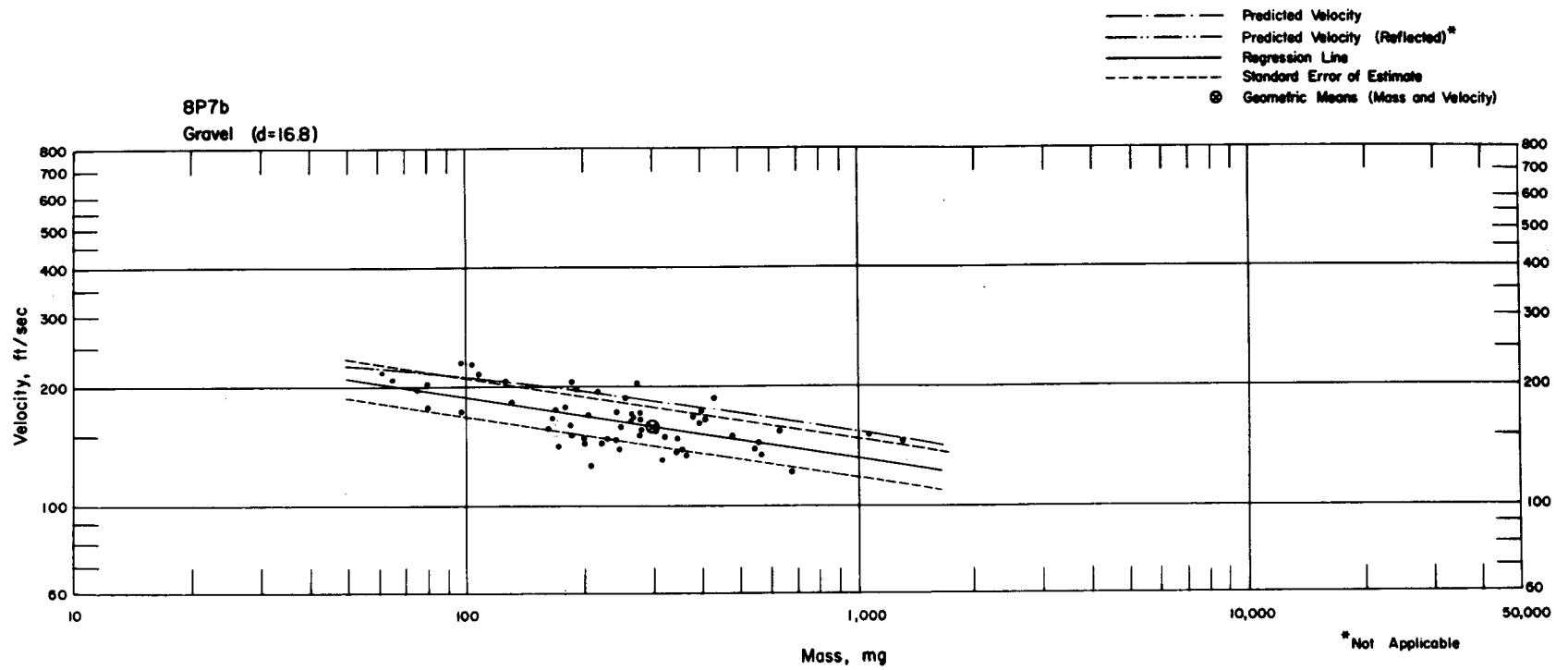


Fig. 4.101—Analysis of gravel missiles from trap 8P7b: $d = 16.8$ ft; $n = 60$; $\log v = 2.5813 - 0.1536 \log m$; $E_{gv} = 1.12$; $M_{50} = 239$ mg; $V_{50} = 164$ ft/sec.

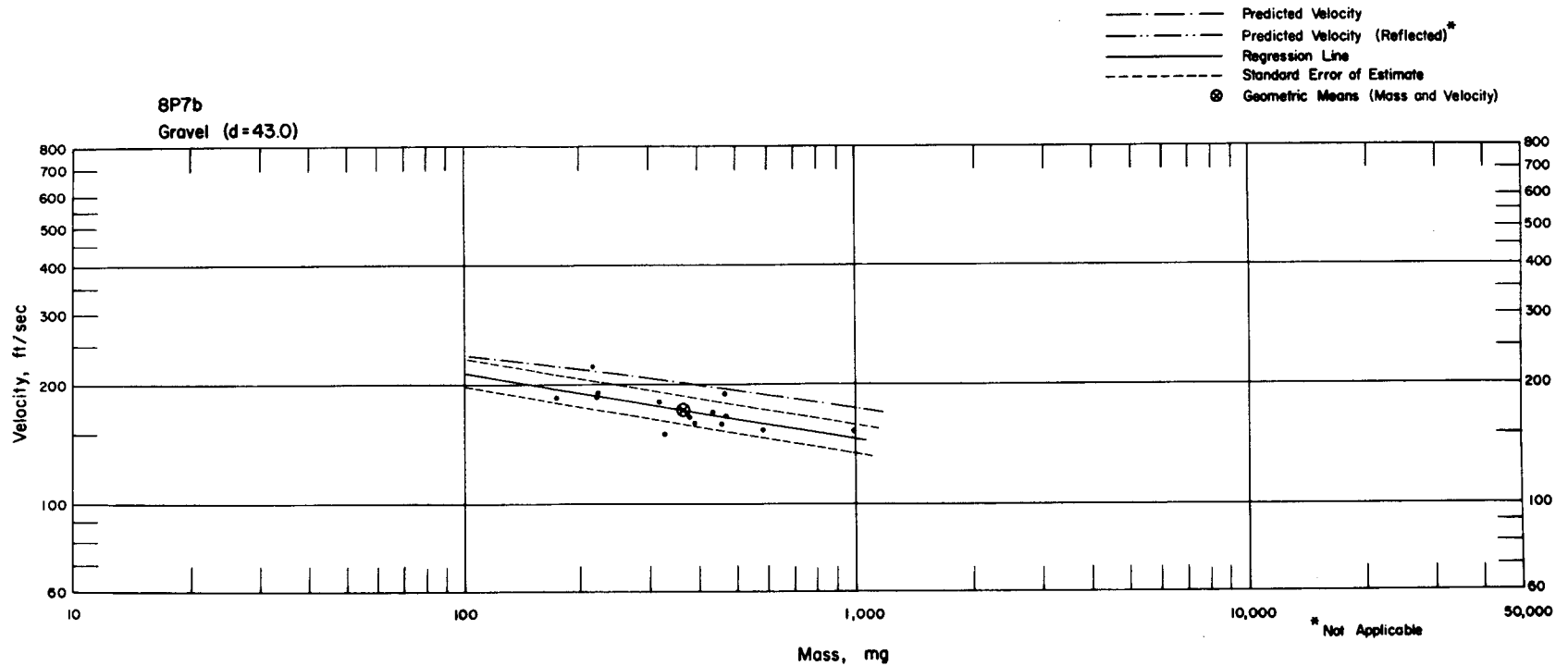


Fig. 4.102—Analysis of gravel missiles from trap 8P7b: $d = 43.0$ ft; $n = 14$; $\log v = 2.6552 - 0.1639 \log m$; $E_{gy} = 1.09$; $M_{50} = 363$ mg; $V_{50} = 172$ ft/sec.

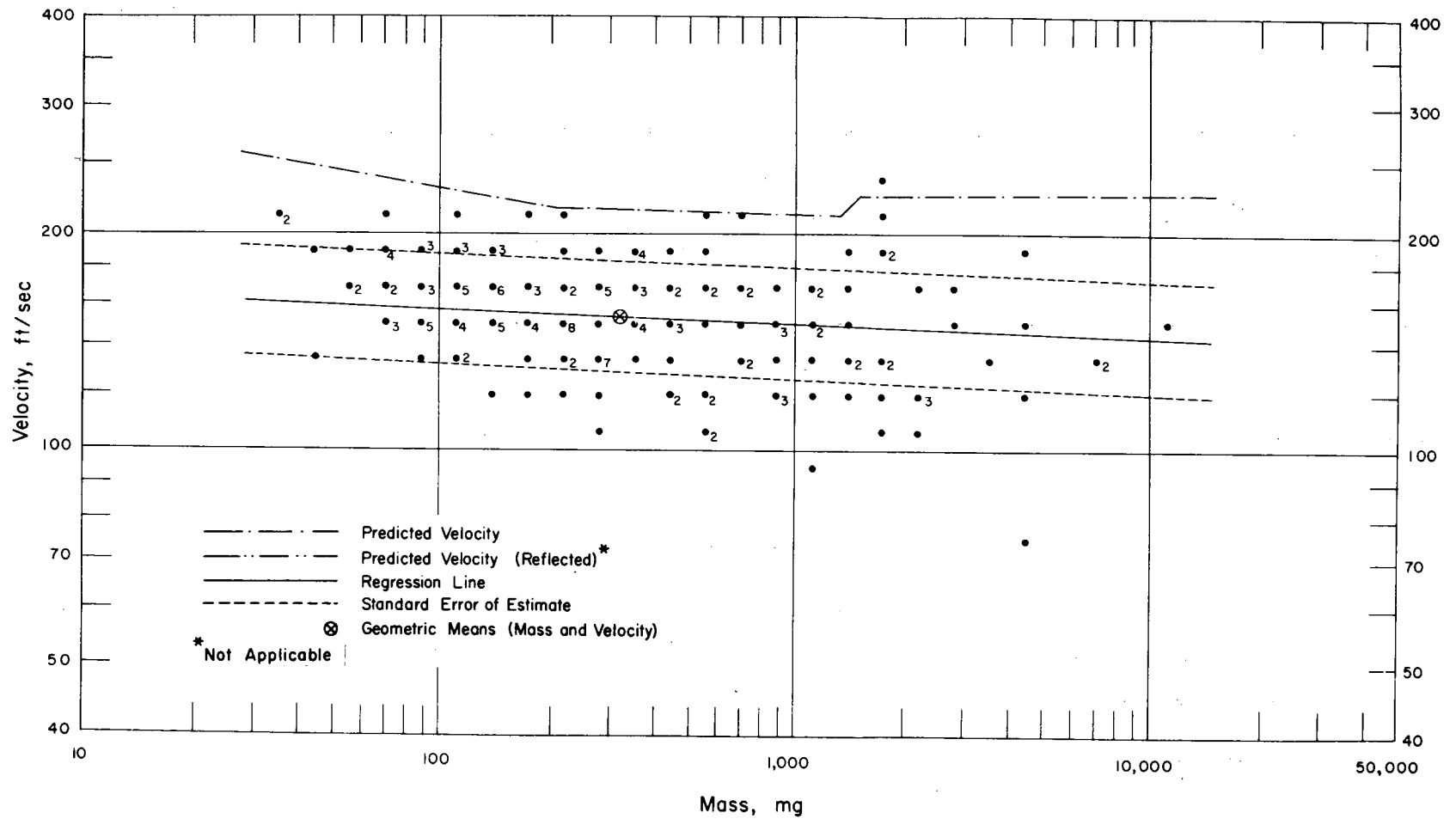


Fig. 4.103—Analysis of window-glass missiles from trap 8P9a: $d = 22.8$ ft; $n = 180$; $\log v = 2.2339 - 0.0191 \log m$; $E_{GV} = 1.19$; $M_{50} = 318$ mg; $V_{50} = 154$ ft/sec.

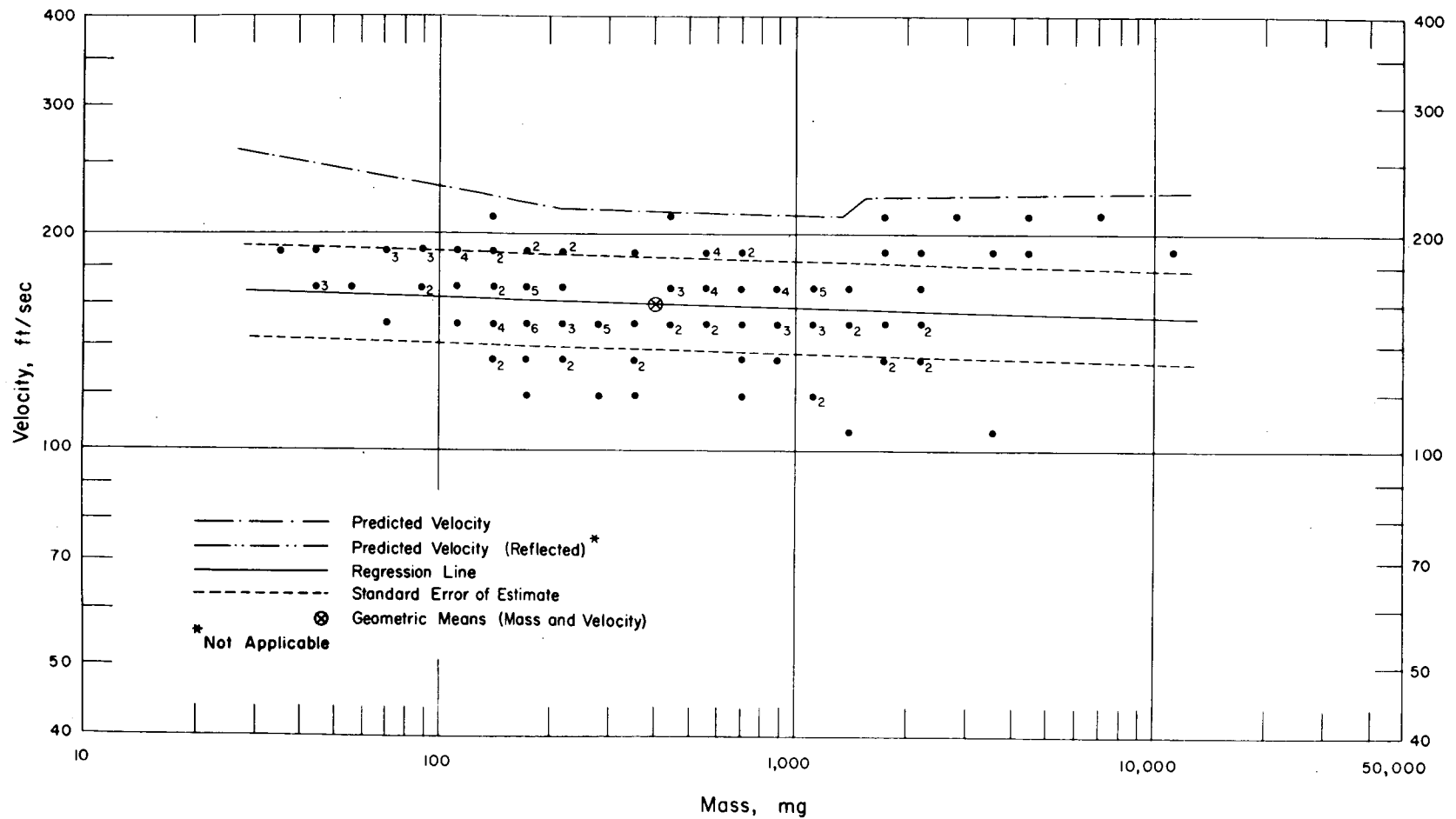


Fig. 4.104—Analysis of window-glass missiles from trap 8P9b: $d = 22.8$ ft; $n = 129$; $\log v = 2.2433 - 0.0143 \log m$; $E_{gv} = 1.16$; $M_{50} = 403$ mg; $V_{50} = 161$ ft/sec.

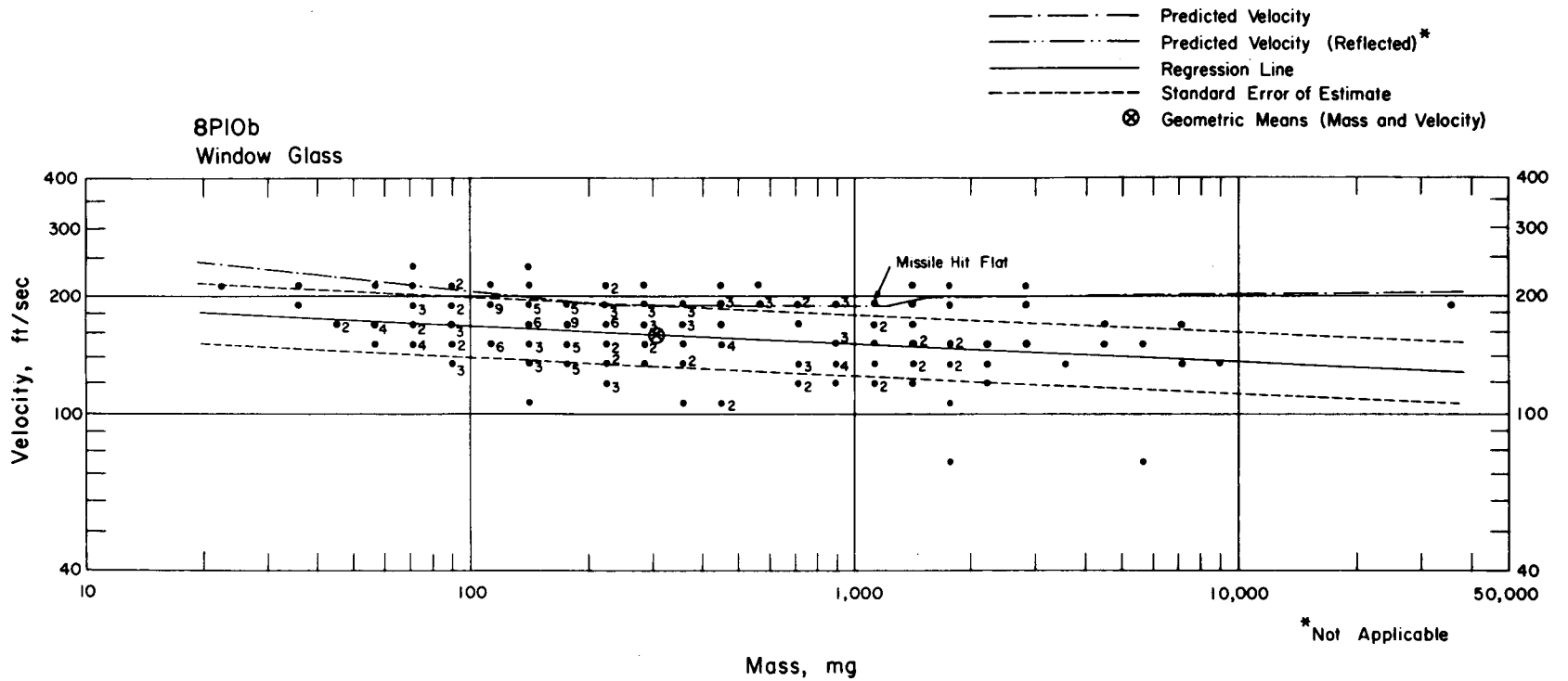


Fig. 4.105—Analysis of window-glass missiles from trap 8PI0b: $d = 12.8$ ft; $n = 204$; $\log v = 2.3216 - 0.0470 \log m$; $E_{gv} = 1.20$; $M_{50} = 302$ mg; $V_{50} = 160$ ft/sec.

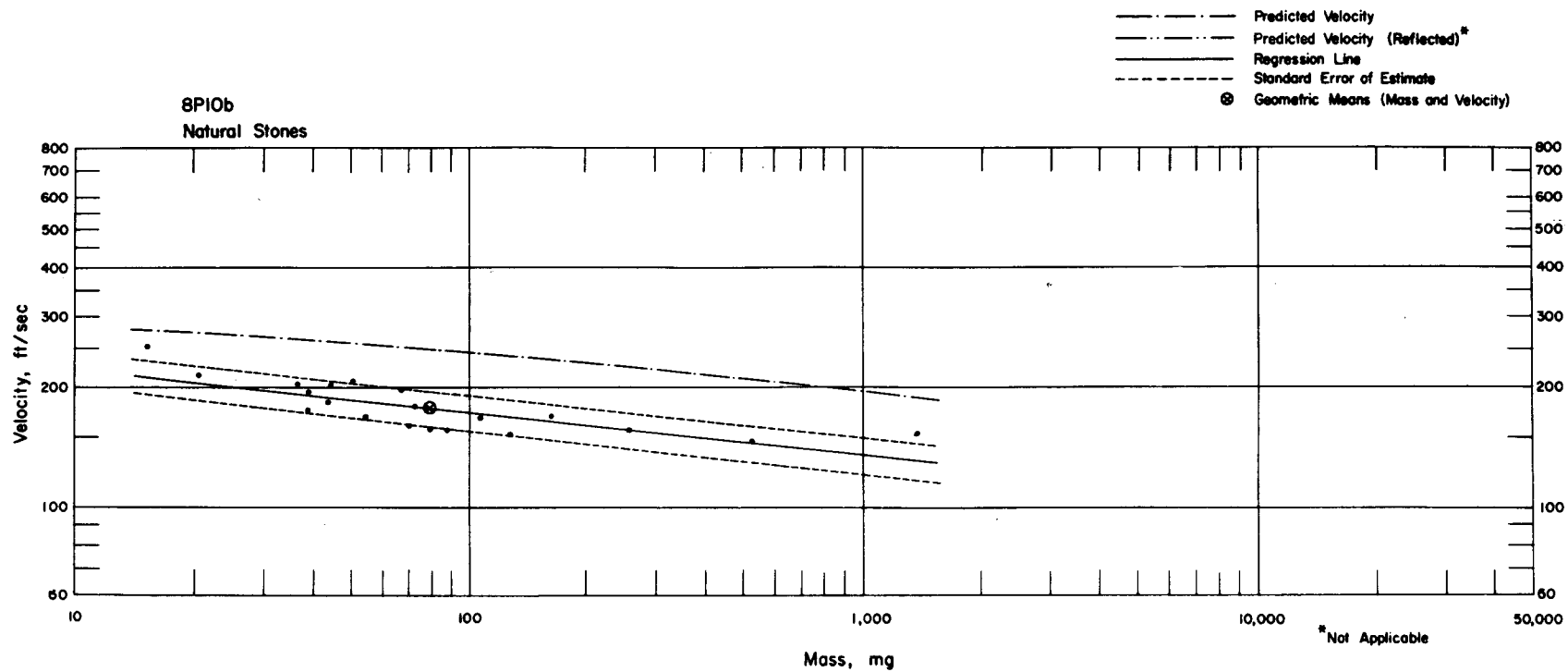


Fig. 4.106—Analysis of natural-stone missiles from trap 8P10b: $n = 20$; $\log v = 2.4586 - 0.1099 \log m$; $E_{gV} = 1.10$; $M_{50} = 79.1$ mg; $V_{50} = 178$ ft/sec.

IOP STATION, RANGE 2730

Note: MD, Gr, and S placed at 7.4', 19.1', and 49.0' from face of traps

MD Military Debris (B) blue
 Gr Gravel (W) white
 S Spheres (Y) yellow

$\frac{1}{12} \text{ ft}^3 \text{ Gr (B)}$
 MD (B)

$\frac{1}{12} \text{ ft}^3 \text{ Gr (B)}$
 MD (B)

$\frac{1}{12} \text{ ft}^3 \text{ Gr (W)}$
 MD (W)

$\frac{1}{12} \text{ ft}^3 \text{ Gr (W)}$
 MD (W)

$\frac{1}{12} \text{ ft}^3 \text{ Gr (Y)}$
 MD (Y)

$\frac{1}{12} \text{ ft}^3 \text{ Gr (Y)}$
 MD (Y)

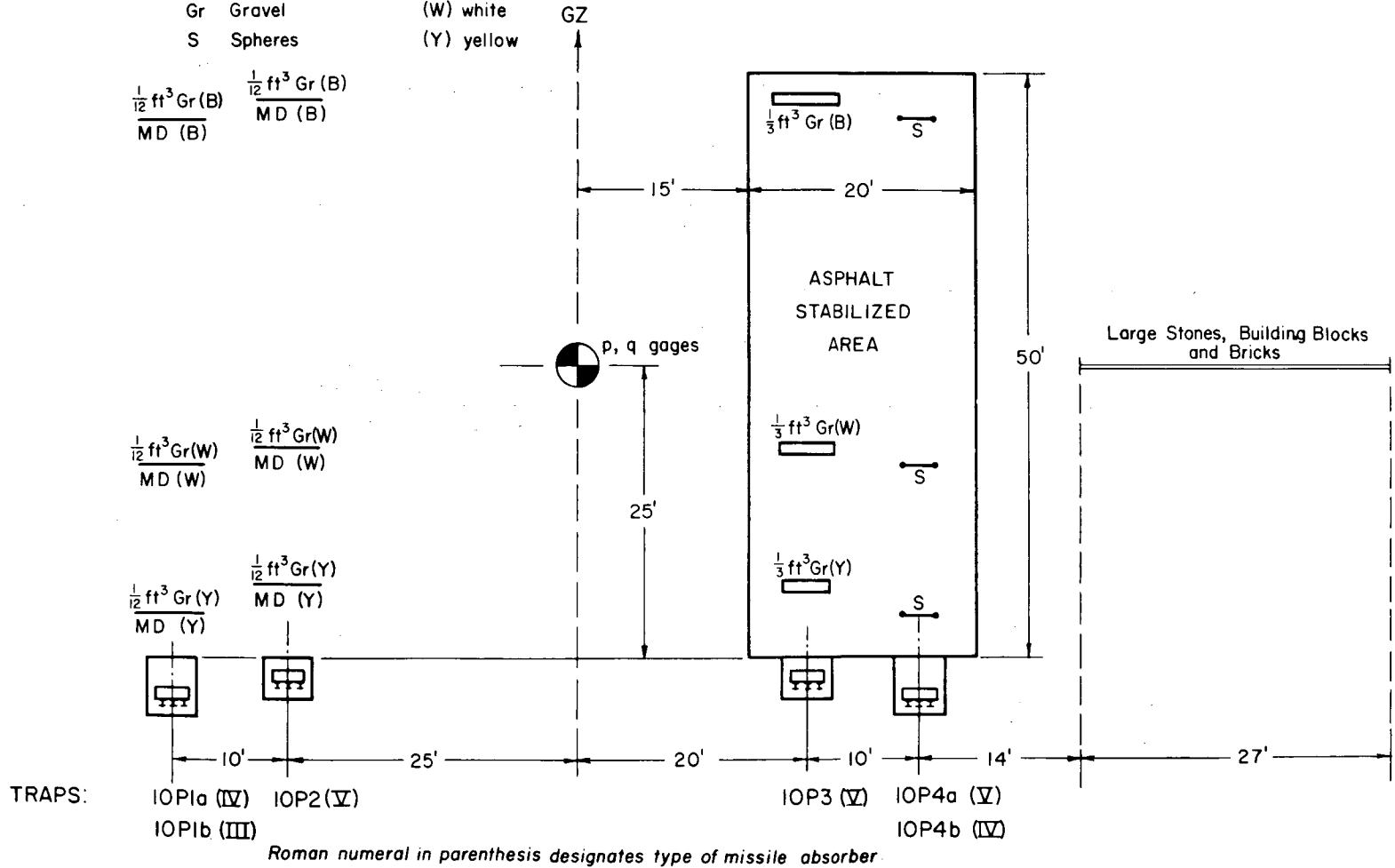


Fig. 4.107—Station 10P layout chart.

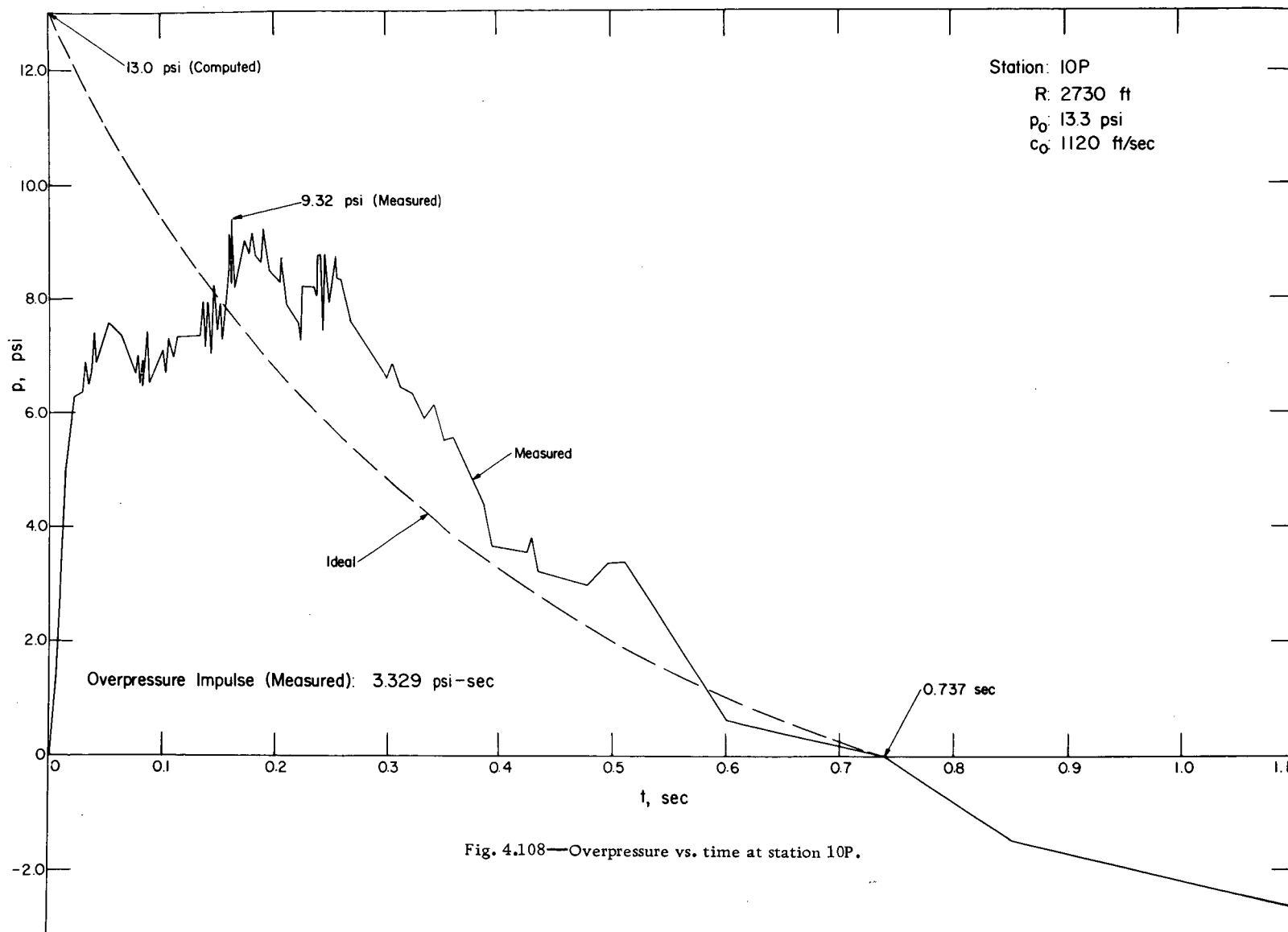


Fig. 4.108—Overpressure vs. time at station 10P.

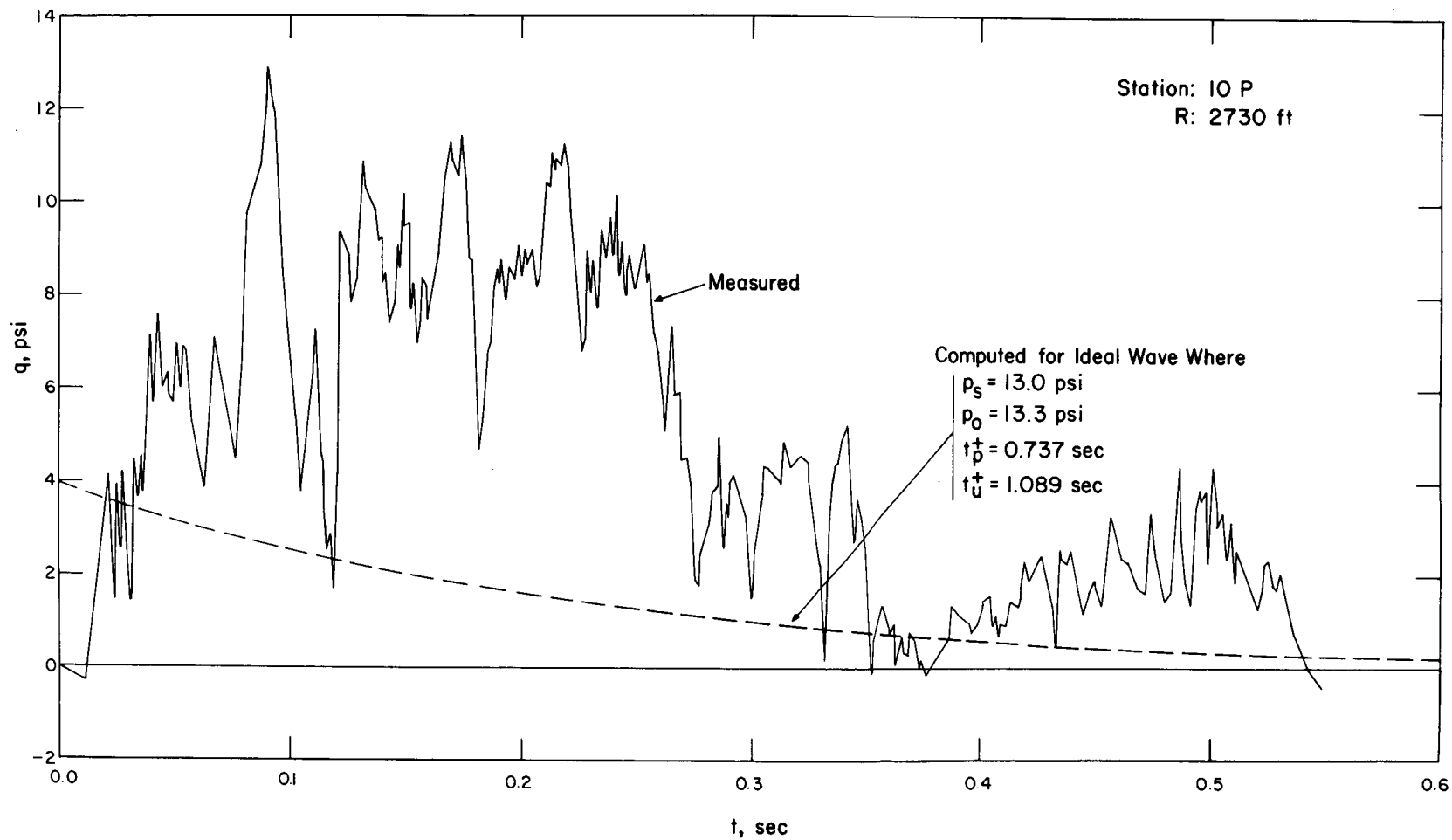


Fig. 4.109—Dynamic pressure vs. time at station 10P.

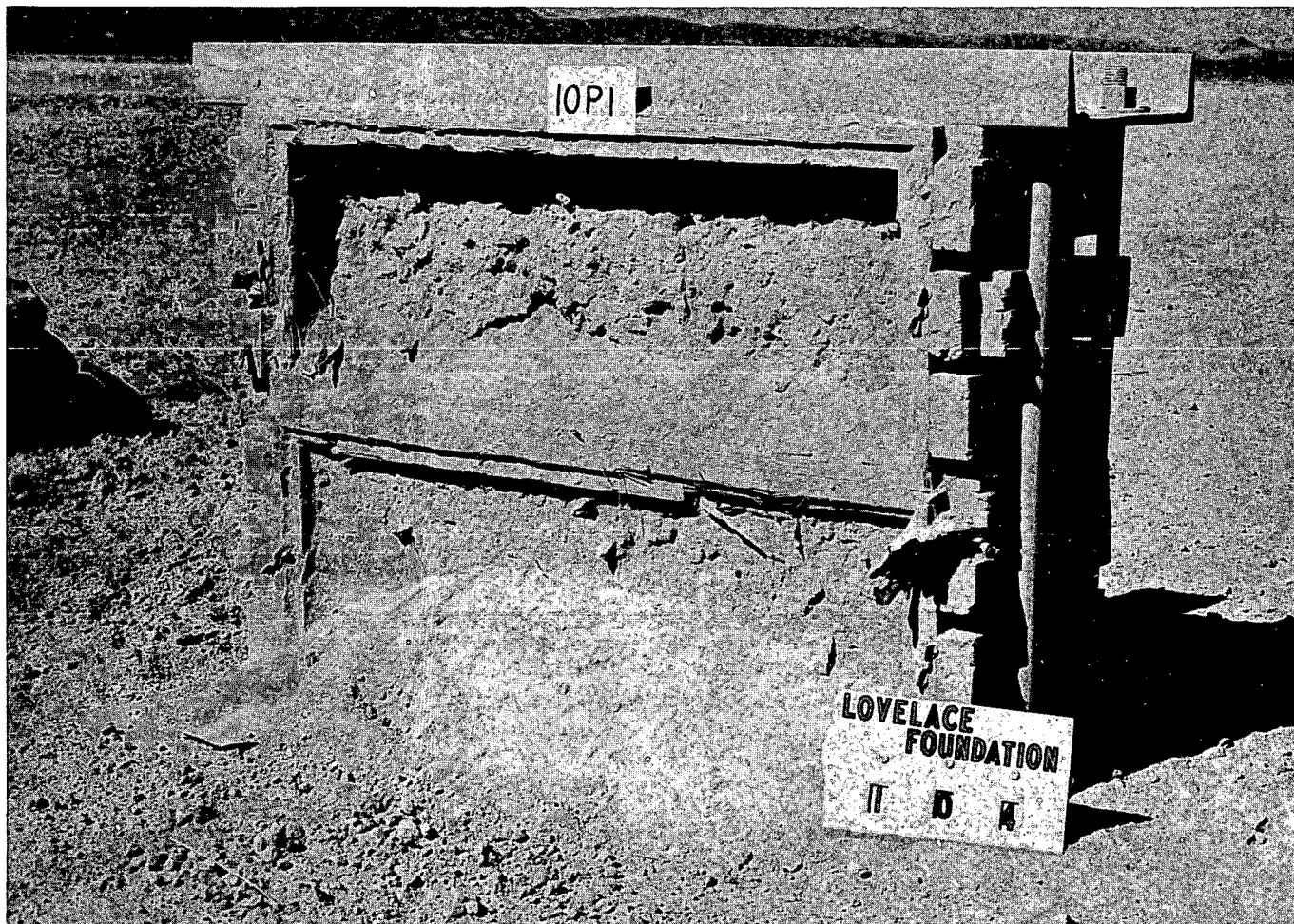


Fig. 4.110—Traps 10P1a and b, postshot.

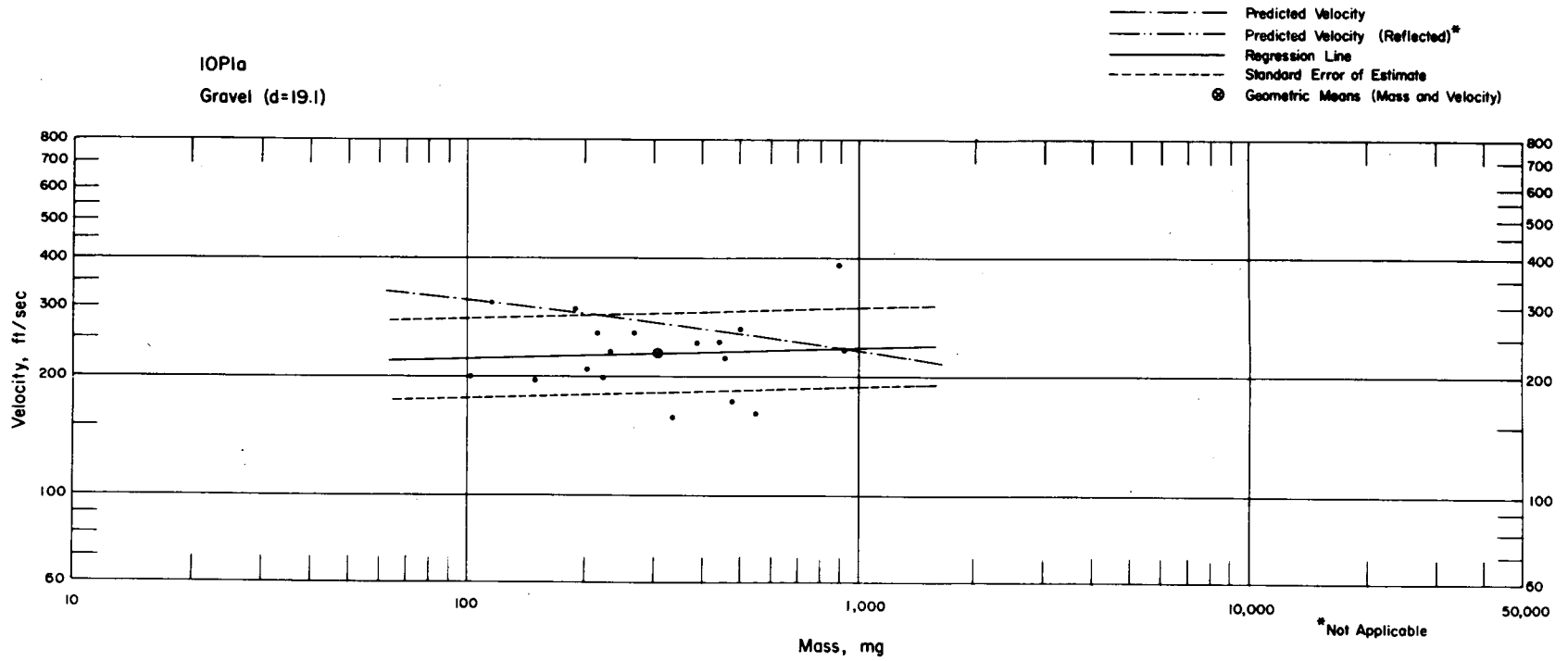


Fig. 4.111—Analysis of gravel missiles from trap 10P1a: $d = 19.1$ ft; $n = 18$; $\log v = 2.2904 + 0.0290 \log m$; $E_{gv} = 1.26$; $M_{50} = 305$ mg; $V_{50} = 230$ ft/sec.

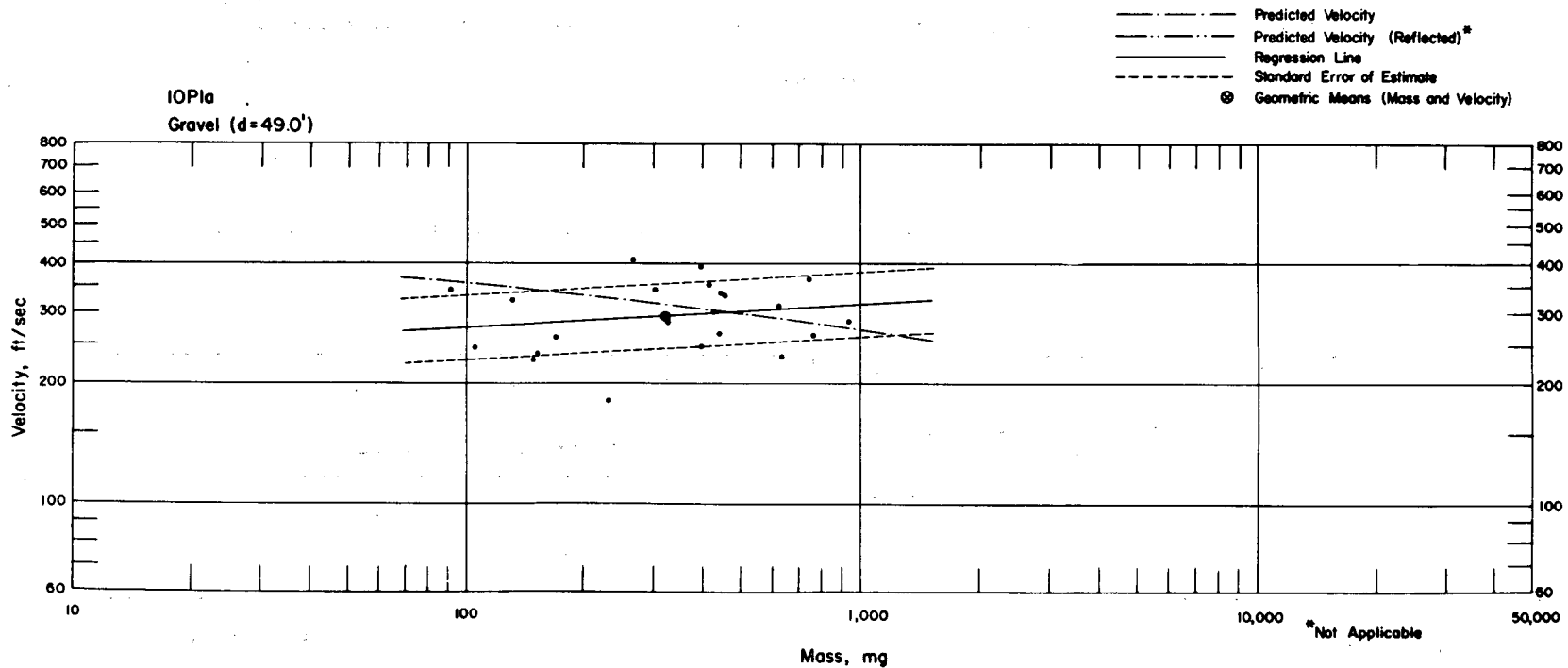


Fig. 4.112—Analysis of gravel missiles from trap 10P1a: $d = 49.0$ ft; $n = 22$; $\log v = 2.3316 + 0.0539 \log m$; $E_{gv} = 1.22$; $M_{50} = 322$ mg; $V_{50} = 293$ ft/sec.

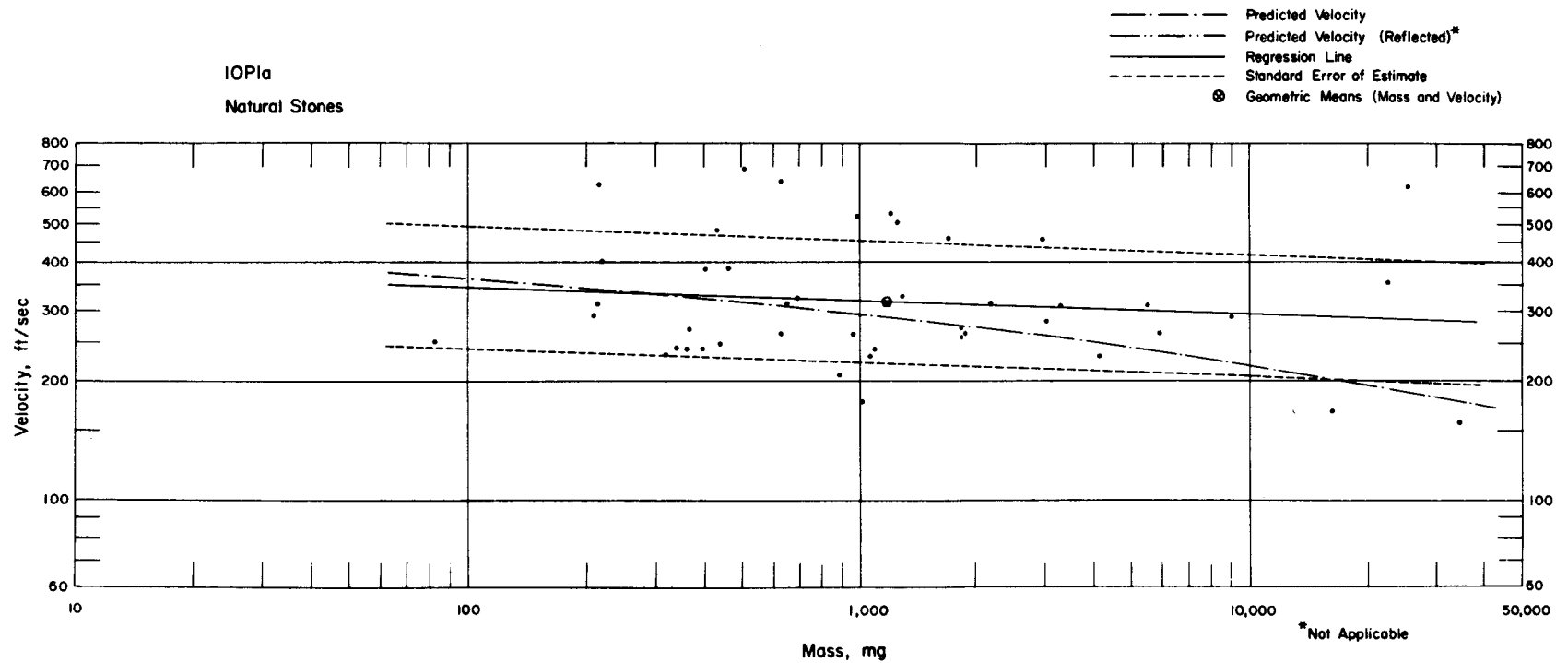


Fig. 4.113—Analysis of natural-stone missiles from trap 10P1a: $n = 44$; $\log v = 2.6137 - 0.0370 \log m$; $E_{gv} = 1.43$; $M_{50} = 1185$ mg; $V_{50} = 316$ ft/sec.

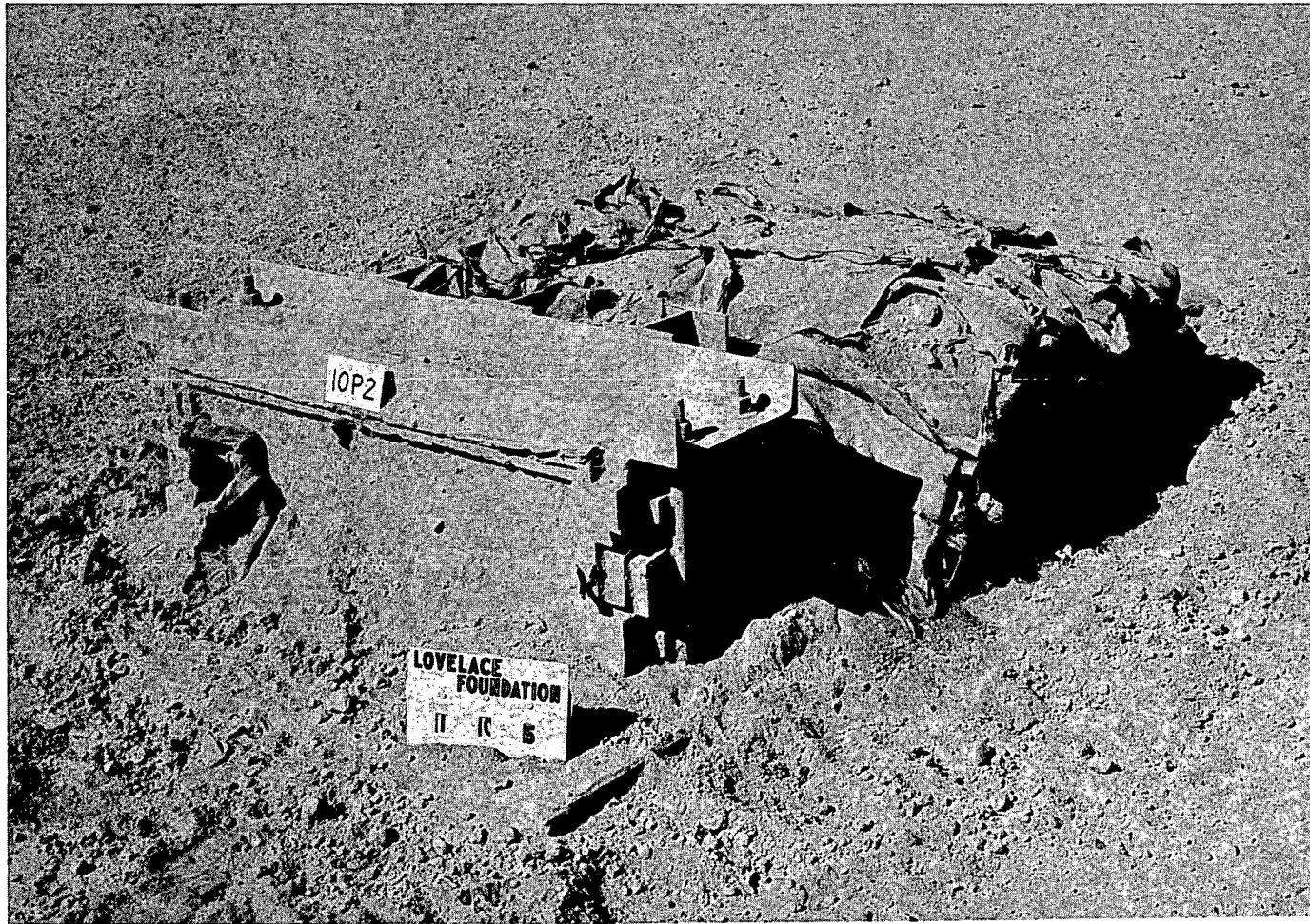


Fig. 4.114—Installation 10P2, postshot.

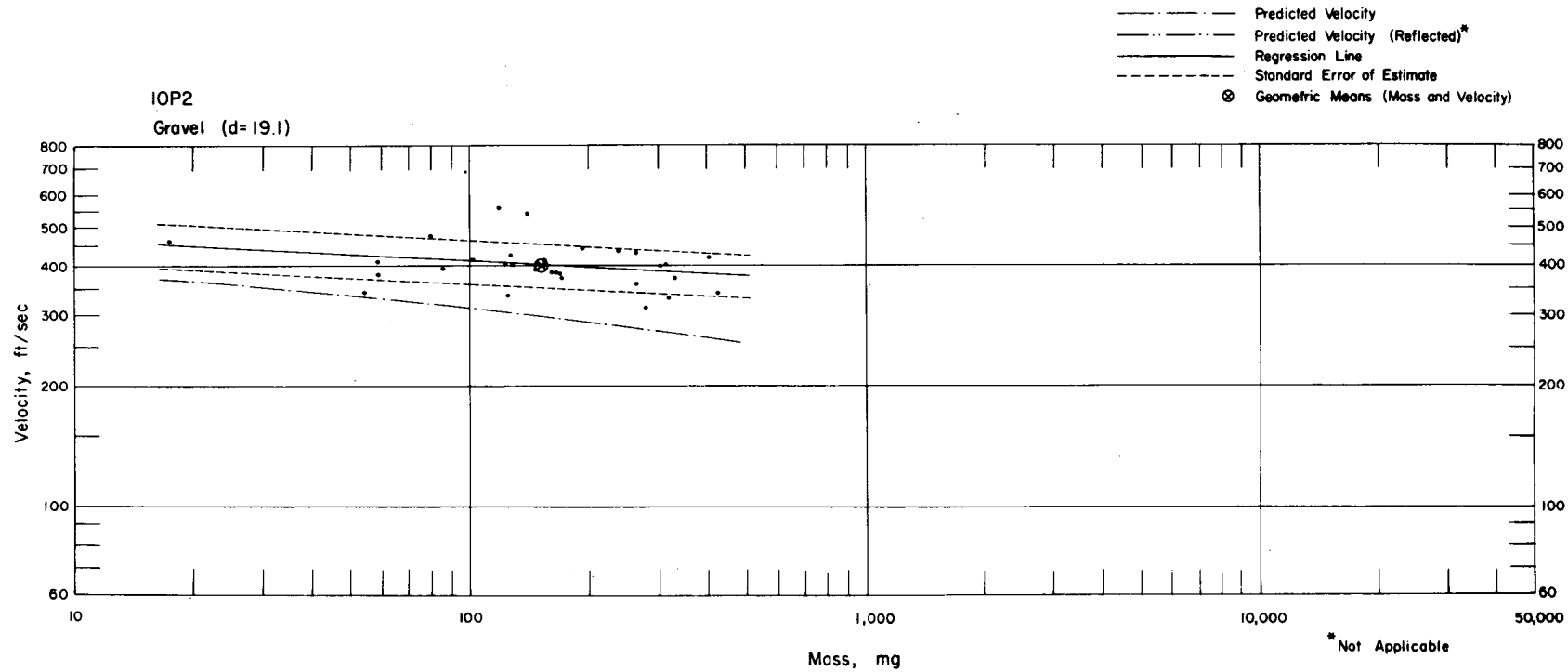


Fig. 4.115—Analysis of gravel missiles from installation IOP2: $d = 19.1$ ft; $n = 31$; $\log v = 2.7155 - 0.0512 \log m$; $E_{GV} = 1.13$; $M_{50} = 151$ mg; $V_{50} = 402$ ft/sec.

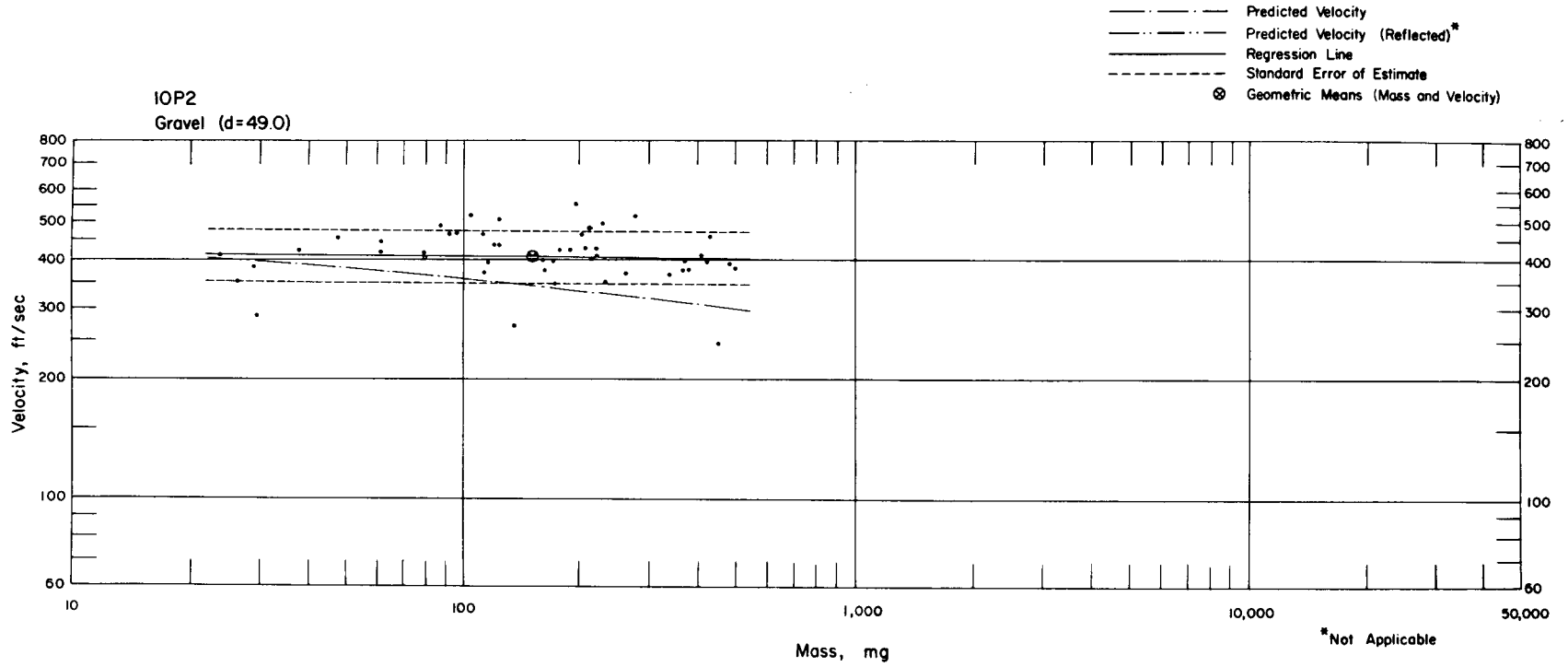


Fig. 4.116—Analysis of gravel missiles from installation 10P2: $d = 49.0$ ft; $n = 48$; $\log v = 2.6245 - 0.0068 \log m$; $E_{gv} = 1.16$; $M_{50} = 148$ mg; $V_{50} = 407$ ft/sec.

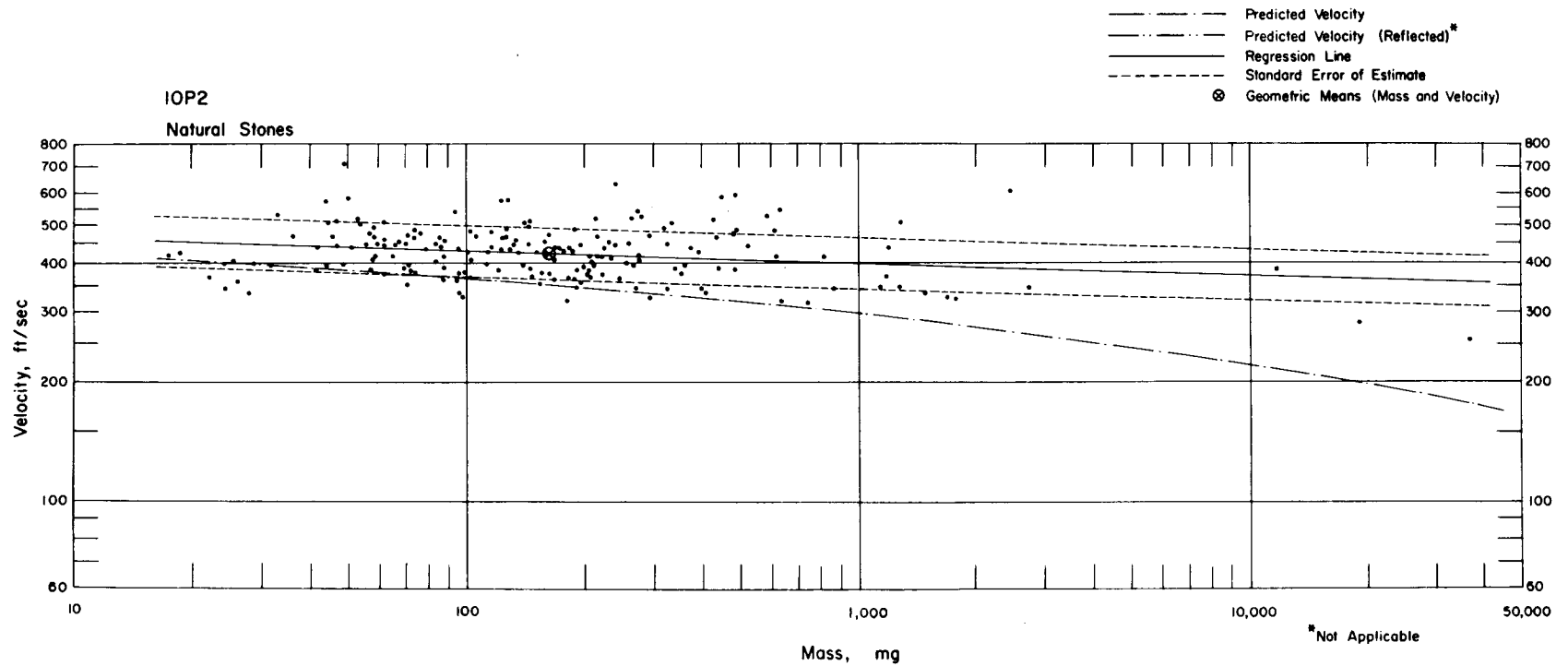


Fig. 4.117—Analysis of natural-stone missiles from installation IOP2: $n = 186$; $\log v = 2.6949 - 0.0312 \log m$; $E_{gv} = 1.16$; $M_{50} = 161$ mg; $V_{50} = 423$ ft/sec.

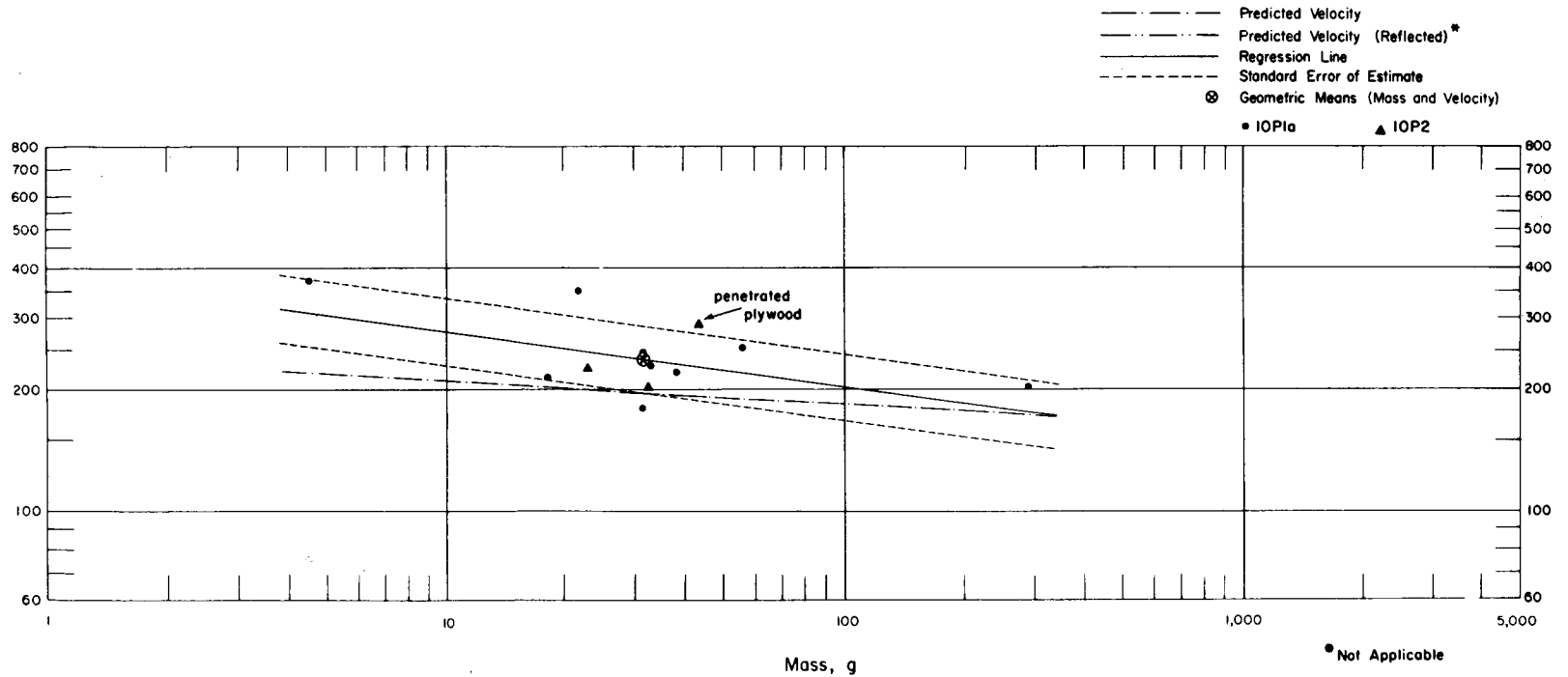


Fig. 4.118—Analysis of military-debris missiles from trap 10P1a and installation 10P2. Data for the missile that penetrated plywood are not included in analysis: $d = 49.0$ ft; $n = 11$; $\log v = 2.9824 - 0.1345 \log m$ (mg); $E_{gv} = 1.21$; $M_{50} = 31.06$ g; $V_{50} = 239$ ft/sec.

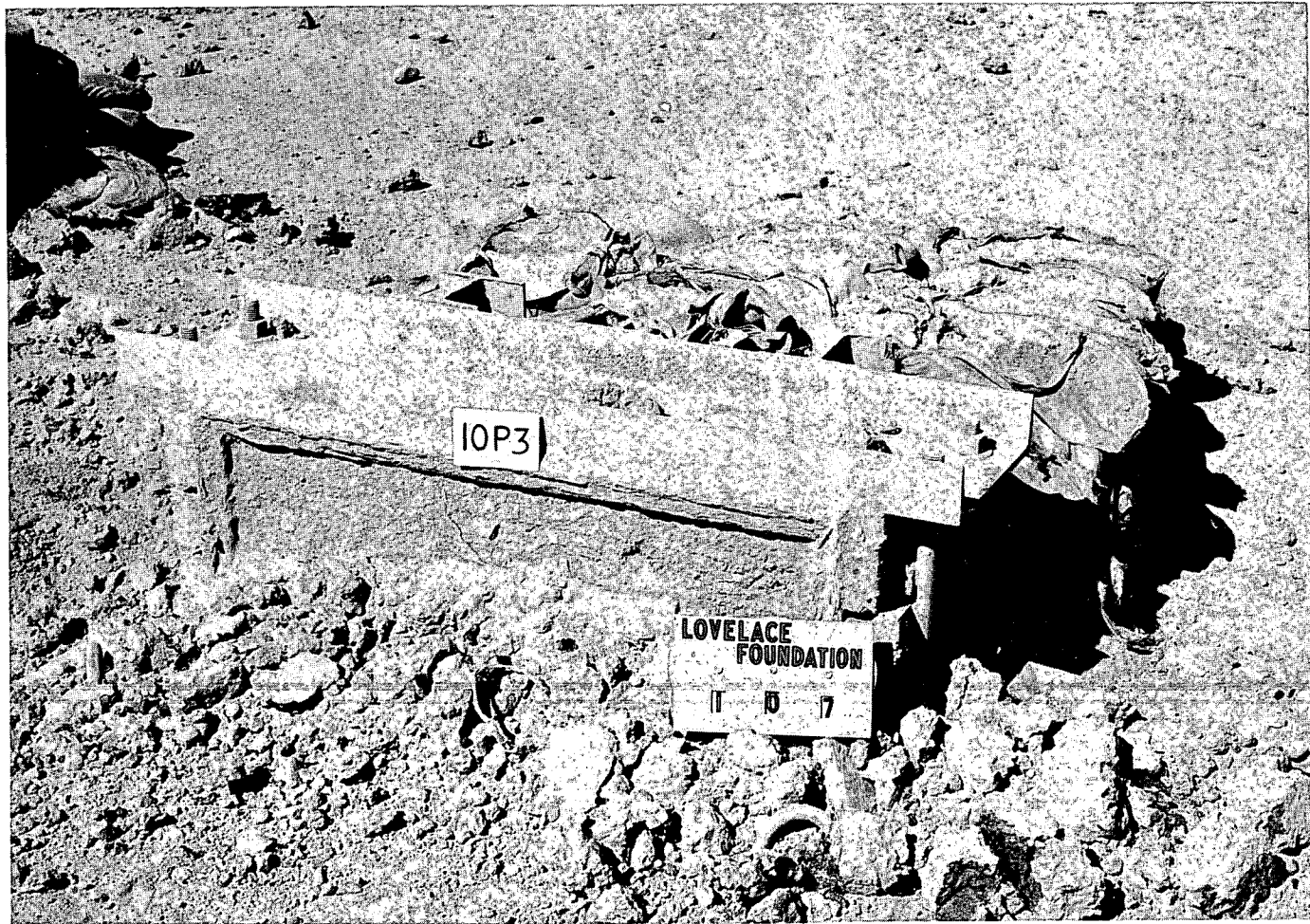


Fig. 4.119—Installation 10P3, postshot.



Fig. 4.120—Installation 10P3 and traps 10P4a and b, postshot.

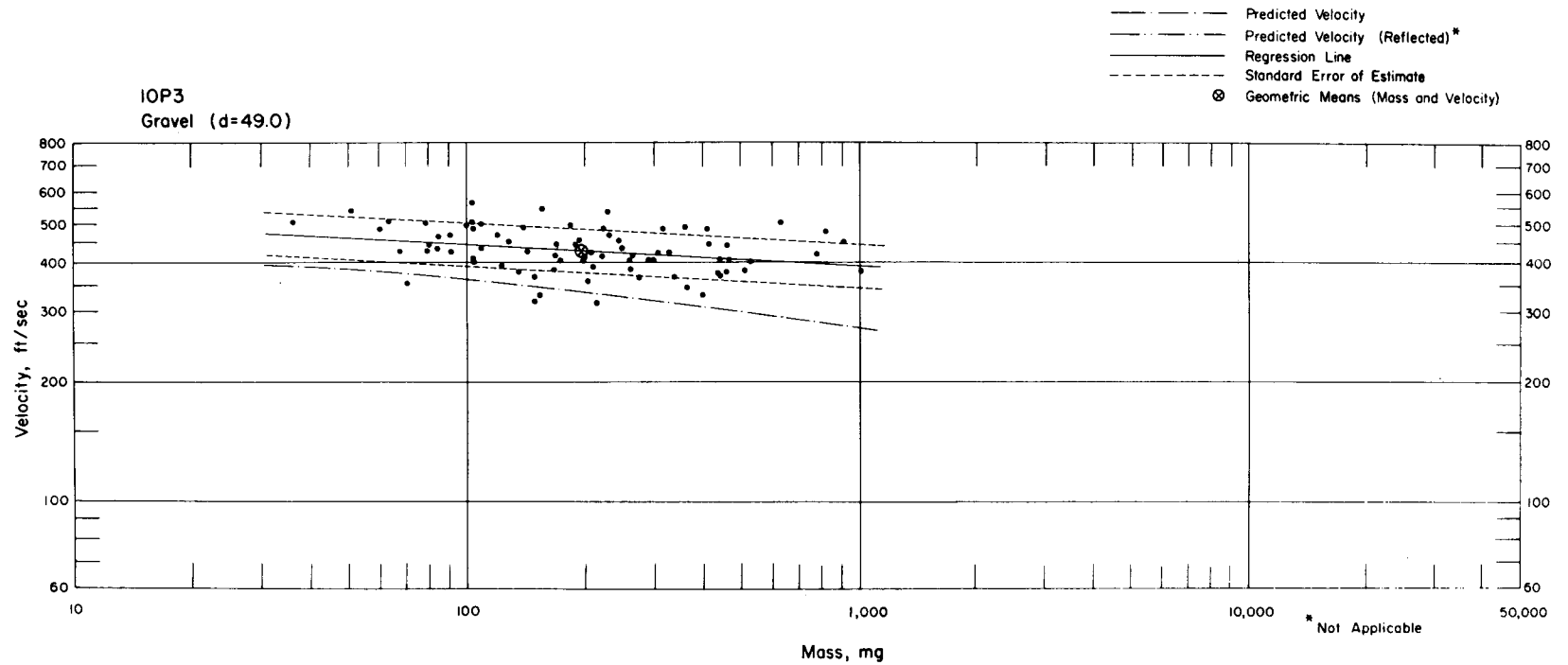


Fig. 4.121—Analysis of gravel missiles from installation IOP3: $d = 49.0$ ft; $n = 78$; $\log v = 2.7511 - 0.0522 \log m$; $E_{gv} = 1.13$; $M_{50} = 195$ mg; $V_{50} = 428$ ft/sec.

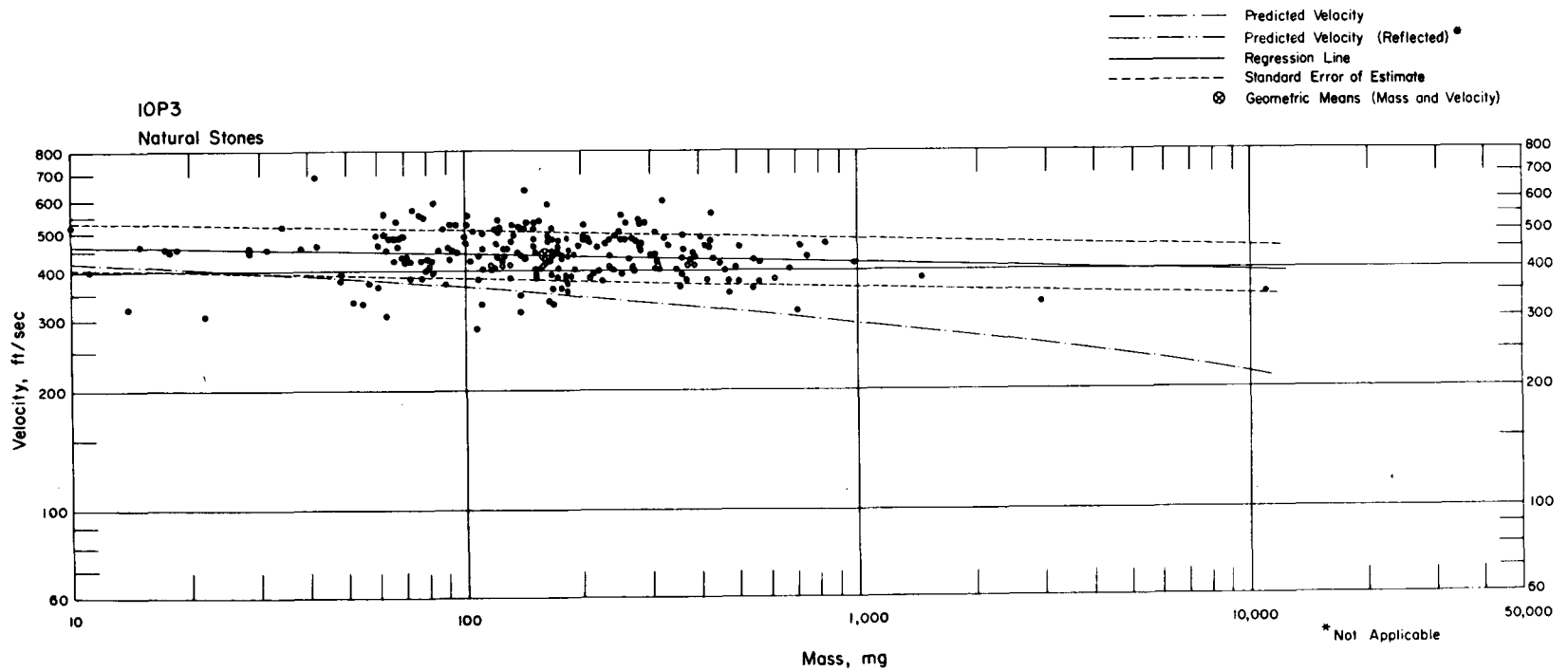


Fig. 4.122—Analysis of natural-stone missiles from installation IOP3: $n = 226$; $\log v = 2.6881 - 0.0217 \log m$; $E_{gV} = 1.15$; $M_{50} = 158$ mg; $V_{50} = 438$ ft/sec.

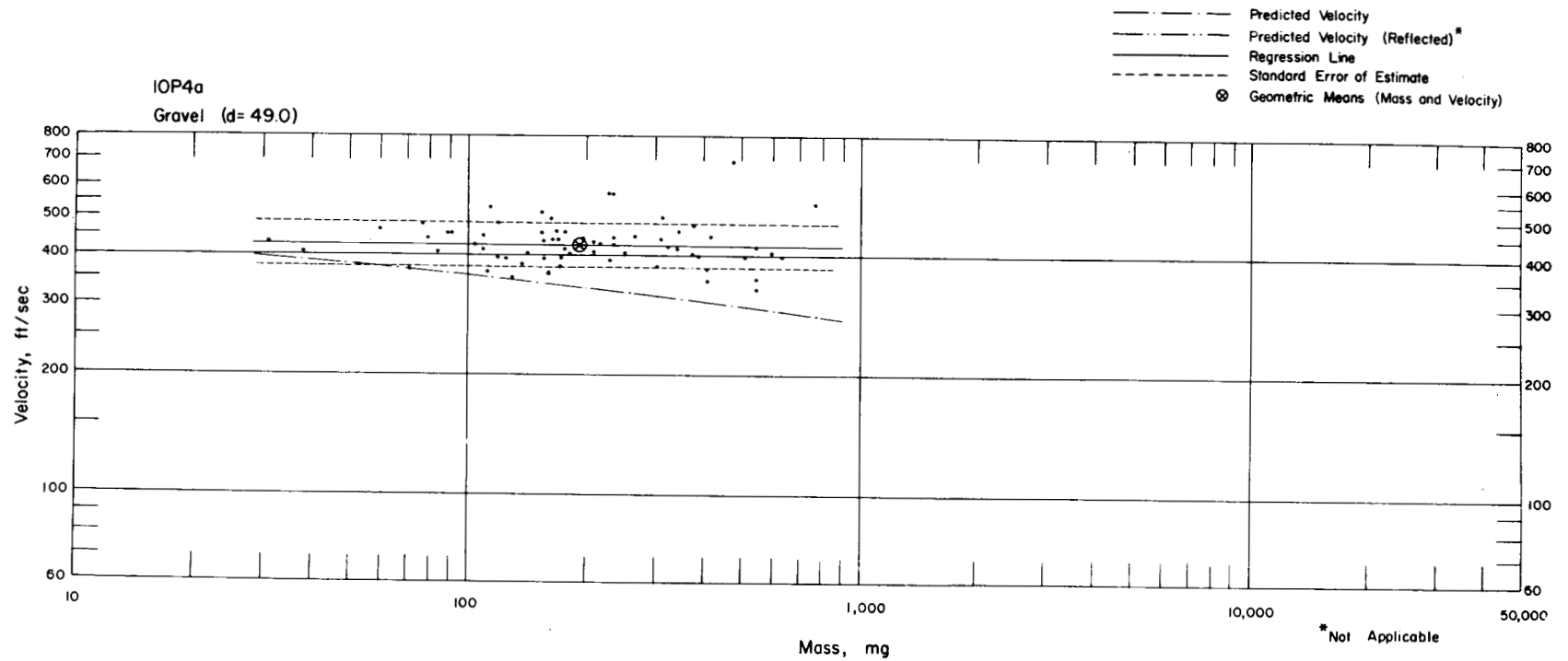


Fig. 4.123—Analysis of gravel missiles from trap IOP4a: $d = 49.0$ ft; $n = 66$; $\log v = 2.6338 - 0.0017 \log m$; $E_{gv} = 1.14$; $M_{50} = 190$ mg; $V_{50} = 427$ ft/sec.

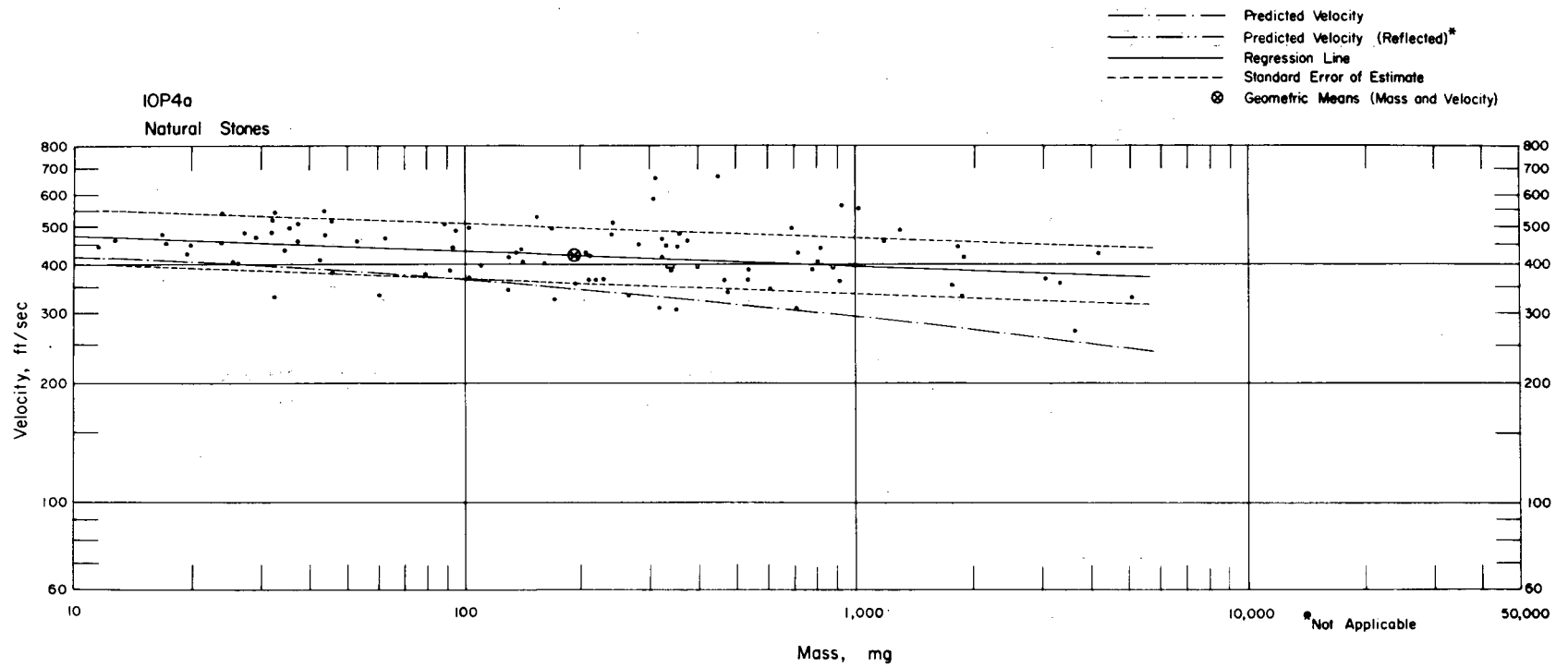
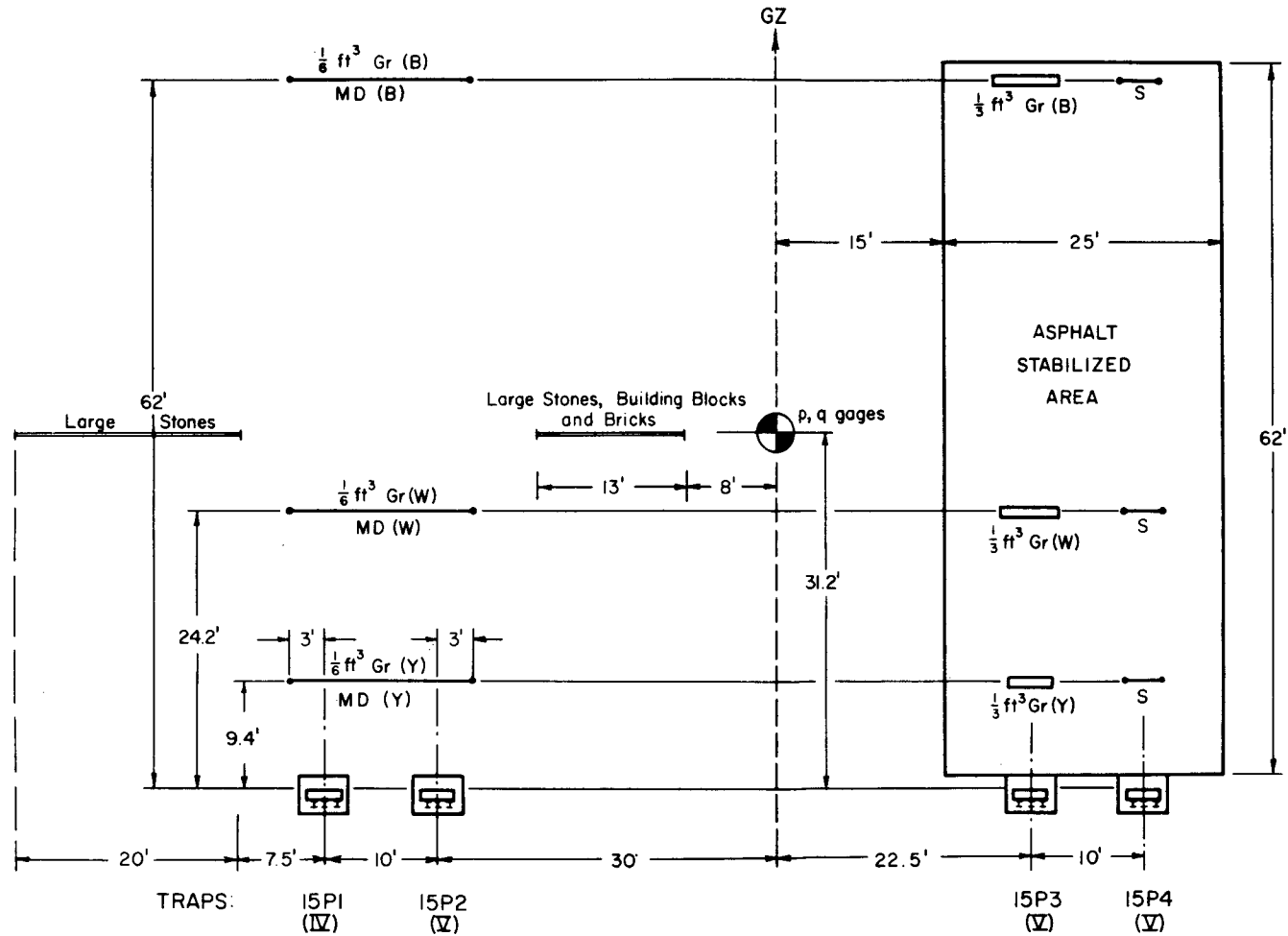


Fig. 4.124—Analysis of natural-stone missiles from trap IOP4a: $n = 96$; $\log v = 2.7112 - 0.0371 \log m$; $E_{GV} = 1.17$; $M_{50} = 188$ mg; $V_{50} = 424$ ft/sec.

15 P STATION, RANGE 2280

MD Military Debris (B) blue
 Gr Gravel (W) white
 S Spheres (Y) yellow



Roman numeral in parenthesis designates type of missile absorber

Fig. 4.125—Station 15P layout chart.

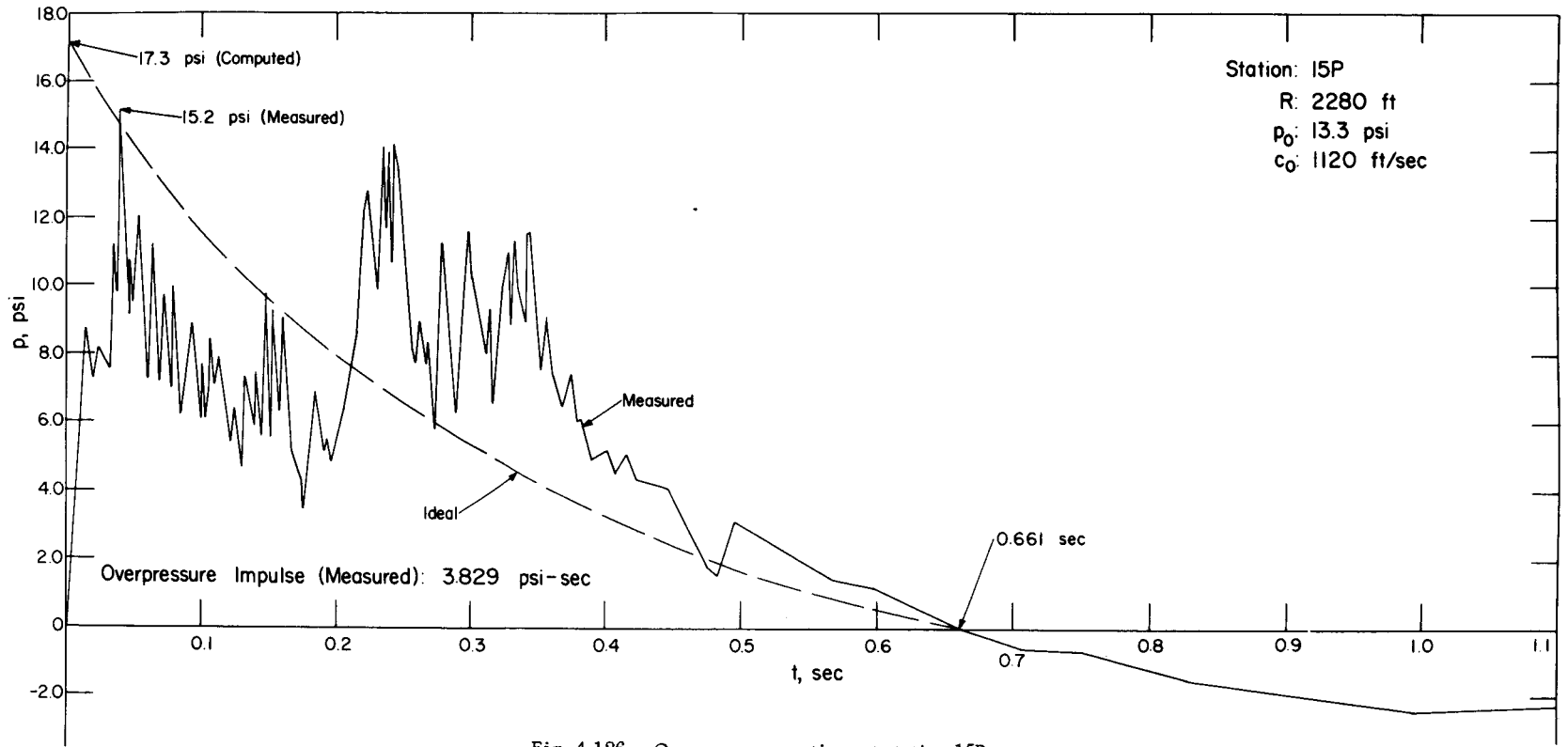


Fig. 4.126—Overpressure vs. time at station 15P.

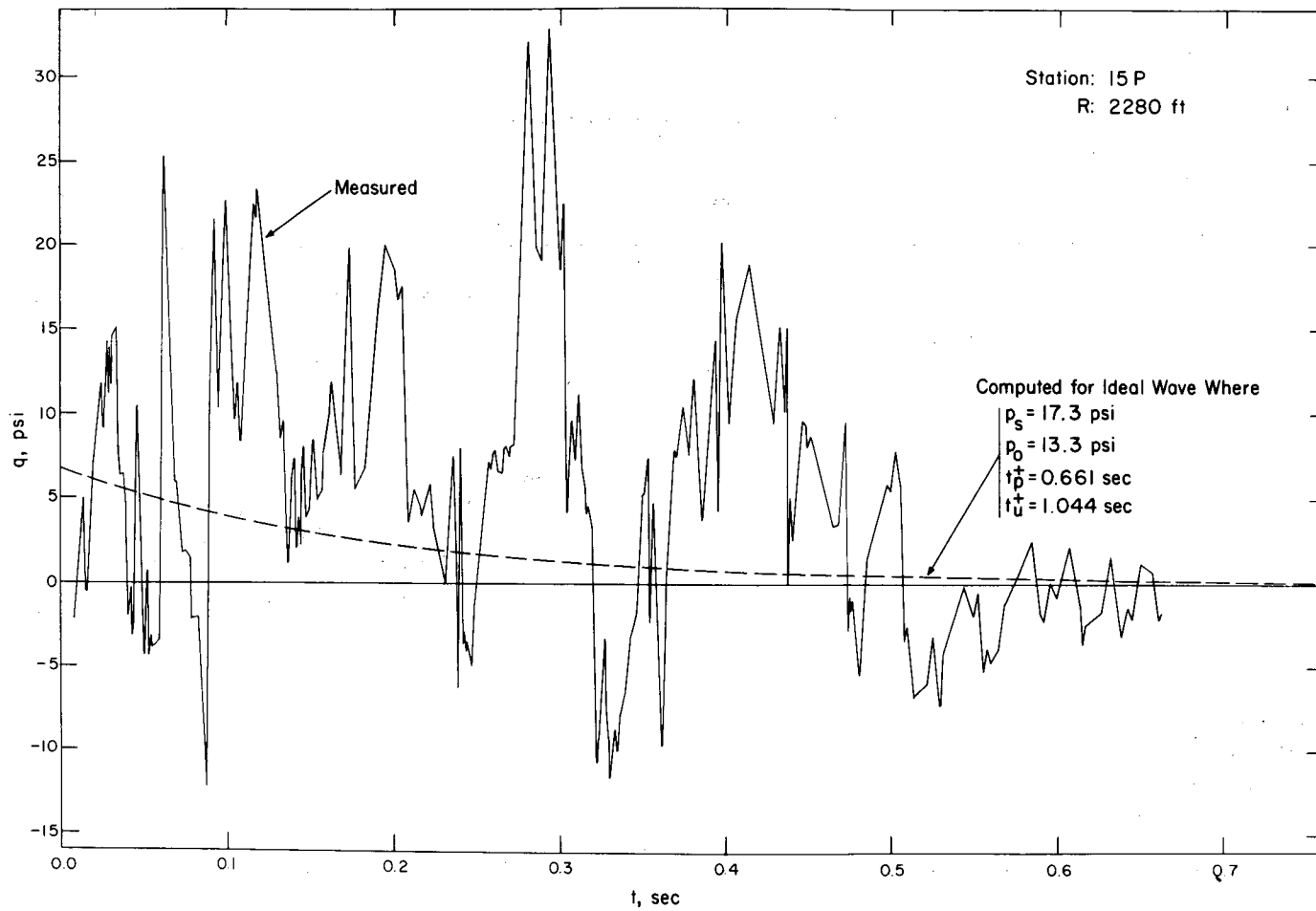


Fig. 4.127—Dynamic pressure vs. time at station 15P.

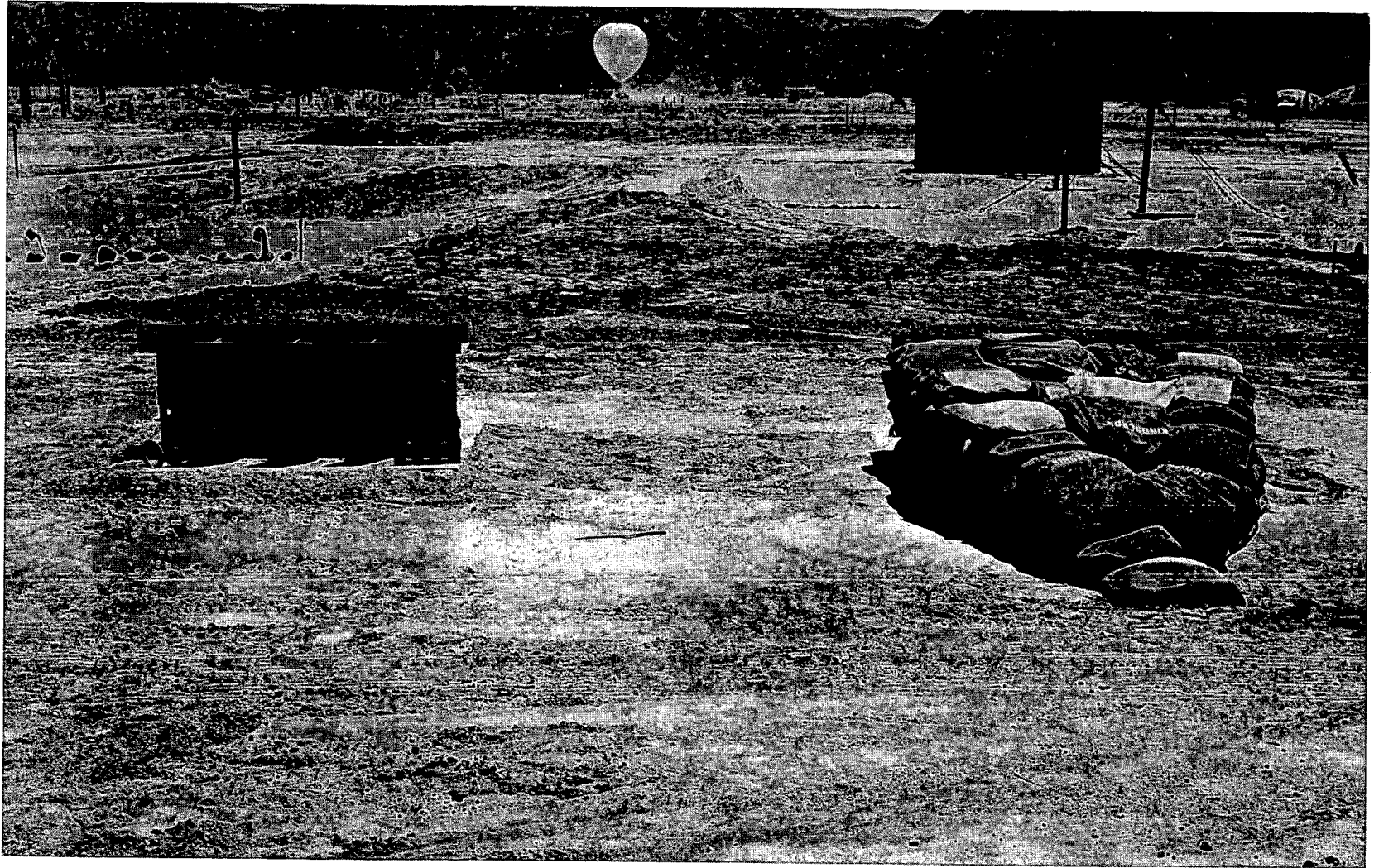


Fig. 4.128—Installations 15P1 (left) and 15P2, preshot. GZ is in background with balloon that carried nuclear device aloft. Installation 15P2 trap is anchored with sand bags.

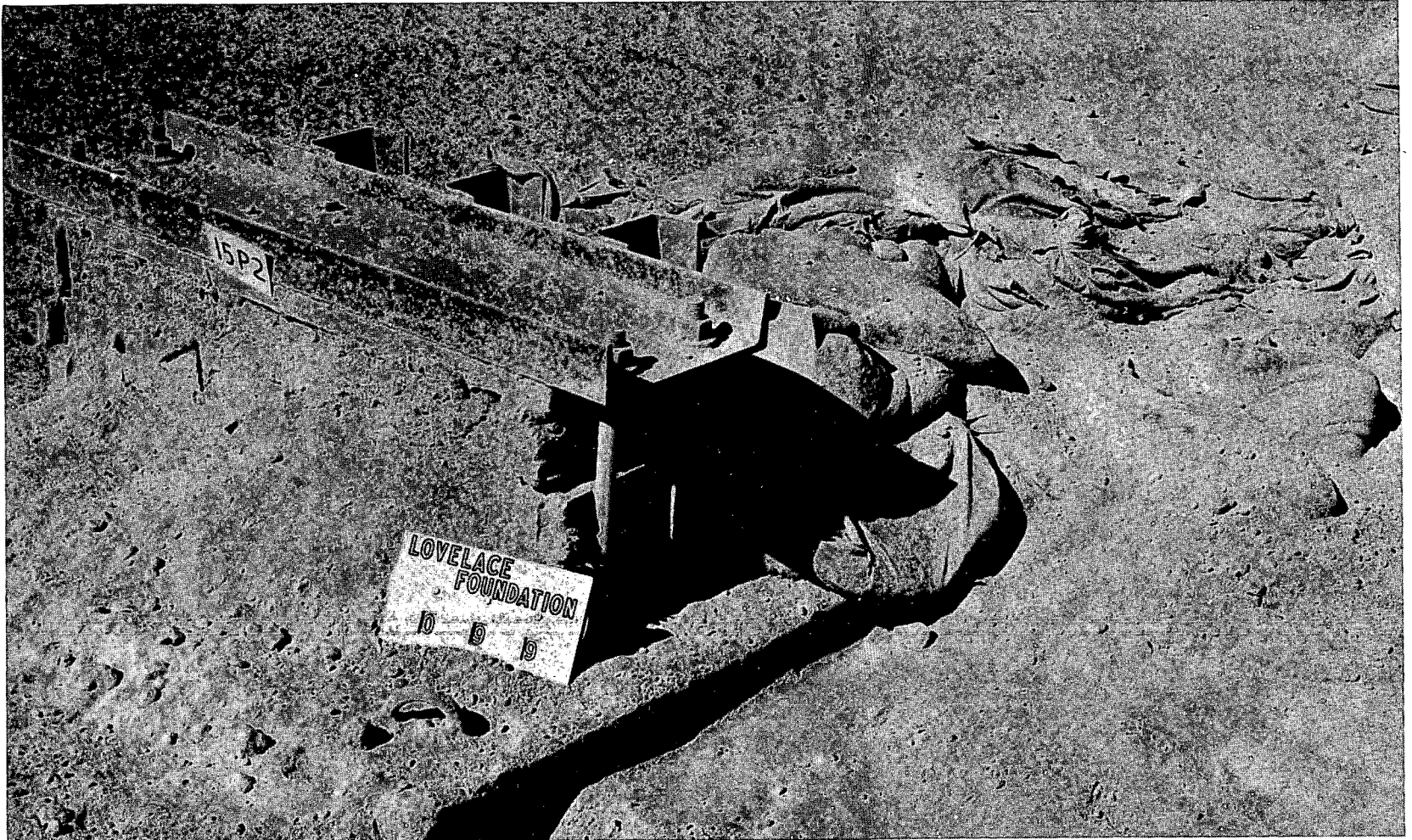


Fig. 4.129—Installation 15P2, postshot. Trap is almost buried by native soil.

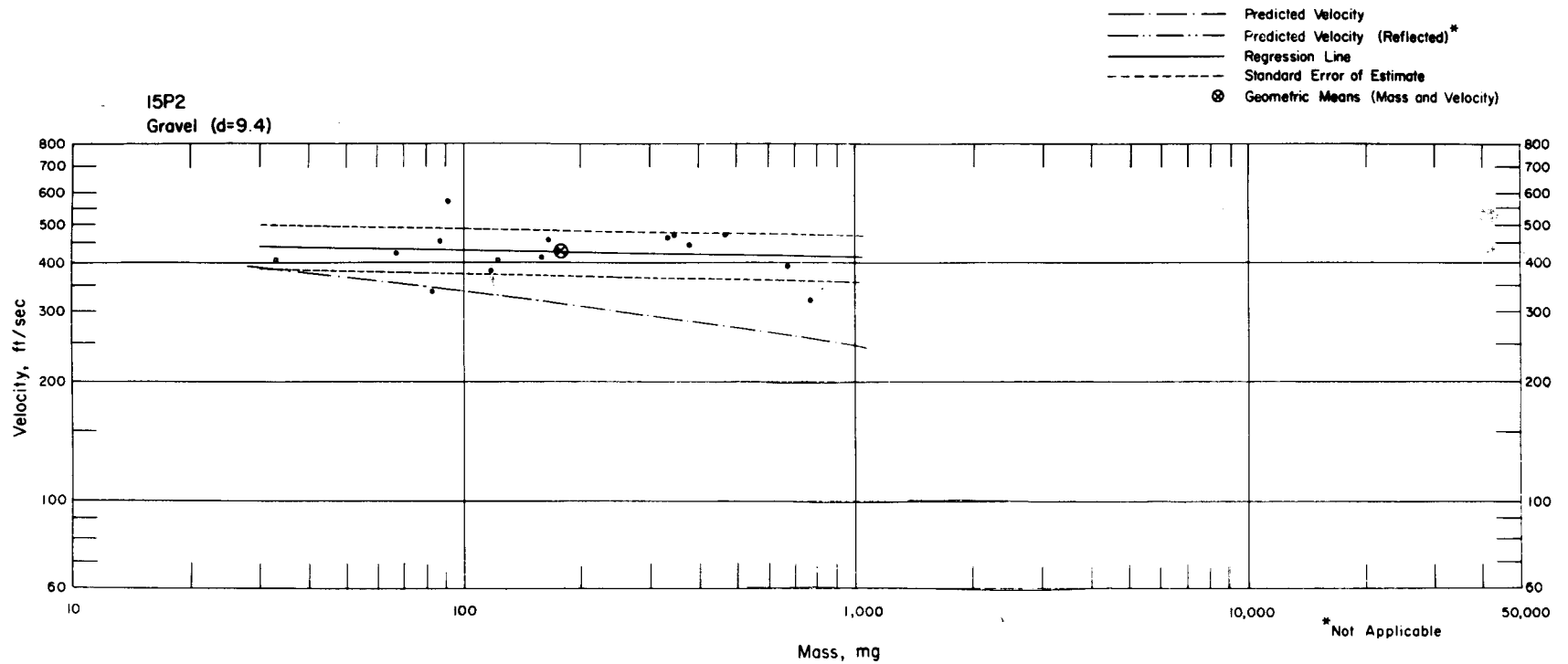


Fig. 4.130—Analysis of gravel missiles from installation 15P2: $d = 9.4$ ft; $n = 16$; $\log v = 2.6707 - 0.0184 \log m$; $E_{gv} = 1.15$; $M_{50} = 177$ mg; $V_{50} = 426$ ft/sec.

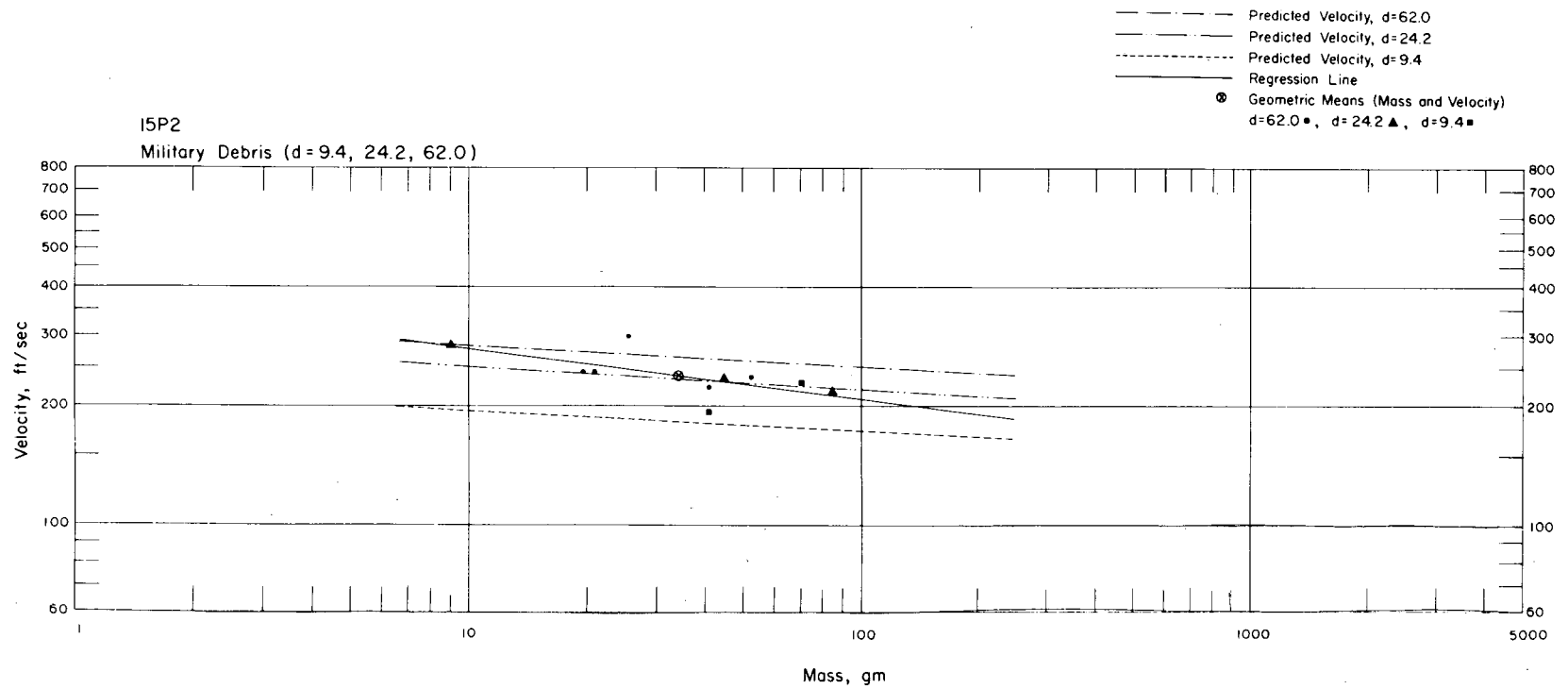


Fig. 4.131—Analysis of military-debris missiles from installation 15P2. Note three predicted velocity lines: $d = 9.4, 24.2,$ and 62.0 ft; $n = 10$; $\log v = 2.5651 - 0.1196 \log m$ (mg); $E_{gv} = 1.10$; $M_{50} = 34.5$ g; $V_{50} = 240$ ft/sec.

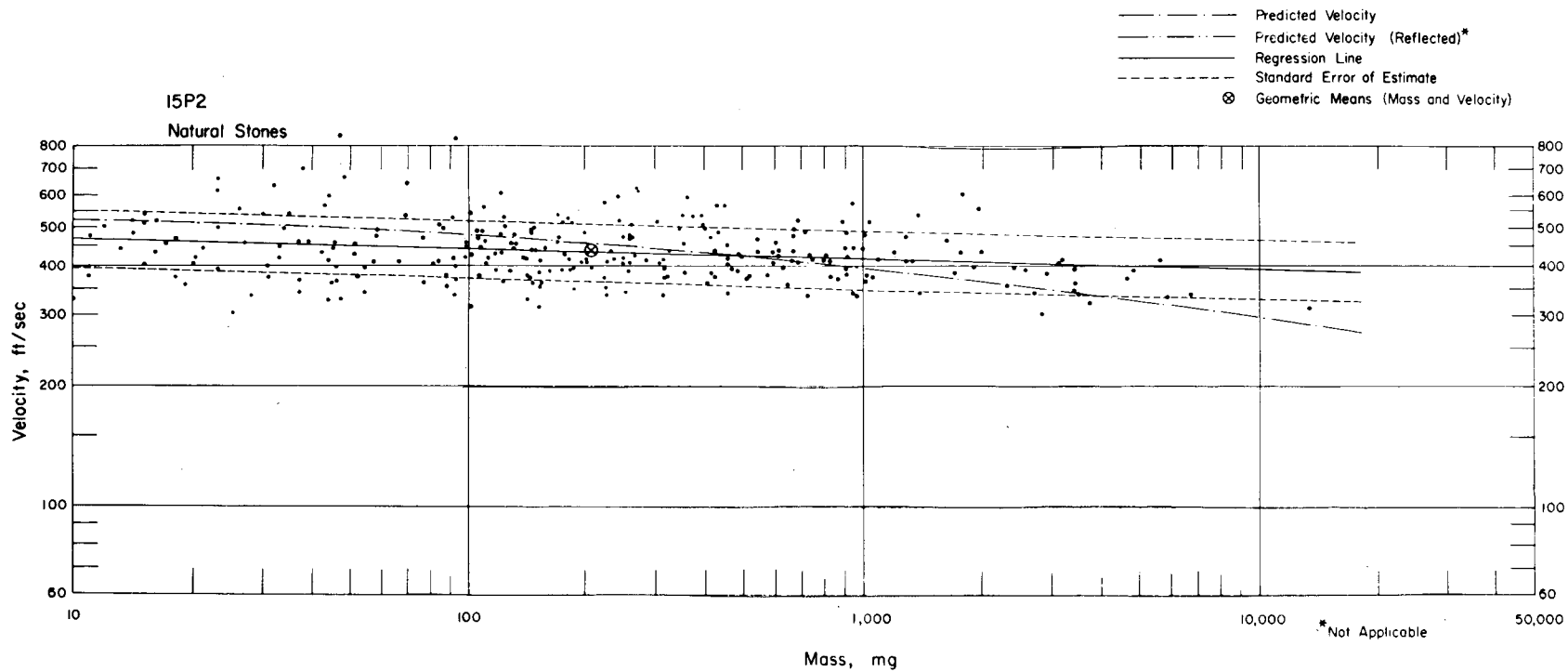


Fig. 4.132—Analysis of natural-stone missiles from installation I5P2: $n = 273$; $\log v = 2.6884 - 0.0229 \log m$; $E_{gv} = 1.18$; $M_{50} = 208$ mg; $V_{50} = 432$ ft/sec. Two large stones that had masses of 9,307 and 19,125 mg passed through the balsa absorber and penetrated the plywood back of the trap. The minimum velocities that they would have had were 458 and 389 ft/sec, respectively. These data were not included in the above analysis.



Fig. 4.133—Stabilized area at station 15P. Gravel installation 15P3 appears on the right and sphere installation 15P4 on the left.



Fig. 4.134—Installations 15P3 and 15P4, preshot.

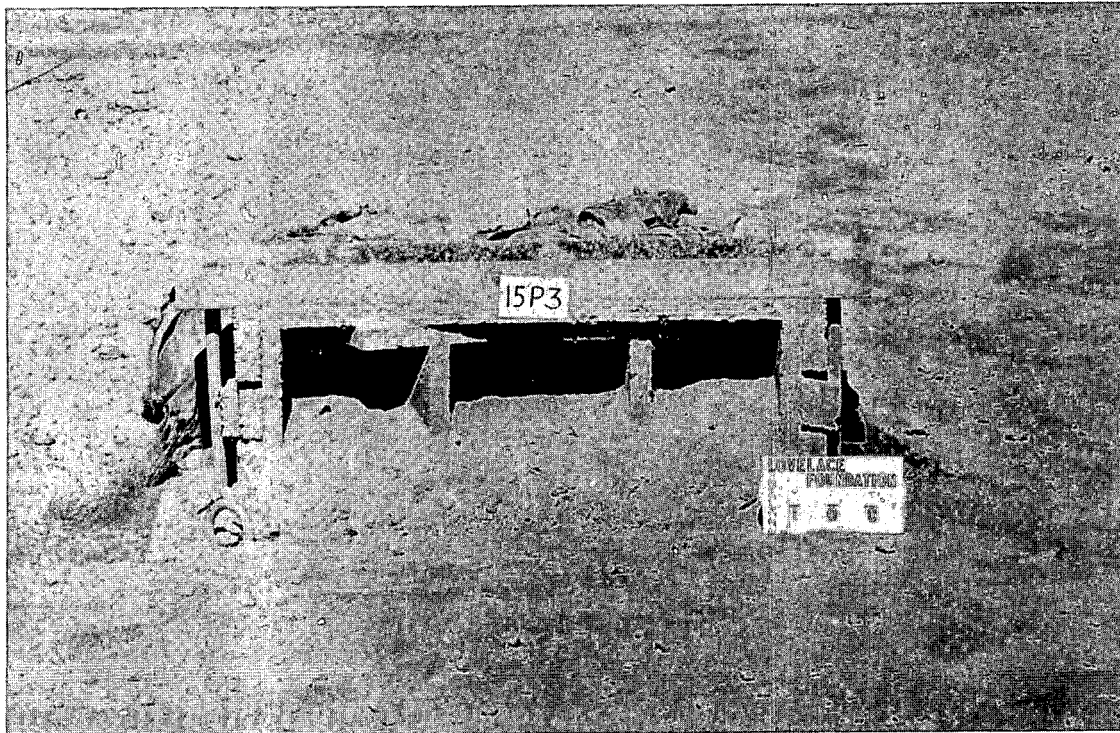


Fig. 4.135 — Installation 15P3, postshot. Installation was destroyed.

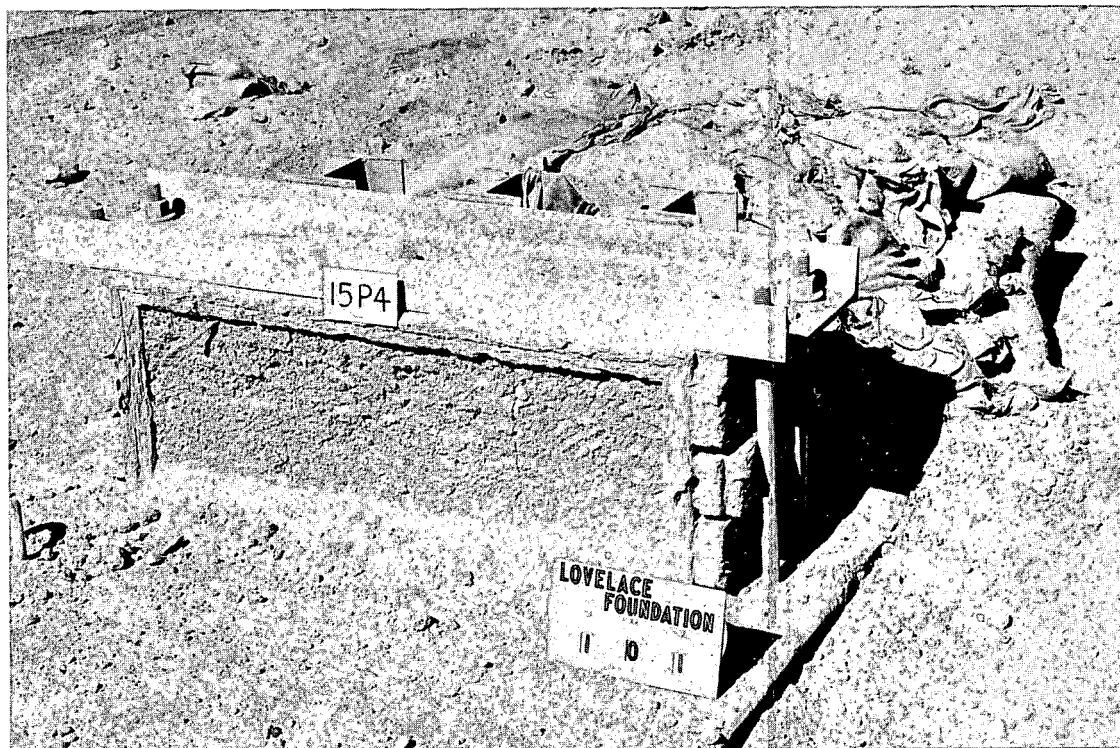


Fig. 4.136 — Installation 15P4, postshot.

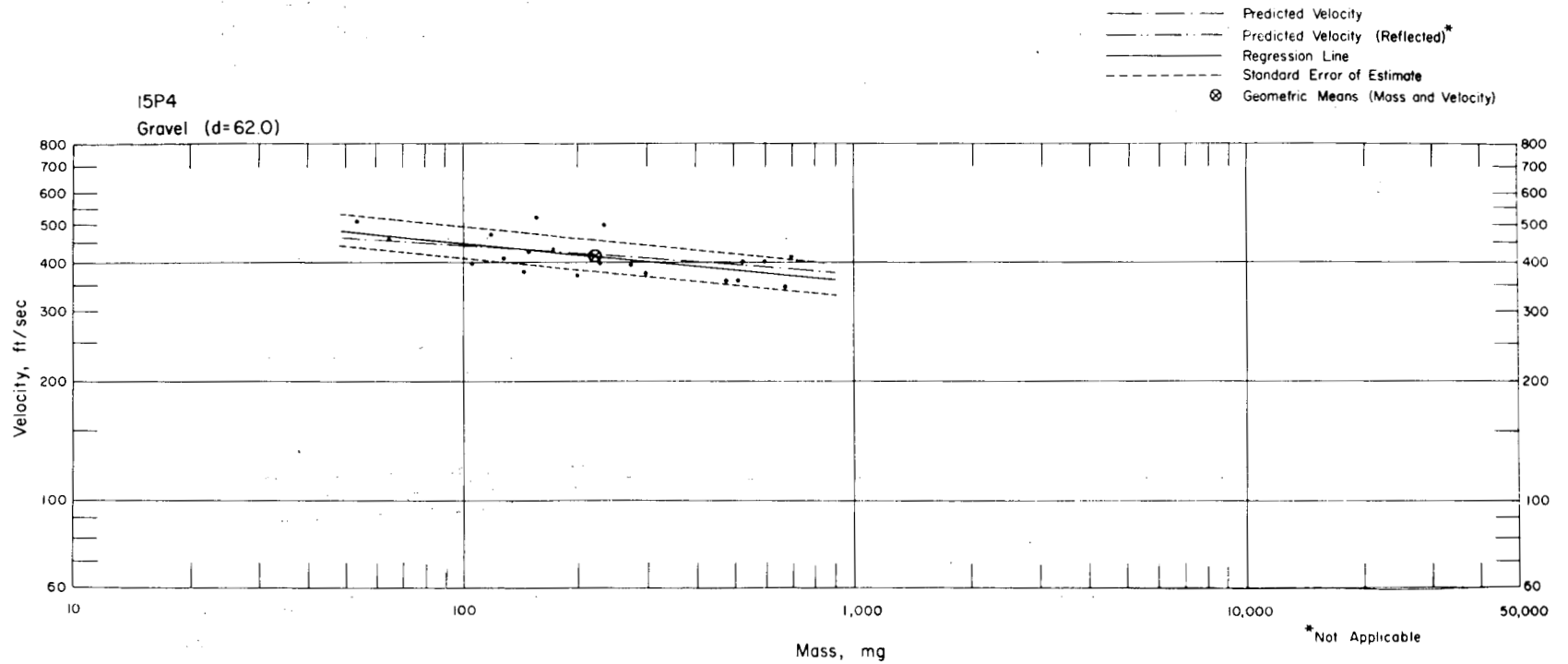


Fig. 4.137—Analysis of gravel missiles from installation 15P4: $d = 62.0$ ft; $n = 20$; $\log v = 2.8394 - 0.0967 \log m$; $E_{gv} = 1.10$; $M_{50} = 223$ mg; $V_{50} = 409$ ft/sec.

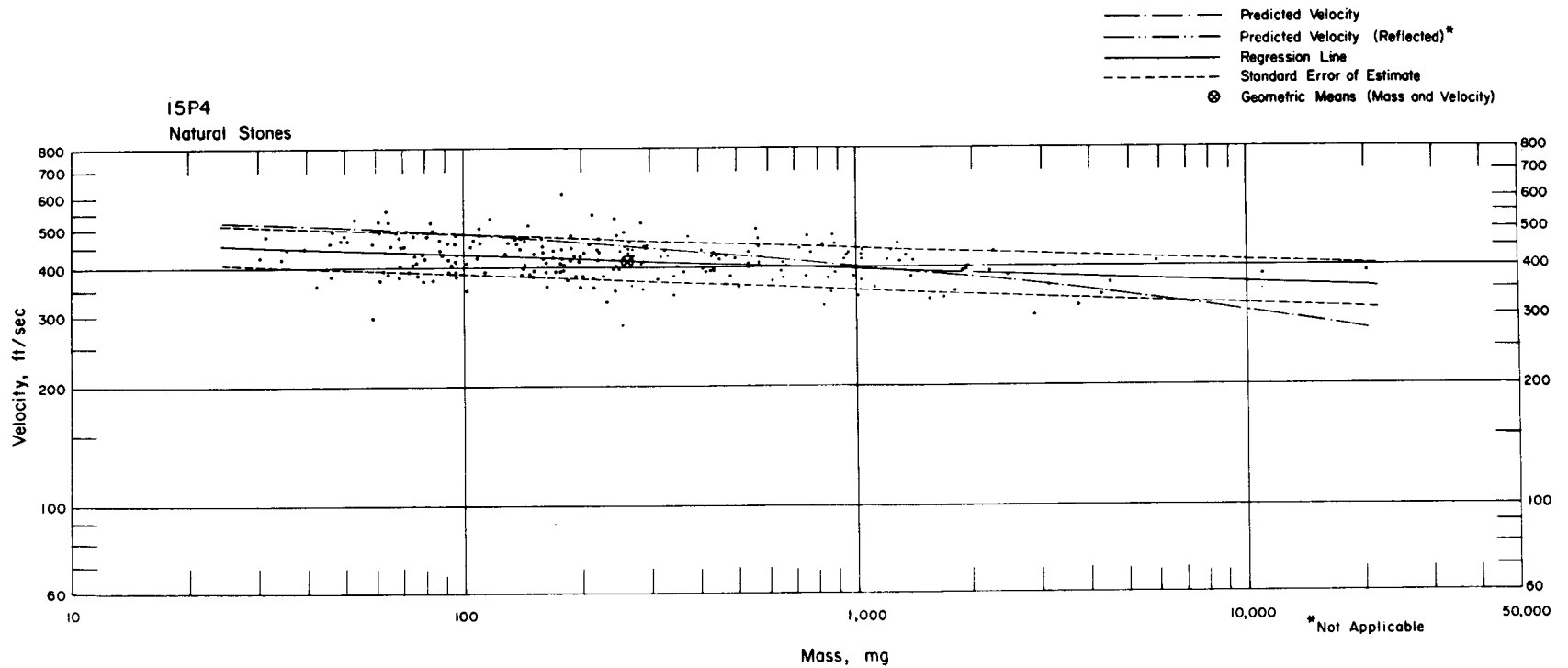


Fig. 4.138—Analysis of natural-stone missiles from installation 15P4: $n = 232$; $\log v = 2.7026 - 0.0361 \log m$; $E_{GV} = 1.12$; $M_{50} = 264$ mg; $V_{50} = 412$ ft/sec.

20 P STATION, RANGE 2030

MD Military Debris (B) blue
 Gr Gravel (W) white
 S Spheres (Y) yellow

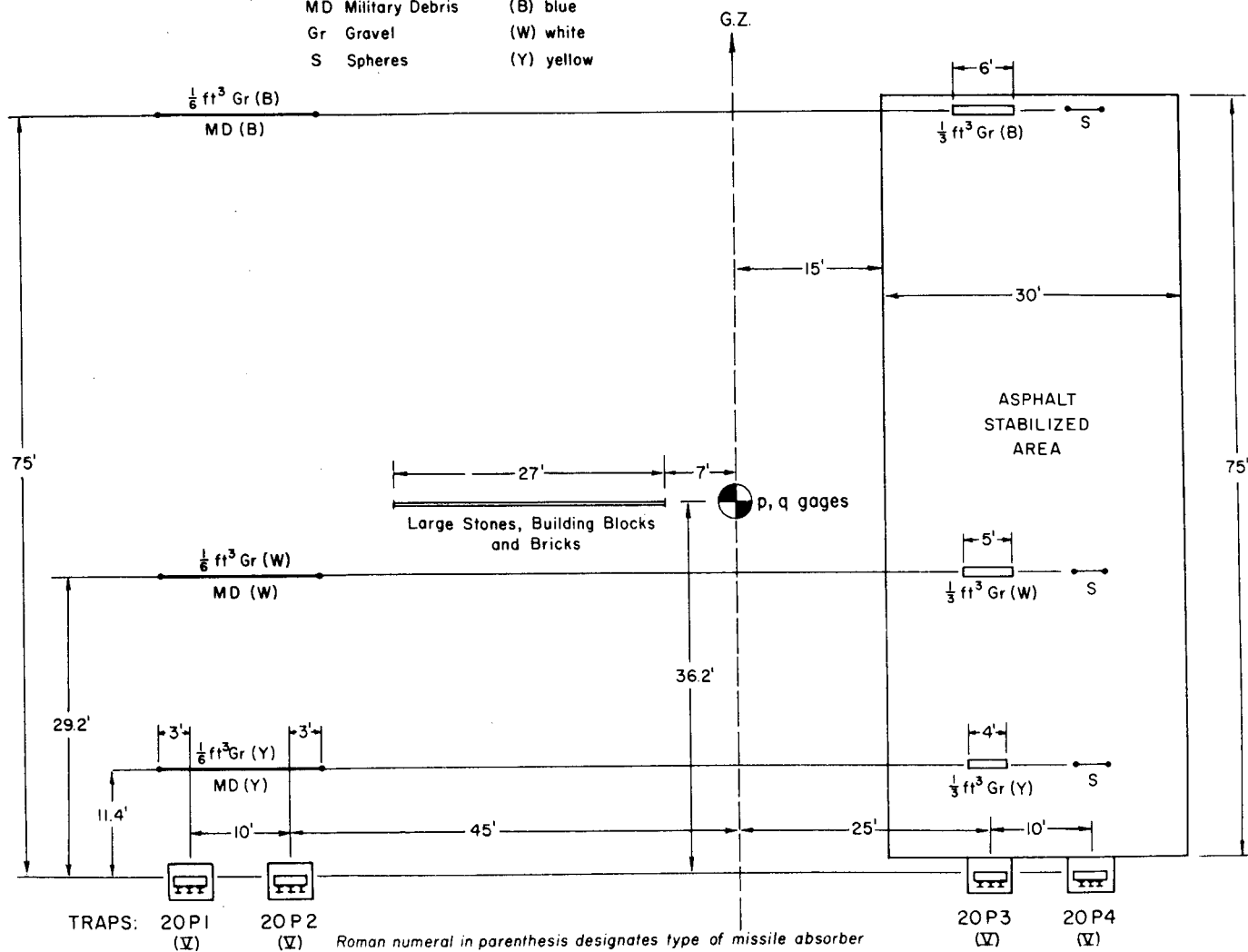
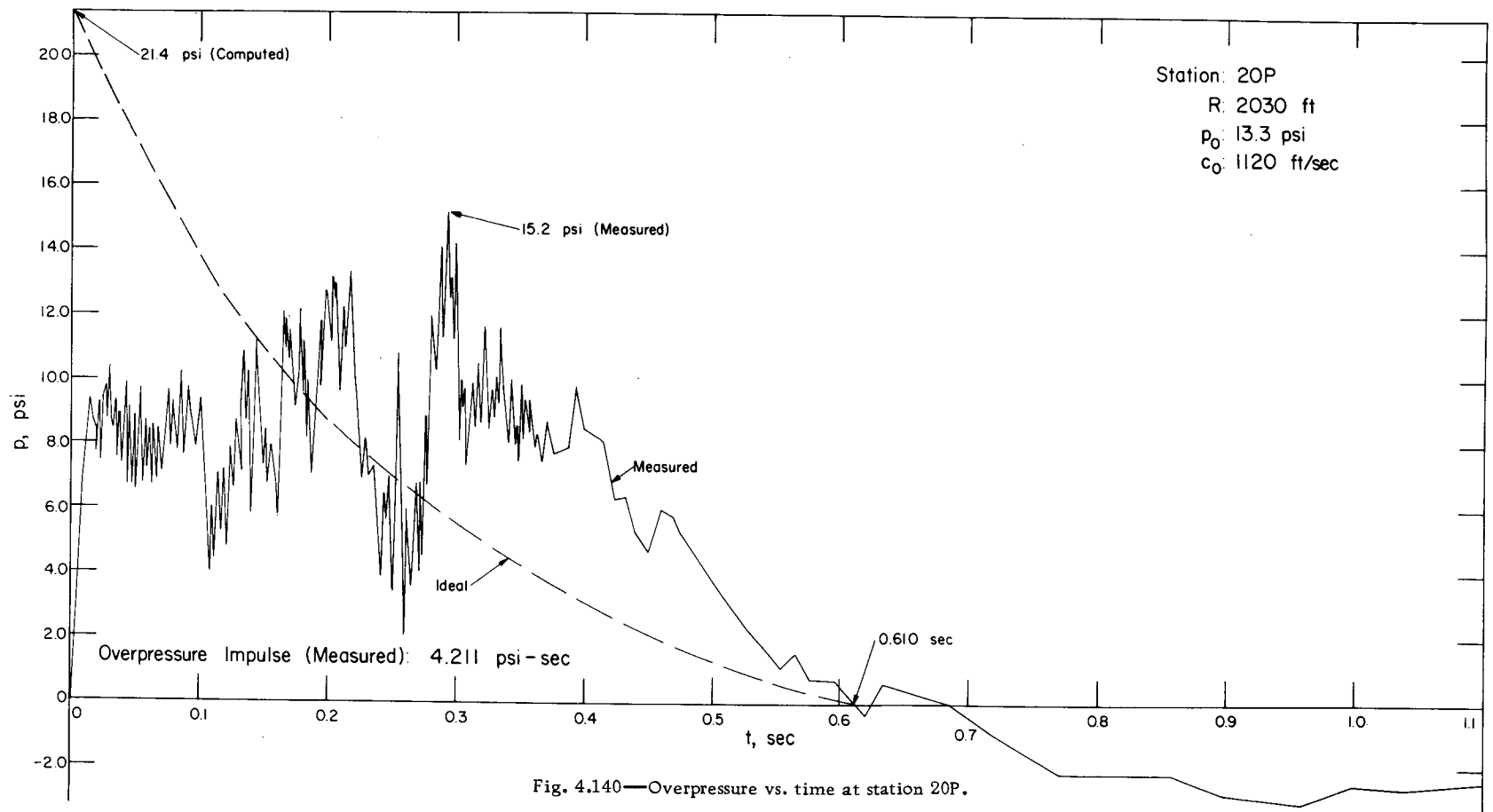


Fig. 4.139—Station 20P layout chart.



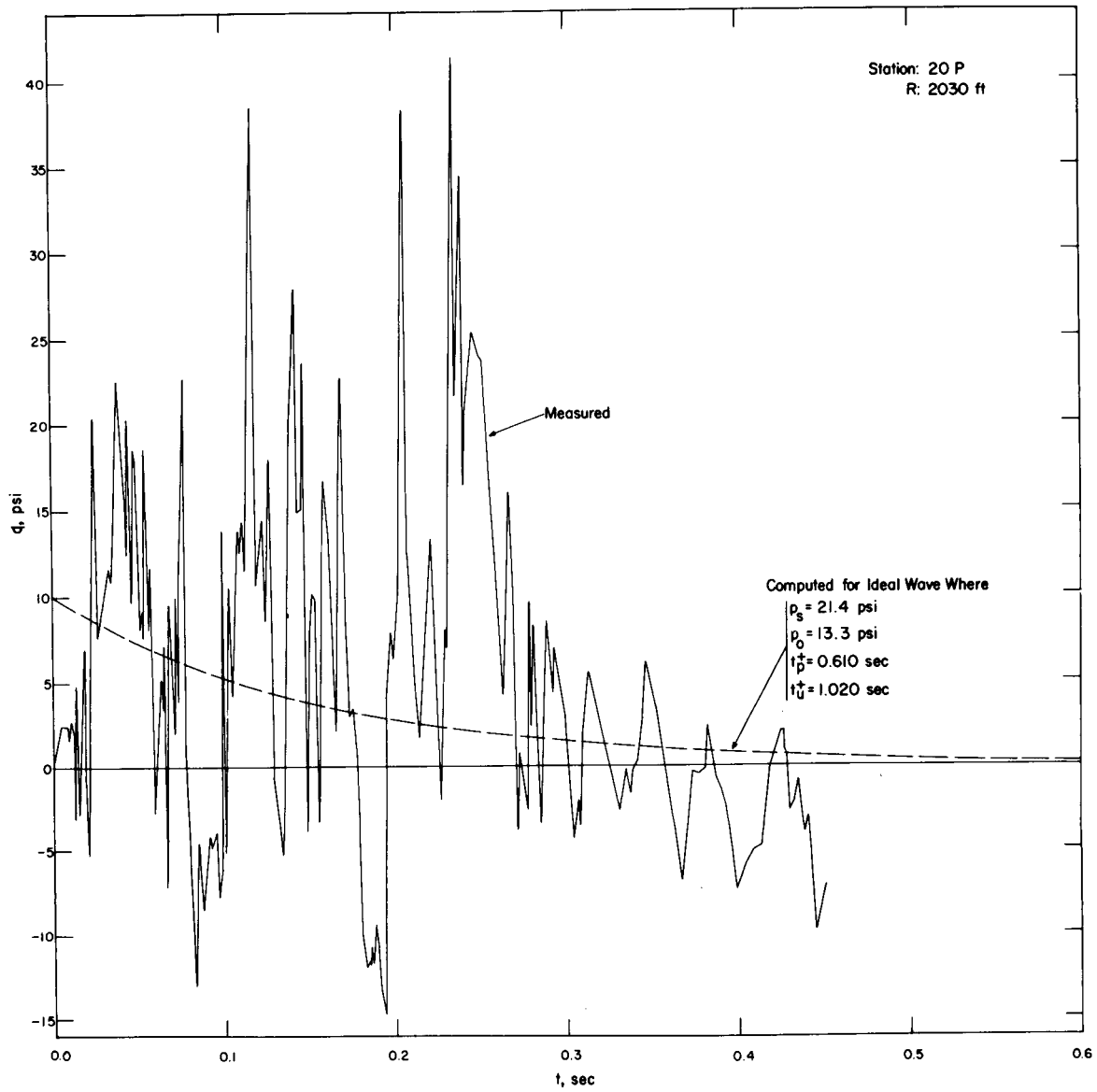


Fig. 4.141—Dynamic pressure vs. time at station 20P.

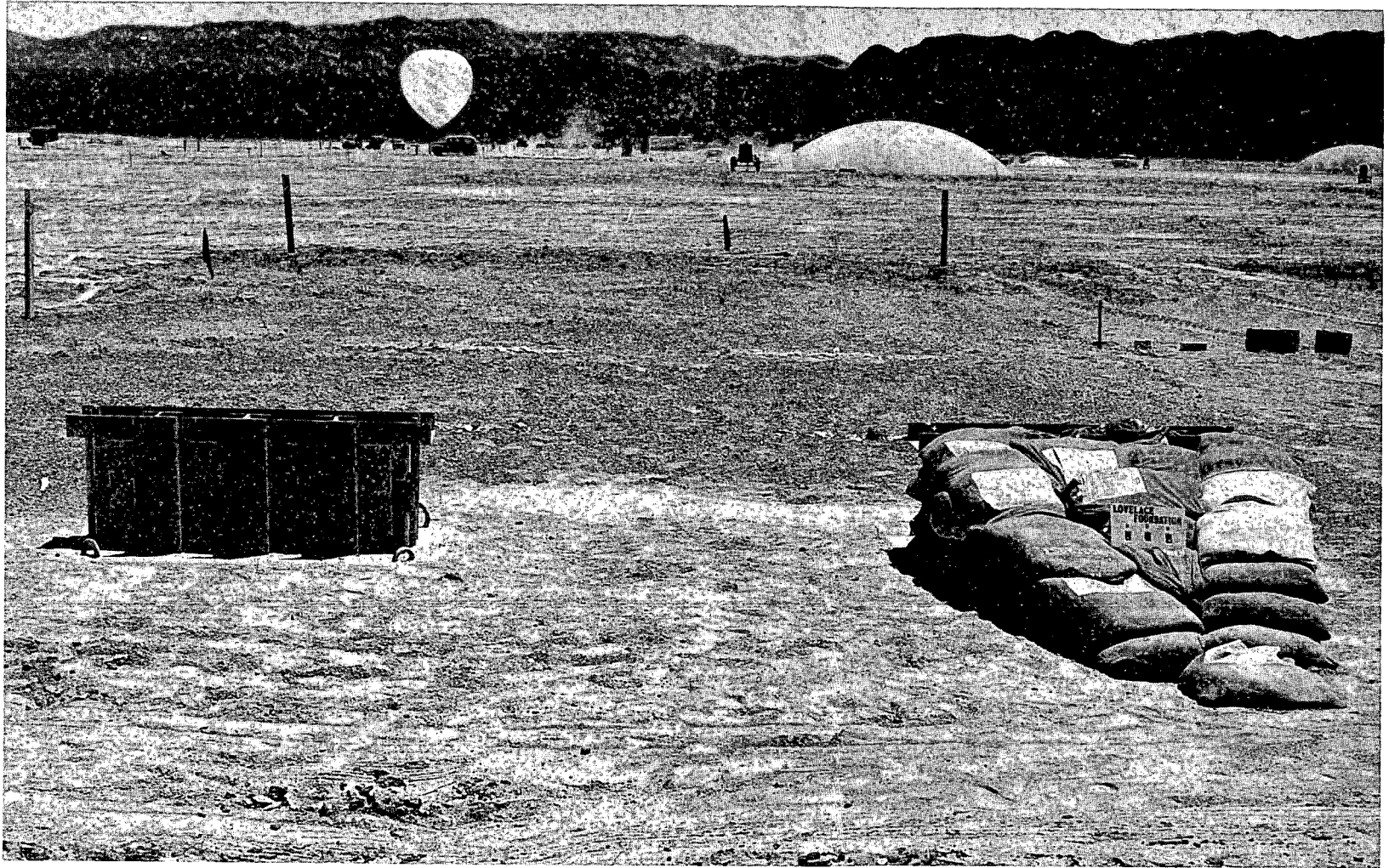


Fig. 4.142—Installations 20P1 and 20P2, preshot, looking toward GZ.

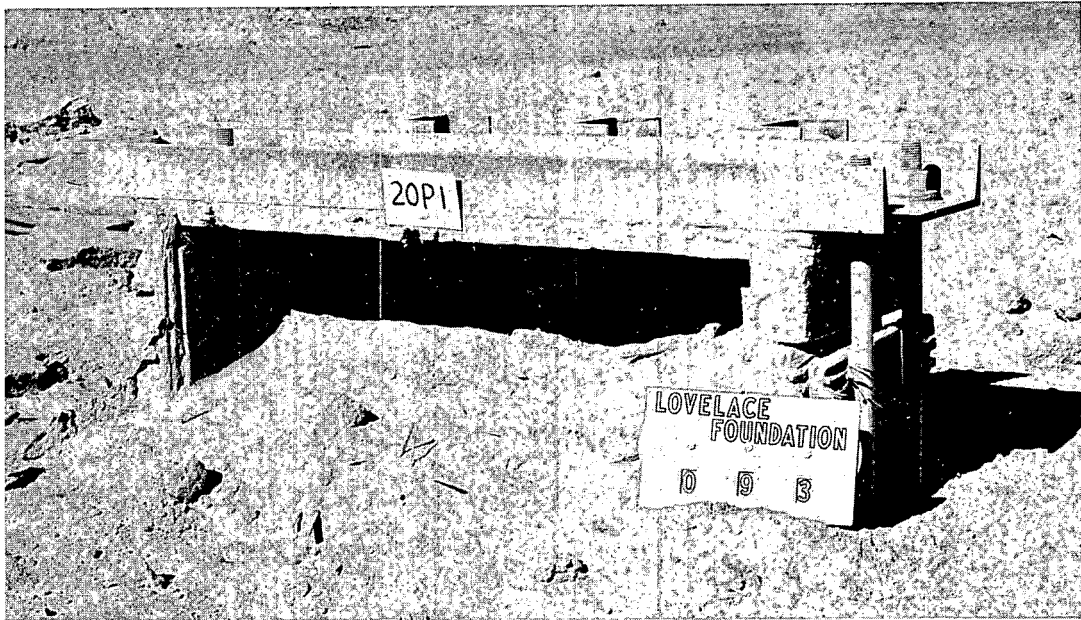


Fig. 4.143— Destroyed installation 20P1, postshot.

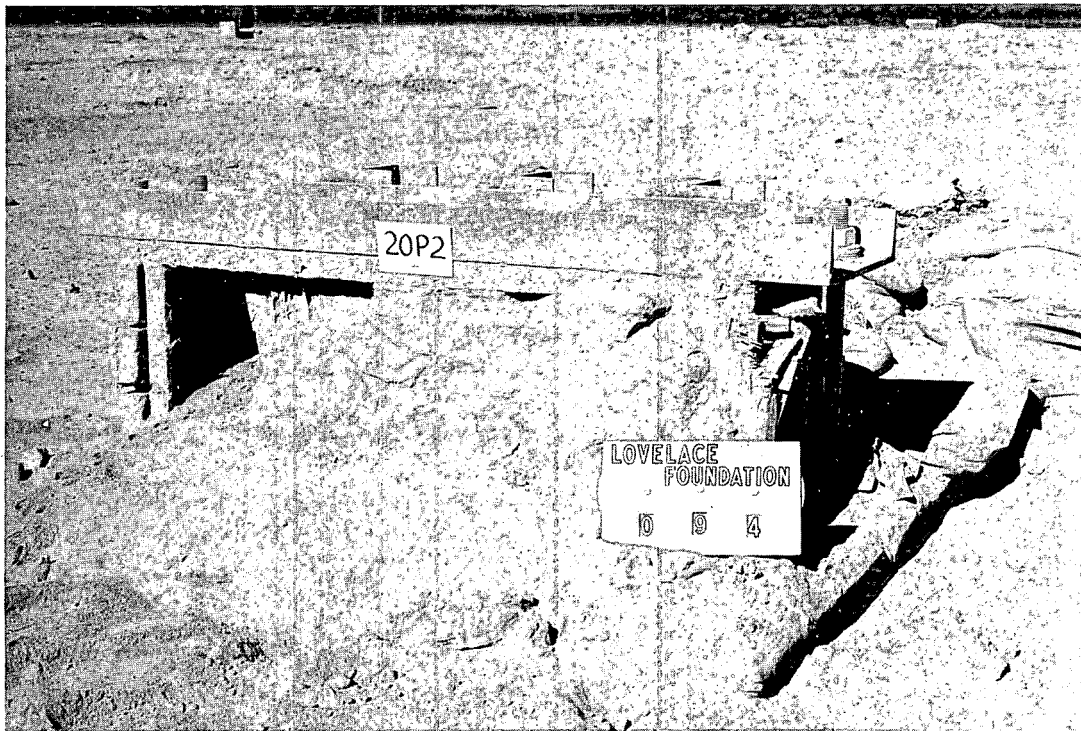


Fig. 4.144— Destroyed installation 20P2, postshot.

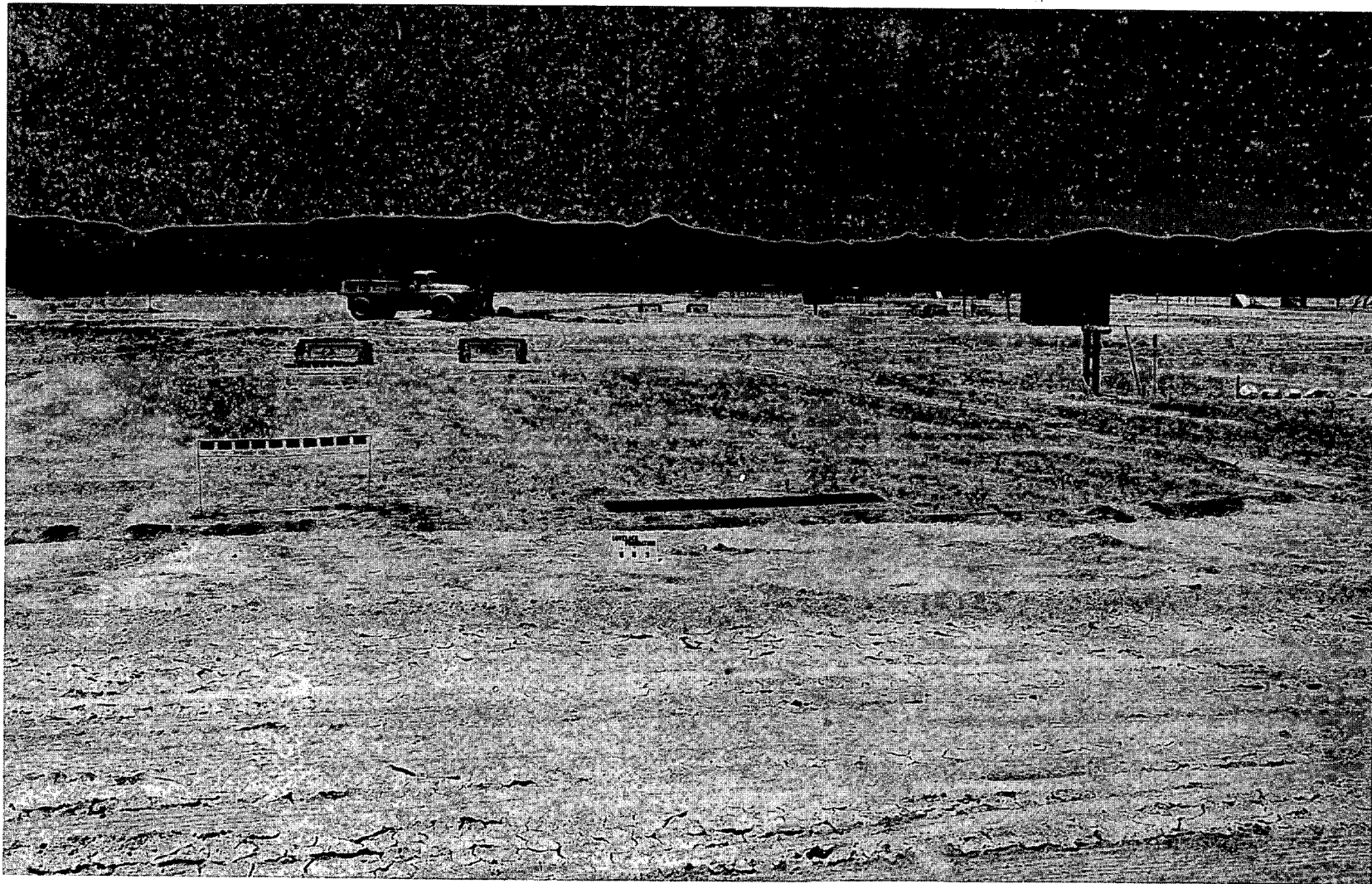


Fig. 4.145—Station 20P, preshot, showing stabilized area and installations 20P3 and 20P4 with spheres and gravel set out.

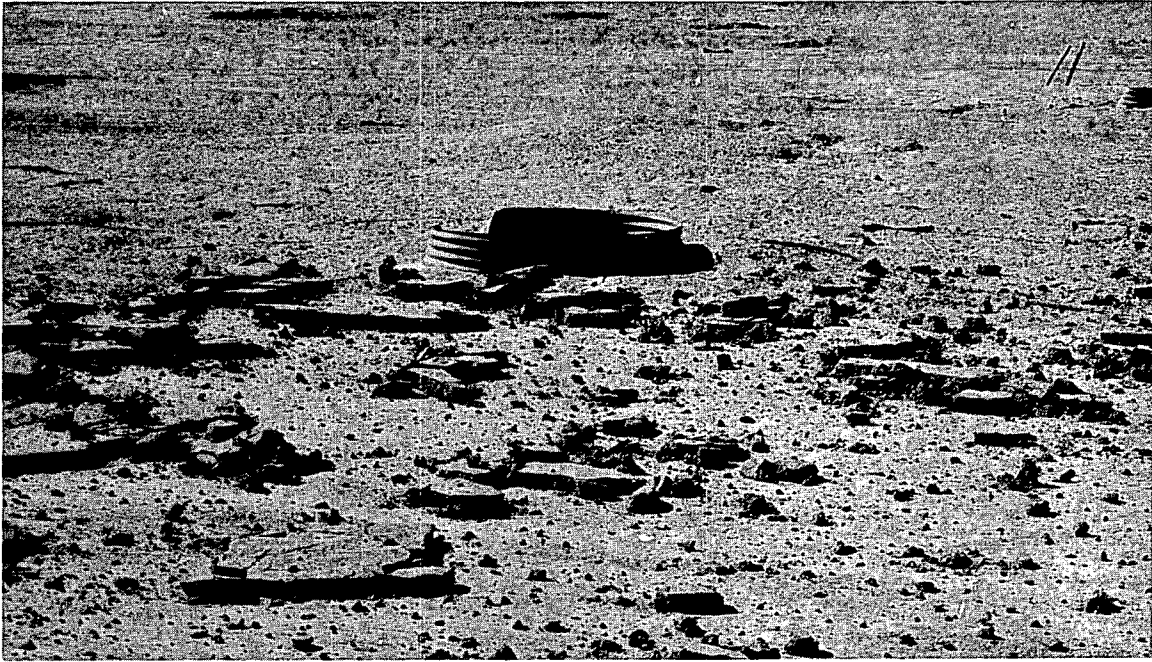


Fig. 4.146—Station 20P, stabilized area, postshot.



Fig. 4.147—Installation 20P3, postshot.

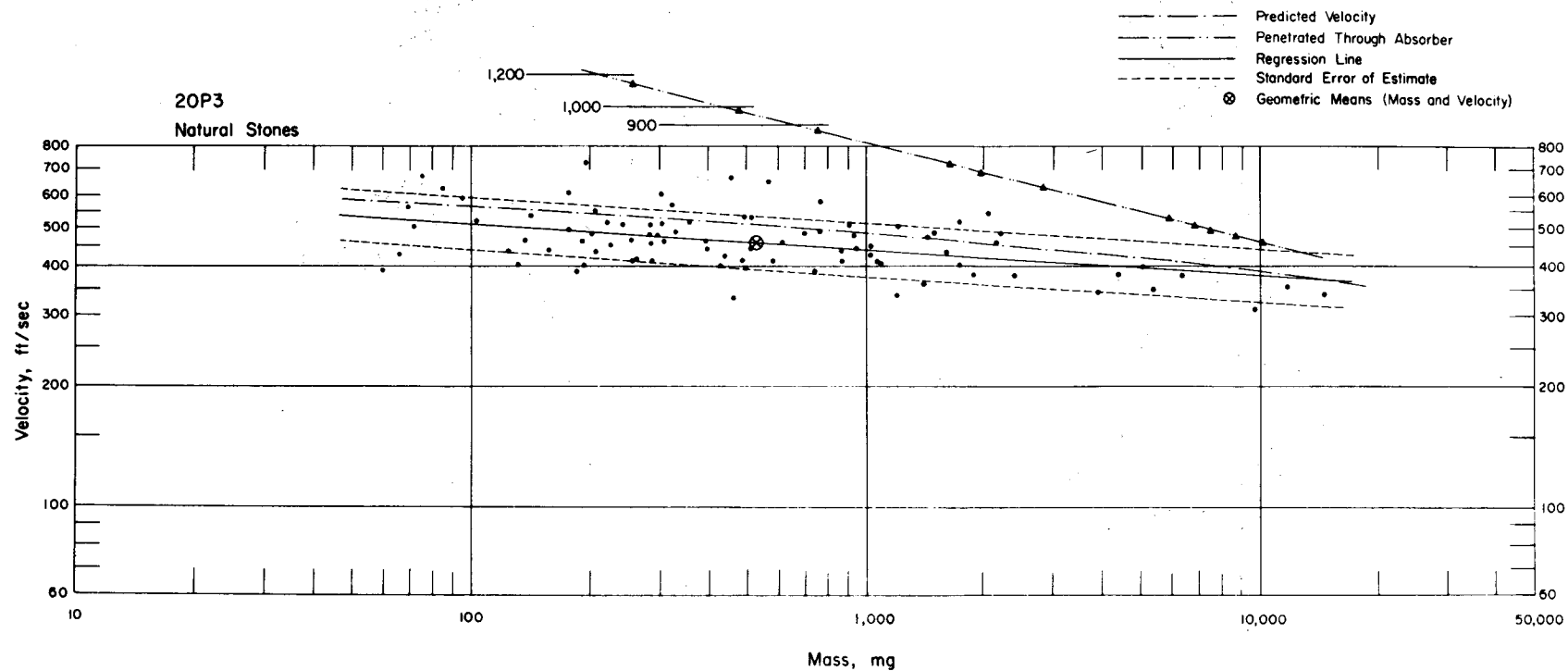


Fig. 4.148—Analysis of natural-stone missiles from installation 20P3: $n = 88$; $\log v = 2.8412 - 0.0659 \log m$; $E_{gV} = 1.16$; $M_{50} = 521$ mg; $V_{50} = 459$ ft/sec. The minimum velocities are plotted for the 11 missiles that penetrated through the absorber into the plywood back of the trap housing. The masses and velocities for those missiles are not included in the analysis.

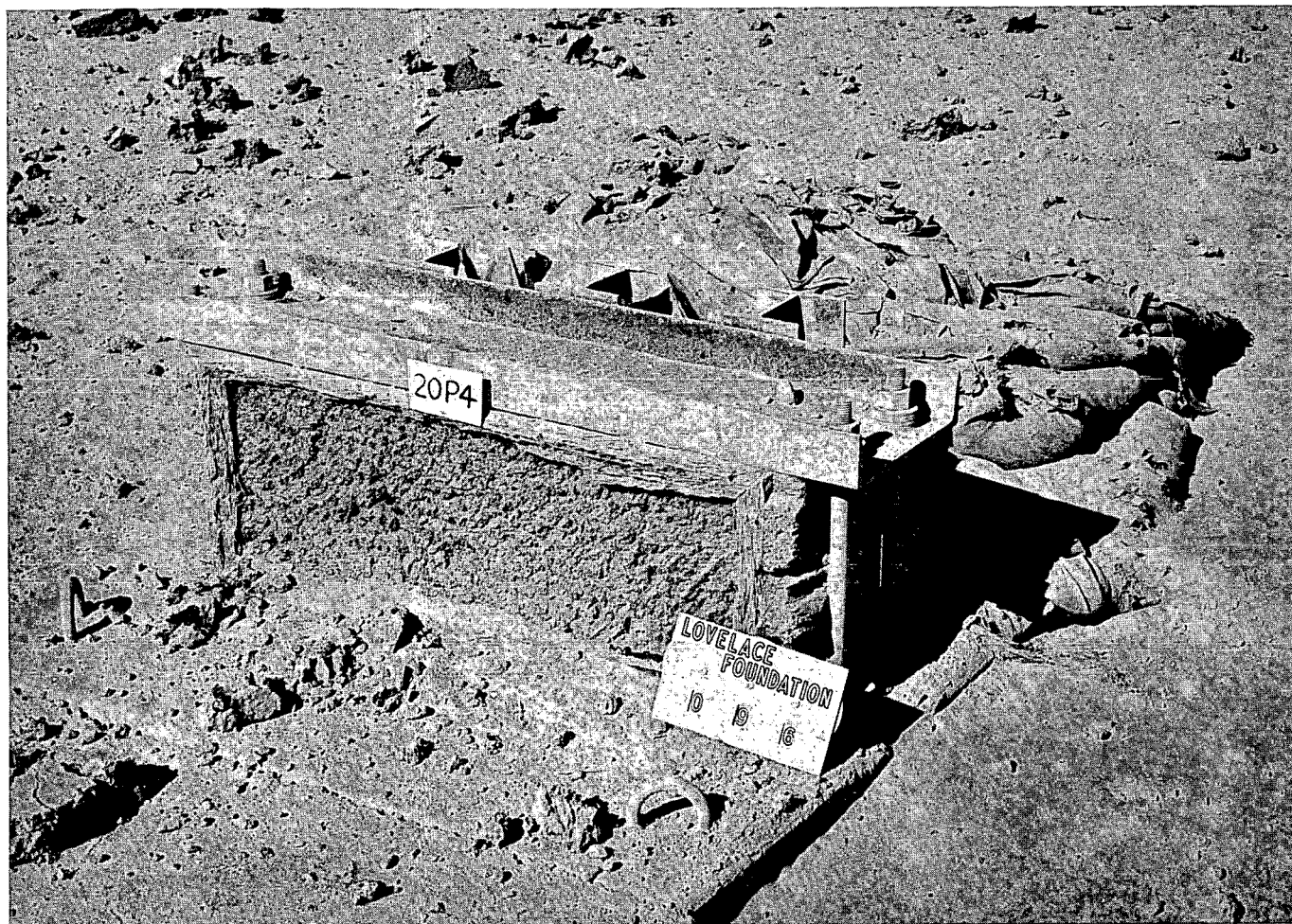


Fig. 4.149—Installation 20P4, postshot (not usable due to erosion).

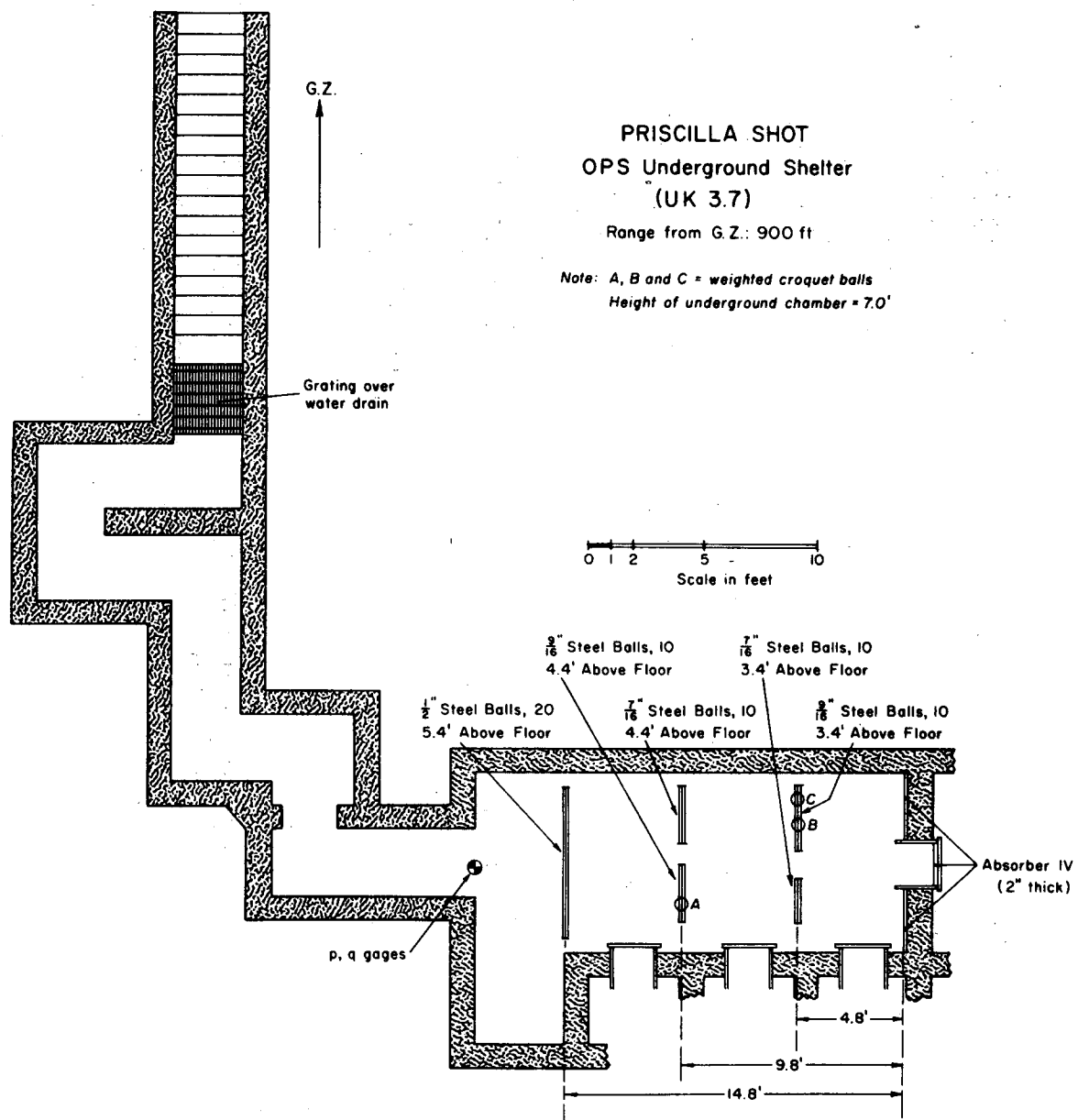


Fig. 4.150—Station OPS layout chart.

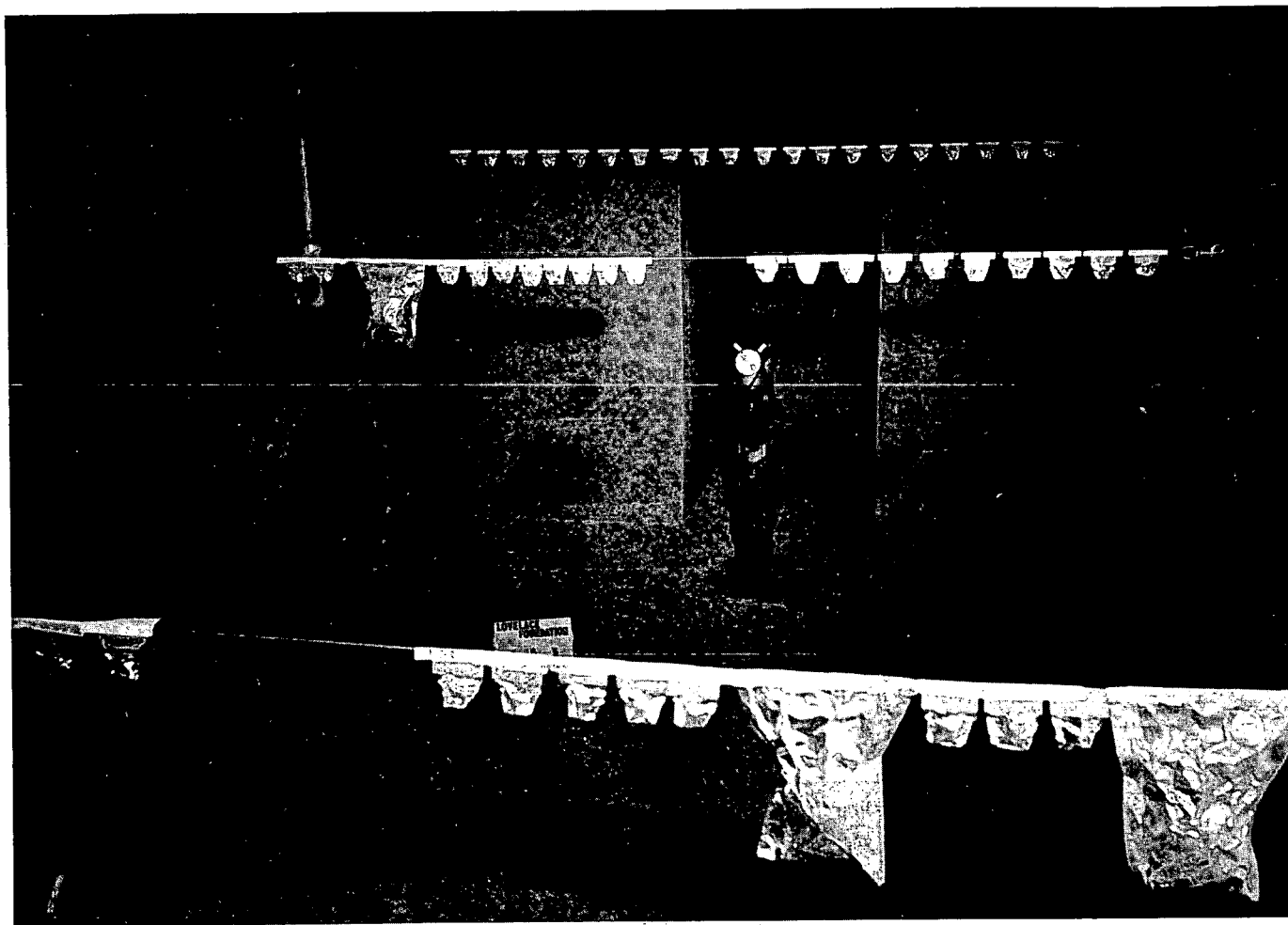


Fig. 4.151—Station OPS, preshot, showing spheres and three croquet balls in foil bags. Photograph was taken near the absorbing material looking toward the entrance.

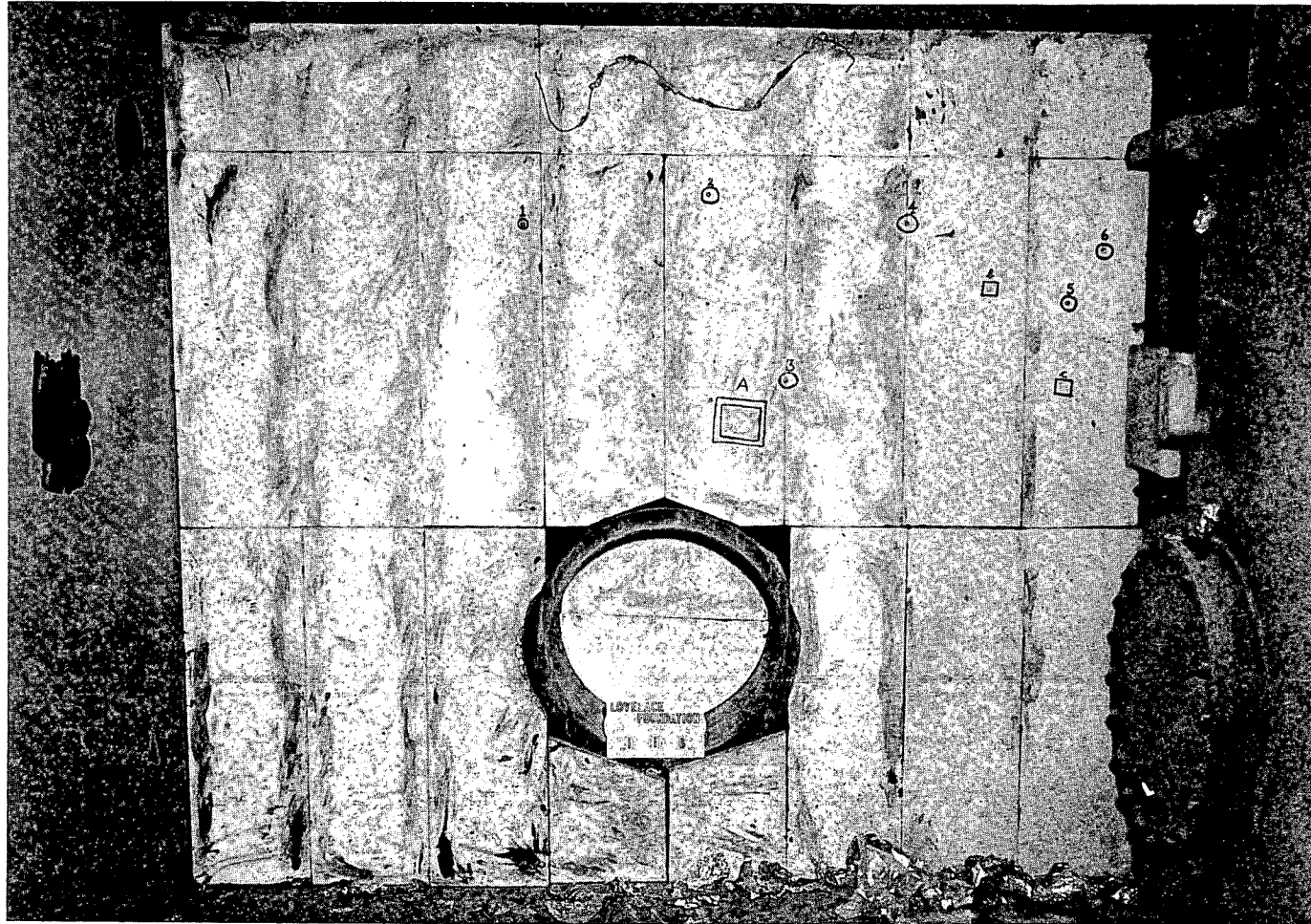


Fig. 4.152—Station OPS, postshot, showing places marked on absorber where spheres and croquet ball impacted. Numbers and letters by impressions correspond to those in Fig. 4.153.

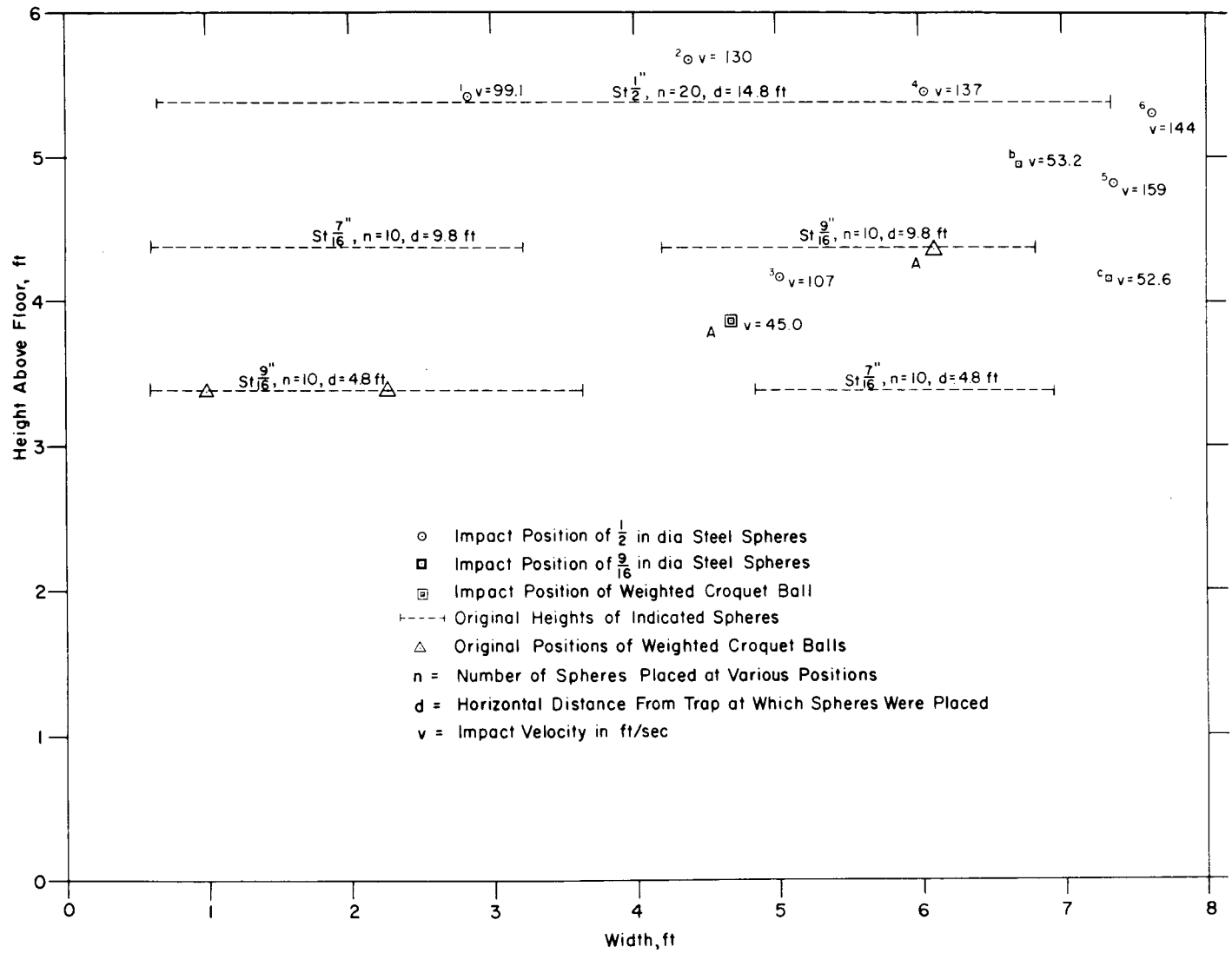


Fig. 4.153—Drawing for station OPS, showing placement of spheres before shot and places on trap surface where spheres impacted. Letters and numbers by recovered spheres correspond with those in Fig. 4.152.

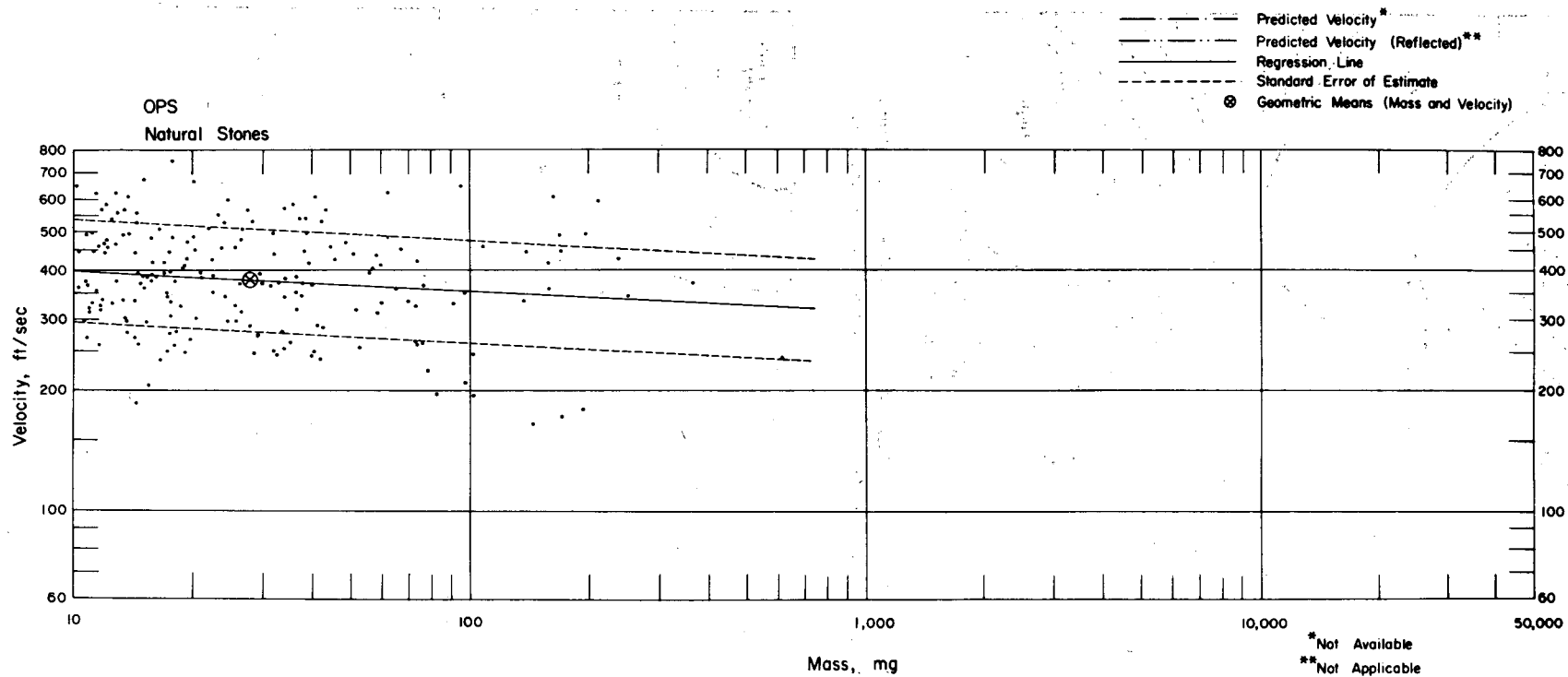


Fig. 4.154—Analysis of natural-stone missiles from station OPS: $n = 194$; $\log v = 2.6493 - 0.0506 \log m$; $E_{gv} = 1.35$; $M_{50} = 28.8$ mg; $V_{50} = 376$ ft/sec.

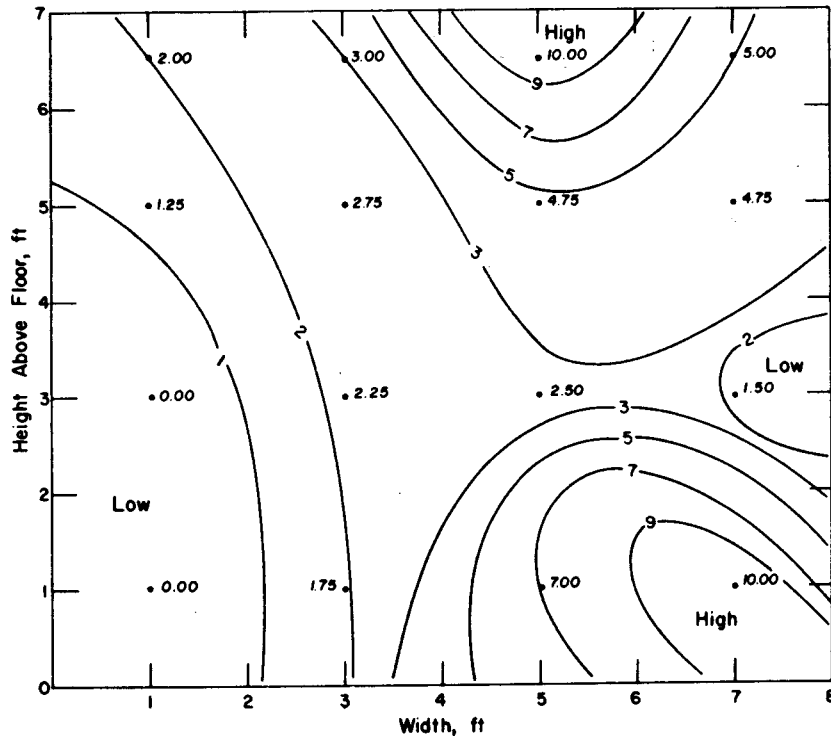


Fig. 4.155—Spatial distribution of natural-stone missiles recovered from station OPS. Numbers indicate missiles per square foot.

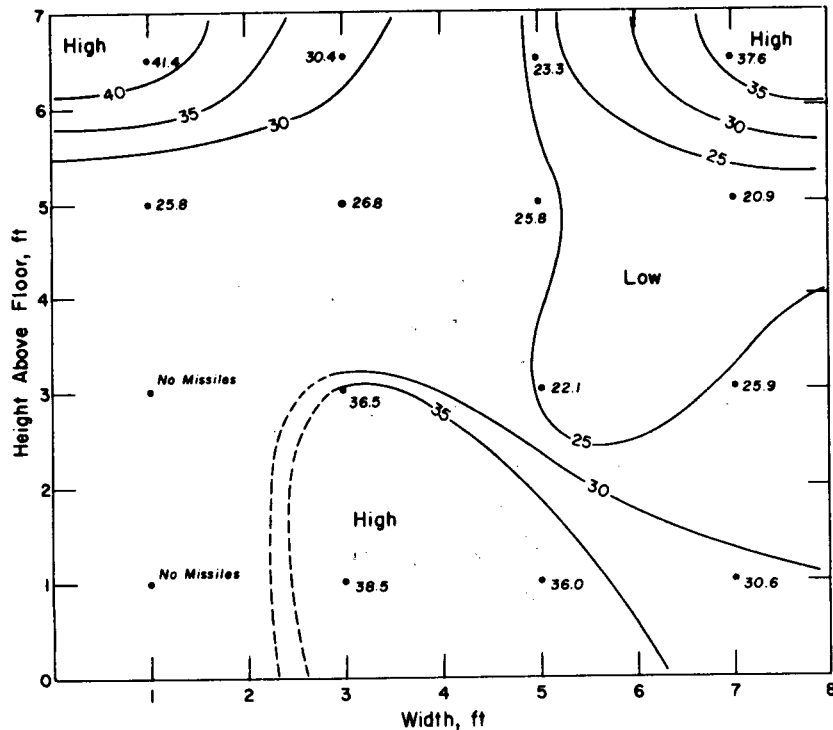


Fig. 4.156—Spatial distribution of the average masses (in mg) of natural-stone missiles recovered from station OPS. The average mass of missiles caught within a particular area segment was plotted at the center of the segment.

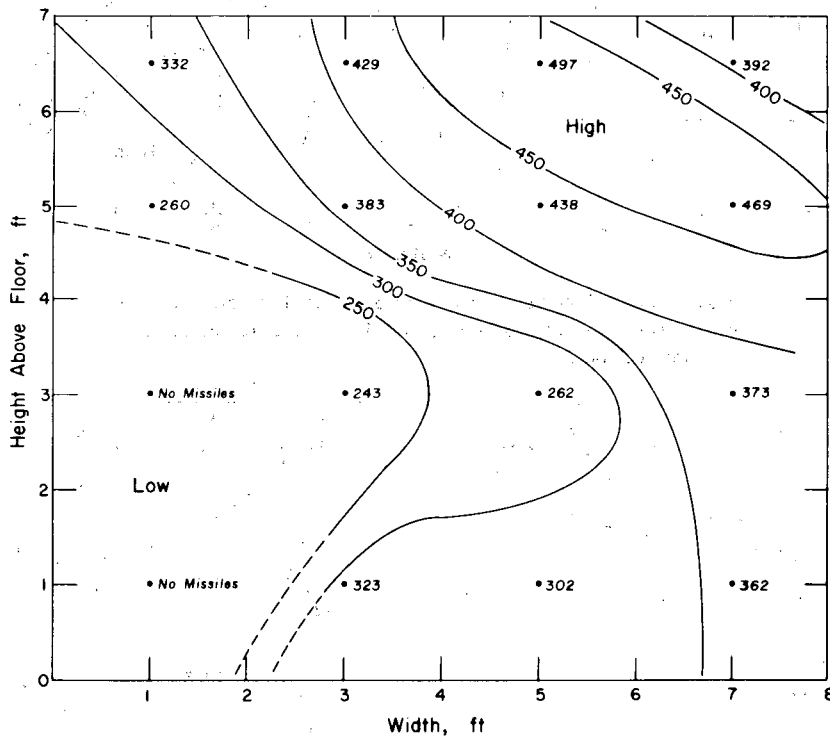


Fig. 4.157—Spatial distribution of the average velocities (in ft/sec) of natural-stone missiles recovered from station OPS. The average velocity of missiles caught within a particular area segment was plotted at the center of the segment.

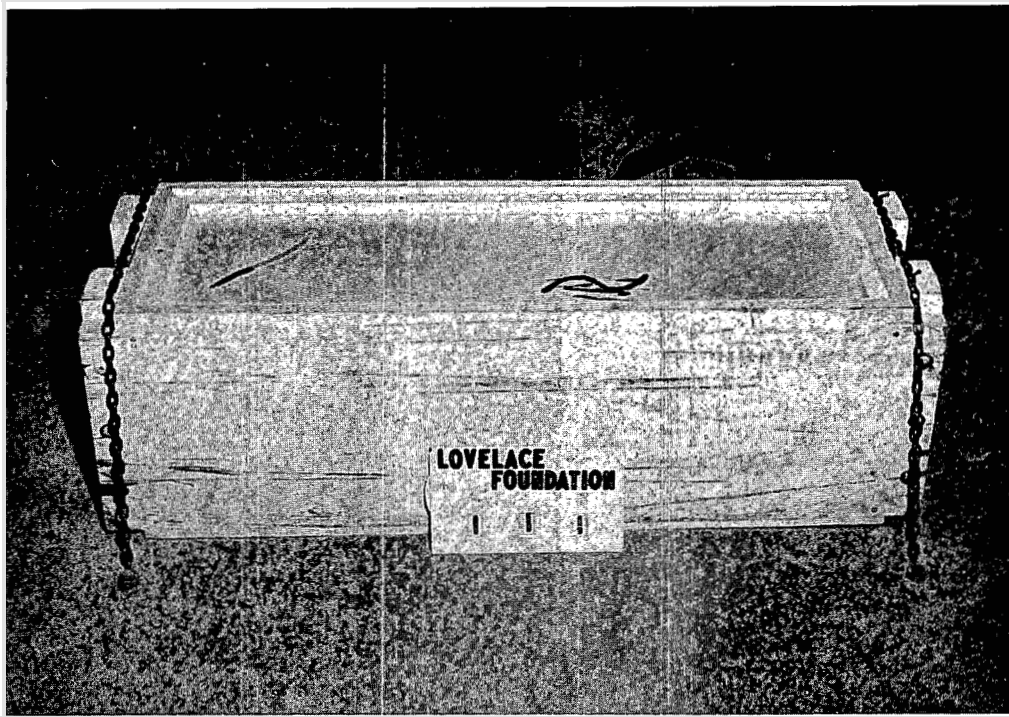


Fig. 4.158— Typical trap installation in arch type shelters. See Ref. 3 for details of shelter construction.



Fig. 4.159— Typical installation of missile absorber in conduit type shelters. See Ref. 4 for details of shelter construction.

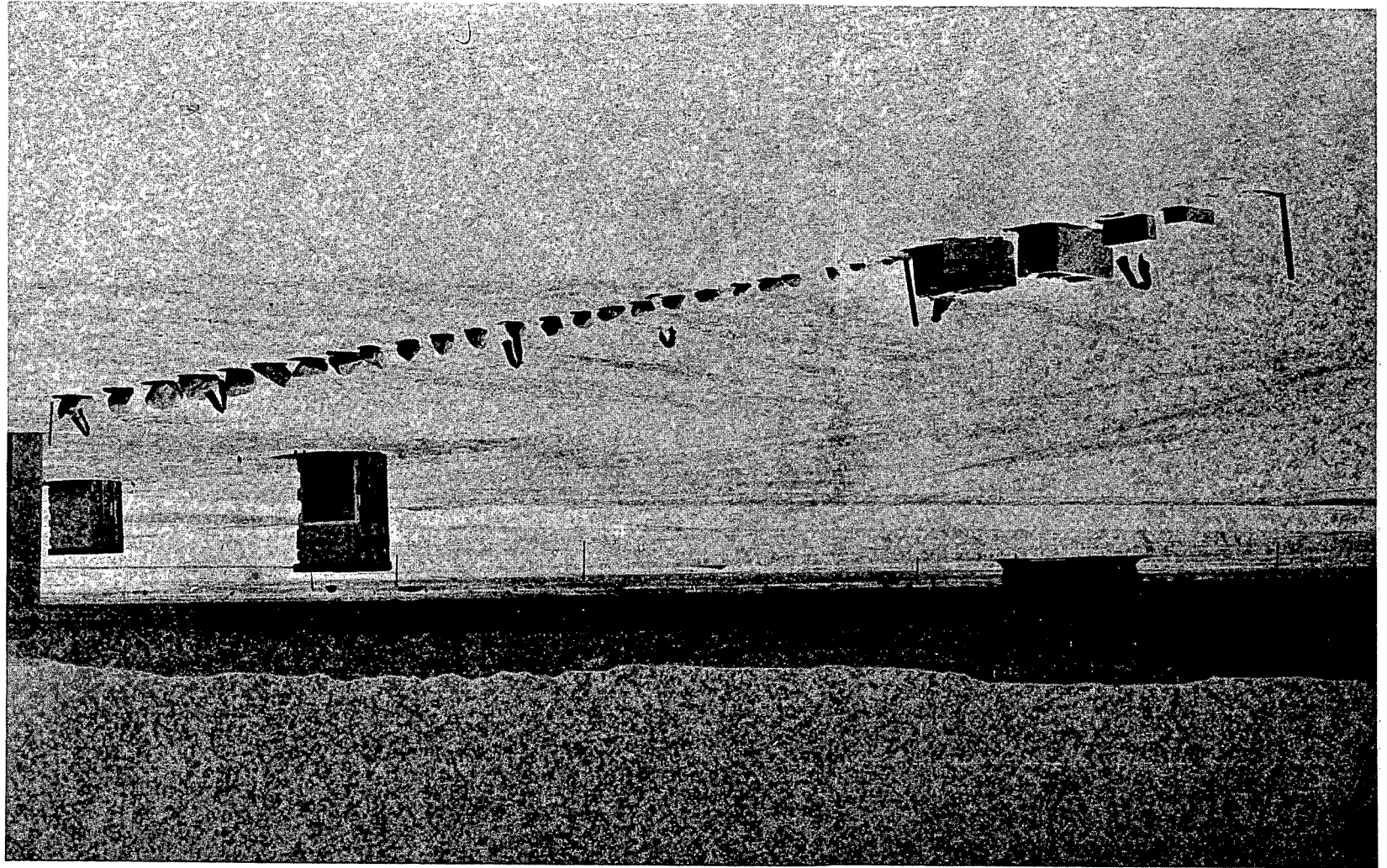


Fig. 4.160—Station 4P and large stones, preshot.



Fig. 4.161—Station 4P and large stones, postshot.

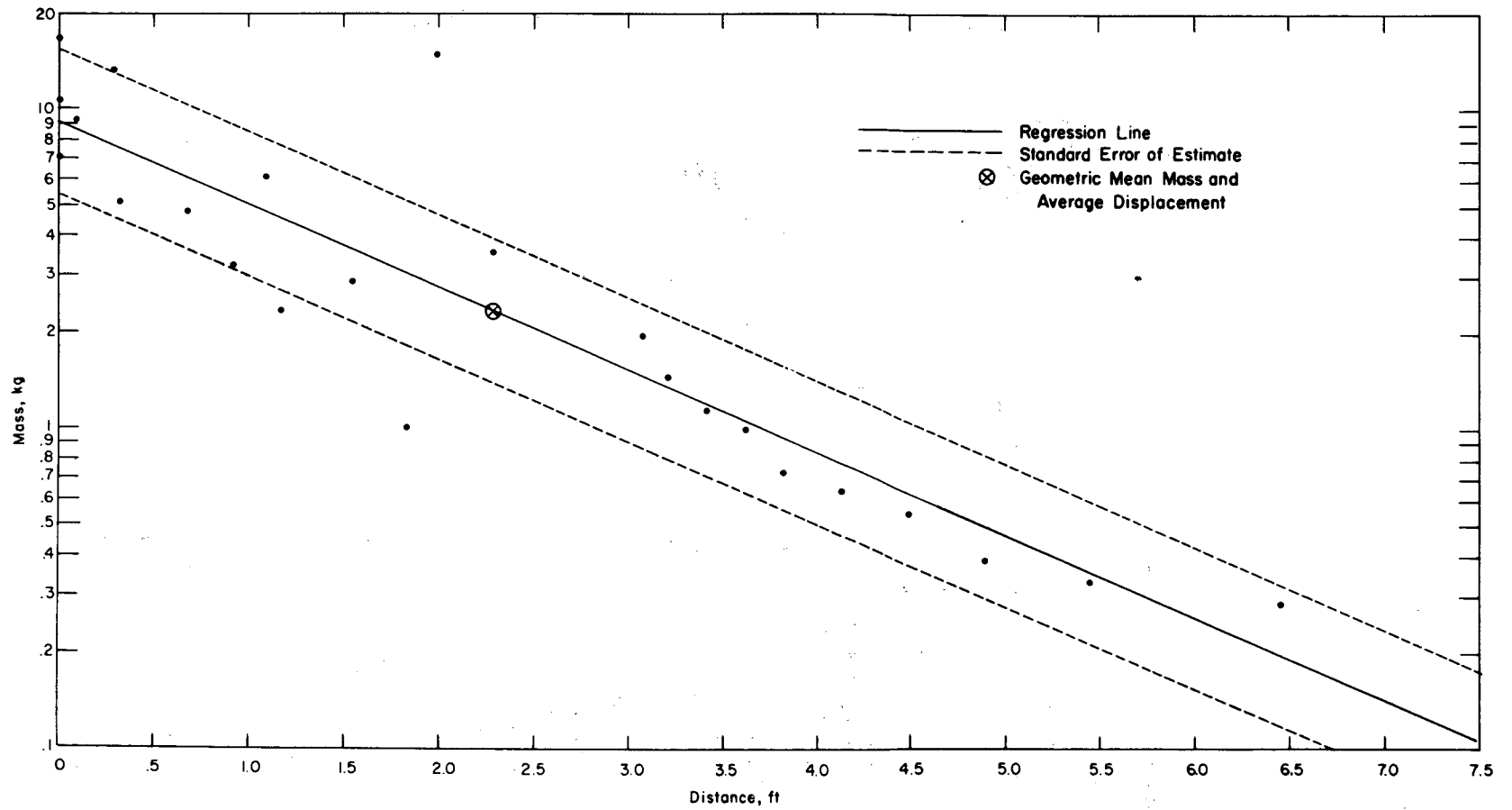


Fig. 4.162—Mass vs. distance for large stones displaced at station 4P: range = 6120 ft; $n = 24$; $\log m = 0.9616 - 0.2579 d$; $E_{gm} = 1.68$; $M_{50} = 2.357$ kg; $\bar{d} = 2.29$ ft.

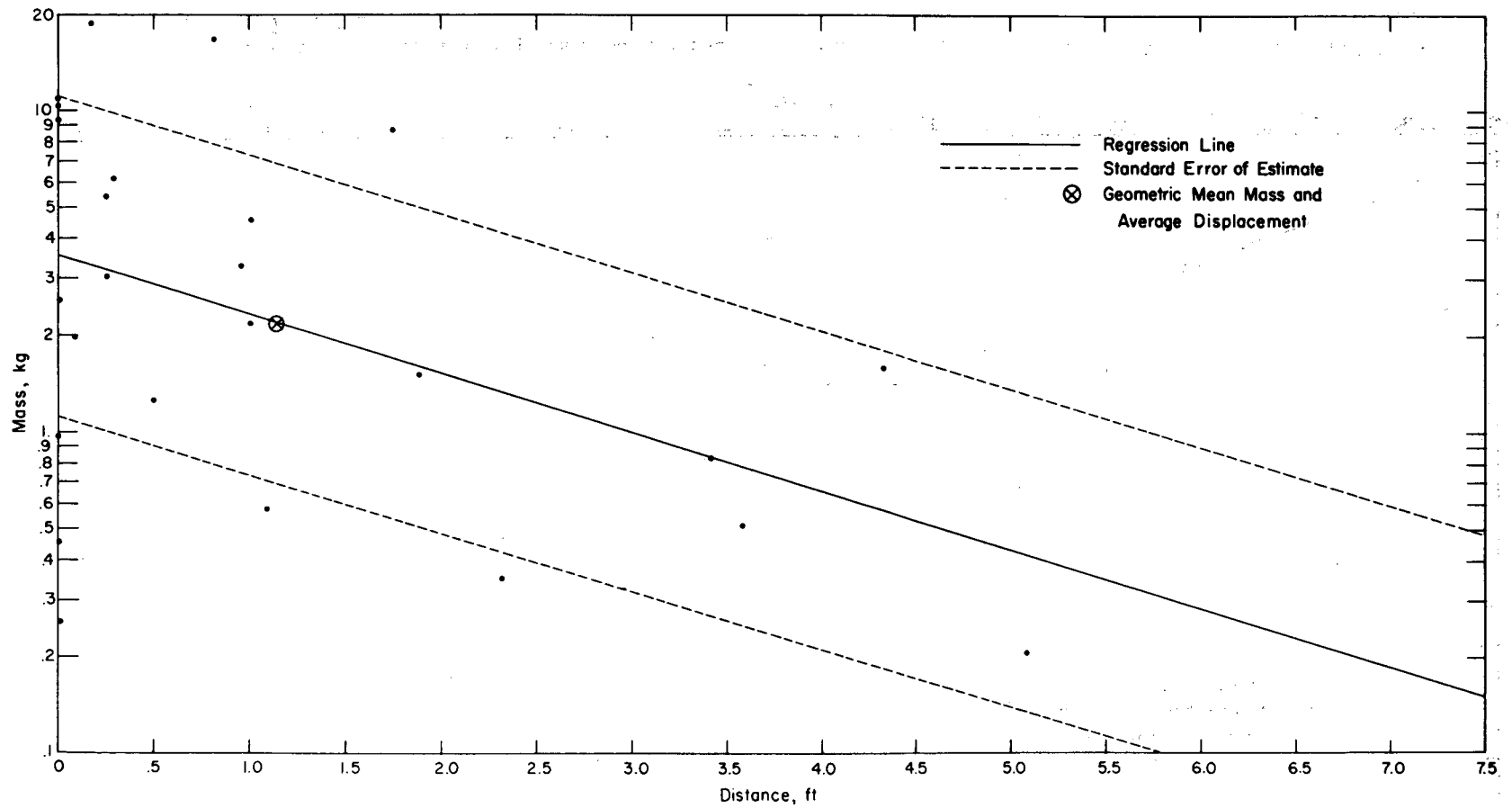


Fig. 4.164—Mass vs. distance for large stones displaced at station 6P: range = 4770 ft; $n = 25$; $\log m = 0.5475 - 0.1817 d$; $E_{gm} = 3.16$; $M_{50} = 2.180$ kg; $\bar{d} = 1.15$ ft.

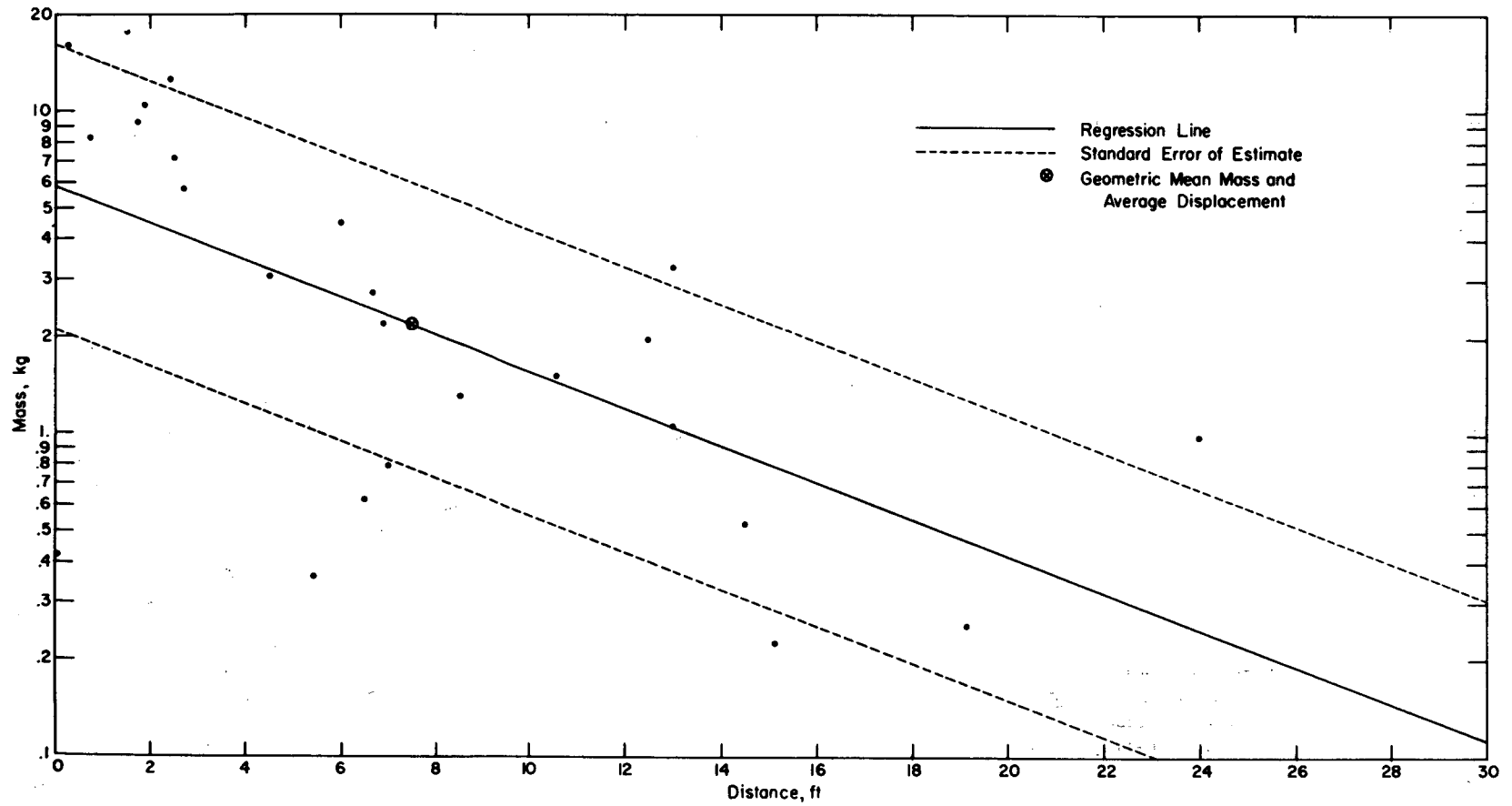


Fig. 4.165—Mass vs. distance for large stones displaced at station 8P: range = 3930 ft; $n = 25$; $\log m = 0.7674 - 0.0573 d$; $E_{gm} = 2.78$; $M_{50} = 2.178$ kg; $\bar{d} = 7.50$ ft.

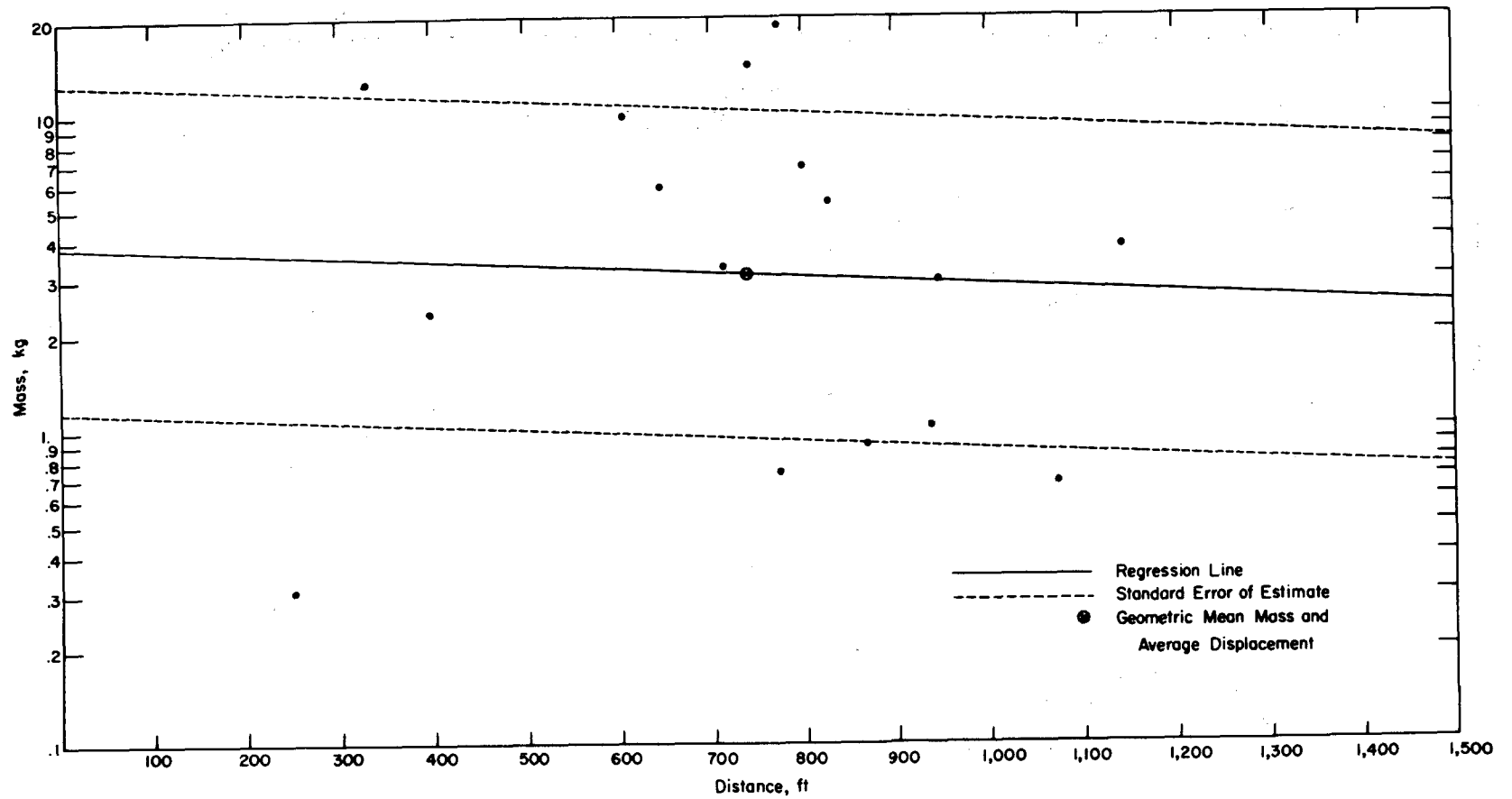


Fig. 4.166—Mass vs. distance for large stones displaced at station 10P: range = 2730 ft; $n = 16$; $\log m = 0.5872 - 0.0001 d$; $E_{gm} = 3.30$; $M_{50} = 3.105$ kg; $\bar{d} = 739$ ft.

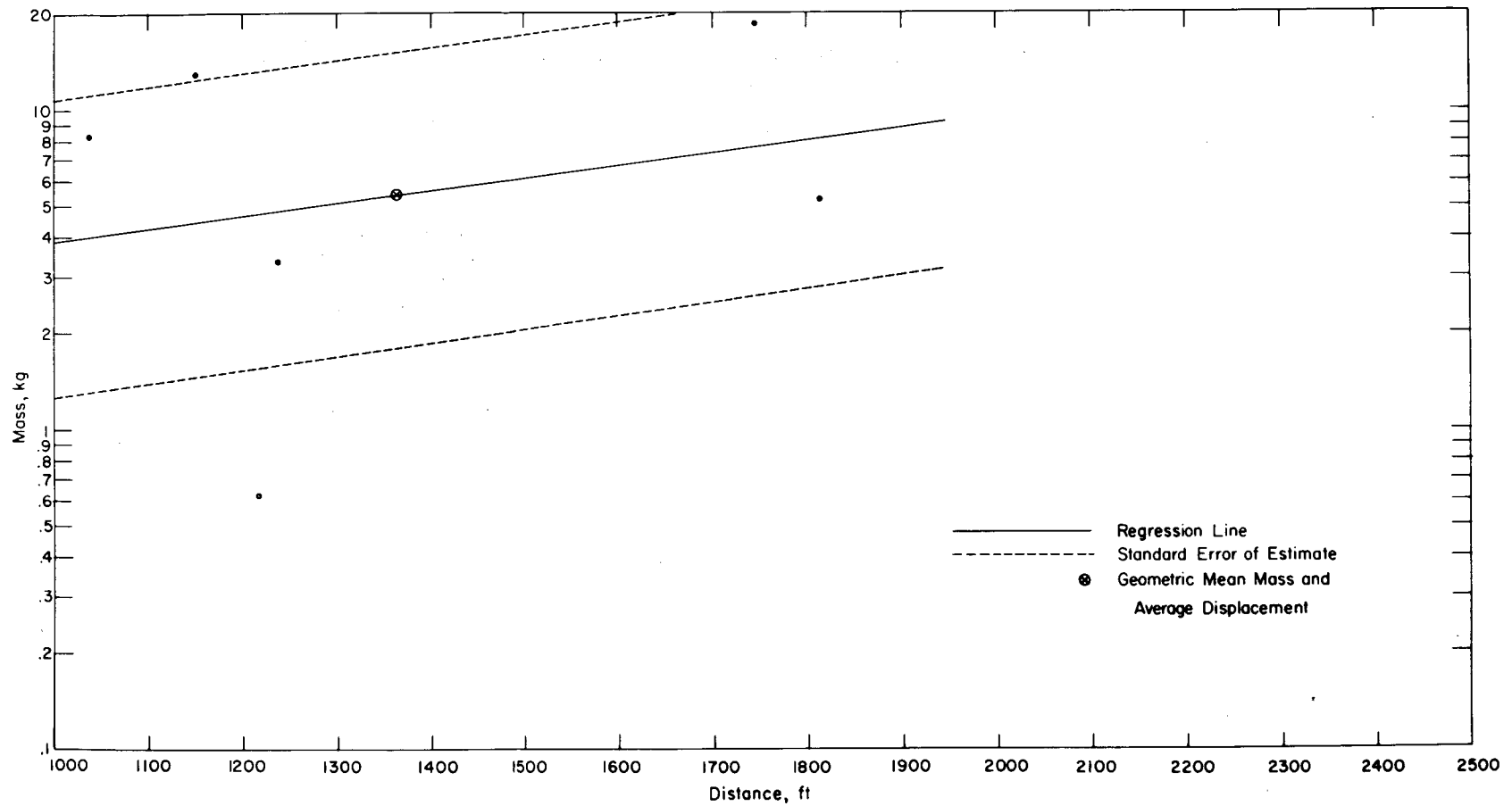


Fig. 4.167—Mass vs. distance for large stones displaced at station 15P: range = 2280 ft; $n = 6$; $\log m = 0.1490 + 0.0004 d$; $E_{gm} = 2.93$; $M_{50} = 5.296$ kg; $\bar{d} = 1367$ ft.

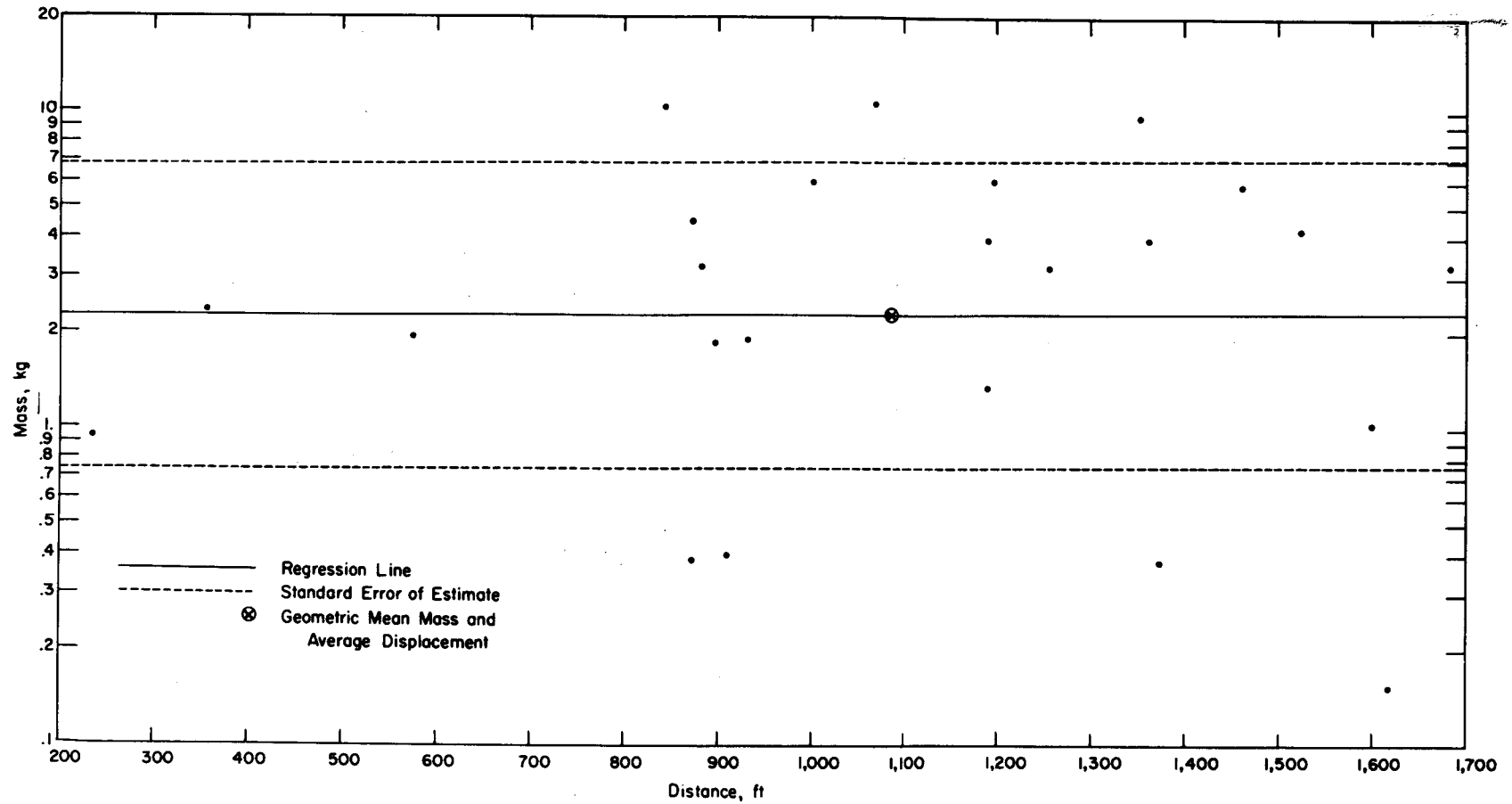


Fig. 4.168—Mass vs. distance for large stones displaced at station 20P: range = 2030 ft; $n = 24$; $\log m = 0.3504 + 0.000009 d$; $E_{gm} = 3.06$; $M_{50} = 2.293$ kg; $\bar{d} = 1094$ ft.

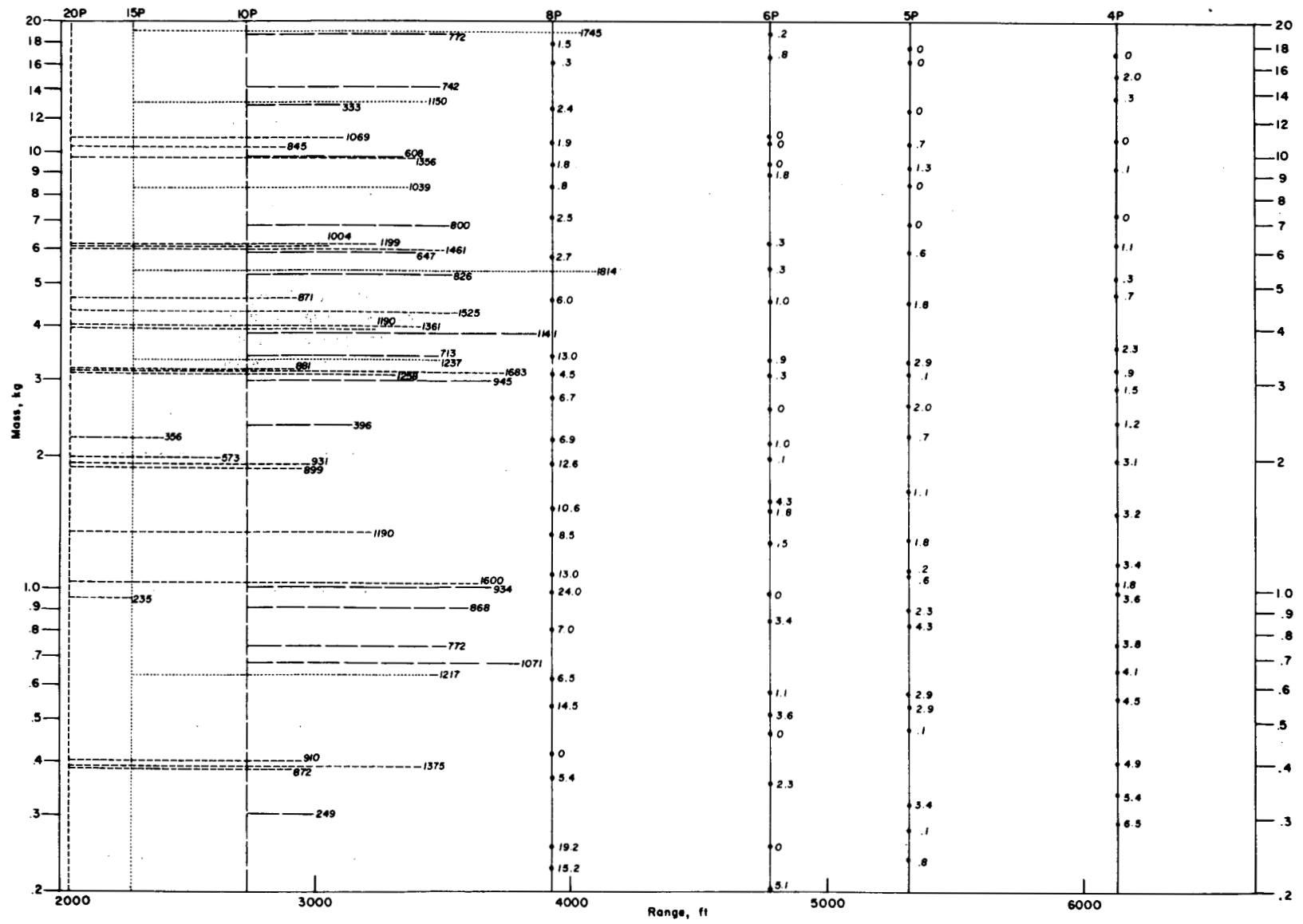


Fig. 4.169—Displacement of marked large stones for seven stations, shot Priscilla.

Chapter 5

SHOT SMOKY, EXPERIMENTAL PROCEDURE AND RESULTS

5.1 GENERAL

The primary purpose for participation in shot Smoky* was to determine the effect of hill-and-dale terrain upon the translation of native (or natural) stones, steel spheres, and military debris. All experiments were made in open areas at ranges of 2548 to 5680 ft, where the measured overpressures varied from about 13 to 5 psi. The yield estimated for this shot, on the basis of certain blast parameters, was 44.5 kt (see Table 5.1).

Locations of the nine stations used in this shot are shown in Fig. 5.1: two on flat terrain on the south blast line, three on hills and three in dales on the northeast line, and one in a dale on the north line. Two trap bases were installed at each station, one base for a single trap and the other for two traps.

A total of 405 steel spheres with diameters of $\frac{7}{16}$, $\frac{1}{2}$, and $\frac{9}{16}$ in. was placed at various distances in front of the traps. In addition, a total of about 3850 pieces of military debris whose masses varied from approximately 1 to 1000 g was set out. Figure 5.2 illustrates a typical placement of debris and spheres. The spheres were placed a short distance above ground level in a shallow trough supported by $\frac{1}{8}$ -in. steel rods.

Experience in shot Priscilla indicated that under certain conditions additional shielding was necessary to protect the absorbing material against thermal radiation. This was accomplished, as illustrated in Fig. 5.3, by mounting 0.0015-in.-thick aluminum foil on a wooden frame about 1 ft in front of the face of the trap. The foil was ruptured and blown aside by the blast, and therefore it presented no obstruction to the missiles striking the traps.

The northeast, south, and north blast lines are discussed in Secs. 5.2, 5.3, and 5.4, respectively. In each section the material pertaining to the terrain of the blast line, along with a discussion of the effects of the terrain on the blast wave, is followed by a station-by-station presentation of the blast-wave and missile data.

A summary of the blast parameters for all stations used in this shot is presented in Table 5.1 (two extra stations are included where there were no missile studies). An explanation of the various parameters tabulated is included in the table. However, the reader is reminded that the computed value of peak overpressure, $(p_s)_c$, was obtained by finding the classical (or ideal) wave whose impulse and duration were equal to those values measured by the BRL gauges.¹ The difference between computed and measured values of overpressure is a rough measure of the nonconformity of the measured wave to an ideal one. This point will be made much clearer upon examination of the overpressure vs. time curves to be presented later in the sections that describe each of the nine stations.

Only 2 of the approximately 3850 pieces of military debris placed in front of the Smoky traps were recovered. Five of 405 steel spheres were recovered. Data pertaining to these 7 objects are presented at the bottom of Table 5.2. Velocities and masses were determined for

* Detonated on a 700-ft tower in Area 2C, Nevada Test Site.

2876 natural-stone missiles caught in the traps placed in this shot. Plots of these data, by trap, will be found in the sections that describe each station. In addition, statistical parameters* for all recovered missiles are summarized in Table 5.2. It should be noted in particular that Table 5.2 also contains the results of a statistical analysis of the data for natural stones combined from all three traps located at each of the nine stations. A mass vs. velocity plot was not made of the combined data at each station.

TABLE 5.1—BLAST PARAMETERS, SHOT SMOKY
(See List of Symbols.)

$p_0 = 12.4 \text{ psi}$ $c_0 = 1118 \text{ ft/sec (15.2°C)}$ Estimated yield: 44.5 kt⁽¹⁾ Terrain: hill, dale, and flat

Station	Range, ft	Blast line	Terrain	$(I_p)_m$, ⁽²⁾ psi-sec	$(I_p)_r$, ⁽³⁾ psi-sec	$(t_p^+)_{m,}$, ⁽²⁾ sec	$(t_p^+)_{r,}$, ⁽⁴⁾ sec	$(p_s)_m$, ⁽²⁾ psi	$(p_s)_c$, ⁽⁵⁾ psi	$(p_s)_r$, ⁽⁶⁾ psi
9S	5680	S	Flat	2.049	2.010	1.118	1.081	5.1	4.80	4.84
8S	4980	NE	Dale	2.280	2.257	0.984	1.014	5.0	6.20	5.92
	4155	S	Flat	2.671	2.645	0.929	0.929	6.5	7.90	7.82
7S	4115	NE	Hill	2.480	2.668	0.932	0.925	7.4	7.25	7.93
	3875	S	Flat	2.840	2.813	0.904	0.899	7.4	8.70	8.70
6S	3739	NE	Dale	3.014	2.902	0.750	0.883	7.7	11.5	9.19
5S	3722	N	Dale	2.883	2.914	0.972	0.881	6.3	8.18	9.25
4S	3406	S	Flat	3.113	3.150	0.868	0.844	6.9	10.1	10.6
3S	3218	NE	Hill	3.071	3.311	0.839	0.821	8.5	10.4	11.6
2S	2914	NE	Dale	4.024	3.612	0.793	0.783	11.5	15.0	13.5
1S	2548	NE	Hill	3.962	4.064	0.728	0.734	13.1	16.4	16.5

⁽¹⁾ Estimation made by comparing overpressure impulse data measured for stations 8S and 9S with data for a surface burst described in *The Effects of Nuclear Weapons*.

⁽²⁾ Determined from BRL mechanical-gauge records.

⁽³⁾ Overpressure impulse computed by regression equation derived from $(I_p)_m$ values

$$\log (I_p)_r = 3.5982 - 0.8776 \log R$$

⁽⁴⁾ Overpressure duration computed by regression equation derived from $(t_p^+)_{m,}$ values

$$\log (t_p^+)_{r,} = -1.7792 + 0.4829 \log R$$

⁽⁵⁾ Peak overpressure computed for a classical blast wave of impulse $(I_p)_m$ and of duration $(t_p^+)_{m,}$.

⁽⁶⁾ Peak overpressure computed by regression equation derived from $(p_s)_c$ values

$$\log (p_s)_r = 6.4370 - 1.5321 \log R$$

5.2 NORTHEAST BLAST LINE

5.2.1 Terrain Effects

A profile of the entire northeast blast line is shown in Fig. 5.4. This chart indicates generally rising land from GZ to the first station (1S). The terrain remains fairly high and hilly until the last station (8S) is reached. This station is on much lower ground and is almost out of the line of sight to the point of detonation.

Selected blast parameters taken from Table 5.1 are also plotted in Fig. 5.4. Overpressure values, p_s , particularly computed ones, $(p_s)_c$, show a marked tendency to be low at the hill stations and high in the dales when compared with the average or regression values. There are no marked deviations of the duration values from the regression line except for station 6S. Here the low measured duration is reflected in a computed maximum overpressure that is particularly high.†

Figures 5.5 and 5.6 (similar to Fig. 5.4) were made to a larger scale to show in more detail the positions of the traps and gauges in relation to the hills and dales. The same blast parameters shown in Fig. 5.4 are plotted on these charts.

* Statistical and analytical procedures were discussed in Chap. 2.

† Since maximum overpressure is computed from measured impulse and duration, this statement has significance if it is assumed that impulse is more accurately determined than the duration.

TABLE 5.2—SUMMARY OF RESULTS, SHOT SMOKY
(See List of Symbols.)

Regression Equation: $\log v = a + b \log m$

Missile	Trap	Absorber		n	\bar{D}_s	a	b	E_{gv}	V_{p50}	V_{50}	\bar{V}	S_{gv}	V_-	V_+	M_{50}	\bar{M}	S_{gm}	M_-	M_+
		type																	
NS	1S1a	VI	238	86.4	2.8102	-0.0664	1.13	482	475	480	1.16	270	683	102	282	3.40	13.6	704 ⁴	
NS	1S1b	VI	174	63.2	2.8191	-0.0557	1.13	470	498	504	1.15	317	704	150	348	3.32	21.3	5905	
NS	1S2	VI	93	33.8	2.8227	-0.0599	1.13	464	486	492	1.16	303	627	181	563	3.46	26.6	13676	
NS	Comb ⁽¹⁾ 1S		505	61.1	2.8061	-0.0568	1.14	472	485	491	1.16	270	704	129	356	3.46	13.6	13676	
NS	2S1	IV	96	34.4	2.6960	-0.0951	1.19	410	286	294	1.25	194	609	327	934	4.33	20.4	9199	
NS	2S2a	VI	307	111.5	2.8089	-0.0658	1.12	460	491	496	1.15	322	680	81.3	159	3.34	10.1	3716	
NS	2S2b	VI	227	82.4	2.7670	-0.0452	1.13	428	460	464	1.15	307	638	203	560	3.76	11.9	14748	
NS	Comb ⁽²⁾ 2S		630	76.3	2.8401	-0.0934	1.22	440	442	454	1.27	194	680	122	421	4.32	10.1	14748	
NS	3S1a	VI	71	25.8	2.9424	-0.1783	1.14	332	434	443	1.24	157	593	51.3	95.4	2.56	11.3	1599	
NS	3S1b	IV	109	39.6	2.6046	-0.0635	1.24	300	286	293	1.26	161	514	219	1000	3.96	38.4	22000	
NS	3S2	VI	95	34.5	2.8475	-0.0872	1.12	328	494	499	1.15	330	772	58.6	122	2.84	12.0	1614	
NS	Comb ⁽³⁾ 3S		275	33.3	2.8914	-0.1549	1.27	319	384	403	1.37	157	772	95.4	463	3.84	11.3	22000	
NS	4S1	VI	43	15.6	2.8446	-0.1044	1.13	318	460	468	1.20	297	670	55.2	348	3.89	10.0	8529	
NS	4S2a	III	81	29.4	2.5473	-0.0890	1.29	287	214	224	1.35	125	511	272	1614	5.76	18.5	27000	
NS	4S2b	III	135	49.0	2.5831	-0.0868	1.29	294	242	253	1.33	131	457	197	1140	5.09	11.0	29500	
NS	Comb ⁽⁴⁾ 4S		259	31.3	2.7025	-0.1285	1.36	297	259	279	1.46	125	670	176	1156	5.55	10.0	29500	
NS	5S1a	II	73	26.5	2.5374	-0.2090	1.09	265	154	159	1.29	67.0	222	47.0	97.4	3.13	10.2	969	
NS	5S1b	II	23	8.4	2.5467	-0.2029	1.08	262	159	162	1.24	95.0	223	51.1	80.3	2.57	11.3	371	
NS	5S2	II	23	8.4	2.5063	-0.1995	1.15	254	129	135	1.37	79.0	220	97.3	249	4.12	10.0	1771	
NS	Comb ⁽⁵⁾ 5S		119	14.4	2.5376	-0.2084	1.11	260	150	155	1.31	67.0	223	54.9	123	3.31	10.0	1771	
NS	6S1a	II	86	30.9	2.3973	-0.0897	1.20	338	159	163	1.24	92.0	290	153	342	3.61	13.1	4052	
NS	6S1b	II	192	69.7	2.4998	-0.1248	1.15	350	177	180	1.22	90.0	274	103	226	3.07	18.5	3182	
NS	6S2	II	259	94.1	2.4594	-0.1056	1.17	338	169	172	1.25	89.0	250	154	319	3.13	12.8	3895	
NS	Comb ⁽⁶⁾ 6S		537	65.0	2.4652	-0.1101	1.19	342	170	174	1.24	89.0	290	133	290	3.23	12.8	4052	
NS	7S1a	III	66	24.0	2.5684	-0.1335	1.19	226	206	214	1.31	113	387	79.4	359	4.58	10.3	6090	
NS	7S1b	III	111	40.3	2.6620	-0.1465	1.20	219	233	242	1.32	116	414	104	375	4.01	10.8	13200	
NS	7S2	III	70	25.4	2.6253	-0.1394	1.17	228	231	238	1.28	131	437	76.3	332	4.09	10.9	6800	
NS	Comb ⁽⁷⁾ 7S		247	29.9	2.6192	-0.1374	1.21	223	225	233	1.31	113	437	88.5	356	4.21	10.3	13200	
NS	8S1	II	26	9.4	2.5214	-0.1906	1.15	197	155	159	1.27	90.0	220	55.2	115	2.98	11.1	1168	
NS	8S2a	II	35	12.7	2.4599	-0.1496	1.14	188	144	149	1.28	84.0	220	103	346	4.25	13.1	4182	
NS	8S2b	II	162	58.8	2.4804	-0.1491	1.14	198	168	172	1.24	83.0	254	51.1	130	3.09	10.6	3507	
NS	Comb ⁽⁸⁾ 8S		223	27.0	2.4856	-0.1560	1.14	196	163	167	1.26	83.0	254	57.5	163	3.34	10.6	4182	
NS	9S1	II	17	6.2	2.4472	-0.1334	1.11	152	168	170	1.16	137	220	45.6	60.9	2.24	12.3	154	
NS	9S2a	II	18	6.5	2.4984	-0.1726	1.09	151	161	165	1.24	108	213	49.3	104	3.26	10.2	604	
NS	9S2b	II	46	16.7	2.4841	-0.1620	1.10	154	167	169	1.16	94.0	239	41.8	67.5	2.51	9.9	345	
NS	Comb ⁽⁹⁾ 9S		81	9.8	2.4844	-0.1614	1.06	152	166	169	1.18	94.0	239	44.2	74.3	2.62	9.9	604	

Missile	Trap	Absorber		d	n	h_1	\bar{h}_2	V_{p50}	$\Delta V\%^{(10)}$	\bar{V}	S_v	V_-	V_+	\bar{M}	$\bar{\alpha}$
		type													
MD	2S1	IV	18.7	1	0	6.5	202	-40.1	121					11580	0.1372
MD	6S2	II	17.1	1	0	10.5	164	-64.1	57 ⁽¹¹⁾					16496	0.1318
St $\frac{7}{16}$	4S2a,b	III	17.1	5	9	9.2	78.0	-3.6	75.2	5.48	69.7	82.7		5597	0.0398

(1) Combination NS from 1S1a,b; 1S2.

(2) Combination NS from 2S1; 2S2a,b.

(3) Combination NS from 3S1a,b; 3S2.

(4) Combination NS from 4S1; 4S2a,b.

(5) Combination NS from 5S1a,b; 5S2.

(6) Combination NS from 6S1a,b; 6S2.

(7) Combination NS from 7S1a,b; 7S2.

(8) Combination NS from 8S1; 8S2a,b.

(9) Combination NS from 9S1; 9S2a,b.

(10) $\Delta V\% = (V - V_{p50}) 100\% / V_{p50}$.

(11) Estimated.

5.2.2 Station 1S

Hill station 1S, which was located at the 2548-ft range on the northeast blast line, was nearer GZ than any other station for shot Smoky. The terrain from GZ to 1S was generally rising, the steepest incline being about 250 ft from the station (see Fig. 5.4). Figure 5.7 indicates the positions of the pressure gauges, military debris, and spheres with respect to the traps. Figure 5.8 is a preshot view of this installation which shows, in addition to the details on the layout chart (Fig. 5.7), a 10-ft pressure-gauge installation and an experimental jeep used by other projects. Note that an extra thermal shield was used on only one trap installation.

Overpressure vs. time measurements at ground level are recorded in Fig. 5.9. The overpressure-vs.-time curve, also shown, for the ideal wave was obtained by procedures outlined in Ref. 1 using the measured values of overpressure impulse (3.962 psi-sec) and of duration (0.728 sec). This curve has a peak overpressure of 16.4 psi, whereas the measured curve was 13.1 psi. The difference between the measured blast wave and the ideal, although significant, was not as great as will be seen for station 4S, which was located at a greater range (3406 ft) on the south blast line. Figure 5.10 is a record of the dynamic pressure obtained 3 ft above the ground. Also shown on this chart is the dynamic pressure associated with the ideal overpressure wave illustrated in Fig. 5.9. Note the latter portion of the measured record, which seems to indicate that the instrument zero was drifting.

Figures 5.11 and 5.12 are closeup photographs of the two trap installations after the detonation. Both photographs show erosion of the wood surfaces, especially the trap housing. Note the absence of the frame for the thermal shield in Fig. 5.11 and the large collection of native debris in front of installation 1S2 (Fig. 5.12). Balsa wood was used as the absorber in all three traps at this station. Thermal damage to the absorber was negligible—even for trap 1S2 which did not have extra thermal protection.

None of the steel spheres (85) or the military debris (about 500 pieces) set out was recovered. Velocity and mass data for natural stones caught by the three traps are plotted in Figs. 5.13 to 5.15. At installation 1S1 the lower trap (1S1a) caught more missiles than the upper trap (238 vs. 174), but the geometric mean velocity for the lower trap was slightly smaller (475 ft/sec vs. 498 ft/sec). Only 93 stones were recovered from installation 1S2, which perhaps indicates shielding by the debris (see Fig. 5.12). These 93 missiles had a geometric mean velocity of 486 ft/sec, which indicated good agreement with the data from installation 1S1 traps. It is of interest to note that on these charts the predicted-velocity curves made on the basis of the ideal blast wave (see Fig. 5.9 and Chap. 3) show fair agreement with the data from all three traps. It should be remembered that the distance of travel for a natural stone is not known; therefore the velocity is predicted assuming the displacement necessary to obtain maximal velocity. All distances of displacement other than this optimum one would result in lower velocities. Thus, ideally, the predicted curve should lie near the top of the velocity distribution. Some scatter above the predicted curve can be explained by variations in the acceleration coefficient for individual missiles as well as by limitations in accuracy inherent in the missile-absorbing technique.

5.2.3 Station 2S

Station 2S was placed in a dale just beyond station 1S (see Figs. 5.4 and 5.5). The experimental arrangement for this station is shown graphically in Fig. 5.16 and pictorially in Fig. 5.17. The two jeeps in Fig. 5.17 were part of another project. Pressure instrumentation had not been installed at the time the photograph was taken.

The measured overpressure vs. time record for station 2S (Fig. 5.18) indicates somewhat closer conformity to the ideal wave than was noted for station 1S. Dynamic pressure vs. time (recorded in Fig. 5.19) is considerably lower than for the hill station (1S) but is just as variable. The dynamic pressure measured between 0.5 and 0.6 sec is of the same order of magnitude as the overpressure (Fig. 5.18) for the same time interval. This undoubtedly indicates an erroneous response of the q gauge.

The postshot photograph of installation 2S1 (Fig. 5.20) indicates that the Styrofoam absorber (type IV) with a thermal protector survived the burst with little damage. Similarly, the balsa absorber (type VI) placed at installation 2S2, but without the extra shield, was in good

condition (Fig. 5.21). Erosion of the trap housing noted in these photographs was considerably less than that for station 1S traps.

Approximately 550 pieces of military debris were placed in front of station 2S traps. One piece originating from a distance of 18.7 ft was caught by trap 2S1. The mass of the piece of debris was 11.58 g and the velocity with which it struck the absorber was estimated to be 121 ft/sec (see Table 5.2).

Natural-stone data obtained from traps 2S1, 2S2a, and 2S2b are presented graphically in Figs. 5.22, 5.23, and 5.24, respectively. It is noteworthy that velocities evaluated using the Styrofoam absorber (type IV at trap 2S1) are somewhat lower than those obtained using the balsa absorber (type VI at traps 2S2a and 2S2b). The threshold velocities for the type IV absorber are lower than for type VI, which results in missiles of lower velocities being caught in type IV (trap 2S1). However, missiles of higher velocities were recorded in the balsa than in the Styrofoam. A recheck of the calibration for each of these absorbers failed to rectify this discrepancy. It has been found that Styrofoam is much more uniform in structure than balsa; therefore more credibility should be given to the data from trap 2S1 than to the other two.

Predicted missile velocities were made from dynamic-pressure data for the ideal wave, which are represented in Fig. 5.19 by a dashed line. Up to about 0.45 sec, the measured curve, although oscillating, corresponds roughly to the ideal-wave curve. The effective dynamic pressure seems to be satisfactorily represented by the "ideal" curve; this is substantiated, in part, by the fact that the predicted-velocity line in Fig. 5.22 lies near the upper limit of the scatter of velocity points.

5.2.4 Station 3S

Station 3S was placed on a hill at the 3218-ft range, slightly higher in elevation than the hill location of station 1S (see Fig. 5.5). The plan for this station is shown diagrammatically in Fig. 5.25. Spheres were not studied, but approximately 550 pieces of military debris were set out. In the preshot photograph of this station (Fig. 5.26), it can be seen that the ground immediately in front of the traps had been leveled with a grader. A thermal shield was used for the installation on the right.

Overpressure and dynamic-pressure records obtained at this station are plotted in Figs. 5.27 and 5.28, respectively. The measured overpressure curve deviates from the ideal curve in that more than 0.1 sec elapsed between arrival of the blast wave and maximum overpressure. The dynamic pressure developed to maximum at an even slower rate, the entire record being characterized by large fluctuations.

The postshot photographs of the installations (Figs. 5.29 and 5.30) indicate that all three traps were in good condition.

No military debris was caught at this station. Data for the 275 natural-stone missiles caught are plotted in Figs. 5.31 to 5.33. That the predicted-velocity line is considerably lower than the higher velocity points for all three traps is consistent with the fact that the measured dynamic pressures were higher than the computed ones for an ideal wave. The lower velocity points for the Styrofoam trap (type IV at trap 3S1b) compared with the low points for the other traps reflect the difference in threshold velocities for the two types of absorbers (refer to Chap. 2). The upper velocities recorded by the two absorber types are nearer the same amount than those observed for station 2S (see Sec. 5.2.3). Absence of small missiles in trap 3S1b data is probably attributable to the fact that they were overlooked when the missiles were extracted from the trap.

5.2.5 Station 6S

The next station on the northeast blast line was 6S, located in a dale at the 3739-ft range (see Figs. 5.4 and 5.6). The experimental plan depicted in Fig. 5.34 indicates that absorber type II, along with extra thermal protection, was used in all three traps. Figure 5.35 is a preshot photograph of this station. The sharp rise in the terrain (shown in the background) which appears to be in the direction of GZ was actually on the right of the blast line looking toward the location of the burst.

Figures 5.36 and 5.37 are records of overpressure and dynamic pressure, respectively, for station 6S. Note that the measured overpressure and dynamic-pressure curves in the

initial portions are lower than the ideal-wave curves. Moreover, the measured dynamic pressures were lower than the computed ones for the ideal wave for most of the duration of the wave.

Figures 5.38 and 5.39 are postshot photographs of the two installations at station 6S. Note the plant stems that stuck to the face of the traps. The frame for the thermal absorber can be seen clearly in Fig. 5.38; however, it was destroyed at the other installation (Fig. 5.39).

The results obtained at this station for natural-stone missiles are presented graphically in Figs. 5.40 to 5.42. The measured missile velocities are generally much lower than those predicted for the ideal wave. This agrees with the fact that the measured dynamic pressure was lower than that computed for the ideal wave (see Fig. 5.37). Note, however, that the velocities for two missiles caught by trap 6S1a (Fig. 5.40) are in agreement with the predicted values. One piece of military debris (about 550 pieces were set out) was caught by trap 6S2. Data for this missile are recorded in Table 5.2.

5.2.6 Station 7S

Station 7S, which was located at the 4115-ft range, was the third of the three hill stations on the northeast blast line. This station was placed on a hill slightly higher and with slopes somewhat greater than the other two (1S and 3S) (see Figs. 5.4 and 5.6).

The plan for this station is shown graphically in Fig. 5.43 and pictorially in Fig. 5.44. Type III absorber, along with thermal shields, was used in all three traps.

The overpressure data presented in Fig. 5.45 indicate that the principal deviation of the measured quantity from that computed for an ideal wave was the longer rise time. Owing to instrument failure, no dynamic pressure was obtained.

Closeup photographs taken after the detonation (Figs. 5.46 and 5.47) indicate that the installations were in good condition.

None of the military debris (about 550 pieces) placed at this station was recovered from the traps. Data for 247 natural stones that were trapped are plotted in Figs. 5.48 to 5.50. Some of the velocity points are higher than the predicted-velocity lines, a result similar to that obtained from the other hill stations, but to a lesser degree. It is interesting to note that velocities obtained at this station correspond roughly with those obtained at station 6S, a dale station 376 ft closer to GZ. Over twice as many missiles were caught at the dale station (6S) than were caught at station 7S. This may be explained in part by the fact that an absorber with a lower density, and thus lower threshold velocities, was used at station 6S.

5.2.7 Station 8S

The last station on the northeast blast line was 8S, located in a long flat dale at the 4980-ft range (see Figs. 5.4 and 5.6). The arrangement at this station (see Fig. 5.51) varied somewhat from others on this line in that the pressure gauges were placed between the two trap installations. Seventy steel spheres, as well as the usual amount of military debris, were placed at this location. Figure 5.52 is a photographic view of installation 8S2 looking away from GZ.

The data plotted in Fig. 5.53 show that even at this range the measured overpressure curve has a fairly long rise time and a flat top which endured for about 0.1 sec. The measured dynamic-pressure curve in Fig. 5.54 is quite erratic, particularly from 0.2 to 0.5 sec.

Postshot photographs (Figs. 5.55 and 5.56) show the two installations to be in good condition. A few plant stems can be seen partly imbedded in the absorber.

No spheres or military debris were caught. Data for the 223 natural-stone missiles that were trapped are plotted in Figs. 5.57 to 5.59. The upper trap, 8S2b, caught 162 missiles in contrast to only 35 for trap 8S2a and 26 for trap 8S1. Unlike the results obtained for the previous dale station (6S), the velocities predicted on the basis of the ideal wave are in fair agreement with the measured ones.

5.3 SOUTH BLAST LINE

The south blast line was flat desert terrain that gradually sloped away from GZ. Figure 5.60 contains a profile of this line, as well as overpressure and duration data for four sta-

tions—only two of which were used for missile studies (4S and 9S). It is interesting to note an actual increase in the measured peak overpressure from station 4S at 3406-ft range to the BRL station at 3875 ft. However, peak overpressures computed for the ideal wave from measured impulses and durations decrease monotonically with increasing range, forming a remarkably smooth curve.

5.3.1 Station 4S

Secondary-missile investigations at station 4S were conducted in cooperation with another project² that was designed to study, by means of motion pictures, the displacement of anthropomorphic dummies simulating 165-lb men. Since efforts to obtain motion pictures failed because of dust obscuration, it was fortunate that some velocity data were obtained in the present study for spheres that also simulated men*—at least insofar as velocity of translation† is concerned.

Figure 5.61 portrays graphically the experimental design for both the missile and dummy projects. An asphalt road that was parallel to the blast line passed between the concrete stabilized area and the pressure instrumentation. Figure 5.62 is a preshot photograph of installation 4S2. The flat terrain characteristic of this blast line can be seen in the background.

The blast data plotted in Fig. 5.63 illustrate a significant deviation of the measured from the ideal-wave overpressures. Since the terrain was flat, it can be assumed that the deviations noted were due to thermal effects. This assumption is strengthened by the fact that the measured dynamic pressure, Fig. 5.64, is significantly higher than the corresponding ideal-wave pressure. Note, however, the low level of measured dynamic pressure for the first 0.05 sec.

The balsa absorber in trap 4S1 suffered little thermal damage (see Fig. 5.65), even without the extra thermal protection. The traps at installation 4S2, portrayed postshot in Fig. 5.66, also endured the thermal effects without serious damage. Absorber type III with a thermal shield, the remains of which can be seen in the photograph, was used at traps 4S2a and b. Figure 5.66 shows four spheres on the right side of the lower trap and one in the upper trap. Velocities of 70, 71, 74, and 83 ft/sec (from left to right) were computed for the $\frac{7}{16}$ -in. steel spheres in the lower trap. Average height of impact was 6.5 in. above the ground. The sphere ($\frac{7}{16}$ -in. steel) in the upper trap had a velocity of 79 ft/sec at an impact height of 20.4 in. These spheres had been placed 9 in. above the ground and 17.1 ft in front of the traps (see Figs. 5.61 and 5.62). The velocity predicted for the spheres (see Table 5.2) was 78 ft/sec.

The average velocity at impact for the five spheres mentioned above was 75.2 ft/sec. If one assumes that the average velocity during transit was between 37.6 and 75.2 ft/sec, the time required to traverse 17.1 ft is found to be between 0.45 and 0.23 sec. Dynamic pressure measured during either of these periods (0 to 0.45 sec or 0 to 0.23 sec) was considerably above that for the ideal wave (see Fig. 5.64), which was the basis for the predicted velocity of 78 ft/sec. From this one might speculate that dynamic pressures as high as those recorded in Fig. 5.64 did not exist at the location of the spheres. It should be noted (see Fig. 5.61) that the initial position of the spheres was only 9 in. above the ground and that the dynamic pressure was measured 3 ft above the surface at a distance of 190 ft from the spheres.

The results obtained for natural-stone missiles caught at this station are plotted in Figs. 5.67 to 5.69. A significant number of missiles whose velocities exceeded the predicted values were caught in each trap. A difference, also noted at other stations, between the response of the absorbers (balsa at installation 4S1 and Styrofoam at traps 4S2a and b) to natural-stone missiles was that the Styrofoam absorber caught missiles that had lower velocities because of its lower threshold velocities. The balsa trap (4S1) caught a larger proportion of small missiles (note position of the geometric mean) whose velocities tended to be somewhat higher than those of the small missiles caught in the Styrofoam traps. The latter yielded a scattering of large missiles which impacted at high velocities, a reasonable result considering the nature of the measured dynamic-pressure curve displayed in Fig. 5.64.

* Total displacements measured after the shot were: standing dummy, 255.7 ft downwind and 43.7 ft to the right; and prone dummy, 160 ft downwind and 31.5 ft to the right.

† The acceleration coefficient of the spheres that were caught is slightly higher than the average value for a tumbling man. References 1 and 3 contain a more complete treatment of this subject.

5.3.2 Station 9S

Figure 5.70 is a layout chart for station 9S. This station was located at the 5680-ft range on the south blast line. The chart indicates the placement of 70 steel spheres and about 550 pieces of military debris. Installation 9S2 is shown in Fig. 5.71.

The overpressure vs. time data (Fig. 5.72) for this station display a closer correspondence of the measured overpressure to that computed for the ideal blast wave than does any other station for shot Smoky. No record of dynamic pressure was obtained.

Figure 5.73 (installation 9S2) is the only postshot photograph of the installations that is reproduced. Note the presence of steel spheres in front of the traps on the concrete surface. Although the two layers of thin foil that were placed over the front surface of the absorber were left intact, they were perforated by natural-stone missiles and a few plant stems.

No military debris or spheres and comparatively few natural stones were caught. Data for the natural stones, presented in Figs. 5.74 to 5.76, indicate a smaller spread in missile velocities than that obtained at stations nearer GZ which used the same type of absorber. Possibly the reason for this was that at 9S there was less difference between the maximum velocity of the missiles and the threshold velocity of the absorber. Thus the predicted-velocity lines are near the low side of the velocity distribution, although they are not unreasonably far from the high side. The largest velocity deviations of the measured from the predicted values are found for the missiles of low mass.

5.4 NORTH BLAST LINE, STATION 5S

The location of station 5S, at the 3722-ft range on the north blast line, is illustrated in Fig. 5.77. The station was located about 900 ft beyond the mountain peak at an elevation approximately 300 ft lower than that of the peak. This was the only station on shot Smoky that was not on a direct line of sight with the point of detonation of the bomb. Hence it was not necessary to use extra thermal protection for the absorbers. The only missiles studied were natural stones (see Fig. 5.78). Figure 5.79 is a view of the station looking up the mountain toward GZ.

Unlike the overpressure records for the other dale stations (see Figs. 5.18, 5.36, and 5.53), Fig. 5.80 illustrates that the initial rise was very sharp—the principal modification being its failure to peak in the manner characteristic of the ideal or classical wave. A dynamic-pressure record was not obtained.

Figures 5.81 and 5.82 show that the foil covering the absorber, except for a small patch on the right side of the lower trap in Fig. 5.81, was still in place after the shot.

Results obtained for the 119 natural-stone missiles caught at this station are presented graphically in Figs. 5.83 to 5.85. Missile velocities were significantly lower than those which could be expected for an ideal wave.

5.5 SUMMARY, SHOT SMOKY

Three traps were placed at each of nine stations located on three blast lines. The station nearest to GZ (1S) had a range of 2548 ft and a measured overpressure of about 13 psi, and the most distant one (9S) had a range of 5680 ft and a measured overpressure of about 5 psi.

Hill-and-dale effects were studied at six stations on the northeast blast line and at one station on the north line. For natural-stone missiles, comparisons were made between measured velocities and the ones predicted on the basis of an ideal blast wave whose overpressure impulse and duration were the same as those measured. In general, the hill stations (1S, 3S, and 7S) produced missiles with velocities that were higher than those predicted, and the dale stations (2S, 5S, 6S, and 8S), lower than predicted. The effect was particularly noticeable at the dale station (5S) on the north line.

Two stations were placed on the south blast line where the terrain was flat. The blast wave incident at the 3406-ft station (4S) was significantly modified by surface thermal effects which resulted in higher dynamic pressures and higher missile velocities than expected for an ideal wave. The blast wave that reached the second station on the south line (9S at 5680 ft) was

almost ideal in form, producing natural-stone velocities in good agreement with those predicted.

A total of 2876 natural-stone missiles was caught by the 27 traps used in this shot: 34 per cent was caught by the lower (a) traps at the installations where the traps were stacked, 41 per cent by the upper (b) traps, and only 25 per cent by the traps not stacked.

About 550 pieces of military debris were placed in front of the traps at each of eight stations. A total of 405 steel spheres ($\frac{1}{16}$ -, $\frac{1}{2}$ -, and $\frac{9}{16}$ -in.-diameter steel) was placed at four stations. Only two pieces of military debris and five spheres were recovered.

Results of the missile studies for shot Smoky are summarized in Table 5.2.* Data resulting from the analysis of all natural stones caught at each station are listed. Some parameters are given here for the first time. The following symbols are used in this table:

$\bar{\alpha}$	Acceleration coefficient of the average mass of the missile sample used to compute predicted values of missile velocity, sq ft/lb
a,b	Regression-equation coefficients
d	Distance of travel of the missile before striking the trap, ft
\bar{D}_s	Spatial density of missiles caught, number per sq ft
$\Delta V\%$	Per cent of difference in average velocity from predicted velocity
E_{gv}	Geometric standard error of estimate in velocity = antilog E_{lv}
h_1	Height above ground at which the missile was placed, in.
\bar{h}_2	Average height above ground at which the missiles struck, in.
MD	Military debris
n	Number of missiles in sample
NS	Natural stone
S_{gv}	Geometric standard deviation of velocity = antilog S_{lv}
St	Steel sphere
V_-	Minimum velocity
V_+	Maximum velocity
\bar{V}	Average velocity
V_{50}	Geometric mean velocity
V_{p50}	Predicted value of velocity for the geometric mean mass

All velocity parameters have units of feet per second. The last five columns of the table contain mass (mg) parameters corresponding to the quantities discussed for velocity.

REFERENCES

1. I. G. Bowen, R. W. Albright, E. R. Fletcher, and C. S. White, A Model Designed to Predict the Motion of Objects Translated by Classical Blast Waves, USAEC Report CEX-58.9, June 29, 1961.
2. R. V. Taborelli, I. G. Bowen, and E. R. Fletcher, Tertiary Effects of Blast—Displacement, Operation Plumbbob Report, WT-1469, May 22, 1959.
3. E. R. Fletcher, R. W. Albright, V. C. Goldizen, and I. G. Bowen, Determinations of Aerodynamic-drag Parameters of Small Irregular Objects by Means of Drop Tests, USAEC Report CEX-59.14, October 1961.

* Table 2.1 describes the absorber types.

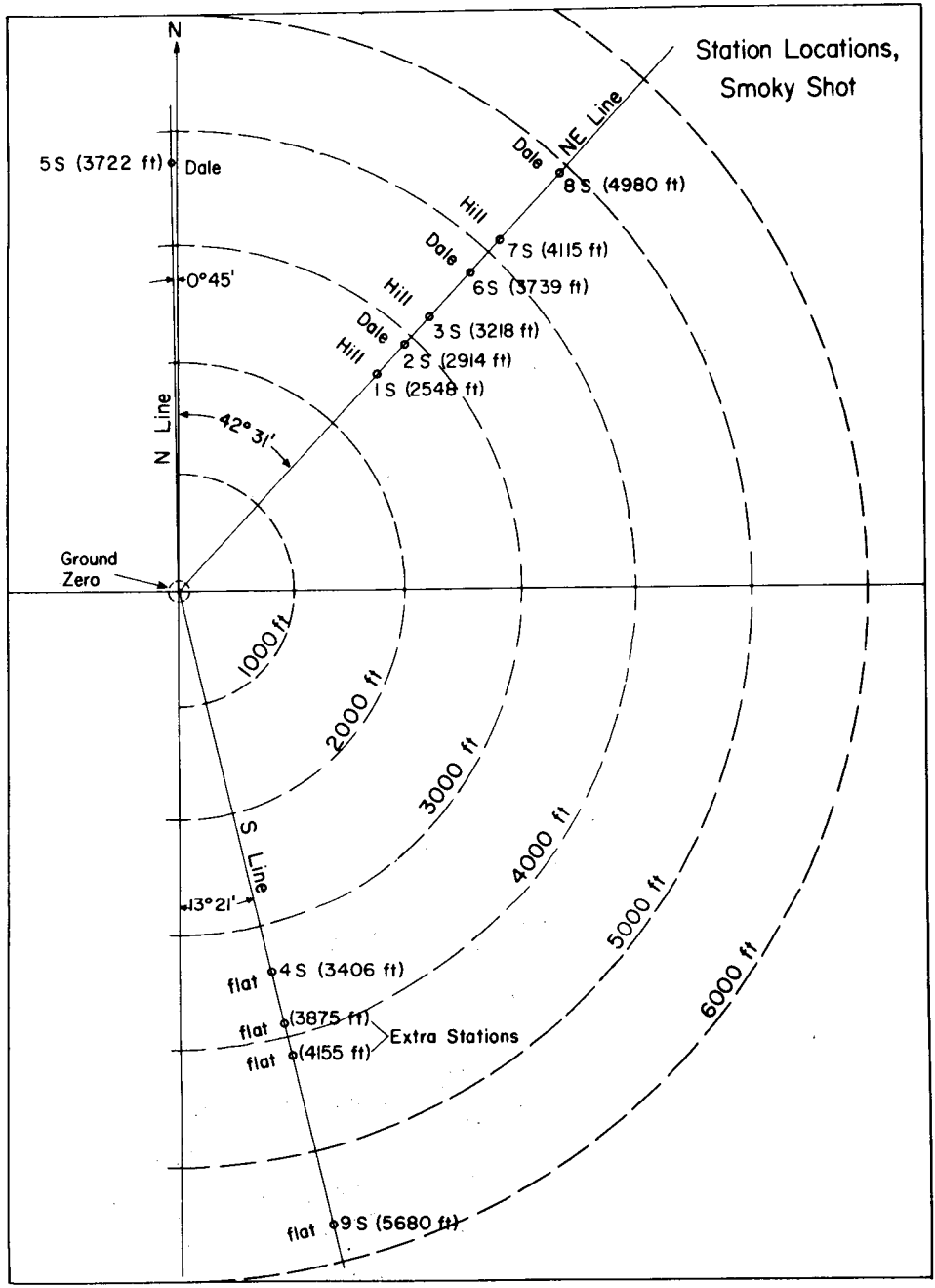


Fig. 5.1—Station locations for shot Smoky in Area 2C, NTS.



Fig. 5.2— Typical placement of military debris and large steel spheres (on trough-like support).

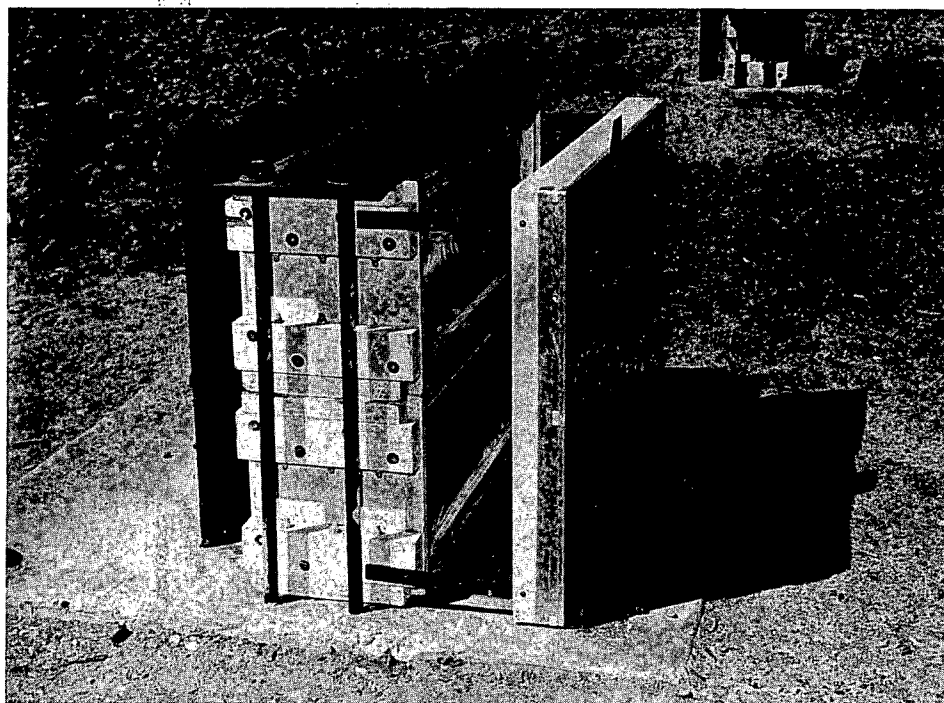


Fig. 5.3— Typical trap installation showing use of extra thermal shield, which consisted of aluminum foil held in frame approximately 1 ft in front of traps.

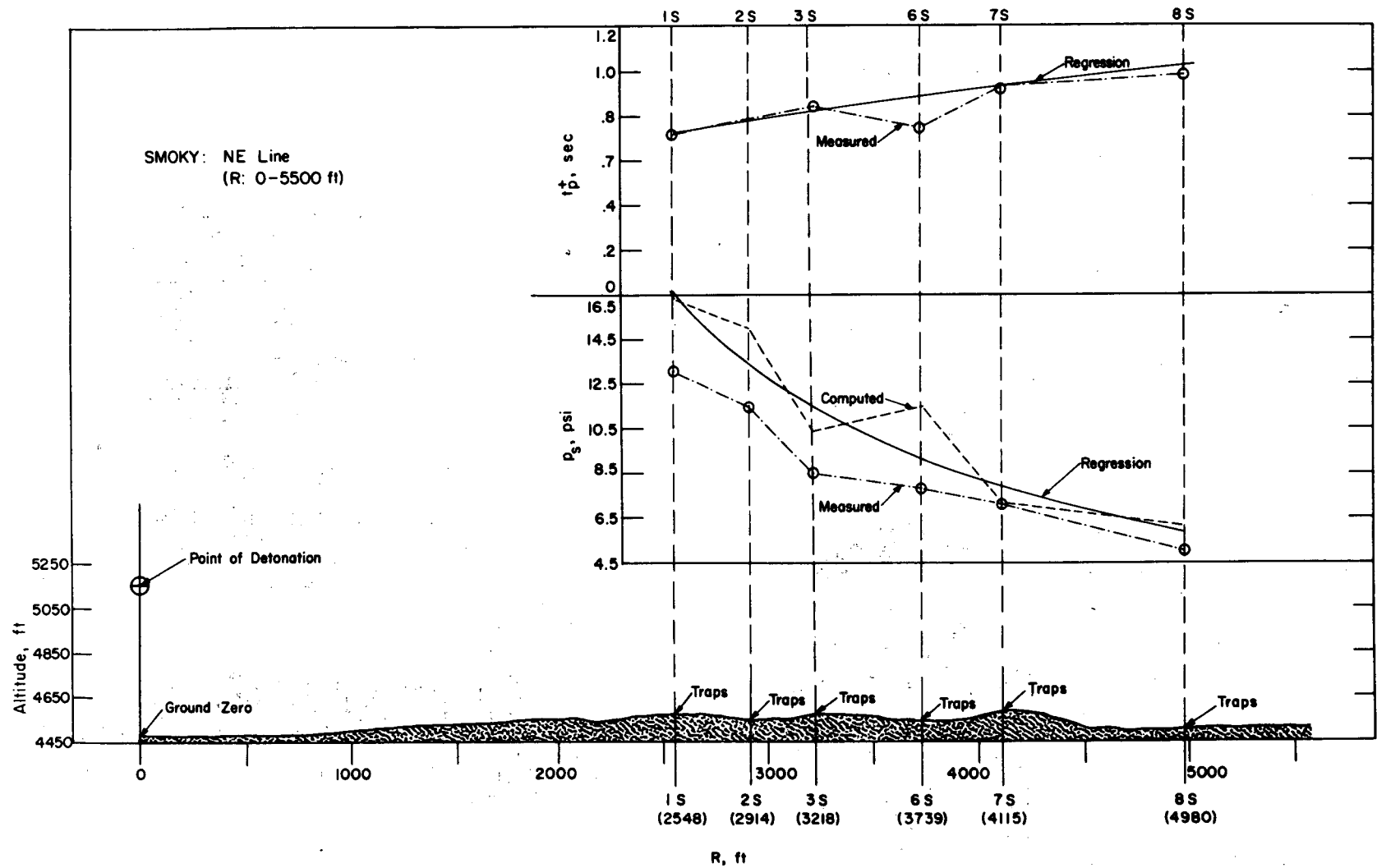


Fig. 5.4—Profile of northeast blast line, shot Smoky. Range: 0 to 5500 ft. Note that the vertical and horizontal scales are the same. See Table 5.1 for explanation of blast-wave parameters.

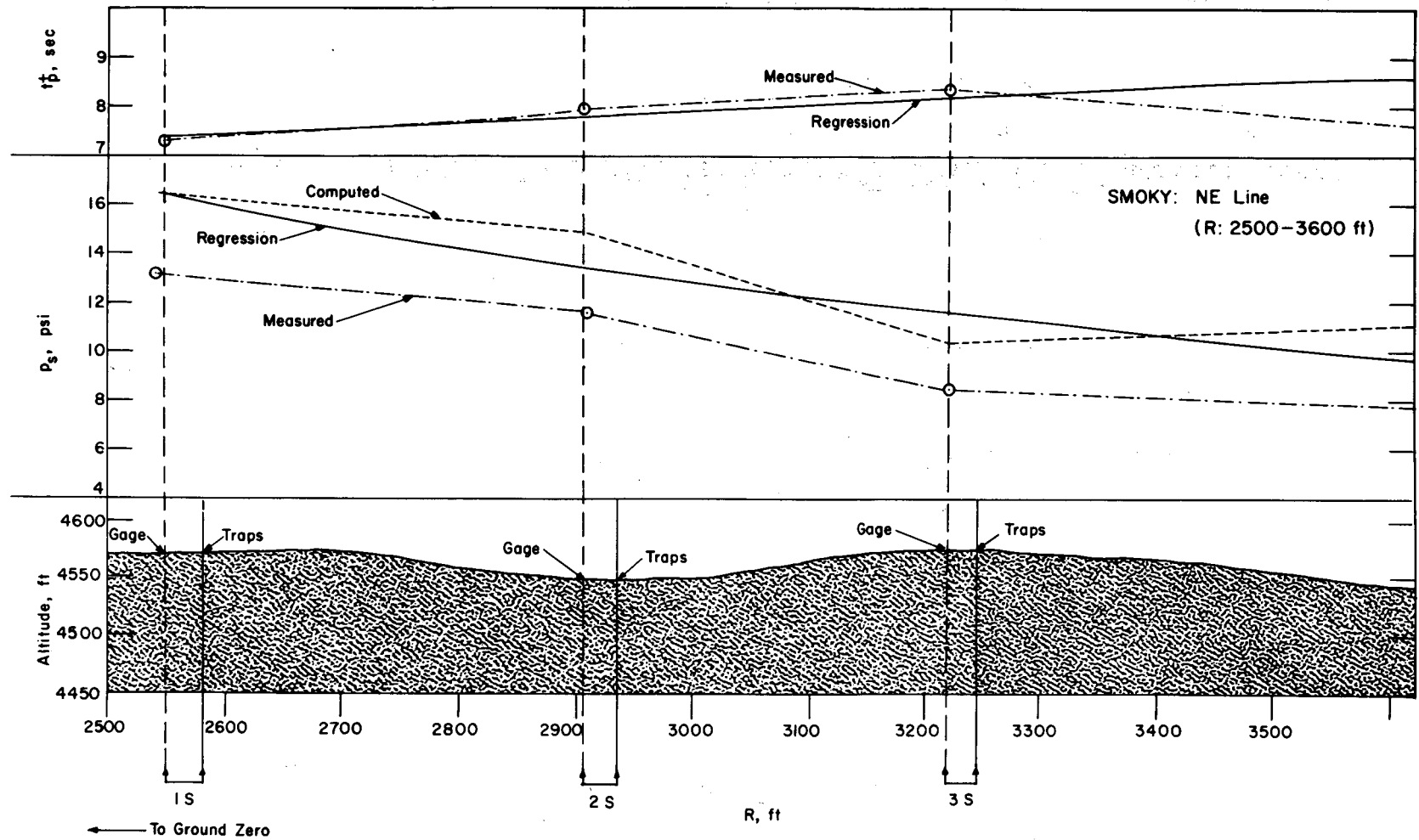


Fig. 5.5—Profile of northeast blast line, shot Smoky. Range: 2500 to 3600 ft. See also Fig. 5.4.

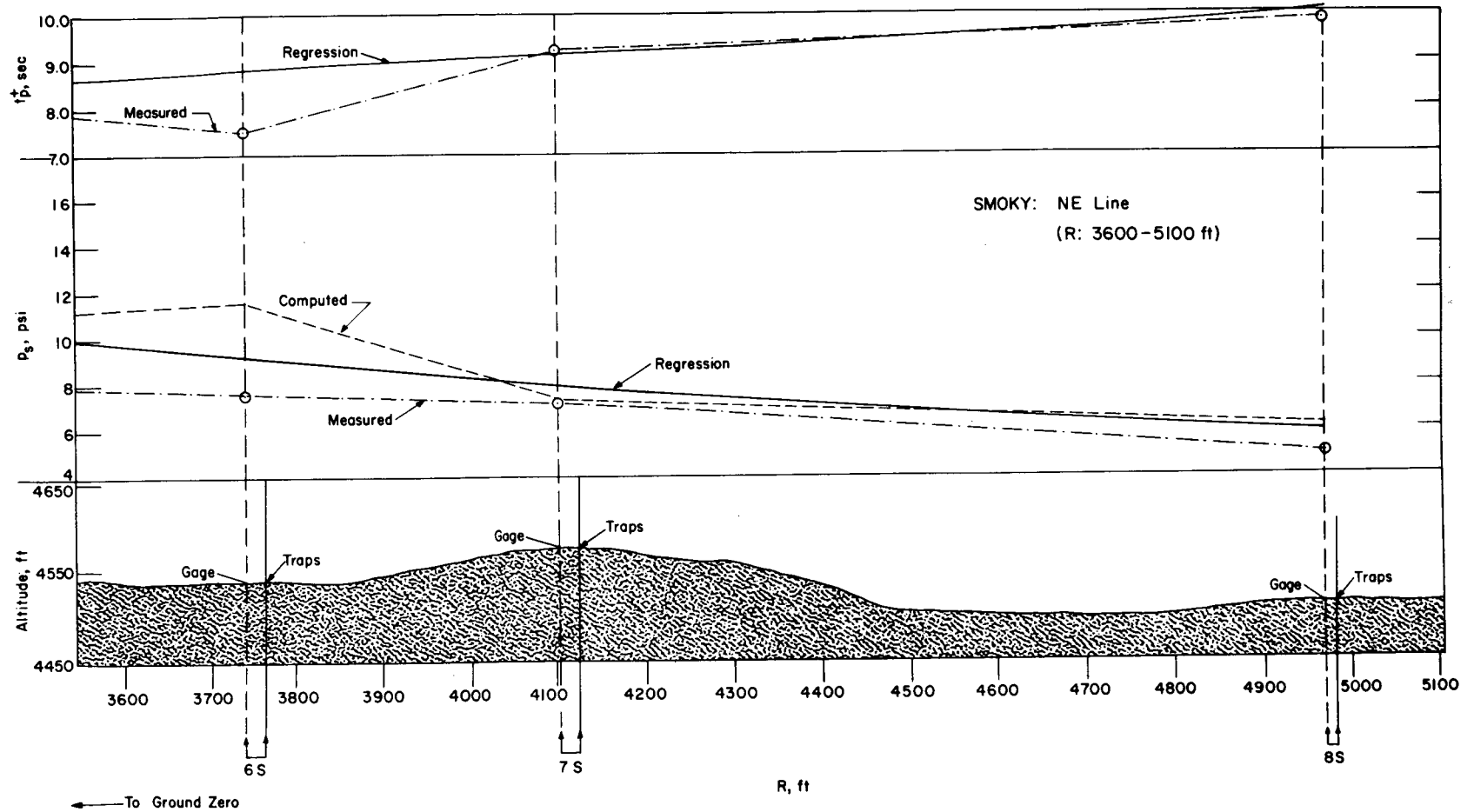


Fig. 5.6—Profile of northeast blast line, shot Smoky. Range: 3600 to 5100 ft. See also Figs. 5.4 and 5.5.

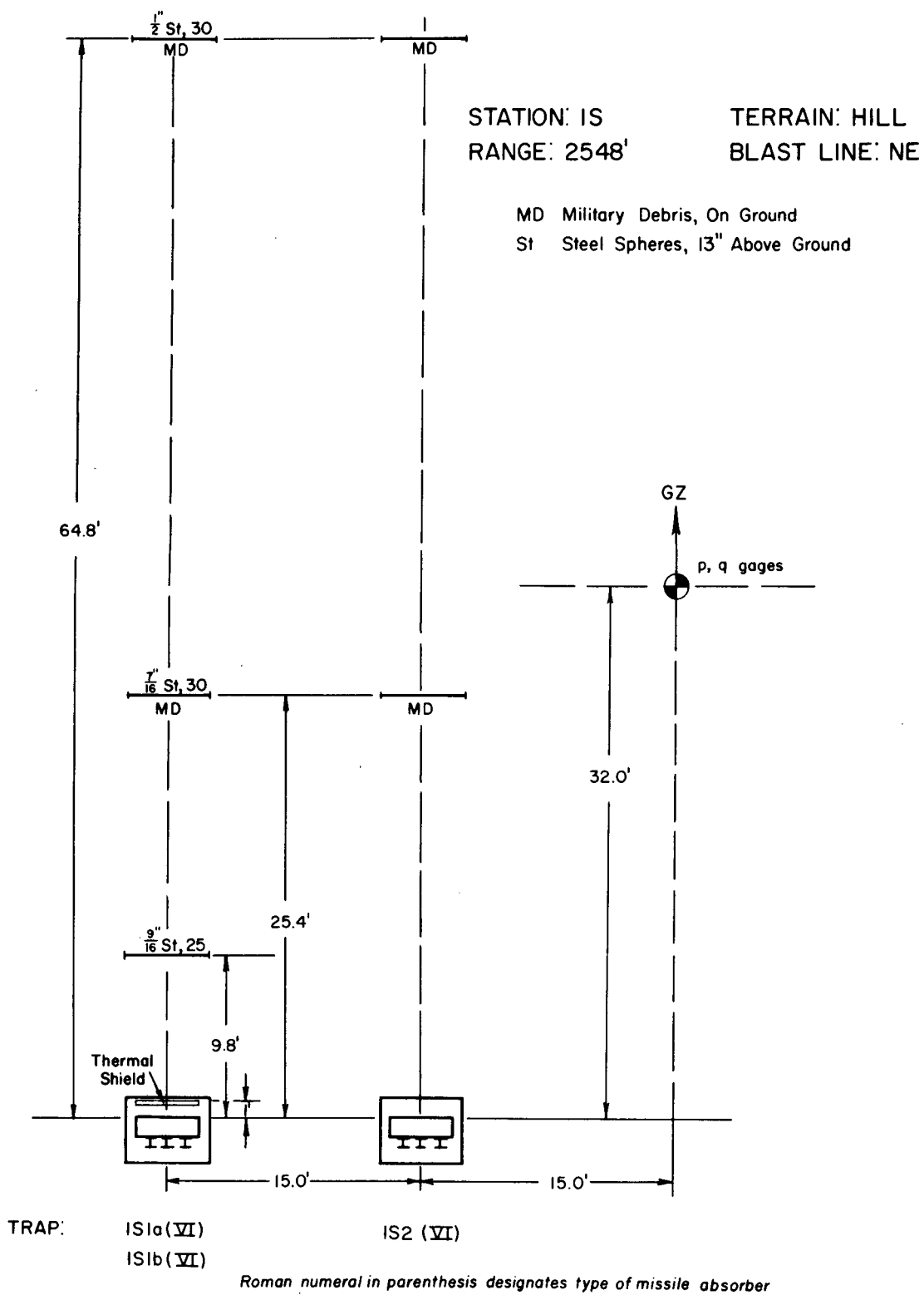


Fig. 5.7—Station 1S layout chart. The small letter suffix by the trap designators indicates level of the stacked traps: "a" for ground level and "b" for one above another trap.

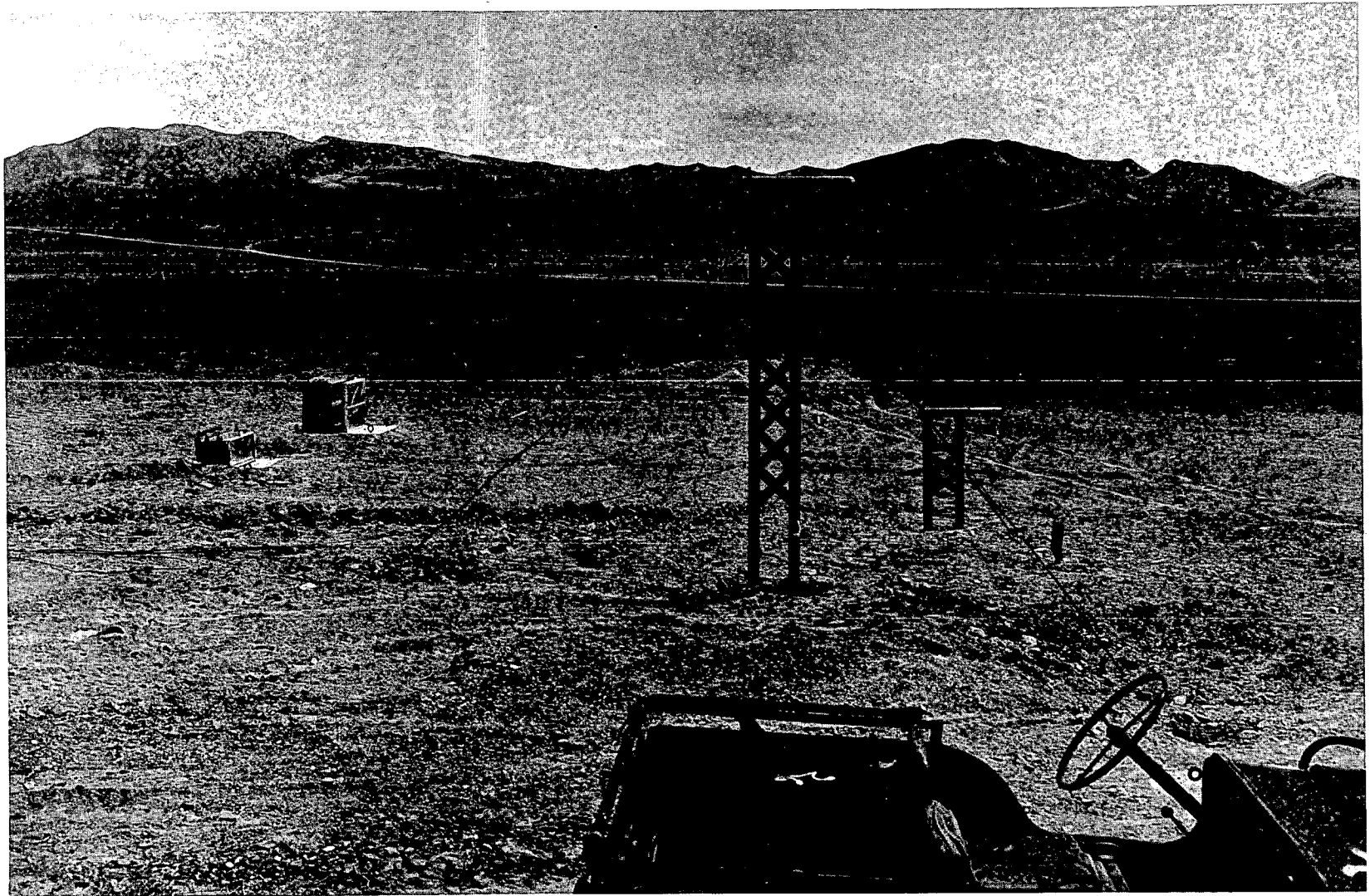


Fig. 5.8—Station 1S, preshot, at 2548-ft range on the northeast blast line.

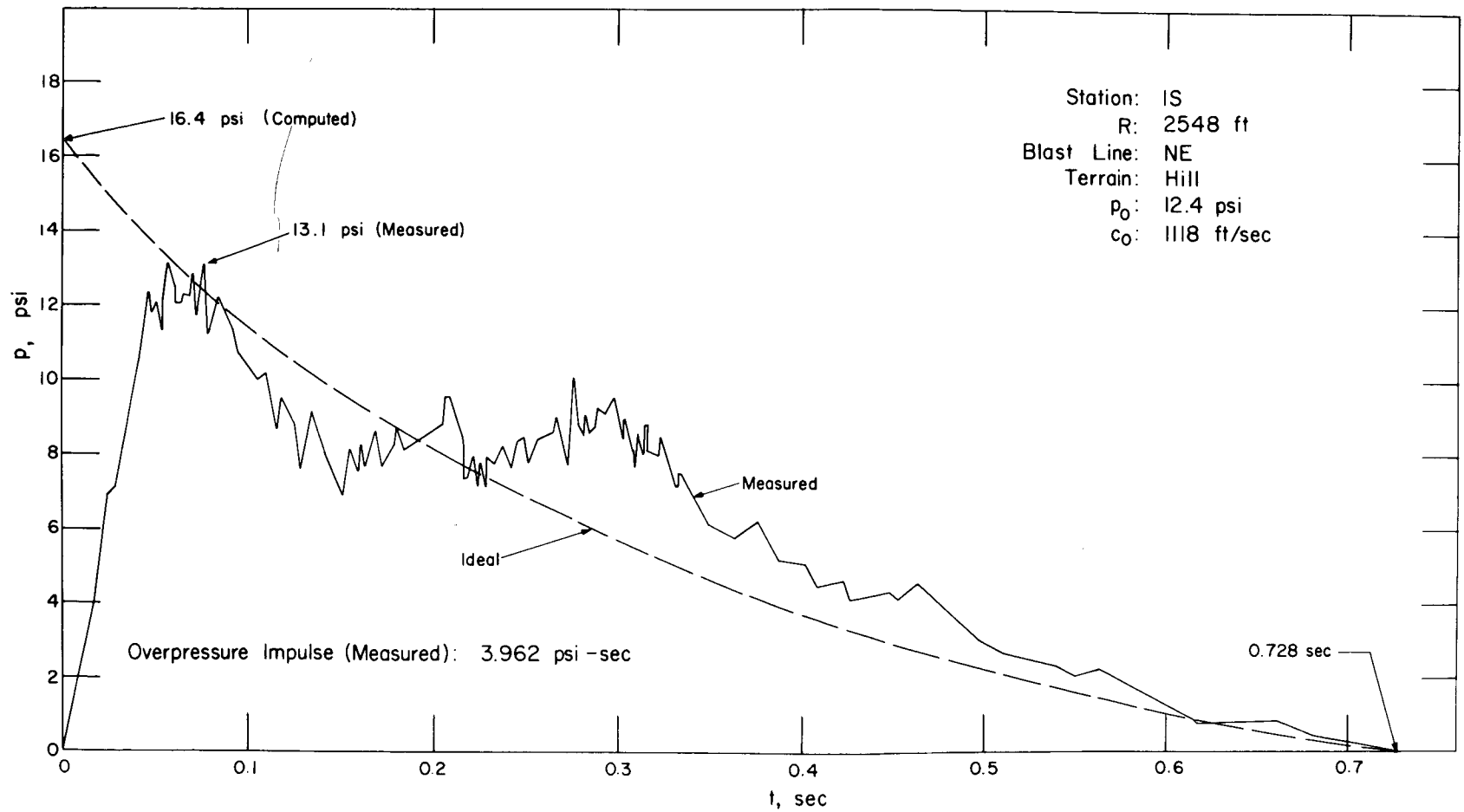


Fig. 5.9—Overpressure vs. time at station 1S.

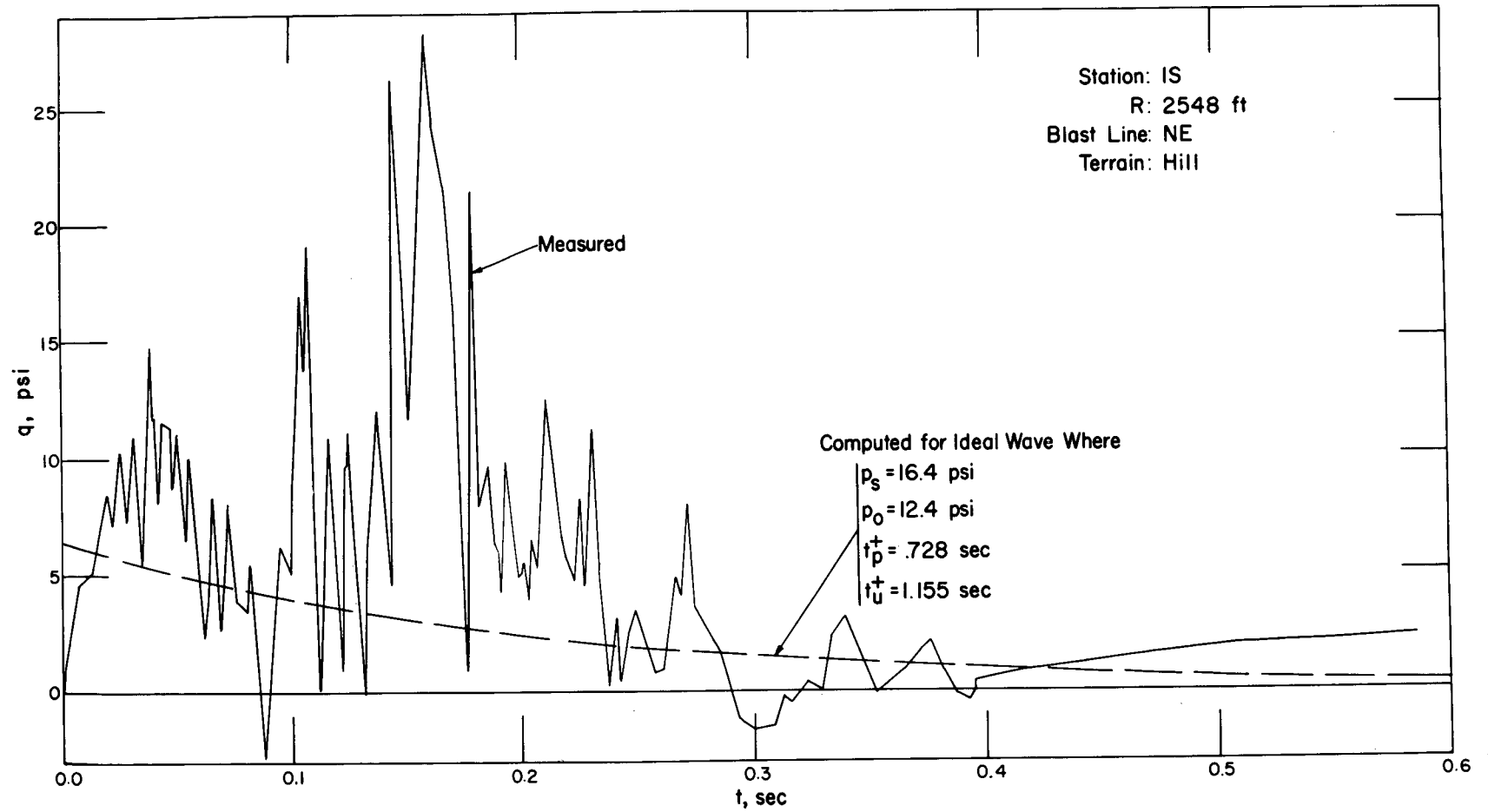


Fig. 5.10—Dynamic pressure vs. time at station 1S.

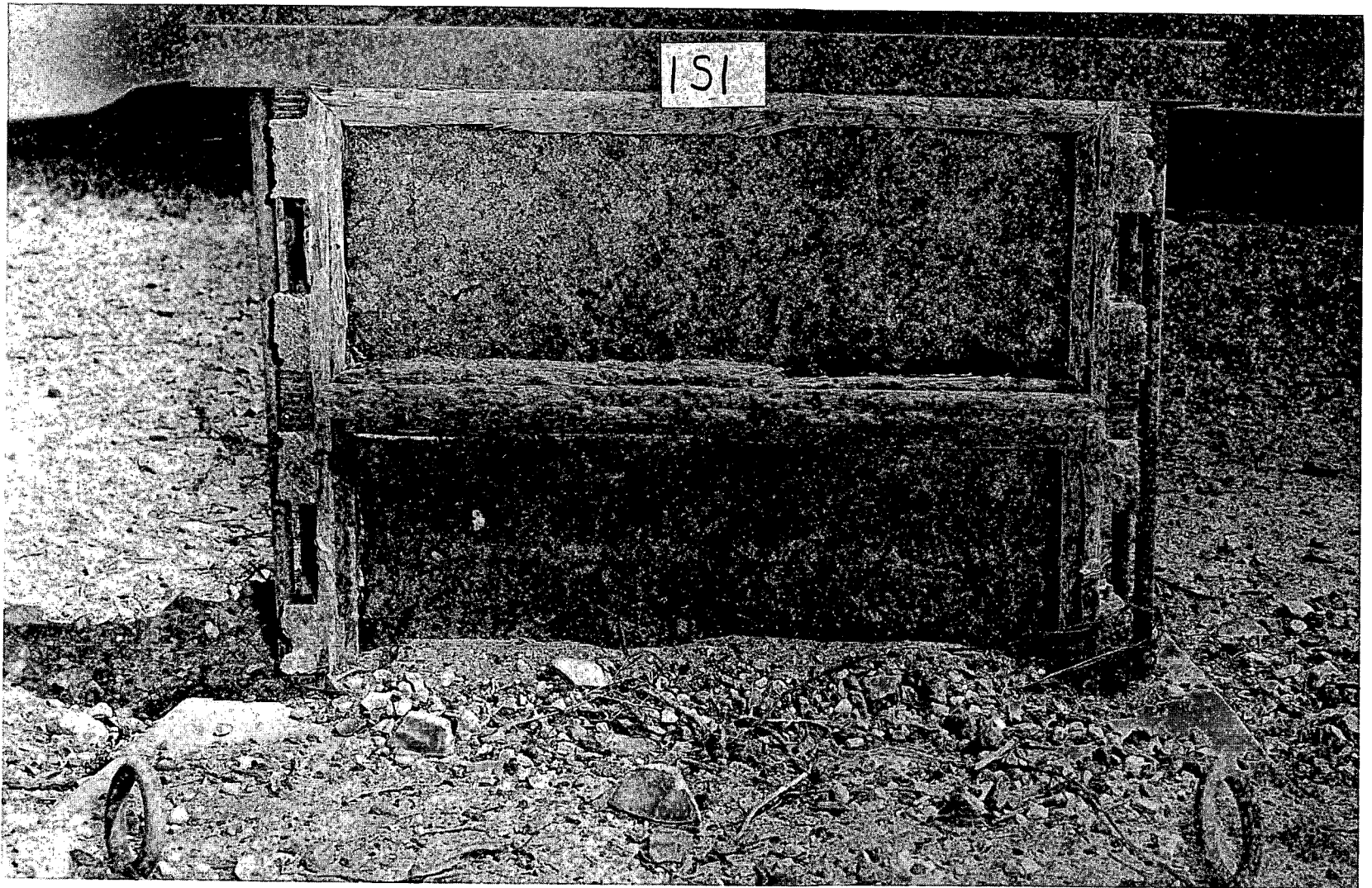


Fig. 5.11—Traps 1S1a and b, postshot. Note debris in front of traps and erosion of trap housing.

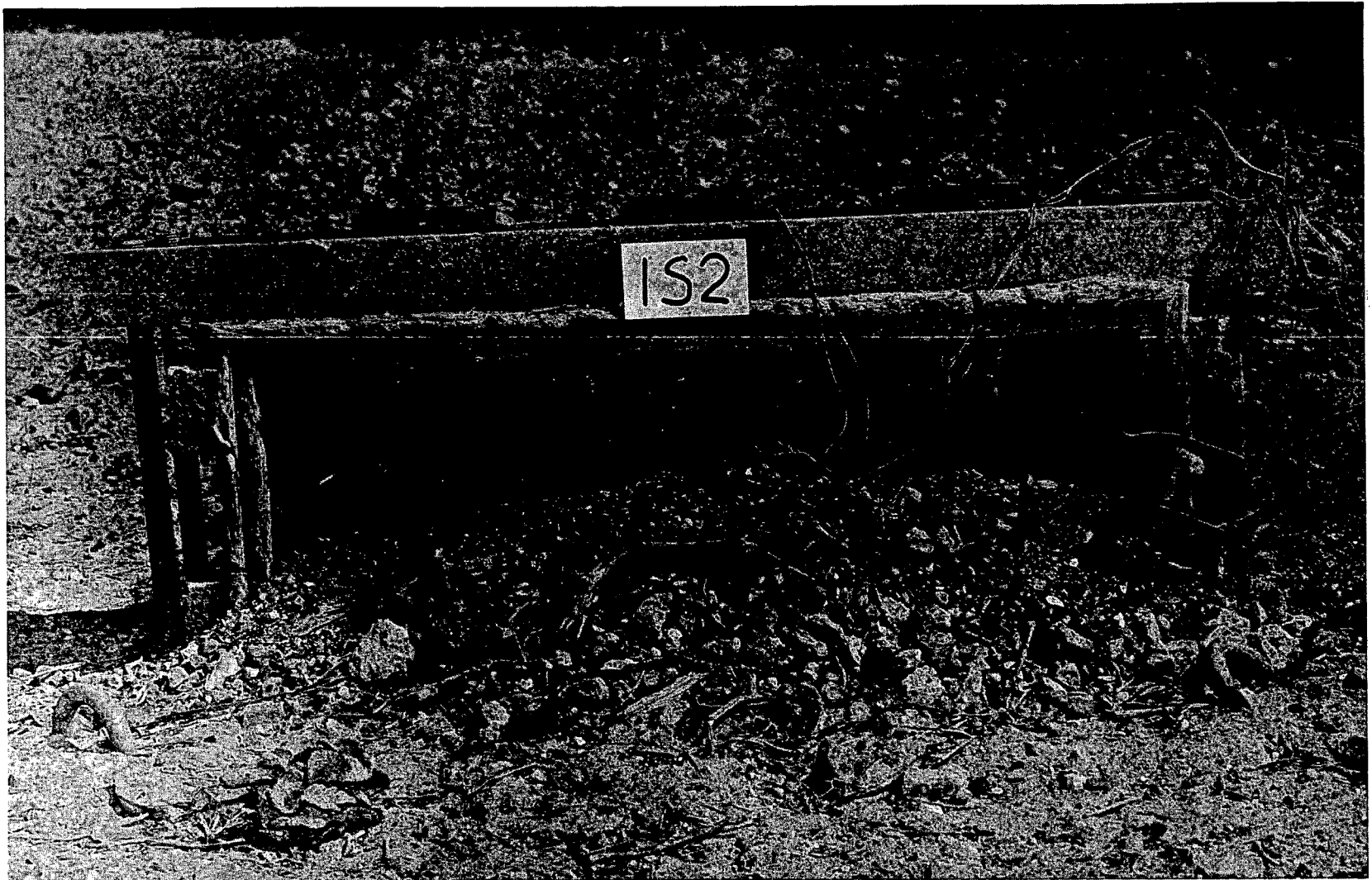


Fig. 5.12—Installation 1S2, postshot. Note debris in front of trap and erosion of trap housing.

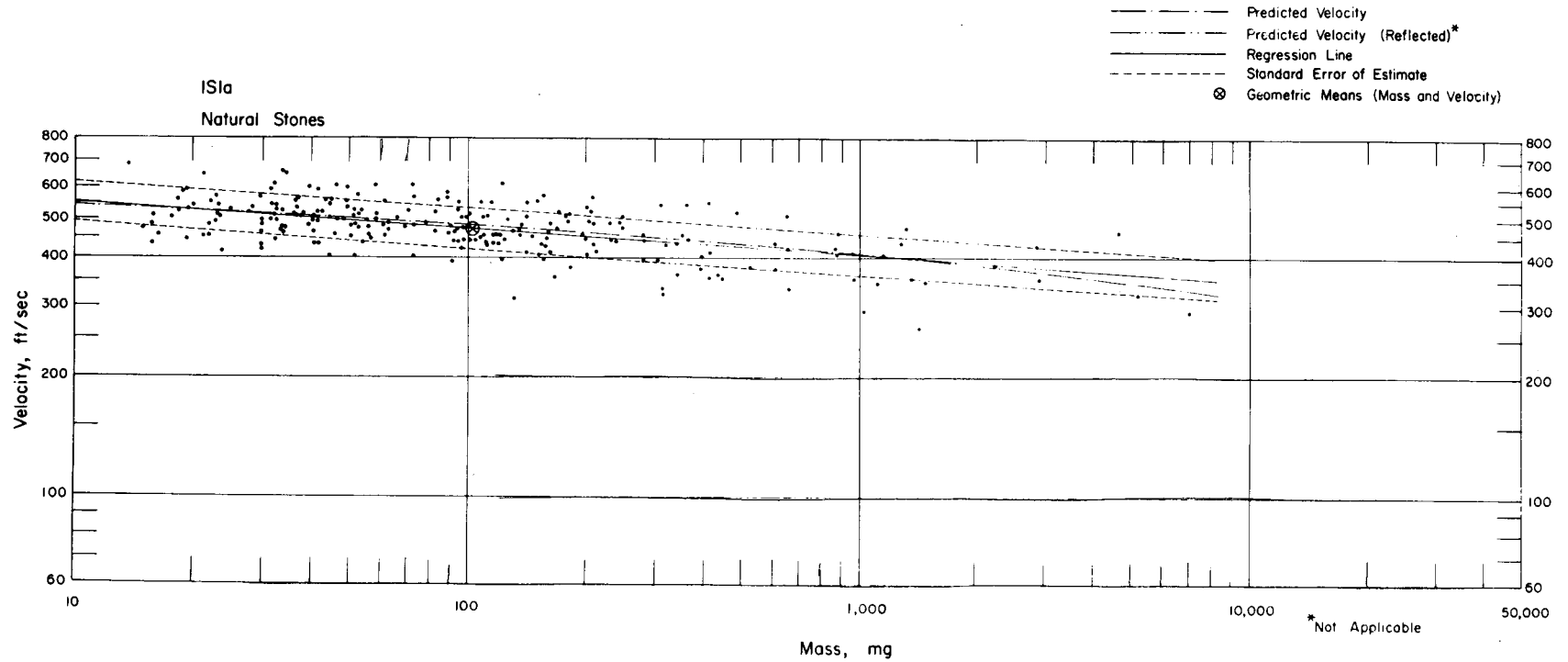


Fig. 5.13—Analysis of natural-stone missiles from trap 1S1a: $n = 238$; $\log v = 2.8102 - 0.0664 \log m$; $E_{gv} = 1.13$; $M_{50} = 102$ mg; $V_{50} = 475$ ft/sec.

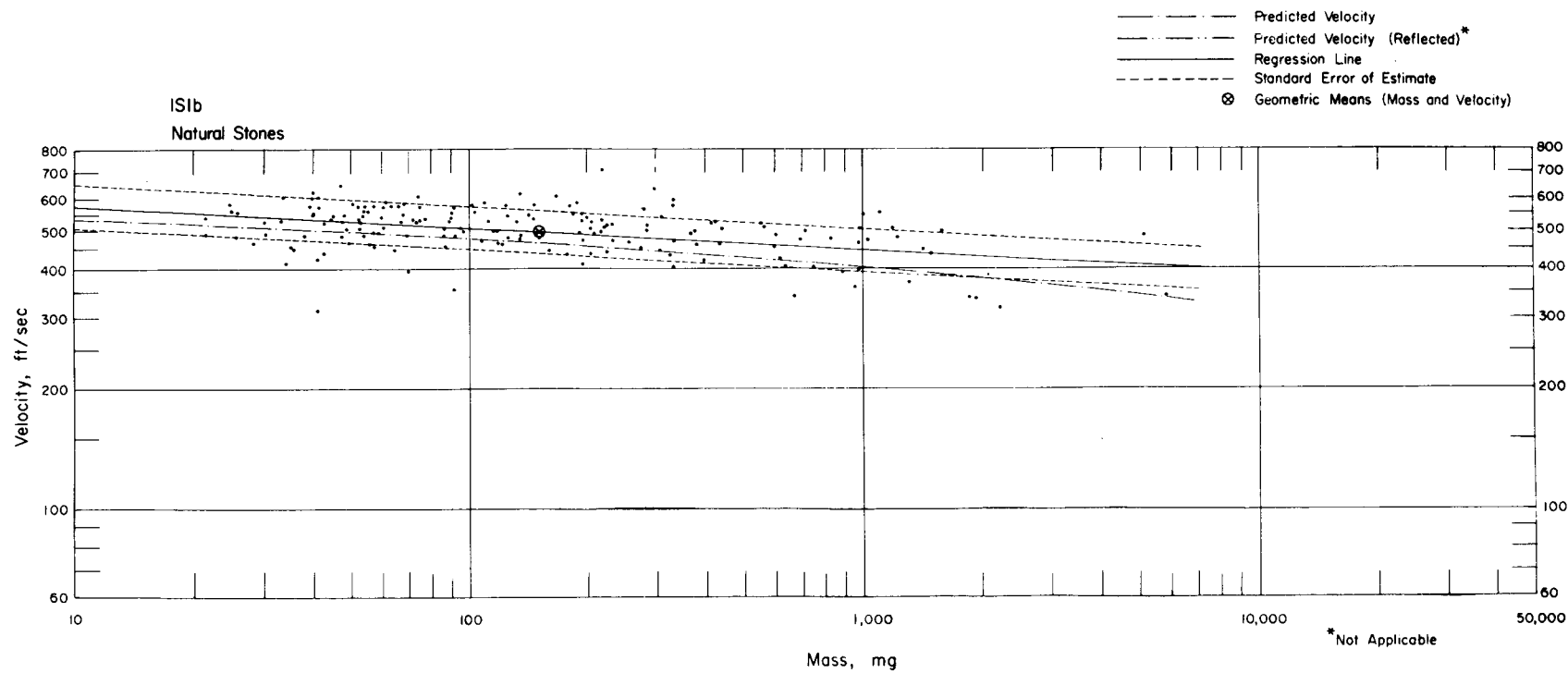


Fig. 5.14—Analysis of natural-stone missiles from trap ISIb: $n = 174$; $\log v = 2.8191 - 0.0557 \log m$; $E_{gv} = 1.13$; $M_{50} = 150$ mg; $V_{50} = 498$ ft/sec.

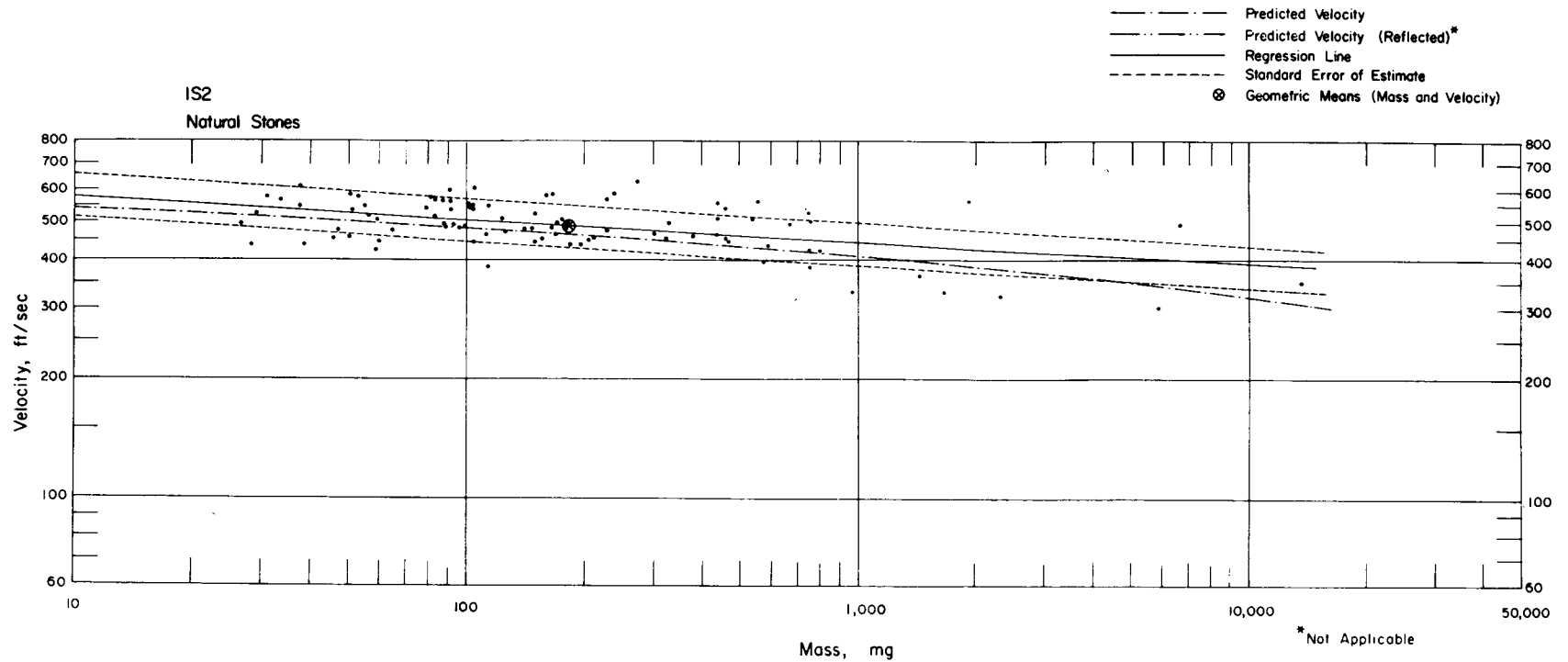


Fig. 5.15— Analysis of natural-stone missiles from trap IS2: $n = 93$; $\log v = 2.8227 - 0.0599 \log m$; $E_{gv} = 1.13$; $M_{50} = 181$ mg; $V_{50} = 486$ ft/sec.

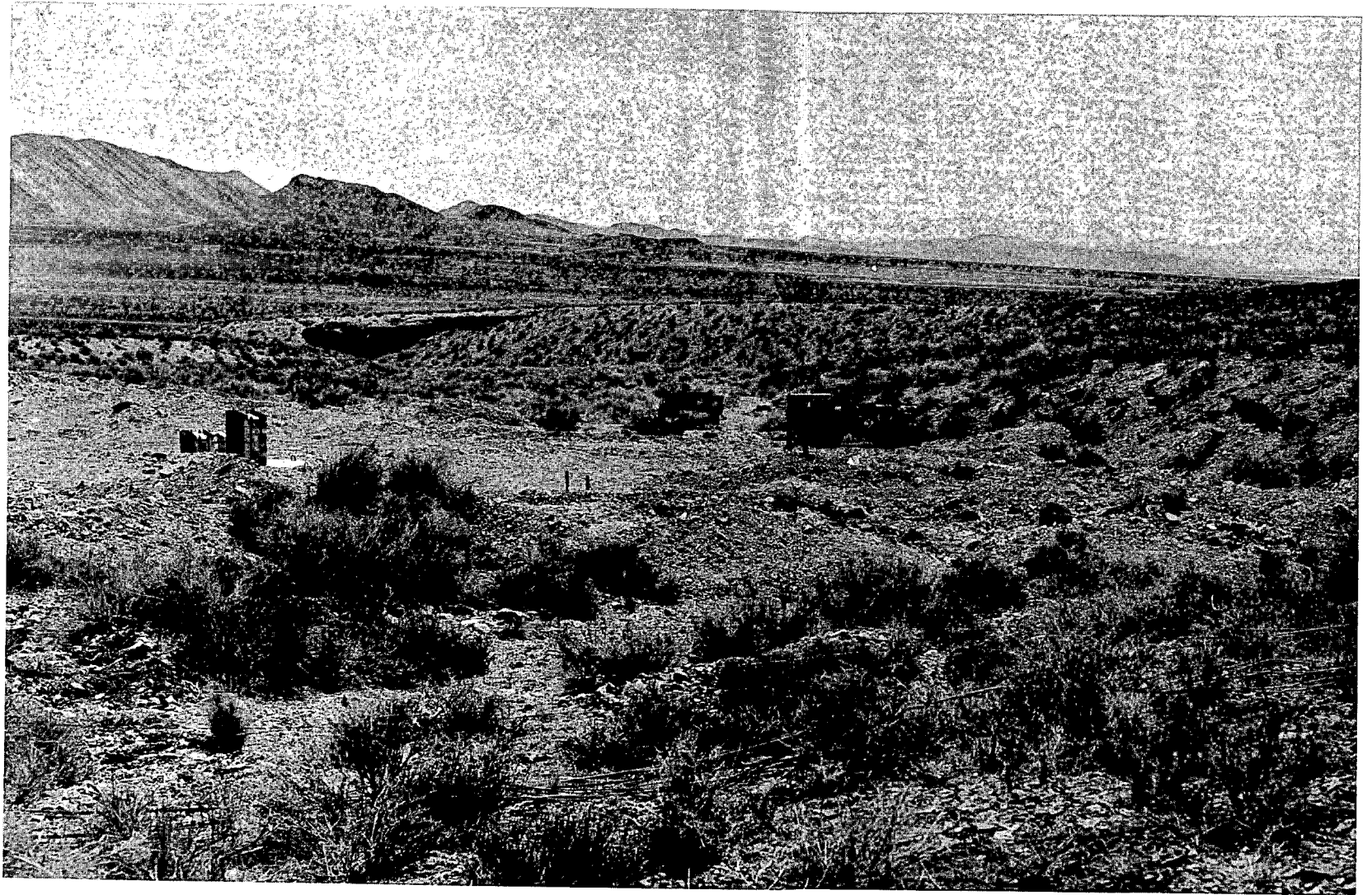


Fig. 5.17—Station 2S, preshot, at 2914-ft range on the northeast blast line.

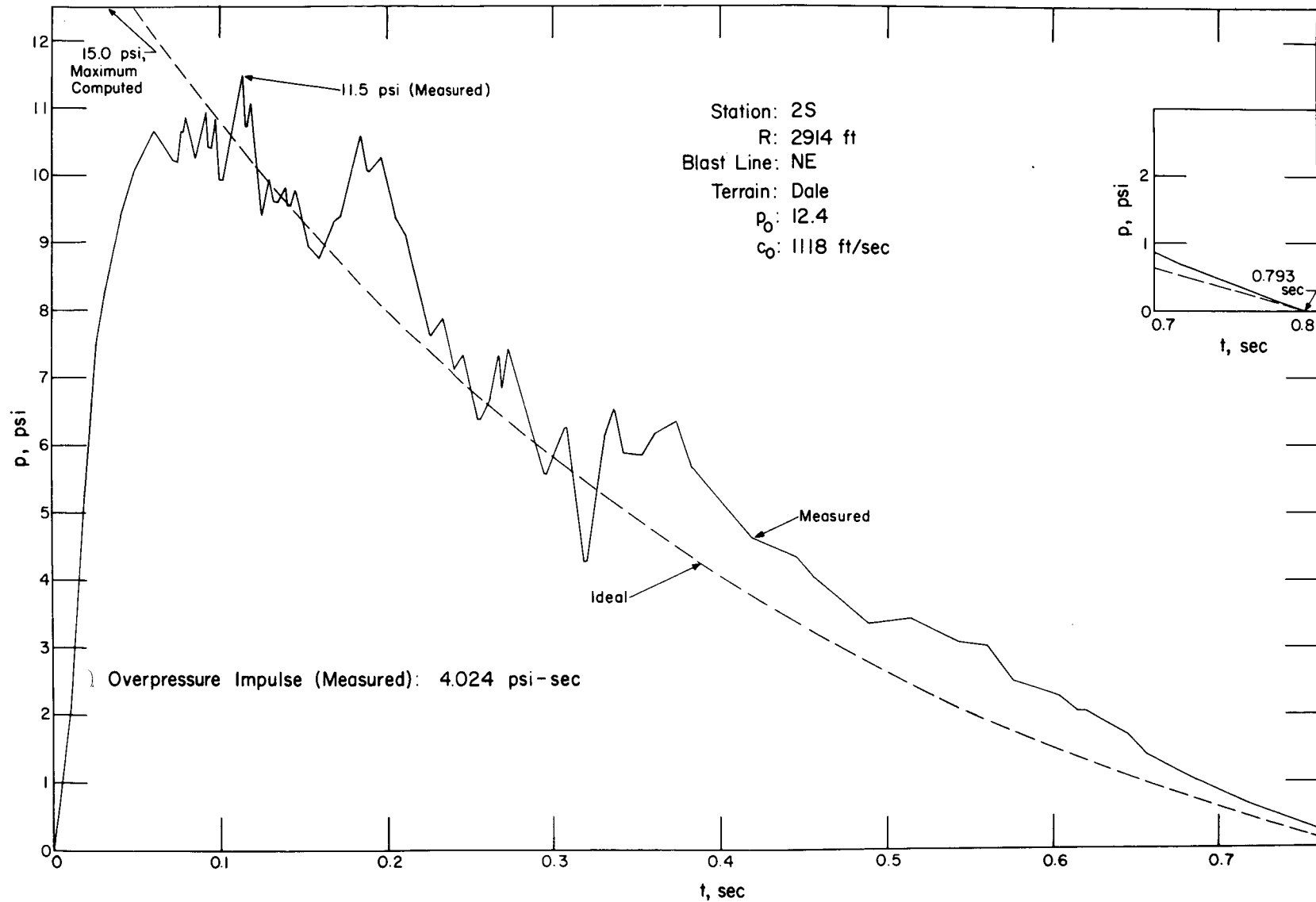


Fig. 5.18—Overpressure vs. time at station 2S.

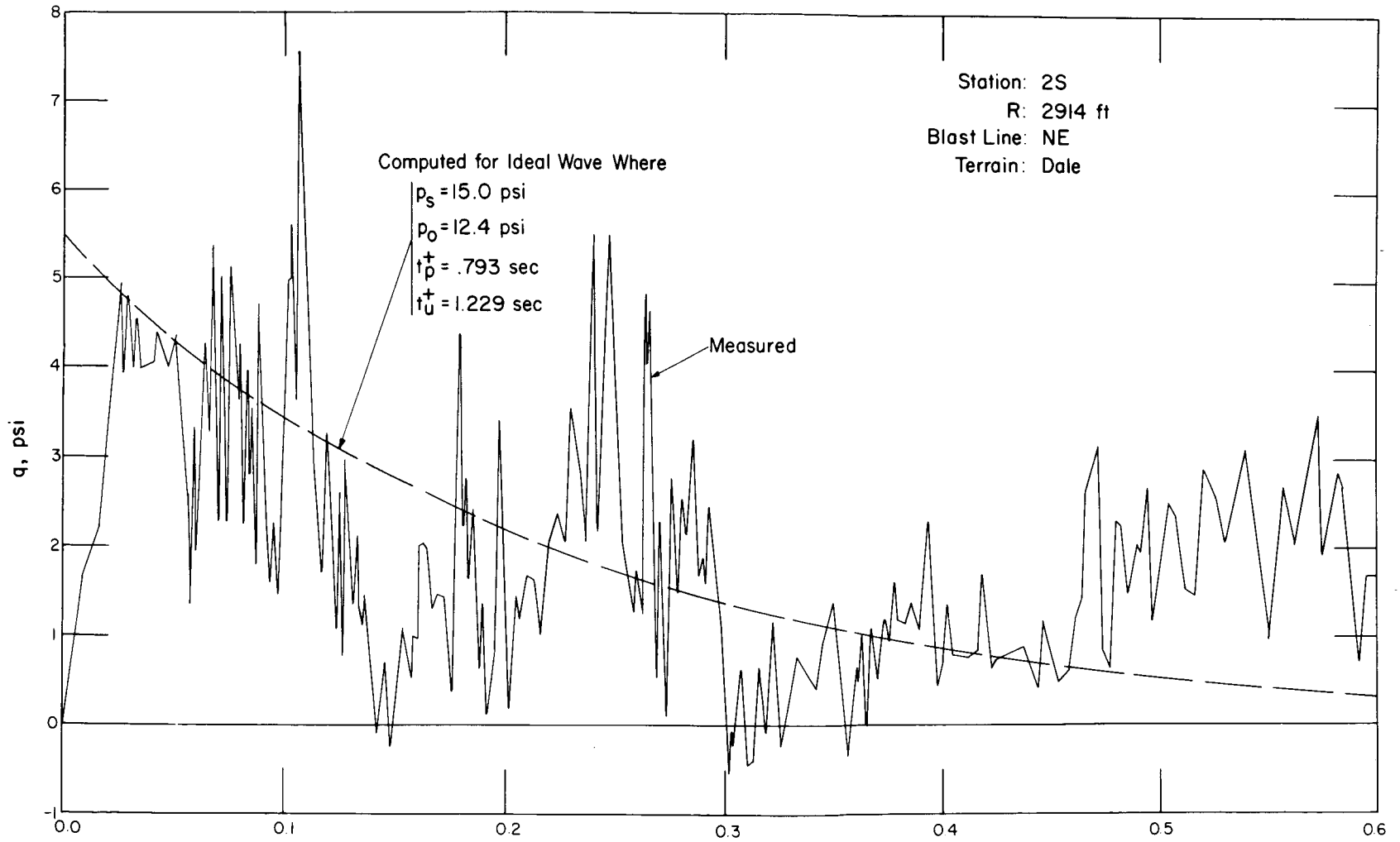


Fig. 5.19—Dynamic pressure vs. time at station 2S.



273

Fig. 5.20—Installation 2S1, postshot. Note debris accumulated in front of trap.

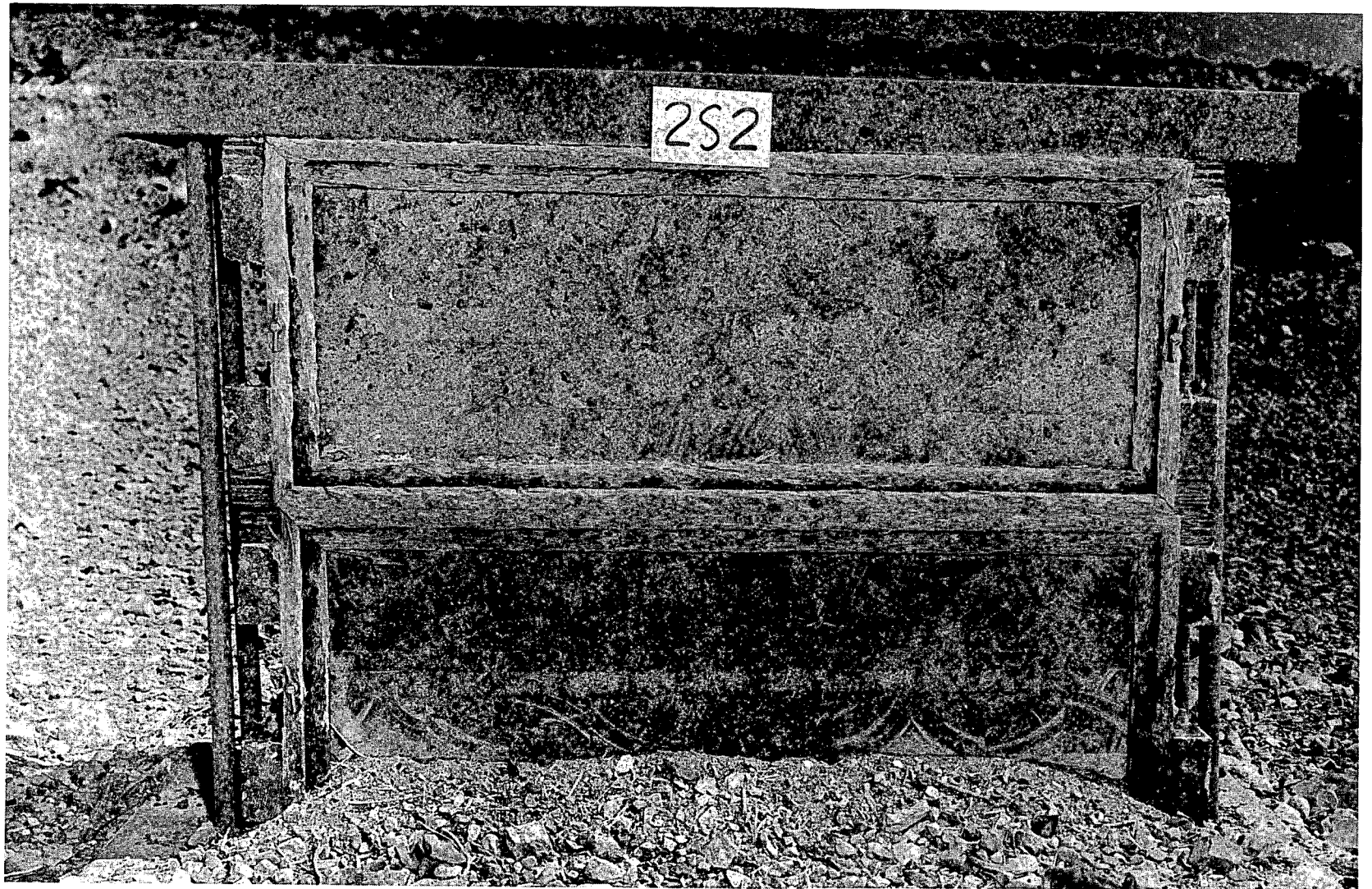


Fig. 5.21—Traps 2S2a and b, postshot.

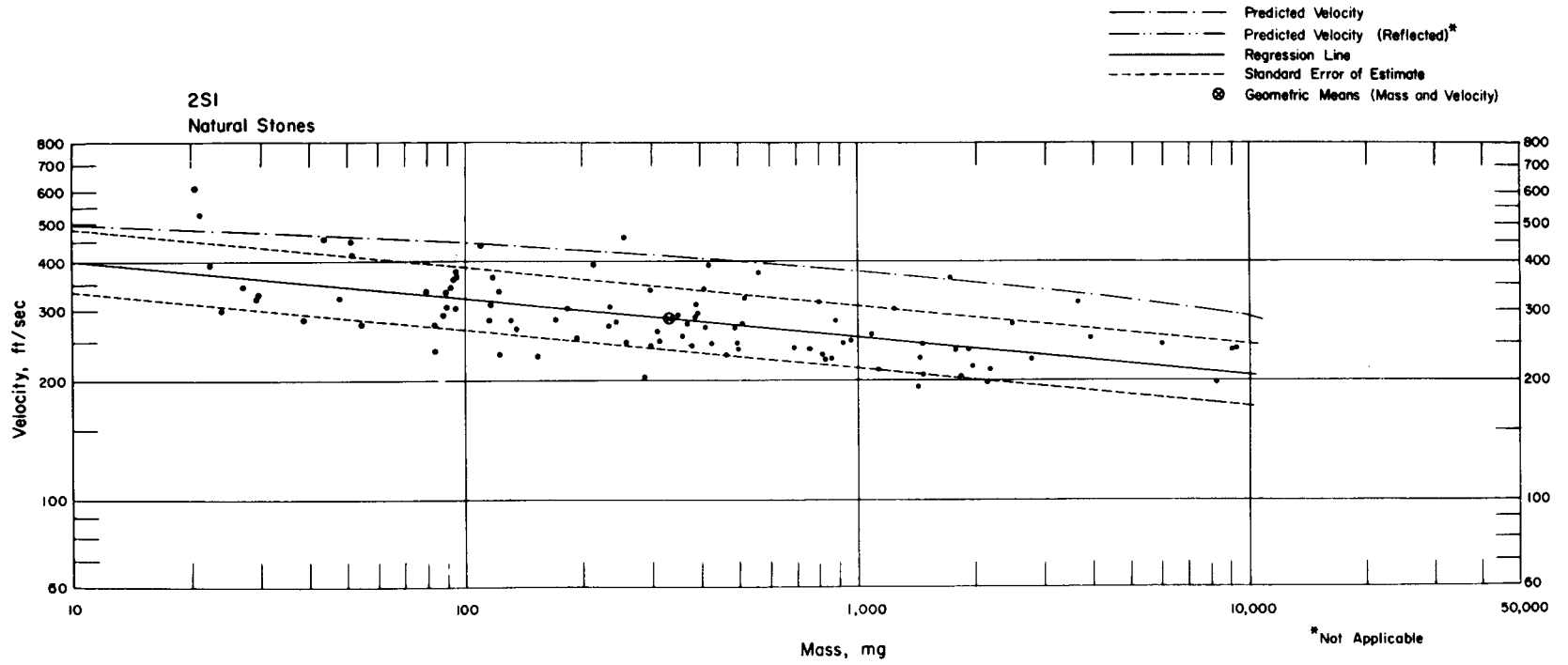


Fig. 5.22— Analysis of natural-stone missiles from installation 2S1: $n = 96$; $\log v = 2.6960 - 0.0951 \log m$; $E_{gv} = 1.19$; $M_{50} = 327$ mg; $V_{50} = 286$ ft/sec.

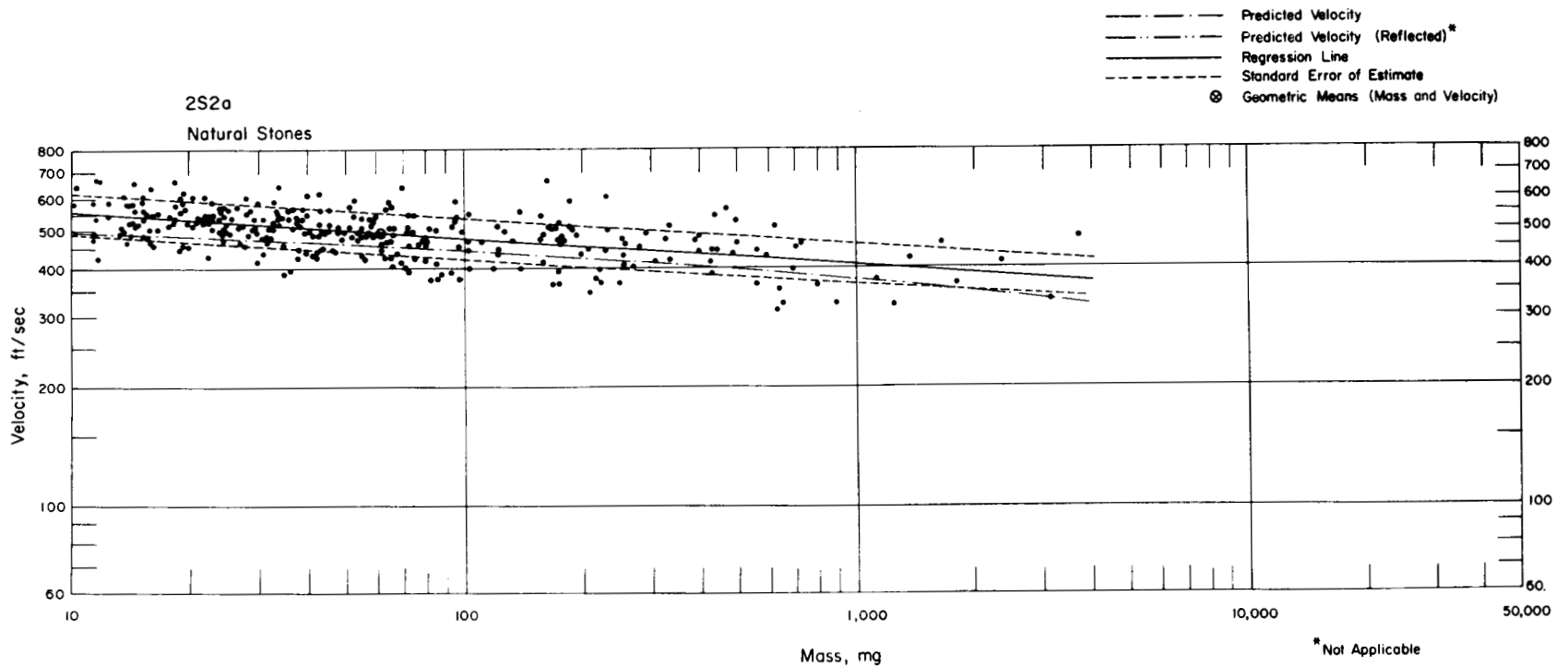


Fig. 5.23—Analysis of natural-stone missiles from trap 2S2a: $n = 307$; $\log v = 2.8089 - 0.0658 \log m$; $E_{gv} = 1.12$; $M_{50} = 61.3$ mg; $V_{50} = 491$ ft/sec.

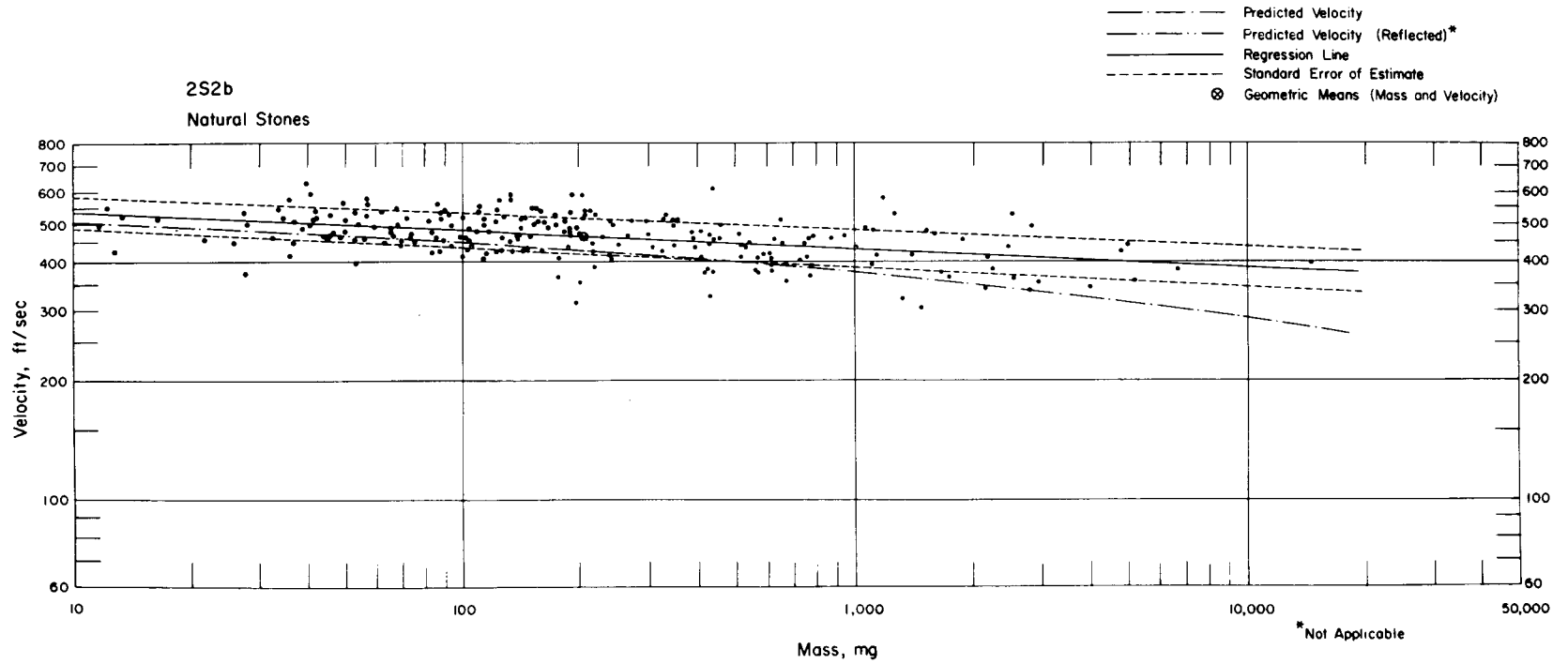


Fig. 5.24—Analysis of natural-stone missiles from trap 2S2b; $n = 227$; $\log v = 2.7670 - 0.0452 \log m$; $E_{gv} = 1.13$; $M_{50} = 203$ mg; $V_{50} = 460$ ft/sec.

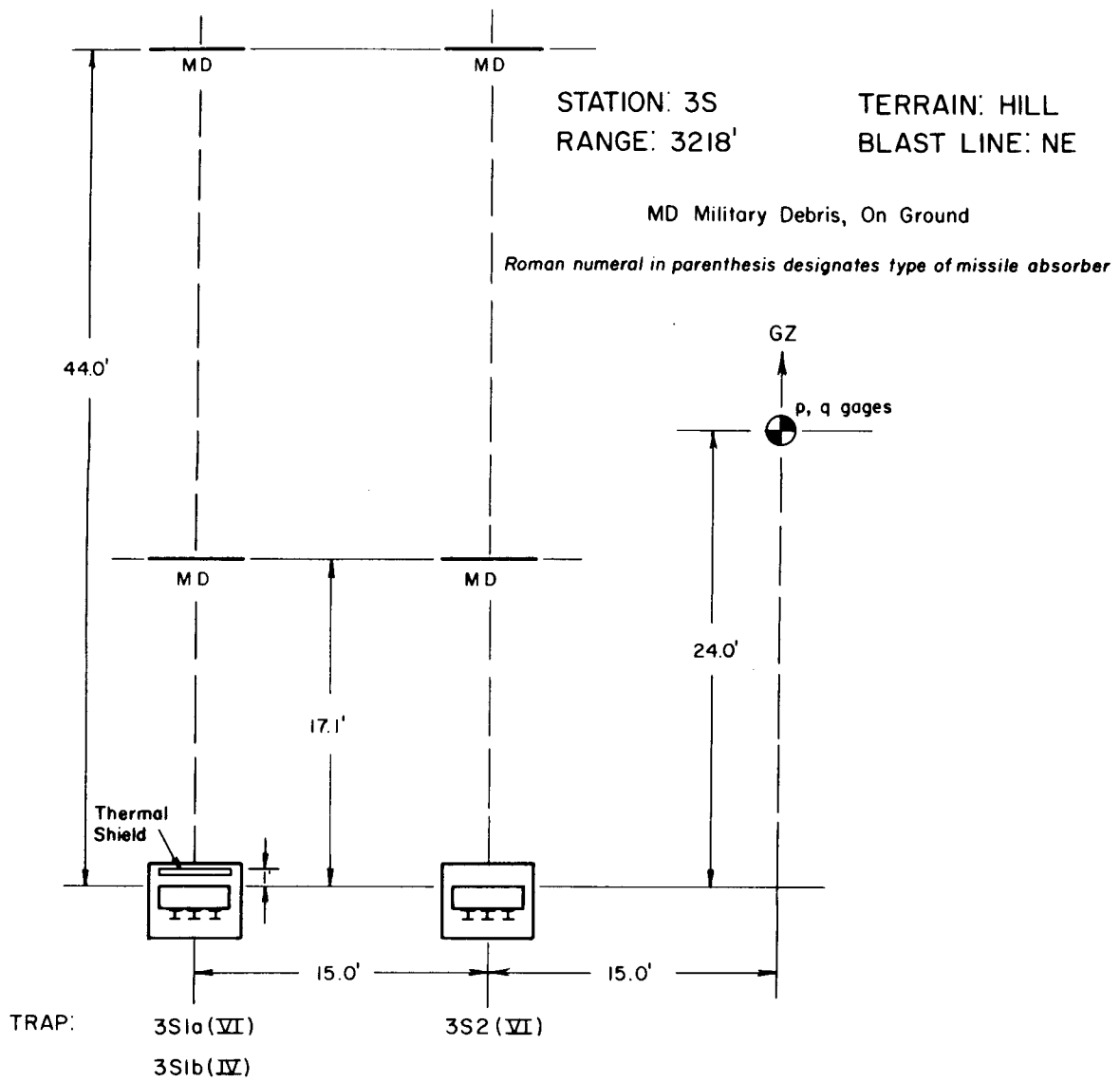


Fig. 5.25—Station 3S layout chart.

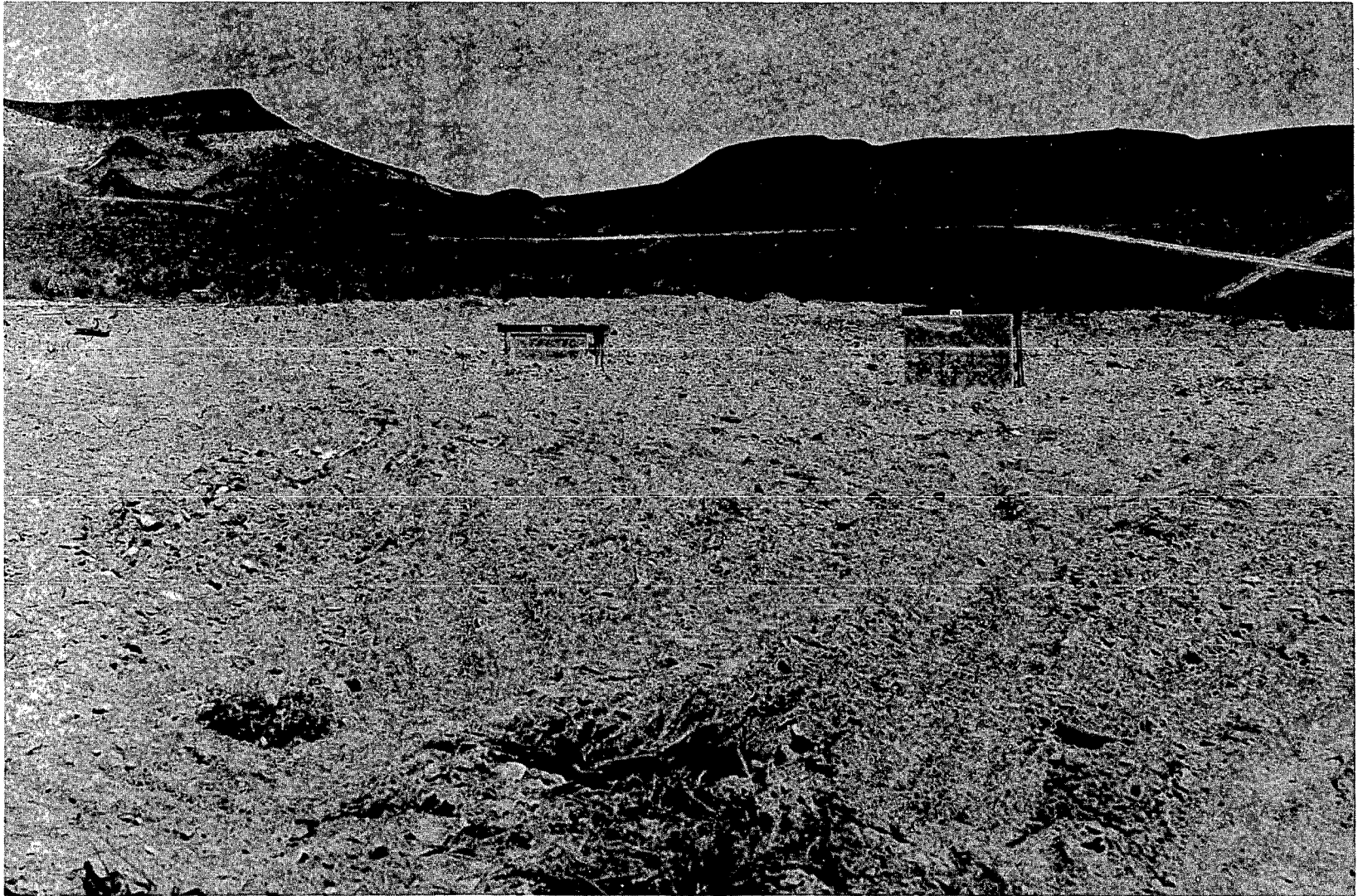


Fig. 5.26—Station 3S, preshot, at 3218-ft range on the northeast blast line.

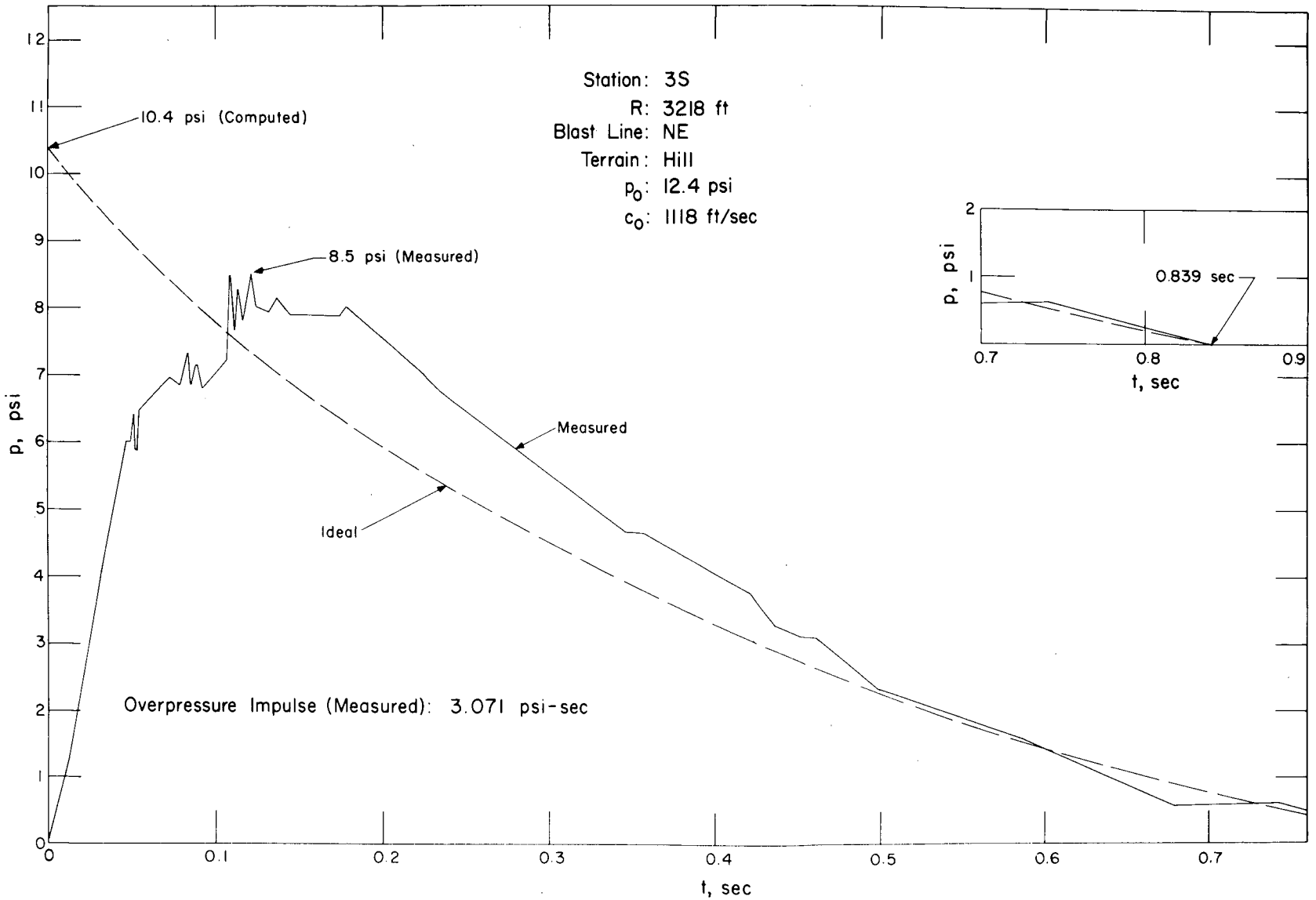


Fig. 5.27—Overpressure vs. time at station 3S.

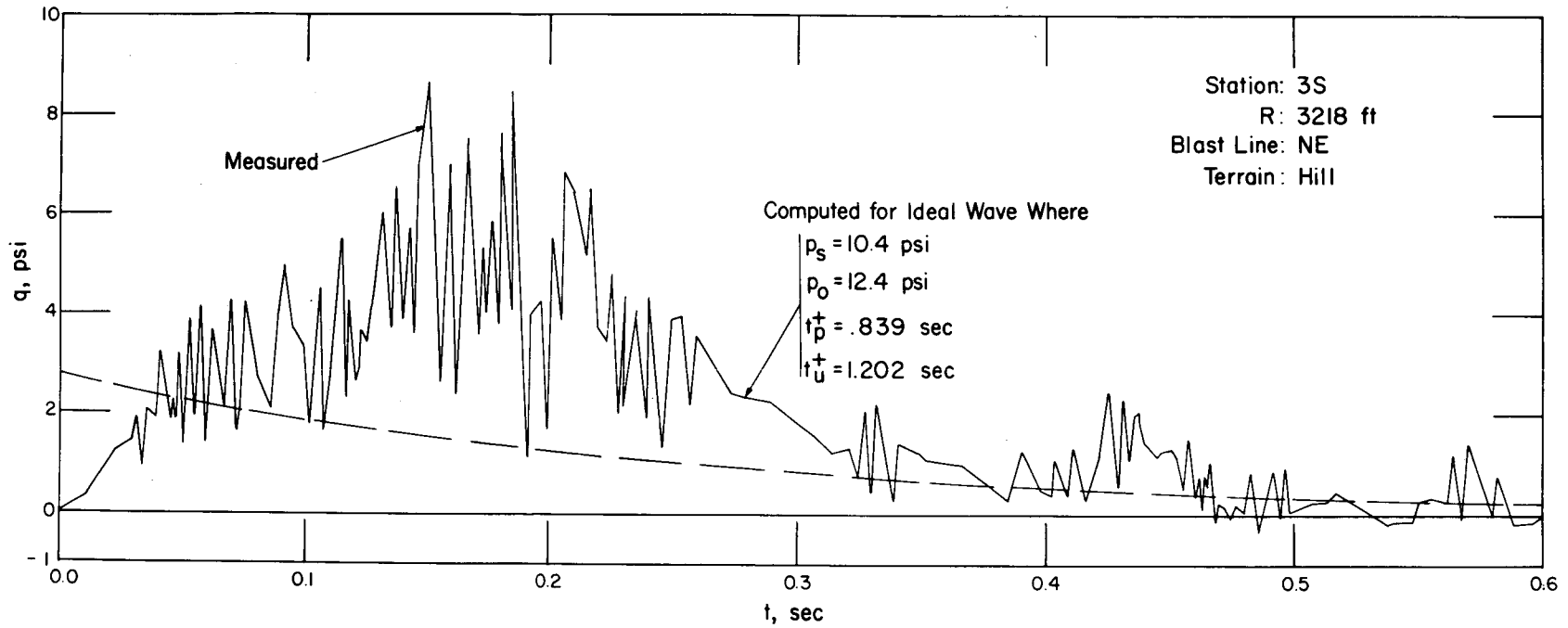


Fig. 5.28—Dynamic pressure vs. time at station 3S.



Fig. 5.29—Traps 3S1a and b, postshot.



Fig. 5.30— Installation 3S2, postshot.

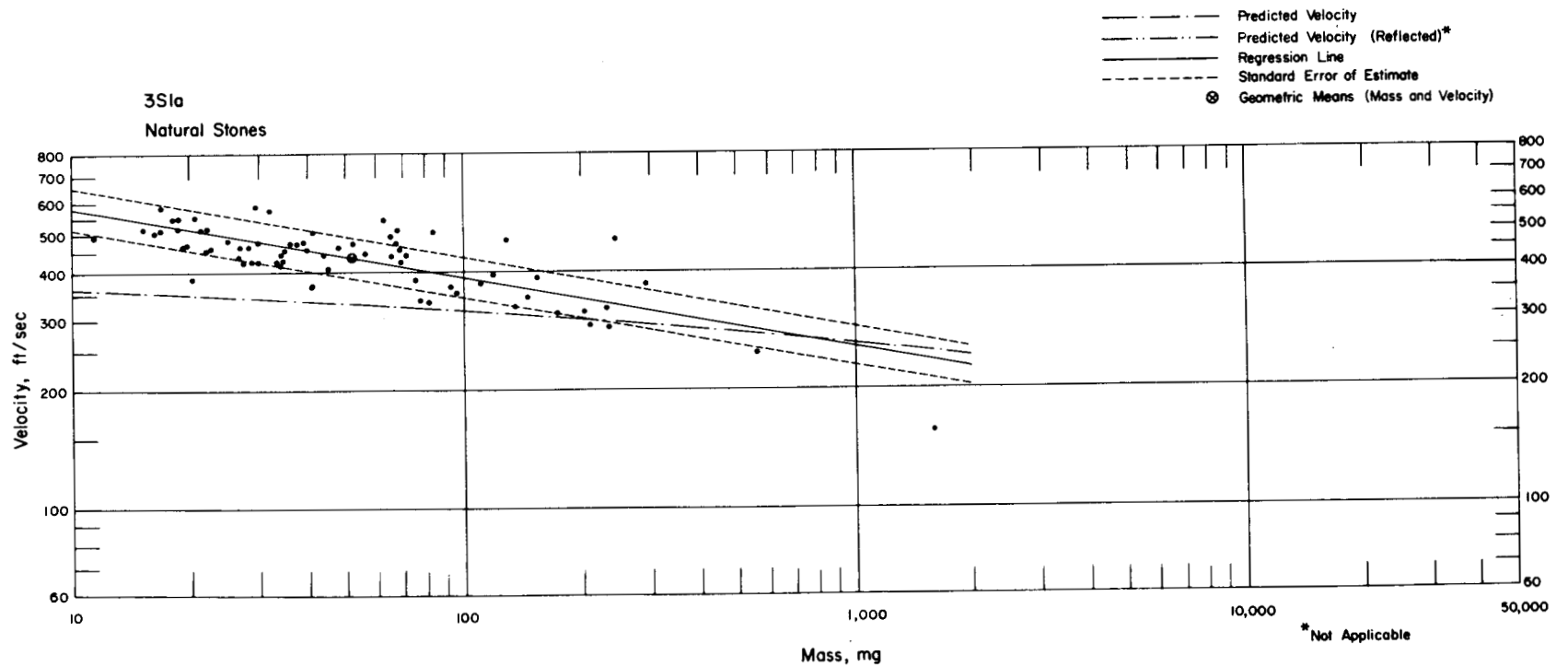


Fig. 5.31—Analysis of natural-stone missiles from trap 3S1a: $n = 71$; $\log v = 2.9424 - 0.1783 \log m$; $E_{GV} = 1.14$; $M_{50} = 51.3$ mg; $V_{50} = 434$ ft/sec.

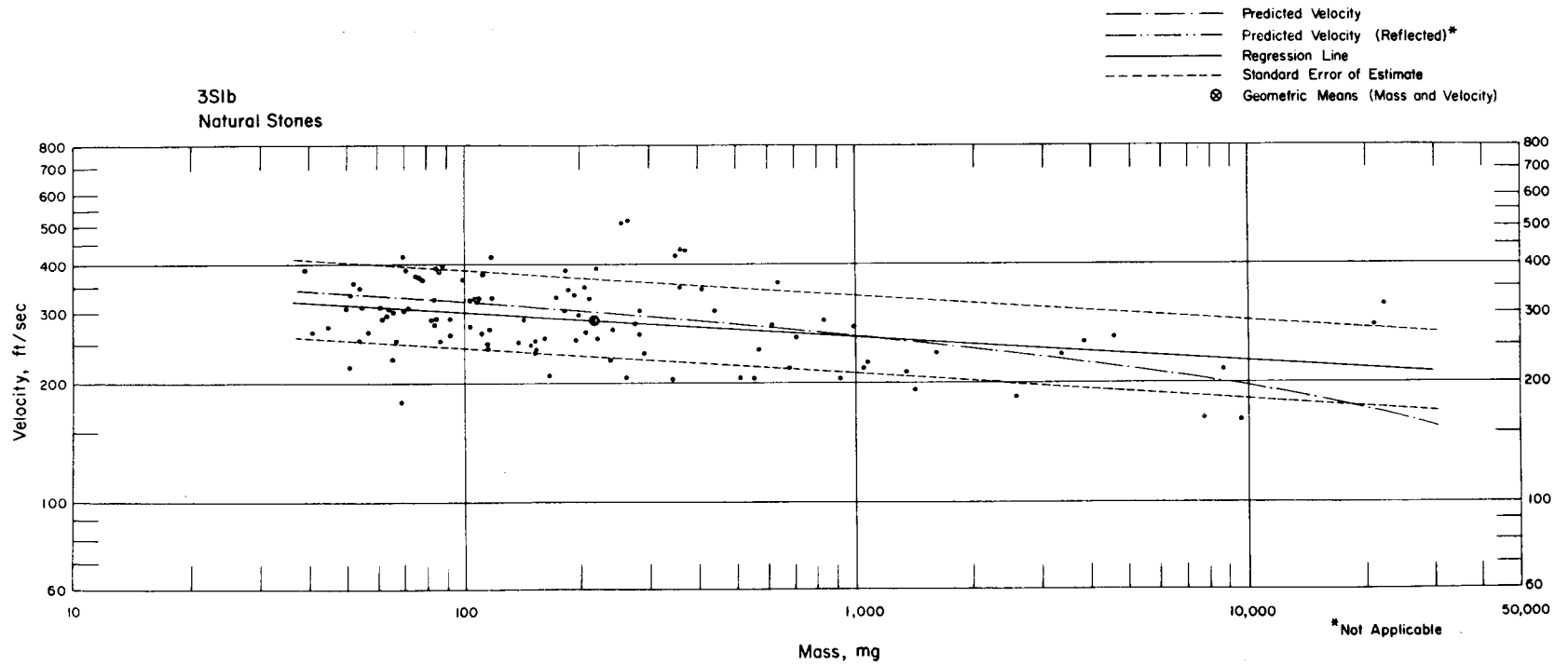


Fig. 5.32— Analysis of natural-stone missiles from trap 3S1b: $n = 109$; $\log v = 2.6046 - 0.0635 \log m$; $E_{GV} = 1.24$; $M_{50} = 219$ mg; $V_{50} = 286$ ft/sec.

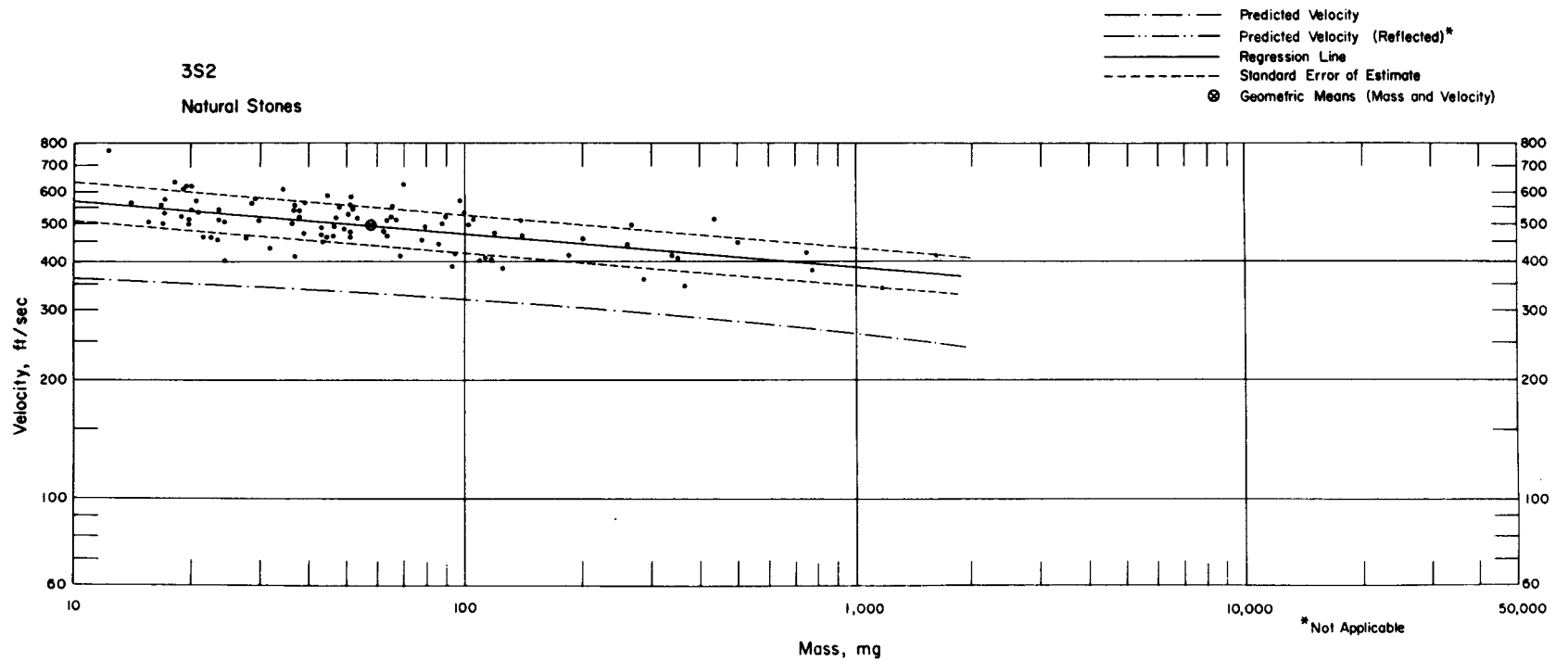


Fig. 5.33— Analysis of natural-stone missiles from installation 3S2: $n = 95$; $\log v = 2.8475 - 0.0872 \log m$; $E_{gv} = 1.12$; $M_{50} = 58.6$ mg;
 $V_{50} = 494$ ft/sec.

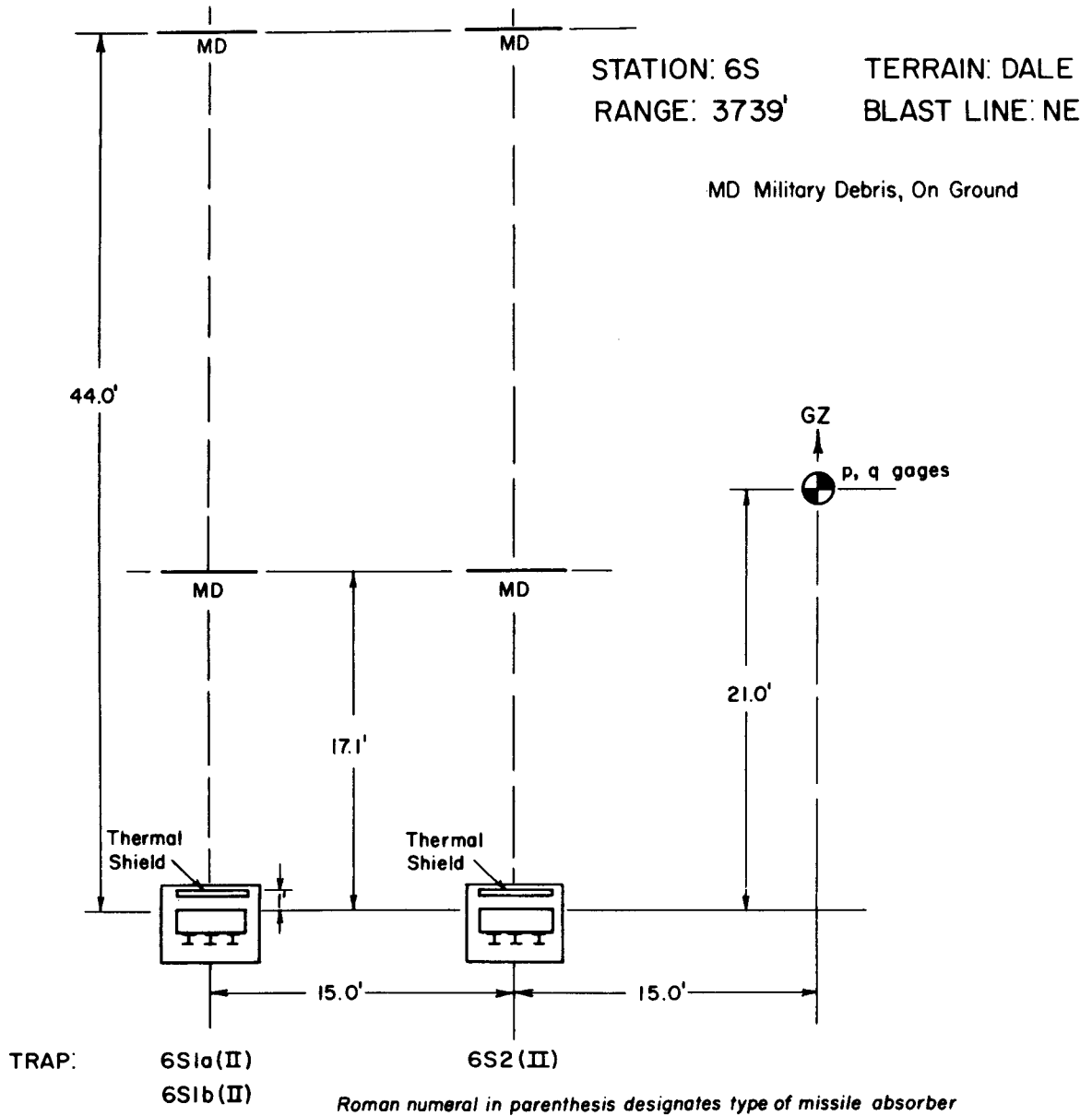


Fig. 5.34—Station 6S layout chart.

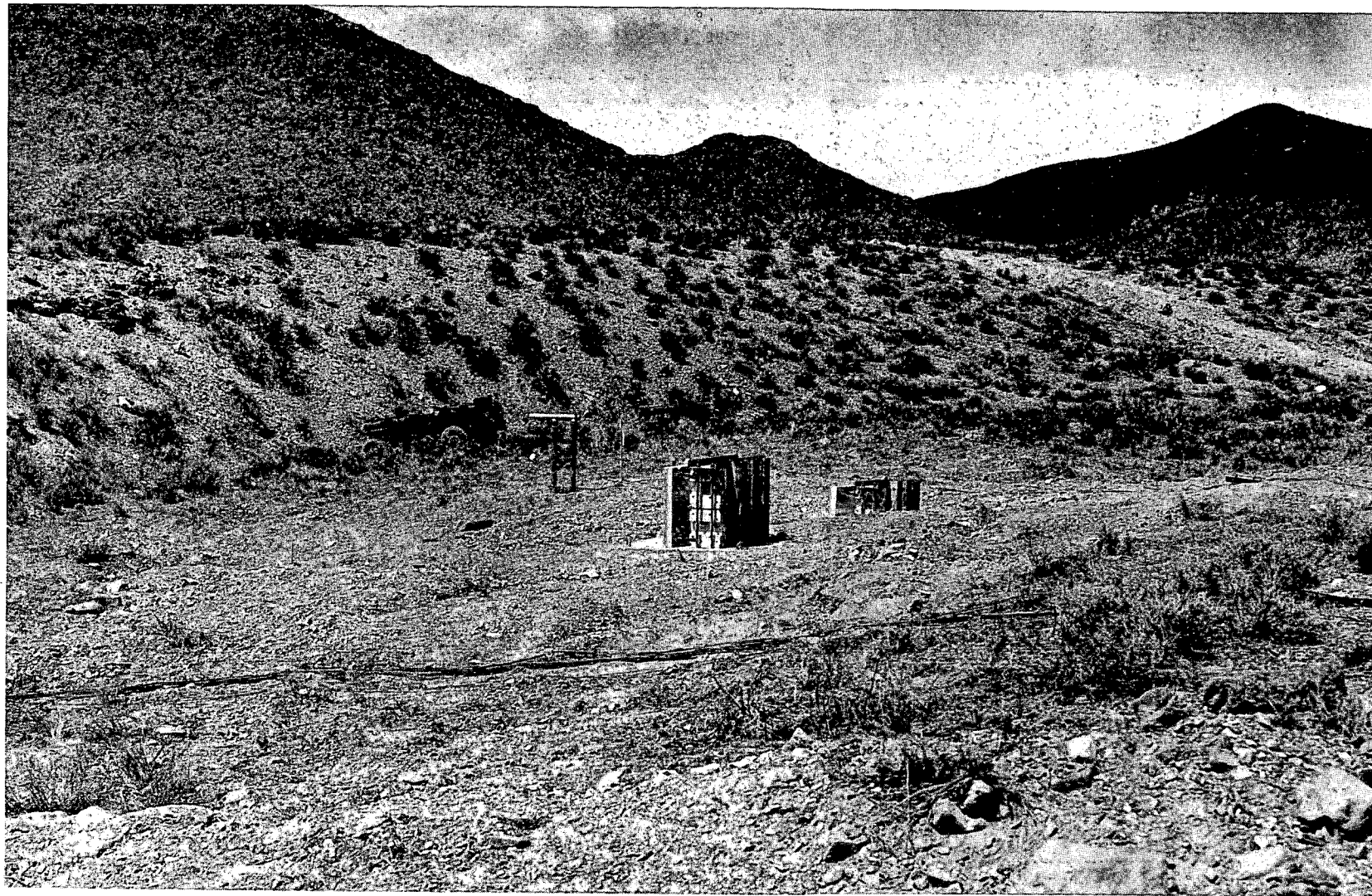


Fig. 5.35—Station 6S, pre-shot, at 3739-ft range on the northeast blast line.

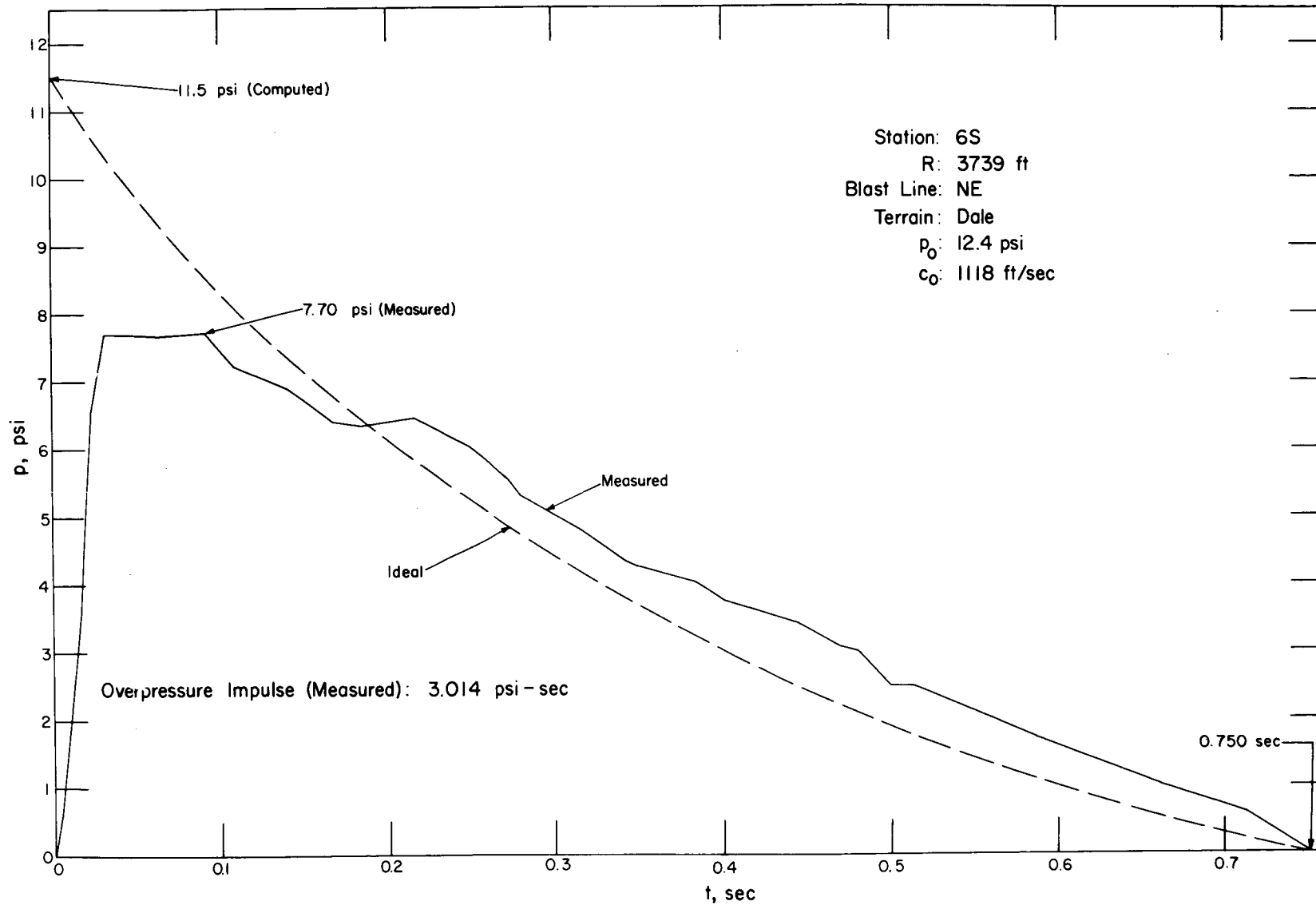


Fig. 5.36—Overpressure vs. time at station 6S.

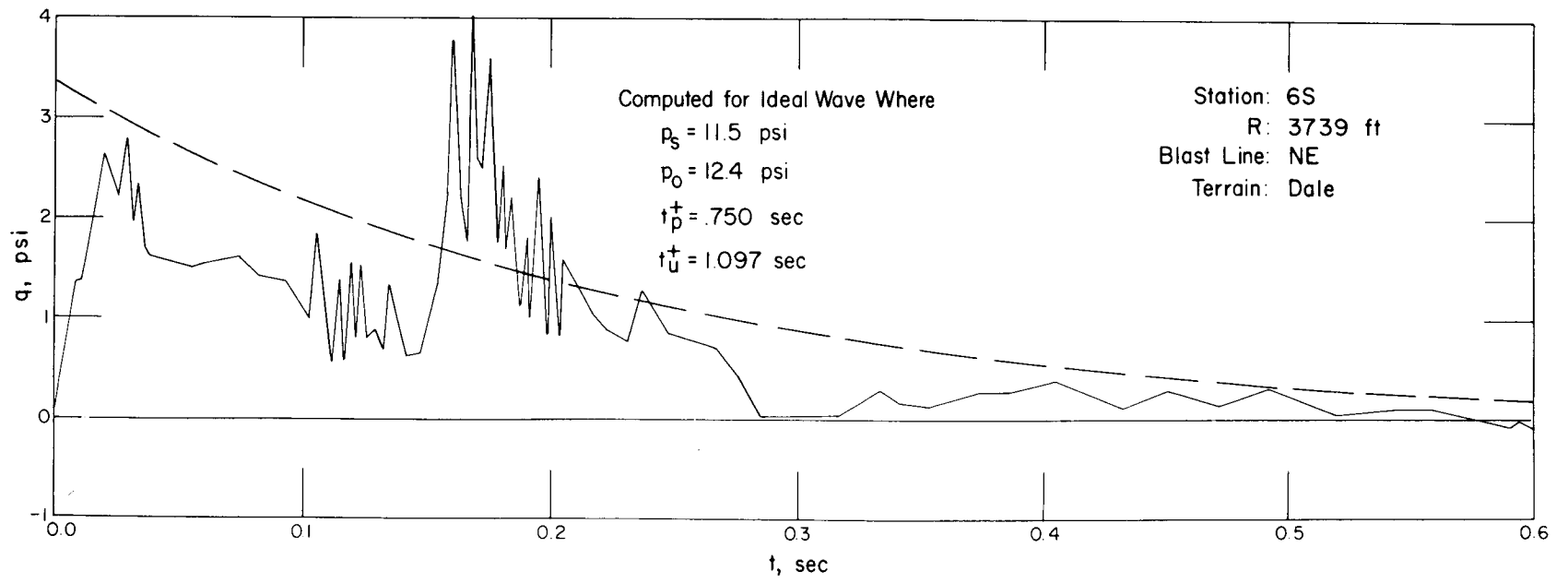


Fig. 5.37—Dynamic pressure vs. time at station 6S.



291

Fig. 5.38—Traps 6S1a, and b, postshot. Note the charred wood. The absorber, however, was undamaged by thermal radiation.

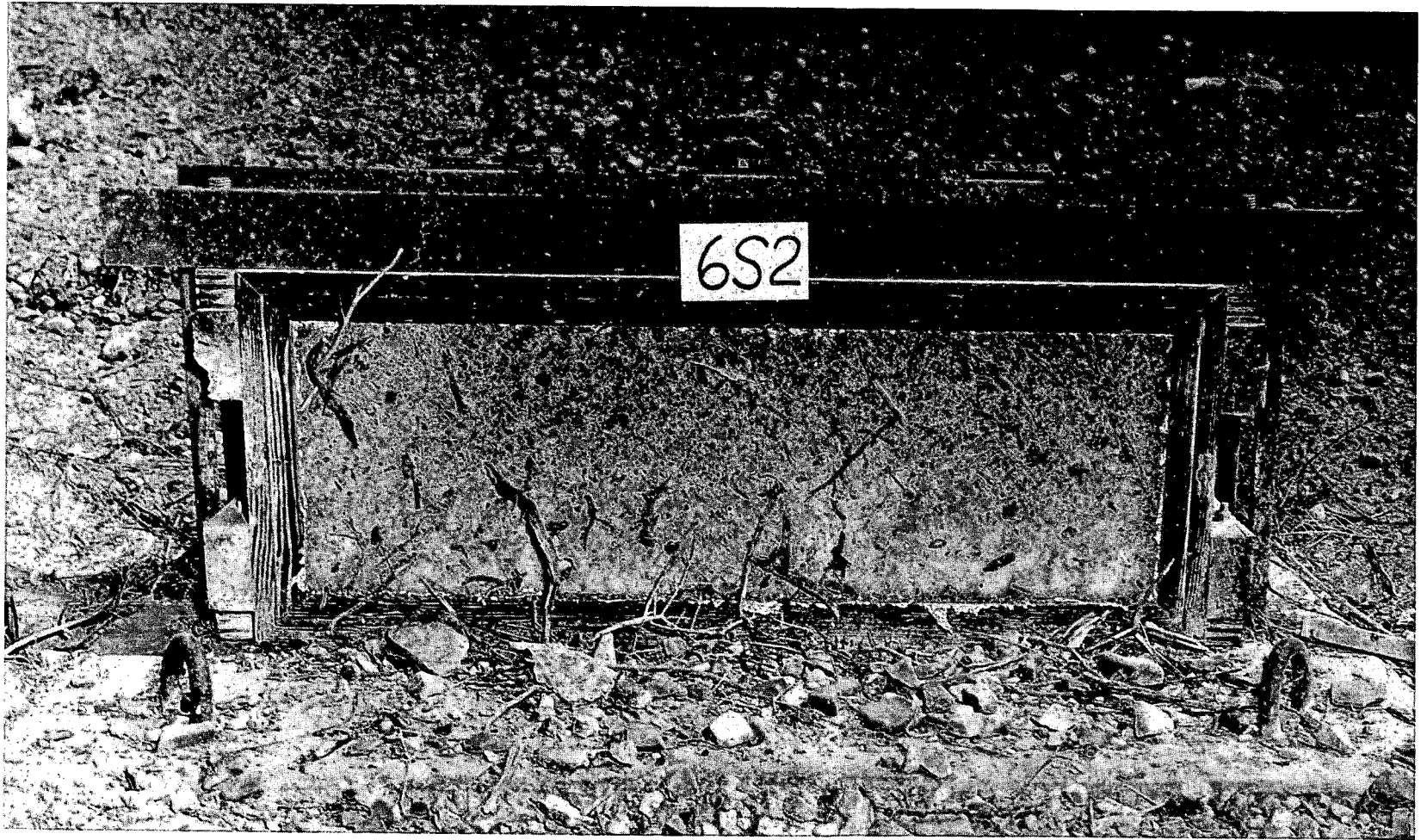


Fig. 5.39—Installation 6S2, postshot. The thermal-shield frame was destroyed.

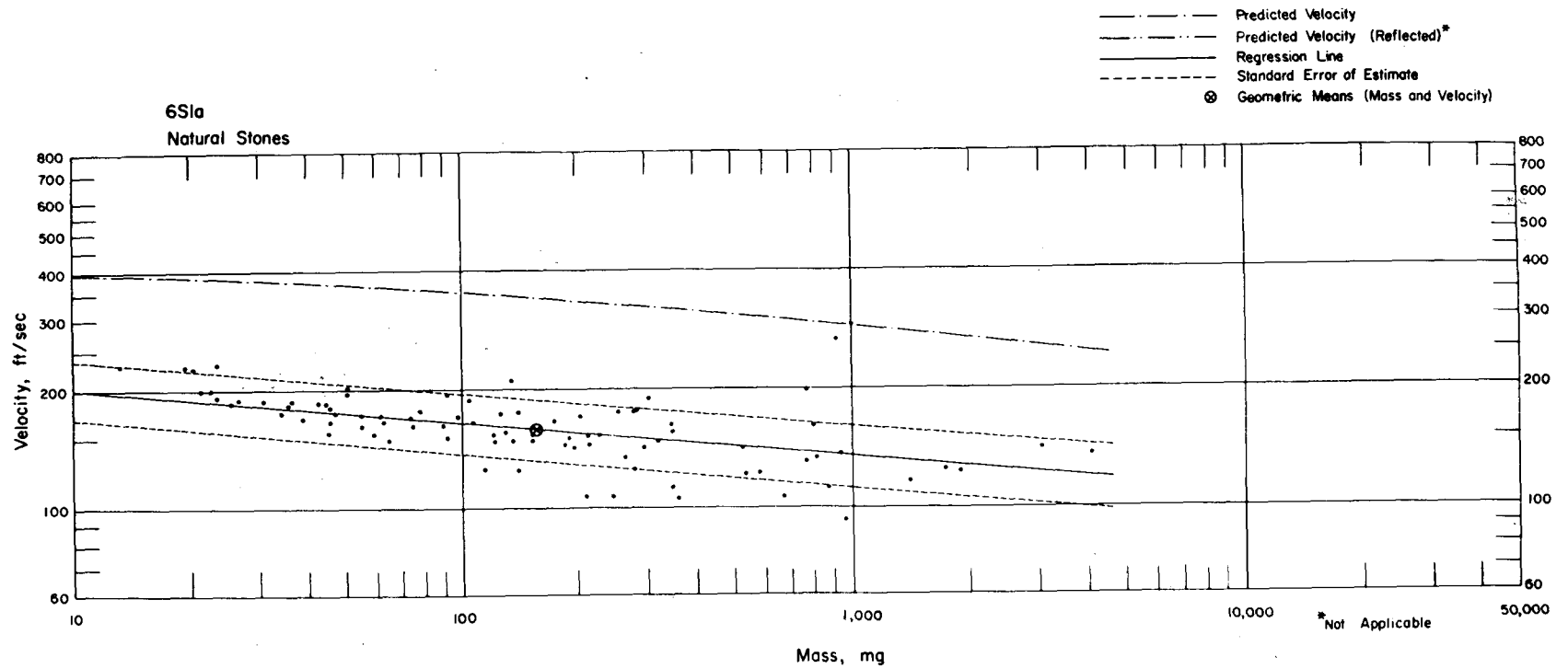


Fig. 5.40—Analysis of natural-stone missiles from trap 6S1a: $n = 86$; $\log v = 2.3973 - 0.0897 \log m$; $E_{GV} = 1.20$; $M_{50} = 153$ mg; $V_{50} = 159$ ft/sec.

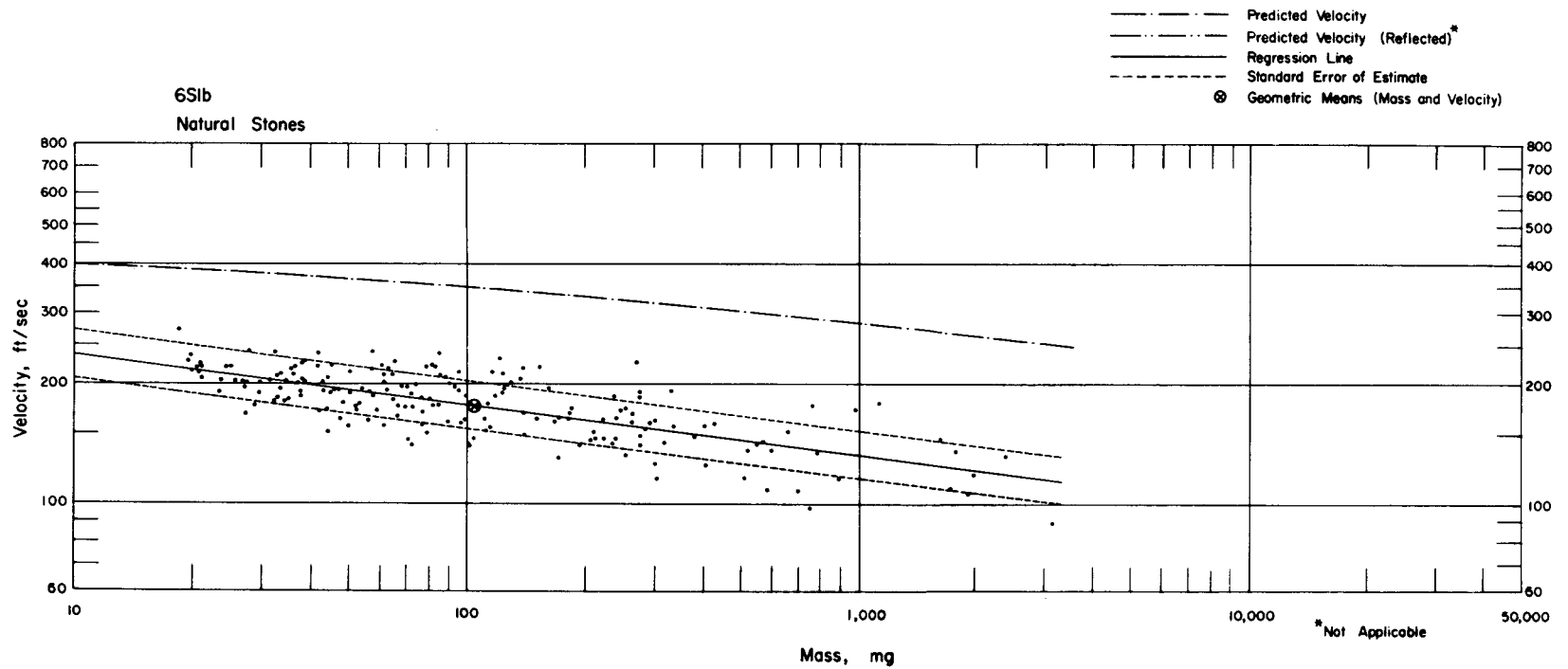


Fig. 5.41—Analysis of natural-stone missiles from trap 6S1b: $n = 192$; $\log v = 2.4998 - 0.1248 \log m$; $E_{gv} = 1.15$; $M_{50} = 103$ mg; $V_{50} = 177$ ft/sec.

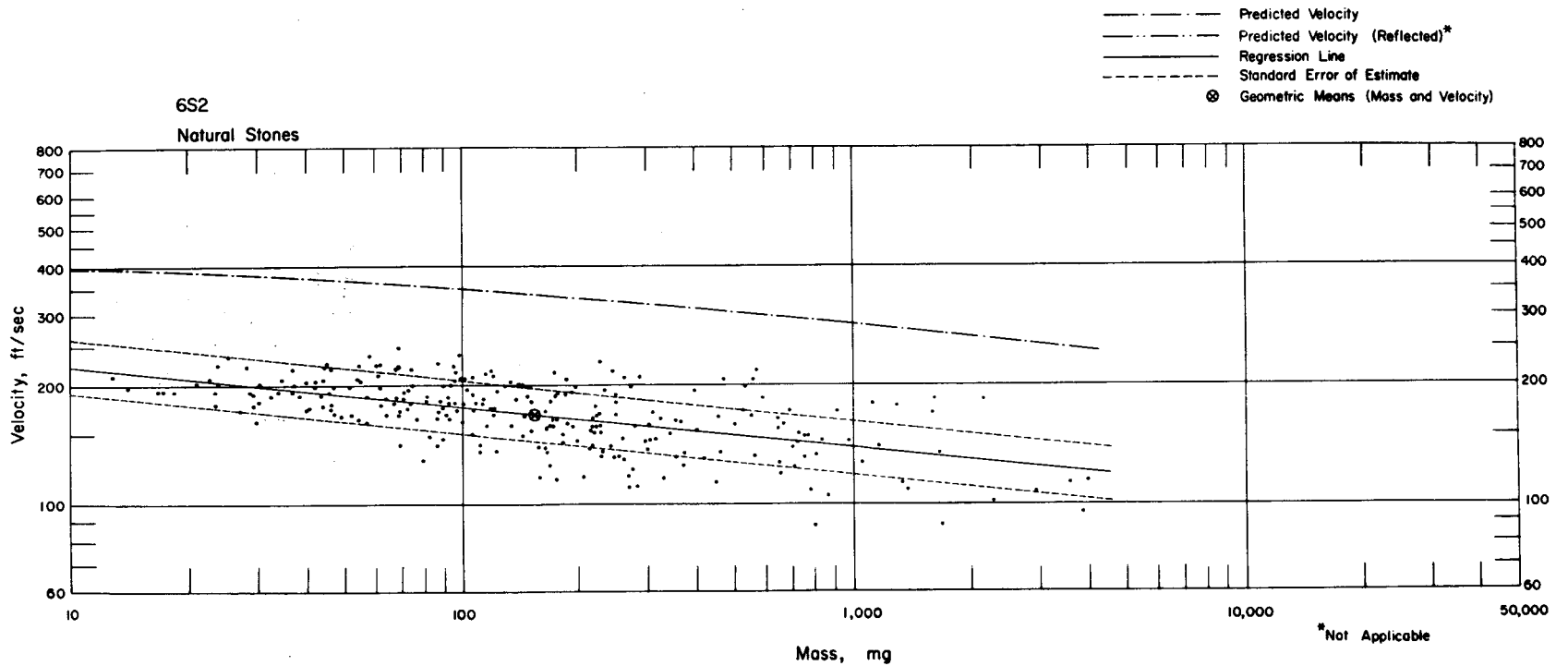


Fig. 5.42—Analysis of natural-stone missiles from installation 6S2: $n = 259$; $\log v = 2.4595 - 0.1056 \log m$; $E_{gv} = 1.17$; $M_{50} = 154$ mg; $V_{50} = 169$ ft/sec.

STATION: 7S
RANGE: 4115'

TERRAIN: HILL
BLAST LINE: NE

MD Military Debris, On Ground

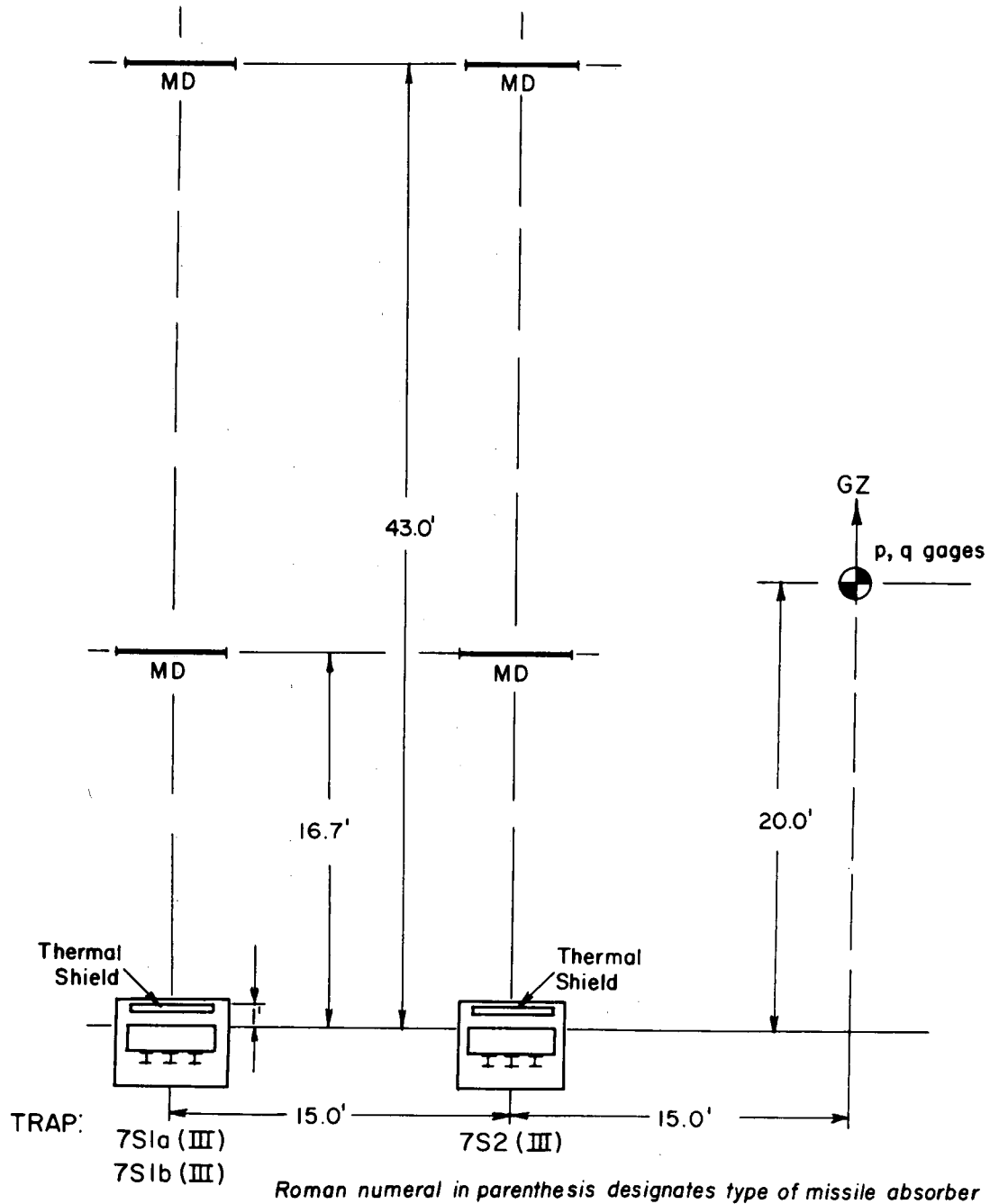


Fig. 5.43—Station 7S layout chart.

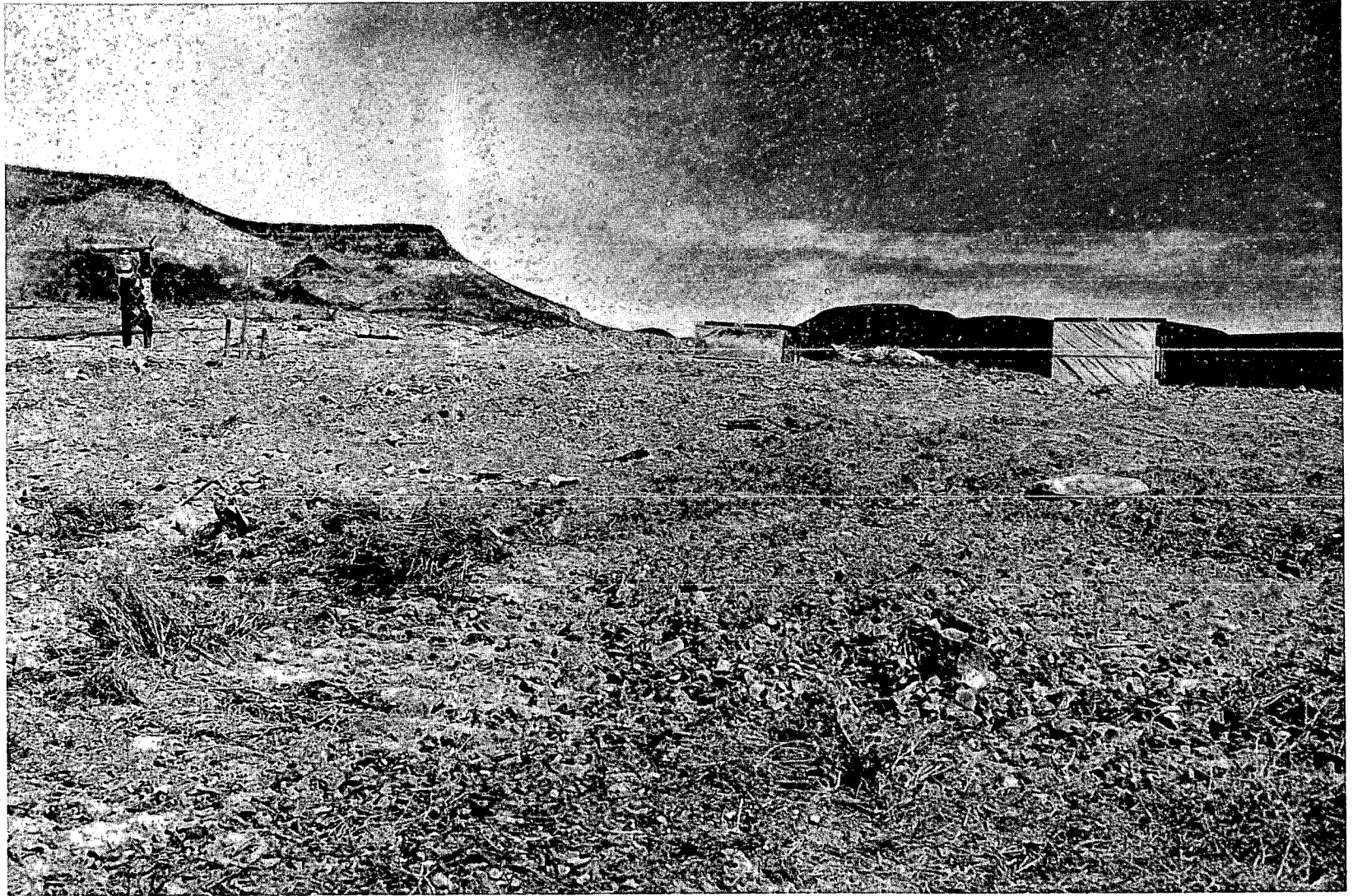


Fig. 5.44—Station 7S, preshot, at 4115-ft range on the northeast blast line.

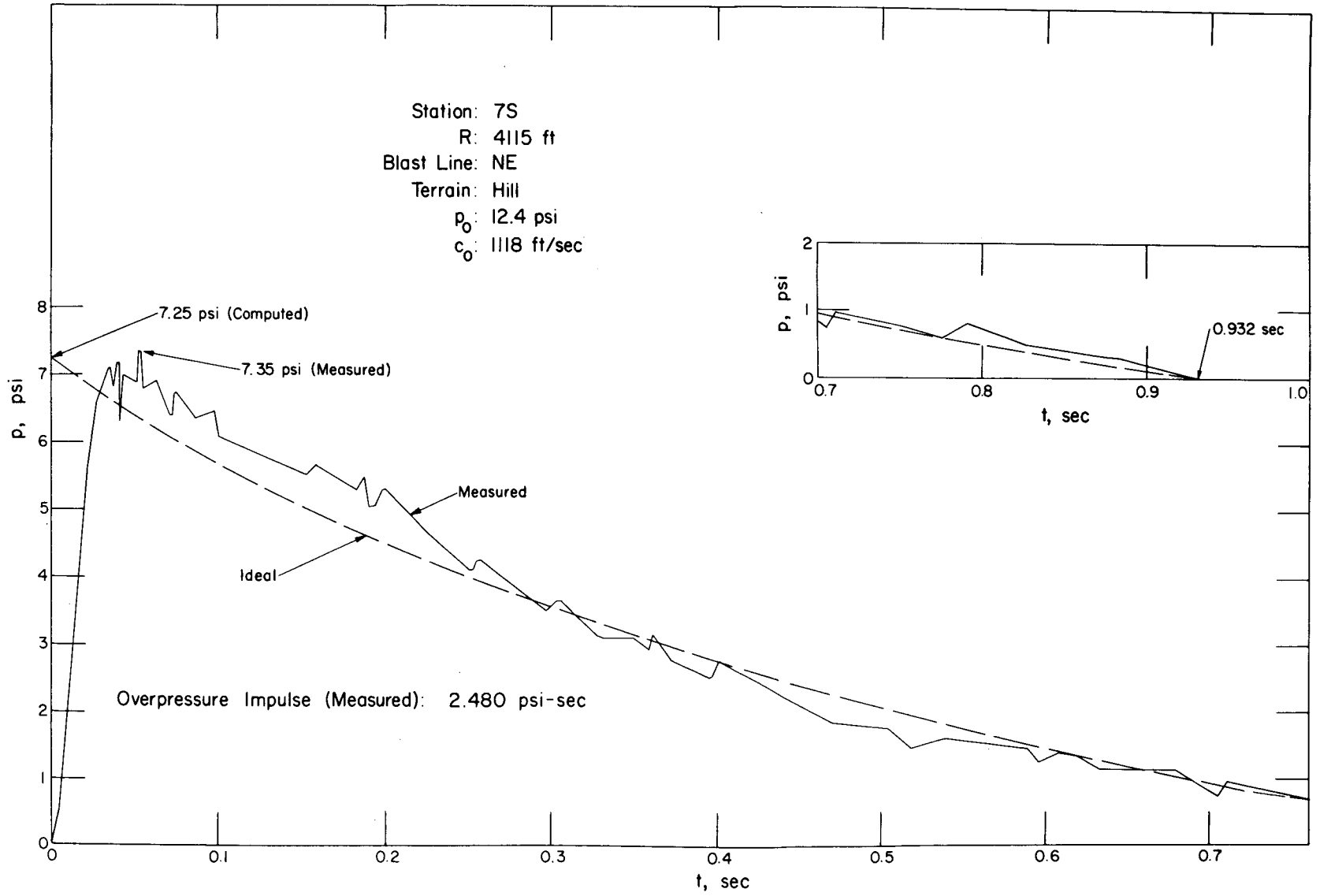


Fig. 5.45—Overpressure vs. time at station 7S.

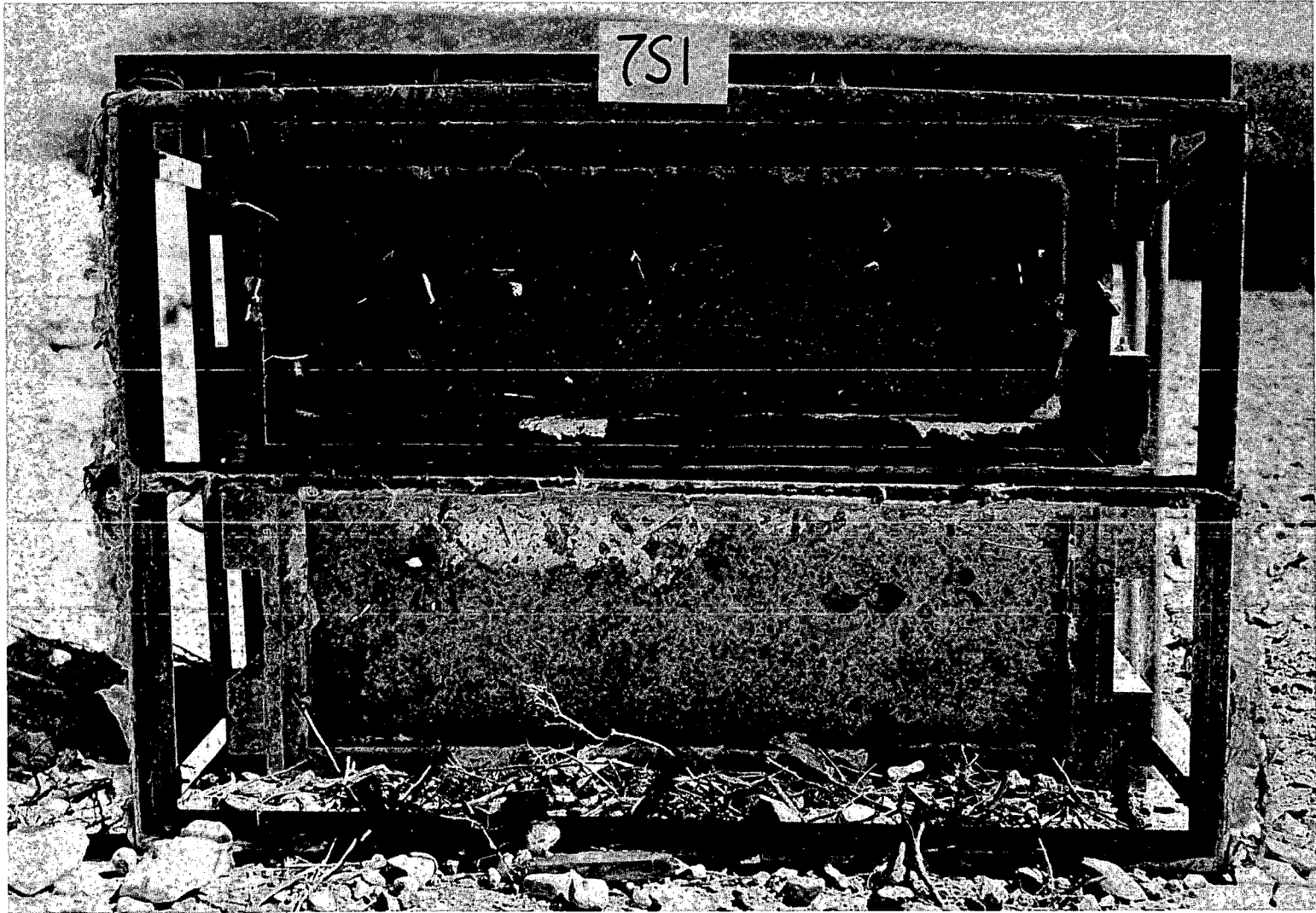


Fig. 5.46—Traps 7S1a and b, postshot, showing thermal-shield frame still in place.



Fig. 5.47—Trap 7S2, postshot. A piece of the thermal-shield support can be seen on the right side of the trap.

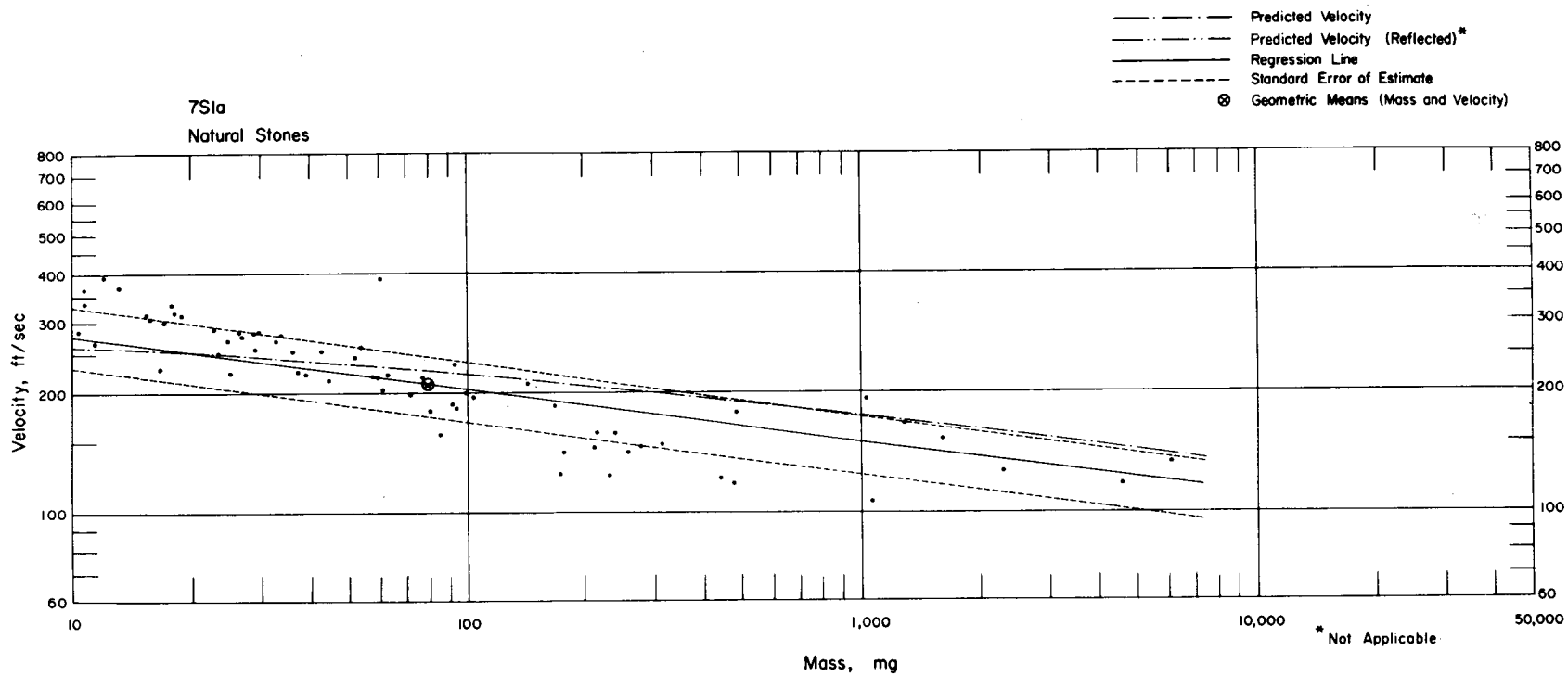


Fig. 5.48—Analysis of natural-stone missiles from trap 7S1a: $n = 66$; $\log v = 2.5684 - 0.1335 \log m$; $E_{gv} = 1.19$; $M_{50} = 79.4$ mg; $V_{50} = 206$ ft/sec.

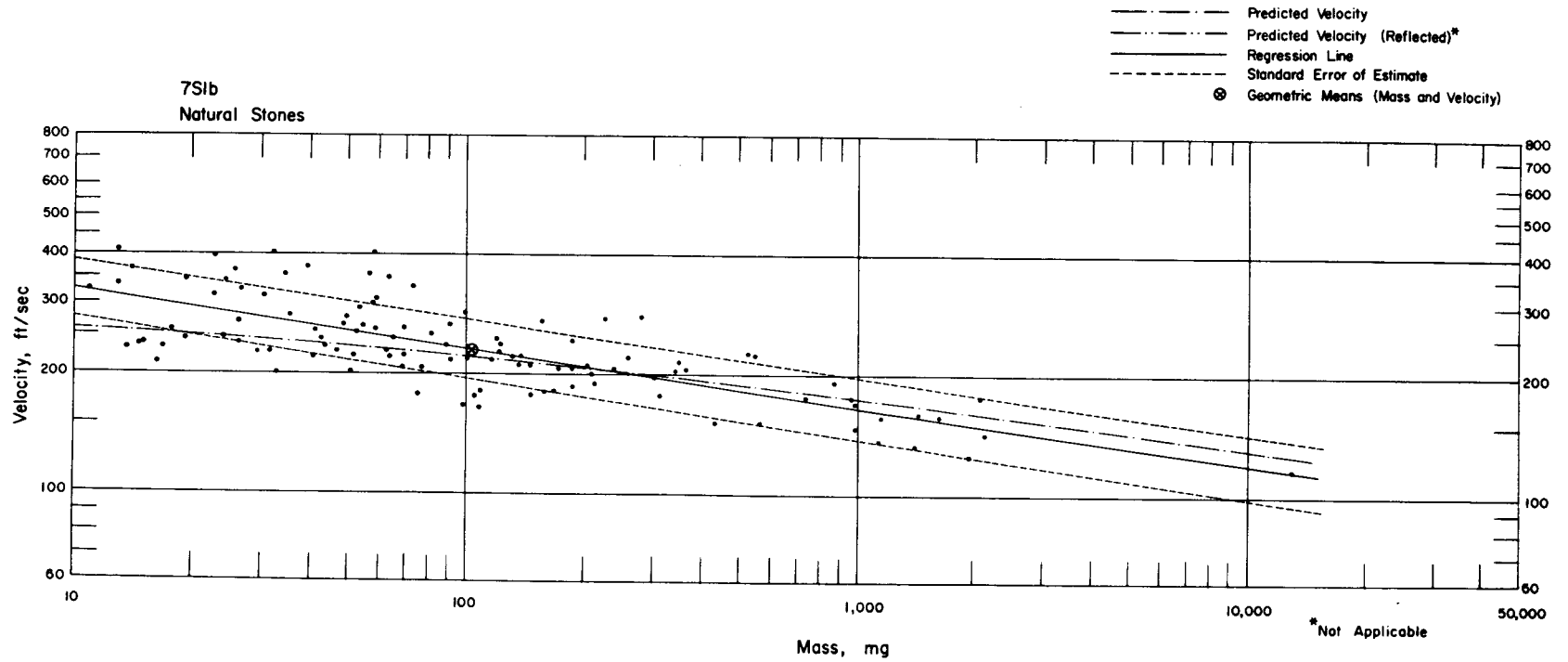


Fig. 5.49—Analysis of natural-stone missiles from trap 7S1b: $n = 111$; $\log v = 2.6620 - 0.1465 \log m$; $E_{gv} = 1.20$; $M_{50} = 104$ mg; $V_{50} = 233$ ft/sec.

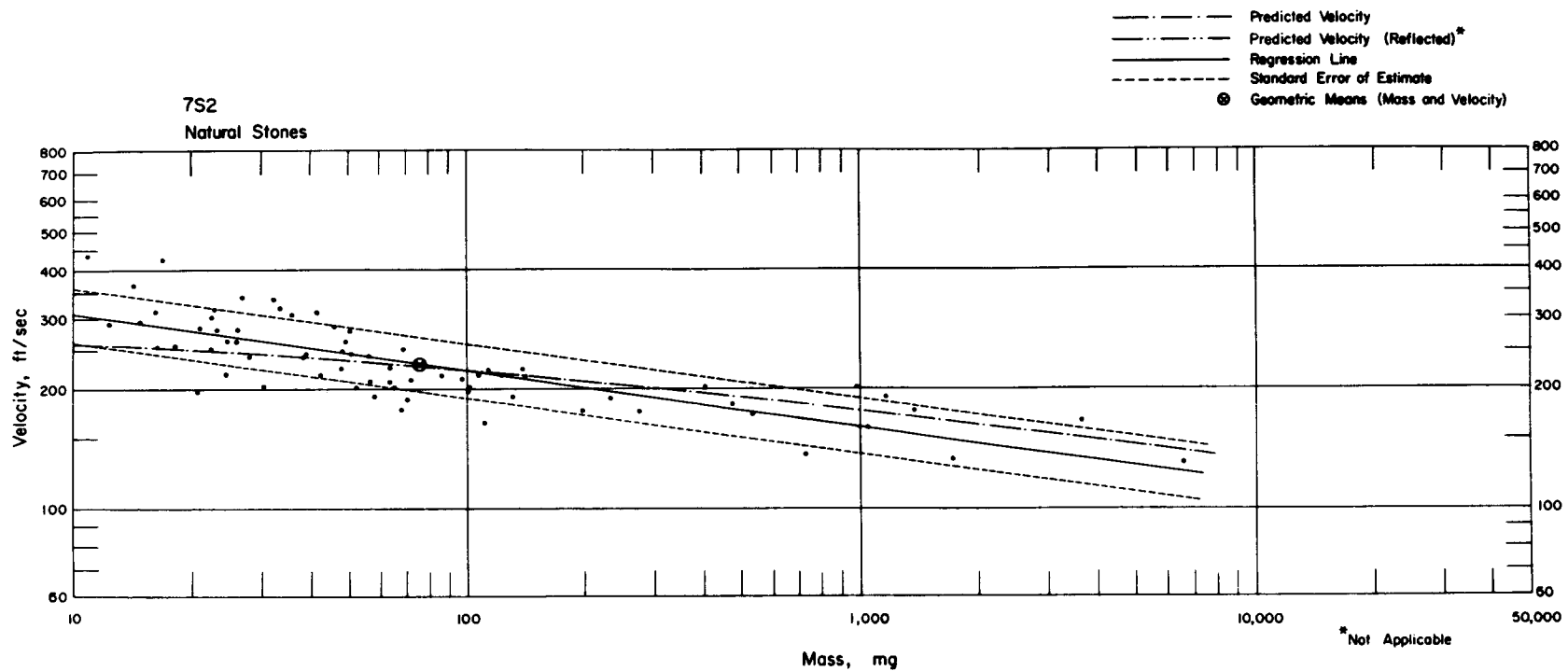


Fig. 5.50—Analysis of natural-stone missiles from trap 7S2: $n = 70$; $\log v = 2.6253 - 0.1394 \log m$; $E_{gv} = 1.17$; $M_{50} = 76.3$ mg; $V_{50} = 231$ ft/sec.

STATION: 8S
RANGE: 4980'

TERRAIN: DALE
BLAST LINE: NE

MD Military Debris, On Ground
St Steel Spheres, 14" Above Ground

Roman numeral in parenthesis designates type of missile absorber

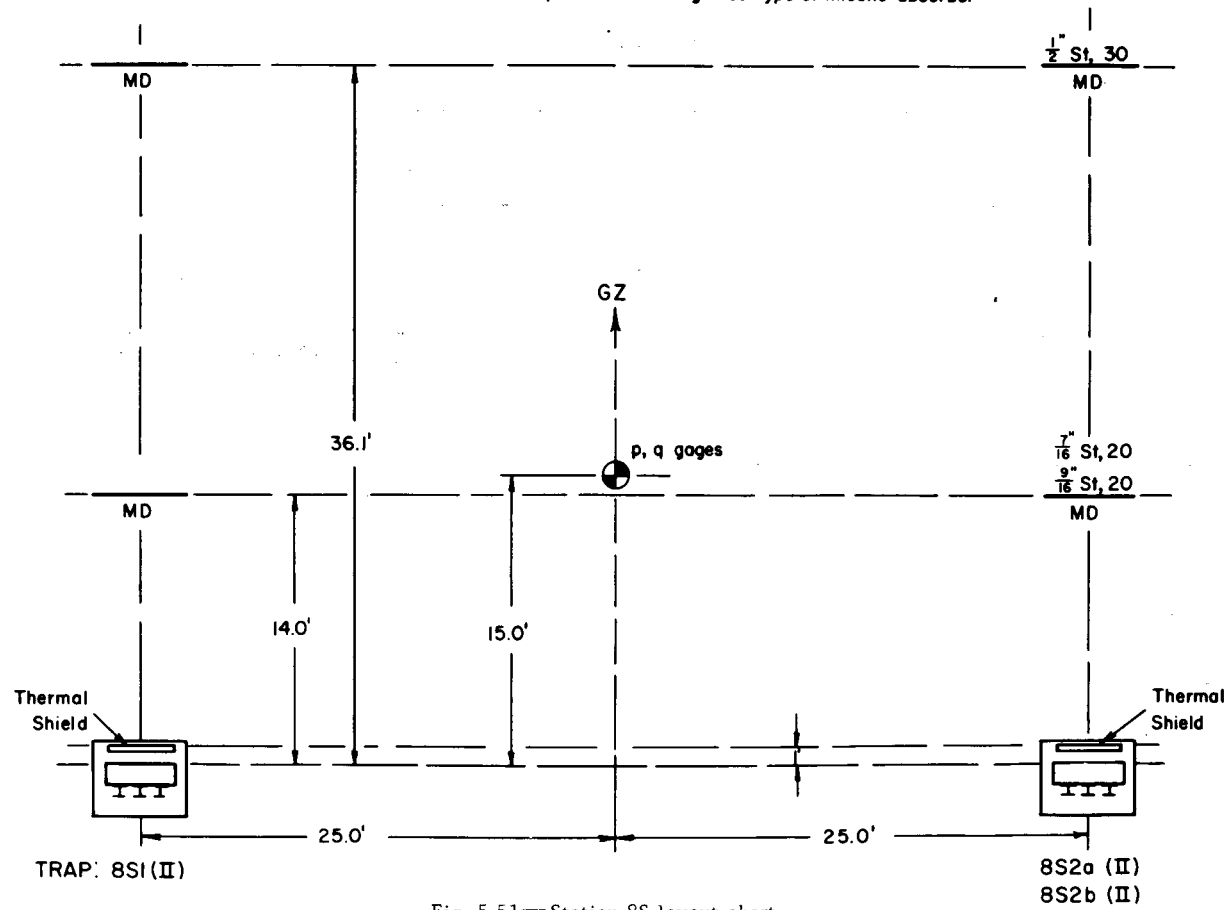


Fig. 5.51—Station 8S layout chart.

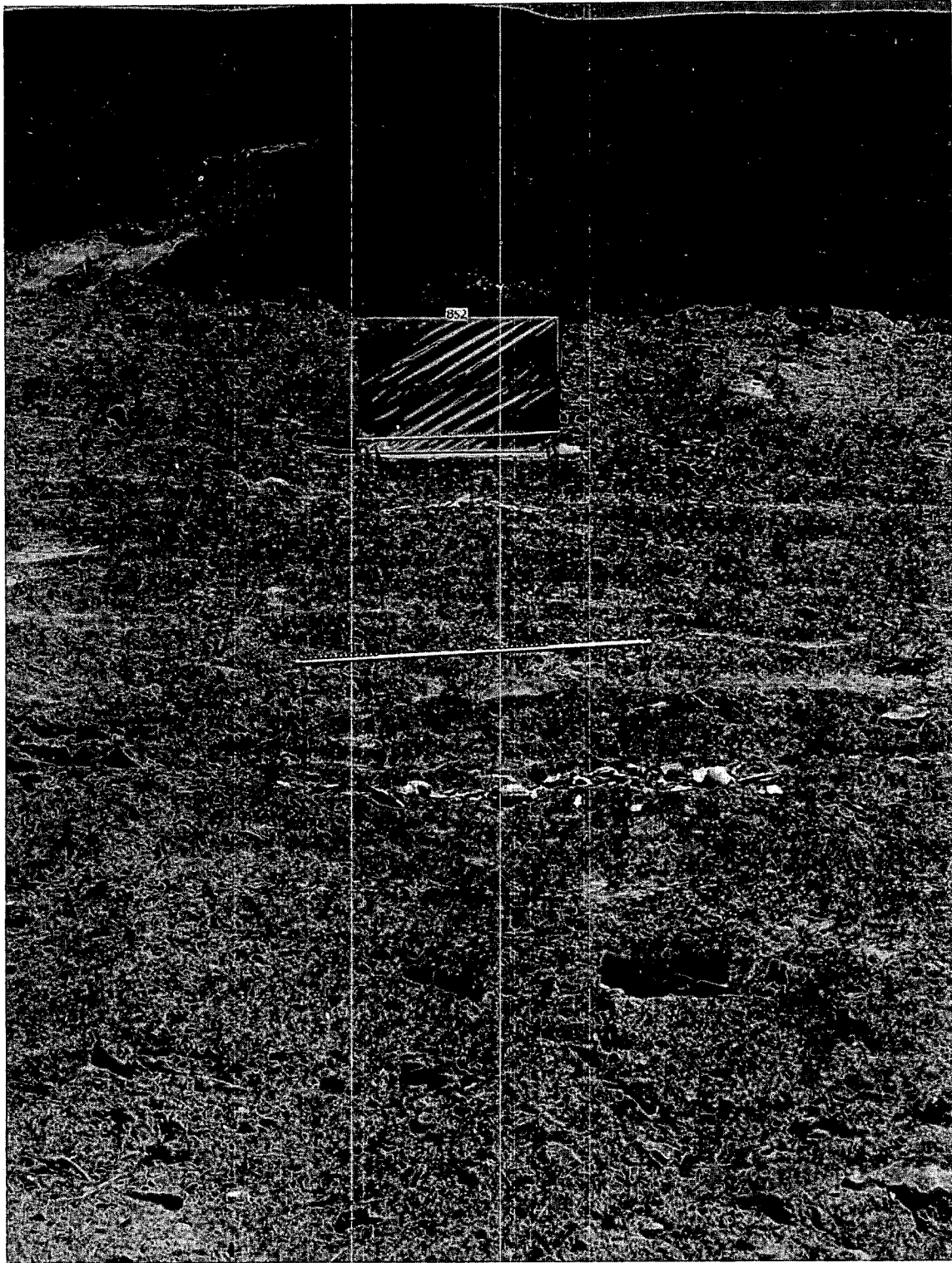


Fig. 5.52—Installation 8S2 at station 8S, 4980-ft range on the northeast blast line.

306

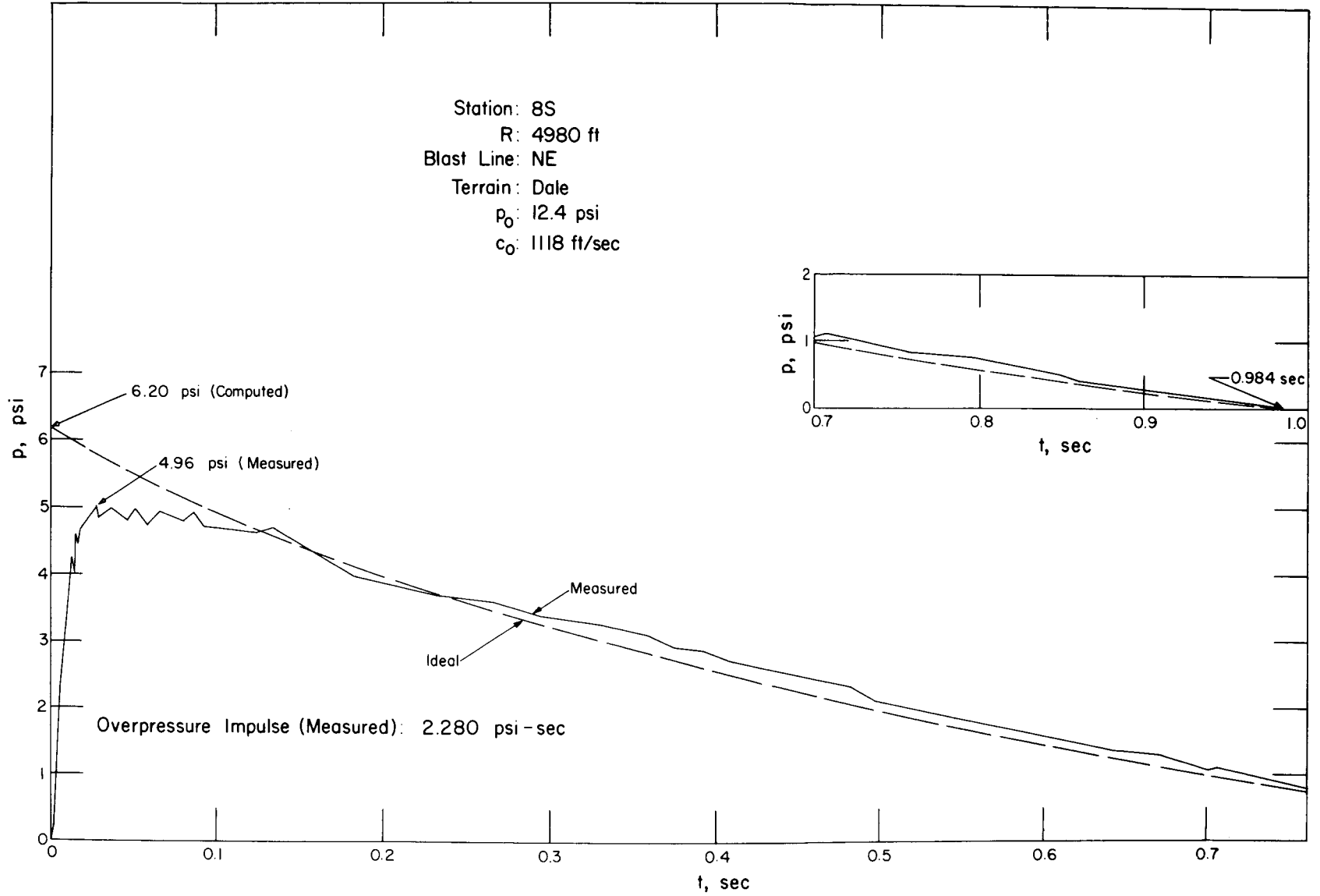


Fig. 5.53—Overpressure vs. time at station 8S.

307

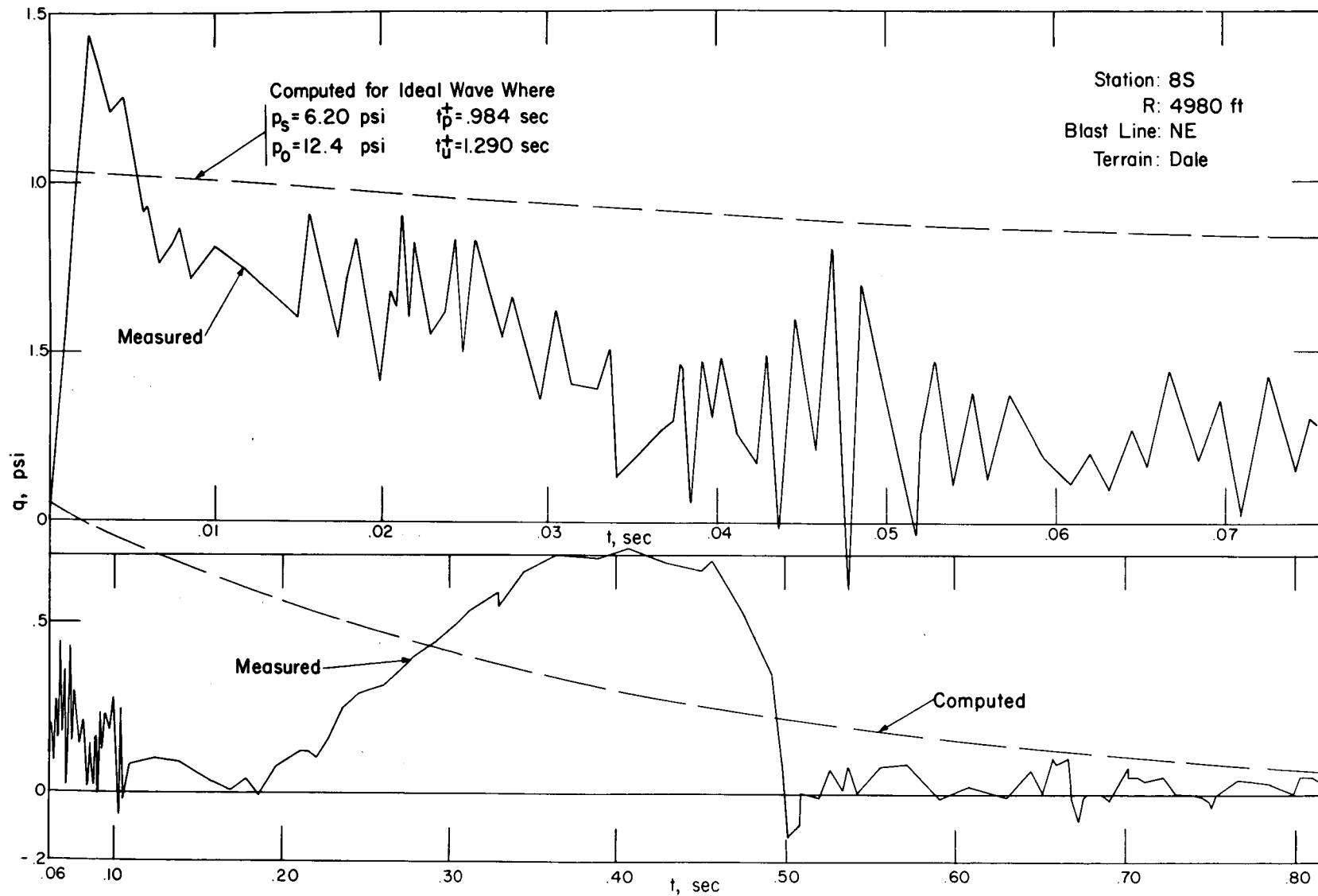


Fig. 5.54—Dynamic pressure vs. time at station 8S.

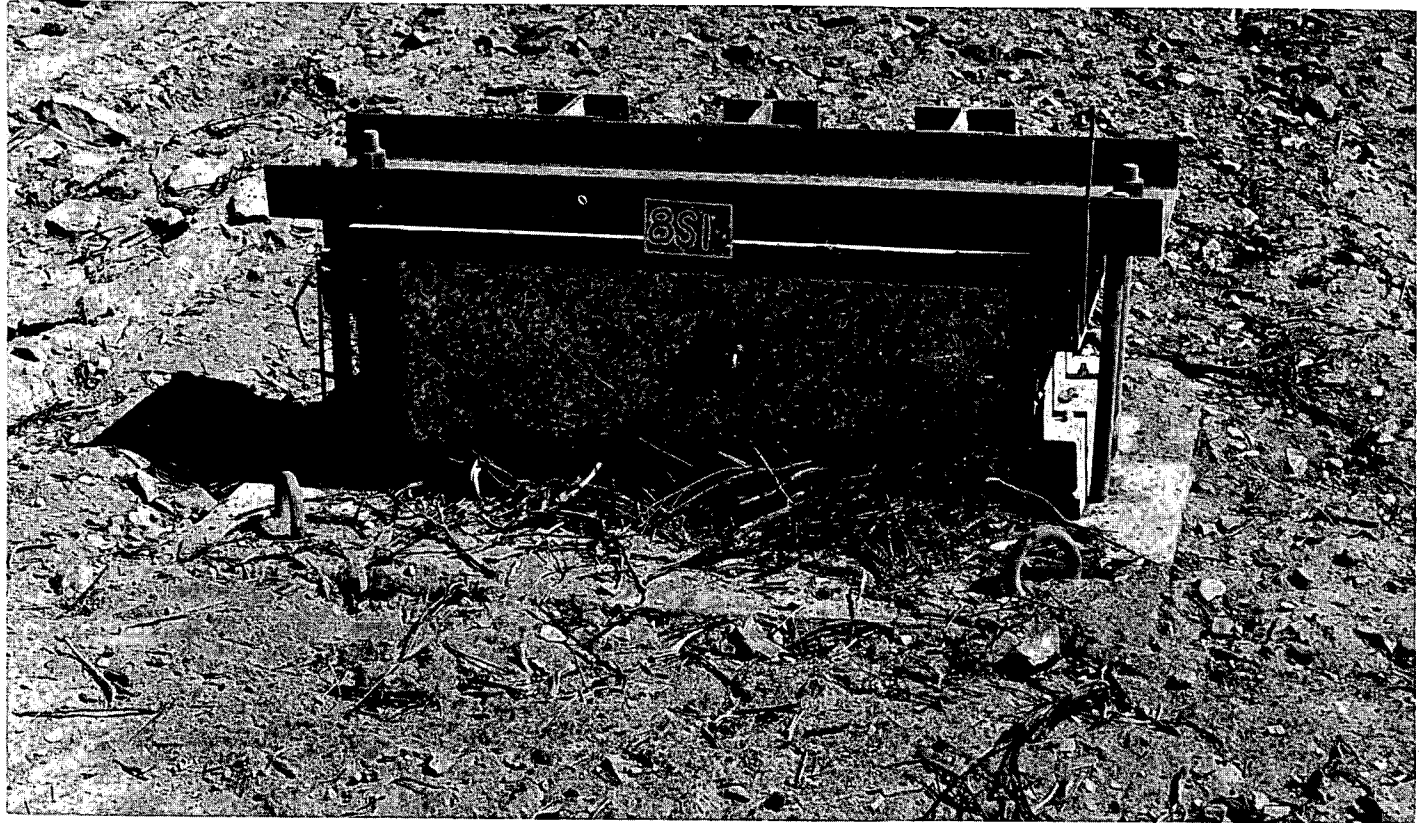


Fig. 5.55—Installation 8S1, postshot.

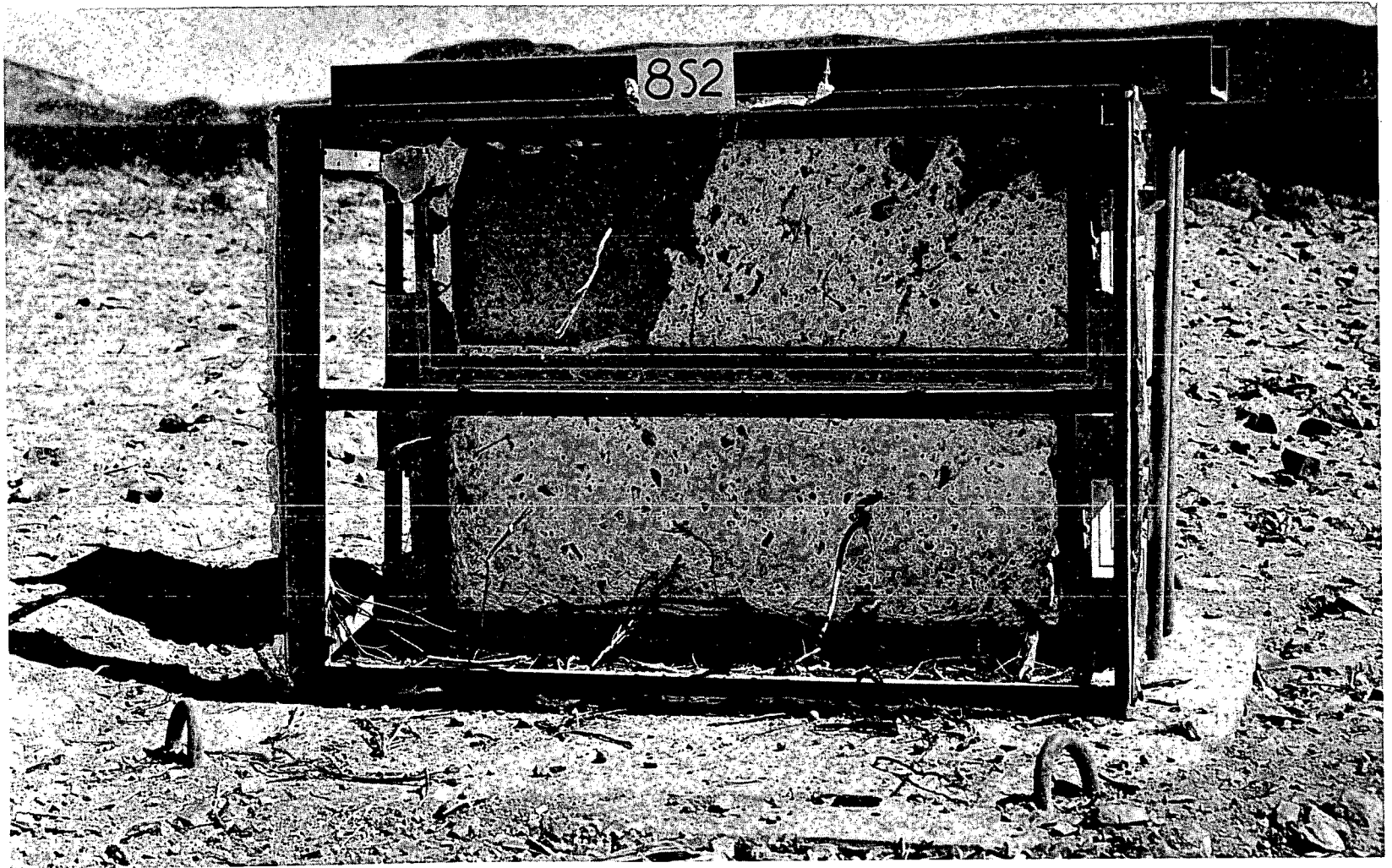


Fig. 5.56—Traps 8S2a and b, postshot.

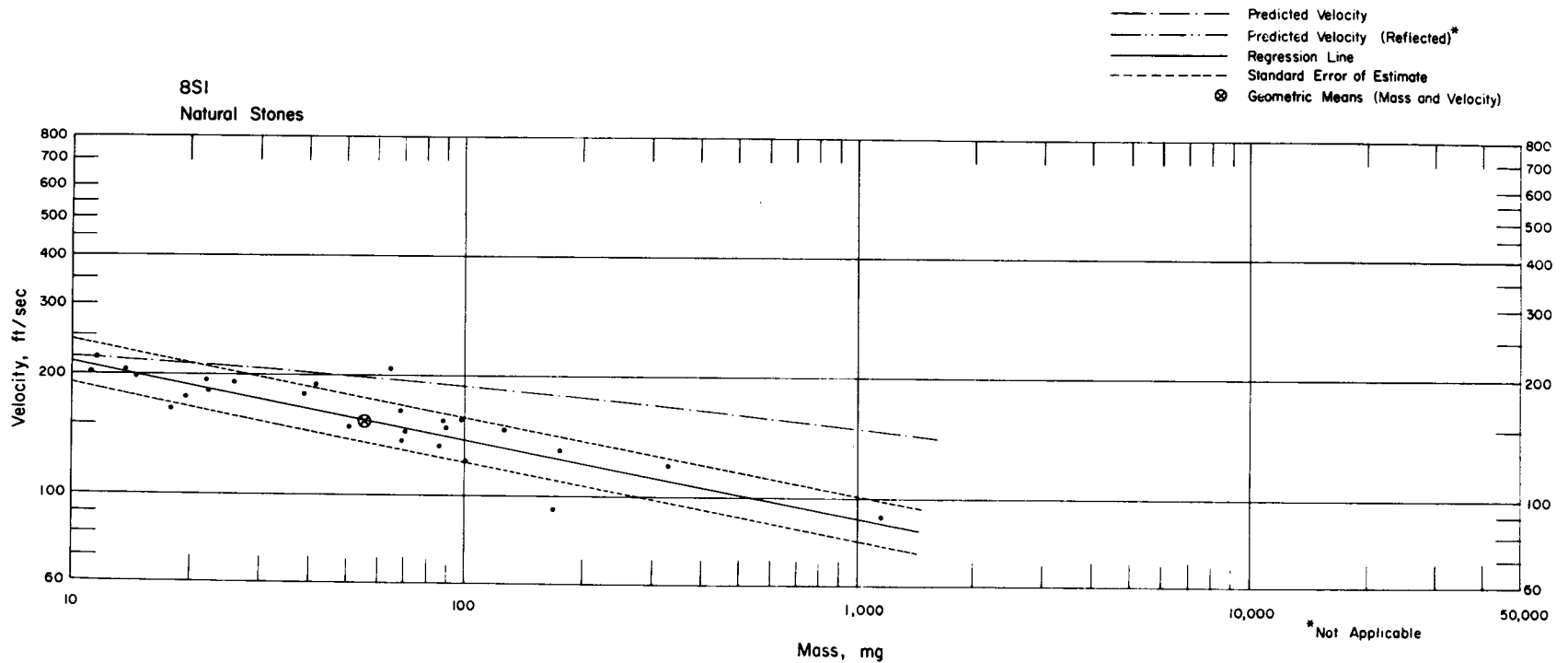


Fig. 5.57—Analysis of natural-stone missiles from installation 8S1: $n = 26$; $\log v = 2.5214 - 0.1906 \log m$; $E_{gv} = 1.15$; $M_{50} = 55.2$ mg; $V_{50} = 155$ ft/sec.

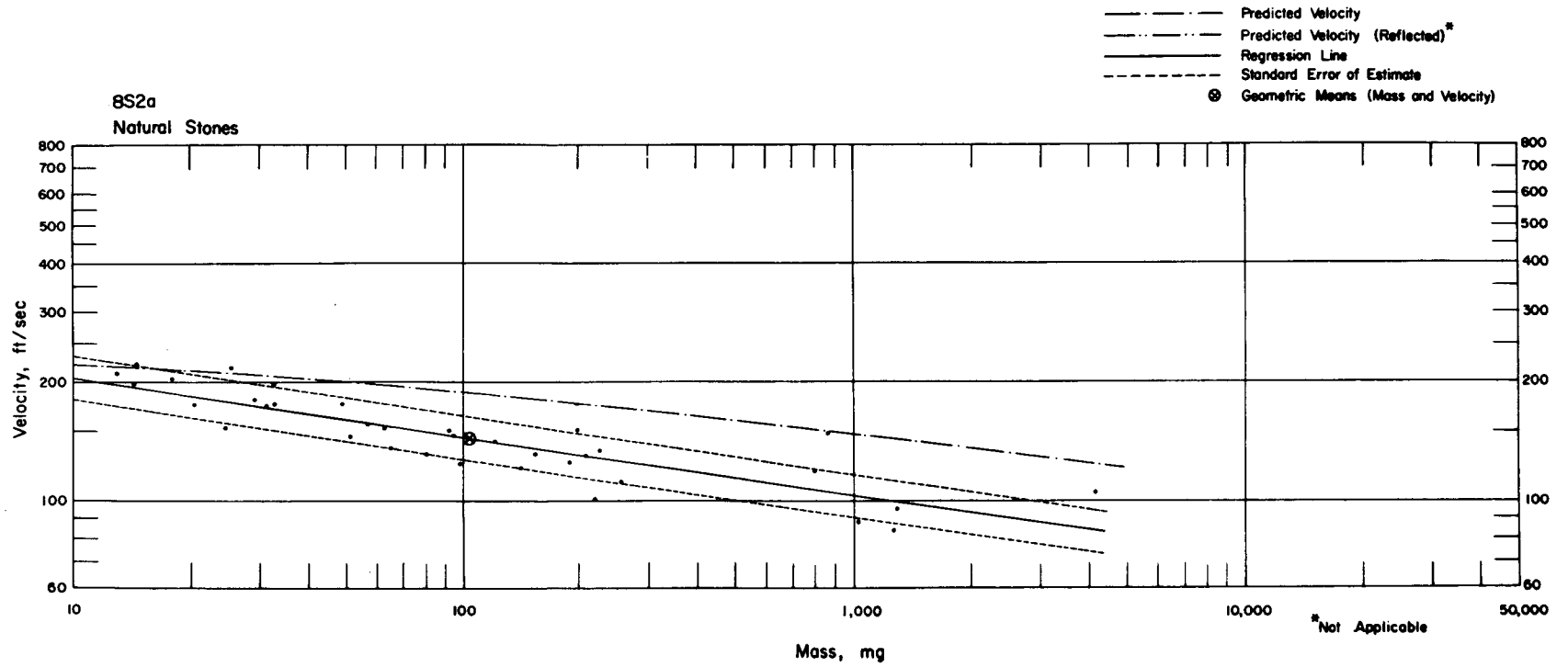


Fig. 5.58—Analysis of natural-stone missiles from trap 8S2a: $n = 35$; $\log v = 2.4599 - 0.1496 \log m$; $E_{gv} = 1.14$; $M_{50} = 103 \text{ mg}$; $V_{50} = 144 \text{ ft/sec}$.

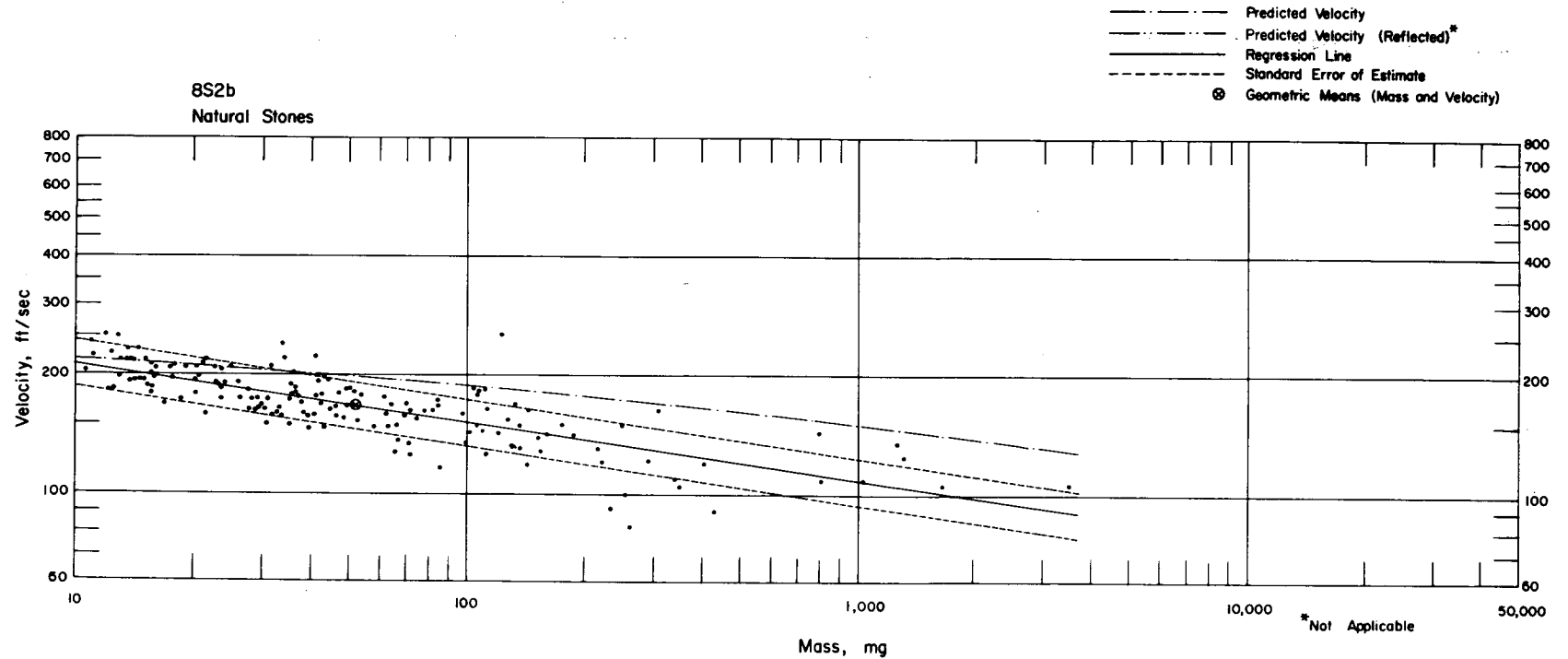


Fig. 5.59—Analysis of natural-stone missiles from trap 8S2b: $n = 162$; $\log v = 2.4804 - 0.1491 \log m$; $E_{gv} = 1.14$; $M_{50} = 51.1$ mg; $V_{50} = 168$ ft/sec.

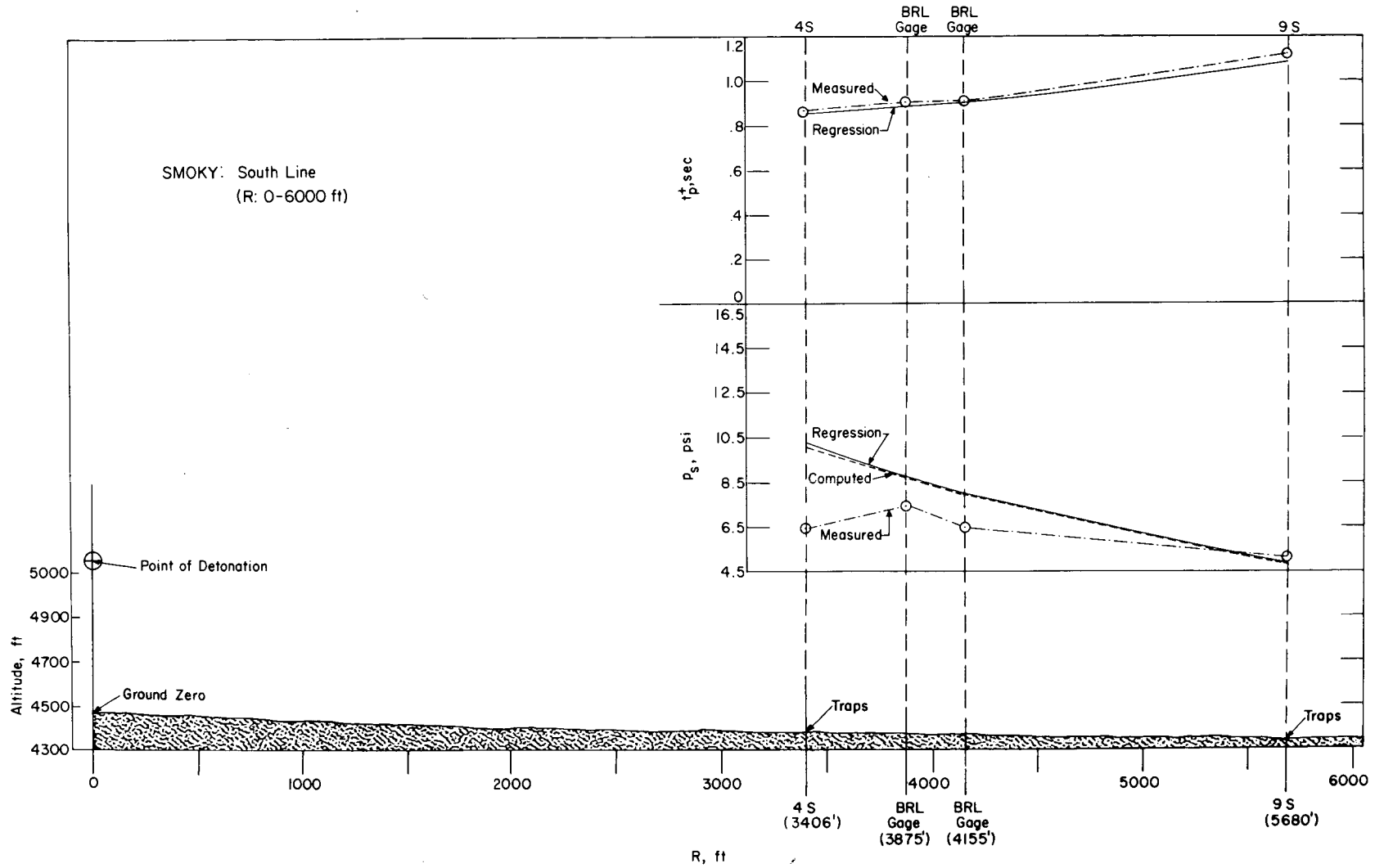


Fig. 5.60—Profile of south blast line, shot Smoky, 0- to 6000-ft range. See Table 5.1 for explanation of blast parameters plotted.

STATION: 4S TERRAIN: FLAT
 RANGE: 3406' BLAST LINE: S

MD Military Debris, On Ground
 S1 Steel Spheres, 9" Above Ground

Roman numeral in parenthesis designates type of missile absorber

314

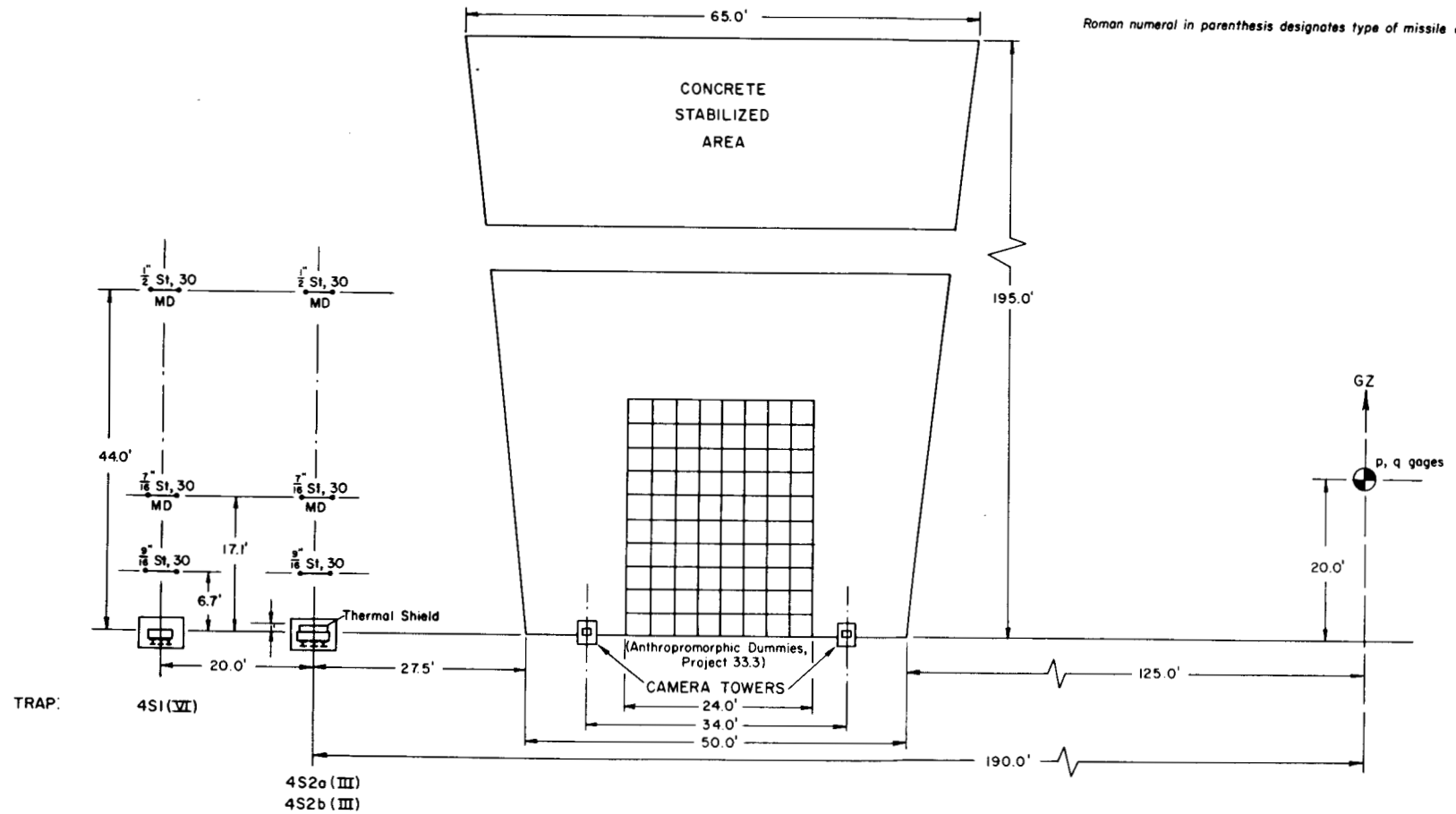


Fig. 5.61—Station 4S layout chart. The concrete stabilized area was used by another project. (See Ref. 2.)

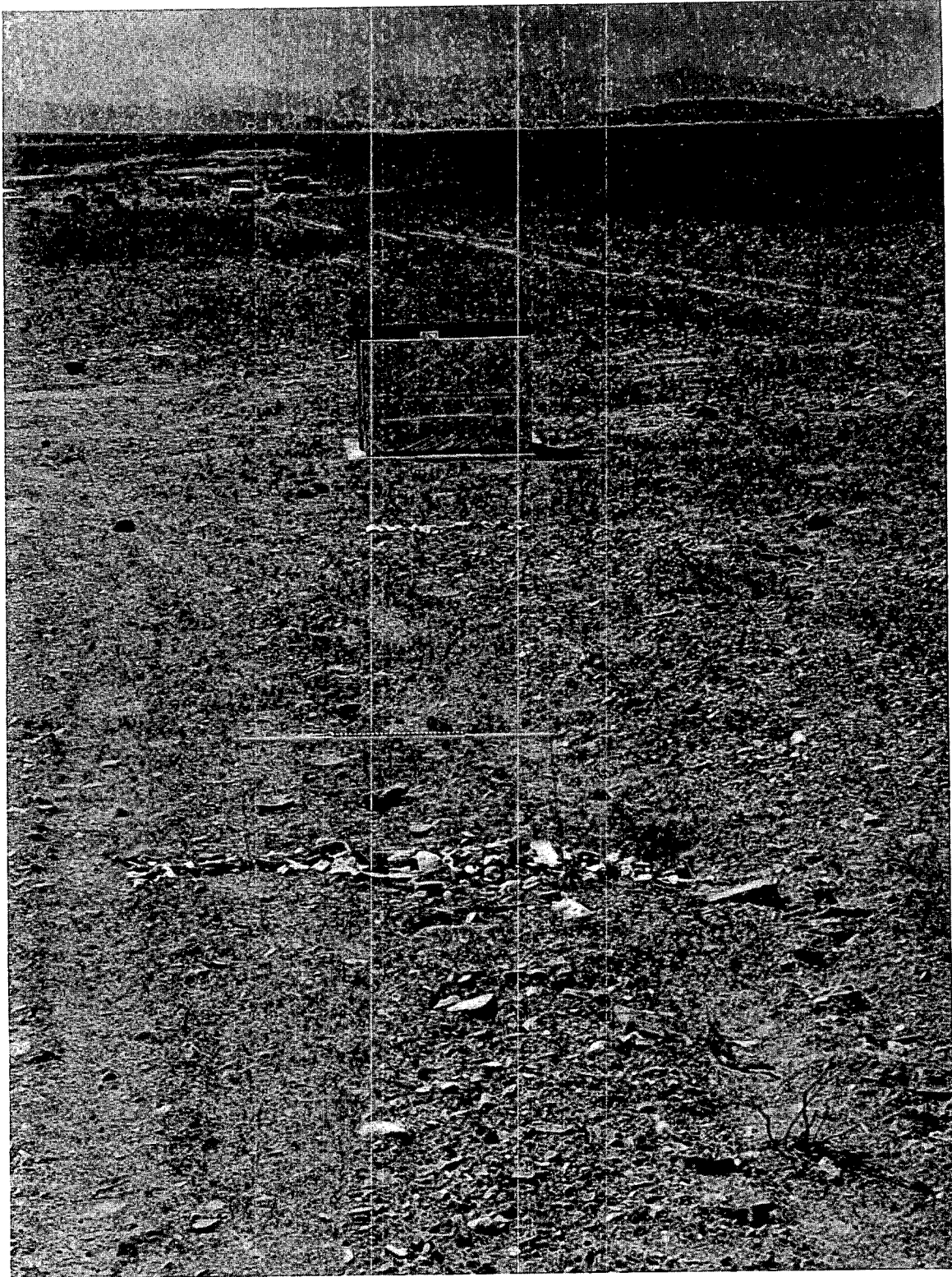


Fig. 5.62—Installation 4S2, preshot, at 3406-ft range on the south blast line.

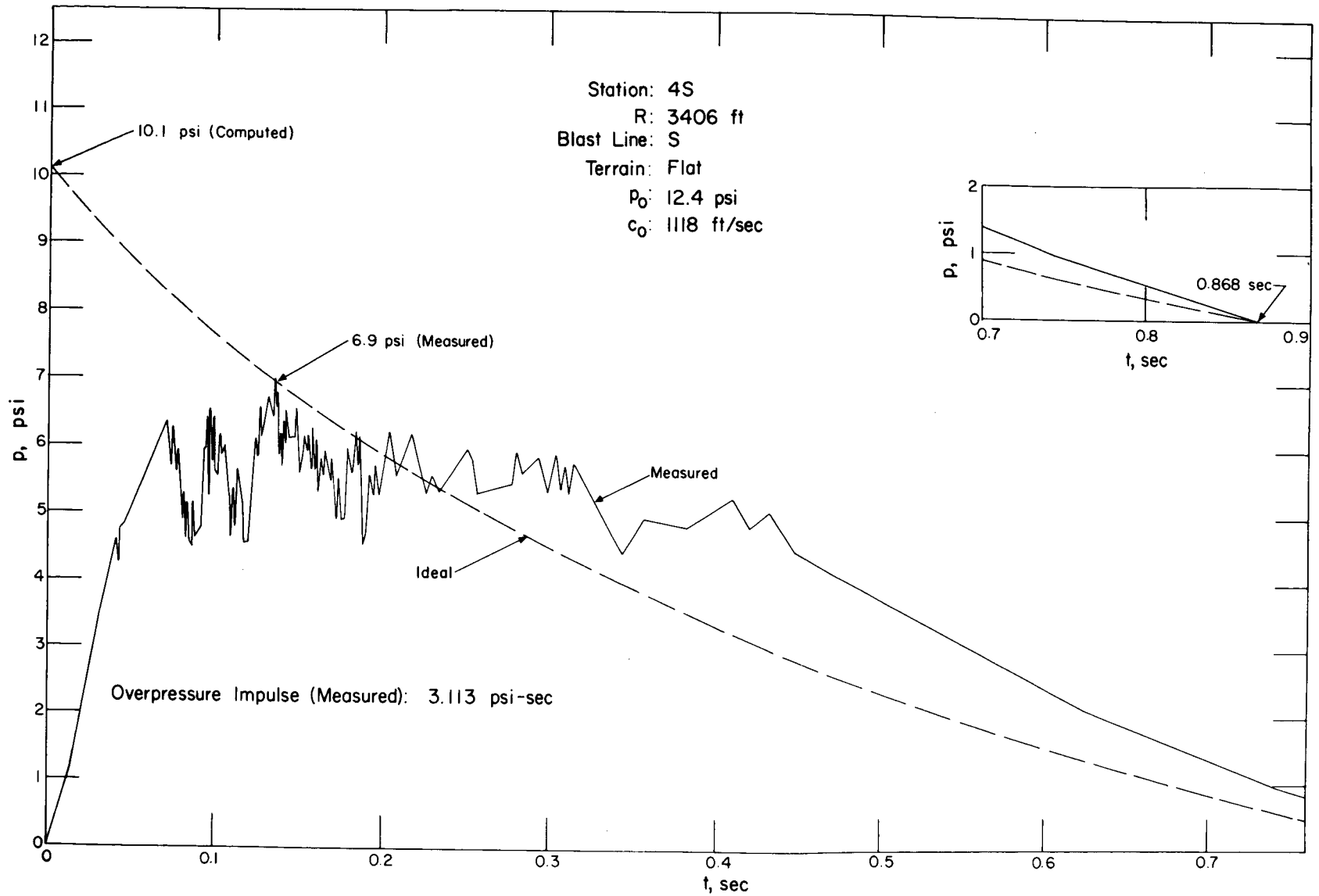


Fig. 5.63—Overpressure vs. time at station 4S.

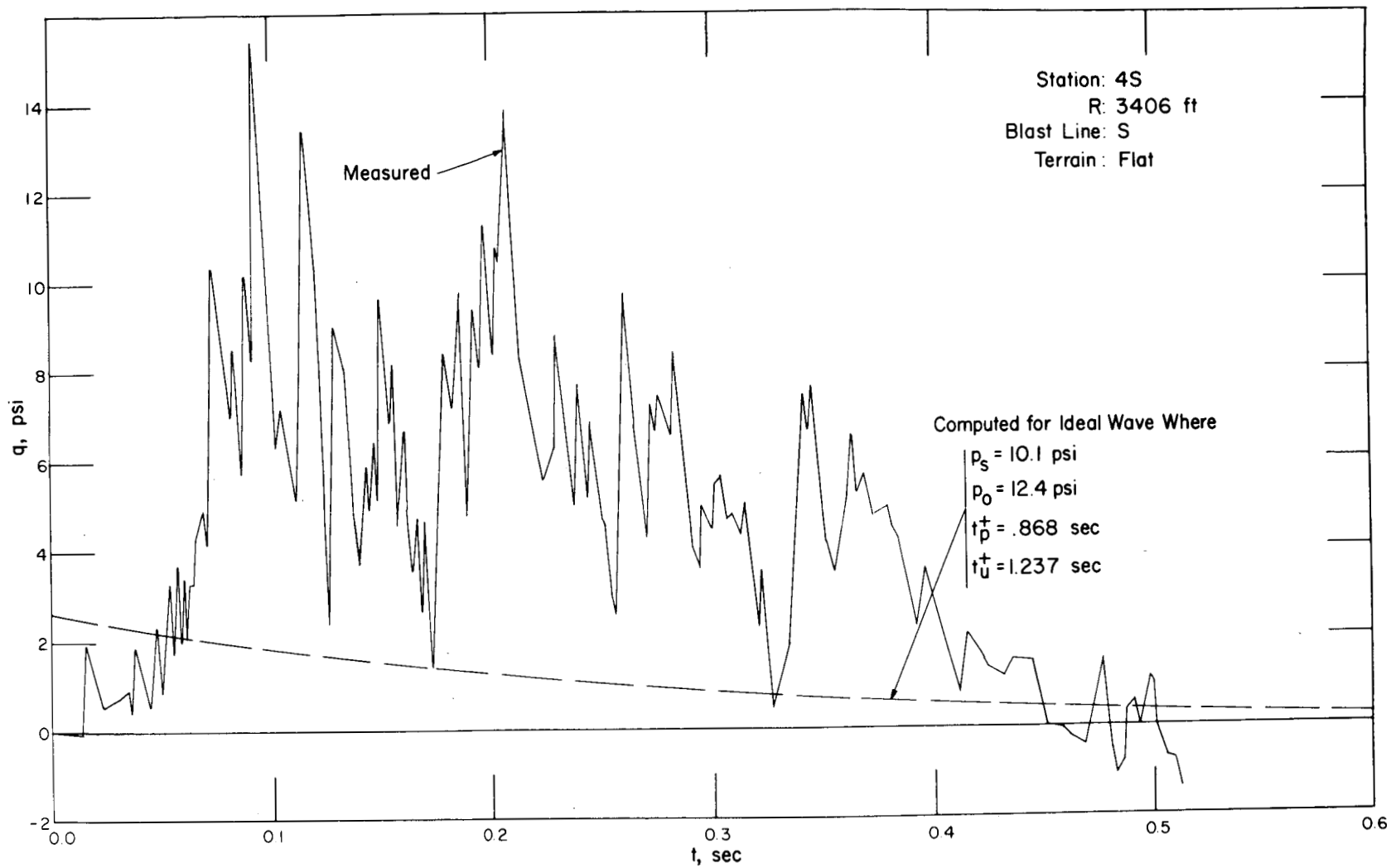


Fig. 5.64—Dynamic pressure vs. time at station 4S.

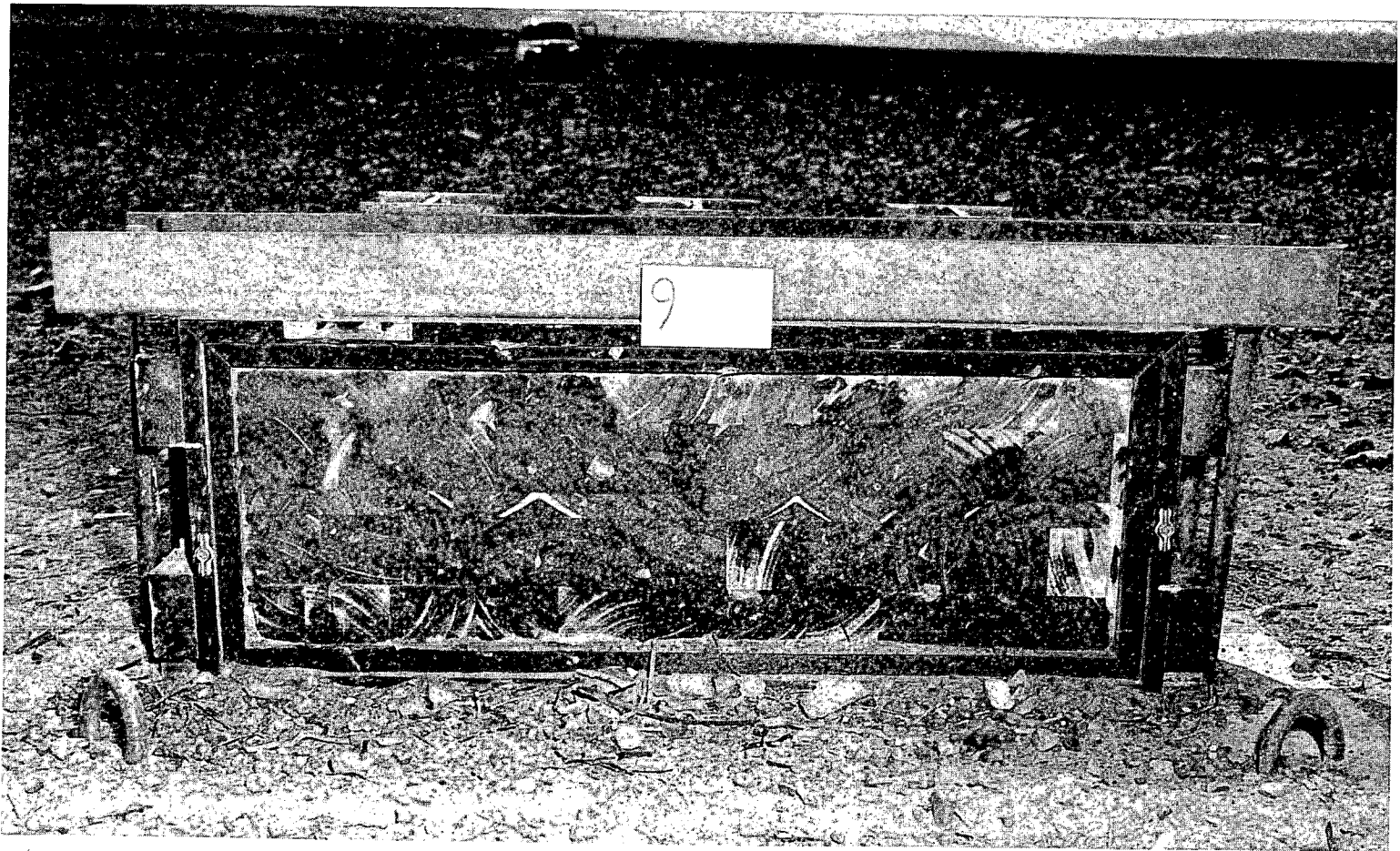


Fig. 5.65—Installation 4S1, postshot. Note effect of thermal scorching on balsa absorber placed end-grain in the trap.

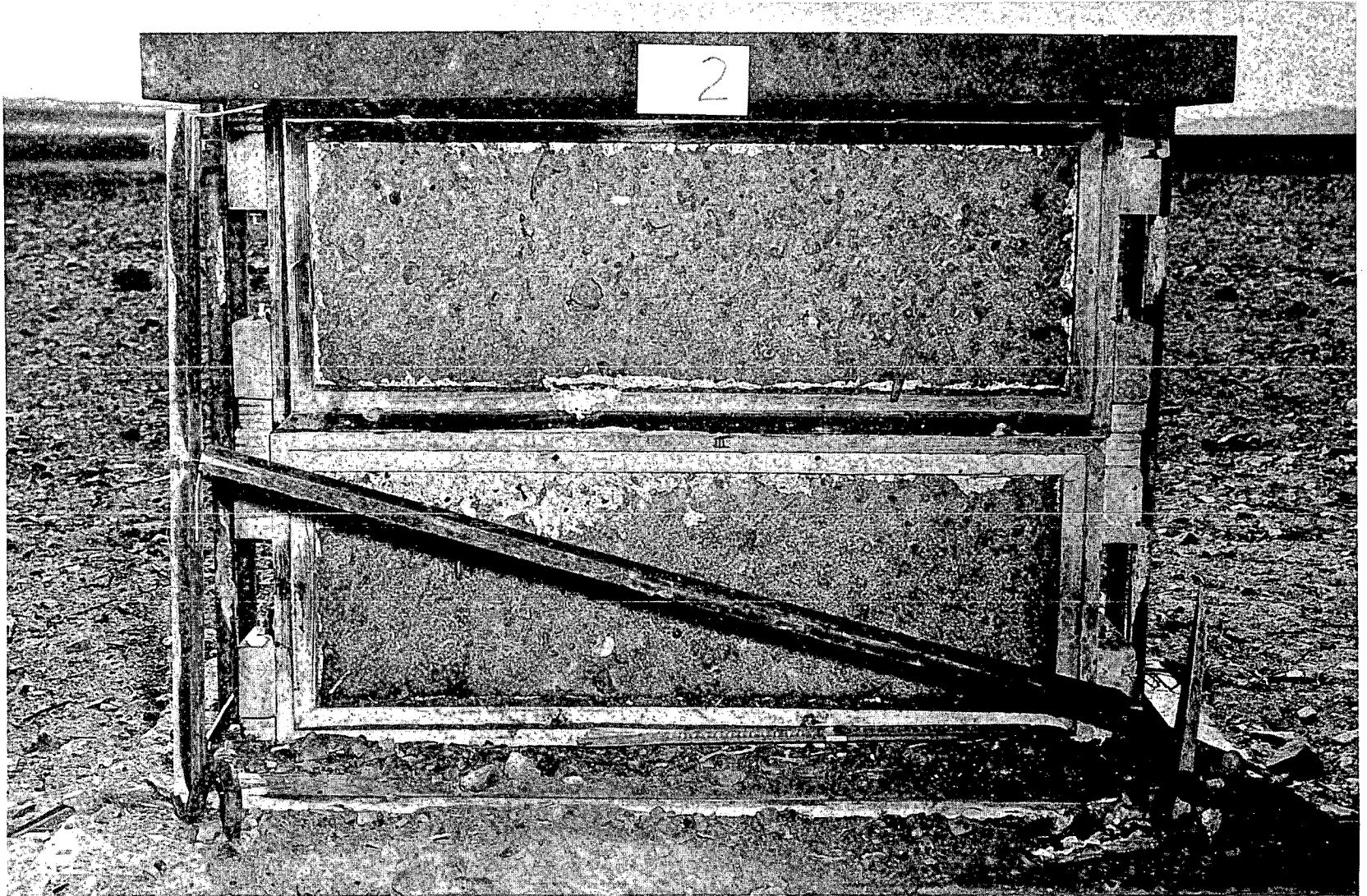


Fig. 5.66—Postshot view of traps 4S2a and b. The thermal-shield frame was partially destroyed. Five large steel spheres were caught in these traps.

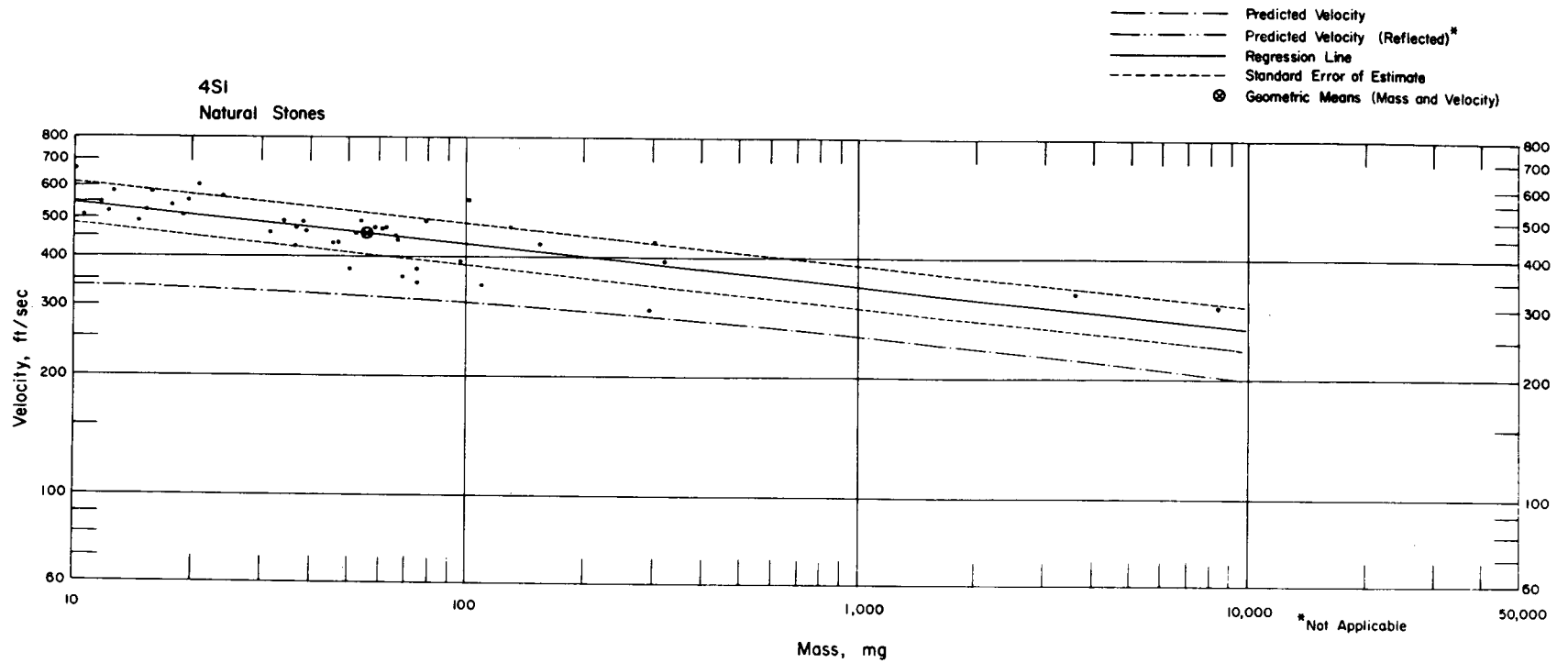


Fig. 5.67—Analysis of natural-stone missiles from installation 4S1: $n = 43$; $\log v = 2.8446 - 0.1044 \log m$; $E_{gv} = 1.13$; $M_{50} = 55.2$ mg; $V_{50} = 460$ ft/sec.

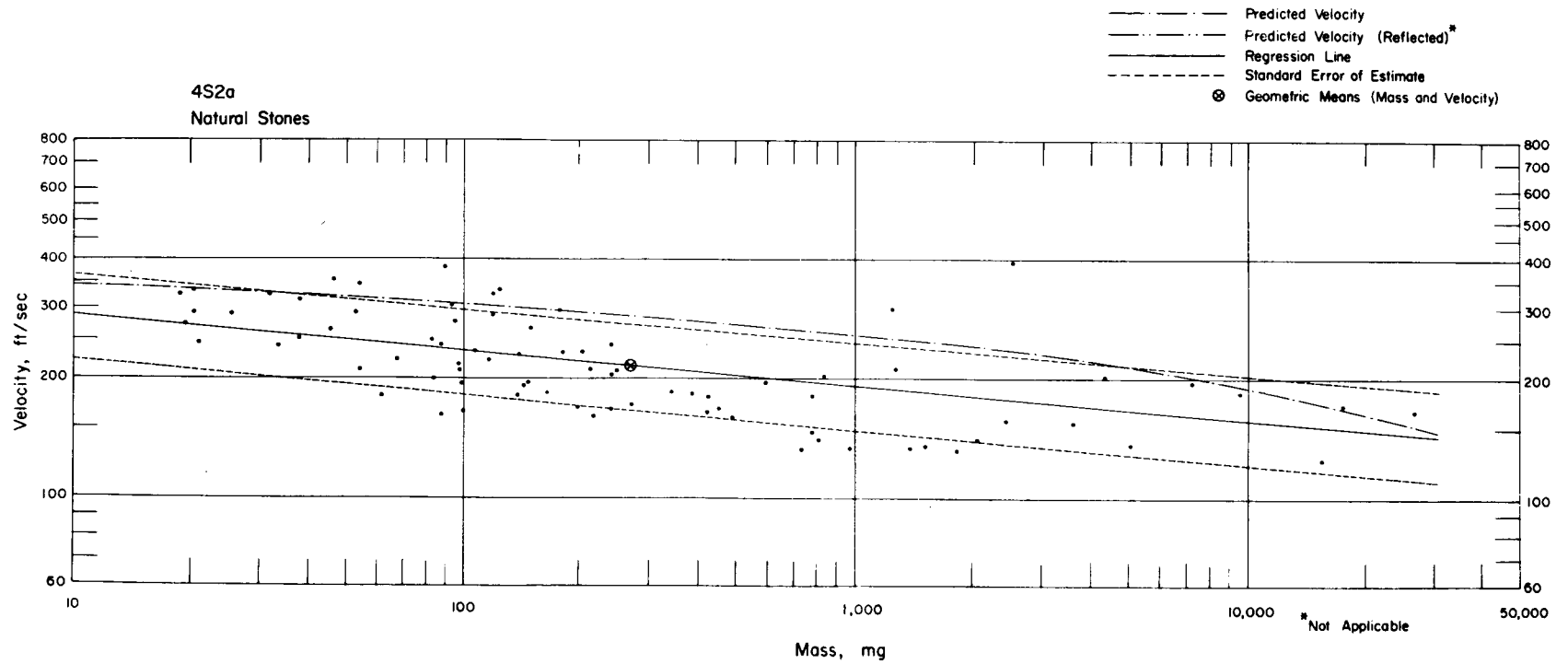


Fig. 5.68—Analysis of natural-stone missiles from trap 4S2a: $n = 81$; $\log v = 2.5473 - 0.0890 \log m$; $E_{gv} = 1.29$; $M_{50} = 272$ mg; $V_{50} = 214$ ft/sec.

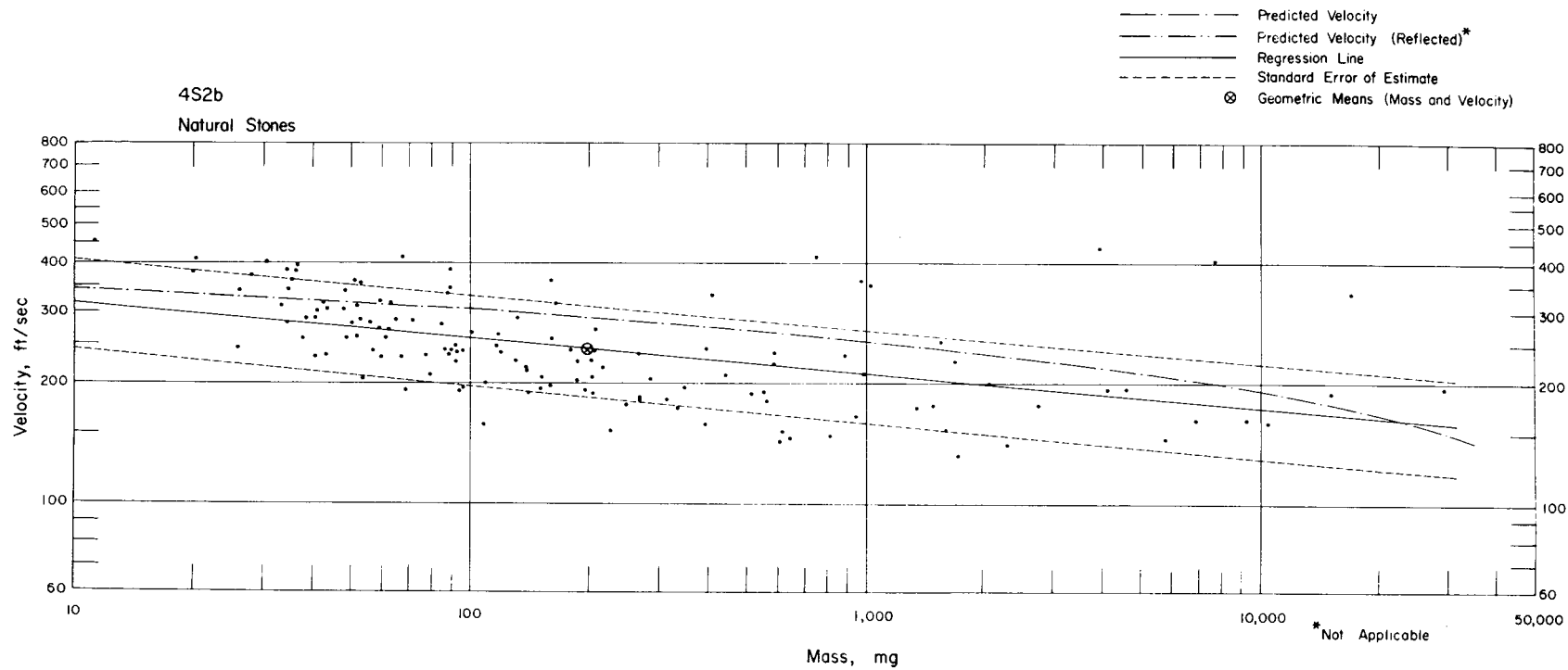


Fig. 5.69—Analysis of natural-stone missiles from trap 4S2b: $n = 135$; $\log v = 2.5831 - 0.0868 \log m$; $E_{gv} = 1.29$; $M_{50} = 197$ mg; $V_{50} = 242$ ft/sec.

STATION: 9S
RANGE: 5680'

TERRAIN: FLAT
BLAST LINE: S

MD Military Debris, On Ground
St Steel Spheres, 9" Above Ground

Roman numeral in parenthesis designates type of missile absorber

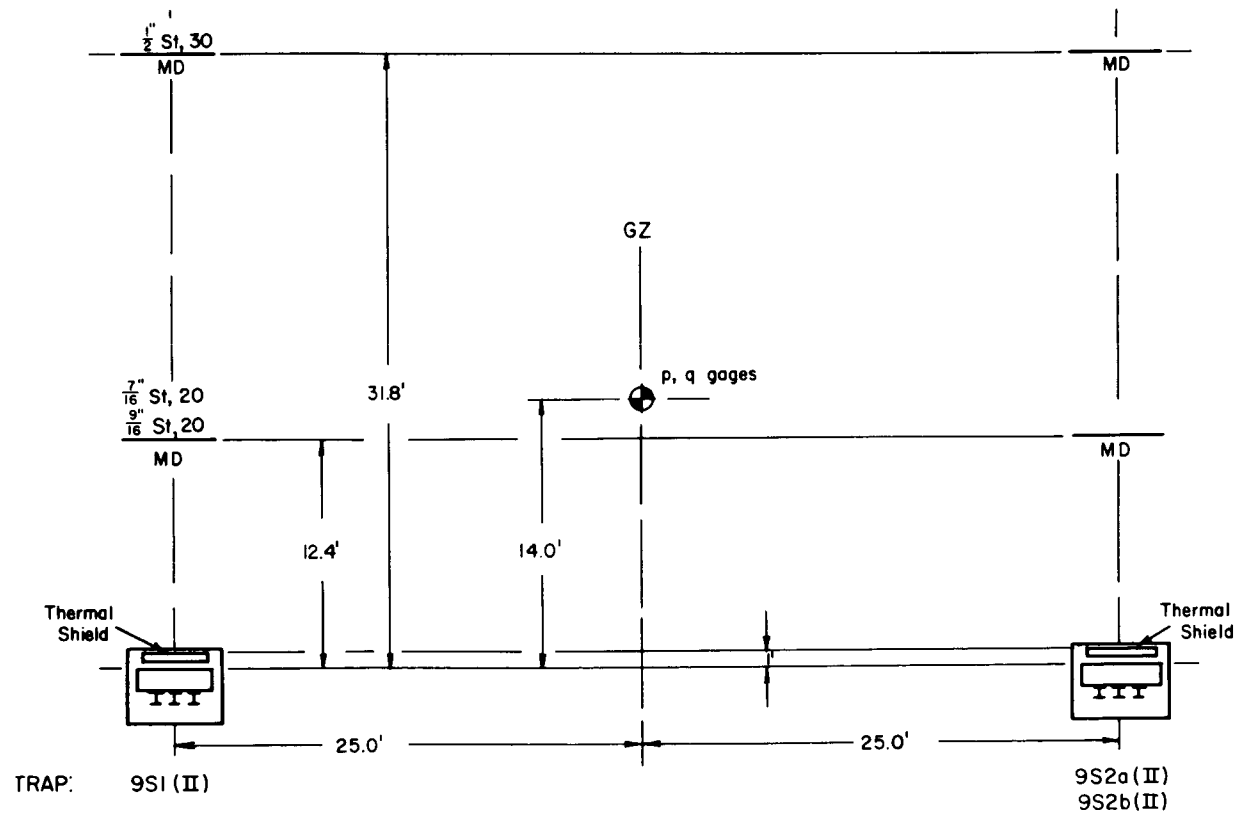


Fig. 5.70—Station 9S layout chart.

323



Fig. 5.71—Traps 9S2a and b, preshot, at 5680-ft range on the south blast line. Note military debris and large steel spheres in the foreground.

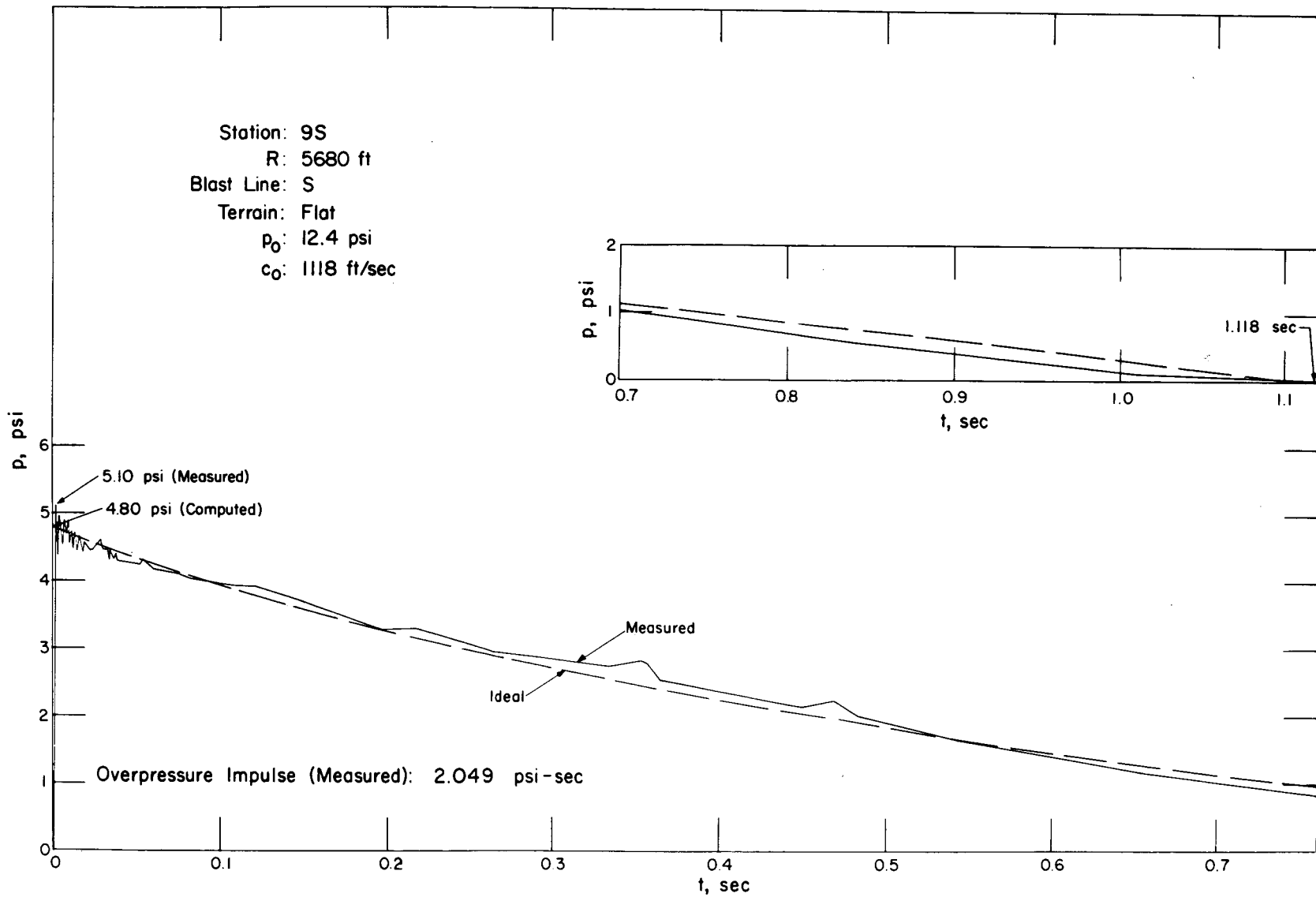


Fig. 5.72—Overpressure vs. time at station 9S.

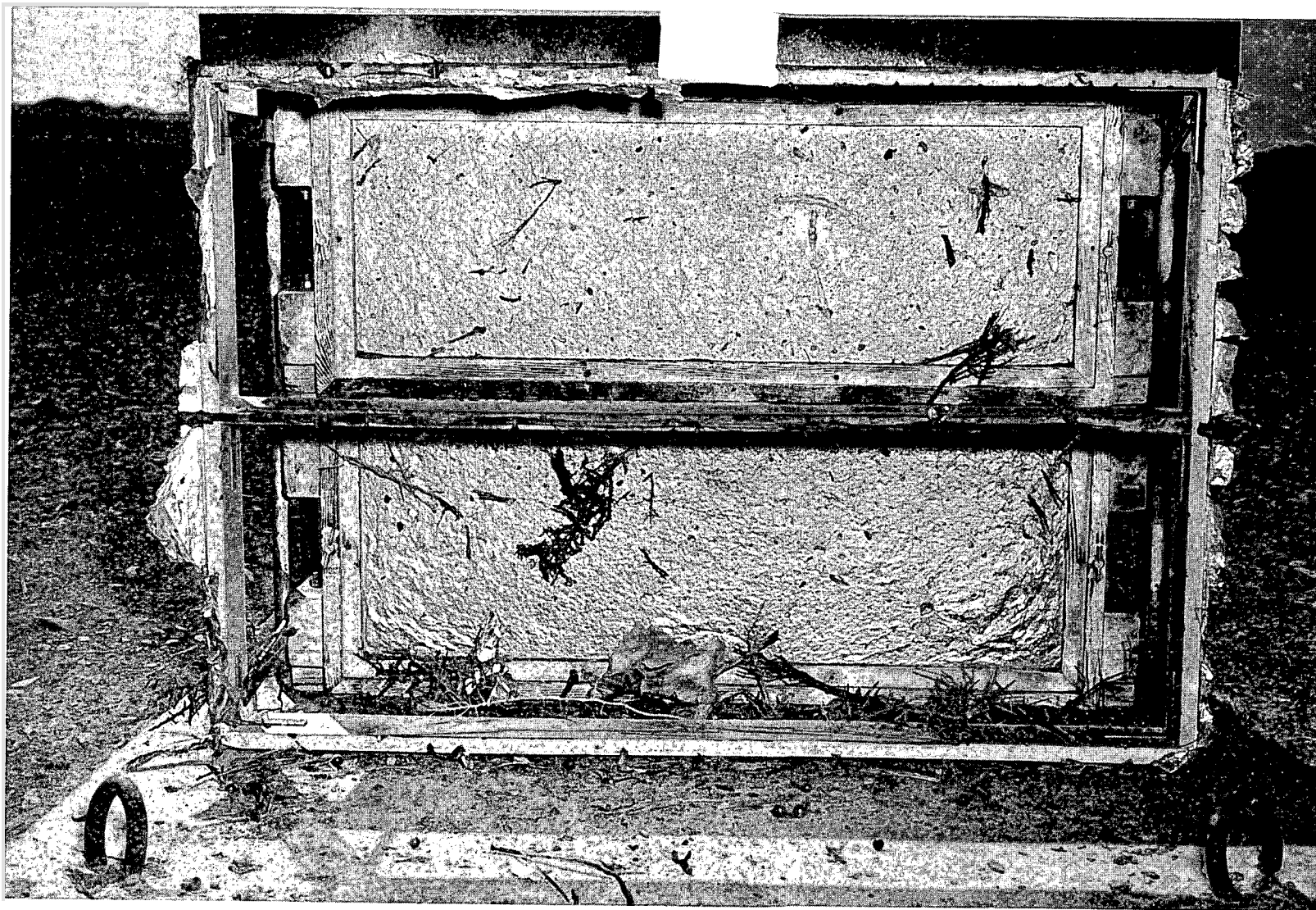


Fig. 5.73—Traps 9S2a and b, postshot. Note steel spheres on concrete base in front of traps.

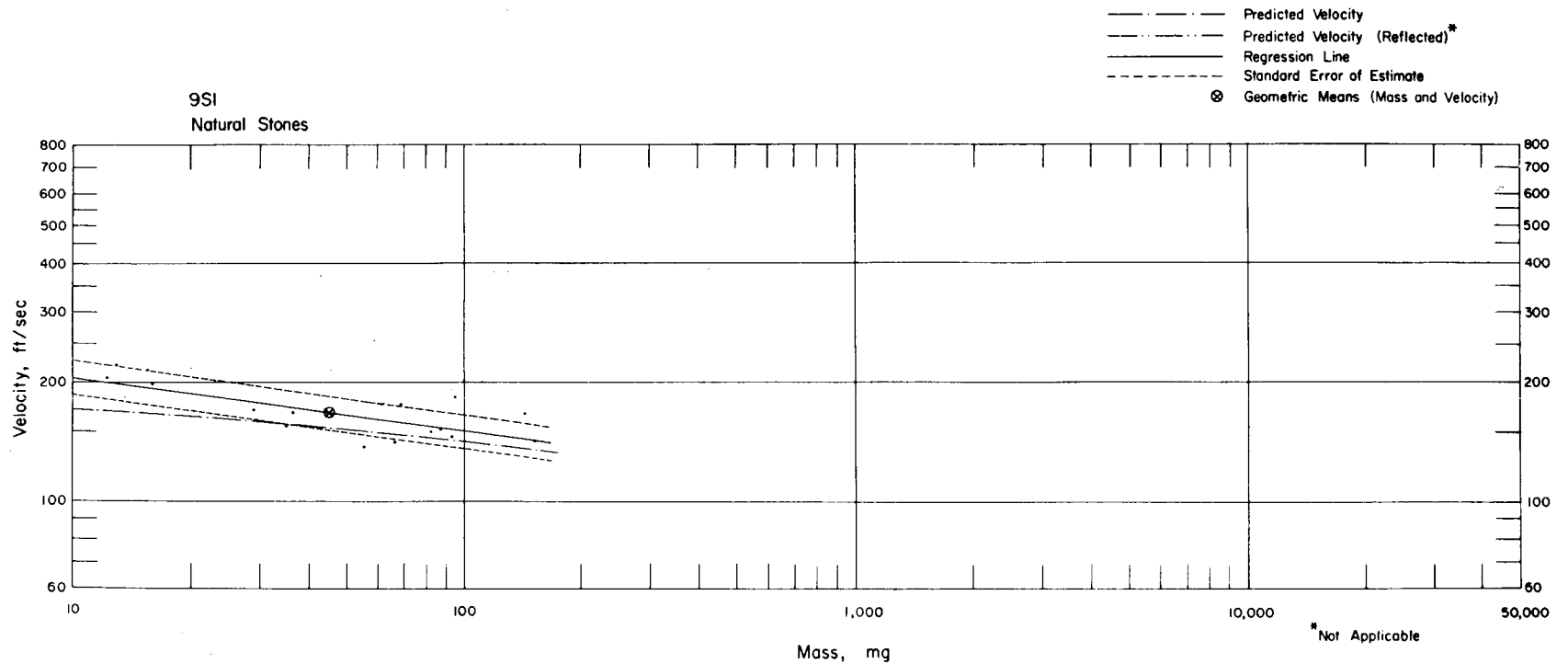


Fig. 5.74—Analysis of natural-stone missiles from installation 9SI: $n = 17$; $\log v = 2.4472 - 0.1334 \log m$; $E_{gv} = 1.11$; $M_{50} = 45.6$ mg; $V_{50} = 168$ ft/sec.

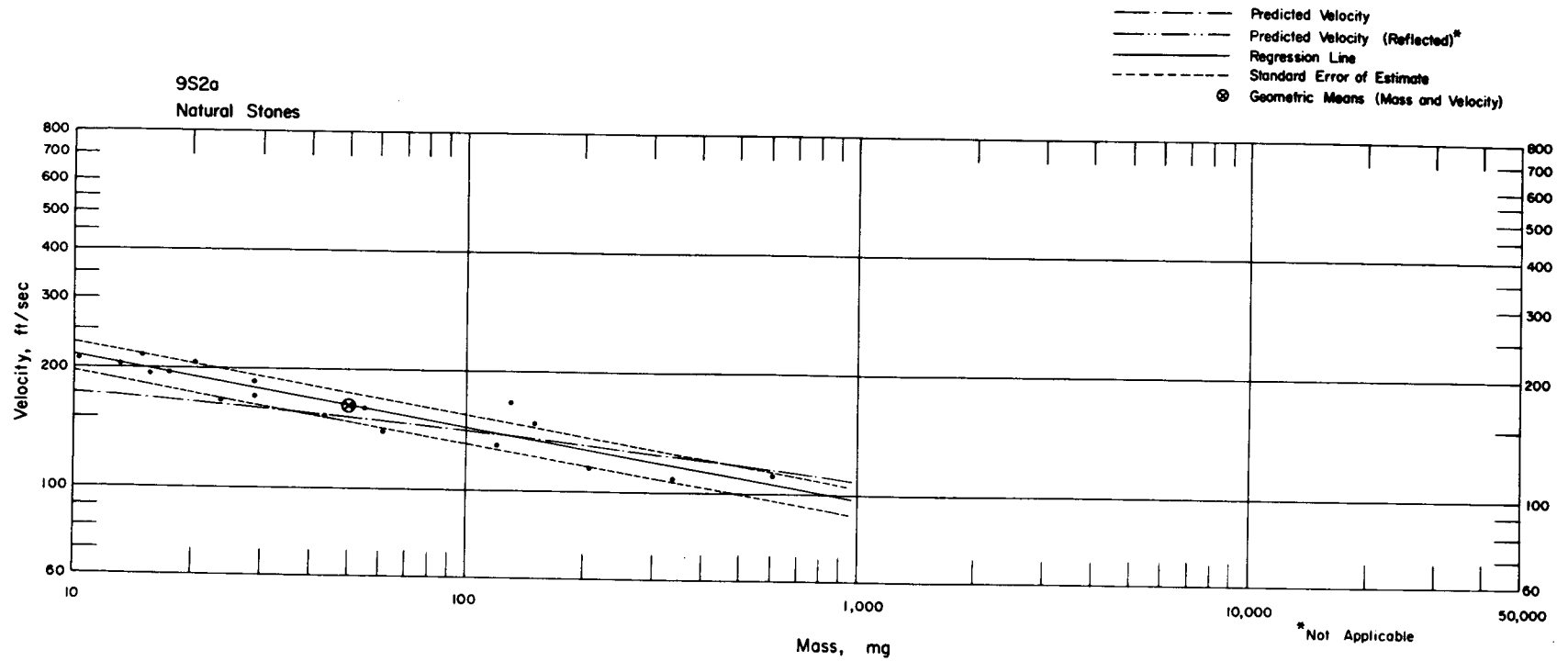


Fig. 5.75— Analysis of natural-stone missiles from trap 9S2a: $n = 18$; $\log v = 2.4984 - 0.1726 \log m$; $E_{GV} = 1.09$; $M_{50} = 49.3$ mg; $V_{50} = 161$ ft/sec.

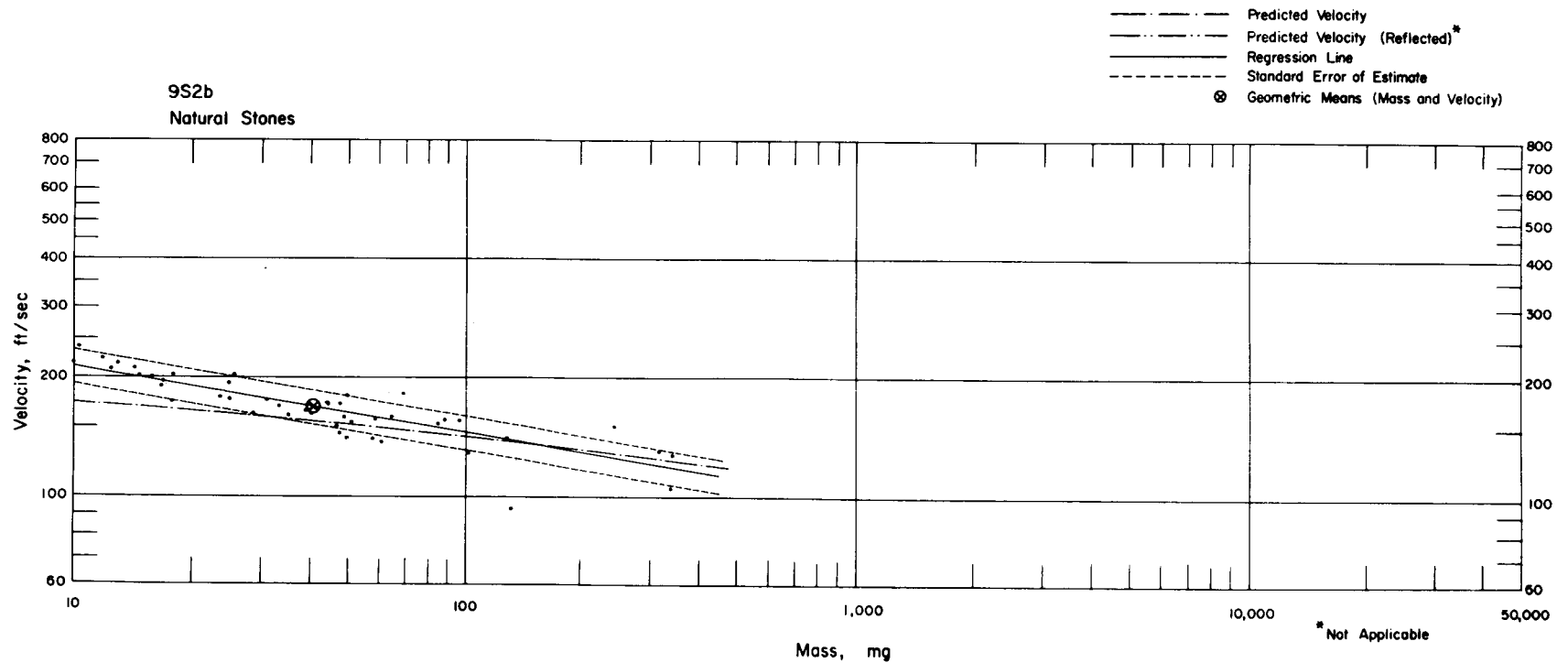


Fig. 5.76—Analysis of natural-stone missiles from trap 9S2b: $n = 46$; $\log v = 2.4841 - 0.1620 \log m$; $E_{gv} = 1.10$; $M_{50} = 41.8$ mg; $V_{50} = 167$ ft/sec.

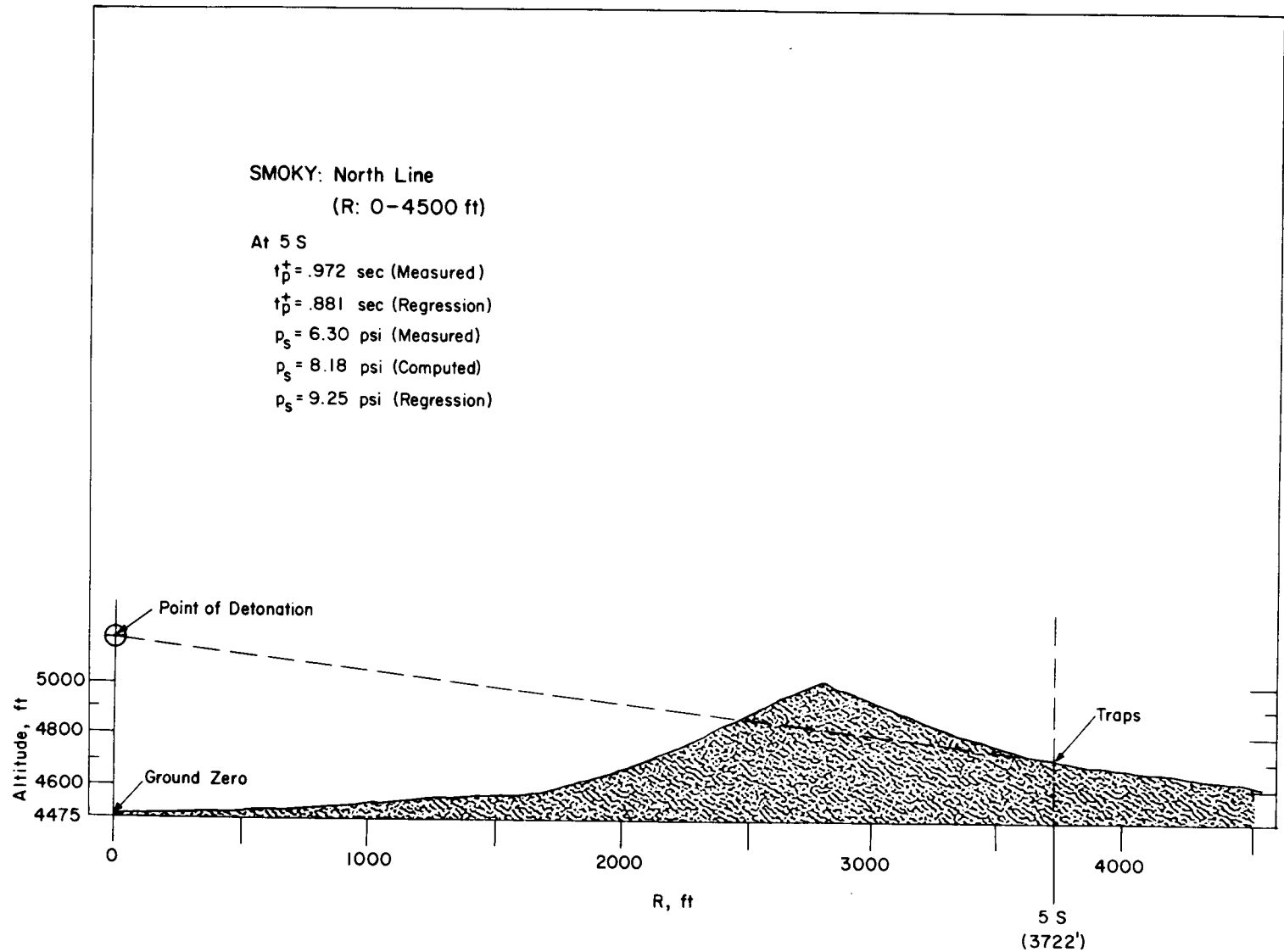


Fig. 5.77—Profile of north blast line, shot Smoky. See Table 5.1 for explanation of blast parameters plotted.

STATION: 5S
RANGE: 3722'

TERRAIN: DALE
BLAST LINE: N

Roman numeral in parenthesis designates type of missile absorber

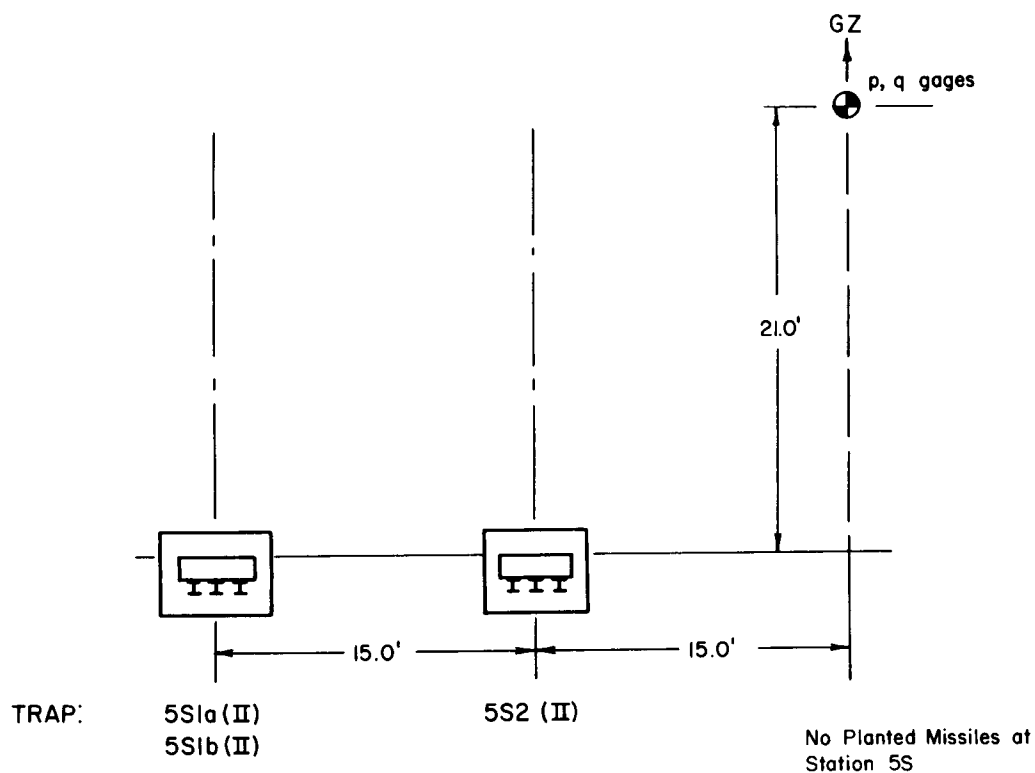


Fig. 5.78—Station 5S layout chart.

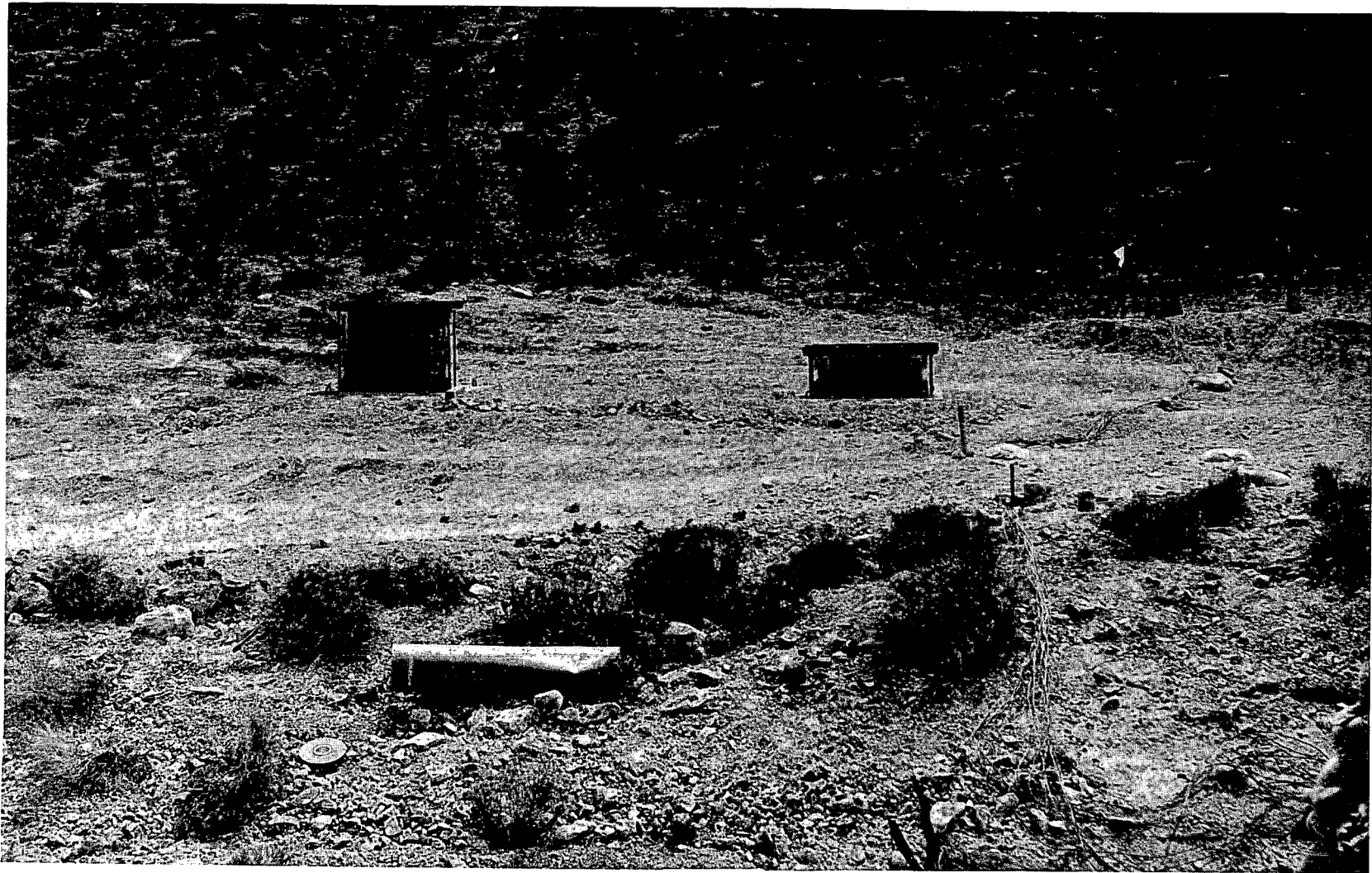


Fig. 5.79—Station 5S, preshot, looking toward GZ. This station was at 3722-ft range on the north blast line and was the only station not in line-of-sight with the point of detonation.

333

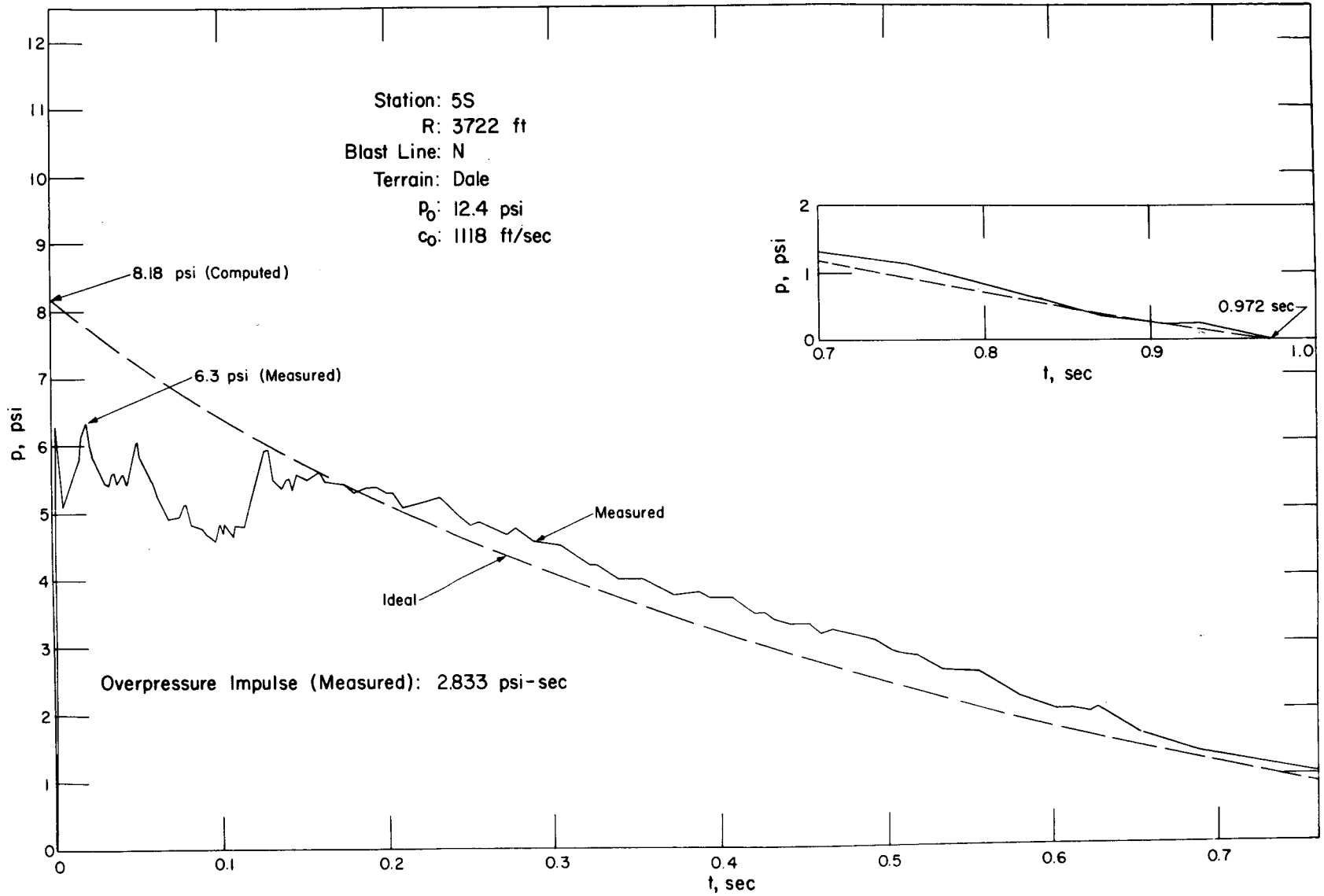


Fig. 5.80—Overpressure vs. time at station 5S.



334

Fig. 5.81—Traps 5S1a and b, postshot.



42



43

44



Fig. 5.82—Installation 5S2, postshot.

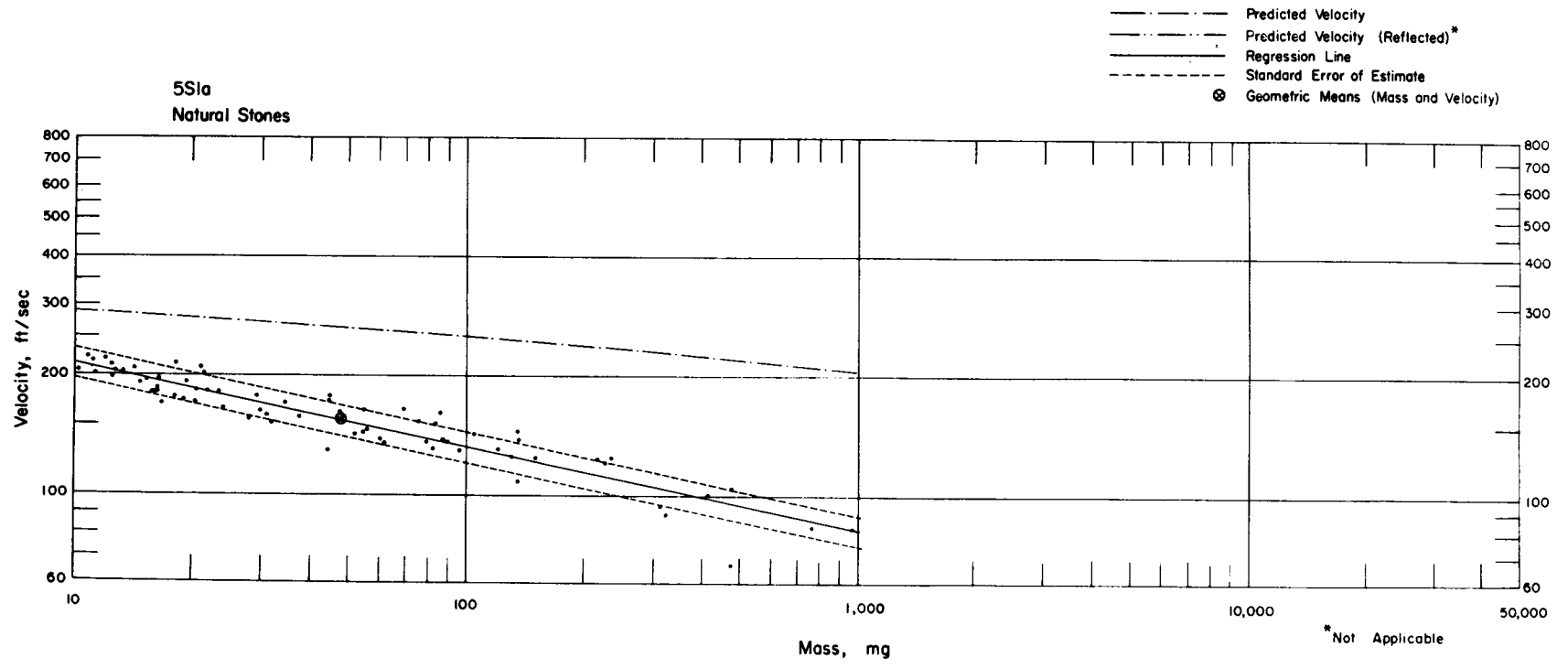


Fig. 5.83—Analysis of natural-stone missiles from trap 5S1a: $n = 73$; $\log v = 2.5374 - 0.2090 \log m$; $E_{gv} = 1.09$; $M_{50} = 47.0 \text{ mg}$; $V_{50} = 154 \text{ ft/sec}$.

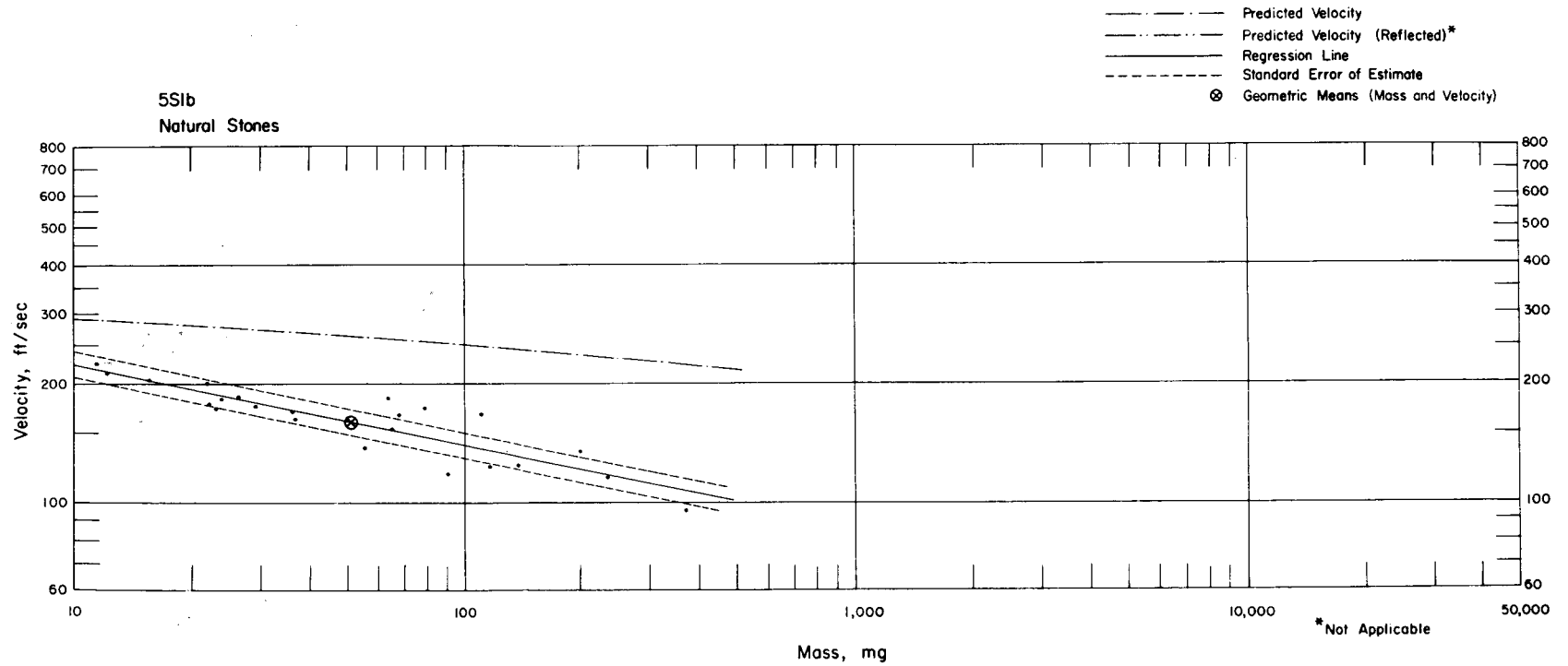


Fig. 5.84—Analysis of natural-stone missiles from trap 5S1b: $n = 23$; $\log v = 2.5467 - 0.2029 \log m$; $E_{gv} = 1.08$; $M_{50} = 51.1 \text{ mg}$; $V_{50} = 159 \text{ ft/sec}$.

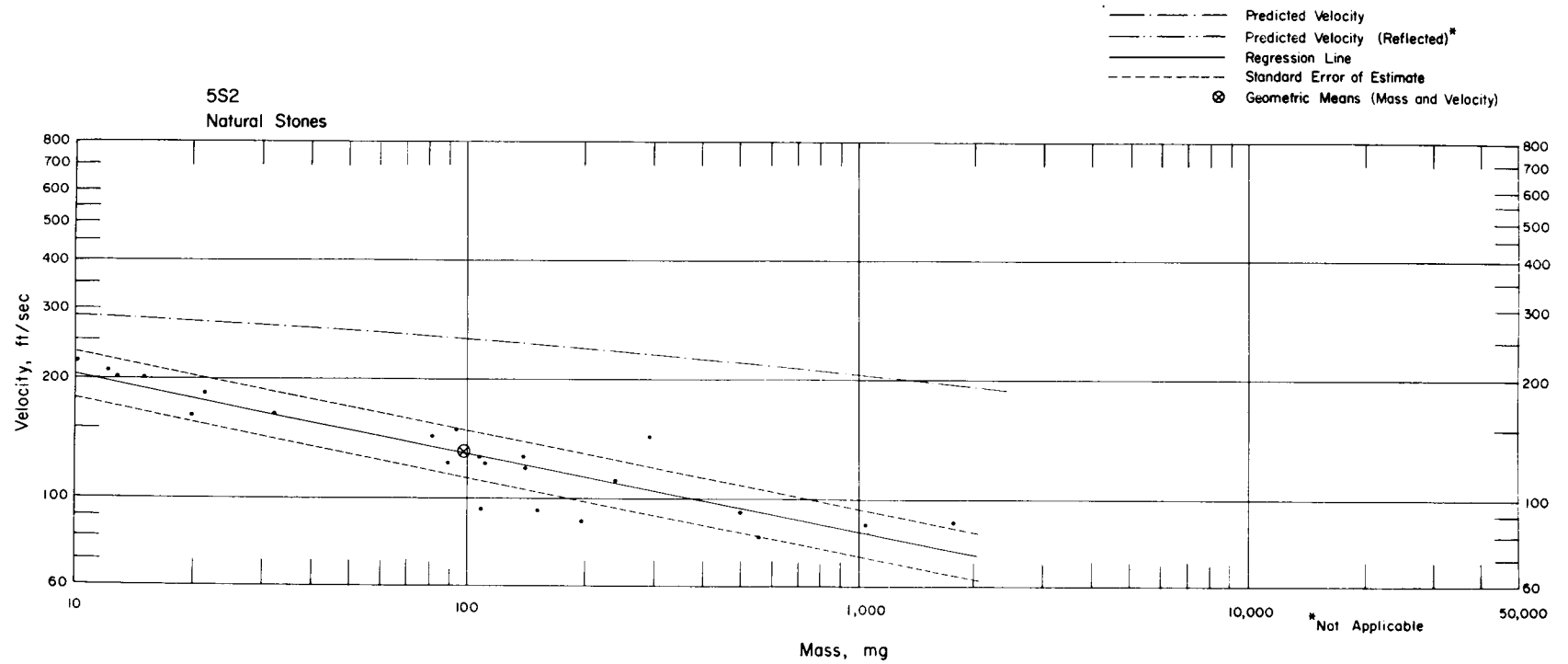


Fig. 5.85—Analysis of natural-stone missiles from installation 5S2: $n = 23$; $\log v = 2.5063 - 0.1995 \log m$; $E_{gv} = 1.15$; $M_{50} = 97.3$ mg; $V_{50} = 129$ ft/sec.

Chapter 6

SHOT GALILEO, EXPERIMENTAL PROCEDURE AND RESULTS

6.1 GENERAL

Participation in shot Galileo involved studies of the translation of (1) fragments from windows mounted in houses and in open areas, (2) natural stone, marked gravel, and spheres in open areas, and (3) debris from a concrete-block wall.

Figure 6.1 is a map of Area 1, NTS, showing the location of the missile stations as well as the blast-wave instrumentation used in this shot. On this chart there was an 8° difference between the azimuth angles of the blast line and of the line of the missile studies. The estimated yield for this shot was 11 kt (see Table 6.1), producing an overpressure at the near range (2750 ft) of about 8.4 psi and at the distant range (4700 ft) of about 3.8 psi. No blast data were obtained at the intermediate range (3750 ft) for station 4.3GTS.

An interesting overall view of all stations used in this shot is shown in Fig. 6.2. This photograph was taken from the 500-ft tower at GZ. Yucca Lake (dry) can be seen in the background. The concrete-block wall was located just left of the rut road at station 7G. At locations 7GTS and 4.3GTS, the tool sheds to the right of the main road were made usable for missile studies by cementing absorbing material on the sides that faced GZ. The houses used in this study can be seen at station 3G: the precast concrete on the left and the reinforced concrete block on the right. Both houses had flat tops.

Data for glass-fragment missiles were obtained at certain locations in cooperation with another project that was studying the penetration effects of this type of missile on biological targets (dogs).¹ The trauma to which a dog was exposed was estimated by placing a trap (or traps) as near the dog installation as possible. A dog was also placed behind the concrete-block wall at station 7G.

The method of presentation used in this chapter is essentially the same as that used in Chaps. 4 and 5. After the description of each installation, or small group of similar installations, the results obtained are discussed and presented graphically. All results are summarized in Table 6.2. In a few cases the missile samples obtained were too small to justify graphical presentations.

6.2 STATION 3G, 4700-FT RANGE

6.2.1 General Discussion and Blast Parameters

Traps were installed at four locations at this station (Fig. 6.1). The first location was a concrete slab that had been the floor of a rambler house destroyed on a previous shot. Marked gravel and spheres were placed on the slab. At the second location traps were installed behind windows in an open area. Natural-stone missiles were also studied. The other two locations were inside the reinforced-block and the precast-concrete (concrete-slab) houses.

TABLE 6.1—BLAST PARAMETERS, SHOT GALILEO
(See List of Symbols.)

$p_0 = 12.7$ psi		$c_0 = 1124$ ft/sec (18.8°C)		Estimated yield: 11 kt ⁽¹⁾		Terrain: flat desert		
Station	Range, ft	$(I_p)_m$, ⁽²⁾ psi-sec	$(I_p)_r$, ⁽³⁾ psi-sec	$(t_p^+)_m$, ⁽²⁾ sec	$(t_p^+)_r$, ⁽⁴⁾ sec	$(p_s)_m$, ⁽²⁾ psi	$(p_s)_c$, ⁽⁵⁾ psi	$(p_s)_r$, ⁽⁶⁾ psi
3G	4700	1.122		0.756		4.5	3.85	
4.3GTS	3750		1.355		0.675		(5.32)	5.34
7G and 7GTS	2750	1.754		0.576		8.7	8.38	

(1) Estimation made by assuming a "typical air burst" as described in *The Effects of Nuclear Weapons*, and by using data for stations 3G and 7G.

(2) Determined from BRL mechanical-gauge records (no gauge at station 4.3GTS).

(3) Overpressure impulse computed by interpolation equation derived from $(I_p)_m$ values

$$\log (I_p)_r = 3.1100 - 0.8333 \log R$$

(4) Overpressure duration computed by interpolation equation derived from $(t_p^+)_m$ values

$$\log (t_p^+)_r = -1.9844 + 0.5073 \log R$$

(5) Peak overpressure computed for a classical blast wave of impulse $(I_p)_m$ and of duration $(t_p^+)_m$. Measured values of impulse and duration were not obtained at station 4.3GTS; therefore regression values $(I_p)_r$ and $(t_p^+)_r$ were used (see text).

(6) Peak overpressure computed by interpolation equation derived from $(p_s)_c$ values for stations 3G and 7G

$$\log (p_s)_r = 5.9122 - 1.4506 \log R$$

Note: The line where missile data were obtained was 150° azimuth from GZ. Blast data were obtained from a line of 158° azimuth.

Blast-wave data obtained for station 3G are plotted in Fig. 6.3. Overpressure vs. time is shown as a solid line for the measured values and as a dashed line for an ideal wave having the same impulse and duration as the measured values (refer to Chap. 3). Agreement between these curves is good except for the early-time periods where, apparently, inertia in the instrumentation delayed the initial rise, caused it to overshoot, and then delayed the return of the recording to a quasistable state. Peak overpressure of the ideal wave (3.85 psi) was used to compute predicted missile velocities. Dynamic pressure was not measured at this station.

The traps used at station 3G, except for trap 3G8b, were the ones used by Project 33.4 in Operation Teapot.² They were different from the others discussed in this report in that the missile-collecting area was square (3.516 sq ft) and the absorber was type I.

6.2.2 Concrete-slab Location, Installations 3G1 to 3G4

Figure 6.4 illustrates the placement of marked gravel and spheres on the concrete slab. Ninety large ($\frac{1}{16}$ -, $\frac{1}{2}$ -, and $\frac{9}{16}$ -in.-diameter) steel spheres were placed in trough-like supports 18 in. above the surface at two locations. One weighted* croquet ball was placed on a 21-in.-high thin rod support (see Figs. 6.5 and 6.6). A total of 13,715 smaller spheres was placed at the eight locations marked in Fig. 6.4. Green, yellow, and black samples contained 2110 spheres each, and red and clear samples, 1055 each. Each sample consisted of the following spheres in the indicated proportions:

*The mass of the croquet ball was increased in order that its acceleration coefficient would correspond roughly to that of a tumbling man (0.035 sq ft/lb). The significance of this concept is treated in Refs. 3 and 4 (see Chap. 3).

$\frac{1}{8}$ -in.-diameter nylon (Ny $\frac{1}{8}$)	5.2%	$\frac{1}{4}$ -in.-diameter steel (St $\frac{1}{4}$)	1.4%
$\frac{1}{8}$ -in.-diameter aluminum (Al $\frac{1}{8}$)	10.4%	36.0 mg (av.) soda glass (Gs)	53.5%
$\frac{3}{16}$ -in.-diameter aluminum (Al $\frac{3}{16}$)	5.2%	72.6 mg (av.) soda glass (Gl)	13.1%
$\frac{1}{4}$ -in.-diameter aluminum (Al $\frac{1}{4}$)	0.7%		
$\frac{3}{8}$ -in.-diameter aluminum (Al $\frac{3}{8}$)	0.1%		
$\frac{1}{8}$ -in.-diameter steel (St $\frac{1}{8}$)	10.4%		

Figure 6.5 is a preshot photograph of the concrete-slab location looking away from GZ. The structure on the left was a reinforced bathroom shelter that was left intact after the remainder of the rambler house originally placed on this slab had been destroyed in Operation Teapot.

Figure 6.6 illustrates typical placement of spheres and gravel at this location. The trough-like support held the large steel spheres, whereas the smaller spheres were placed in the tissue-paper bags beneath the steel spheres and the croquet ball.

Figure 6.7 is a closeup photograph of installation 3G3 taken after the detonation. This installation, as well as others on this shot, was in good condition, and no signs of thermal or blast damage were seen.

Because so few missiles were caught at this location, the data were not prepared in the plotted form. The small number caught was undoubtedly the result of their low velocities relative to the threshold values of the absorber. Note the gravel left in front of the trap in Fig. 6.7. Installation 3G1 caught one natural stone and four pieces of gravel (see Table 6.2 for results). Data were obtained for two natural stones, six pieces of gravel, and one $\frac{1}{8}$ -in. steel sphere from installation 3G4 (Table 6.2). No results were obtained for installations 3G2 or 3G3.

6.2.3 Open Area, Installations 3G5 to 3G9

Figure 6.8 illustrates diagrammatically the plan for missile studies for five installations (3G5 to 3G9) that were placed in an open area between the concrete slab and the reinforced-block house (see Fig. 6.1). Installation 3G5, the only one not behind a window, was meant for the study of natural-stone missiles.

Four of the installations at this location are shown in Fig. 6.9 (installation 3G5 is not shown). The reinforced block house can be seen on the left side of the photograph. The trap installation that was second from the left consisted of an empty box. A dog was later placed in this box. The trap above the box (3G8b) was the small size similar to those used at the other stations.

Figures 6.10 (3G6 catching window glass) and 6.11 (3G7 behind plate glass) are postshot photographs of two representative installations. In Fig. 6.11 the impressions of fragments that struck the trap flat can be seen.

Nothing was caught in installation 3G5. Installation 3G6, which was located 4.6 ft behind a window, caught 42 fragments. The velocities and masses for these fragments are plotted in Fig. 6.12. Note two predicted-velocity lines shown on this and subsequent charts for glass-fragment data at station 3G. The lower line was computed for an ideal blast wave similar to that depicted in Fig. 6.3. The upper line was computed for an ideal wave whose peak overpressure is equal to the reflected value (assuming normal incidence and perfect reflection) of the peak overpressure of the incident ideal wave. The duration was assumed to be the same as that measured. This "reflected" assumption* results in a prediction line that is compatible with the data from installation 3G6 (Fig. 6.12) since the predicted values are near the top of distribution of the measured ones.

Seven fragments of plate glass were recovered from installation 3G7. The plot shown in Fig. 6.13 indicates that the measured velocities lie between the two prediction lines discussed above.

Trap 3G8b, placed 10.9 ft behind the window and above the dog installation, which was 31.5 in. high, caught 15 fragments. The regression line relating velocity to mass for these

*For a more complete discussion of this assumption see Chap. 3.

missiles is shown in Fig. 6.14. The slope of the line appears to be "wild" owing to a small range in mass along with a relatively large range in velocity.

Data for 16 fragments of window glass from installation 3G9 are plotted in Fig. 6.15. Because the distance the missiles traveled was greater than that for trap 3G8b, discussed above, the predicted-velocity lines are slightly higher for installation 3G9. The geometric mean of the measured velocities was also somewhat greater for the missiles traversing the longer distance—104 compared with 96 ft/sec for installation 3G9 and trap 3G8b, respectively.

6.2.4 Reinforced Concrete-block House, Traps 3G10a to 3G11e

(a) *General.* Locations of the seven traps used in the concrete-block house are indicated on the floor plan presented in Fig. 6.16. Elevation views of the stacked traps are shown at the bottom of the figure. The bedroom window facing GZ, which was 3 ft high and 6 ft wide, was 3 ft 7 in. above floor level. There were three panes in the horizontal direction and three in the vertical. Each pane was 23.5 in. wide and 11.5 in. high. Panes in the living-room window were the same size. This window consisted of 20 panes: five in the horizontal direction and four in the vertical. The window, which was 10 ft wide and 4 ft high, was 2 ft 7 in. above floor level.

(b) *Bedroom Traps, 3G10a to 3G10c.* The traps that were placed in the bedroom are shown in Fig. 6.17. Note the iron straps holding the traps together and the chain used to anchor the stack against the wall.

The missile-collecting area of each trap was divided into nine segmental areas, and the number of missiles caught per square foot was computed for each. These numbers were plotted at the midpoint of the appropriate areas as illustrated in Fig. 6.18. Contour lines were then drawn to connect points of equal spatial density. The heights of the top and the bottom of the bedroom window from which the missiles originated are indicated as dashed lines. The highest density (82 missiles per square foot) occurred just below the height of the bottom of the window and the lowest (12 missiles per square foot) near the center-height of the window.

Data for the bottom trap of the trio are presented in Fig. 6.19. Predicted-velocity lines were computed for glass in normal orientation (flat) to the wind. However, on this chart predicted velocities are also shown for fragments in edgewise orientation, indicating a surprisingly small effect due to orientation with respect to the wind.⁴

Figures 6.20 and 6.21 contain the data obtained for the middle and top traps, respectively. Though the number of missiles caught in each trap was different, the velocities measured were quite similar and the masses were only slightly different (missiles in the top trap were somewhat heavier).

(c) *Living-room Traps, 3G11a to 3G11e.* Figure 6.22 is a postshot view of installation 3G11. Two traps are shown on the floor, a dog trap (empty) above them, and two more traps on top. This assembly was held together and to the wall with angle iron.

A spatial-distribution chart similar to the one described for installation 3G10 is presented in Fig. 6.23 for missiles caught at installation 3G11. Unfortunately, no data were obtained in the most interesting region, the central region occupied by the dog trap. The contour lines (dashed) extrapolated to this region are of dubious value. A total of 500 missiles was caught in the lower traps, whereas only 354 were recovered from the upper two. This indicates a tendency for the fragments to fall during transit.

Velocity and mass data for the 854 missiles caught at installation 3G11 are plotted by trap in Figs. 6.24 to 6.27. In general, the velocity points lie between the two predicted-velocity lines, based on blast waves with peak overpressures of 3.85 (see Fig. 6.3) and 8.66 psi (reflected value for incident shock overpressure of 3.85 psi).

Attention is called to the results of two additional analyses which were made for the data from trap 3G11e (Fig. 6.27). Whether or not the slope of the regression line should be the same for large as for small fragments was determined by making one analysis for missiles with masses less than 219.5 mg and another for those with masses greater than 219.5 mg. The regression slopes found were somewhat different. This may be attributed in part to the variation of threshold velocity with missile mass: the fact that the smaller fragments have higher threshold velocities tends to increase the average velocity of the small missiles that were

caught (Fig. 2.6). Another factor to be considered is that the smaller fragments have slightly higher acceleration coefficients⁴ (note higher predicted velocities for the smaller missiles, e.g., in Fig. 6.27).

6.2.5 Precast-concrete House, Traps 3G12a to 3G13e

(a) *General.* The plan for missile studies in the precast-concrete (concrete slab) house illustrated in Fig. 6.28 was essentially the same as that described in the last section for the concrete-block house. There were, however, some differences in the size of the rooms and windows. The bedroom window facing GZ was identical to the one in the bedroom of the concrete-block house except that in the present case it was only 3 ft 6 in. above the floor. The living-room windows of the two houses had the same number of panes of the same size, the difference being in the arrangement. For the precast-concrete house there were four panes in the horizontal direction and five in the vertical. This window, which was 5 ft high and 8 ft wide, was 1.5 ft above the floor. Note that installation 3G13 was centered behind the window; thus it was necessary to provide support independent of the wall on one side (Fig. 6.28).

(b) *Bedroom Traps, 3G12a to 3G12c.* Figure 6.29 is a postshot view of installation 3G12. The scorching on the upper trap did not result from the thermal effects of this shot but from exposure on another occasion.

A total of 425 fragments was retrieved from the three traps at installation 3G12 in the precast-concrete house compared to 444 from the similar installation (3G10) in the concrete-block house. The spatial-distribution chart (Fig. 6.30) indicates that the highest missile densities occurred in the middle trap, which was from 2.5 to 4.4 ft above the floor. Fewer fragments were caught on the right (looking away from GZ) than on the left side of the traps. This may be attributed to air flow through the side window (see Fig. 6.28) which would deflect the missiles to the left.

Velocity and mass data for missiles caught in installation 3G12 traps are presented in Figs. 6.31 to 6.33. The geometric mean velocity was slightly lower for the bottom trap, 132 ft/sec vs. 145 and 144 ft/sec for the middle and upper traps, respectively.

(c) *Living-room Traps, 3G13a to 3G13e.* Figure 6.34 is a postshot view of installation 3G13. This illustration, as well as Fig. 6.35, serves to illustrate the quantity of glass fragments found on the floor after the detonation. Also shown in Fig. 6.35 is the outside door for the living room (see Fig. 6.28), which was found, strangely enough, along the wall closest to GZ.

A total of 707 missiles was retrieved from the four traps at installation 3G13: 361 from the upper traps, 346 from the lower traps, 304 from the two on the left, and 403 from those on the right. Results of a more detailed spatial-distribution analysis are presented in Fig. 6.36. Although iso-density lines were extrapolated to the region occupied by the dog, their validity is doubtful. It appears that a general downward trajectory of the fragments compensated for the average window height being nearer the upper traps (see dashed lines in Fig. 6.36) since about the same spatial densities were observed in the lower as in the upper traps.

Velocity and mass data for installation 3G13 traps are presented in Figs. 6.37 to 6.40. In agreement with data from the other traps located in houses, the velocity points, in general, lie between the velocities predicted for the incident peak overpressure and its reflected value. Slightly lower geometric mean velocities were found for the lower traps: 133 and 134 ft/sec for traps 3G13a and 3G13b vs. 142 and 144 ft/sec for traps 3G13d and 3G13e.

6.2.6 Analysis of Combined Data Obtained in Houses

Because the experimental conditions for the traps placed in the two houses were quite similar, an analysis of the combined data was made. The results for 2523 fragments of window glass are set forth in Fig. 6.41. Essentially the same features are evident on this chart as were seen on the plots for the individual traps (e.g., Figs. 6.19 and 6.20).

Use was made of the large quantity of data obtained in houses to test the validity of the log-normal assumption for the velocity and mass distributions. The graphical test used is shown in Fig. 6.42. The ordinate of this chart is marked on the right in geometric-standard-

deviation units drawn to a linear scale and on the left in the corresponding percent-of-total-sample units used to plot the experimental data. The abscissa is a logarithmic scale used for both mass and velocity. The straight lines are a graphical representation of computed values of the geometric mean and geometric standard deviations.* Thus a comparison between the sample points (taken at arbitrary intervals) and the lines indicates that the log-normal assumption is reasonable. However, the points for small masses fall below the line. The reason for this may be that some of the small fragments were overlooked since they were difficult to locate in the absorber.

6.3 STATION 4.3GTS, 3750-FT RANGE

6.3.1 General

The tool-shed shelter used at this station was constructed and tested by a project in Operation Teapot (1955). The structure survived the original test and was made available in the next operation for the study of secondary missiles. The diagram in Fig. 6.43 indicates the placement of marked gravel and spheres as well as the location and size of the shelter. A 2-in.-thick layer of type II absorber was cemented† to the structure on the side facing GZ. The total missile-collecting area was 7 by 7 sq ft, equivalent to more than 16 small traps. A double layer of aluminum foil similar to that used in the other traps for thermal protection was placed over the absorber.

A total of 2328 spheres was placed at this location. Three of these were weighted croquet balls (described in Sec. 6.2.2) and 90 were $\frac{7}{16}$ -, $\frac{1}{2}$ -, and $\frac{9}{16}$ -in.-diameter steel spheres (placed as indicated in Fig. 6.43). A total of 2110 small spheres was evenly divided between the two locations indicated.‡ In addition to these, 125 "extra large" soda-glass spheres with an average mass of 243 mg were placed at the 11.4-ft distance.

The placement of marked gravel indicated in Fig. 6.43 is illustrated in Fig. 6.44. Also depicted are the steel spheres in the trough-like support, the croquet ball on a long thin rod, and the tissue-paper packets on the ground containing smaller spheres.

Since the blast line was not instrumented at the range of this station (3750 ft), interpolated values of peak overpressure and duration were used to compute predicted missile velocities. These interpolated quantities, recorded in Table 6.1, were 5.34 psi and 0.675 sec for peak overpressure and duration, respectively.

Figure 6.45 is a postshot photograph of station 4.3GTS. Shreds of aluminum foil can be seen hanging on the absorber, which was found to be in good condition. Some of the impressions made by the missiles that struck this trap are visible.

6.3.2 Marked-gravel Data

Data for 16 pieces of gravel placed 11.4 ft from the station are presented in Fig. 6.46. Since both the average acceleration coefficient as a function of missile mass⁴ and the distance of travel are known for these stones, the predicted-velocity line should pass through the center of the measured velocity points. For all stones having masses less than 100 mg, however, the measured velocities were higher than those predicted. Missiles with lower velocities were probably present but were not caught because of insufficient impact velocity (refer to threshold-velocity chart, Fig. 2.8).

Data for gravel missiles originating 29.2 ft from the station are shown in Fig. 6.47. The predicted velocities are higher than in the previous instance (cf. with Fig. 6.46) because the

*The straight lines were determined as follows: The geometric mean mass (M_{50}), for example, was plotted at zero geometric-standard-deviation units. The quantities $M_{50} \cdot S_{gm}$ and M_{50}/S_{gm} were plotted at +1 and -1 geometric-standard-deviation units, respectively, where S_{gm} is the geometric standard deviation of mass.

†A commercial linoleum cement was used.

‡The small spheres placed at 29.2 ft were painted blue; those at 11.4 ft were not painted and are labeled in Fig. 6.43 as "clear." The percentages of the various types of spheres used in each sample were the same as those set forth in Sec. 6.2.2.

distance of travel was greater. There is little evidence of the threshold-velocity effect that was noted at the smaller distance. The average measured and predicted velocities are in good agreement.

A spatial-distribution chart similar to that described in Sec. 6.2.4 is presented in Fig. 6.48 for the gravel placed at 29.2 ft. High spatial densities of missiles tend to be near the bottom of the trap due to gravity and near the outside edges due to wind streaming around the trap. It is remarkable that some missiles were caught near the top of the trap, indicating an average trajectory about 13.5° from the horizontal.

Spatial-distribution charts were also prepared for the average masses and velocities of the gravel missiles discussed in the preceding paragraph. The region of high mass at the top of the chart (Fig. 6.49) is somewhat surprising. However, examination of the previous figure reveals that the number of missiles on which this "high" was based was comparatively small. The velocity-distribution chart (Fig. 6.50) shows a marked tendency for the missiles that struck high on the trap to have high velocities.

6.3.3 Natural-stone Data

Velocity and mass data for 586 natural stones trapped at station 4.3GTS are presented in Fig. 6.51. The predicted-velocity line lies reasonably near the top of the distribution of measured velocity points* except for the missiles of higher mass where the predicted-velocity line is too high relative to the measured points.

The spatial-distribution chart for natural stones (Fig. 6.52) indicates that maximum densities occurred about 3 ft from the ground at the left and right edges and in the center of the trap. As the blast winds streamed around the installation, the winds oriented toward the center of the obstacle would be diverted at a shorter distance from the trap than were the winds on either side. For this reason one might expect to find a region of high density in the center of the trap as well as on either edge. In the spatial distribution of gravel (Fig. 6.48), the fact that the high in the center was missing may be explained by the manner in which gravel was placed in front of the trap, as illustrated in Fig. 6.44.

Unlike the situation for gravel, there was a marked tendency for the heavier natural stones to impact at a relatively low level above ground (see Figs. 6.49 and 6.53). Since, for the same blast exposure, small stones acquire higher velocities than do large ones, it is not surprising to find (in Fig. 6.54) a region of high velocity at the top of the trap and a region of low velocity at the bottom. In fact, it is generally true that (see Figs. 6.53 and 6.54) regions of high or low velocity correspond to regions of low or high mass, respectively.

6.3.4 Sphere Data

Complete statistical data for 18 spheres caught at this location are presented in Table 6.2. The average velocity for the largest sample caught (14 small glass spheres) was 29.2 per cent higher than predicted. This may be explained by the fact that the spheres of lower velocities were not caught due to insufficient penetration; i.e., the distribution of missile velocities obtained was distorted due to the inability of the trap to catch missiles whose velocities were below threshold values (see threshold-velocity chart, Fig. 2.11).

6.4 STATION 7GTS, 2750-FT RANGE

6.4.1 General

The overpressure vs. time data obtained at the 2750-ft range for stations 7GTS and 7G are presented in Fig. 6.55. Correspondence between the curves for overpressure (computed for an ideal wave and measured) is generally good, the computed curve yielding a more realistic value of peak overpressure for use in predicting missile velocities. However, the measured

*Predicted velocities were made for natural stones on the assumption of optimum distance of travel for maximum velocity. Any other distance of travel would result in missile velocities being lower than the predicted values.

dynamic-pressure record (Fig. 6.56) is considerably different from the computed curve for an ideal wave, particularly for the first 0.15 sec.

The experiment at this station was similar to the one at station 4.3GTS. The diagram in Fig. 6.57 indicates positions of placement for gravel and spheres as well as the amount of gravel used. The number (2328) and distribution of spheres were exactly the same as those described in the second paragraph of Sec. 6.3.1 (see also Fig. 6.44). It is to be noted, however, that the distances of placement were greater at station 7GTS since a stronger blast wave was expected at this location than at station 4.3GTS.

It was not feasible to place an extra thermal shield before the absorber as was done at selected 7G installations placed at the same range; therefore a heavier and more thermal-resistant Styrofoam (absorber type III) was used here than at station 7G. As evidenced by the postshot photograph (Fig. 6.58), the absorber suffered no significant damage. As shown in this photograph, two members of one of the trough-like sphere supports are imbedded in the absorber. The dark appearance of the absorber was due mostly to impregnation of a thin outer layer of Styrofoam by dust associated with the blast wave.

6.4.2 Marked-gravel Data

Results obtained for 42 pieces of gravel placed 15.5 ft from the trap are graphed in Fig. 6.59. The prediction line lies quite close to the upper standard error of estimate line, which is itself about 12 per cent above the regression line. Similar data obtained for gravel placed at 39.5 ft are shown in Fig. 6.60. Again the predicted-velocity line and the upper standard error of estimate line are near each other. The deviation of the prediction curve from the regression line is about the same as noted above for the gravel arriving from the 15.5-ft distance.

A spatial-distribution chart (Fig. 6.61) was prepared for the 294 pieces of gravel caught which originated 39.5 ft from the trap. Maximum missile densities occurred about 3 ft from the ground, one on the left and the other on the right (compare Figs. 6.48 and 6.52). Missiles striking the trap 7 ft above ground level had an average trajectory about 10° from the horizontal. The spatial-distribution plot for average masses of the gravel missiles (Fig. 6.62) does not show any definite trends. The region of high mass at the upper left is somewhat surprising. It should be remembered that in this region the missile density was low, and thus the average mass (948 mg) producing this "high" was based on relatively few missiles. Comparison of Figs. 6.62 and 6.63 shows, in general, regions of high or low velocity which correspond to regions of low or high mass, respectively. This agrees with observations made for natural stones caught at station 4.3GTS (refer to Sec. 6.3.3 and Figs. 6.53 and 6.54).

6.4.3 Natural-stone Data

Log velocity vs. log mass is plotted in Fig. 6.64 for 1238 natural stones caught at this location. Two predicted-velocity lines are shown on this and subsequent charts for natural stones caught at station 7G. The upper line was prepared using acceleration coefficients determined for a sample of natural stones from station 4.3GTS. Because it was uncertain whether or not natural stones at other stations in the Galileo shot (Area 1, NTS) were similar to the stones at station 4.3GTS, another predicted-velocity line was prepared using acceleration coefficients for the marked gravel. The greatest difference between predicted velocities indicated by these lines occurs for the missiles of high masses. Both lines were computed for the maximum velocity attained; i.e., distance of displacement was assumed to be that which would result in maximum velocity being attained. For the large natural stones, the predicted-velocity line for gravel agrees with the measured data better than does the other prediction line. However, the reverse could be said for the missiles of low masses.

The spatial-distribution chart of natural stones caught at station 7GTS (Fig. 6.65) indicates that the highest missile densities occurred between 2.5 and 4 ft above ground level. The same three regions of high density noted for natural stones at station 4.3GTS (cf. Fig. 6.52) are present on this chart; however, in the present case the outside "highs" are farther from the edges of the trap than those observed for the station at lower overpressure.

Figure 6.66, the spatial-distribution chart, indicates that there was no definite trend in average mass of the missiles as a function of location in the trap. Owing to the fairly uniform

distribution of missile masses, there is little correspondence between regions of high or low average velocity (Fig. 6.67) and those of low or high mass, respectively.

6.4.4 Sphere Data

Velocities were obtained for three $\frac{7}{16}$ -in.-diameter steel spheres* at this location. Because the data were not significantly different from those obtained for three similar spheres at station 7G, analysis was made for the combined lot and is presented in Table 6.2. It is interesting that, although velocities evaluated for the six spheres varied from 33 to 56 ft/sec, the average was 44.5—just 0.5 ft/sec less than that predicted.

Statistical data for 19 "extra large" (Gx with average mass of 243 mg) and 7 small glass spheres caught at station 7GTS are listed in Table 6.2. The deviation of the measured from the predicted velocities for the larger glass spheres (-13 per cent) is about the same as that noted for the marked gravel. The average velocity determined for the seven small spheres, however, was only 1.1 per cent less than that predicted.

6.5 STATION 7G, 2750-FT RANGE

6.5.1 General

The blast-wave measurements presented for station 7GTS in Sec. 6.4 (Figs. 6.55 and 6.56) also apply for station 7G, which was located near 7GTS (see Figs. 6.1 and 6.2) and at the same range.

The design chart in Fig. 6.68 indicates the placement of a concrete-block wall, window and plate glass, and marked gravel and spheres. The total number of spheres and amount of gravel used are specified for each location. Each sample of colored spheres consisted of the same proportions of the various types described in Sec. 6.2.2.

6.5.2 Concrete-block Wall, Traps 7G1a to 7G3b

(a) *General.* Figure 6.69 is a preshot view of the concrete-block wall and associated traps. Trap installations were located 10.2, 20.2, and 40.2 ft from the wall. The installation that was 20.2 ft from the wall consisted of a missile trap placed over a dog installation.¹ Extra thermal shields were installed at the two most distant locations but not at the near position, which was protected from thermal radiation by the wall itself.

Figures 6.70 and 6.71 illustrate the scatter of blocks and fragments from the wall. The absorber at the installation 10.2 ft from the wall (Fig. 6.72) was ruined by the impaction of blocks and large fragments. Installation 7G2, which was 40.2 ft from the wall (Fig. 6.73), was relatively undamaged in spite of numerous blocks that came to rest nearby. Some damage was noted on the right side of trap 7G3b (Fig. 6.74) resulting from impact of a large object. The debris that accumulated before the more distant traps, 7G2a and b and 7G3b (Figs. 6.73 and 6.74), appears to be less fragmented than that in front of the near traps, 7G1a and b (Fig. 6.72).

(b) *Block-wall Results.* Final resting positions for the larger wall fragments (whole, half, and joined blocks) are plotted in Fig. 6.75.† One block (not plotted, but indicated at the top of the chart) was found as far as 403 ft downwind and 170 ft left of the center of the wall. Note the absence of blocks behind the trap installations. A study of the downwind displacement, d_x , of these wall fragments (illustrated in Fig. 6.76) indicated an approximate log-normal distribution.‡ This analysis yielded a value for the geometric mean of the downwind displacement d_{x50} ,

*The significance of translation data for spheres of this type was discussed in Secs. 4.9.6 and 5.3.1.

†It was estimated that the wall originally contained 236 blocks. Without mortar the dimensions of each block were approximately 7.5 by 7.5 by 16 in. The average weight of the blocks left whole after the detonation was 33.9 lb. This weight includes that of the mortar which adhered to the blocks; the total weight of the concrete-block wall before the detonation was estimated to have been more than 4.2 tons.

‡A description of this type of analysis was presented in Sec. 6.2.6.

of 38.34 ft (also plotted on Fig. 6.75), which means that half of the missiles were translated more than this distance and half, less. As shown in Fig. 6.76, about 10 per cent of the 155 whole and multiple blocks was displaced downwind more than 100 ft.

An additional analysis was made using all wall fragments weighing more than 0.1 lb. The plot of the mass distribution of these 1528 fragments (shown in Fig. 6.77) illustrates an approximate log-normal distribution with a geometric mean mass of 1.366 lb. The reason for the abrupt percentage increase between mass points at 31 and 39 lb is that the mass of whole blocks, some with adhering mortar, was between these values.

When all wall fragments were considered, it was found that the downwind displacement, d_x , was neither a log-normal distribution (as was found for the larger fragments, Fig. 6.76) nor a linear-normal one. In the plot presented in Fig. 6.78 of d_x vs. per cent of total sample, the experimental points were fitted by "eye" with a smooth curve. The usefulness of this plot will be made clear in the following paragraph.

Dispersion of wall fragments in a direction perpendicular to the blast wind (crosswind or d_y) was studied in the following manner: The grid illustrated in Fig. 6.75 was divided into 10-ft-wide strips in the d_x direction and extended as far as necessary in the d_y direction to include all fragments. Assuming that the mean d_y displacement of fragments found in each 10-ft d_x strip to be along a line perpendicular to the center of the wall ($\bar{d}_y = 0$), a standard deviation in linear d_y , S_{d_y} , was computed for each 10-ft d_x interval. There was considerable variability in the computed standard deviations. However, it was found that a plot of S_{d_y} as a function of the square of the corresponding d_x values resulted in a scatter of points through which a straight line could be drawn. This procedure is illustrated in Fig. 6.79. Note that the quantity plotted on the ordinate was devised so that negative d_x values squared would remain negative.

The data represented in Figs. 6.78 and 6.79 were used in the following way to determine the smoothed contour lines shown in Fig. 6.80 which connect points on the grid plane where the spatial densities of wall fragments are the same: Sample percentages were evaluated at each 10-ft d_x interval with the chart in Fig. 6.78. The number of fragments within each 10-ft interval was determined from these figures. The spatial distribution of fragments in each strip was assumed to be gaussian with a mean d_y displacement of zero and standard deviation equal to that determined by the straight line in Fig. 6.79. Thus, by use of normal distribution tables, it was possible to compute spatial density as a function of d_y for each 10-ft strip. Values of d_y were determined for spatial densities of 0.3, 1, 3, 10, and 30 fragments per 100 sq ft, as illustrated in Fig. 6.80. For the smaller densities the d_y dispersion became greater as the downwind distances from the wall increased. The 10-line, however, shows the opposite effect. The points on this chart were plotted at the center of 10-ft squares (100 sq ft), and the associated figures represent the number of fragments found in each square. Probably owing to inaccurate extrapolation, the contours to the left of the wall extend to regions where missiles were not found. The fact that the missiles found upwind of the wall were small is demonstrated by the absence of points on the chart (Fig. 6.75) in that area for whole, half, and joined blocks.

The smoothed contour lines described above and illustrated in Fig. 6.80 present a description of the average displacement of fragments to be expected from repeated experiments of a similar nature, even though they fail to describe the measured data in every detail. It is useful to note that there was no significant difference in the mass distributions for missiles displaced a short distance compared to those translated greater distances except for those small fragments displaced upwind which were discussed above.

(c) *Trap Results.* No data were obtained from the traps at installation 7G1 since the absorber suffered large-scale deformation from the impaction of blocks and block fragments (Fig. 6.72). Natural-stone data were obtained for the remaining three traps placed at greater distances behind the wall. These data are presented in Figs. 6.81 to 6.83. Since considerably more natural stones were caught at the locations that were uninfluenced by the wall, comparison with data presented in Sec. 6.5.3 for installations 7G4 and 7G5 indicates that the traps behind the wall may have experienced some shielding. Velocities obtained for stones from the behind-the-wall traps are generally low compared to those predicted for natural stones or for gravel for station 4.3GTS (refer to Sec. 6.4).

6.5.3 Spheres and Natural Stones, Traps 7G4a to 7G5b

The two installations in the foreground of Fig. 6.84 were designed to study the translation of spheres and natural stones. The five installations appearing in the background will be discussed in succeeding sections. Figures 6.85 and 6.86 depict the appearance of installations 7G4 and 7G5 after the detonation. The thermal-shield frames were left relatively undamaged, and the absorber was found to be in good condition.

The placement of spheres for these installations was described in Fig. 6.68 and Sec. 6.5.1. Data for 196 spheres that were caught (10,730 were placed) are presented in Table 6.2. Since the experimental conditions were approximately the same, corresponding data for spheres from all four traps were combined in every case. Data for each type of sphere are presented separately. Since there was no significant difference between their impact velocities, no distinction was made between the small metal and nylon spheres placed at 15.5 ft and those placed at 39.5 ft. Predicted velocity and percentage deviation from the predicted velocity are listed in Table 6.2 for each distance of translation—even for the cases where the data from two or three distances were combined.

Larger samples were obtained for the glass spheres than for the other types, and the average velocities obtained for those translated 39.5 ft were significantly higher than for those arriving from 15.5 ft. It is interesting that the average velocities measured for these spheres were 10 to 15 per cent lower than those predicted—about the same deviation found for marked gravel at station 7GTS (see Figs. 6.59 and 6.60).

Natural-stone data obtained for the four traps at this location are plotted in Figs. 6.87 to 6.90. The upper* traps at each installation caught more missiles whose velocities were generally higher than did the lower traps. The maximum velocity line predicted for gravel (see Sec. 6.4) generally agrees with the higher missile velocities obtained for the upper traps. However, velocities evaluated from the ground-level traps were all considerably lower than predicted.

6.5.4 Window-glass and Plate-glass Installations, Traps 7G6a to 7G9b

(a) *General.* Four installations were used at station 7G to investigate the translation of fragments from windows mounted in open areas (see Figs. 6.68 and 6.84). Three of these used ordinary double-strength window glass placed 21.2, 11.2, and 6.2 ft from the trap, and the fourth used plate glass at a distance of 11.2 ft. Studies of the penetration of dogs by glass fragments were conducted by another project¹ at the two 11.2-ft installations. Natural-stone data were also obtained by all traps in this group.

(b) *Installation 7G6.* Figure 7G6 is a postshot view of the 7G6 traps. These traps were located 21.2 ft behind the window. Data for 221 fragments caught by the lower trap and 229 by the upper one are displayed in Figs. 6.92 and 6.93, respectively. Note that in each case the predicted-velocity line, which was computed under the assumption of no reflection, satisfactorily defines the upper limit of measured velocities. These results differ markedly from those from station 3G, especially for the traps placed inside houses where most of the velocities were above this line (e.g., see Fig. 6.41).

A few fragments at this installation struck the traps flat. It is quite probable that these missiles were oriented perpendicular to the wind during the entire trajectory from the window to the trap. A separate calibration (see Chap. 2) made for fragments impacting in this manner showed more reliability than did the general calibration for glass fragments. This was largely due to the elimination of the variable of orientation for the missiles that struck flat. Thus, for the reasons stated above, the velocities obtained for fragments that impacted flat could be expected to exhibit less variability than those for missiles that rotated during transit or after impact. Although the velocities for four flat-impact missiles caught at this location (plotted in Fig. 6.94) were fairly consistent with the predicted line, more consistent data were obtained at other locations at station 7G (discussed later in this section).

Data for natural-stone missiles caught at this installation are presented in Figs. 6.95 and 6.96. The number of missiles caught and their average velocities were lower than for the

*The designator for upper traps ends with "b" and for lower traps, with "a."

traps at stations 7G4 and 7G5 where windows were not present. One reason that fewer missiles were recovered from the traps behind the windows was "over saturation" of the absorber; i.e., velocity could not be determined for an object striking the absorber at the same location where another object had previously impacted. Too, it is possible that the window-frame installation afforded some shielding of the traps from natural-stone missiles originating at greater distances from the traps than that at which the window was placed.

(c) *Traps 7G7b and 7G8b.* Traps 7G7b and 7G8b, which were placed above dog traps (31.5 in. high), were located 11.2 ft behind glass installations—plate glass for trap 7G7b and window glass for trap 7G8b.

At the plate-glass installation, the absorber suffered extensive deformation from the flat impaction of large fragments. A postshot photograph was not made. However, the appearance of trap 7G7b was similar to that of the traps for installation 8P3 (shown in Fig. 4.86). Installation 7G8, which was located behind window glass, is shown in Fig. 6.97.

The data for the plate glass from trap 7G7b were divided into two groups: those for 28 fragments whose orientations in the absorber were random (Fig. 6.98) and those for 4 fragments impacting flat (Fig. 6.99). The larger sample of randomly oriented missiles showed considerable variation in velocity when compared to the smaller sample of missiles striking flat. For the group that impacted flat, the regression line passes very close to all four velocity points and is almost parallel to the predicted-velocity line. The measured velocities were about 8.7 per cent lower than those predicted. As shown by this chart (Fig. 6.99), both measured and predicted velocities are slightly higher for the larger fragments than are the corresponding velocities for the smaller missiles.

Velocities were determined for 127 fragments of window glass caught in trap 7G8b. These data, plotted in Fig. 6.100, show that the higher velocities conform roughly with the predicted line.

Data for natural stones caught in traps 7G7b and 7G8b are plotted in Figs. 6.101 and 6.102, respectively. Traps 7G7b and 7G8b were placed higher above the ground* than other stacked traps that were behind windows (7G6b and 7G9b). It is interesting to note that the traps placed higher above the ground recorded higher velocities for natural stones (compare Figs. 6.101 and 6.102 with Figs. 6.96 and 6.109).

(d) *Traps 7G9a and 7G9b.* The 7G9 window-glass installation† is shown in Fig. 6.103. The window and traps were 6.2 ft apart. Figure 6.104 depicts the condition of the traps after the detonation. Plant stems can be seen imbedded in the absorber and collected on the surface in front of the installation.

This installation was identical to 7G6 except for the distance between the window and the trap—21.2 ft for installation 7G6 and 6.2 ft for installation 7G9. A comparison of the results obtained from the two installations (see Figs. 6.105 and 6.106) indicates that the geometric mean velocities for the fragments traveling the greater distance were somewhat higher. This could be expected from theory.³ More missiles were caught at the greater distance, possibly because their higher velocities were more important than the increased spatial dispersion which also increased with distance. This argument depends on the observation that the percentage of a sample of a given missile caught in a trap depends on the average velocity at impact: missiles striking the trap at velocities less than the threshold velocity are not caught.

Another interesting comparison between installations 7G6 and 7G9 is that only 4 of 454 fragments struck the traps flat for the longer distance of translation (21.2 ft for installation 7G6), whereas 18 of 403 fragments did so for the shorter distance (6.2 ft for installation 7G9). The velocity data for the later missile sample presented in Fig. 6.107 indicates a close correspondence, in general, with the predicted velocities. The velocities measured for the larger fragments, however, were somewhat higher than predicted.

*At station 7G the "b" traps above the "A," or dog traps, were 31.5 in. above ground and those above "a" traps were 15 in. above ground.

†The window panes were painted different colors for the purpose of identification of the source. However, a separate analysis for different colored fragments was not made for this report.

Results obtained for natural stones at traps 7G9a and 7G9b are graphed in Figs. 6.108 and 6.109. Velocities for the ground-level trap were generally lower than for the other Trap.

6.5.5 Marked-gravel and Natural-stone Installation 7G10

The placement of marked gravel at this installation is indicated in Fig. 6.68. Figure 6.110 depicts the appearance of the two traps after the detonation. The frame that held the aluminum-foil thermal shield was left intact by the blast wave.

Results obtained for gravel placed 15.5 ft from the installation are presented in Figs. 6.111 and 6.112 for the lower and upper traps, respectively. For the lower trap the velocity predicted for stones with masses equal to that of the geometric mean, 302 mg, is 169 ft/sec (refer to Table 6.2). The measured geometric mean velocity, however, was only 113 ft/sec—33 per cent lower than that predicted. A corresponding comparison for the upper trap indicates that the geometric mean of measured velocities was 22 per cent lower than predicted. Gravel placed at 39.5 ft was caught in significant numbers only in the upper trap (Fig. 6.113). As in the previous instances, measured velocities proved to be lower than those predicted (about 24 per cent).

Since the gravel experiment at installation 7G10 was practically identical to that at station 7GTS, a comparison of the results obtained at the two locations is appropriate. For each of the gravel samples at station 7GTS, the geometric mean velocity was only 13 per cent lower than the velocity predicted compared to 33 and 22 per cent quoted in the last paragraph for 7G10 traps. One reason for this discrepancy is illustrated by a comparison of the data in Fig. 6.112 with those in Fig. 6.59. The type II absorber used at installation 7G10 caught lower velocity missiles than did the more dense absorber, III, used at station 7GTS. On the other hand, the higher velocity missiles represented on these charts are in good agreement. Thus the greater spread in velocities to the low side resulted in a lower geometric mean for installation 7G10 than for station 7GTS.

Velocities for 51 natural stones caught in trap 7G10a and for 133 caught in trap 7G10b are plotted in Figs. 6.114 and 6.115, respectively. In agreement with other natural-stone samples caught at this station, the predicted velocities made for gravel defines with reasonable accuracy the upper limit for the velocities measured.

6.6 ANALYSIS OF COMBINED DATA FROM STATIONS 7G AND 7GTS

Since the blast conditions at stations 7G and 7GTS were about the same, analyses were made of combined data for gravel obtained at the two locations. The results for gravel translated 15.5 and 39.5 ft are given in Table 6.2 but are not presented in graphical form.

Natural-stone data were obtained from every trap at station 7G except those at the 7G1 installation, which were made unusable by impactation of blocks from the wall. The results of an analysis for these missiles (1139) are recorded in Table 6.2.

6.7 SUMMARY AND DISCUSSION, SHOT GALILEO

6.7.1 Blast Parameters

The production of secondary missiles by a nuclear-produced blast wave was studied at four stations placed at three different ranges from GZ. Station designators, ranges, and pertinent blast-wave parameters are given in Table 6.1, page 340. Interpolated figures are recorded for station 4.3GTS since no blast measurements were made at this range. The interpolation equations used were of the same form used in the regression analysis of the Priscilla and Smoky blast data. The method for obtaining computed values of peak overpressure, $(p_s)_c$, was discussed in Chap. 3. For station 4.3GTS, where blast measurements were not available, $(p_s)_c$ was obtained from interpolated values of overpressure impulse, $(I_p)_r$, and overpressure duration, $(t_p^+)_r$. The computed values of maximum overpressure were 3.85, 5.32, and 8.38 psi for ranges of 4700, 3750, and 2750 ft, respectively.

Assuming that shot Galileo* could be characterized as the "typical air burst" described in *Effects of Nuclear Weapons*,⁵ the yield was estimated to be 11 kt (using the blast data tabulated for stations 3G and 7G).

6.7.2 Tabulated Results

A summary of all data obtained for shot Galileo except that for the concrete-block wall (Sec. 6.5.2) is given in Table 6.2.†

Since more than one type of missile was caught at many of the installations, the same trap may be listed at several locations in the table.

6.7.3 Station 3G, 4700-ft Range

An attempt was made at this station to record the velocities of marked gravel, natural stones, and various types of spheres. However, only 1 sphere ($\frac{1}{8}$ -in.-diameter steel), 10 pieces of gravel, and 3 natural stones were trapped. The "catch" was low because of insufficient impact velocity to cause effective penetration.‡ It was observed that the stones that remained in the absorber did so because they happened to strike the trap with a sharp point or edge forward. The average velocities evaluated for samples biased in this manner were too high since the absorbers were calibrated for random orientations at impact.

The translation of fragments from windows was investigated at station 3G by mounting windows in open regions and by using conventional windows in two houses. Double-strength window glass ($\frac{1}{8}$ in. thick) was used at all locations except for one outside the installation; $\frac{1}{4}$ -in.-thick plate glass was used at this location. Impact velocities were obtained at station 3G for a total of 2603 glass fragments: 2523 of these were caught in the houses by 14 traps placed, facing GZ, about 10 ft from windows; 73 were caught in 3 traps behind window installations in open areas; and 7 were from the plate-glass installation mounted in an open area.

It was noted that the double-strength glass mounted in open areas produced much larger (M_{50} ranged from 1.44 to 3.69 g) but fewer missiles than did the same type of glass used in the conventional manner in houses (M_{50} ranged from 0.227 to 0.557 g). The impact velocities, however, were generally higher in the houses than in the open regions.

For both types of installations the measured velocities were higher than those which could be explained by the usual method for predicting velocities of secondary missiles. It was found that velocities for most of the fragments were between the values predicted by the usual method and those predicted assuming the maximum overpressure to be equal to the reflected value of the incident maximum overpressure.

6.7.4 Station 4.3GTS, 3750-ft Range

This station consisted of one large trap constructed by cementing a 2-in. layer of absorber on the GZ side of a cubical structure. The missile-collecting area was 7 ft wide and 7 ft high (see Fig. 6.45). Marked gravel and spheres were placed 11.4 and 29.2 ft in front of the trap.

Velocities were obtained for 765 missiles at this location— 161 pieces of marked gravel, 586 natural stones, and 18 spheres. In general, the measured and predicted velocities were in good agreement for the gravel and natural stones. The average velocity of the largest sample of spheres (14 soda-glass spheres) caught, however, was 29 per cent higher than the predicted velocity. This discrepancy was probably due to the relatively high threshold velocity of the absorber, i.e., spheres of lower velocity may have struck the trap but were not caught because of insufficient penetration.

6.7.5 Station 7GTS, 2750-ft Range

The missile trap used at this station was similar to station 4.3GTS. Marked gravel and spheres were placed 15.5 and 39.5 ft from the trap. Impact velocities were determined for 336

*Burst height was 500 ft.

†See Table 2.1 for description of absorber types.

‡See discussion of threshold velocities in Sec. 2.5.

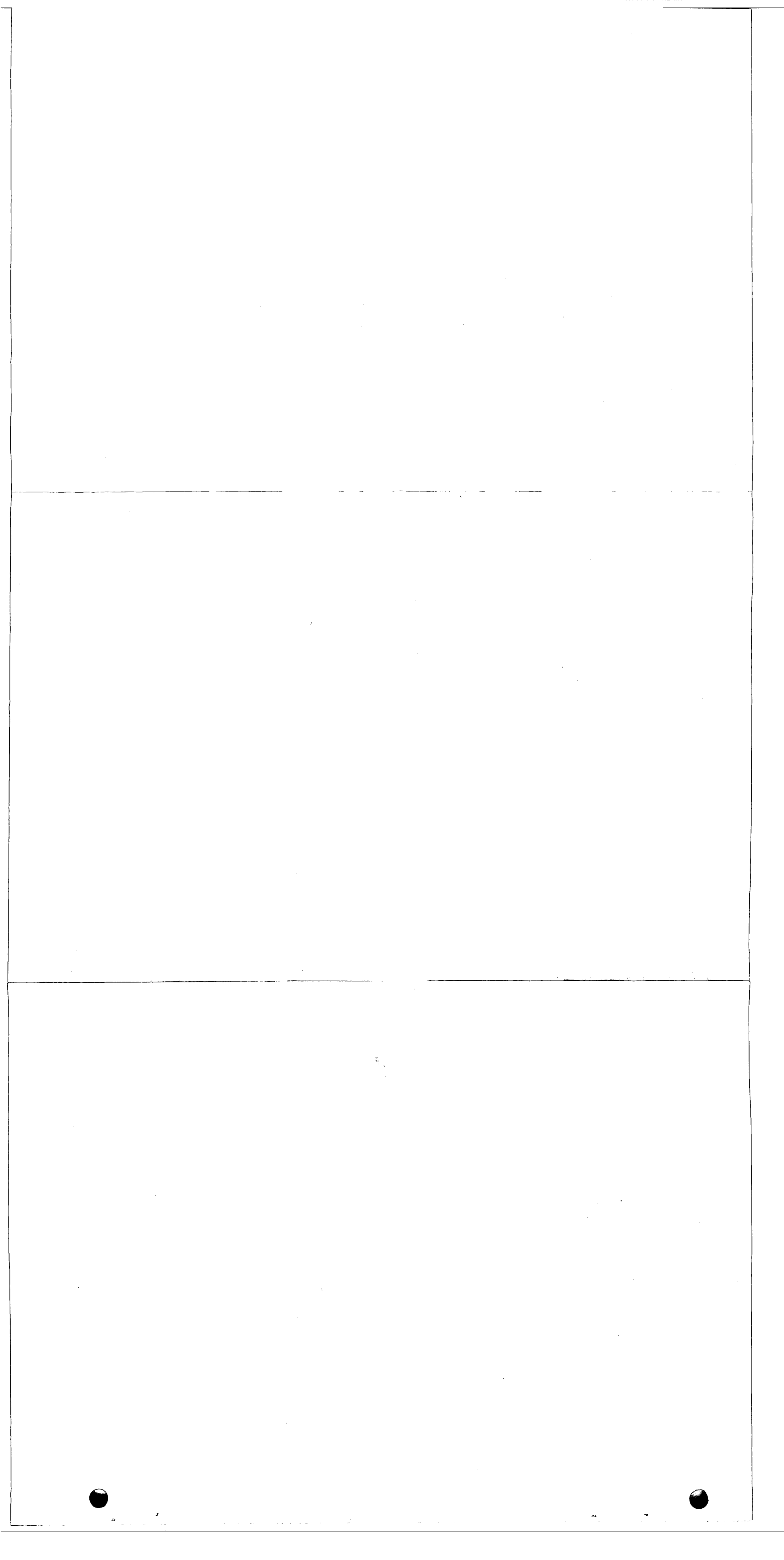
TABLE 6.2—SUMMARY OF RESULTS, SHOT GALILEO
(See List of Symbols)

Regression Equation: $\log v = a + b \log m$

Missile	Trap	Absorber type*	d	n	\bar{D}_s	a	b	E_{gv}	V_{p50}	$(V_{p50})_R$	V_{50}	\bar{V}	S_{gv}	V_-	V_+	M_{50}	\bar{M}	S_{gm}	M_-	M_+
WG	3G6	I	4.6	42	11.9	2.0540	0.0097	1.21	66	152	122	123	1.21	84.1	168	1440	2066	2.46	178	8913
WG	3G8b	II	10.9	15	5.4	2.7679	-0.2300	1.32	86	200	96	100	1.37	53.1	150	2620	3245	2.06	563	7317
WG	3G9	I	19.5	16	4.6	2.0453	-0.0079	1.21	92	224	104	106	1.20	66.9	150	3692	5018	2.31	604	16530
PG	3G7	I	9.6	7	2.0	2.2374	-0.0631	1.26	63	162	104	107	1.26	84.1	168	2965	7372	4.54	214	28494
WGH	3G10a	I	10.0	70	19.9	2.1173	0.0172	1.20	77	187	145	147	1.21	84.1	237	333	615	3.05	44.7	3548
WGH	3G10b	I	10.0	240	68.3	2.1278	0.0150	1.16	78	188	146	148	1.16	106	266	314	538	2.73	35.5	5623
WGH	3G10c	I	10.0	134	38.1	2.0297	0.0497	1.21	77	186	144	147	1.22	84.1	266	404	769	2.80	35.5	8913
WGH	3G11a	I	10.0	164	46.6	2.1153	0.0136	1.21	78	188	141	143	1.21	84.1	211	303	567	3.07	17.8	8913
WGH	3G11b	I	10.0	336	95.6	2.0923	0.0104	1.19	78	189	131	133	1.20	84.1	237	236	545	3.73	11.2	8913
WGH	3G11d	I	10.0	278	79.1	2.0628	0.0337	1.18	77	187	141	143	1.19	84.1	211	355	644	3.00	22.4	5623
WGH	3G11e	I	10.0	169	48.1	2.2480	-0.0435	1.20	78	189	140	142	1.20	84.1	237	227	454	3.28	35.5	4467
WGH	3G12a	I	10.7	74	21.1	2.0902	0.0127	1.19	79	190	132	134	1.18	94.4	188	299	614	3.09	28.2	7079
WGH	3G12b	I	10.7	228	64.8	2.0791	0.0320	1.19	78	189	145	148	1.20	94.4	266	383	665	2.71	56.2	8913
WGH	3G12c	I	10.7	123	35.0	2.1055	0.0201	1.24	78	188	144	148	1.24	75.0	237	495	886	2.88	35.5	7079
WGH	3G13a	I	10.7	196	55.7	2.0258	0.0405	1.19	79	190	133	136	1.19	84.1	237	281	544	3.02	17.8	8913
WGH	3G13b	I	10.7	150	42.7	2.0638	0.0268	1.19	79	190	134	136	1.19	84.1	211	252	527	3.19	17.8	8913
WGH	3G13d	I	10.7	207	58.9	2.1197	0.0124	1.18	79	189	142	144	1.18	94.4	237	328	651	3.19	17.8	7079
WGH	3G13e	I	10.7	154	43.8	2.0971	0.0221	1.20	78	188	144	146	1.20	94.4	237	557	970	2.82	44.7	7079
WGH	Comb ⁽¹⁾ 3G	I	10.3	2523	51.3	2.0913	0.0216	1.20	78	188	140	142	1.20	75.0	266	321	628	3.16	11.2	8913
Gr	3G4	I	8.0	6	2.2				62					83.3	145		326		162	597
Gr	3G1	I	22.5	4	1.4				67					113	150		201		71.2	306
NS	3G1, 3G4	I		3	0.5				123					150	203		54.8		9.8	136
Gr	4.3GTS	II	11.4	16	0.3	2.5852	-0.2323	1.14	107		115	120	1.31	88.0	204	182	269	2.81	13.6	1227
Gr	4.3GTS	II	29.2	145	3.0	2.5803	-0.2227	1.13	109		108	110	1.23	73.5	187	288	394	2.19	54.9	3190
NS	4.3GTS	II		586	12.0	2.4969	-0.1691	1.12	180		172	176	1.29	75.0	266	35.2	68.5	2.69	11.2	1000
WG	7G6a	II	21.2	221	80.2	2.2117	-0.0248	1.19	202		141	143	1.19	84.1	211	323	776	2.94	28.2	8913
WG	7G6b	II	21.2	229	83.2	2.2502	-0.0234	1.15	202		155	156	1.15	106	237	355	643	2.65	35.5	8913
WG	7G8b	II	11.2	127	46.1	2.2133	-0.0220	1.18	180		142	143	1.19	75.0	237	604	1560	3.43	44.7	44670
WG	7G9a	II	6.2	192	69.7	2.1827	-0.0211	1.17	157		134	136	1.18	75.0	211	442	1177	3.45	44.7	28180
WG	7G9b	II	6.2	193	70.1	2.2084	-0.0304	1.18	157		134	136	1.18	75.0	211	454	990	3.30	28.2	14130
FWG	7G6a,b	II	21.2	4	0.7	1.7958	0.1253	1.04	218		199	200	1.12	176	237	10387	14528	2.30	3082	33290
FWG	7G9a,b	II	6.2	18	6.5	1.9735	0.0675	1.05	170		170	170	1.07	146	189	6223	8428	2.28	791	23858

Missile	Trap	Absorber type*	d	n	\bar{D}_s	a	b	E_{gv}	V_{p50}	$(V_{p50})_R$	V_{50}	\bar{V}	S_{gv}	V_-	V_+	M_{50}	\bar{M}	S_{gm}	M_-	M_+
PG	7G7b	II	11.2	28	10.2	2.2144	-0.0459	1.22	152		118	121	1.23	75.0	188	1189	4126	5.07	112	28180
FPG	7G7b	II	11.2	4	1.4	2.0829	0.0161	1.00	161		147	147	1.02	142	150	151 ⁽²⁾	280 ⁽²⁾	1.36	24.8	596 ⁽²⁾
Gr	7G10a	II	15.5	51	18.5	2.7053	-0.2634	1.14		169	113	115	1.23	82.0	195	302	363	1.85	11.0	1215
Gr	7G10b	II	15.5	117	42.5	2.5716	-0.1828	1.13		173	135	138	1.20	94.0	210	255	334	2.14	37.5	1516
Gr	7GTS	III	15.5	42	0.8	2.4966	-0.1318	1.12		175	153	154	1.16	111	222	236	306	2.07	41.1	1451
Gr	Comb ⁽³⁾		15.5	210	3.8	2.6084	-0.2009	1.16		172	133	136	1.23	82.0	222	261	336	2.06	37.5	1516
Gr	7G10a	II	39.5	4	1.4				184		116	118	1.24	96.0	162	296	357	1.82	162	730
Gr	7G10b	II	39.5	18	6.5	2.5056	-0.1462	1.14		197	149	150	1.16	113	182	190	233	1.89	77.9	556
Gr	7GTS	III	39.5	294	5.8	2.5533	-0.1397	1.14		190	166	167	1.18	107	317	239	311	2.11	18.8	1184
Gr	Comb ⁽⁴⁾		39.5	316	5.7	2.5461	-0.1389	1.15		191	165	165	1.19	96.0	317	237	307	2.09	18.8	1184
NS	7G2a	II		26	9.4	2.4759	-0.1489	1.10	280	238	169	172	1.20	107	243	45.7	96.4	2.90	11.3	808
NS	7G2b	II		38	13.8	2.5761	-0.1926	1.12	283	245	189	194	1.26	105	249	35.9	101	2.87	12.4	1999
NS	7G3b	II		31	11.3	2.5407	-0.1592	1.09	284	246	198	200	1.16	143	277	34.6	46.3	2.11	11.2	171
NS	7G4a	II		73	26.5	2.5126	-0.1730	1.11	277	235	164	168	1.26	88.9	256	53.1	158	3.36	10.2	3079
NS	7G4b	II		244	88.6	2.5393	-0.1660	1.14	281	244	190	194	1.24	90.7	289	36.9	70.8	2.71	10.0	1671
NS	7G5a	II		54	19.6	2.5215	-0.1893	1.11	272	228	148	151	1.24	91.7	238	71.5	127	2.63	10.9	1640
NS	7G5b	II		236	85.7	2.5609	-0.1826	1.14	277	236	178	183	1.26	63.9	283	49.8	104	2.73	10.6	3262
NS	7G6a	II		26	9.4	2.5112	-0.1729	1.11	264	215	143	146	1.25	94.0	245	116	248	3.19	12.8	2096
NS	7G6b	II		30	10.9	2.4875	-0.1441	1.12	265	216	156	158	1.18	103	213	112	154	2.27	19.2	602
NS	7G7b	II		101	36.7	2.5475	-0.1608	1.16	282	245	198	202	1.23	87.4	292	36.3	65.0	2.56	10.1	764
NS	7G8b	II		29	10.5	2.4335	-0.0954	1.16	273	228	182	184	1.19	117	240	67.2	108	2.62	11.0	575
NS	7G9a	II		42	15.2	2.4539	-0.1479	1.12	261	208	137	140	1.22	100	206	140	282	3.00	19.2	2222
NS	7G9b	II		25	9.1	2.4198	-0.1138	1.22	261	208	150	153	1.26	68.5	204	141	324	3.43	19.7	2271
NS	7G10a	II		51	18.5	2.4807	-0.1590	1.14	272	226	153	157	1.27	87.3	222	73.3	176	3.39	10.6	2004
NS	7G10b	II		133	48.3	2.5193	-0.1471	1.16	276	233	183	187	1.24	91.1	265	56.6	116	3.00	10.0	1468
NS	7GTS	III		1238	24.6	2.5314	-0.1201	1.17	280	241	218	222	1.21	92.5	422	40.5	76.5	2.67	11.2	2240
NS	Comb ⁽⁵⁾ 7G			1139	27.6	2.5419	-0.1727	1.15	278	235	176	181	1.27	63.9	292	52.2	117	3.40	10.0	3262

Missile	Trap	Absorber type*	n, d ⁽⁶⁾	n	\bar{h}_z ⁽⁷⁾	V_{p50}	$\Delta V\%$ ⁽⁸⁾	\bar{V}	S_v	V_-	V_+	\bar{M}	S_m	M_-	M_+	$\bar{\alpha}$
St 1/8	3G4	I	1, 22.5	1		38	+128.9	87				130.8				0.1389
Al 1/8	4.3GTS	II	2, 29.2	2	13.6	107	+11.2	119	8.5	113	125	47.34				0.3839
Al 3/16	4.3GTS	II	1, 29.2	1	12.9	89	+27.0	113				153.7				0.2660
Gx	4.3GTS	II	1, 11.4	1	23.1	85	+35.2	115				231				0.240
Gs	4.3GTS	II	14, 29.2	14	30.6	112	+29.5	145	4.5	138	152	39.8	4.3	31.7	48.7	0.435
Ny 1/8	7G4a, b	II	5, 15.5	9	17.7	224	+5.4	236	11.7	222	259	19.73				0.9210
	7G5b	II	4, 39.5			240	-1.7									
Al 1/8	7G4a, b	II	5,													



pieces of gravel, 1238 natural stones, and 29 spheres—a total of 1603 missiles. In general, the correspondence of measured velocities with those predicted was good; e.g., the geometric mean velocity for 294 pieces of gravel displaced 39.5 ft was 166 ft/sec—12.6 per cent lower than the predicted velocity.

6.7.6 Station 7G, 2750-ft Range

Experimental studies at station 7G involved the translation of (1) debris from a concrete-block wall, 40 ft long and 64 in. high, (2) marked spheres and gravel, (3) fragments from windows mounted in open areas, and (4) natural stones.

Trap installations were placed 10.2, 20.2, and 40.2 ft behind the concrete-block wall mentioned above. The absorber in the traps at the 10.2-ft installation was ruined by the impaction of blocks and block fragments. Natural stones (no block fragments) were retrieved from the traps at the other installations. Final resting positions were determined for 1528 wall fragments whose weights ranged from 0.1 to more than 100 lb (multiple blocks). The greatest downwind displacement measured for a whole block (about 34 lb) was 403 ft. Fifty per cent of the whole and multiple blocks was found more than 38 ft from the original position of the wall. Spatial-distribution charts were prepared which illustrate the dispersion of the wall fragments crosswind as well as downwind.

Velocities were determined for 1016 fragments from four windows (one plate glass) mounted in open areas 6.2 to 21.2 ft from the trap installations. The higher velocities measured were adequately explained by the velocities predicted, using the incident maximum overpressure (8.38 psi). Velocities for 26 fragments that struck the absorber flat were, in general, only slightly less than those predicted.

Data for 1139 natural stones were obtained from 15 traps at station 7G. Two traps caught 190 pieces of gravel. Most of the measured velocities for stone (including gravel) were about the same as, or less than, those predicted.

One hundred and ninety-six spheres were caught by four traps. The largest sample of a particular type of sphere consisted of 47 small soda-glass spheres with an average mass of 41 mg. The average measured velocity for these spheres was 166 ft/sec, 10.3 per cent less than the predicted velocity of 185 ft/sec.

REFERENCES

1. V. C. Goldizen, D. R. Richmond, T. L. Chiffelle, I. G. Bowen, and C. S. White, *Missile Studies with a Biological Target, Operation Plumbbob Report, WT-1470, Jan. 23, 1961.*
2. I. G. Bowen, A. F. Strehler, and M. B. Wetherbe, *Distribution and Density of Missiles from Nuclear Explosions, Operation Teapot Report, WT-1168, December 1956.*
3. I. G. Bowen, R. W. Albright, E. R. Fletcher, and C. S. White, *A Model Designed to Predict the Motion of Objects Translated by Classical Blast Waves, USAEC Report CEX-58.9, June 29, 1961.*
4. E. R. Fletcher, R. W. Albright, V. C. Goldizen, and I. G. Bowen, *Determinations of Aerodynamic-drag Parameters of Small Irregular Objects by Means of Drop Tests, USAEC Report CEX-59.14, October 1961.*
5. Samuel Glasstone (Ed.), *The Effects of Nuclear Weapons*, Superintendent of Documents, U. S. Government Printing Office, Washington 25, D. C., June 1957.

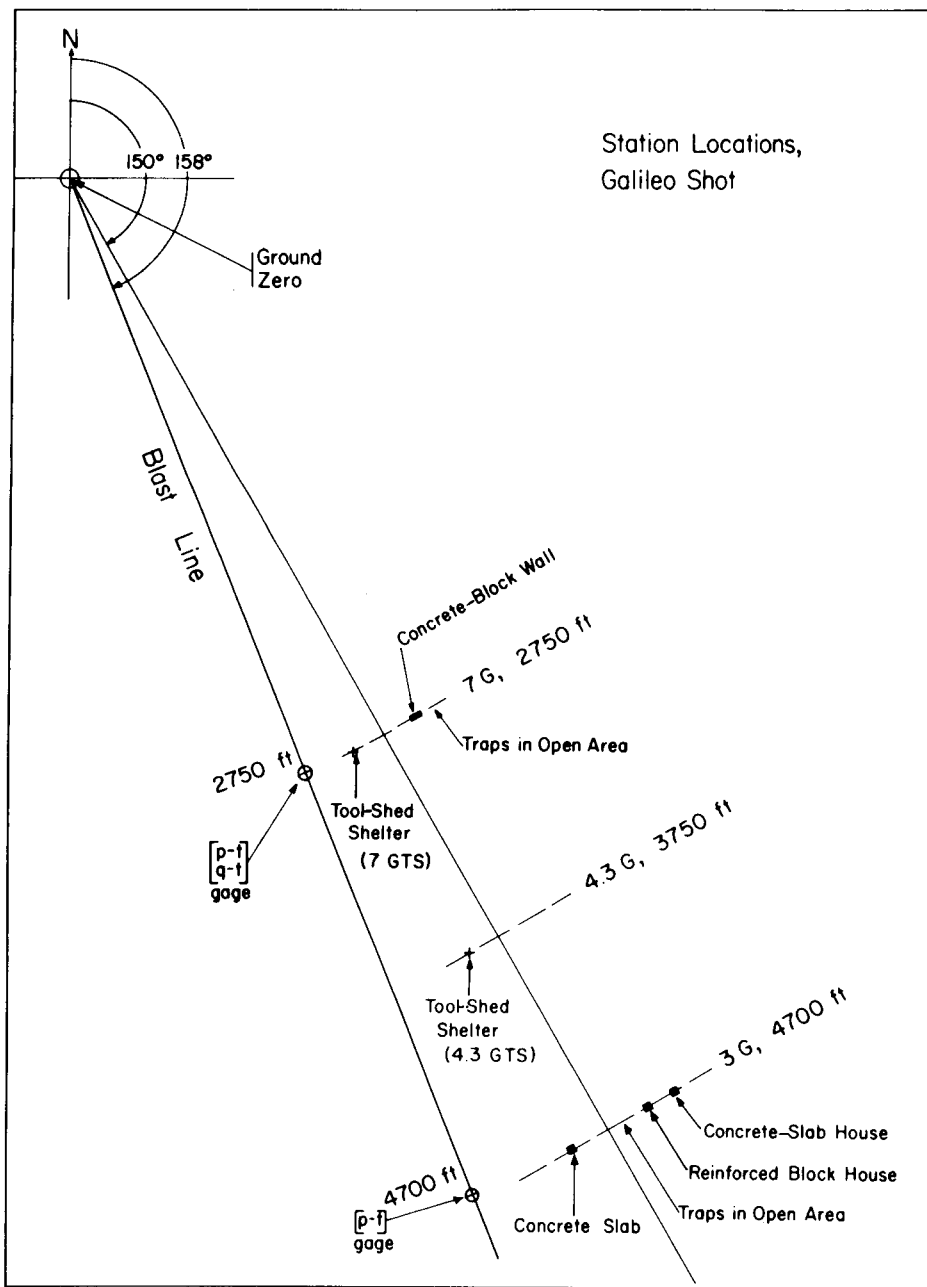


Fig. 6.1—Station locations for shot Galileo in Area 1, NTS.

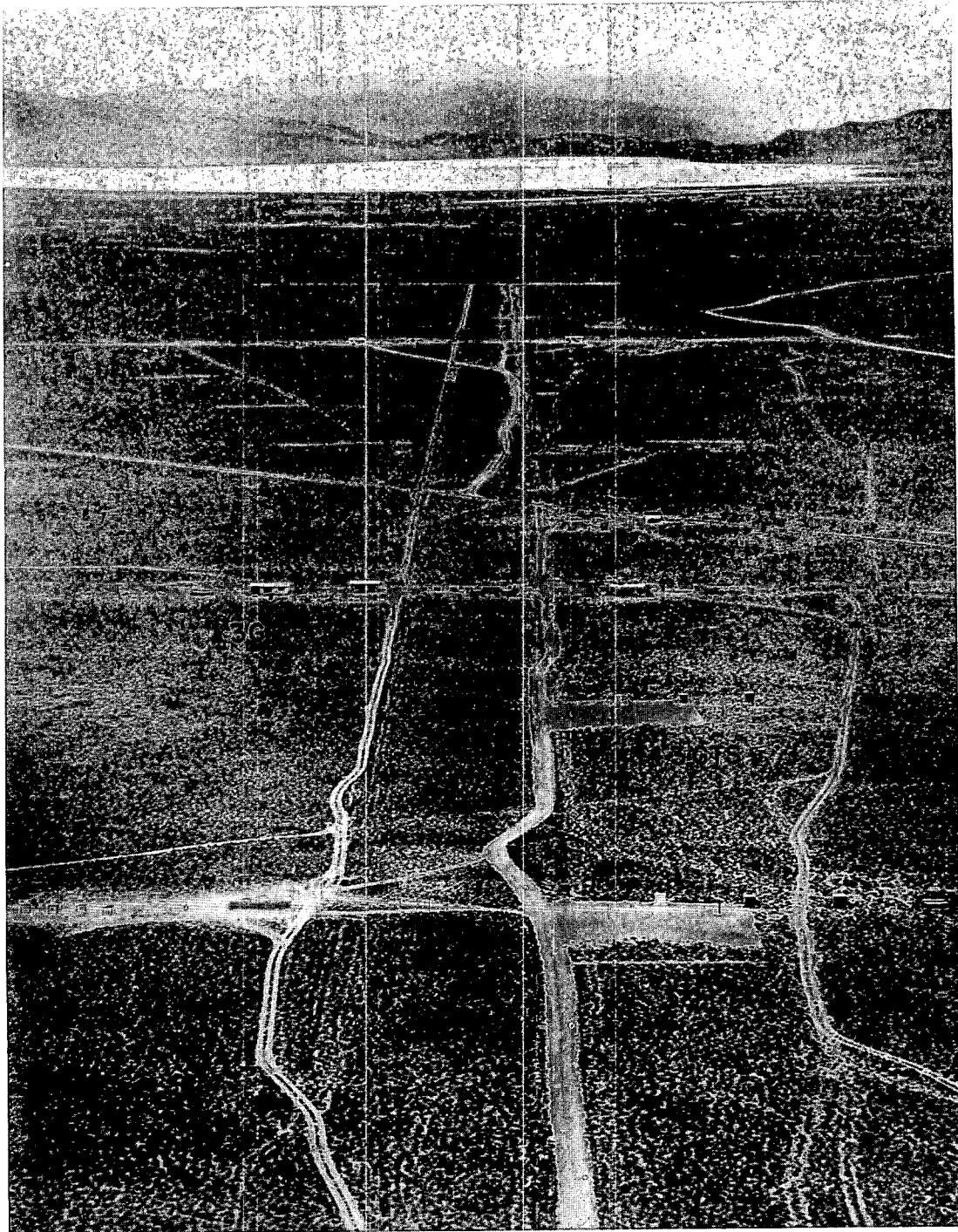


Fig. 6.2— Photograph of Galileo installations taken from the 500-ft tower at GZ. Dry lake bed can be seen in the background.

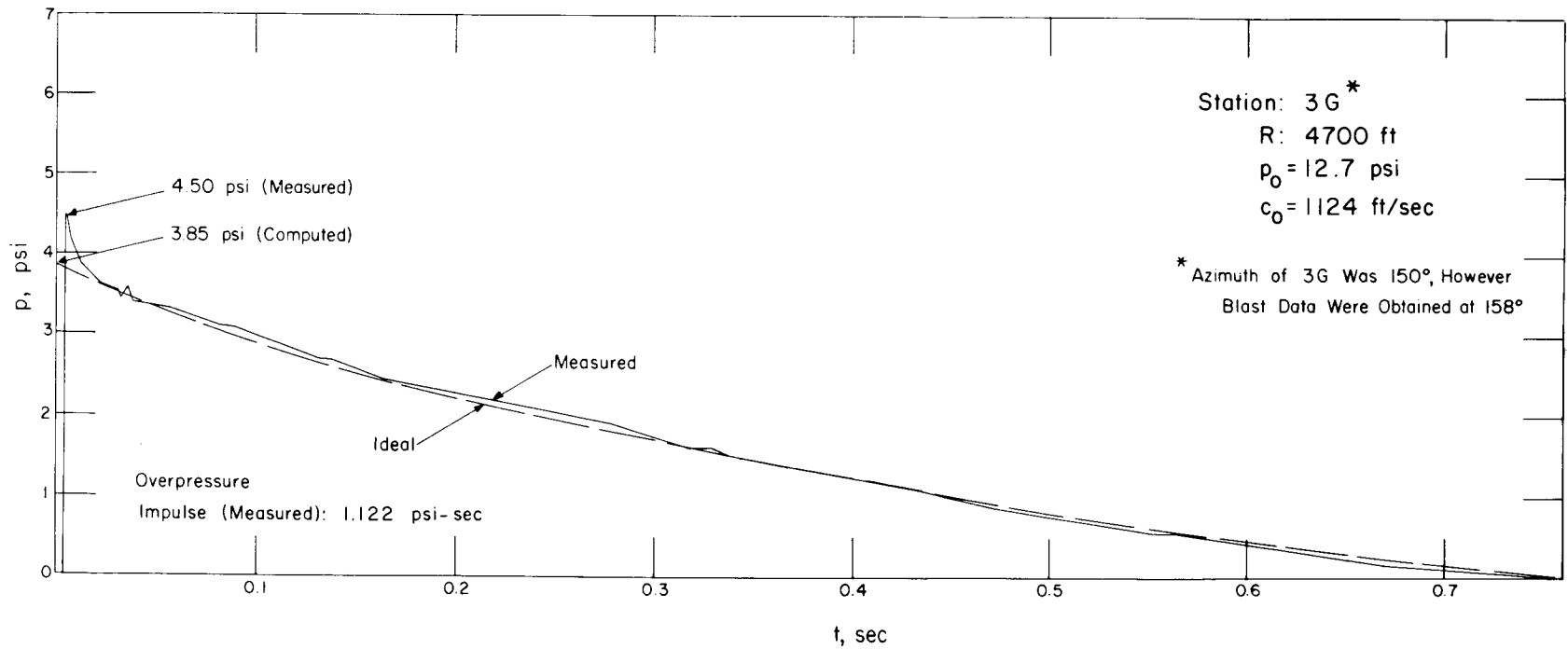


Fig. 6.3—Overpressure vs. time at station 3G.

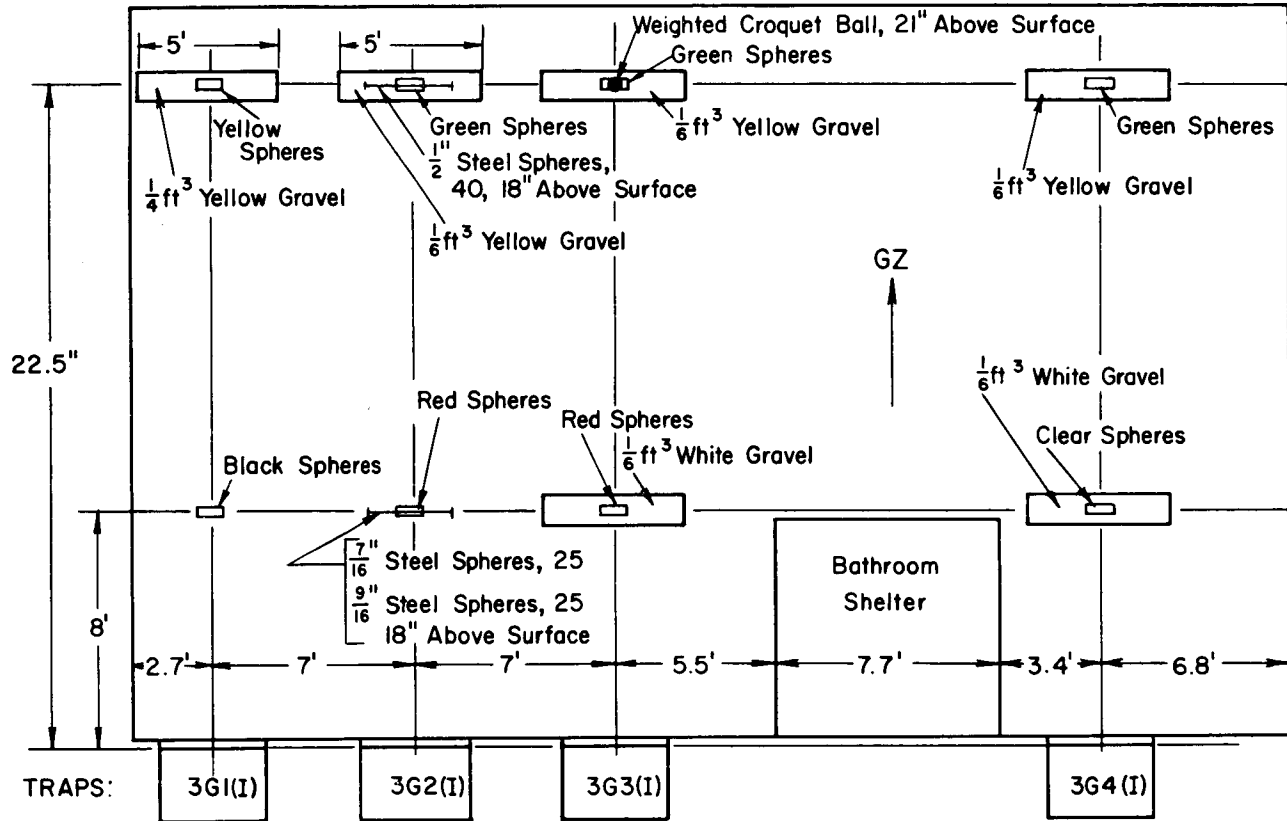


Fig. 6.4—Layout chart for installations 3G1, 3G2, 3G3, and 3G4. The level of the missile bases is 3 in. below slab height; the bathroom shelter is 8 ft high. Roman numeral in parentheses designates type of missile absorber.

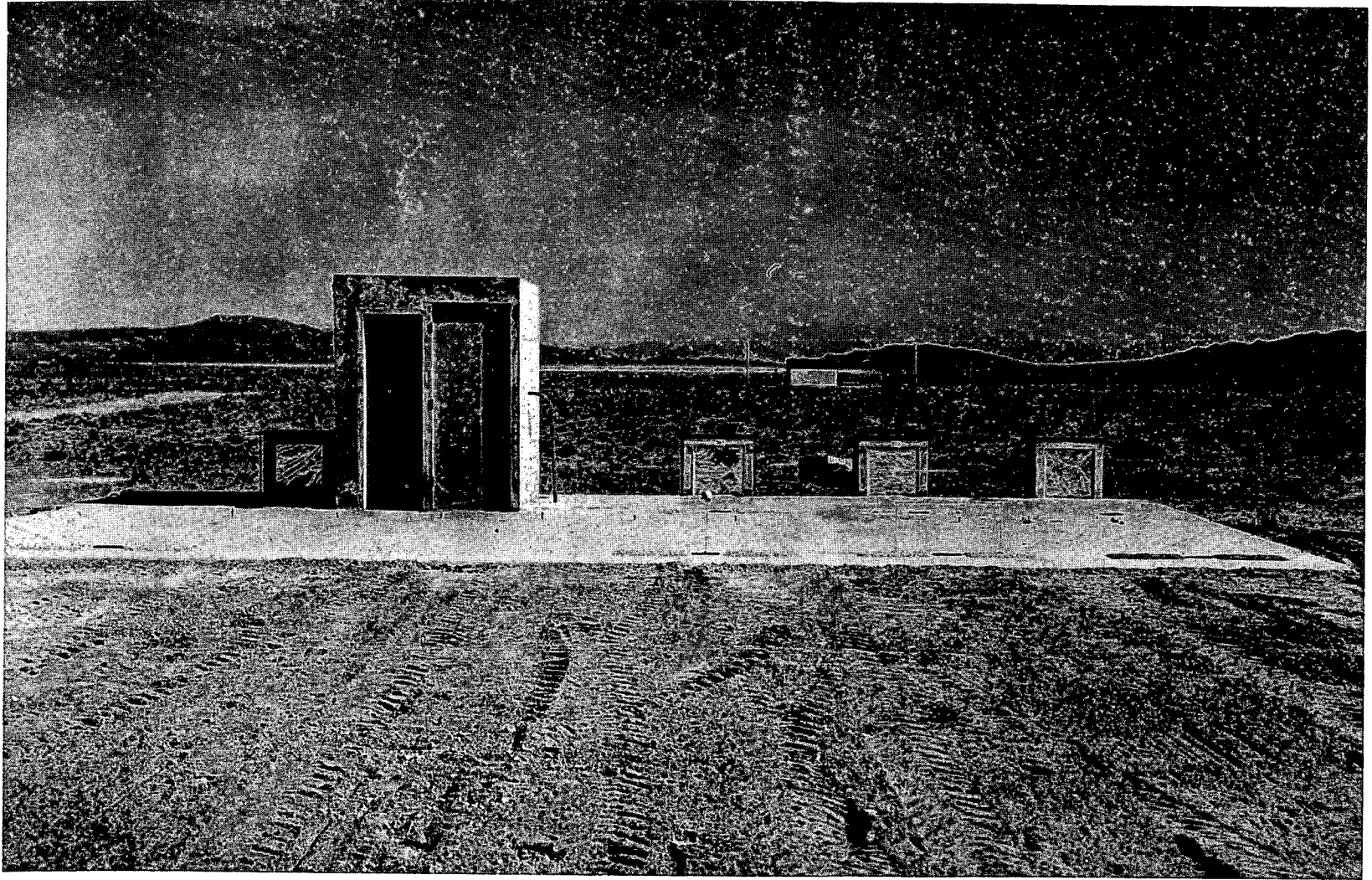


Fig. 6.5—Preshot view of installations 3G1, 3G2, 3G3, and 3G4 (from right to left). The concrete pad and bathroom shelter were remains of a rambler house that was used in Operation Teapot.

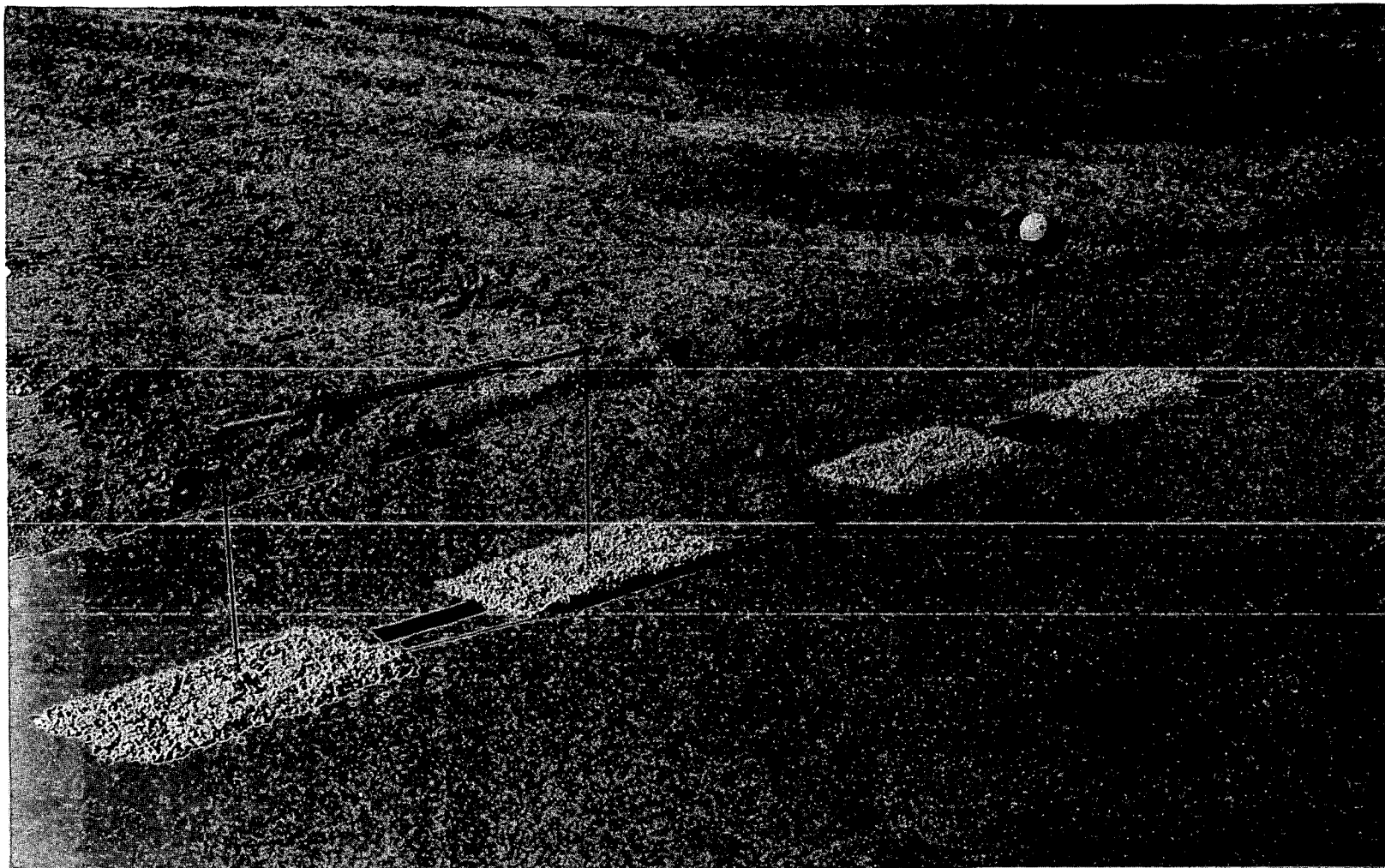


Fig. 6.6—Missiles that were set out 22.5 ft in front of installations 3G2 and 3G3. Large steel spheres can be seen on the trough-like support on the left. The support on the right holds a weighted croquet ball. Piles of marked gravel and packets of spheres are on the concrete surface.

362

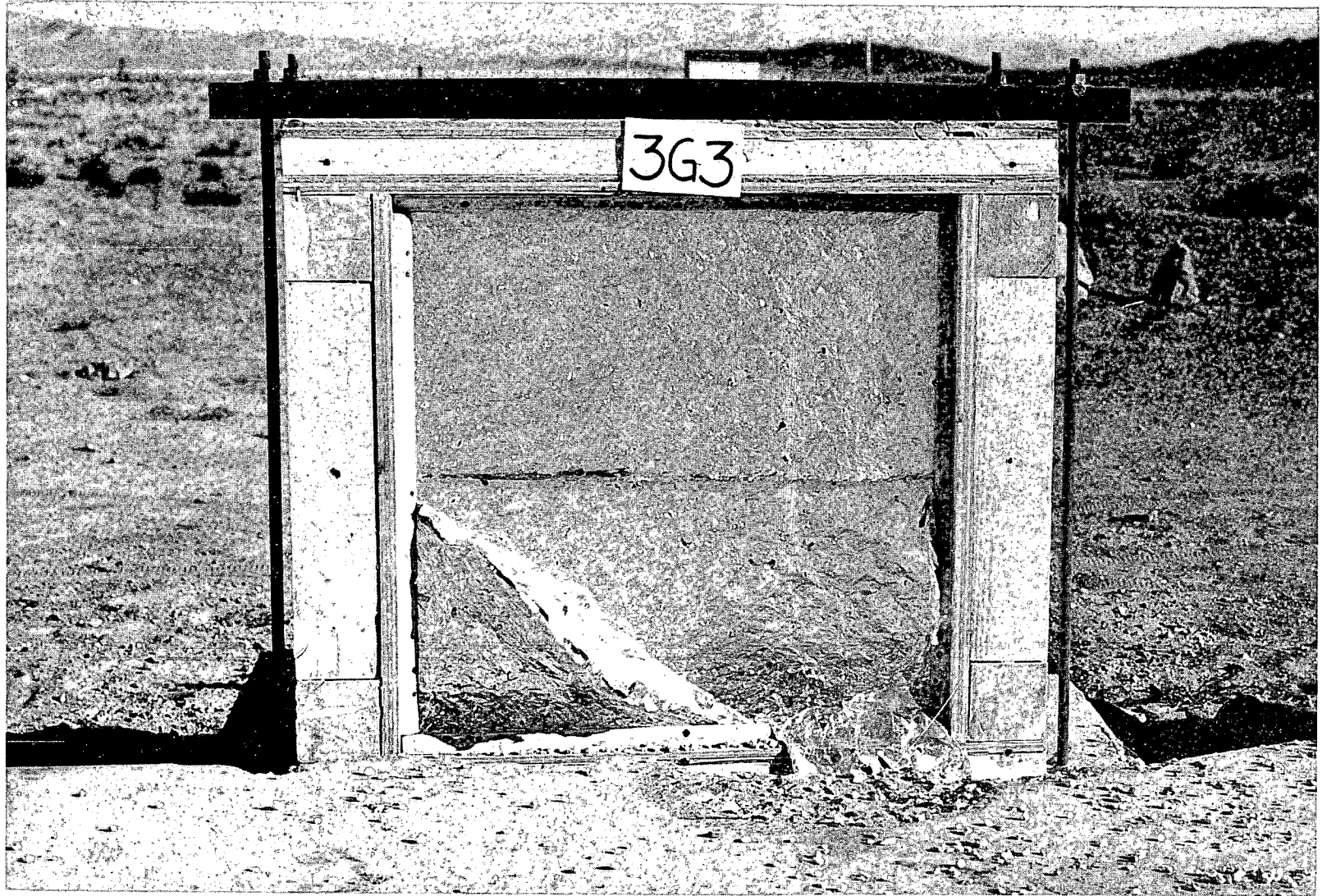
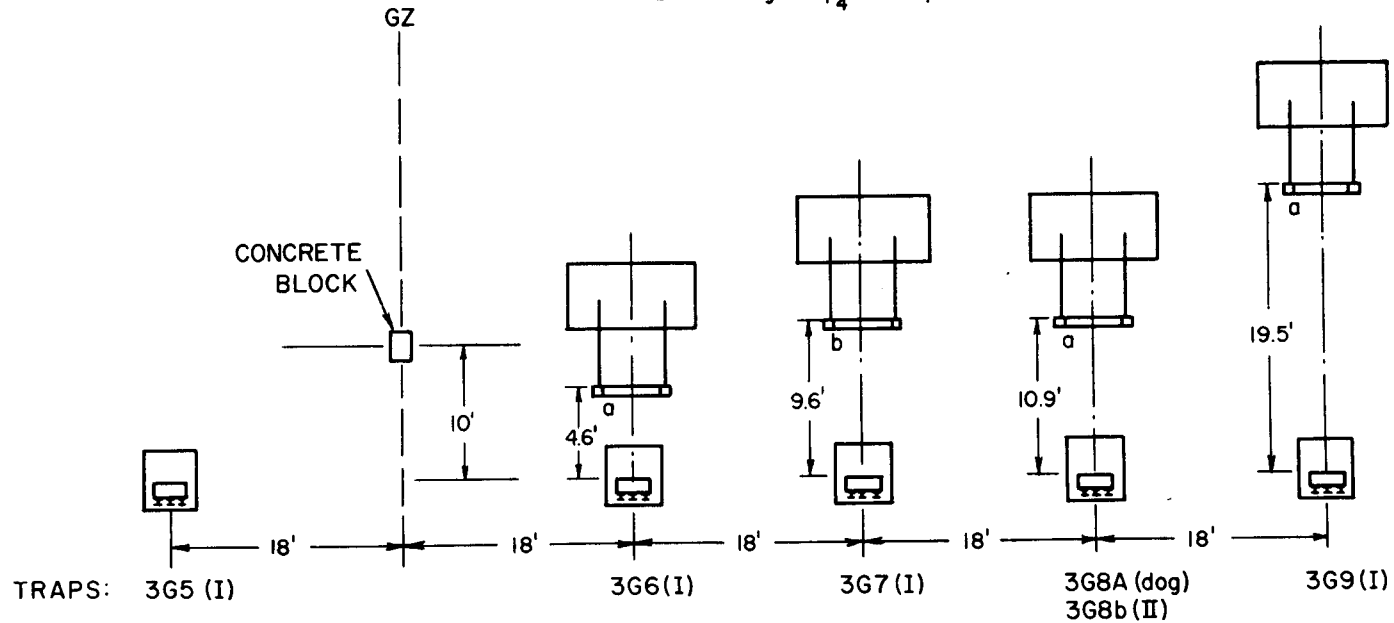


Fig. 6.7—Installation 3G3, postshot. Note marked gravel scattered in front of the trap.

STATION 3G
 Installations 3G5-3G9
 RANGE: 4700

a—Window glass, $\frac{1}{8}$ " thick, framed and mounted
 b—Plate glass, $\frac{1}{4}$ " thick, framed and mounted

363



Roman numeral in parenthesis designates type of missile absorber

Fig. 6.8—Layout chart for installations 3G5, 3G6, 3G7, 3G8b, and 3G9. Trap 3G8b is stacked above 3G8A.

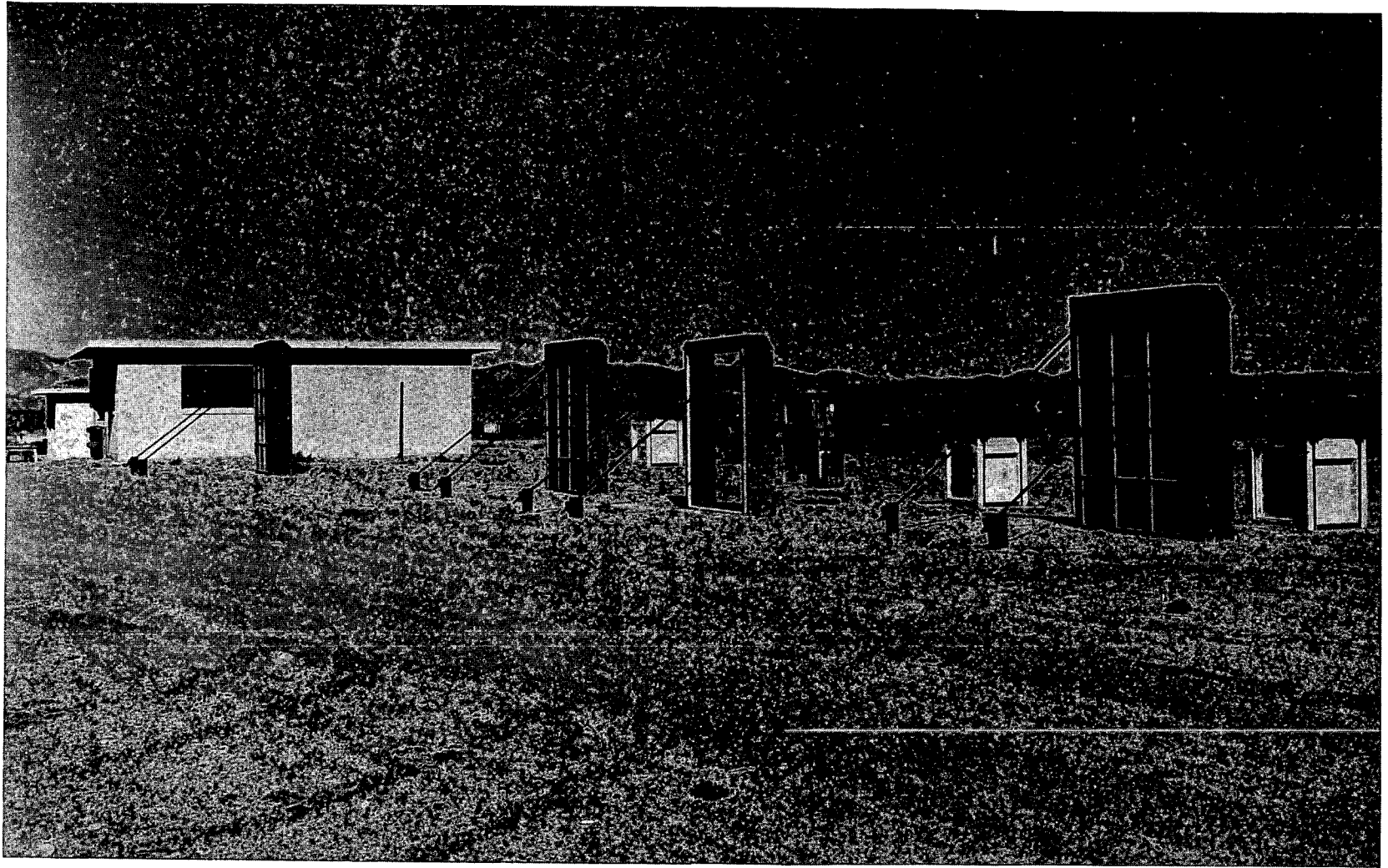


Fig. 6.9—Preshot view of installations 3G6, 3G7, 3G8b, and 3G9. The reinforced-block house in which trap installations 3G10 and 3G11 were located and a corner of the precast-concrete house in which 3G12 and 3G13 were located are also shown.

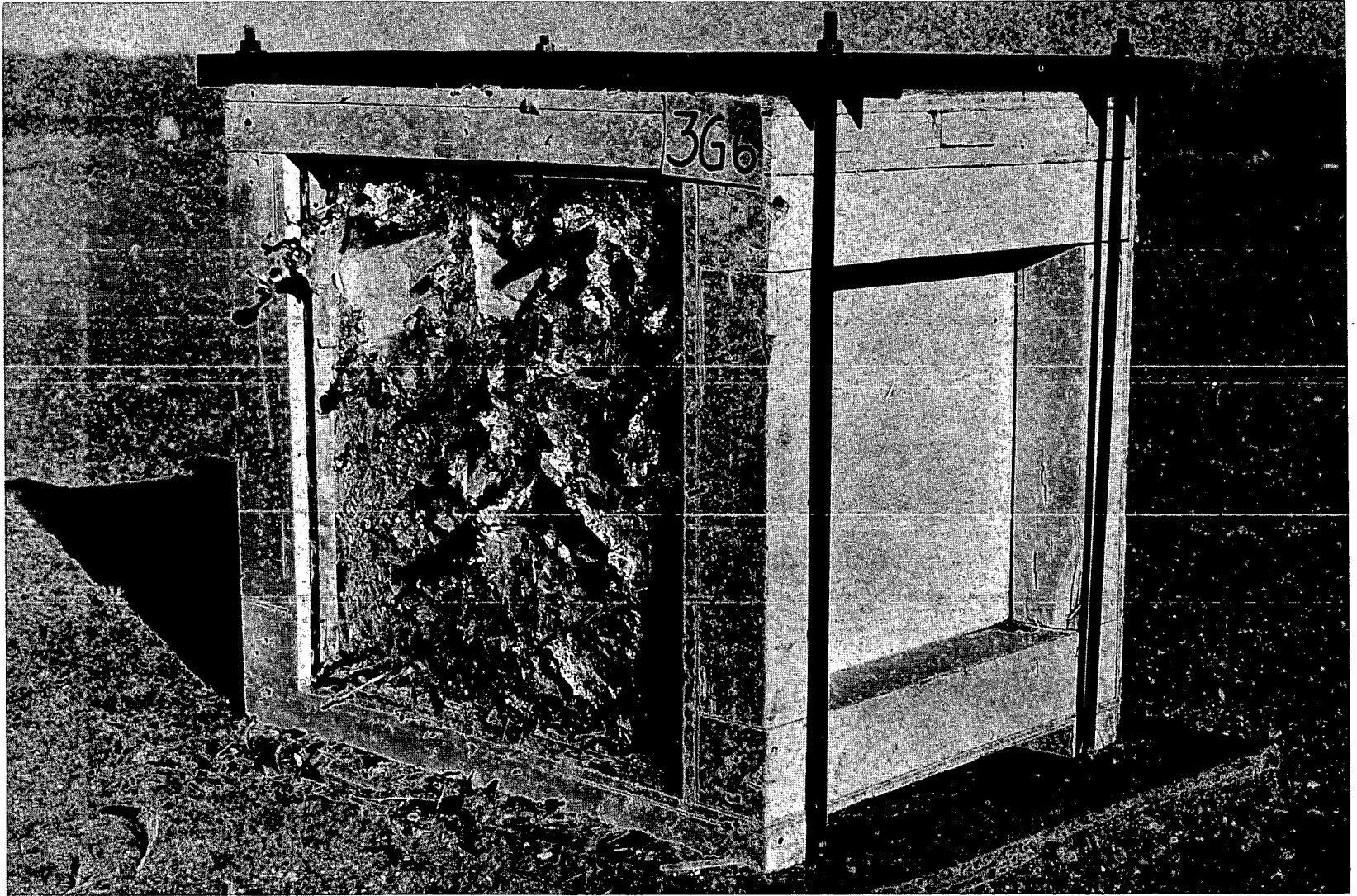


Fig. 6.10—Installation 3G6, postshot, placed 4.6 ft behind window-glass installation. Torn aluminum foil can be seen on the face of the trap.



Fig. 6.11—Installation 3G7, postshot, placed 9.6 ft behind plate-glass installation. Note dents made in absorber by missiles that were not captured.

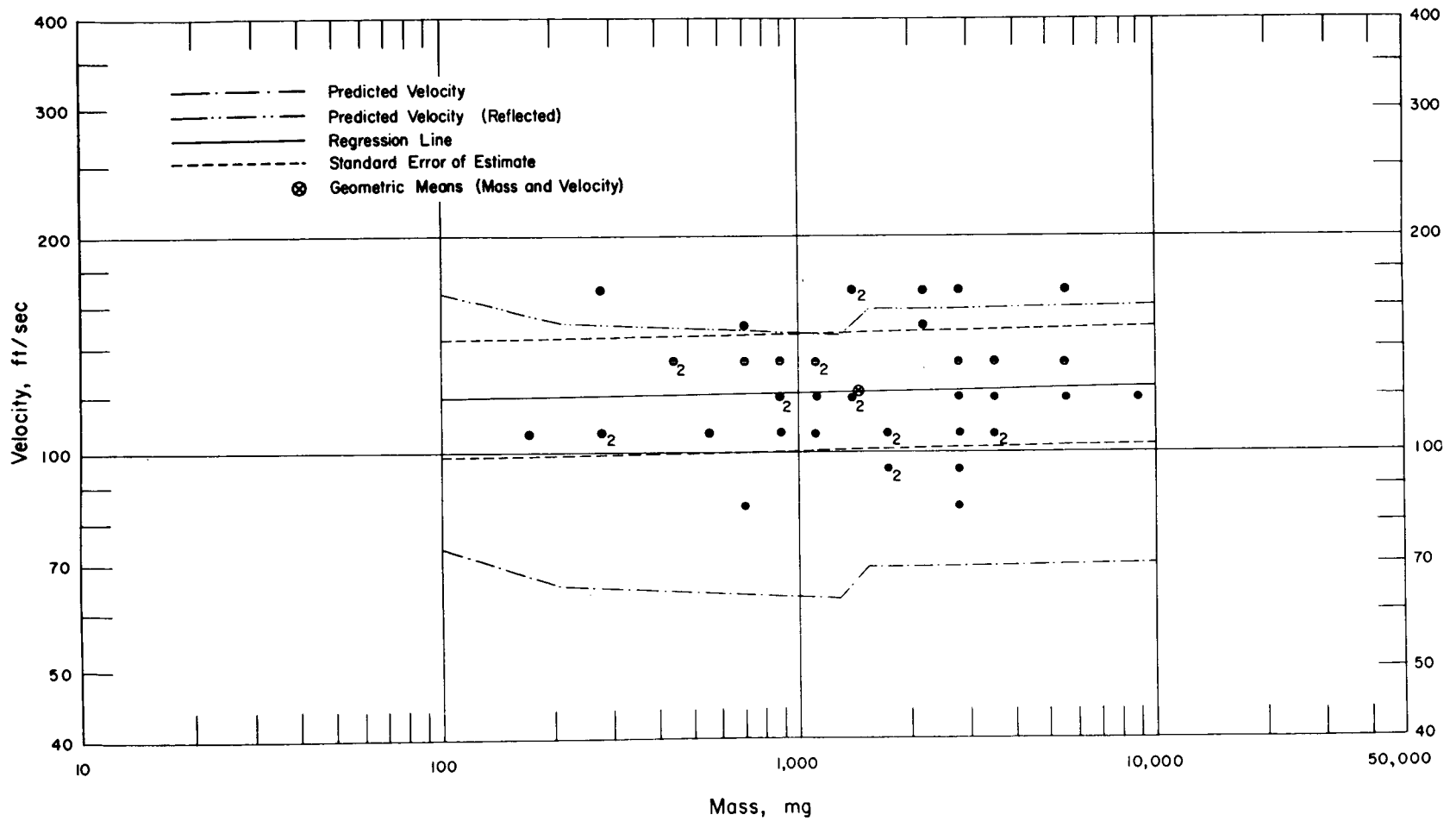


Fig. 6.12—Analysis of window-glass missiles from installation 3G6: $d = 4.6$ ft; $n = 42$; $\log v = 2.0540 + 0.0097 \log m$; $E_{gv} = 1.21$; $M_{50} = 1440$ mg; $V_{50} = 122$ ft/sec.

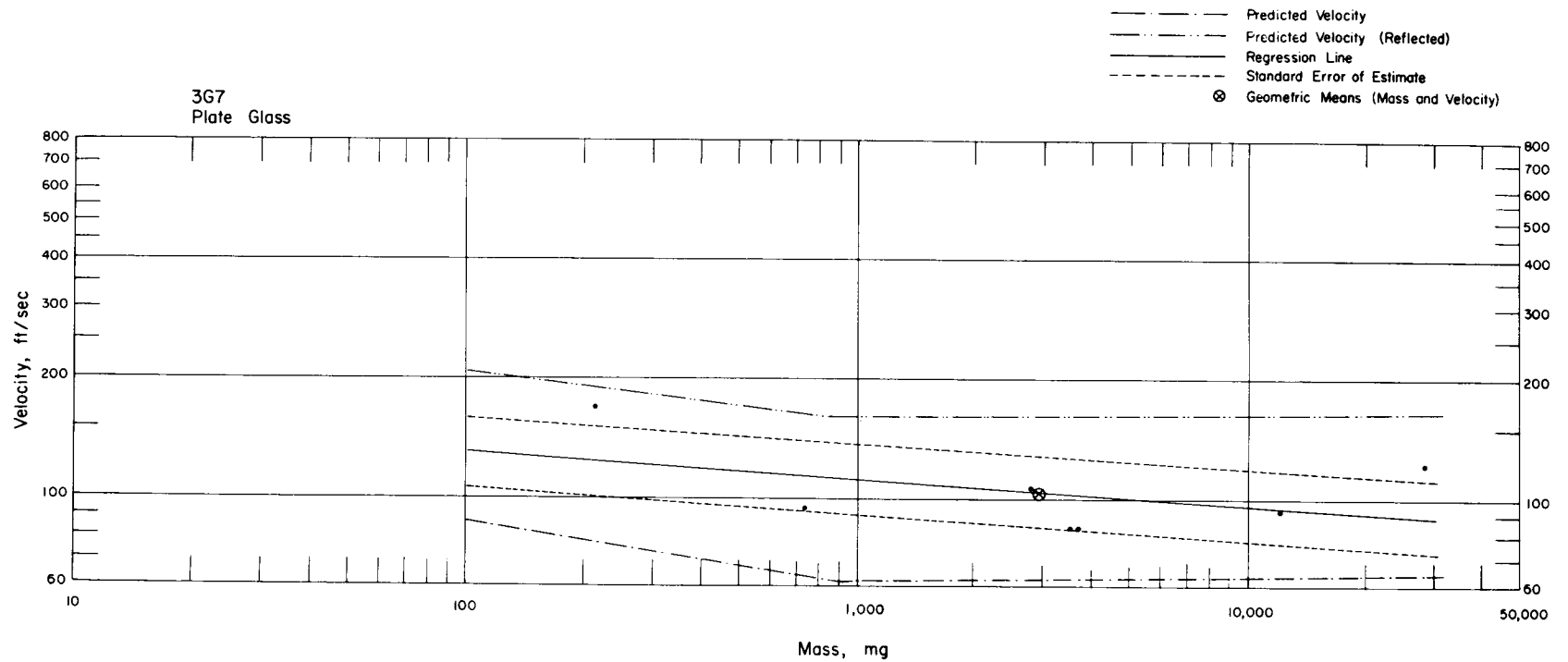


Fig. 6.13—Analysis of plate-glass missiles from installation 3G7: $d = 9.6$ ft; $n = 7$; $\log v = 2.2374 - 0.0631 \log m$; $E_{gv} = 1.26$; $M_{50} = 2965$ mg; $V_{50} = 104$ ft/sec.

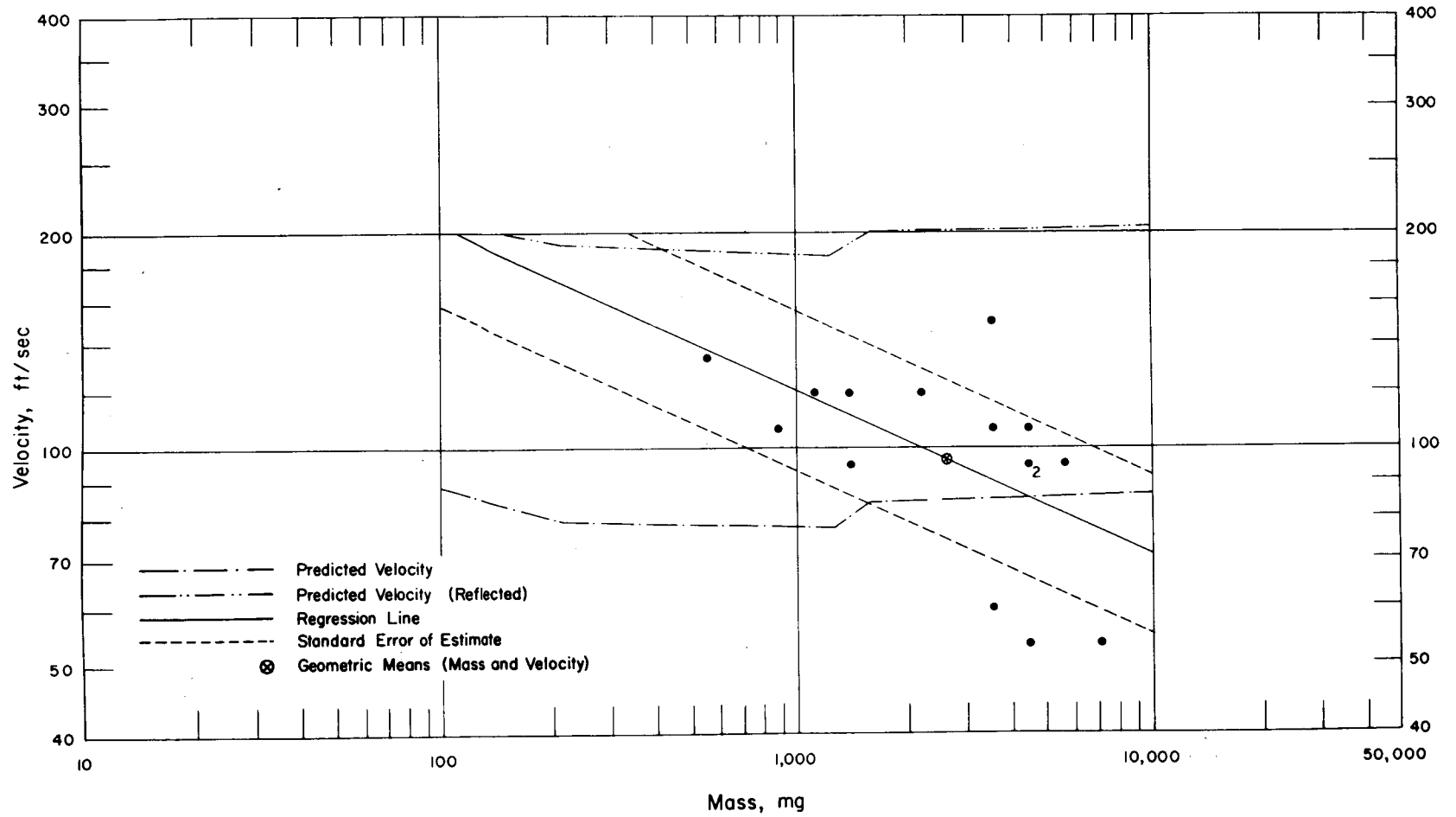


Fig. 6.14—Analysis of window-glass missiles from trap 3G8b: $d = 10.9$ ft; $n = 15$; $\log v = 2.7679 - 0.2300 \log m$; $E_{GV} = 1.32$; $M_{50} = 2620$ mg; $V_{50} = 96$ ft/sec.

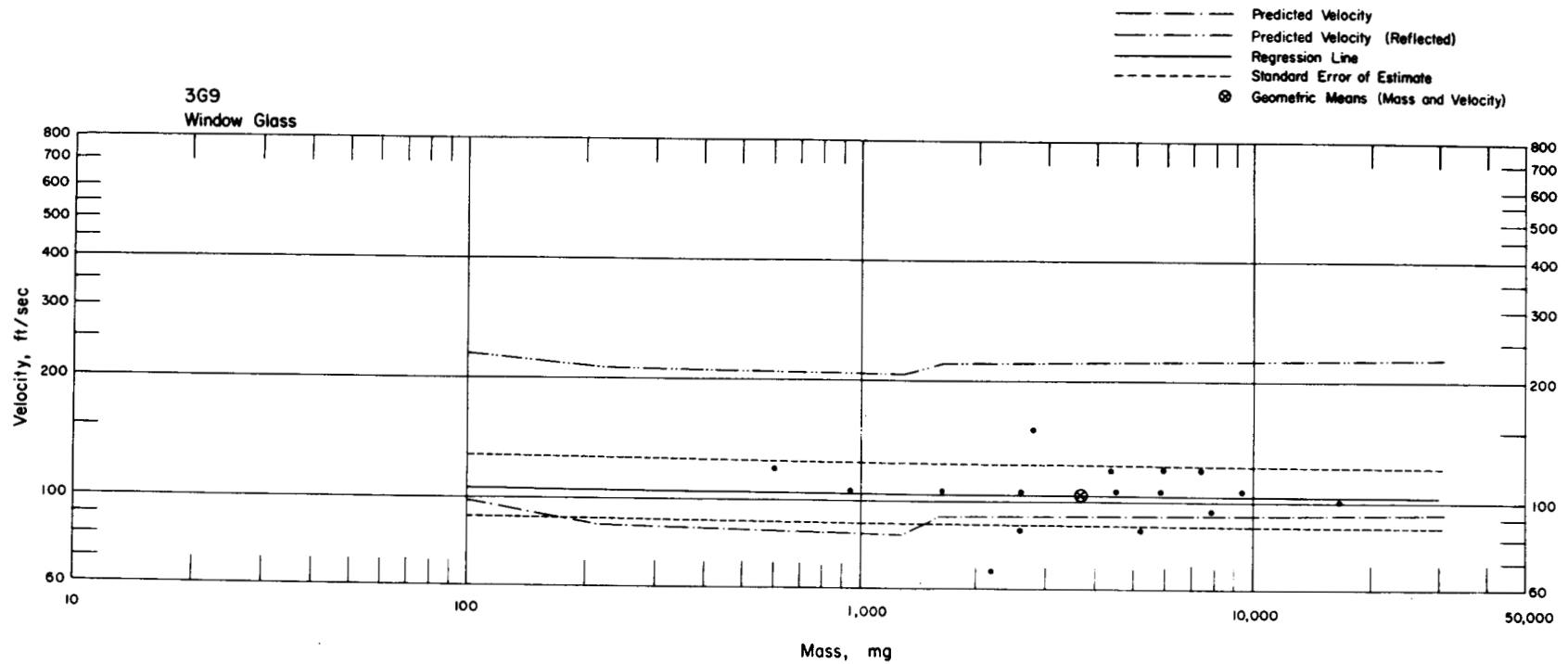


Fig. 6.15—Analysis of window-glass missiles from installation 3G9: $d = 19.5$ ft; $n = 16$; $\log v = 2.0453 - 0.0079 \log m$; $E_{gv} = 1.21$; $M_{50} = 3692$ mg; $V_{50} = 104$ ft/sec.

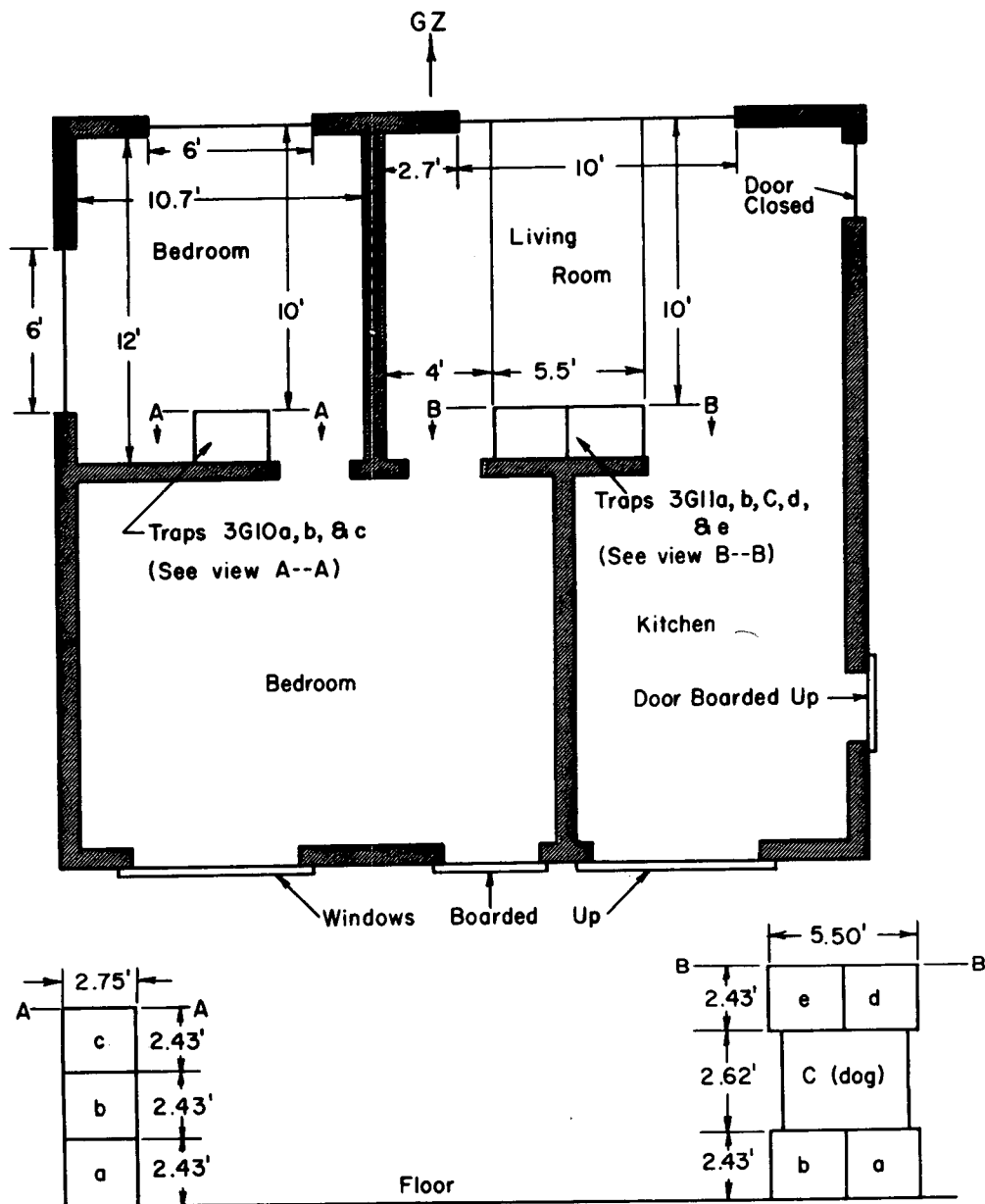


Fig. 6.16—Floor plan of reinforced concrete-block house, 4700-ft range. Traps 3G10a, b and c, and 3G11a, b, d and e all have type I absorbers. The bedroom window opposite traps 3G10a, b and c is 3 ft 7 in. above the floor, has nine 11.5- by 23.5-in. panes, and is 6 by 3 ft. The living-room window opposite traps 3G11a, b, d and e is 2 ft 7 in. above the floor, has twenty 11.5- by 23.5-in. panes, and is 10 by 4 ft.

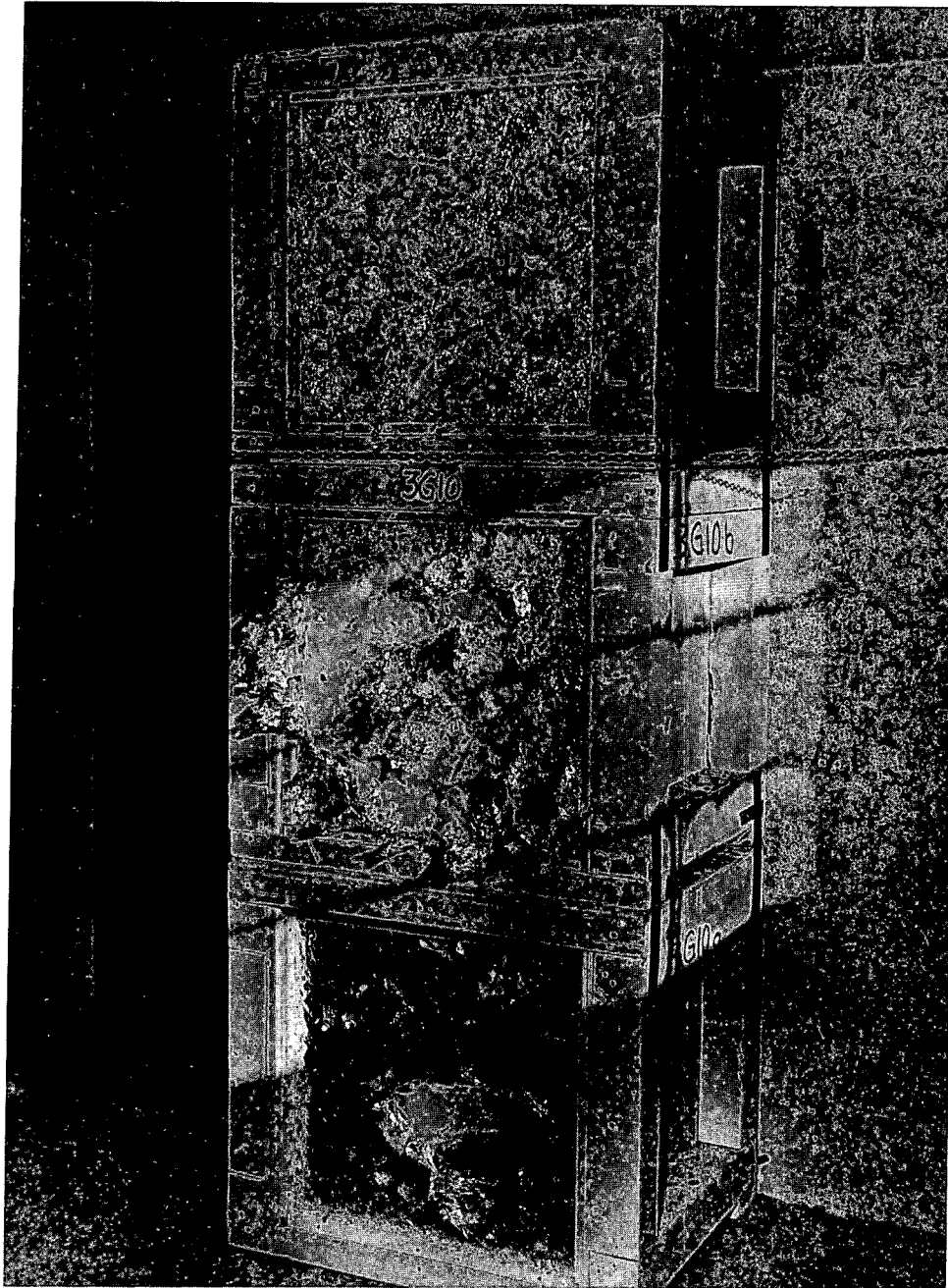


Fig. 6.17—Traps 3G10a, b and c, postshot, placed in front bedroom of the reinforced concrete-block house.

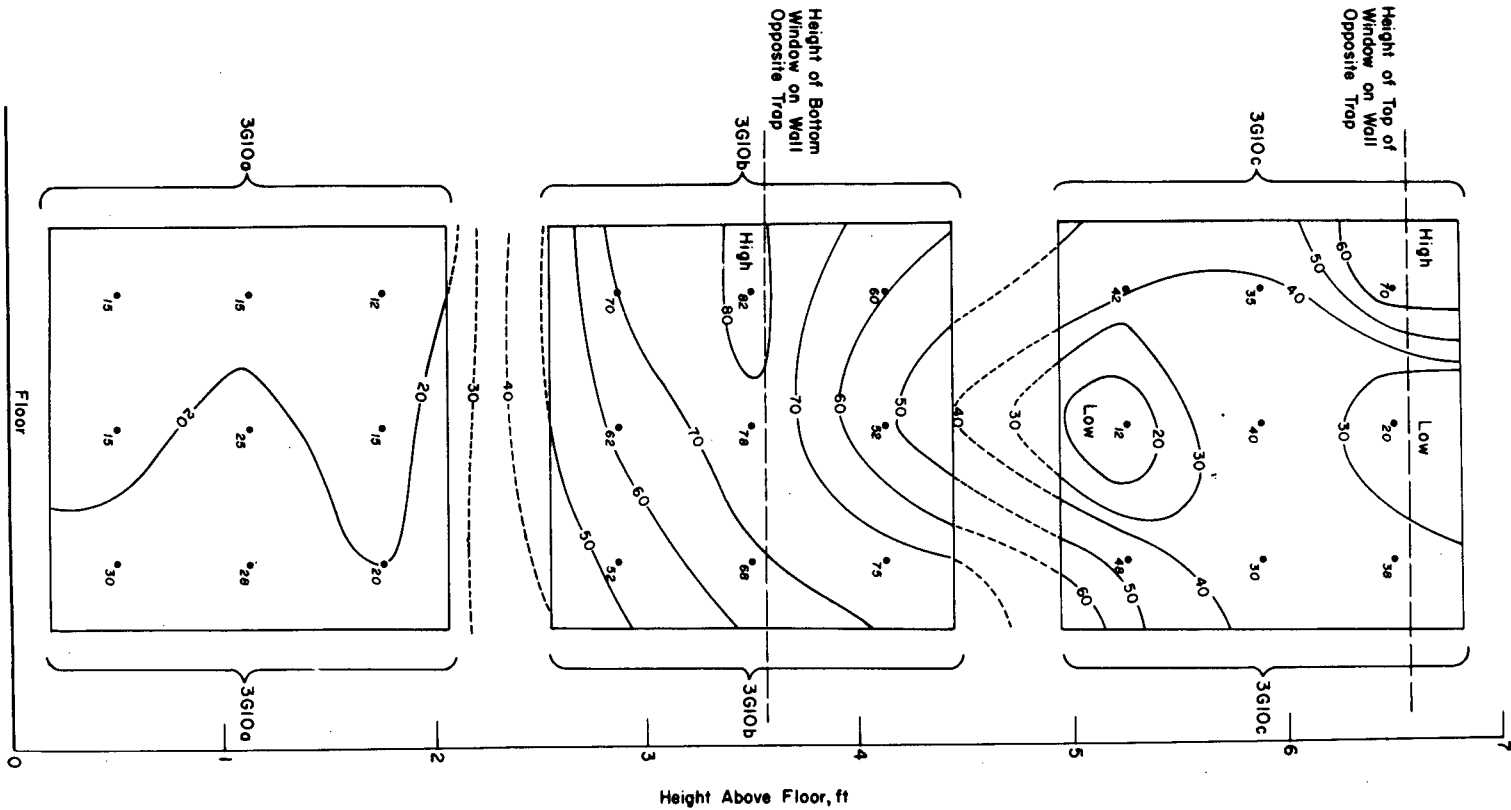


Fig. 6.18—Spatial distribution of window-glass missiles in installation 3G10 traps. Numbers indicate missiles per square foot.

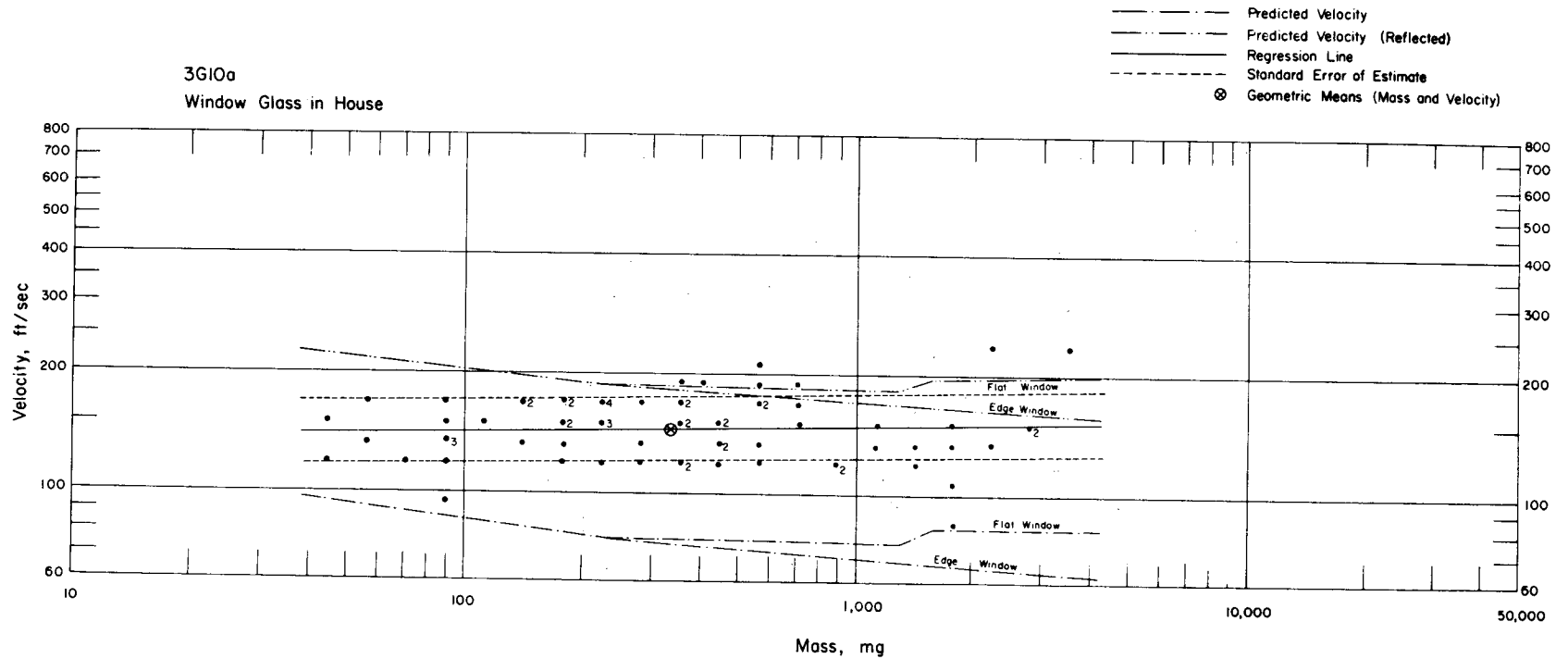


Fig. 6.19—Analysis of window-glass missiles from trap 3G10a: $d = 10.0$ ft; $n = 70$; $\log v = 2.1173 + 0.0172 \log m$; $E_{gv} = 1.20$; $M_{50} = 333$ mg; $V_{50} = 145$ ft/sec. Additional analysis was made for mass region above 219.5 mg.

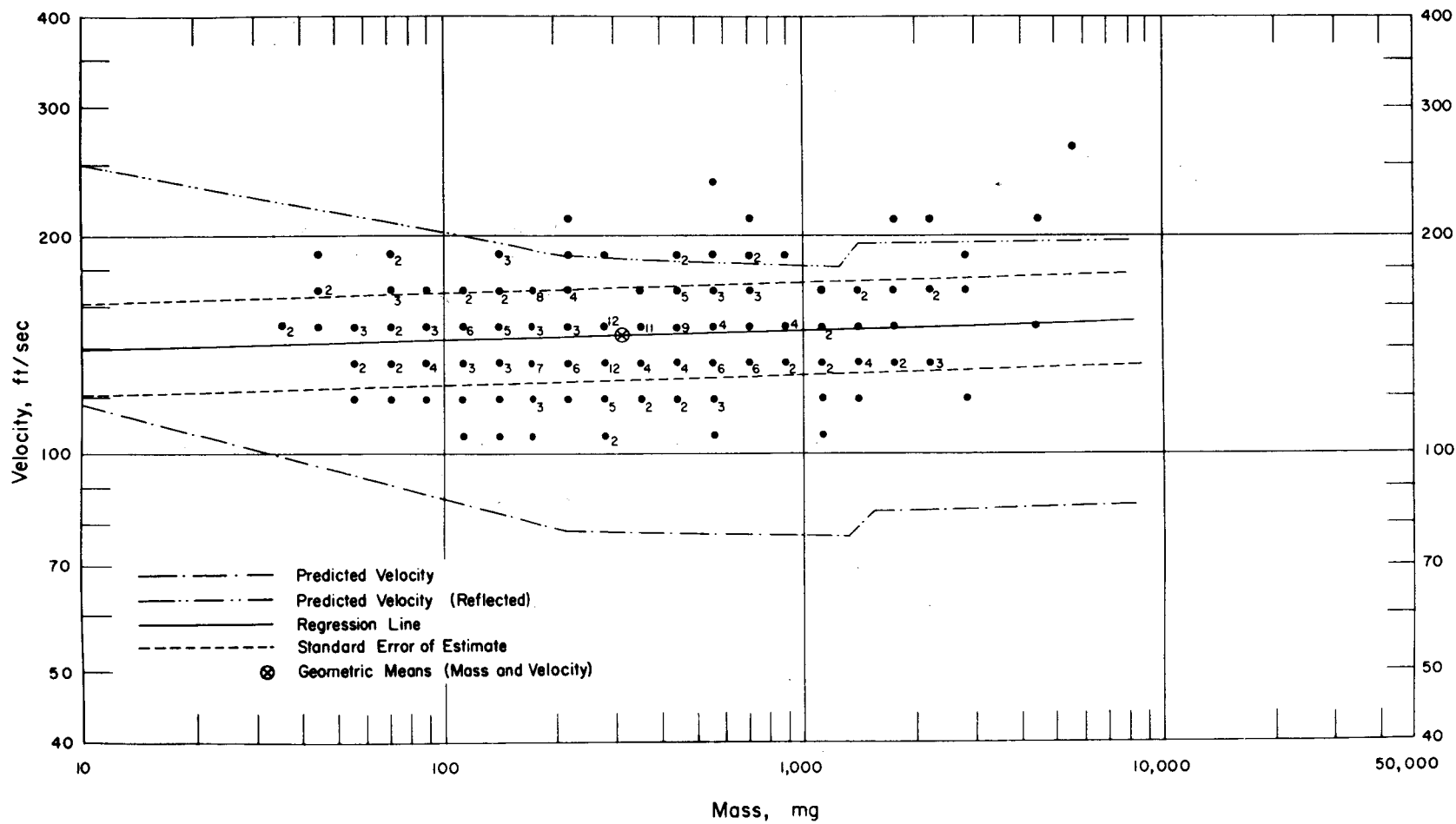


Fig. 6.20—Analysis of window-glass missiles from trap 3G10b: $d = 10.0$ ft; $n = 240$; $\log v = 2.1278 + 0.0150 \log m$; $E_{gv} = 1.16$; $M_{50} = 314$ mg; $V_{50} = 146$ ft/sec.

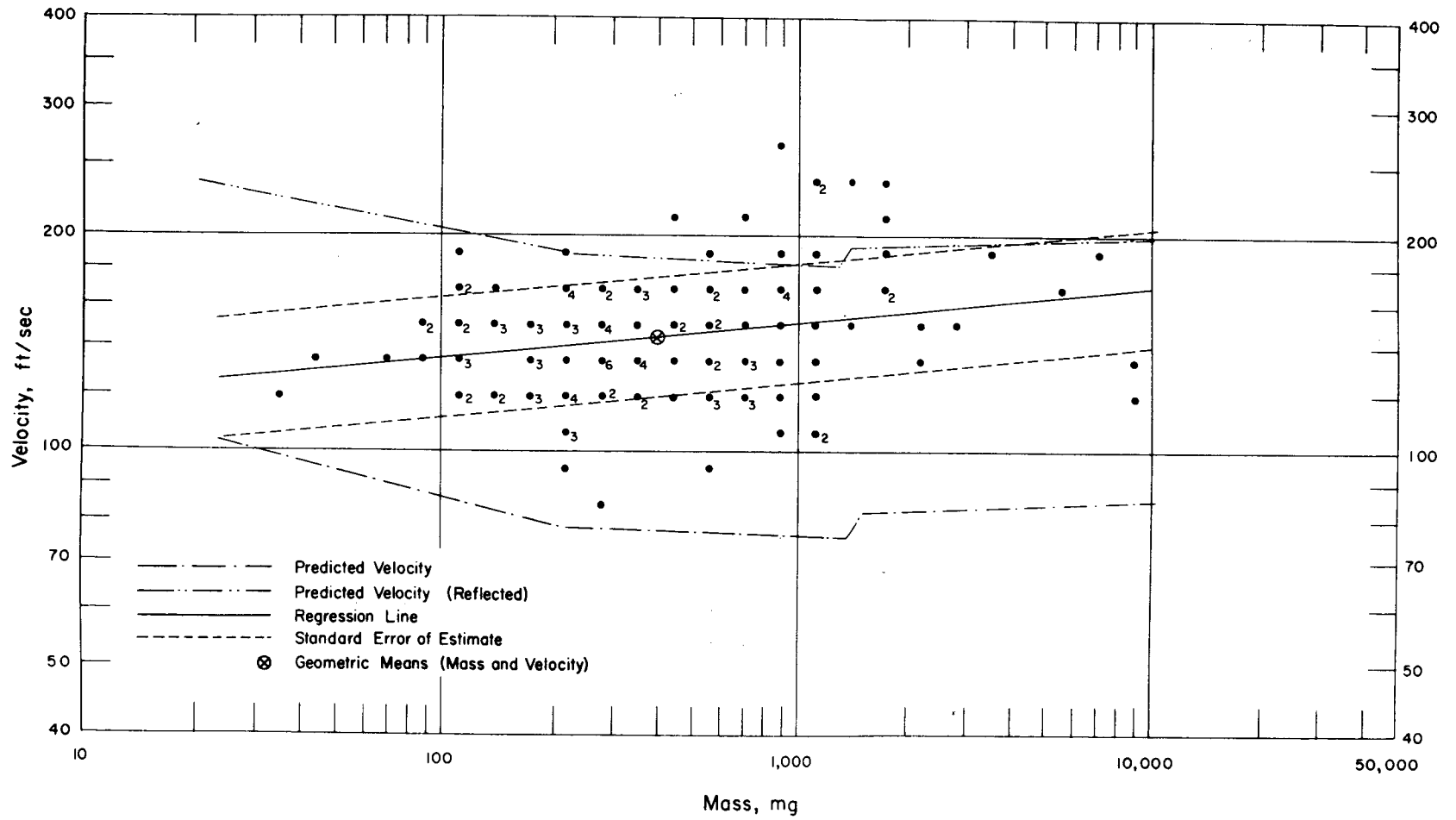


Fig. 6.21—Analysis of window-glass missiles from trap 3G10c: $d = 10.0$ ft; $n = 134$; $\log v = 2.0297 + 0.0497 \log m$; $E_{gV} = 1.21$; $M_{50} = 404$ mg; $V_{50} = 144$ ft/sec.

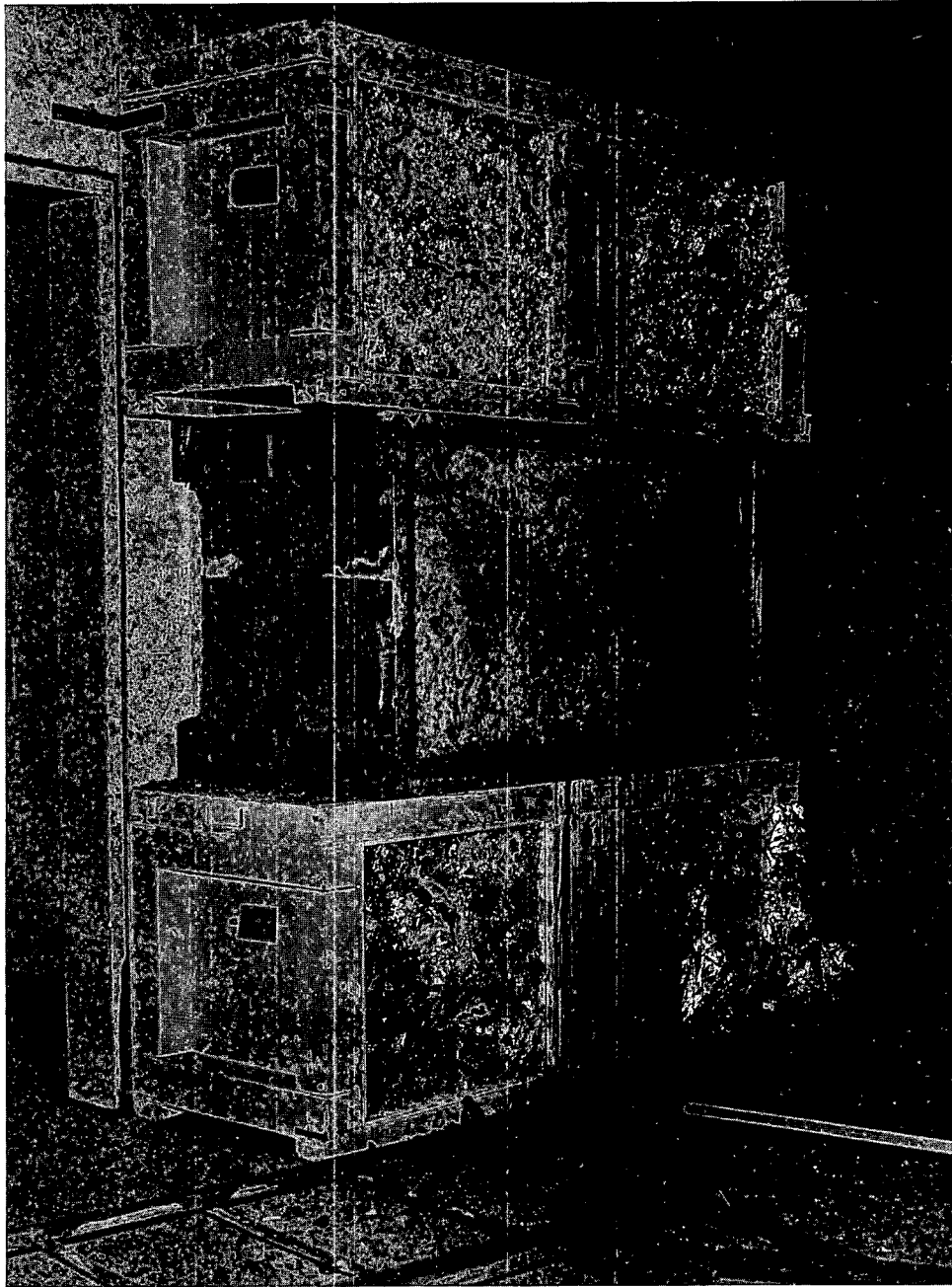


Fig. 6.22—Traps 3G11a, b, d and e, postshot, placed in living room of the reinforced concrete-block house. The box between the upper and lower traps contained a dog (Project 33.4). Note window frame that was dislodged by the blast wave.

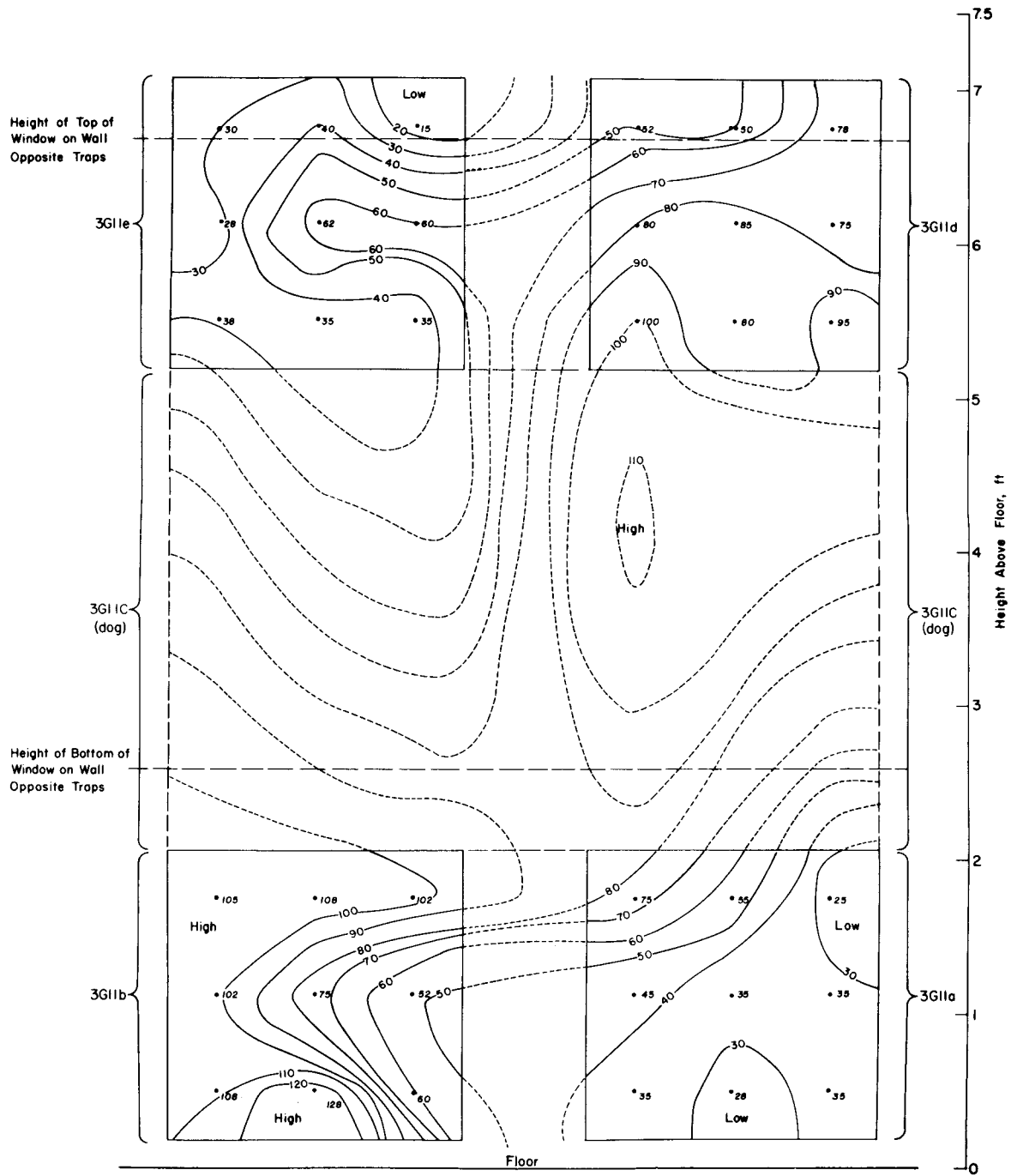


Fig. 6.23—Spatial distribution of window-glass missiles in installation 3G11 traps. Numbers indicate missiles per square foot.

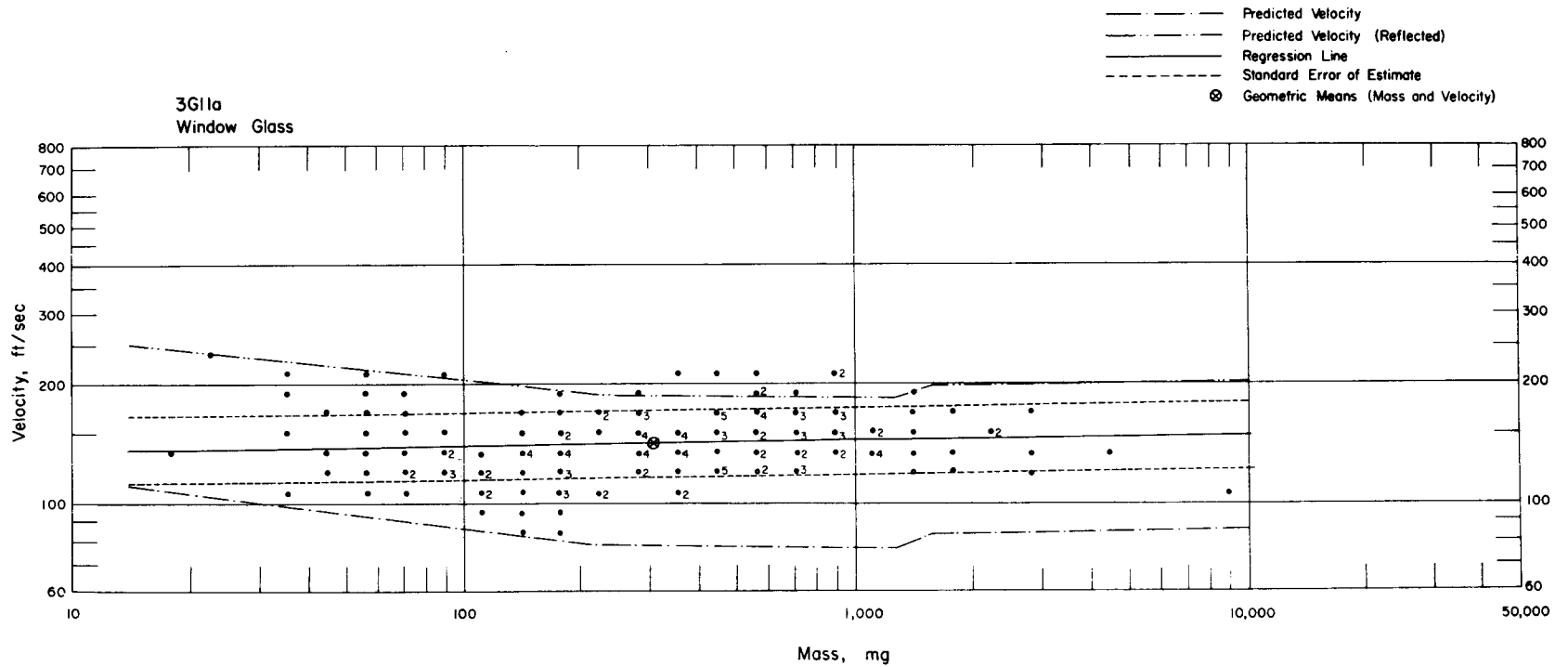


Fig. 6.24—Analysis of window-glass missiles from trap 3G11a: $d = 10.0$ ft; $n = 164$; $\log v = 2.1153 + 0.0136 \log m$; $E_{gv} = 1.21$; $M_{50} = 303$ mg; $V_{50} = 141$ ft/sec.

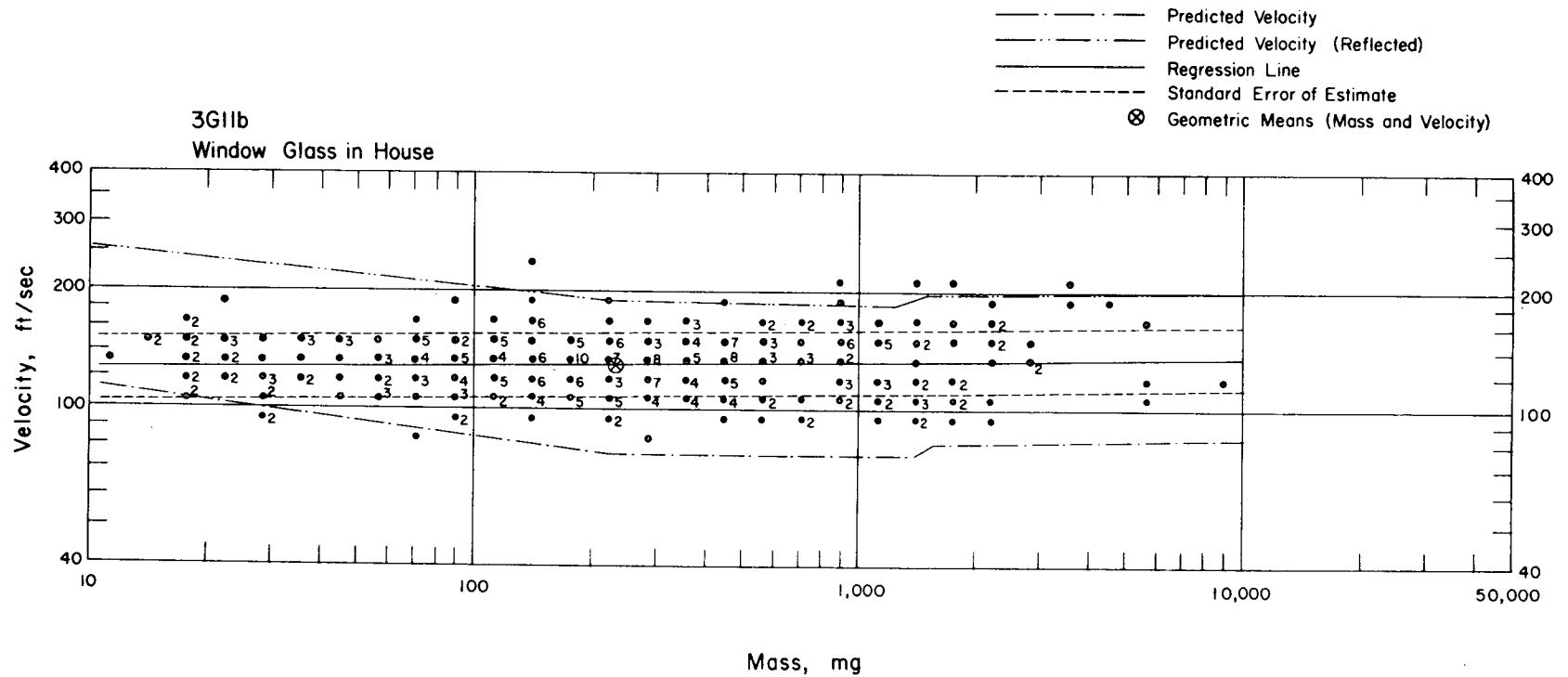


Fig. 6.25—Analysis of window-glass missiles from trap 3G11b: $d = 10.0$ ft; $n = 336$; $\log v = 2.0923 + 0.0104 \log m$; $E_{gV} = 1.19$; $M_{50} = 236$ mg; $V_{50} = 131$ ft/sec.

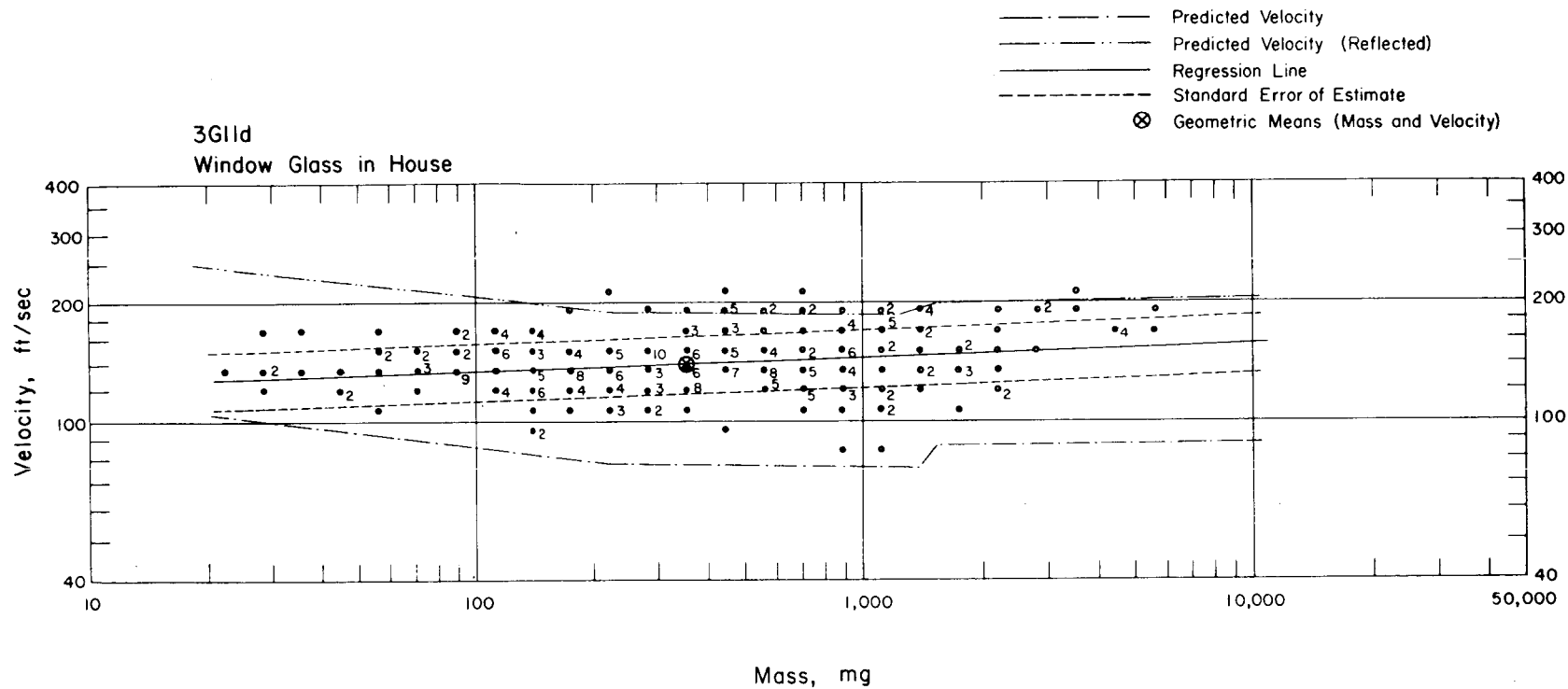


Fig. 6.26—Analysis of window-glass missiles from trap 3G11d: $d = 10.0$ ft; $n = 278$; $\log v = 2.0628 + 0.0337 \log m$; $E_{GV} = 1.18$; $M_{50} = 355$ mg; $V_{50} = 141$ ft/sec.

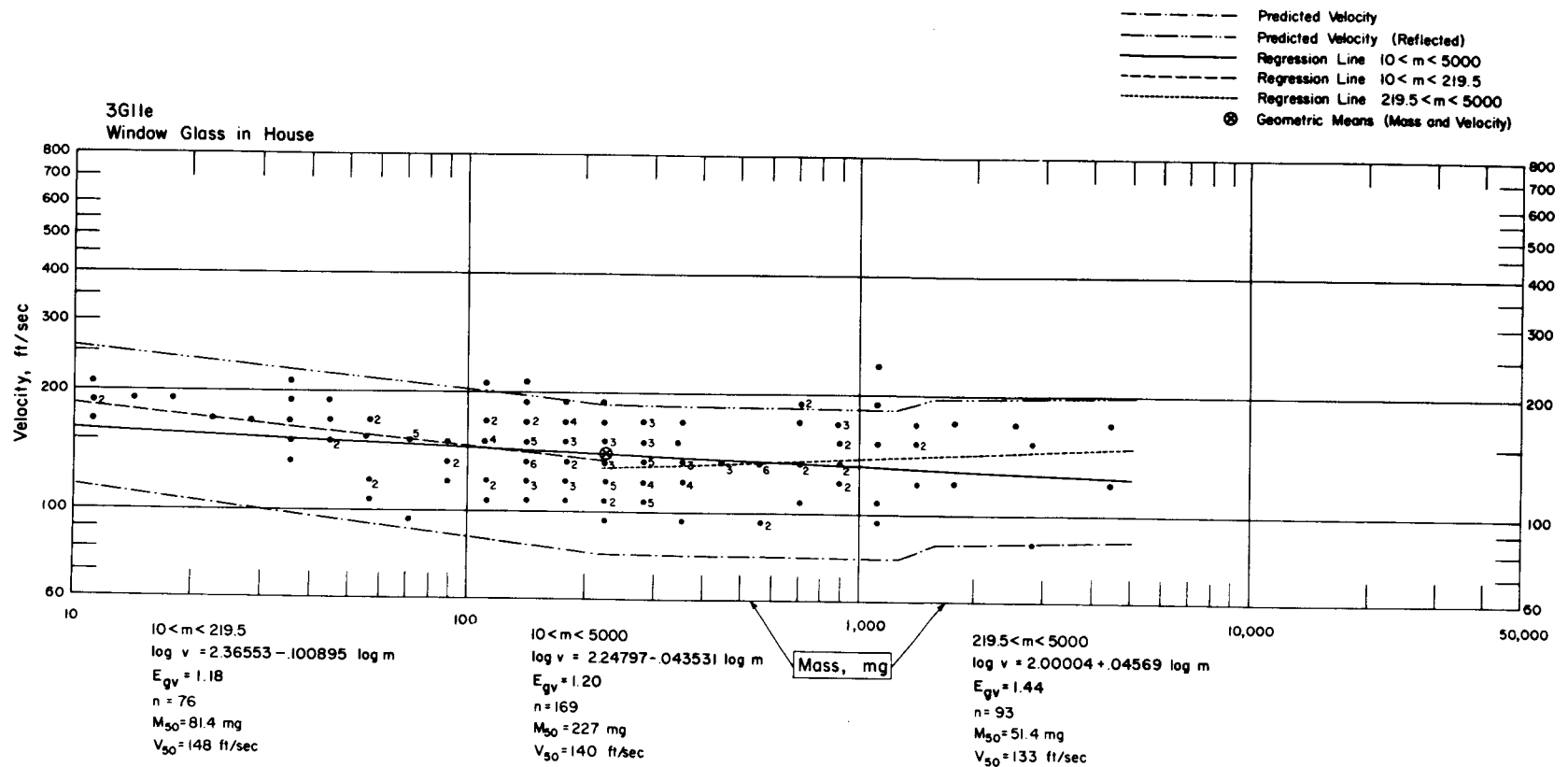


Fig. 6.27—Analyses of window-glass missiles from trap 3G11e. Three analyses were made: one for total mass-range; one for smaller masses; and one for larger masses. $d = 10 \text{ ft}$.

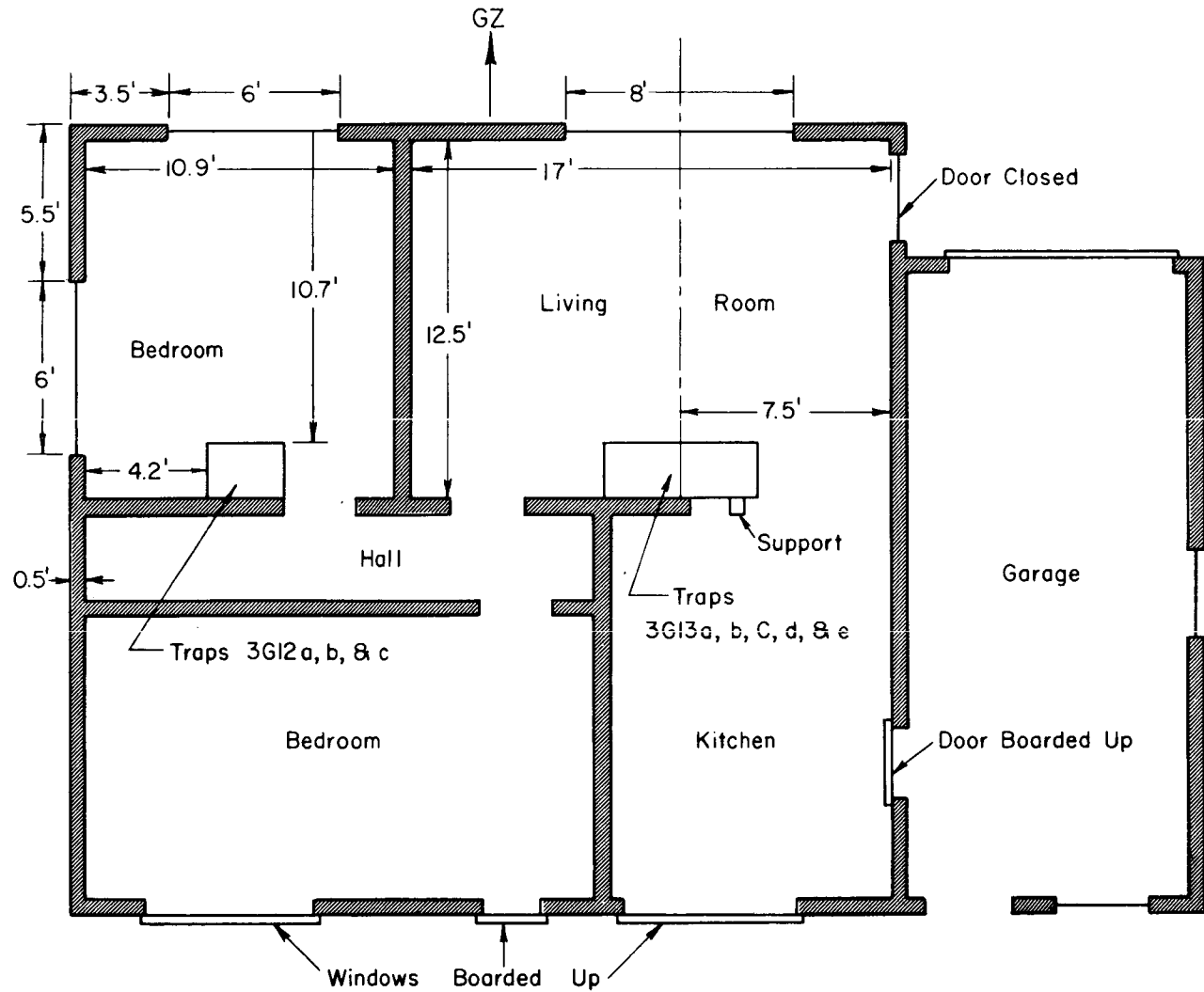


Fig. 6.28—Floor plan of precast-concrete house, 4700-ft range. Traps 3G12a, b and c and 3G13a, b, d and e all have type I absorbers. Trap 3G13C is a dog trap. The bedroom window opposite traps 3G12a, b and c has nine 11.5- by 23.5-in. panes, is 6 by 3 ft, and is 3 ft 6 in. above the floor. The living-room window opposite traps 3G13a, b, d and e, has twenty 11.5- by 23.5-in. panes, is 8 by 5 ft, and is 1 ft 6 in. above the floor. The trap elevations are the same as those in the reinforced concrete-block house. (See Fig. 6.16.)

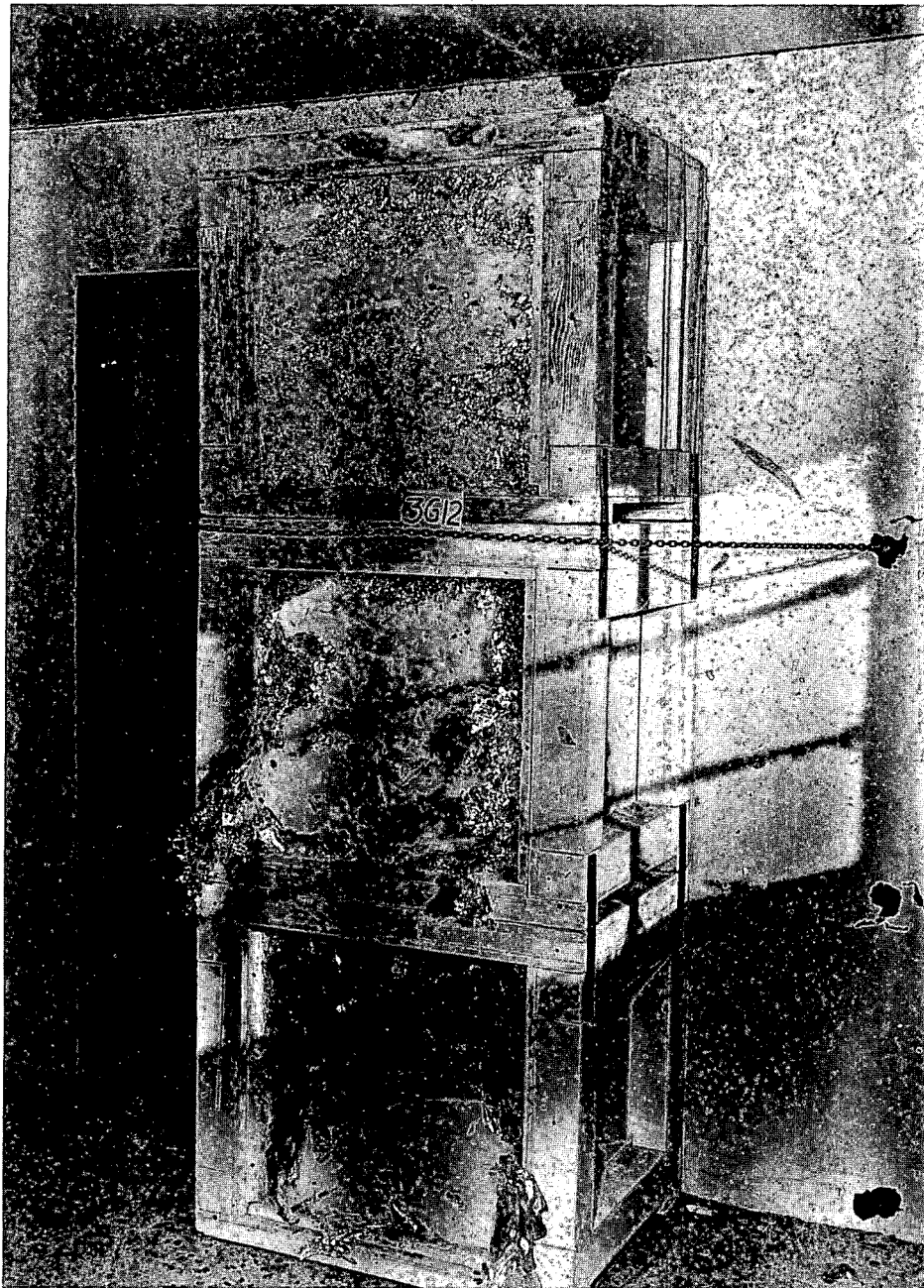


Fig. 6.29 — Traps 3G12a, b and c, postshot, placed in the front bedroom of the precast-concrete house.

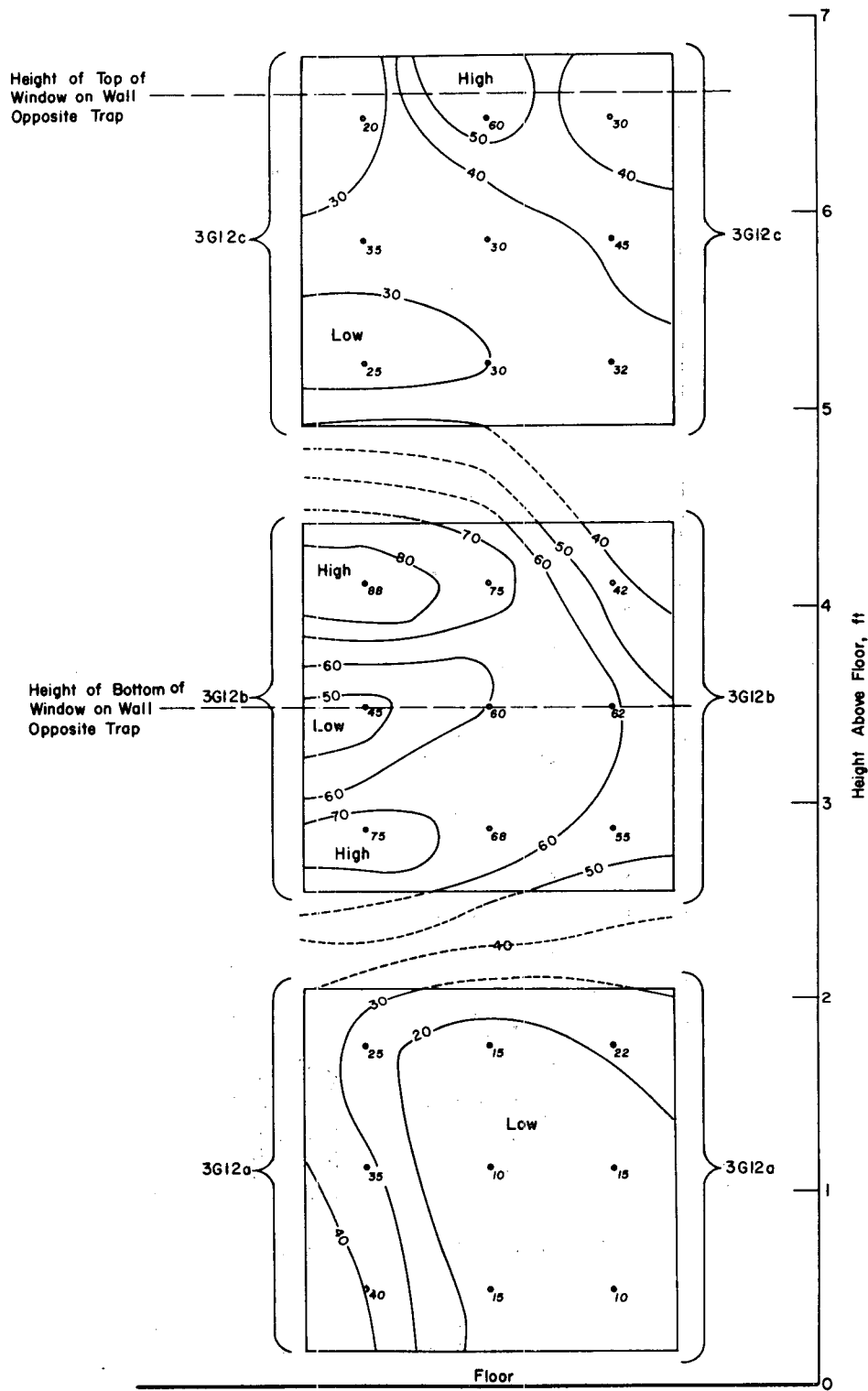


Fig. 6.30—Spatial distribution of window-glass missiles in installation 3G12 traps. Numbers indicate missiles per square foot.

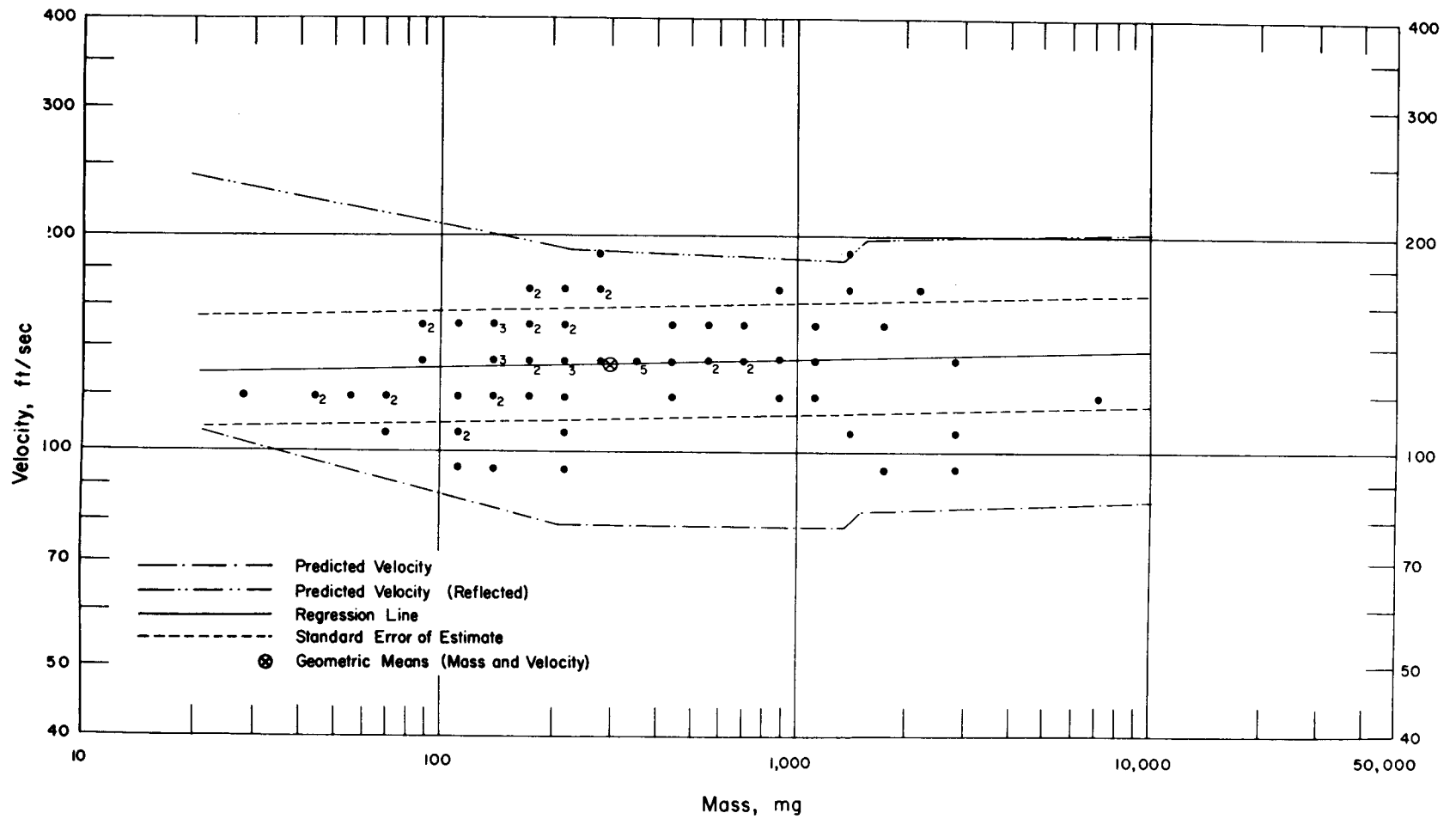


Fig. 6.31—Analysis of window-glass missiles from trap 3G12a: $d = 10.7$ ft; $n = 74$; $\log v = 2.0902 + 0.0127 \log m$; $E_{gv} = 1.19$; $M_{50} = 299$ mg; $V_{50} = 132$ ft/sec.

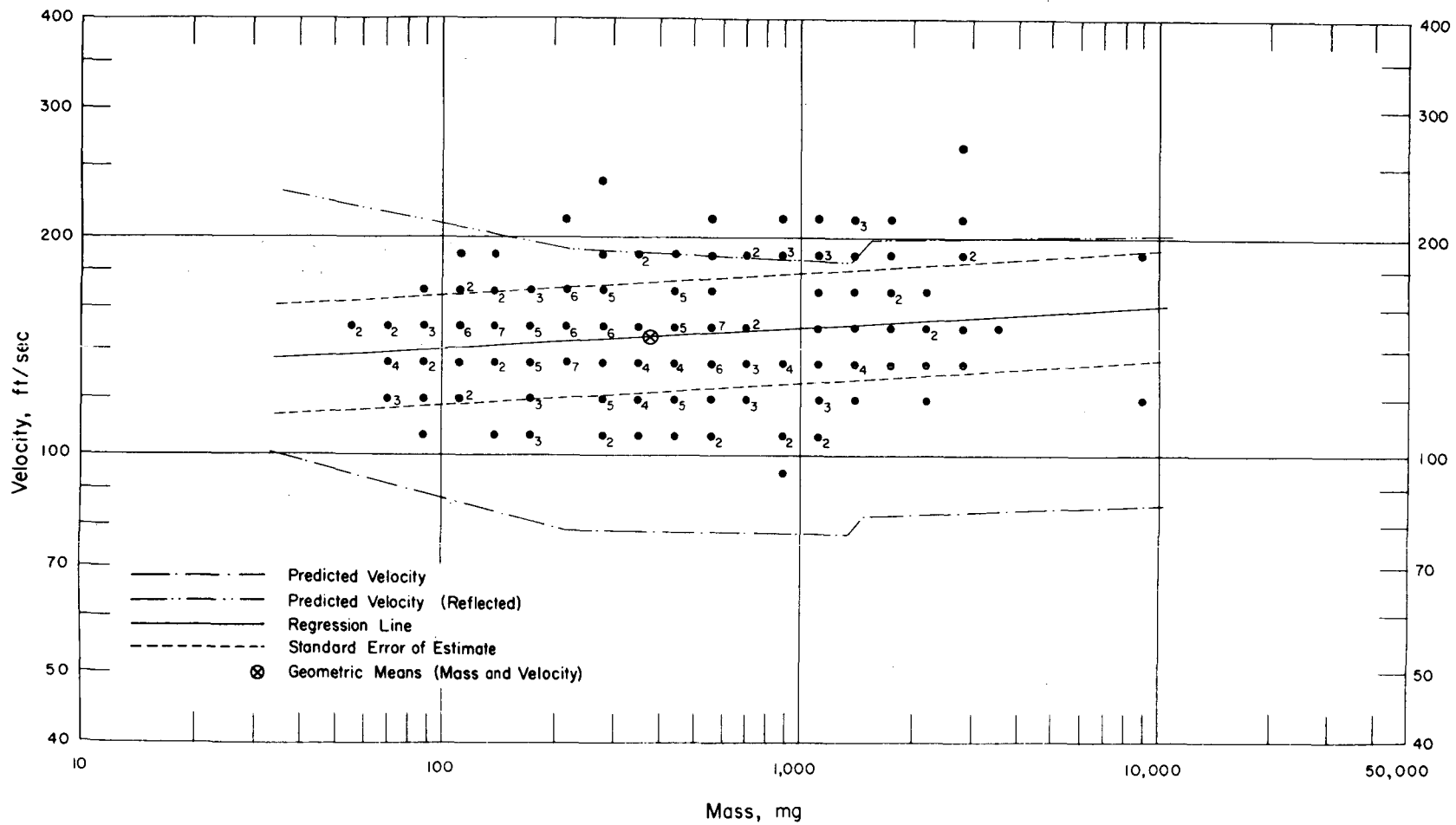


Fig. 6.32—Analysis of window-glass missiles from trap 3G12b: $d = 10.7$ ft; $n = 228$; $\log v = 2.0791 + 0.0320 \log m$; $E_{gv} = 1.19$; $M_{50} = 383$ mg; $V_{50} = 145$ ft/sec.

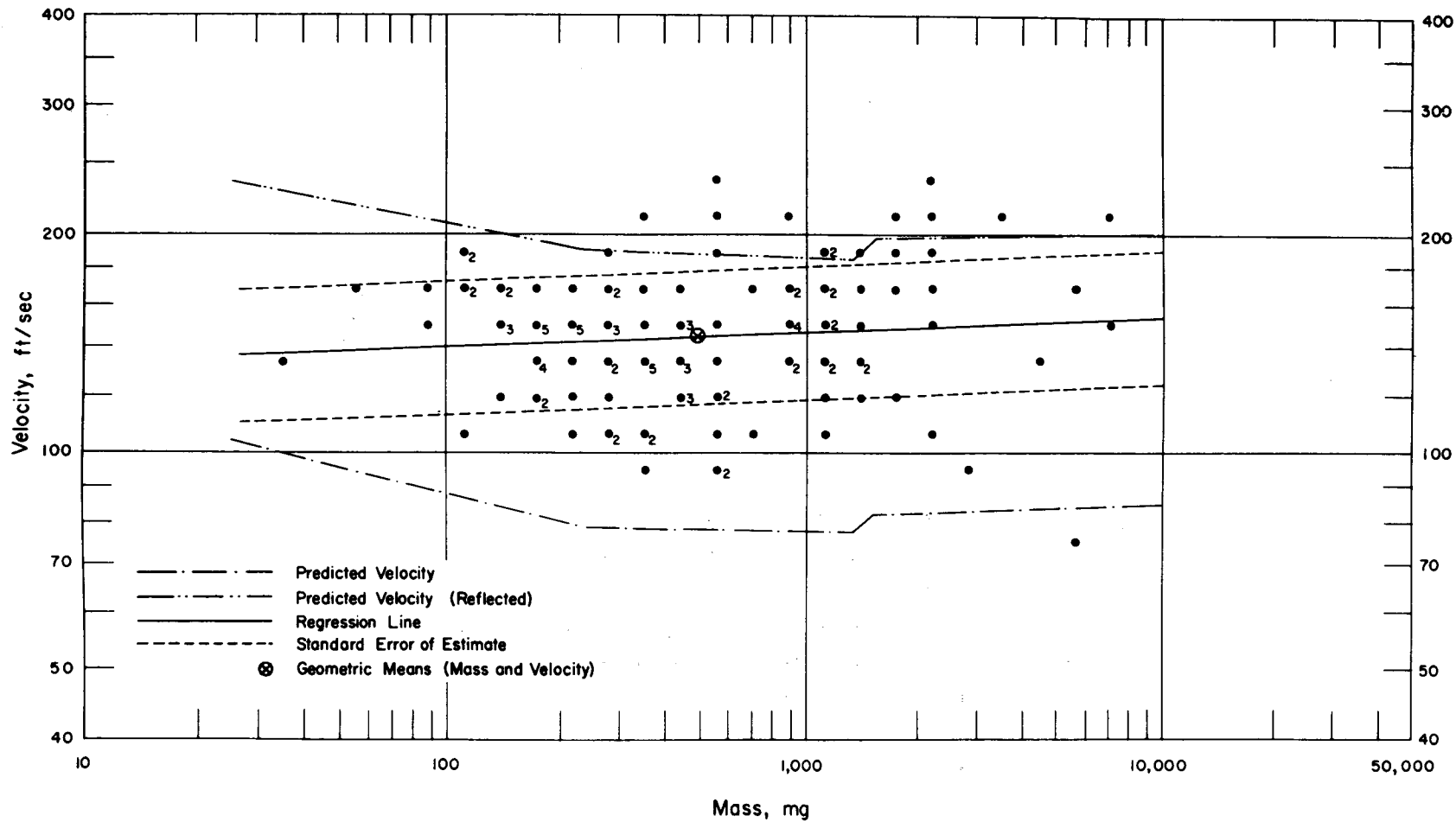


Fig. 6.33—Analysis of window-glass missiles from trap 3G12c: $d = 10.7$ ft; $n = 123$; $\log v = 2.1055 + 0.0201 \log m$; $E_{gV} = 1.24$; $M_{50} = 495$ mg; $V_{50} = 144$ ft/sec.

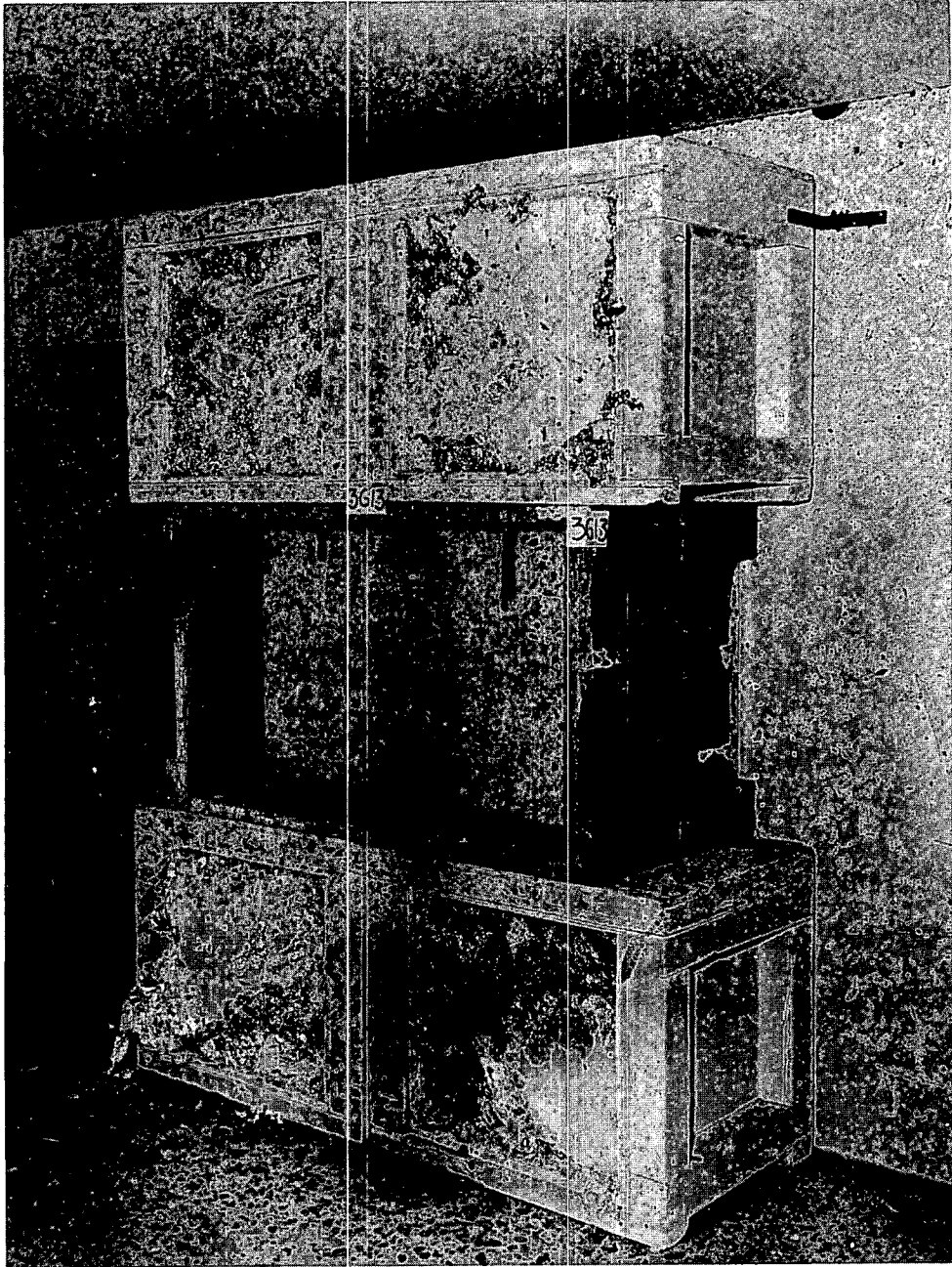


Fig. 6.34—Traps 3G13a, b, d and e, postshot, placed in the living room of the precast-concrete house. The box between upper and lower traps contained a dog (Project 33.4).

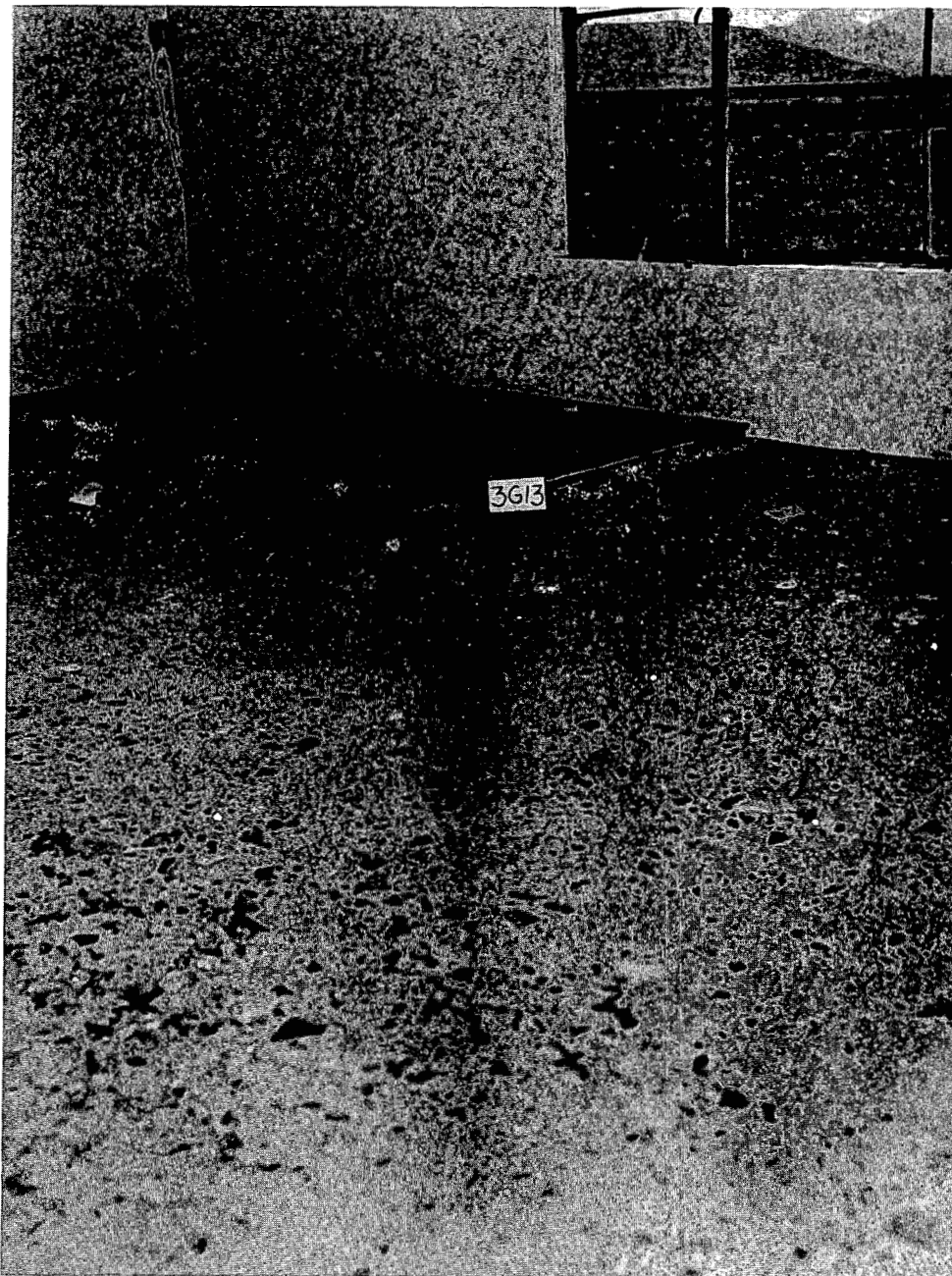


Fig. 6.35— Postshot view of the living room of the precast-concrete house where traps 3G13a, b, d, and e were located. The window looks toward GZ. The door shown in the corner was blown from its original closed position on the right side of the room. The debris on the floor consisted of mostly fragments of window glass.

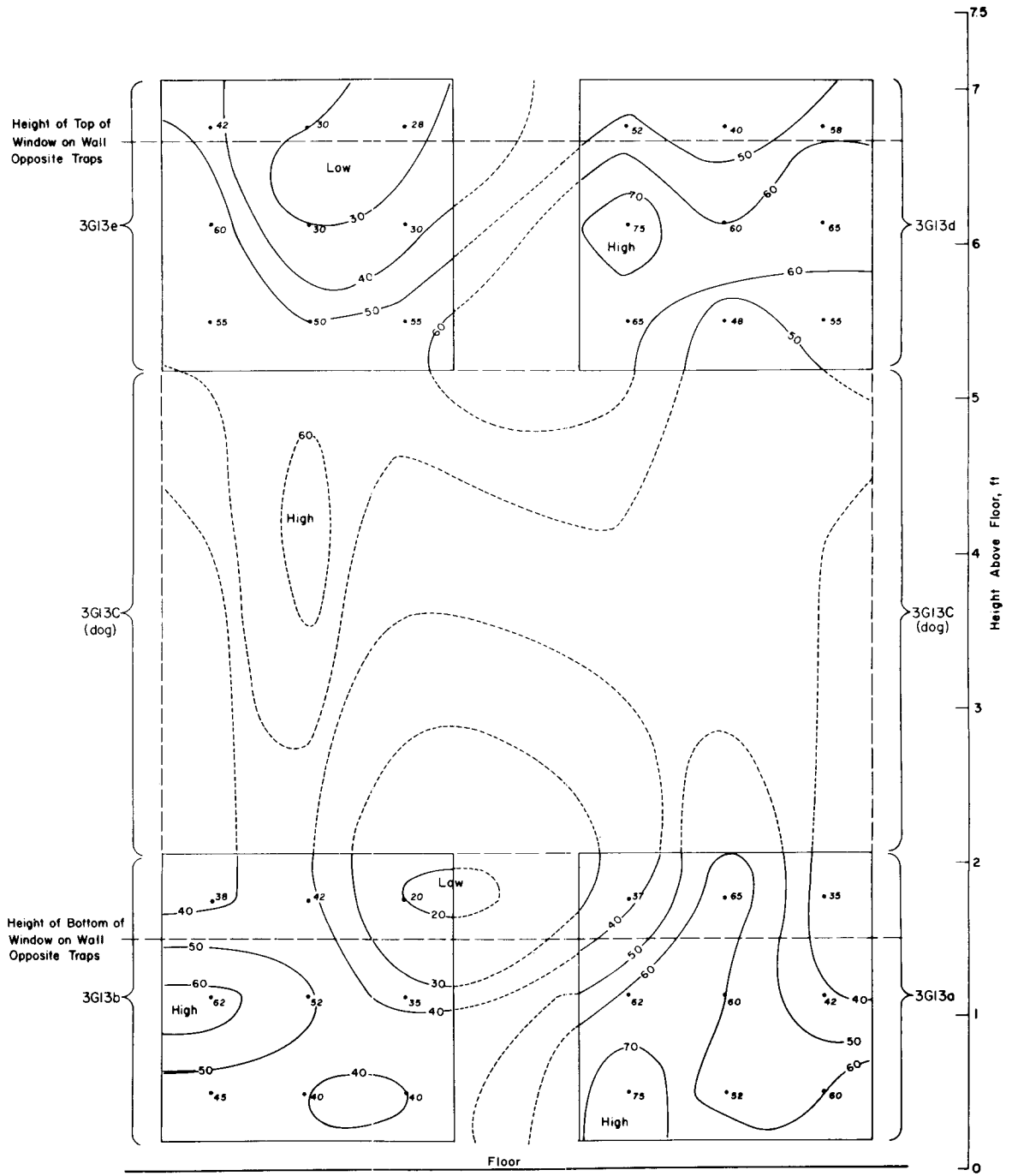


Fig. 6.36—Spatial distribution of window-glass missiles in installation 3G13 traps. Numbers indicate missiles per square foot.

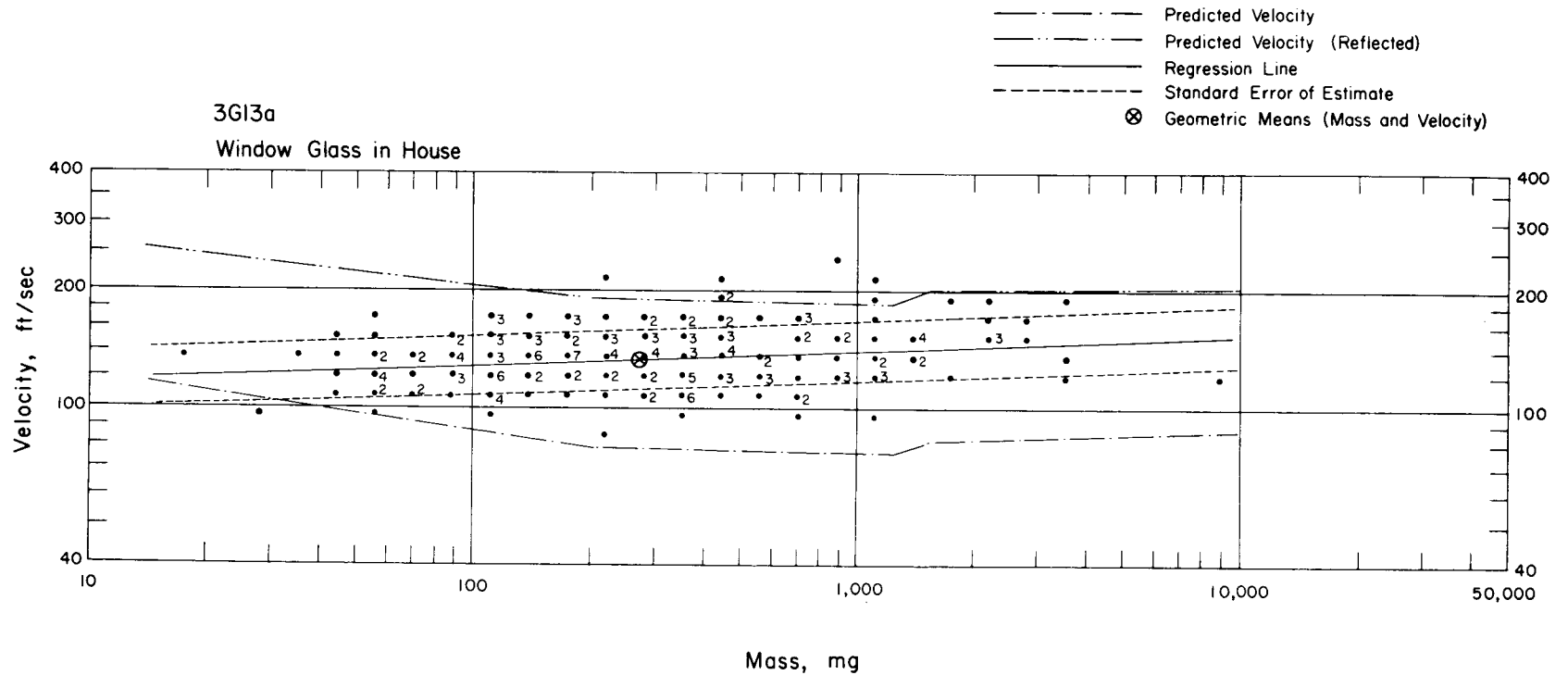


Fig. 6.37—Analysis of window-glass missiles from trap 3G13a: $d = 10.7$ ft; $n = 196$; $\log v = 2.0528 + 0.0405 \log m$; $E_{gv} = 1.19$; $M_{50} = 281$ mg; $V_{50} = 133$ ft/sec.

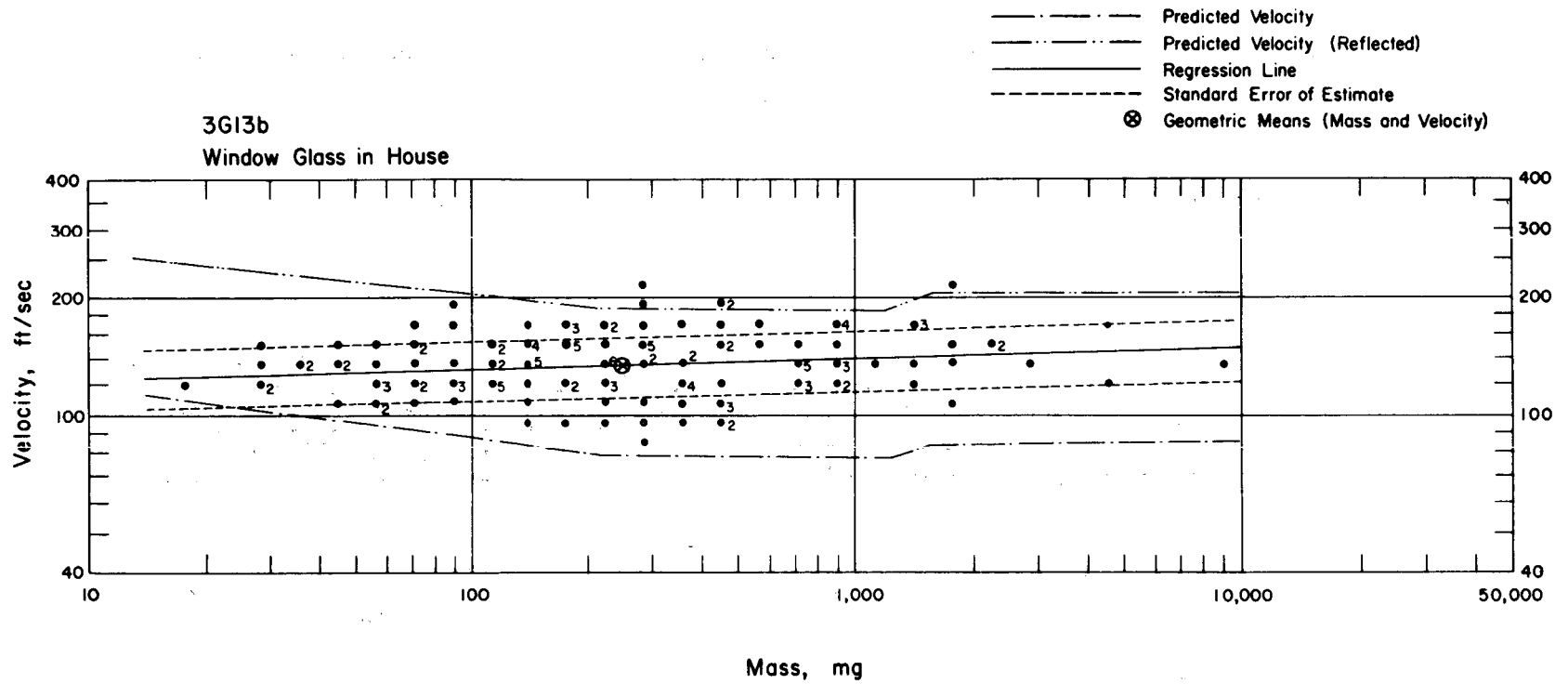


Fig. 6.38—Analysis of window-glass missiles from trap 3G13b: $d = 10.7$ ft; $n = 150$; $\log v = 2.0638 + 0.0268 \log m$; $E_{gv} = 1.19$; $M_{50} = 252$ mg; $V_{50} = 134$ ft/sec.

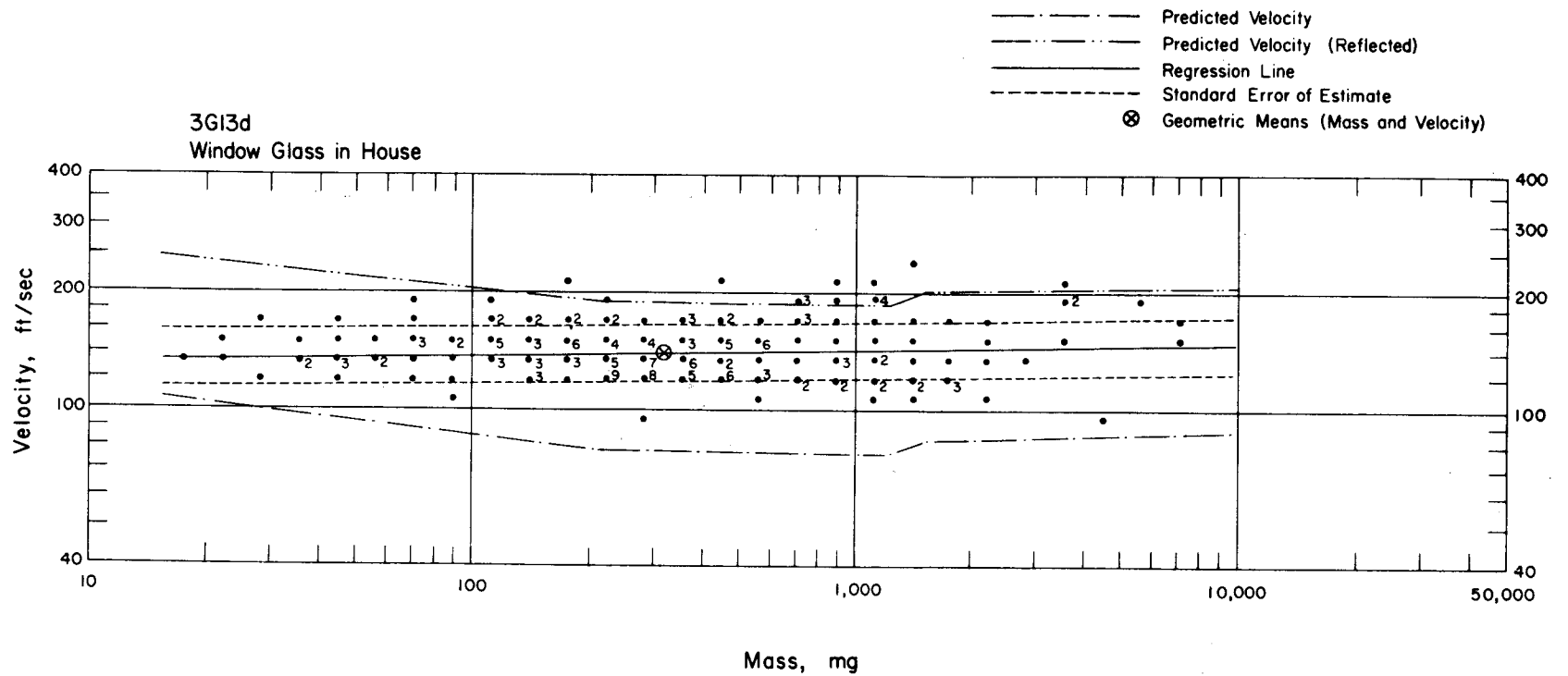


Fig. 6.39—Analysis of window-glass missiles from trap 3G13d: $d = 10.7$ ft; $n = 207$; $\log v = 2.1197 + 0.0124 \log m$; $E_{gv} = 1.18$; $M_{50} = 328$ mg; $V_{50} = 142$ ft/sec.

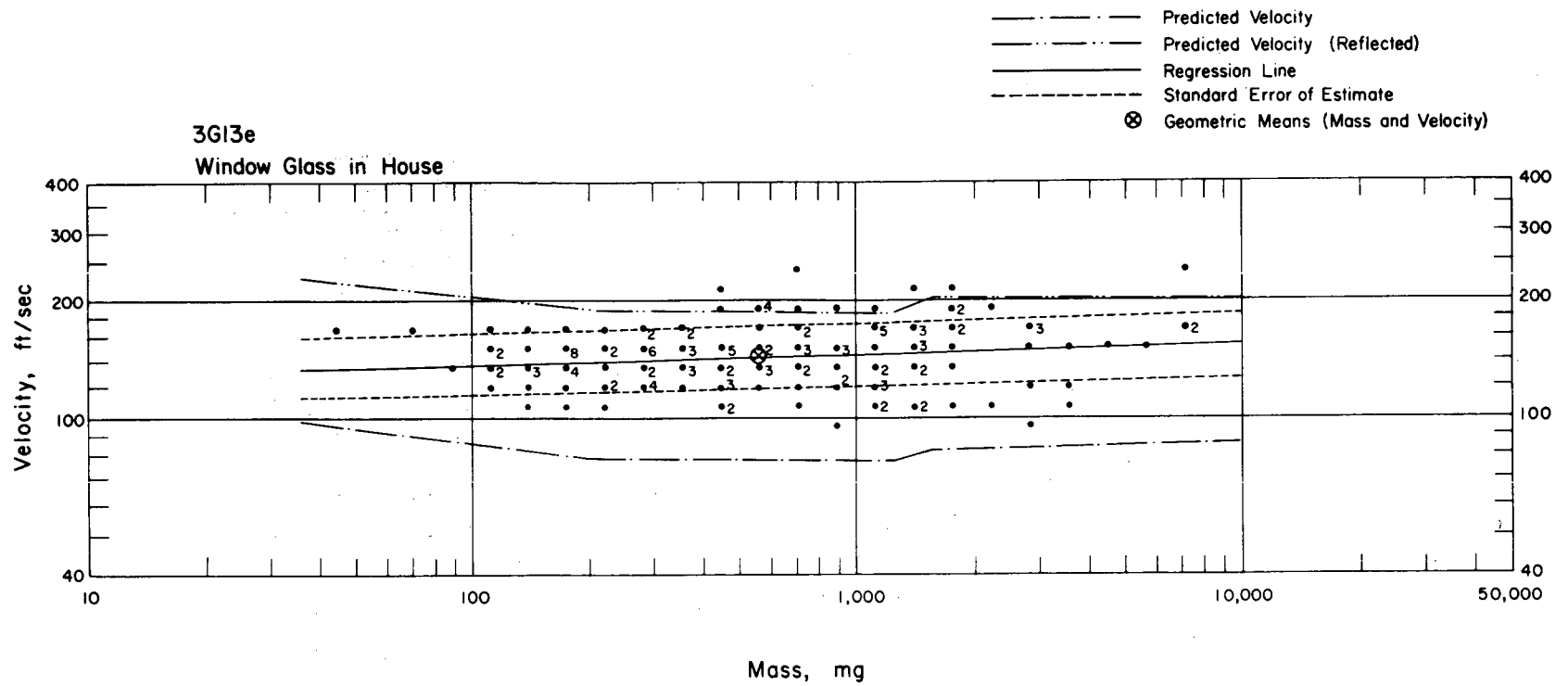


Fig. 6.40—Analysis of window-glass missiles from trap 3G13e: $d = 10.7$ ft; $n = 154$; $\log v = 2.0971 + 0.0221 \log m$; $E_{gv} = 1.20$; $M_{50} = 557$ mg; $V_{50} = 144$ ft/sec.

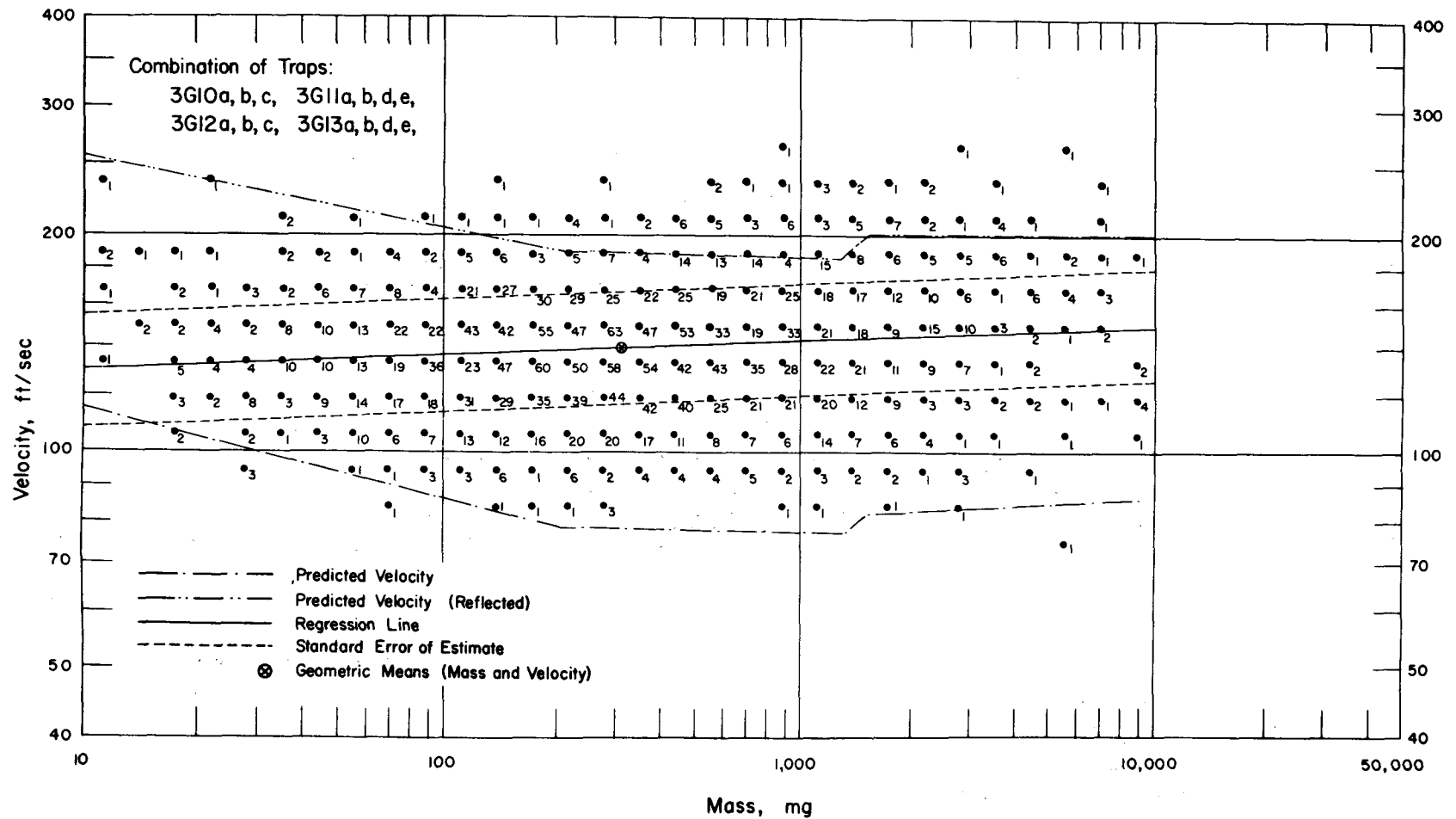


Fig. 6.41—Analysis of window-glass missiles from 14 traps (stations 3G10, 3G11, 3G12, and 3G13): d (average) = 10.3 ft; n = 2523; $\log v = 2.0913 + 0.0216 \log m$; $E_{GV} = 1.20$; $M_{50} = 321$ mg; $V_{50} = 140$ ft/sec.

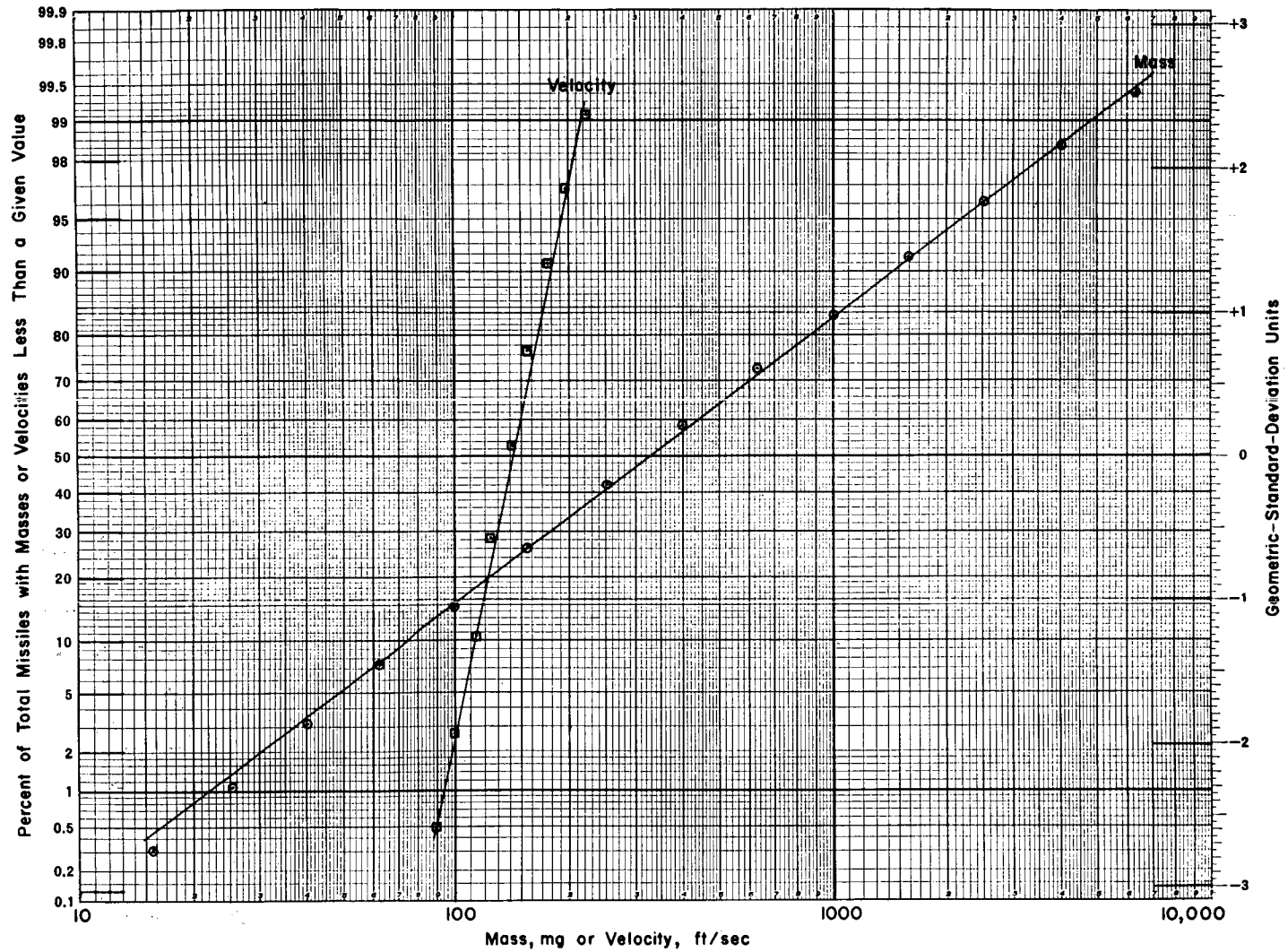
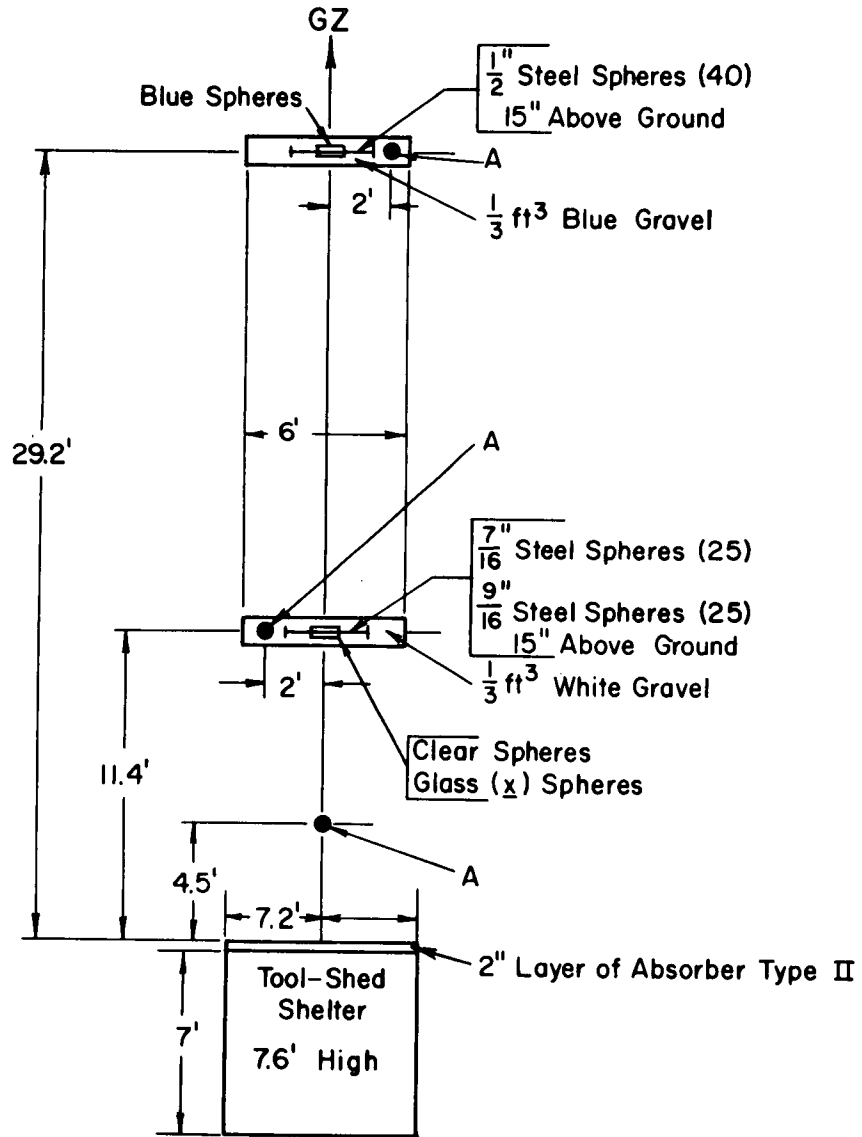


Fig. 6.42—Glass-fragment data for 14 traps in houses showing per cent of total missiles with masses or velocities less than a given value.
 $n = 2523$.

STATION: 4.3GTS
 RANGE: 3750'
 BLAST LINE: S 30° E of GZ



A = Weighted Croquet Ball, 40 $\frac{1}{2}$ " Above Ground

Fig. 6.43—Layout chart for station 4.3GTS.



Fig. 6.44—Preshot photograph of station 4.3GTS planted missiles. Large steel spheres are on trough-like support; weighted croquet ball, on rod support; marked gravel, in piles on the ground; small spheres, in packets between gravel piles.

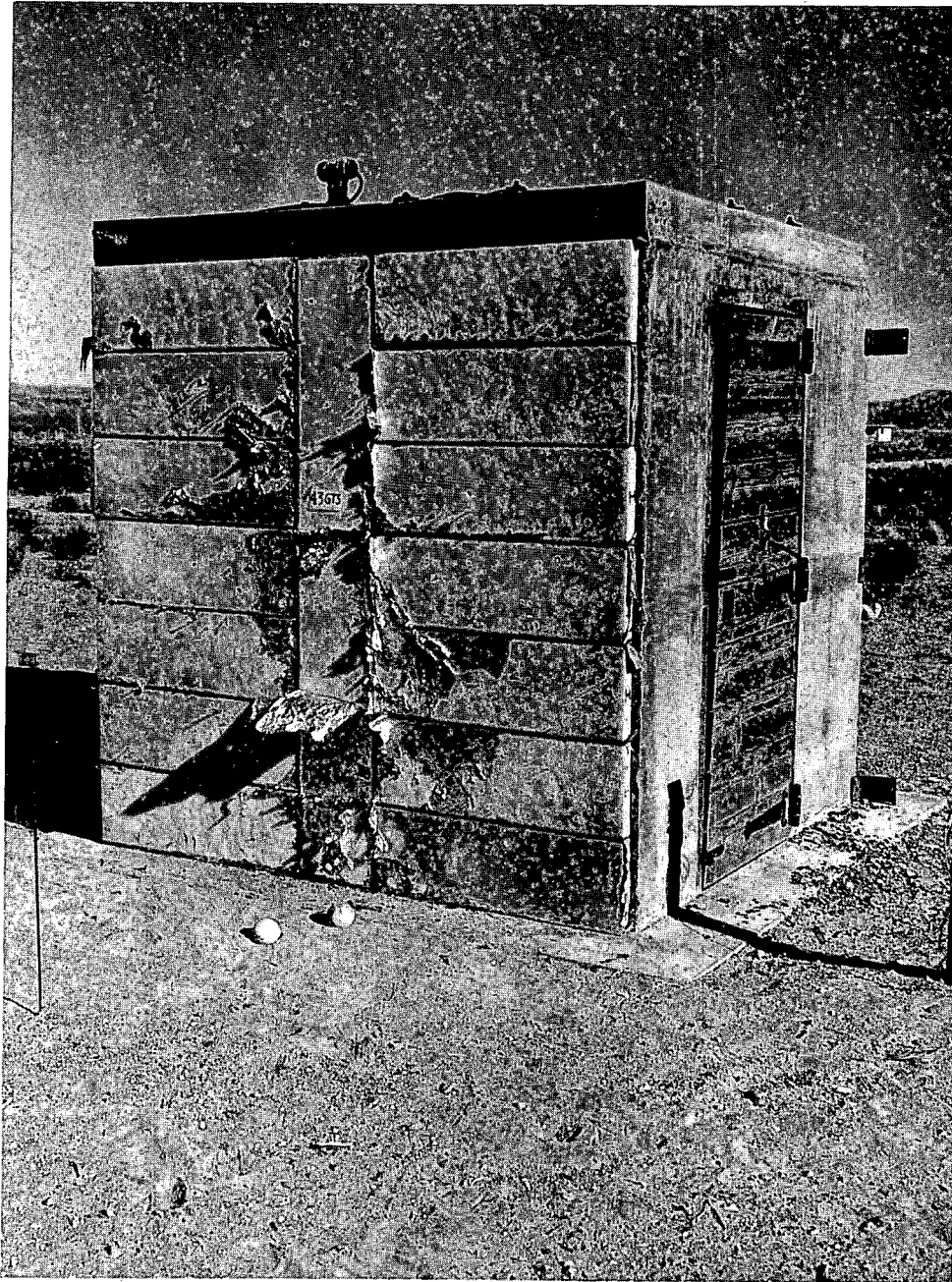


Fig. 6.45— Postshot photograph of station 4.3GTS installation. A 2-in.-thick layer of type II missile absorber was cemented to the side facing GZ of a tool-shed shelter.

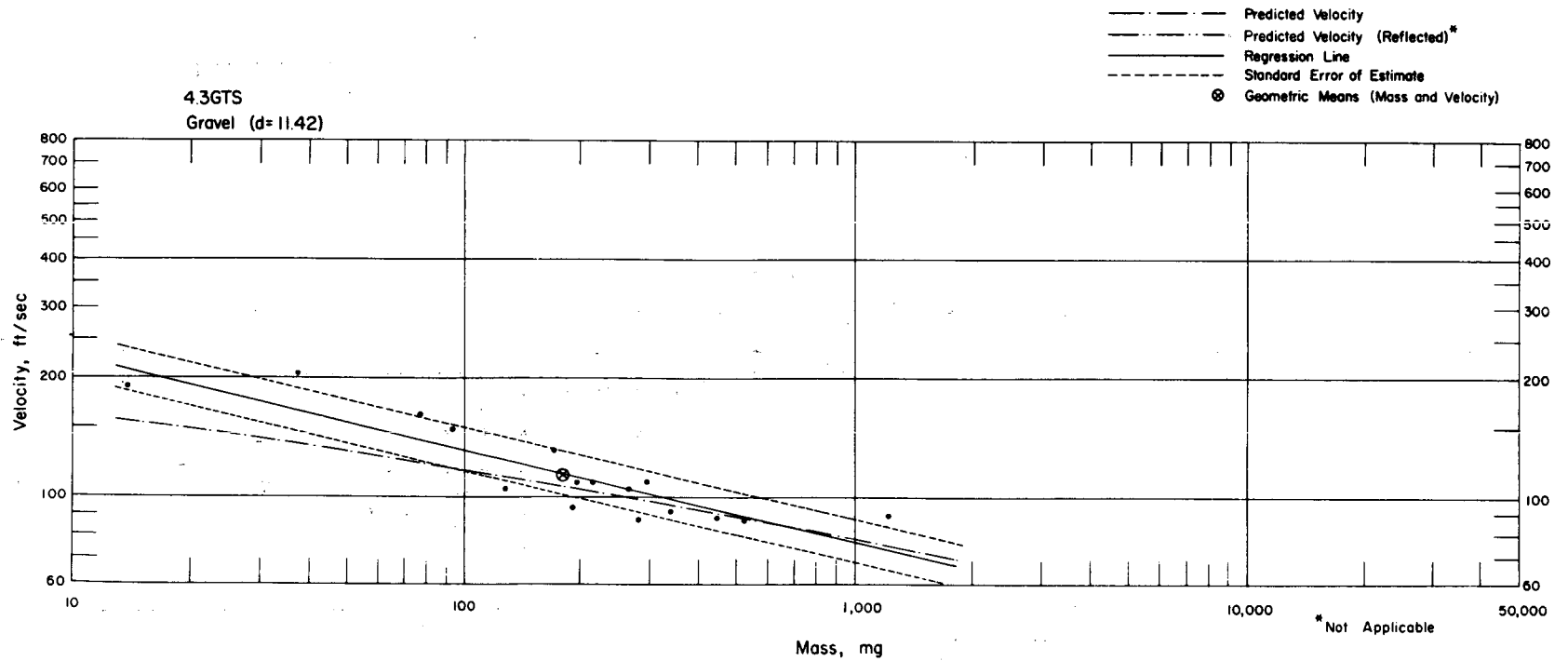


Fig. 6.46—Analysis of gravel missiles from station 4.3GTS: $d = 11.4$ ft; $n = 16$; $\log v = 2.5852 - 0.2323 \log m$; $E_{gv} = 1.14$; $M_{50} = 182$ mg; $V_{50} = 115$ ft/sec.

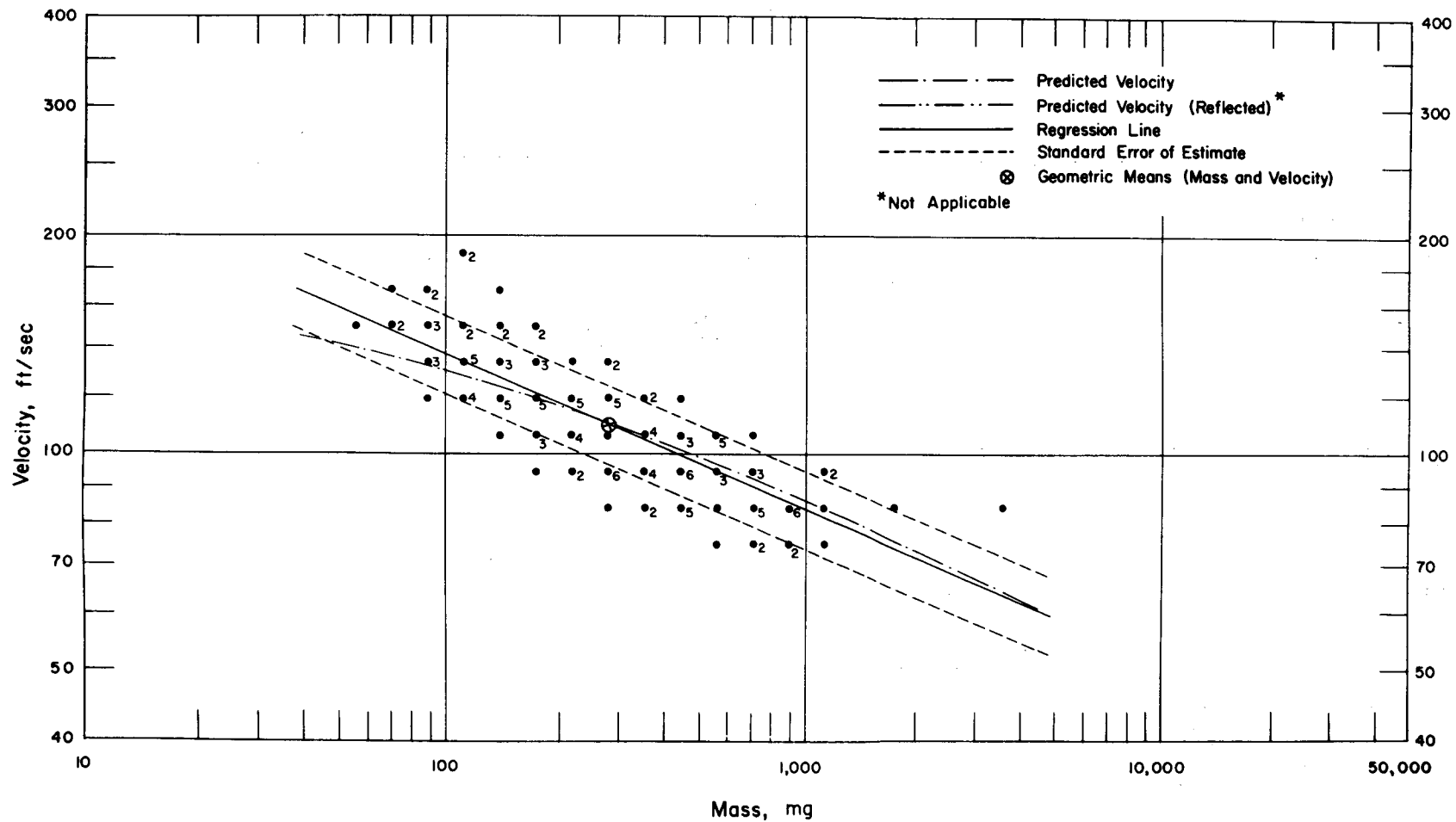


Fig. 6.47—Analysis of gravel missiles from station 4.3GTS: $d = 29.2$ ft; $n = 145$; $\log v = 2.5803 - 0.2227 \log m$; $E_{gv} = 1.13$; $M_{50} = 288$ mg; $V_{50} = 108$ ft/sec.

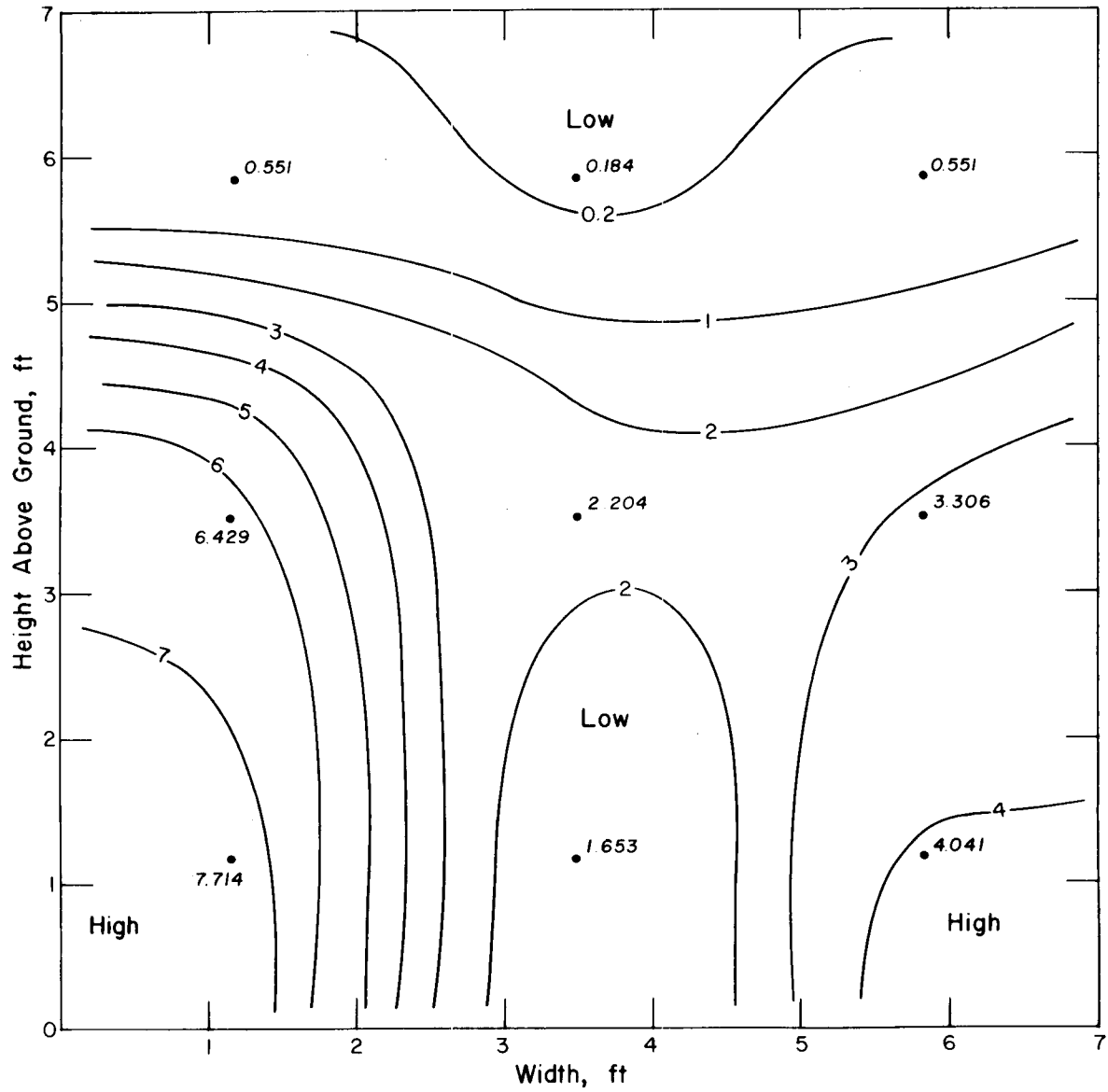


Fig. 6.48—Spatial distribution of gravel missiles, $d = 29.2$ ft, recovered from station 4.3GTS. The numbers refer to the number of missiles per square foot passing through the front surface of the trap.

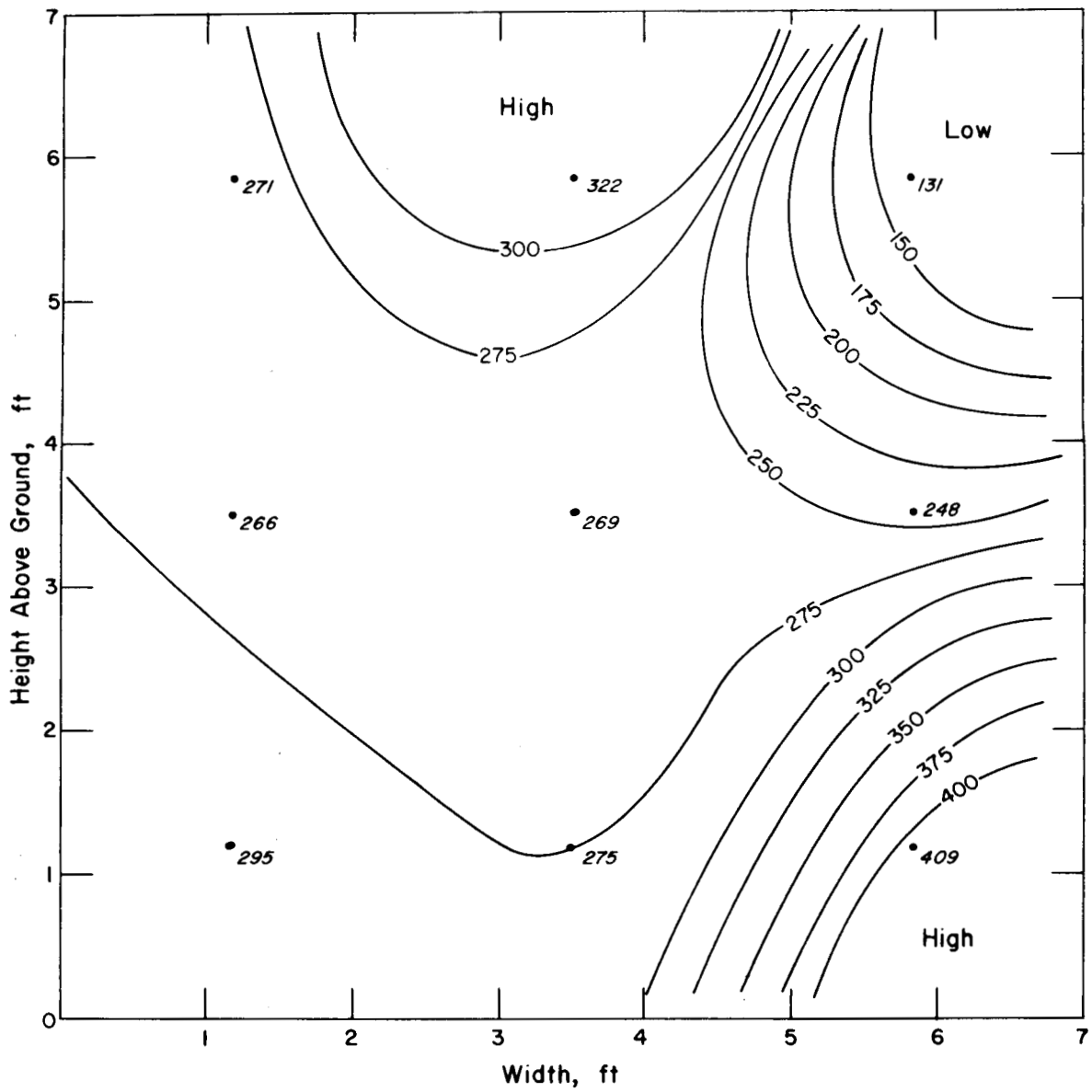


Fig. 6.49—Spatial distribution of the average masses (in mg) of gravel missiles, $d = 29.2$ ft, recovered from station 4.3GTS. The average mass of missiles caught within a particular area segment was plotted at the center of the segment.

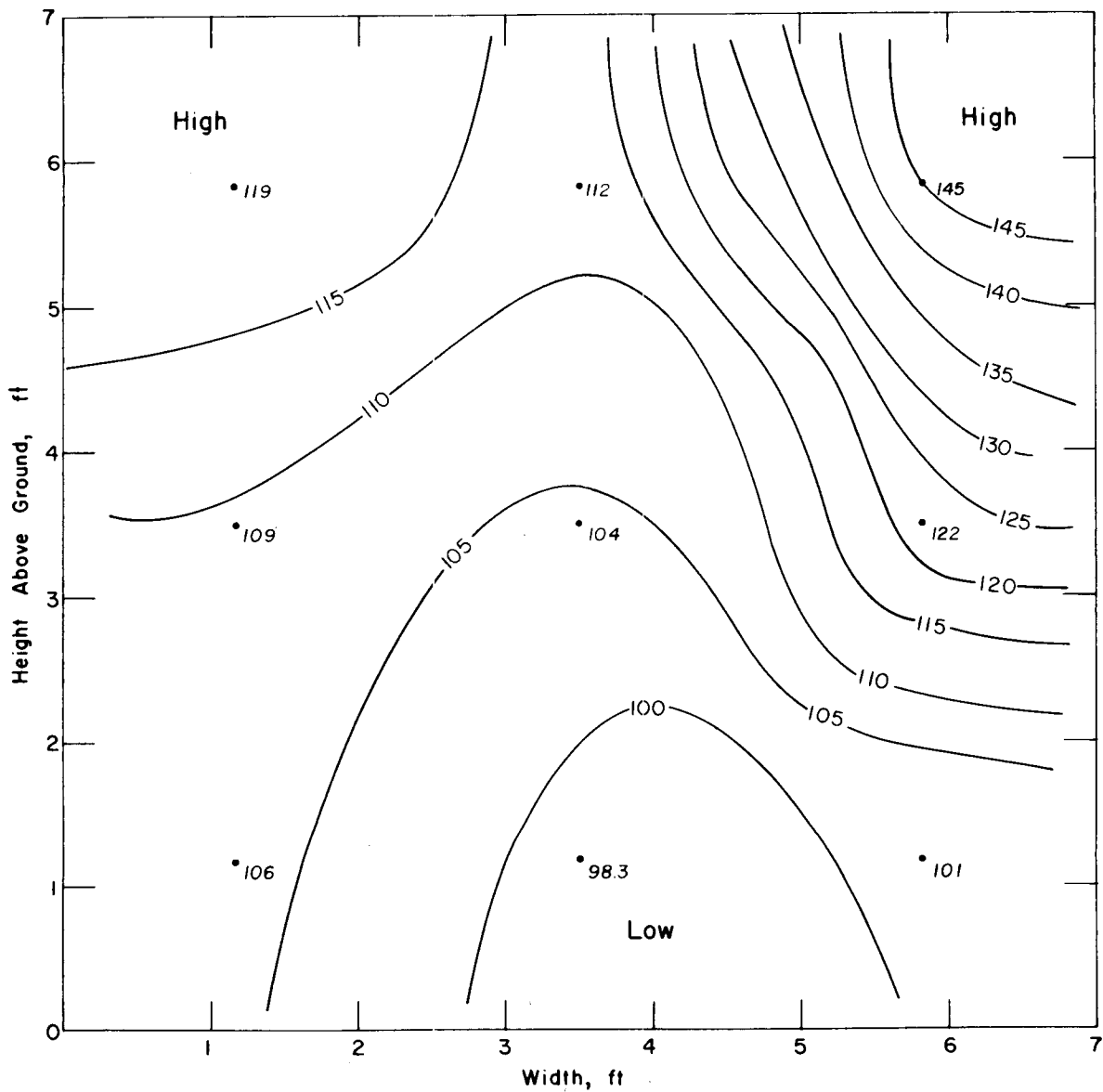


Fig. 6.50—Spatial distribution of the average velocities (in ft/sec) of gravel missiles, $d = 29.2$ ft, recovered from station 4.3GTS. The average velocity of missiles caught within a particular area segment was plotted at the center of the segment.

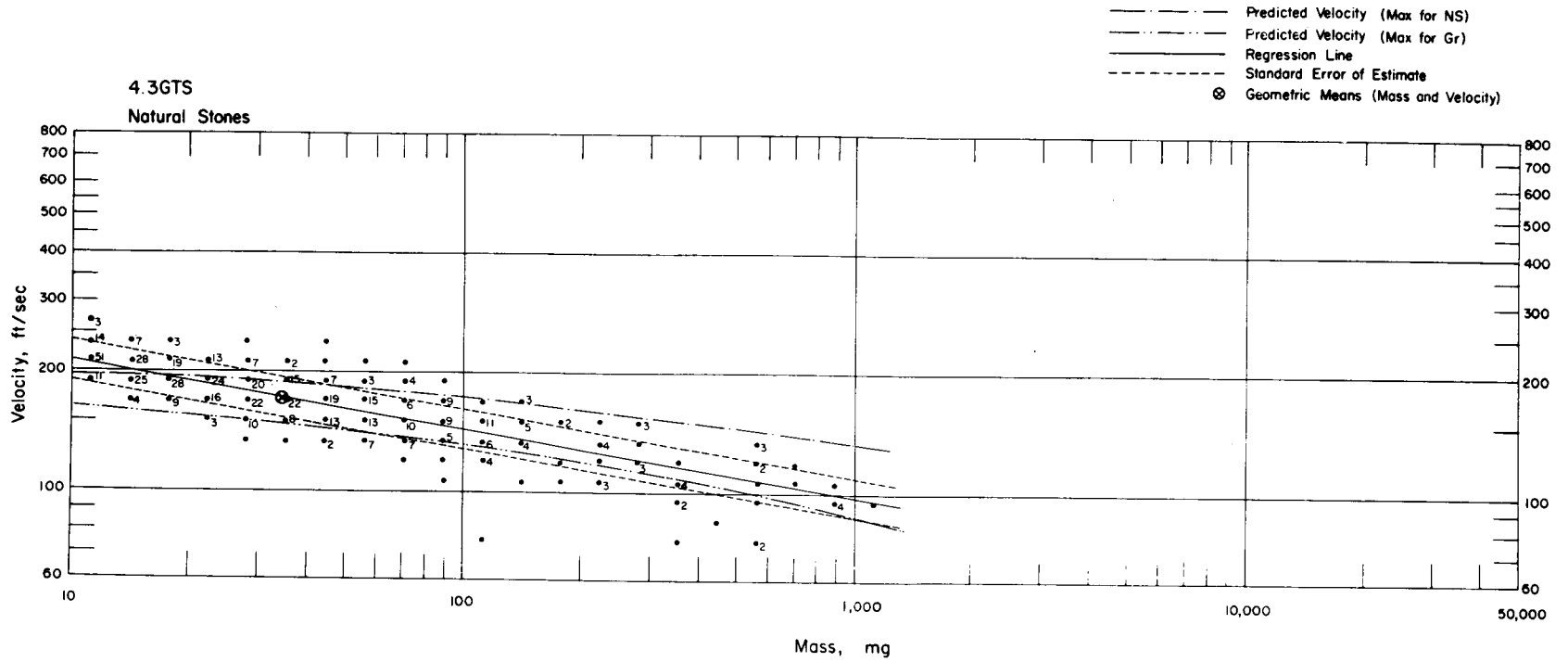


Fig. 6.51—Analysis of natural-stone missiles from station 4.3GTS: $n = 586$; $\log v = 2.4969 - 0.1691 \log m$; $E_{gv} = 1.12$; $M_{50} = 35.2$ mg; $V_{50} = 172$ ft/sec.

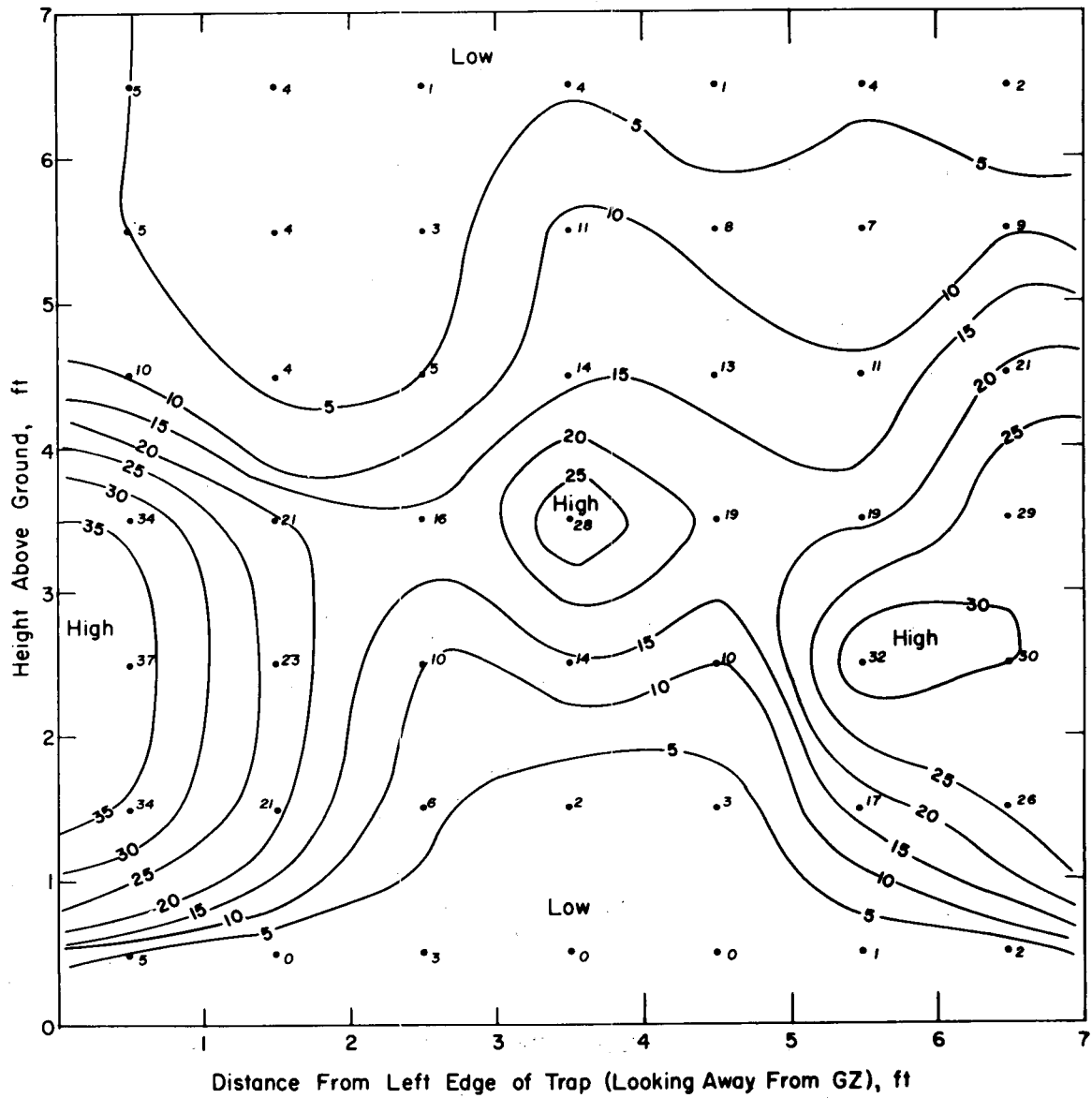


Fig. 6.52—Spatial distribution of natural-stone missiles recovered from station 4.3GTS. Numbers indicate missiles per square foot.

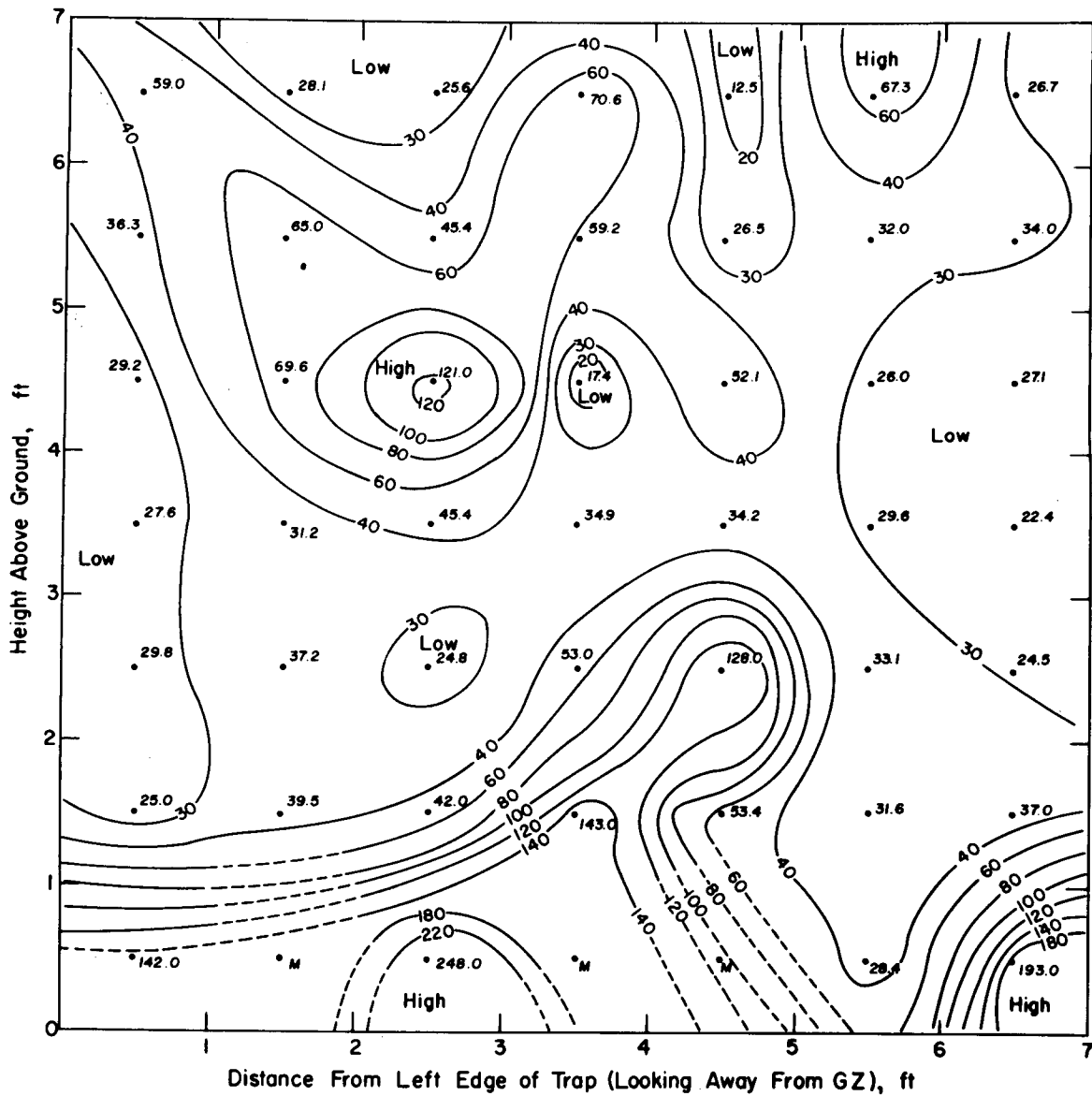


Fig. 6.53—Spatial distribution of the average masses (in mg) of natural-stone missiles recovered from station 4.3GTS. The average mass of missiles caught within a particular area segment was plotted at the center of the segment.

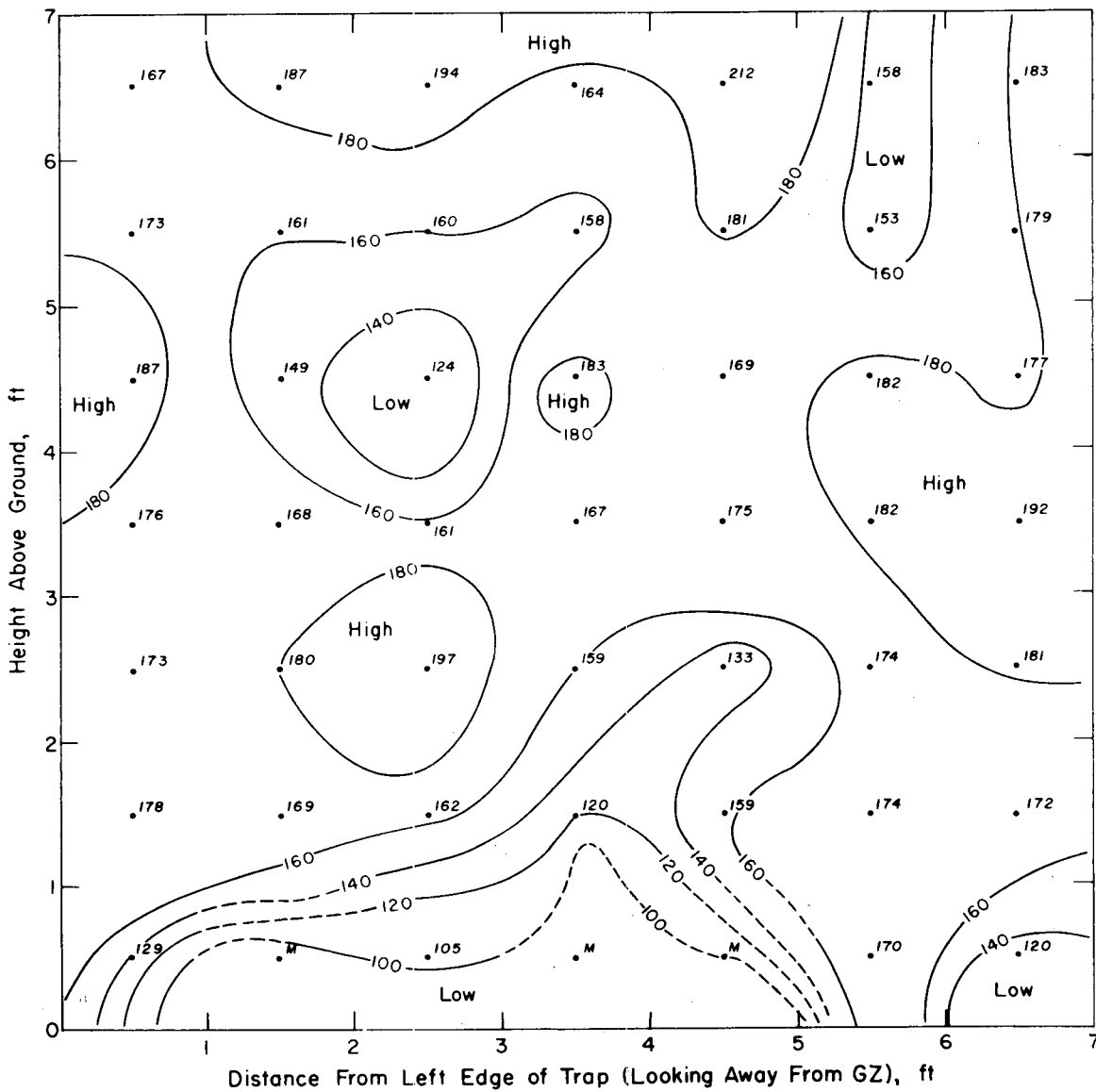


Fig. 6.54—Spatial distribution of the average velocities (in ft/sec) of natural-stone missiles recovered from station 4.3GTS. The average velocity of missiles caught within a particular area segment was plotted at the center of the segment.

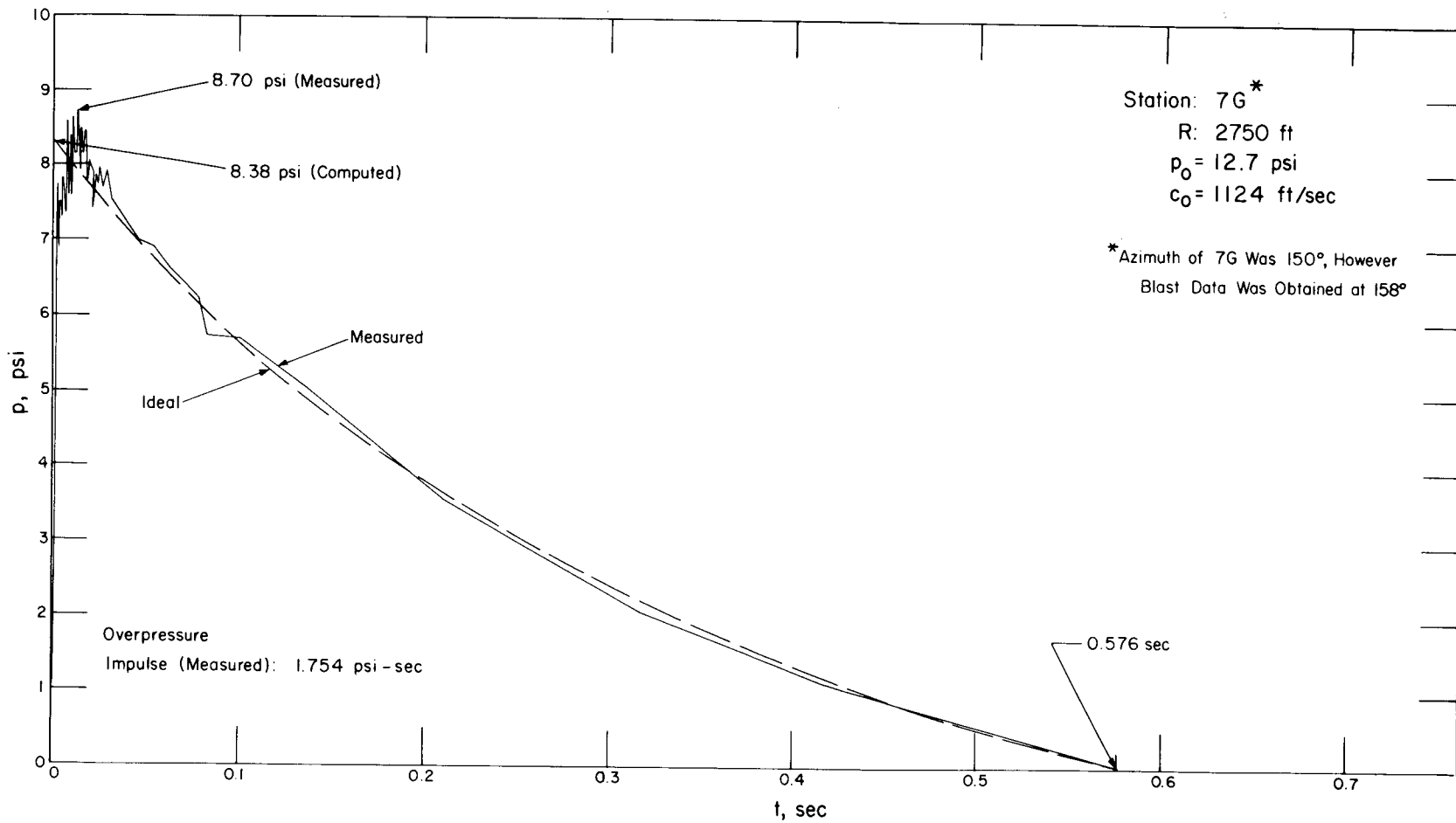


Fig. 6.55—Overpressure vs. time for stations 7GTS and 7G.

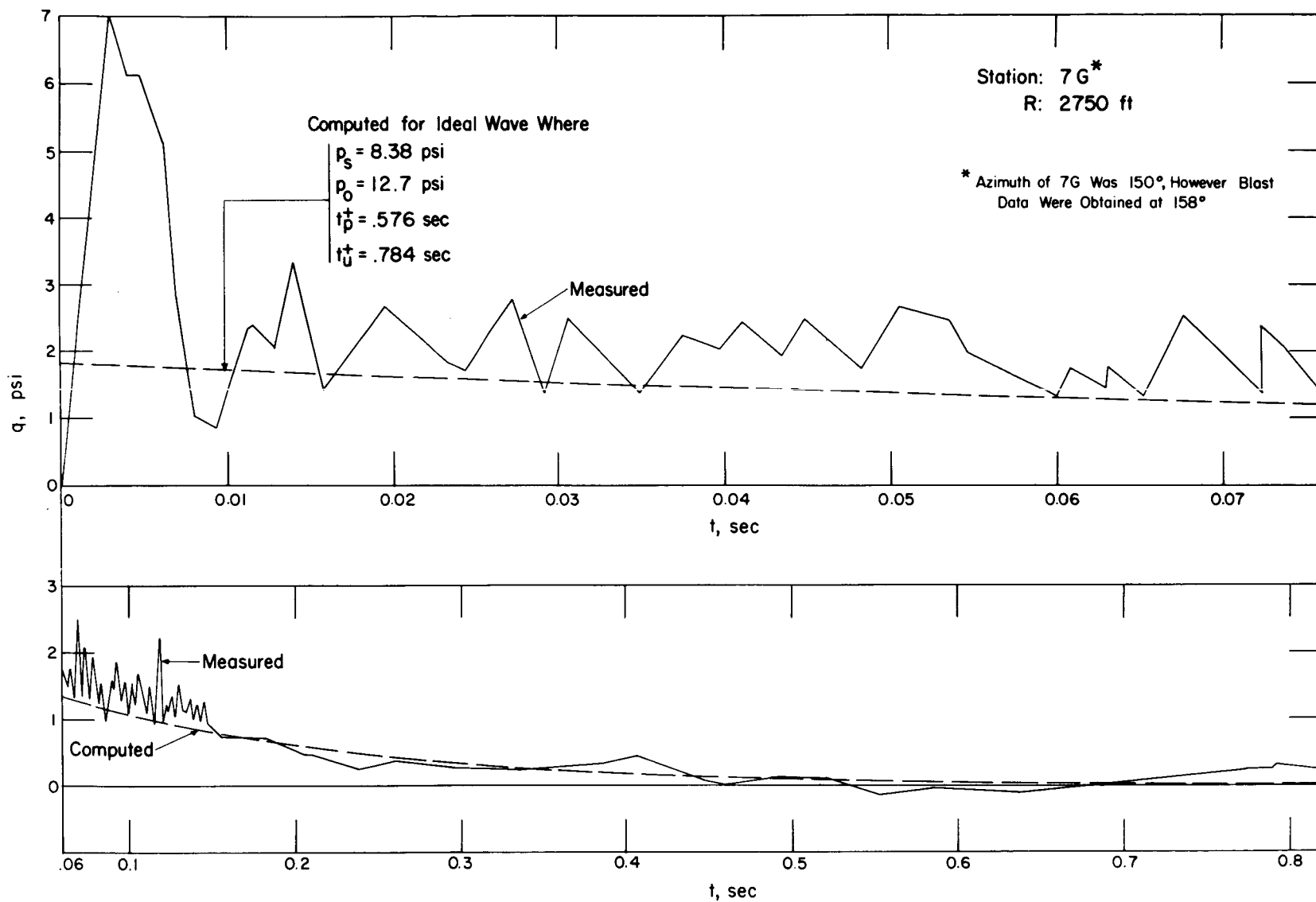
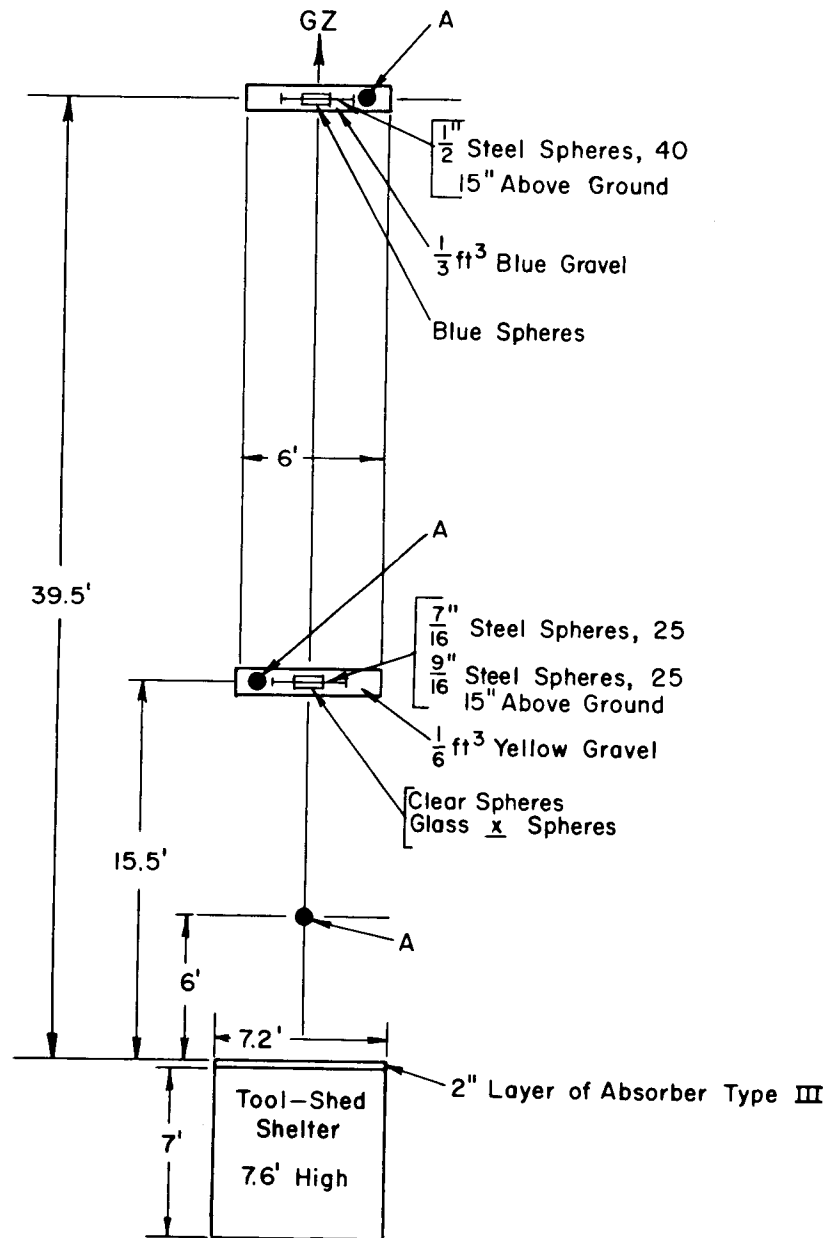


Fig. 6.56—Dynamic pressure vs. time for stations 7GTS and 7G.

STATION: 7GTS
 RANGE: 2750'
 BLAST LINE: S 30° E of GZ



A = Weighted Croquet Ball, 40 ¹/₂" Above Ground

Fig. 6.57—Layout chart for station 7GTS.

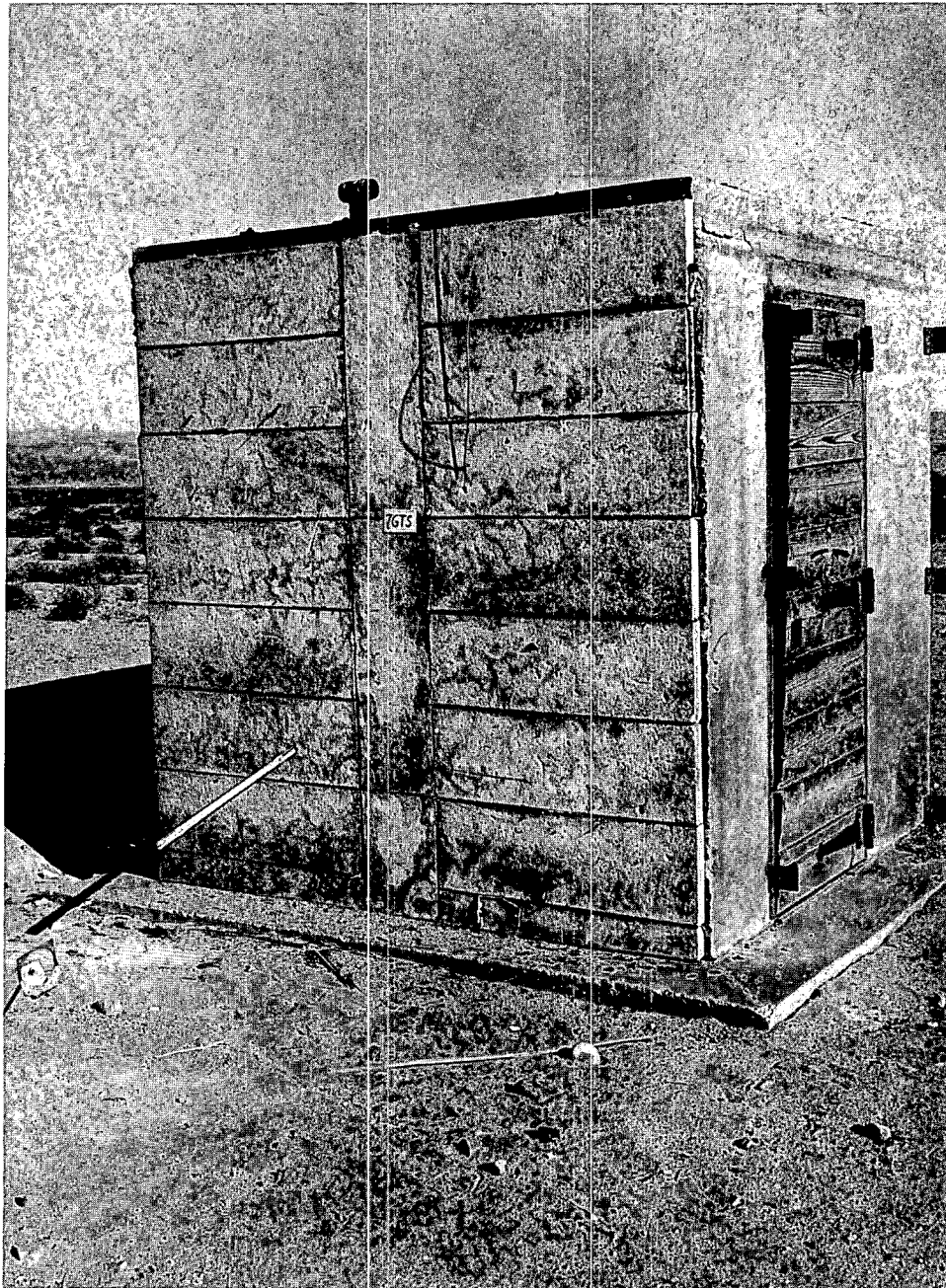


Fig. 6.58 — Station 7GTS, postshot. This station used a 2-in.-thick layer of type III absorber cemented to the side of the tool shed which faced GZ.

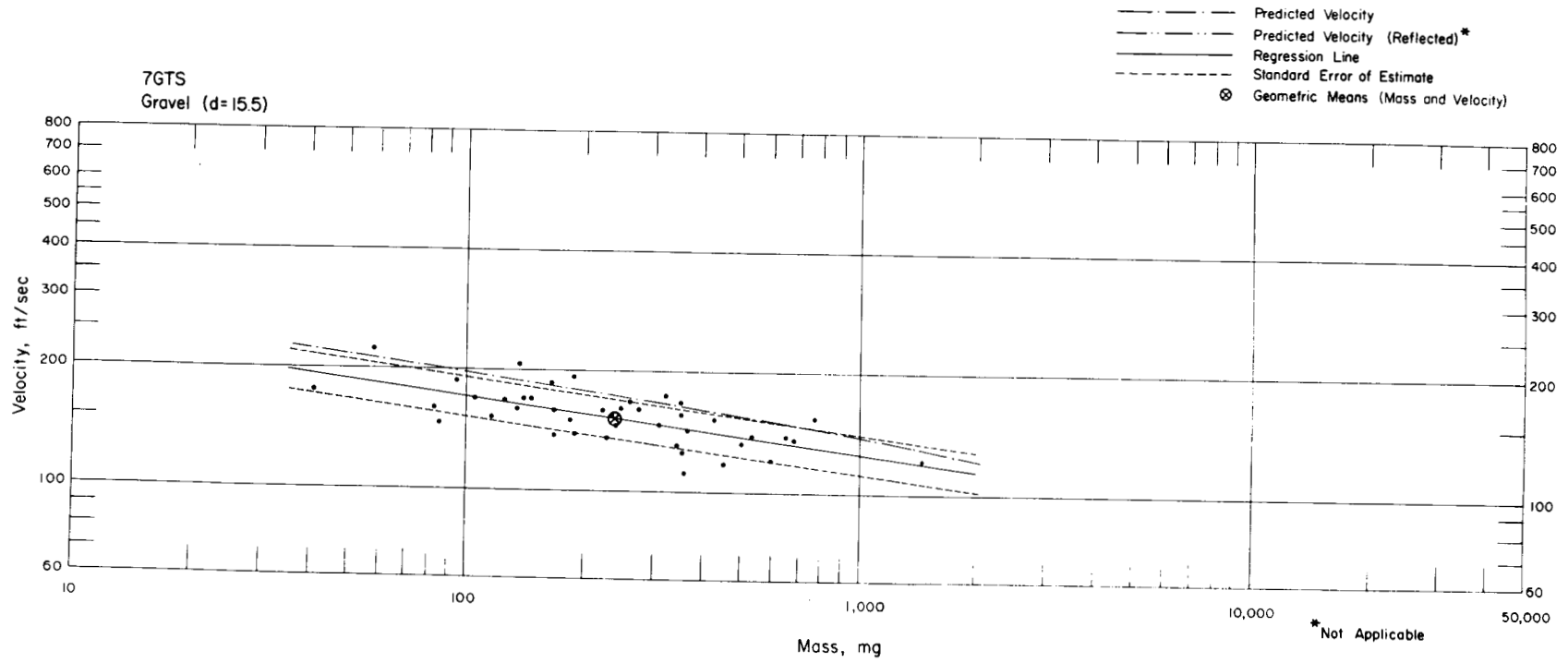


Fig. 6.59—Analysis of gravel missiles from station 7GTS: $d = 15.5$ ft; $n = 42$; $\log v = 2.4966 - 0.1318 \log m$; $E_{gv} = 1.12$; $M_{50} = 236$ mg; $V_{50} = 153$ ft/sec.

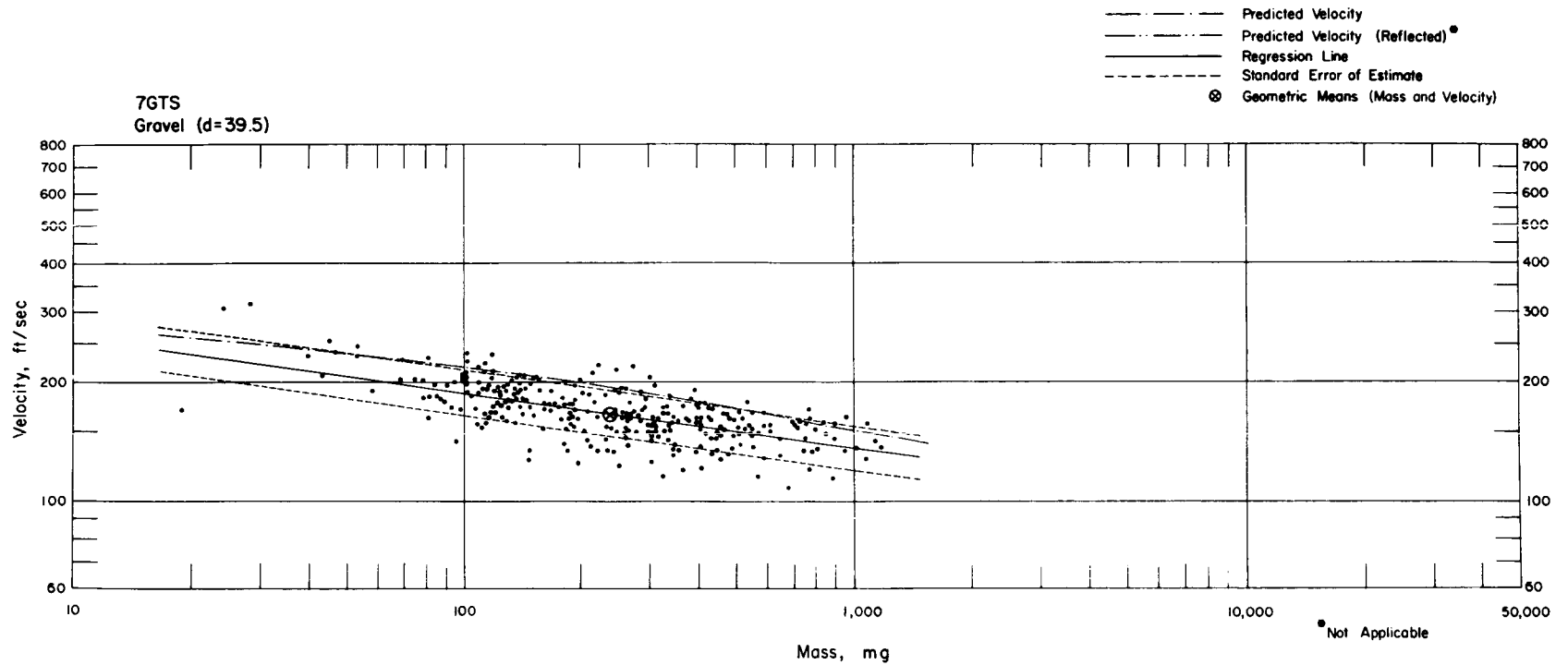


Fig. 6.60—Analysis of gravel missiles from station 7GTS: $d = 39.5$ ft; $n = 294$; $\log v = 2.5533 - 0.1397 \log m$; $E_{gv} = 1.14$; $M_{50} = 239$ mg; $V_{50} = 166$ ft/sec.

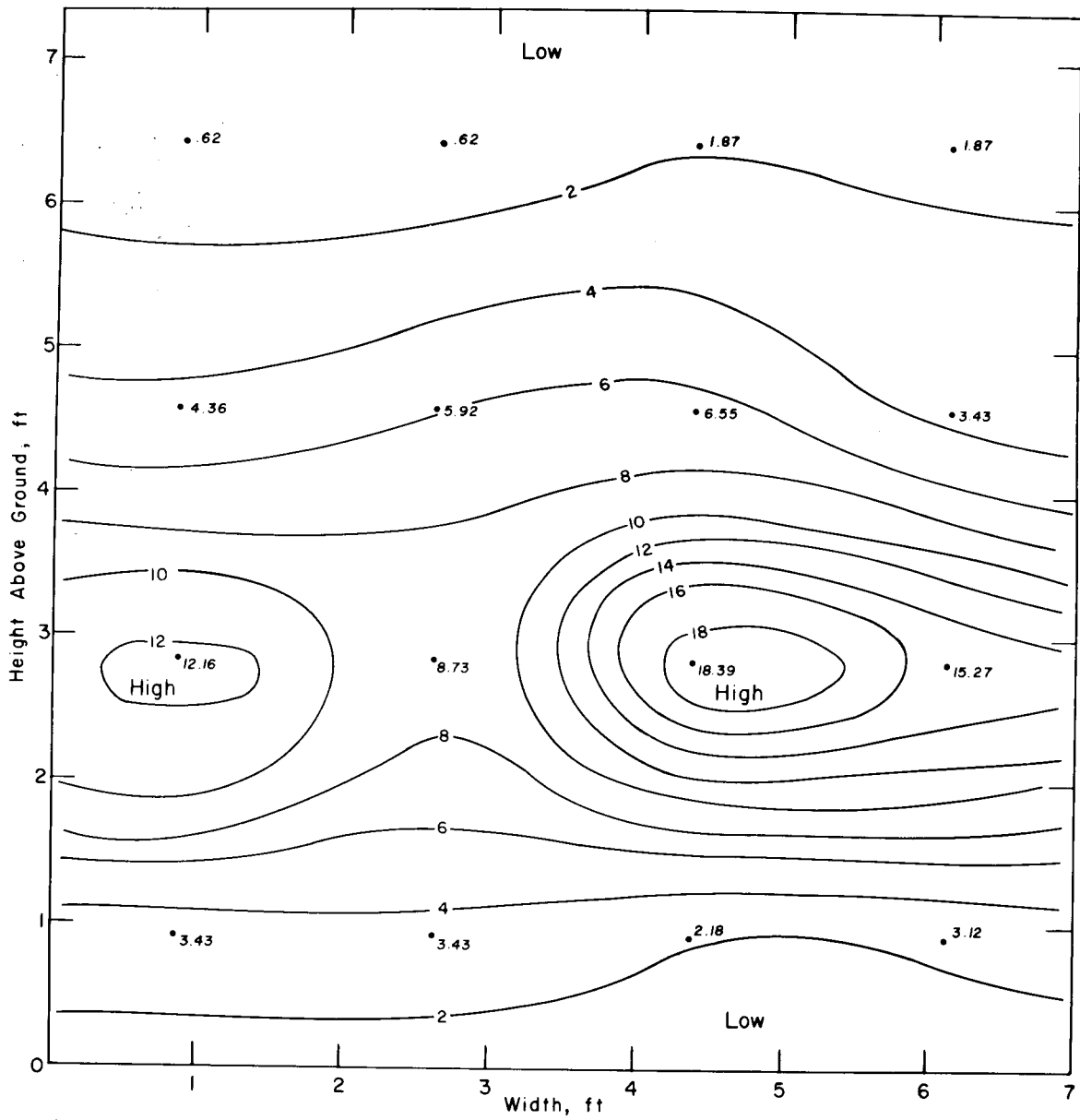


Fig. 6.61—Spatial distribution of gravel missiles, $d = 39.5$ ft, recovered from station 7GTS. Numbers indicate missiles per square foot.

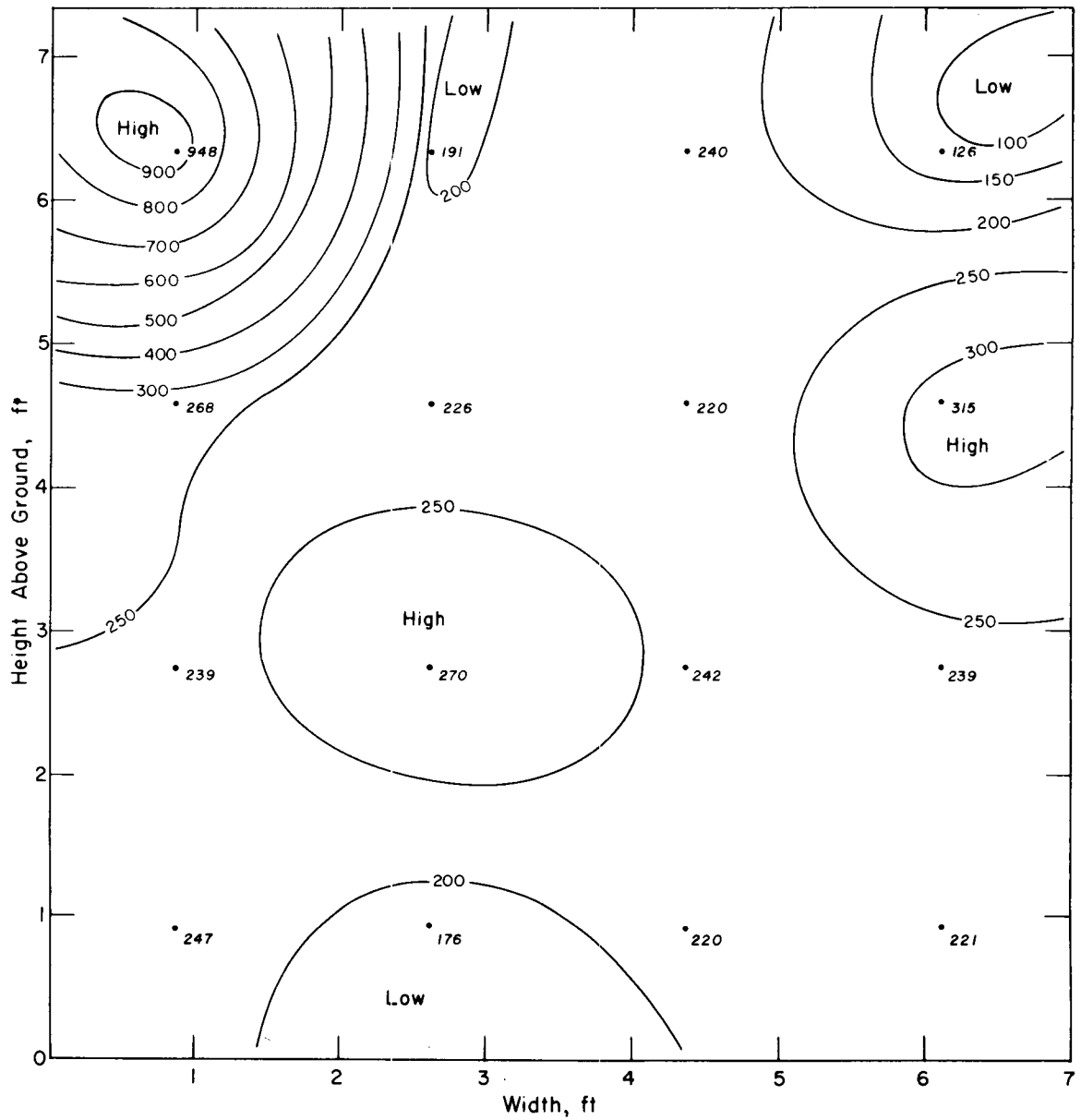


Fig. 6.62—Spatial distribution of the average masses (in mg) of gravel missiles, $d = 39.5$ ft, recovered from station 7GTS. The average mass of missiles caught within a particular area segment was plotted at the center of the segment.

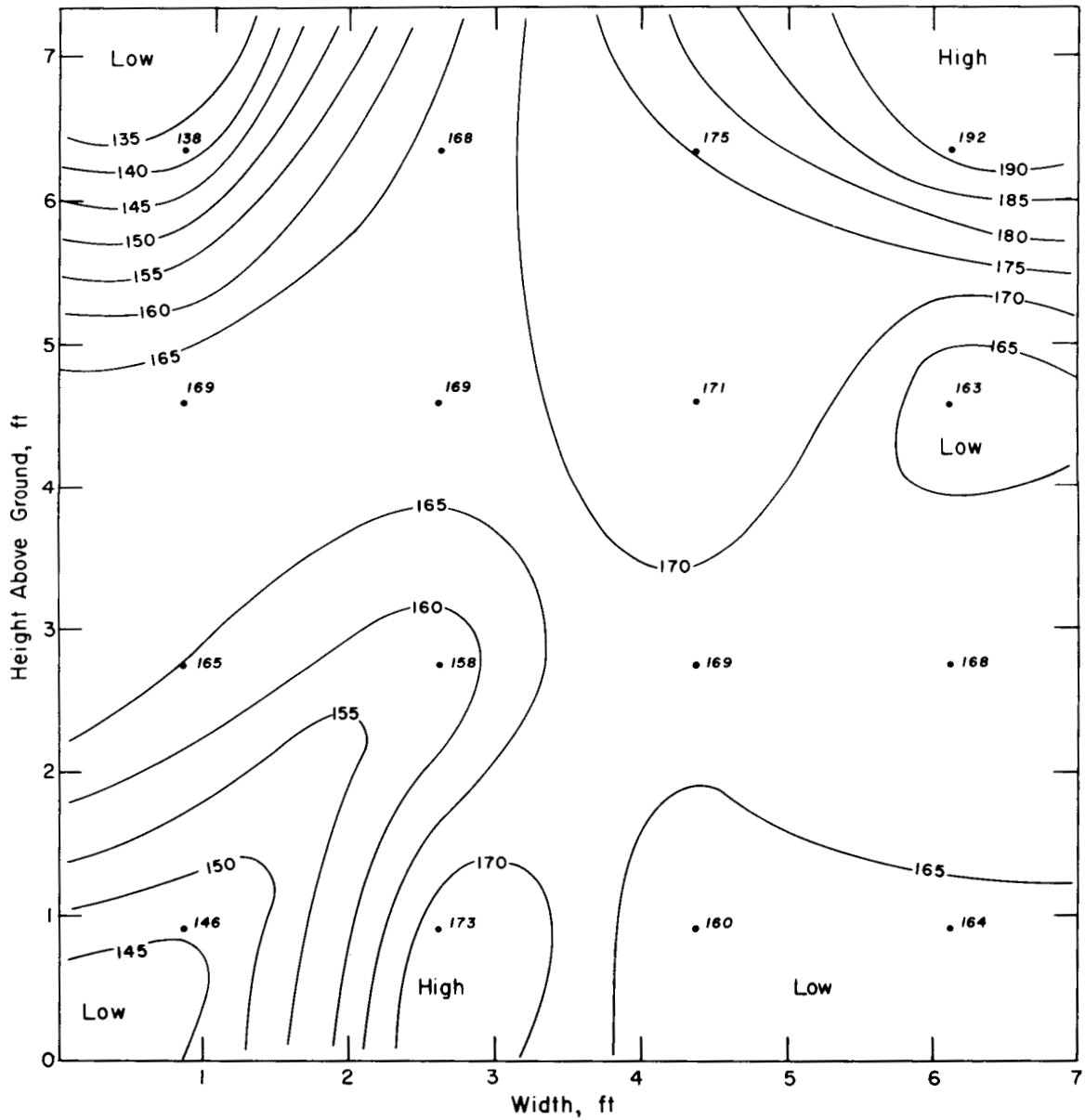


Fig. 6.63—Spatial distribution of the average velocities (in ft/sec) of gravel missiles, $d = 39.5$ ft, recovered from station 7GTS. The average velocity of missiles caught within a particular area segment was plotted at the center of the segment.

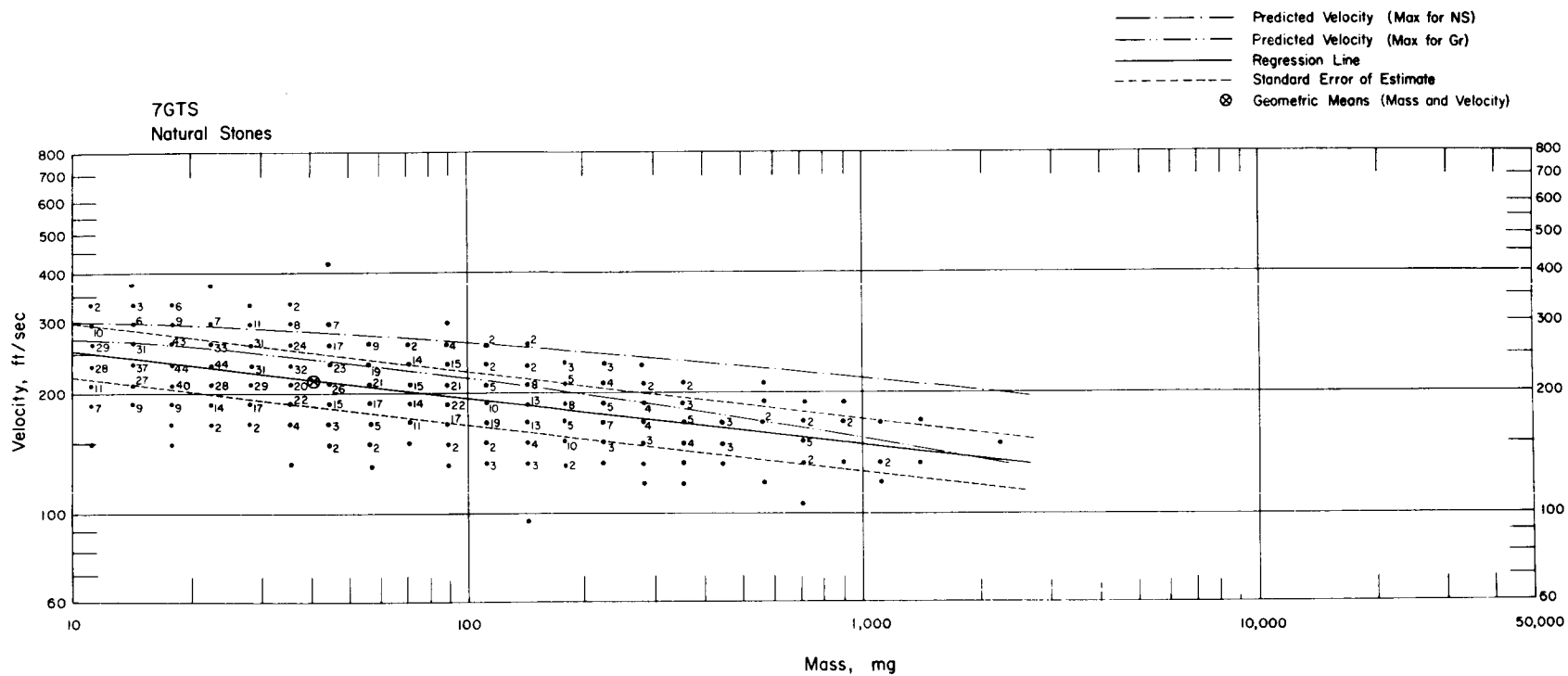


Fig. 6.64—Analysis of natural-stone missiles from station 7GTS: $n = 1238$; $\log v = 2.5314 - 0.1201 \log m$; $E_{gv} = 1.17$; $M_{50} = 40.5$ mg; $V_{50} = 218$ ft/sec.

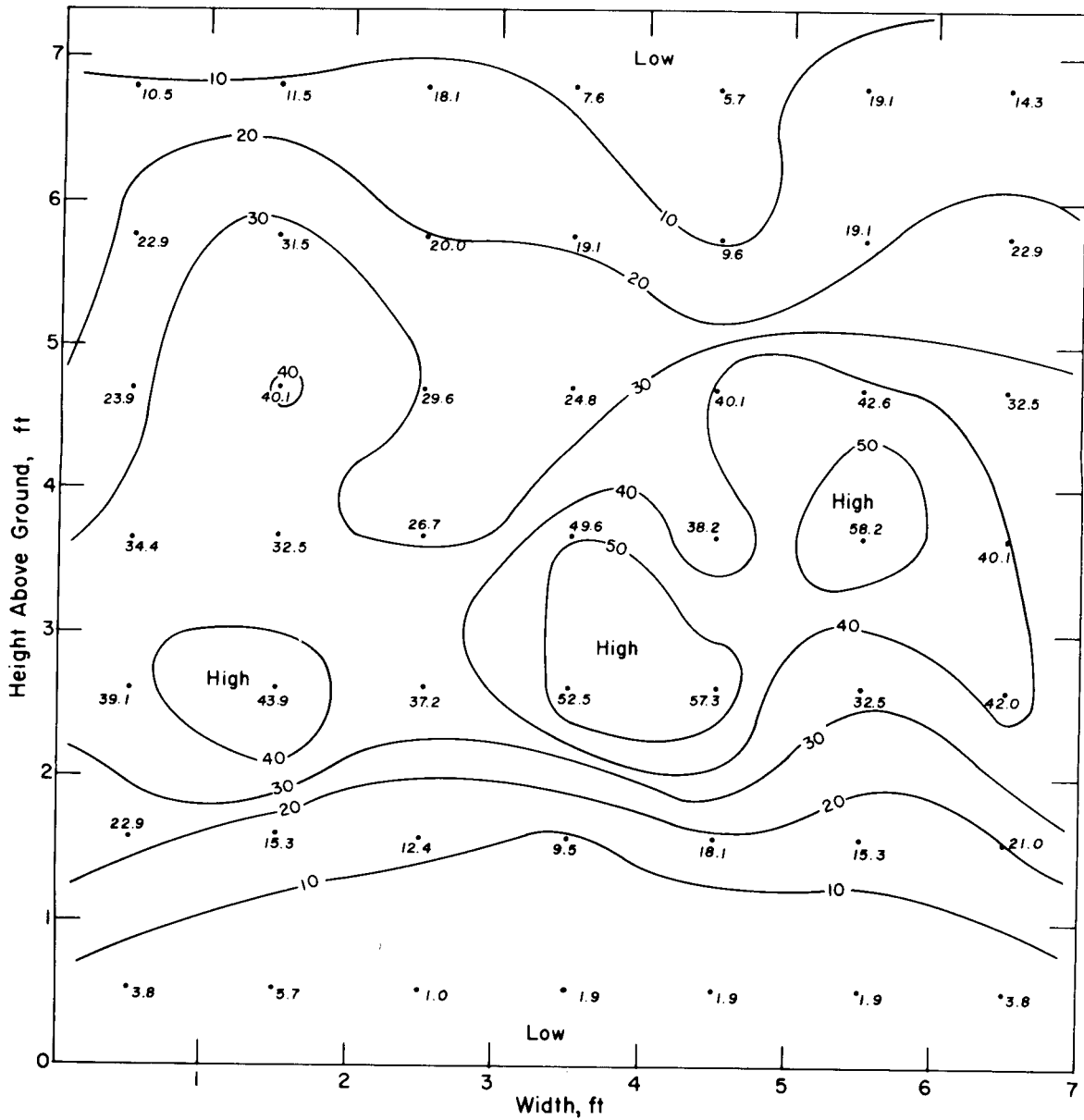


Fig. 6.65—Spatial distribution of natural-stone missiles recovered from station 7GTS. Numbers indicate missiles per square foot.

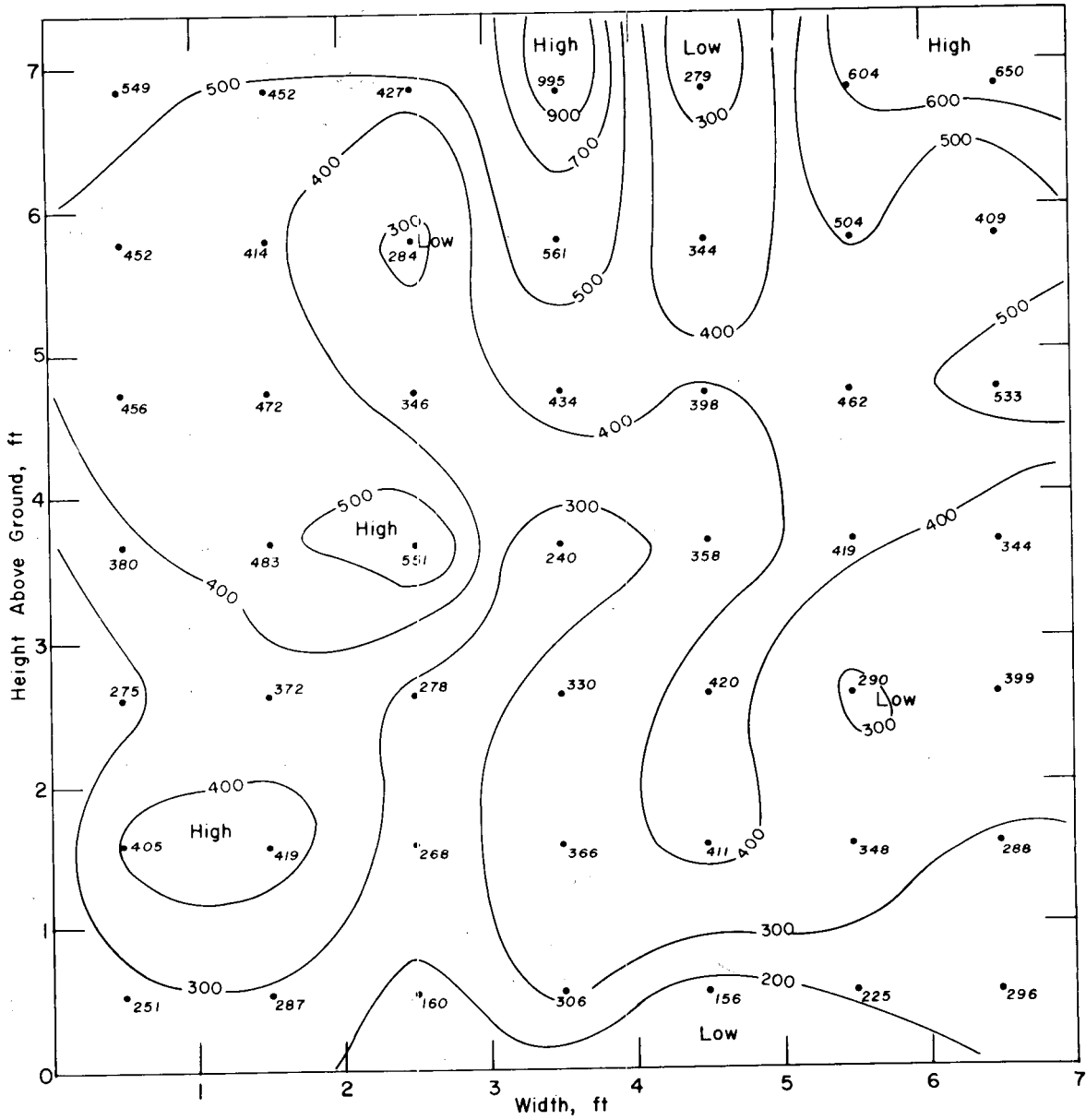


Fig. 6.66—Spatial distribution of the average masses (in mg) of natural-stone missiles recovered from station 7GTS. The average mass of missiles caught within a particular area segment was plotted at the center of the segment.

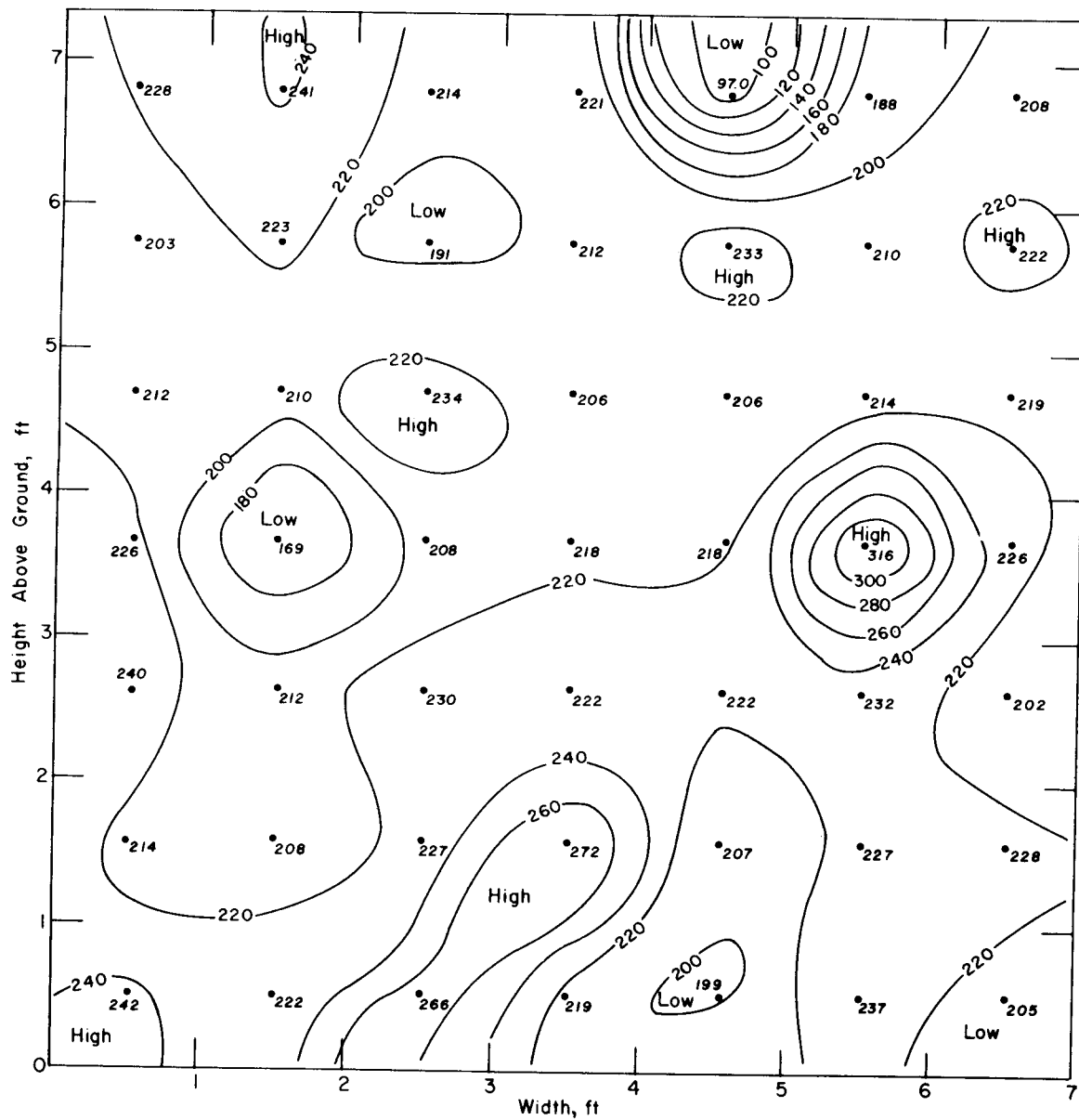


Fig. 6.67—Spatial distribution of the average velocities (in ft/sec) of natural-stone missiles recovered from station 7GTS. The average velocity of missiles caught within a particular area segment was plotted at the center of the segment.

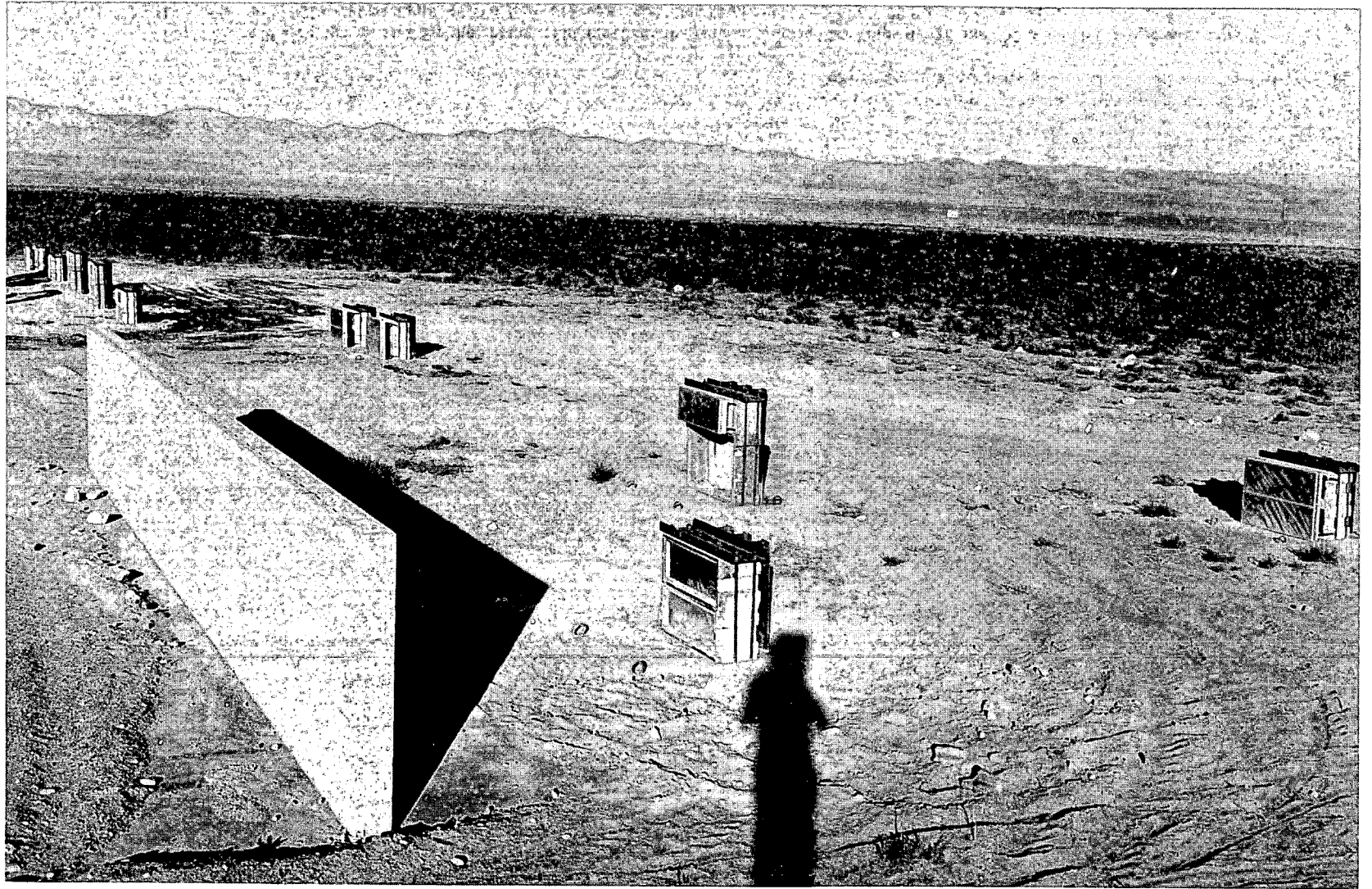


Fig. 6.69—Concrete-block wall (64 in. high, 40 ft long, and 7.5 in. thick) at station 7G, preshot.

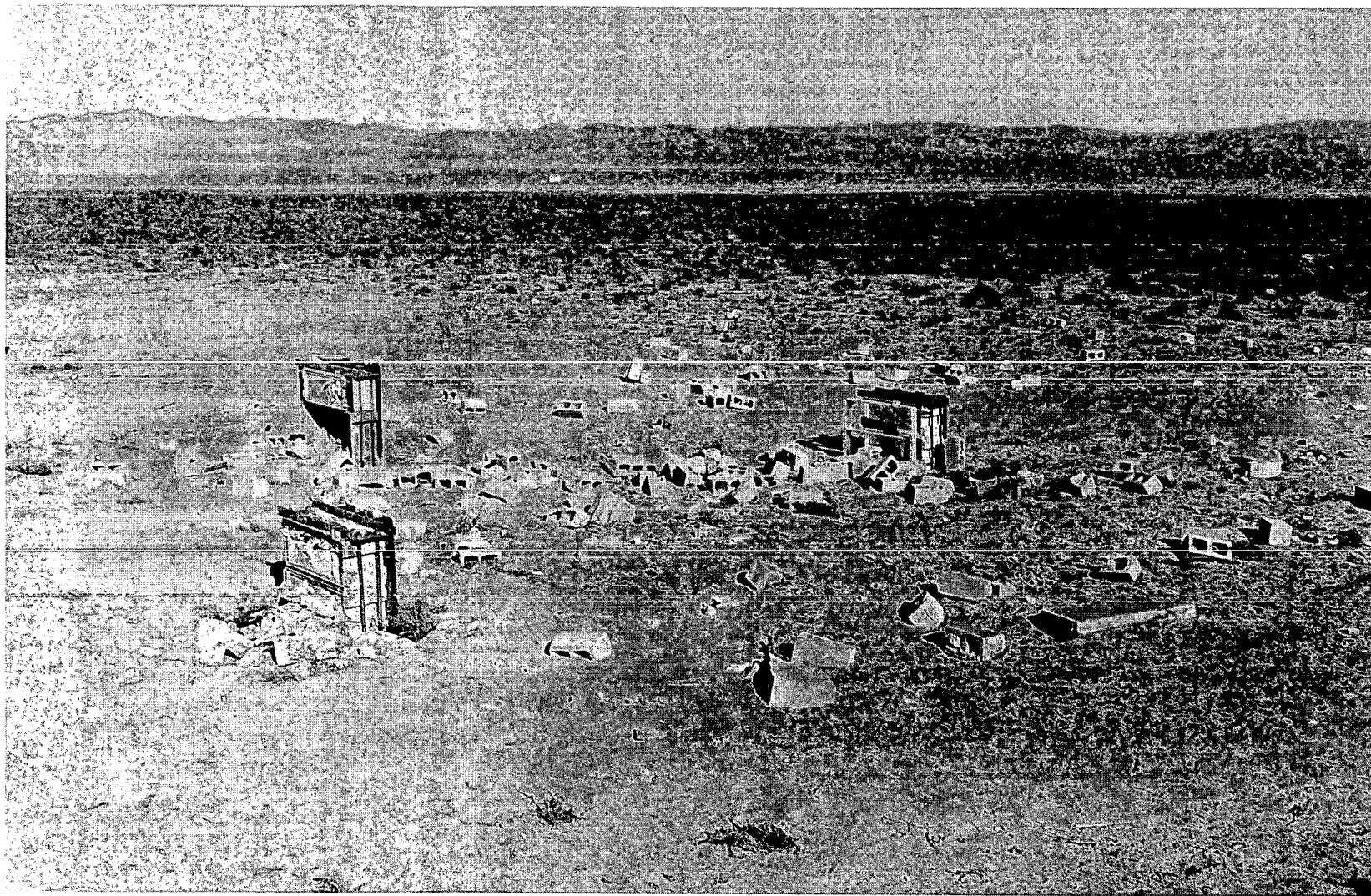


Fig. 6.70—Photograph illustrating the scatter of blocks from the wall at station 7G. Traps shown are: 7G1a and b (foreground), 10.2 ft from the wall; 7G2a and b (right), 40.2 ft from the wall; and 7G3b (behind 7G1a and b), 20.2 ft from the wall.

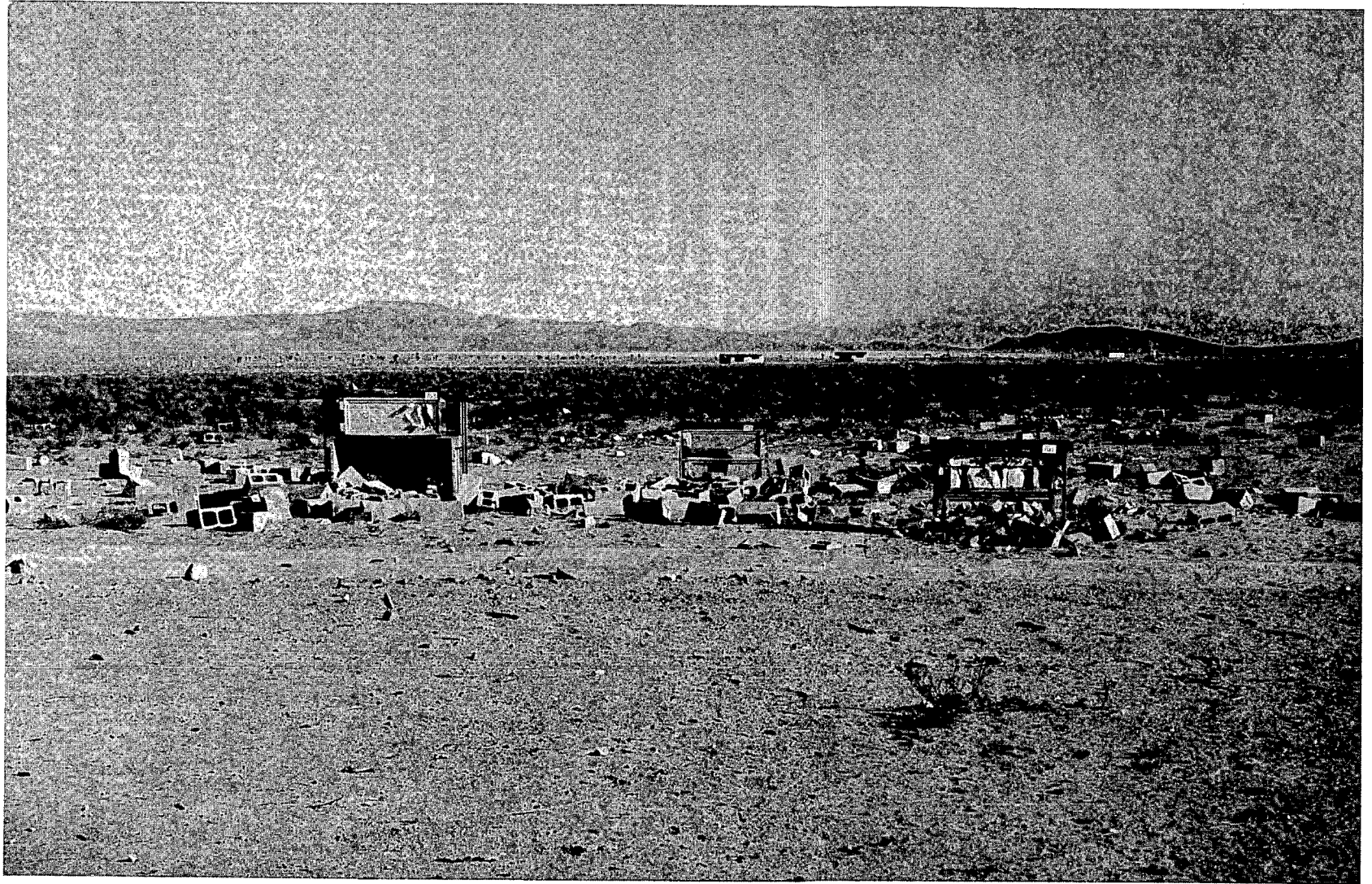


Fig. 6.71—Blocks from the concrete-block wall and traps 7G1a and b, 7G2a and b, and 7G3b, postshot.



427

Fig. 6.72—Traps 7G1a and b (foreground) and 7G2a and b (background). The absorbers in the installation 7G1 traps, 10.2 ft behind the wall, were ruined by the impact of the large heavy blocks.

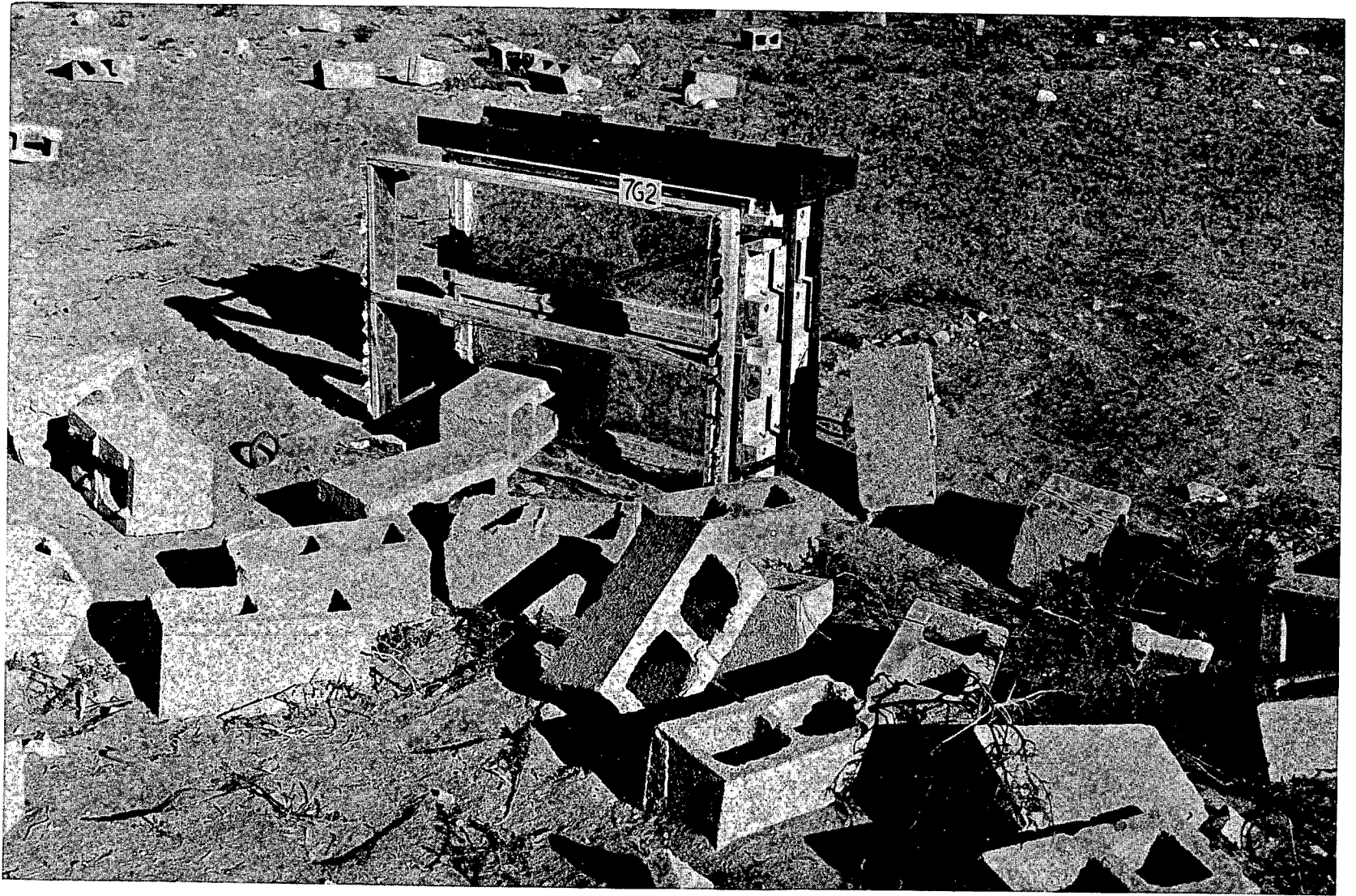


Fig. 6.73—Traps 7G2a and b, 40.2 ft behind the concrete-block wall, postshot.



Fig. 6.74—Trap 7G3b, placed above the dog installation (Project 33.4), 20.2 ft from the concrete-block wall.

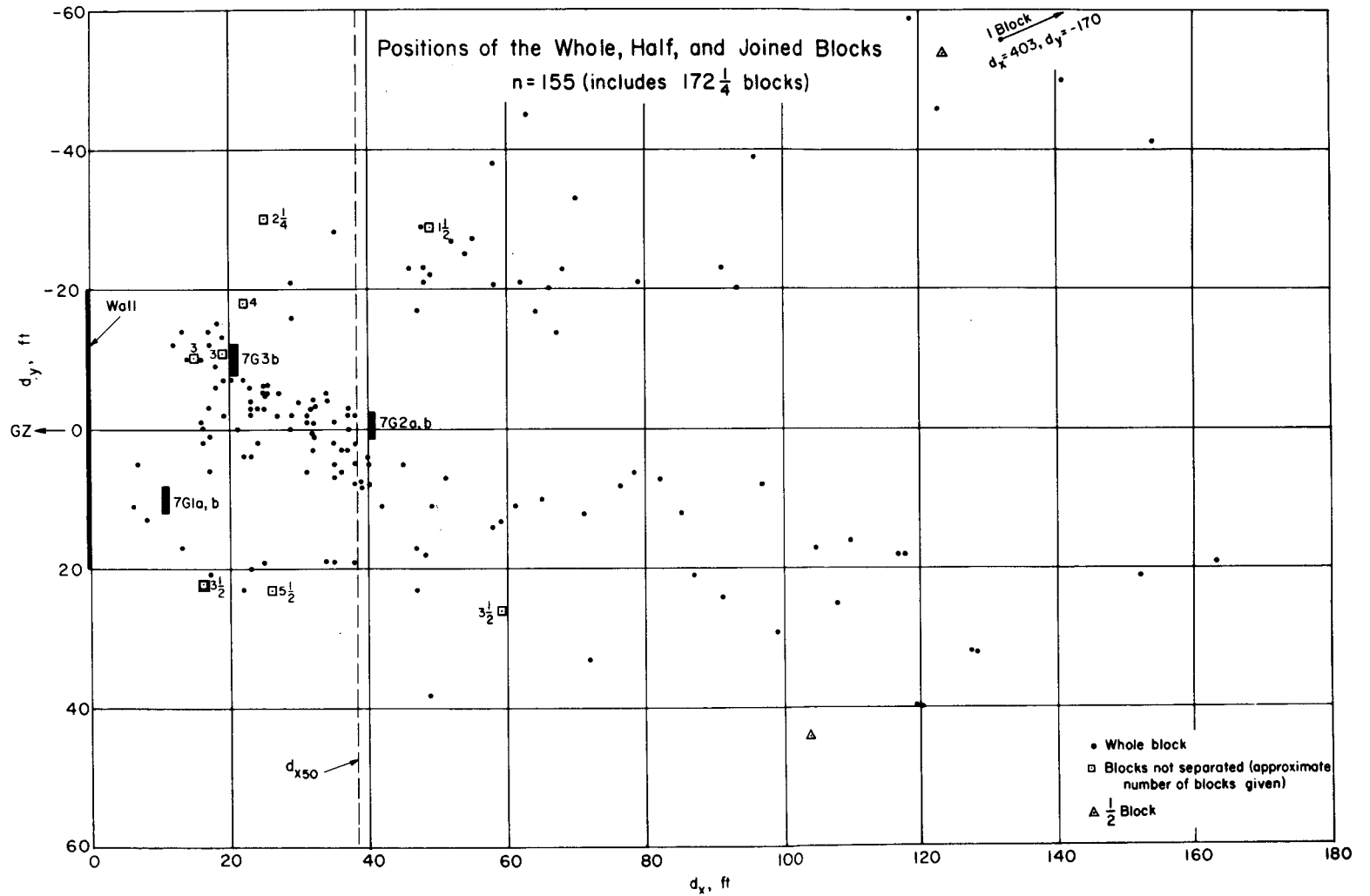


Fig. 6.75—Final positions of whole, half, and joined blocks from the concrete-block wall.

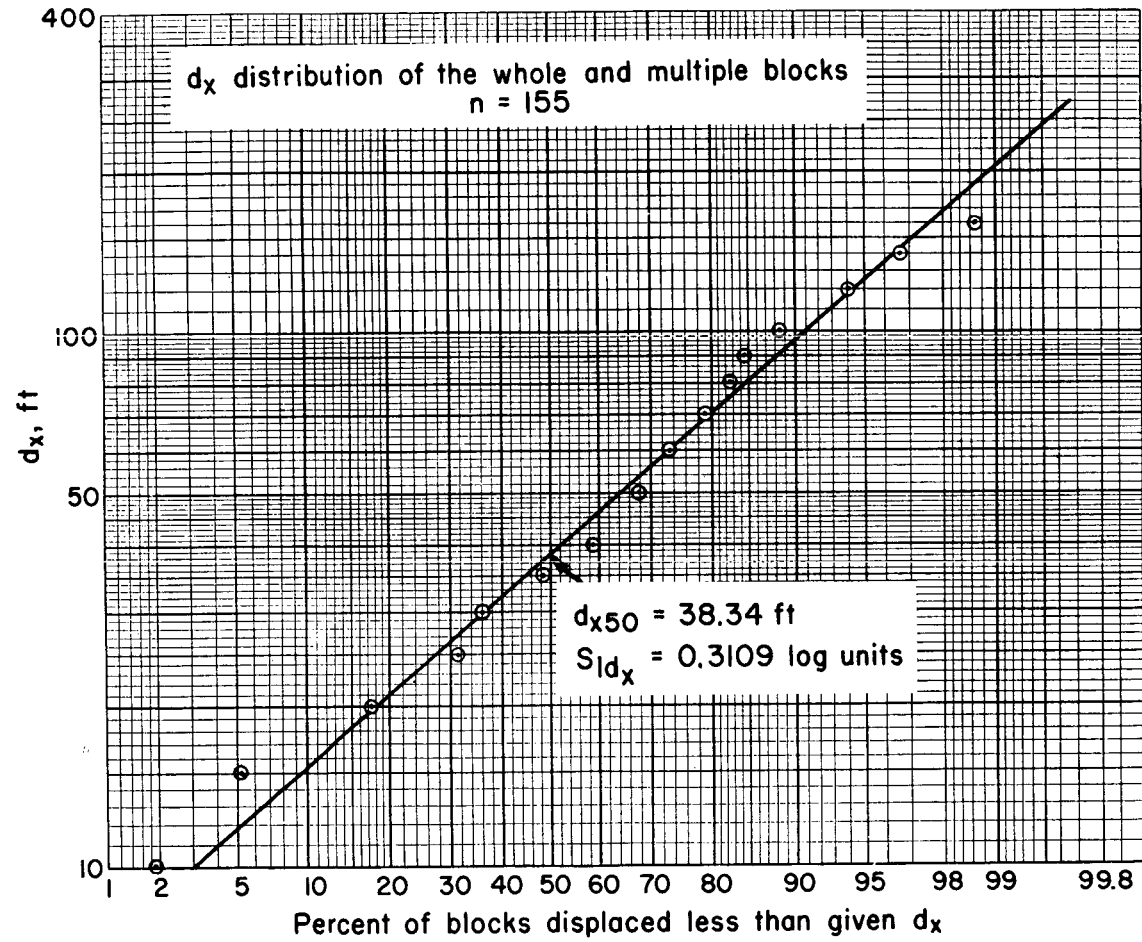


Fig. 6.76—Downwind distribution of the whole, half, and joined blocks from the concrete-block wall.

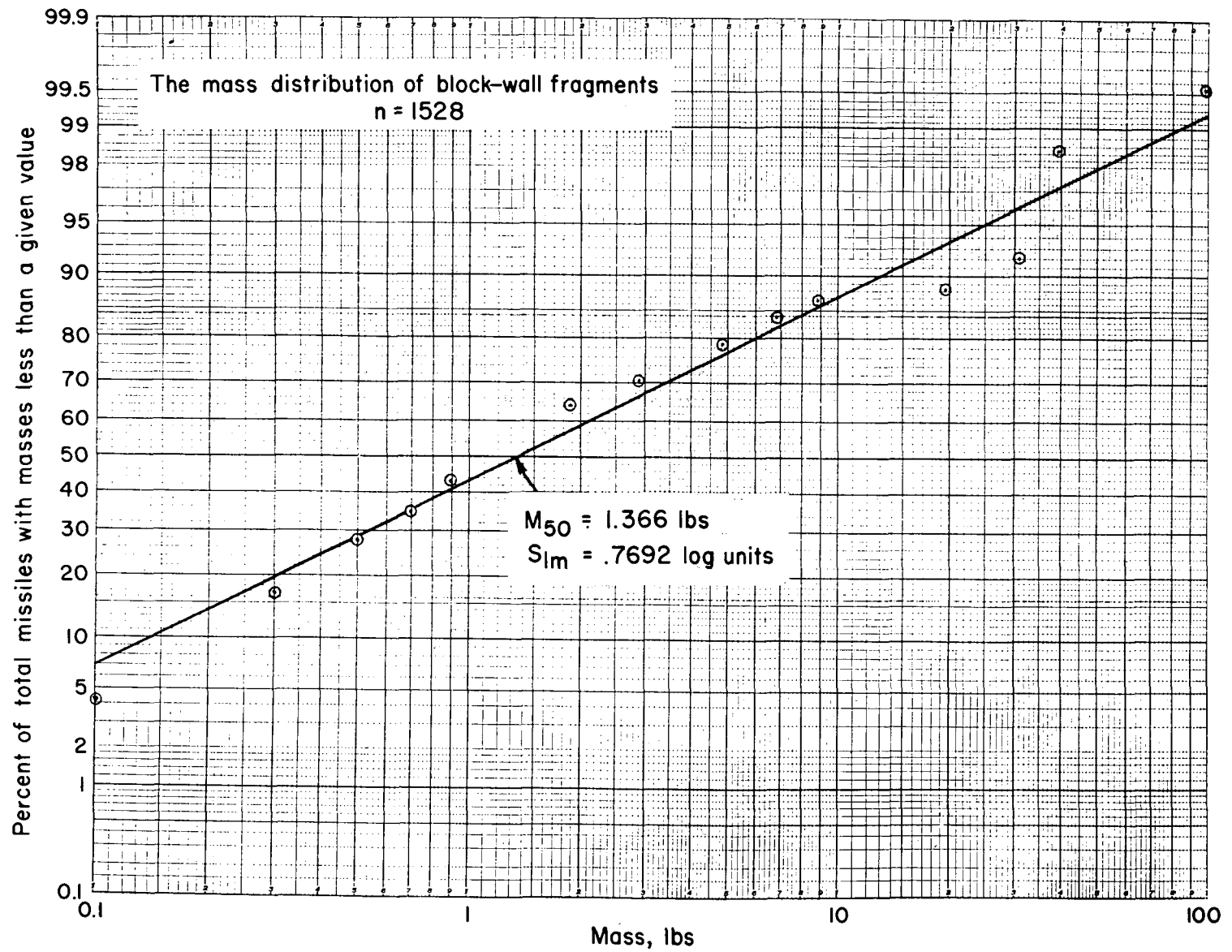


Fig. 6.77—The mass distribution of all fragments with masses over 0.1 lb from the concrete-block wall.

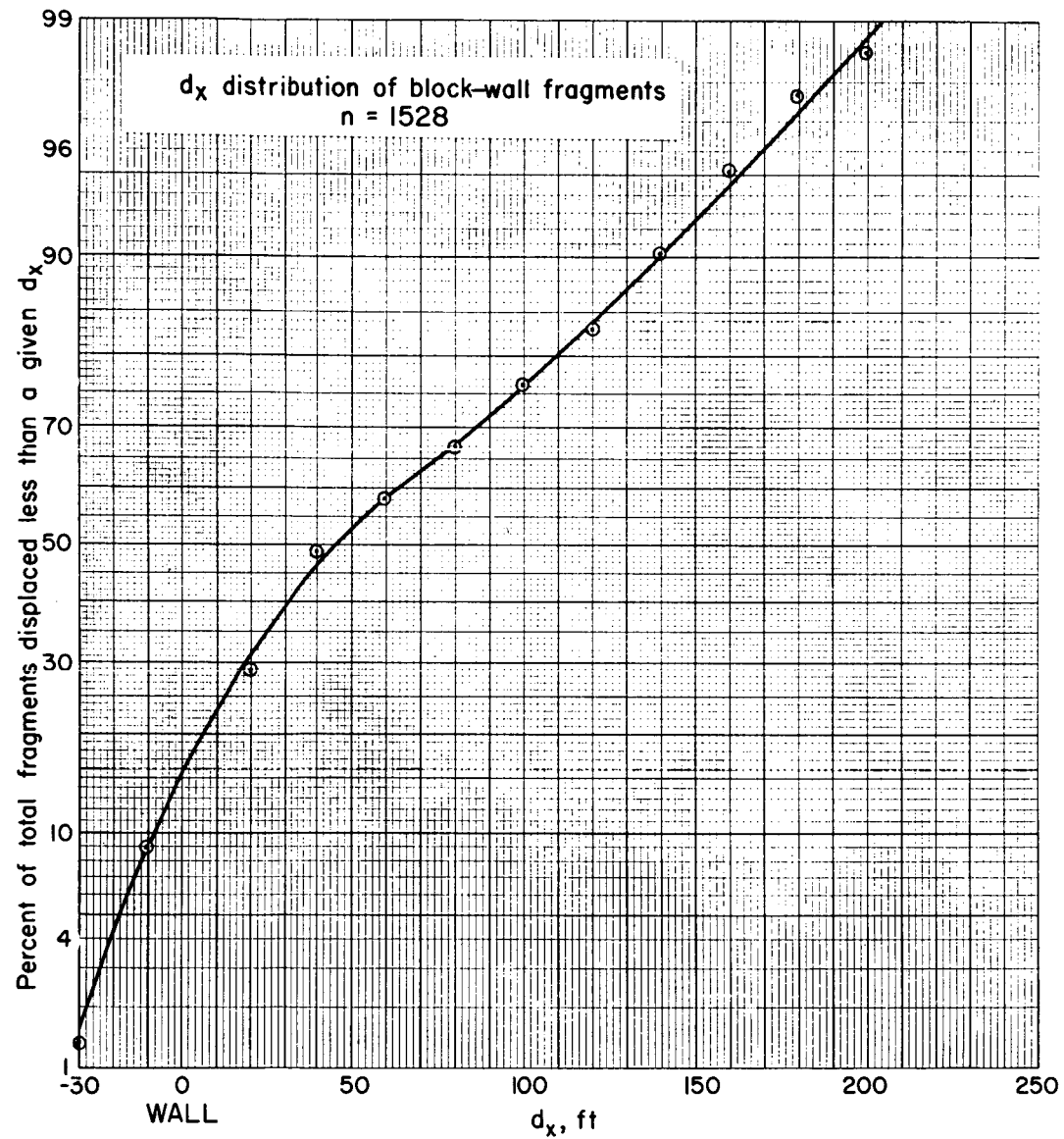


Fig. 6.78—The downwind distribution of all fragments with masses over 0.1 lb from the concrete-block wall.

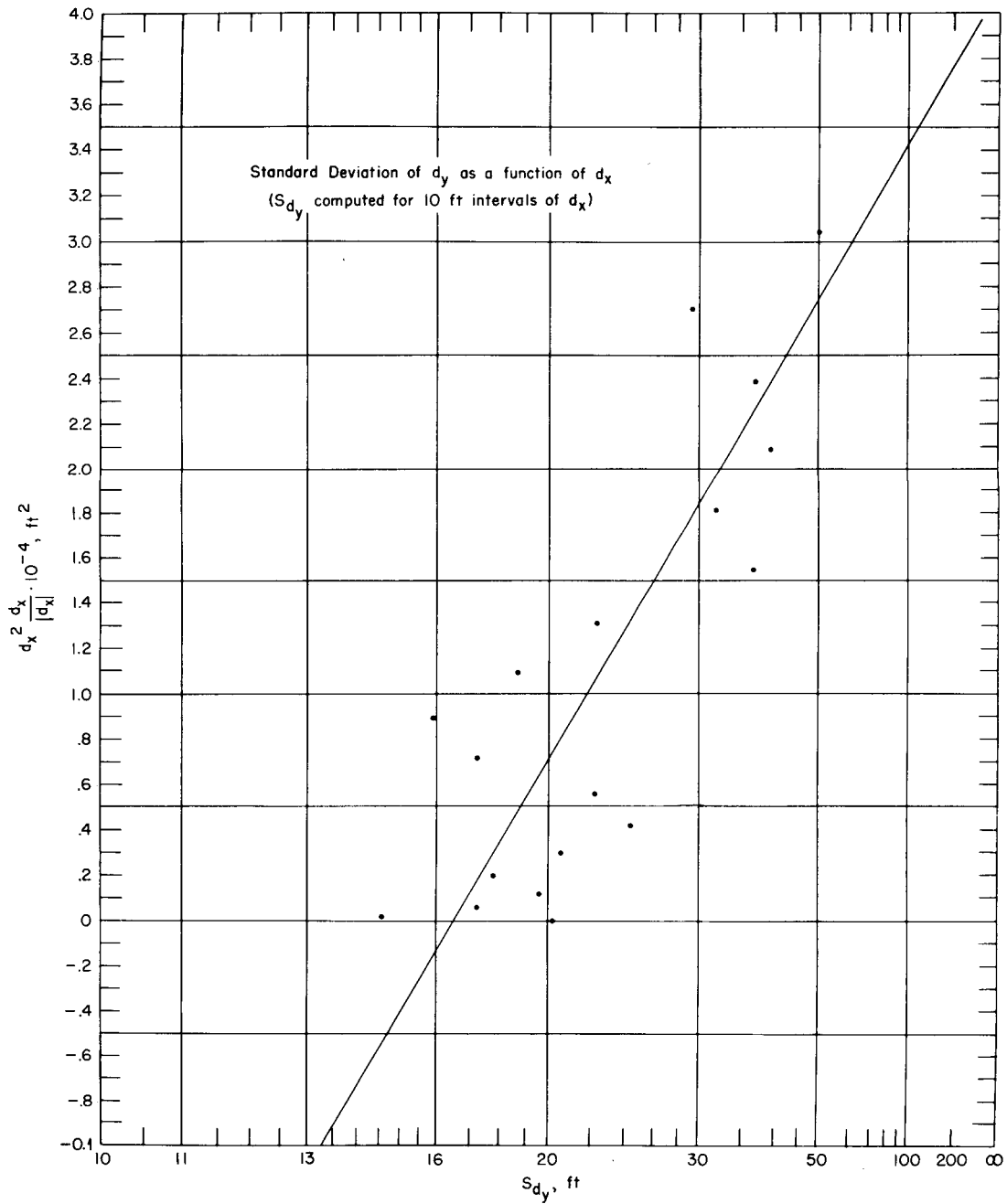


Fig. 6.79— Standard deviation of crosswind displacement (S_{d_y}) vs. downwind displacement squared ($d_x^2 \cdot d_x/|d_x|$) for all fragments with masses over 0.1 lb from the concrete-block wall.

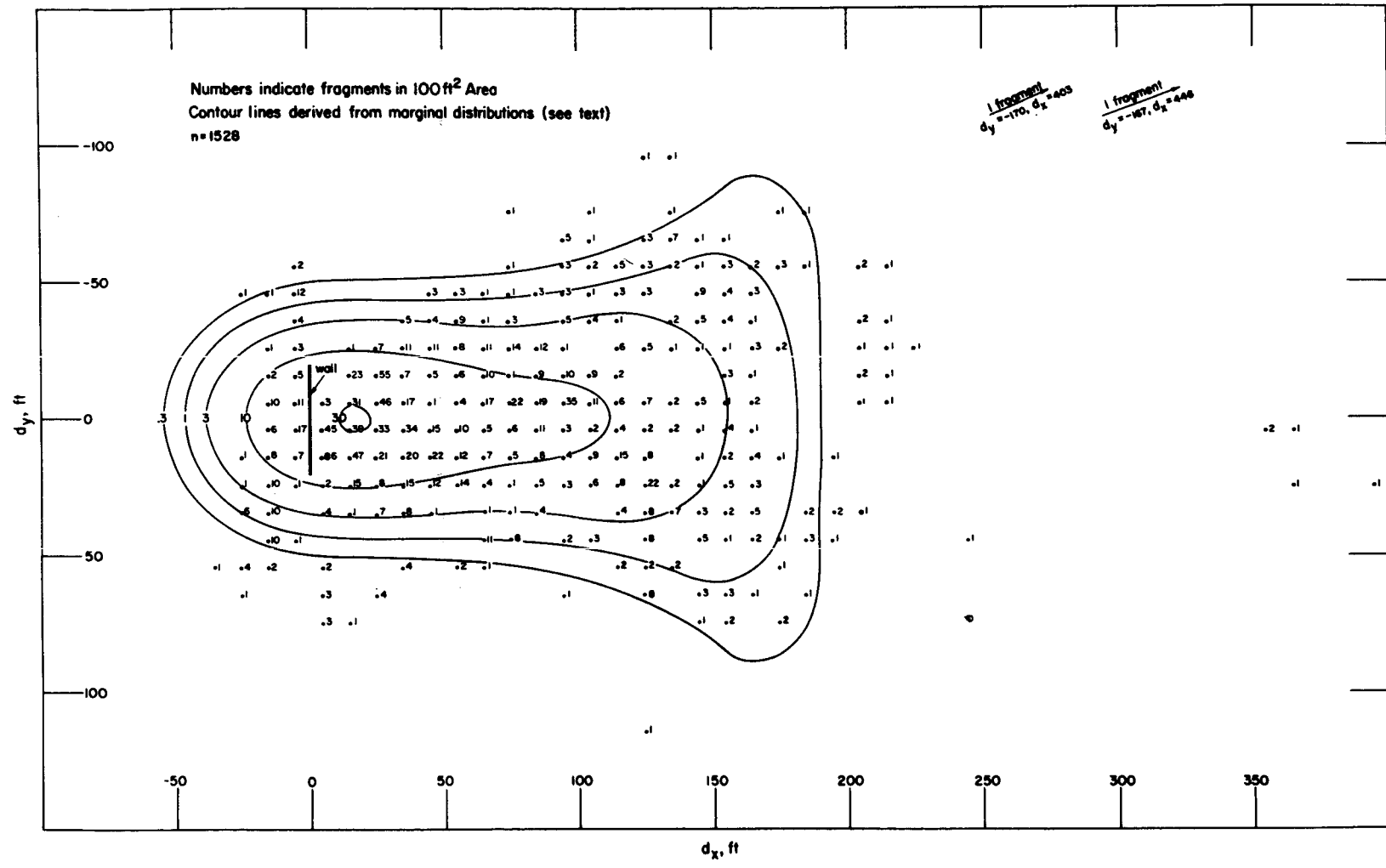


Fig. 6.80—Spatial distribution of all fragments with masses over 0.1 lb from the concrete-block wall.

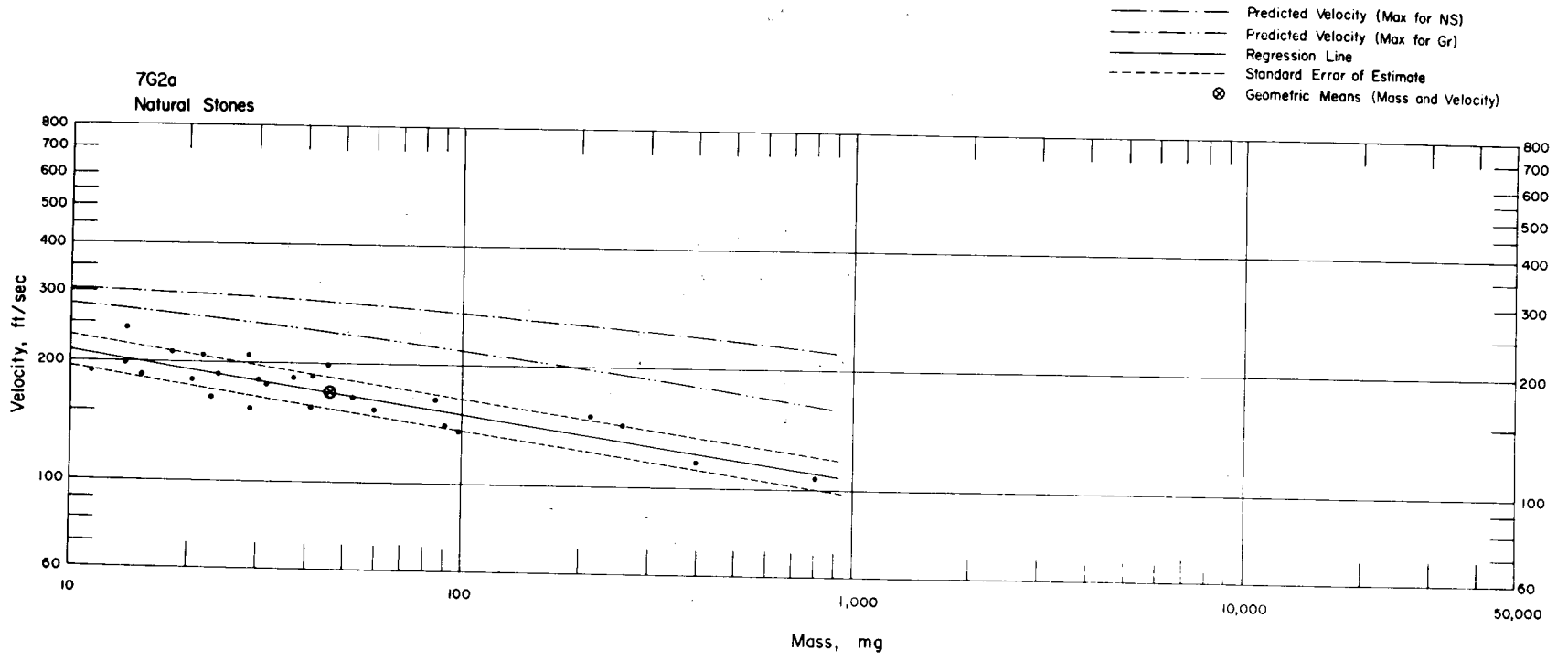


Fig. 6.81—Analysis of natural-stone missiles from trap 7G2a: $n = 26$; $\log v = 2.4759 - 0.1489 \log m$; $E_{GV} = 1.10$; $M_{50} = 45.7 \text{ mg}$; $V_{50} = 169 \text{ ft/sec}$.

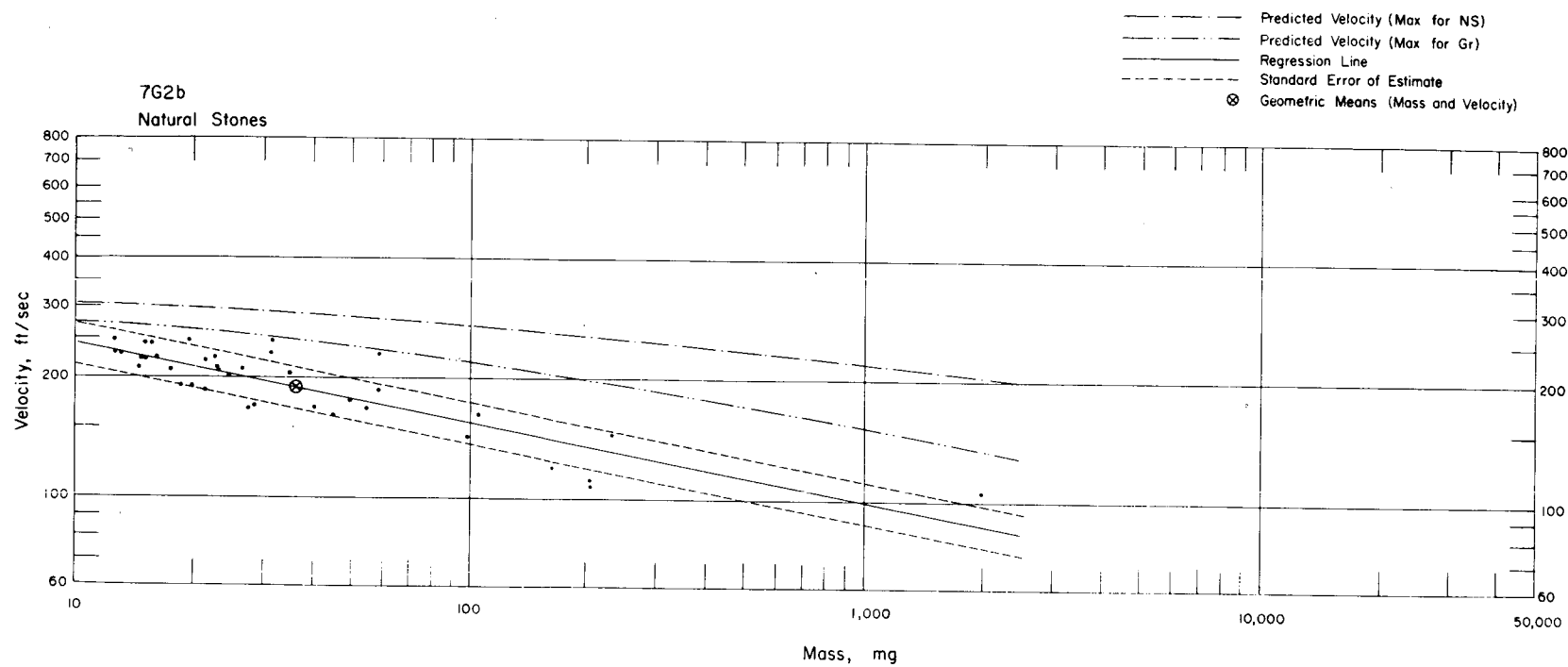


Fig. 6.82—Analysis of natural-stone missiles from trap 7G2b: $n = 38$; $\log v = 2.5761 - 0.1926 \log m$; $E_{gv} = 1.12$; $M_{50} = 35.9$ mg; $V_{50} = 189$ ft/sec.

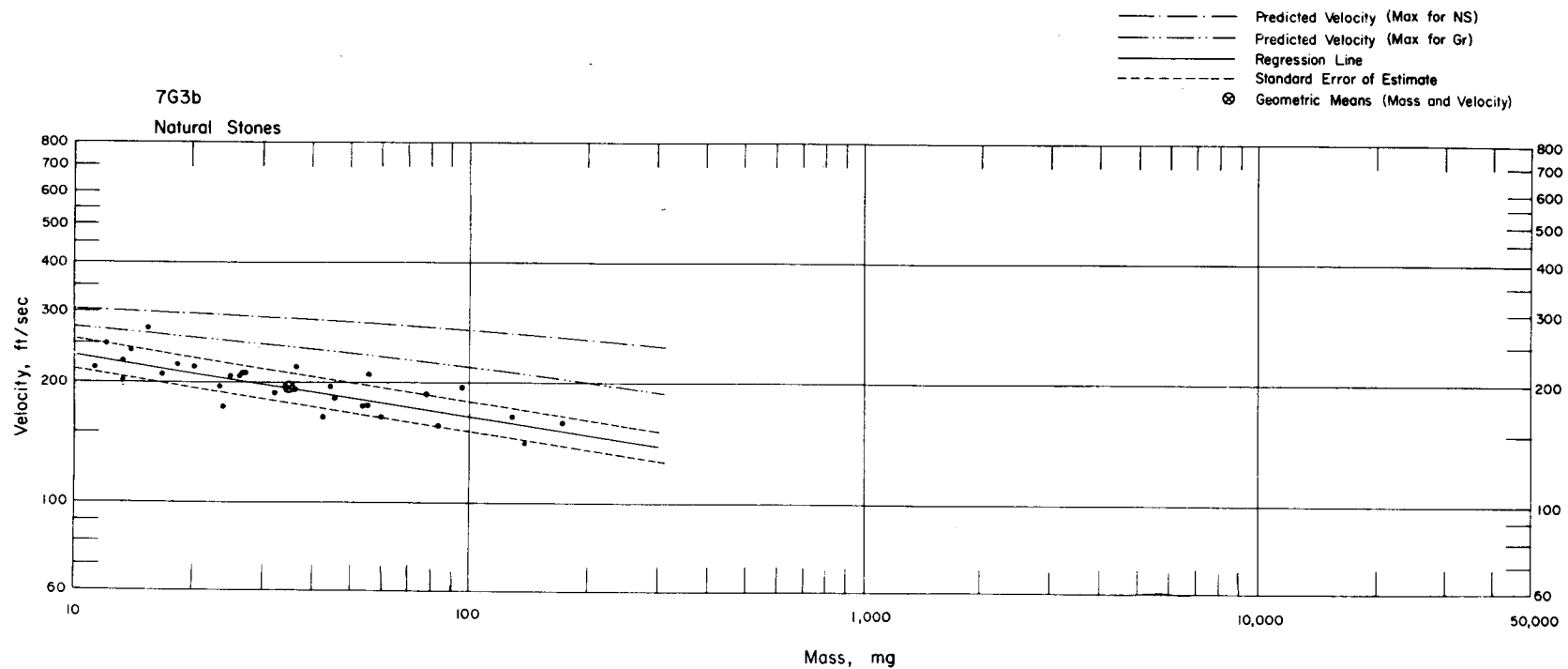
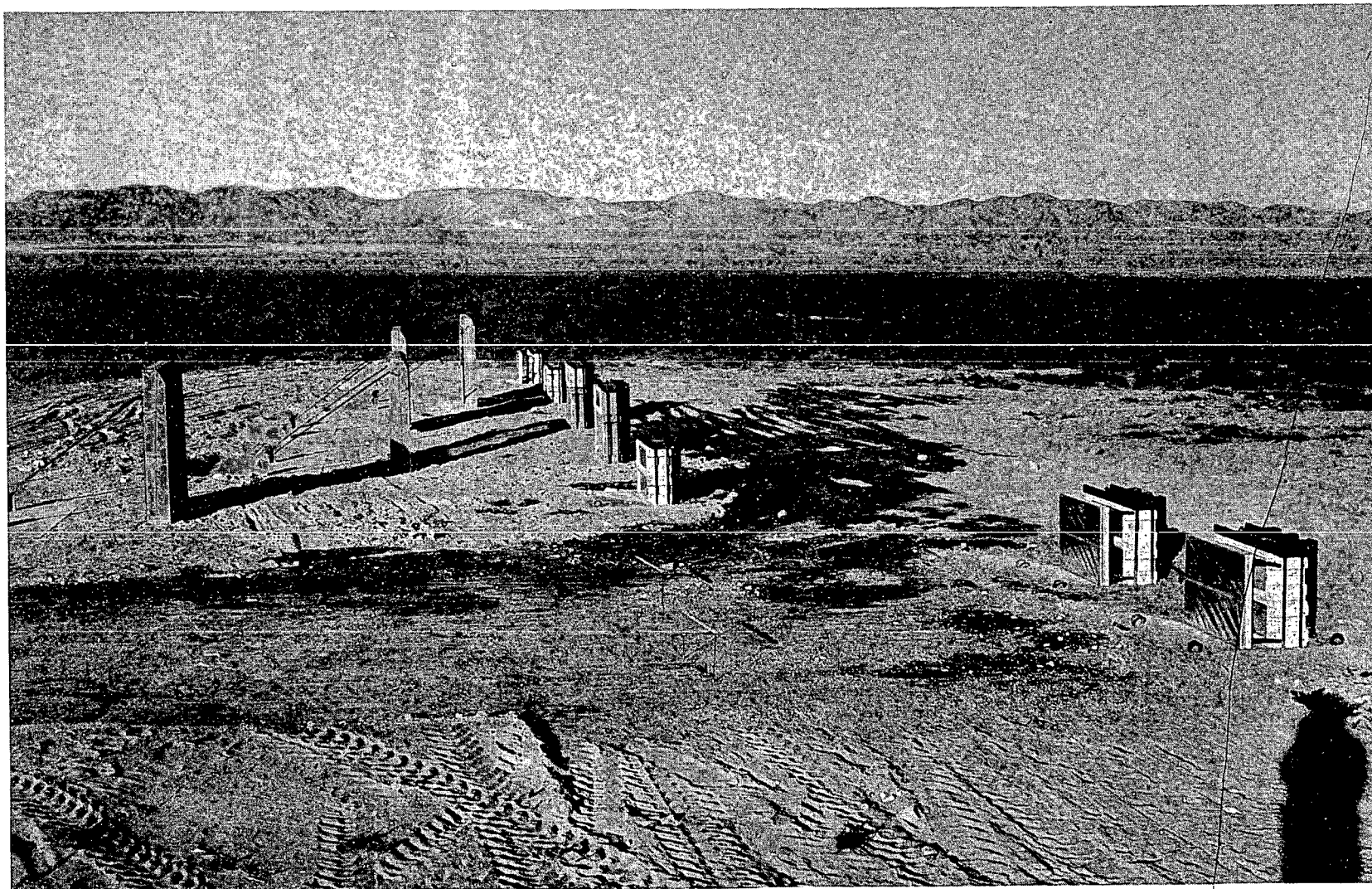


Fig. 6.83—Analysis of natural-stone missiles from trap 7G3b: $n = 31$; $\log v = 2.5407 - 0.1592 \log m$; $E_{gv} = 1.09$; $M_{50} = 34.6$ mg; $V_{50} = 198$ ft/sec.



439

Fig. 6.84— Station 7G installation from traps 7G4a and b (in the foreground on the right) through traps 7G10a and b (in the background), preshot.

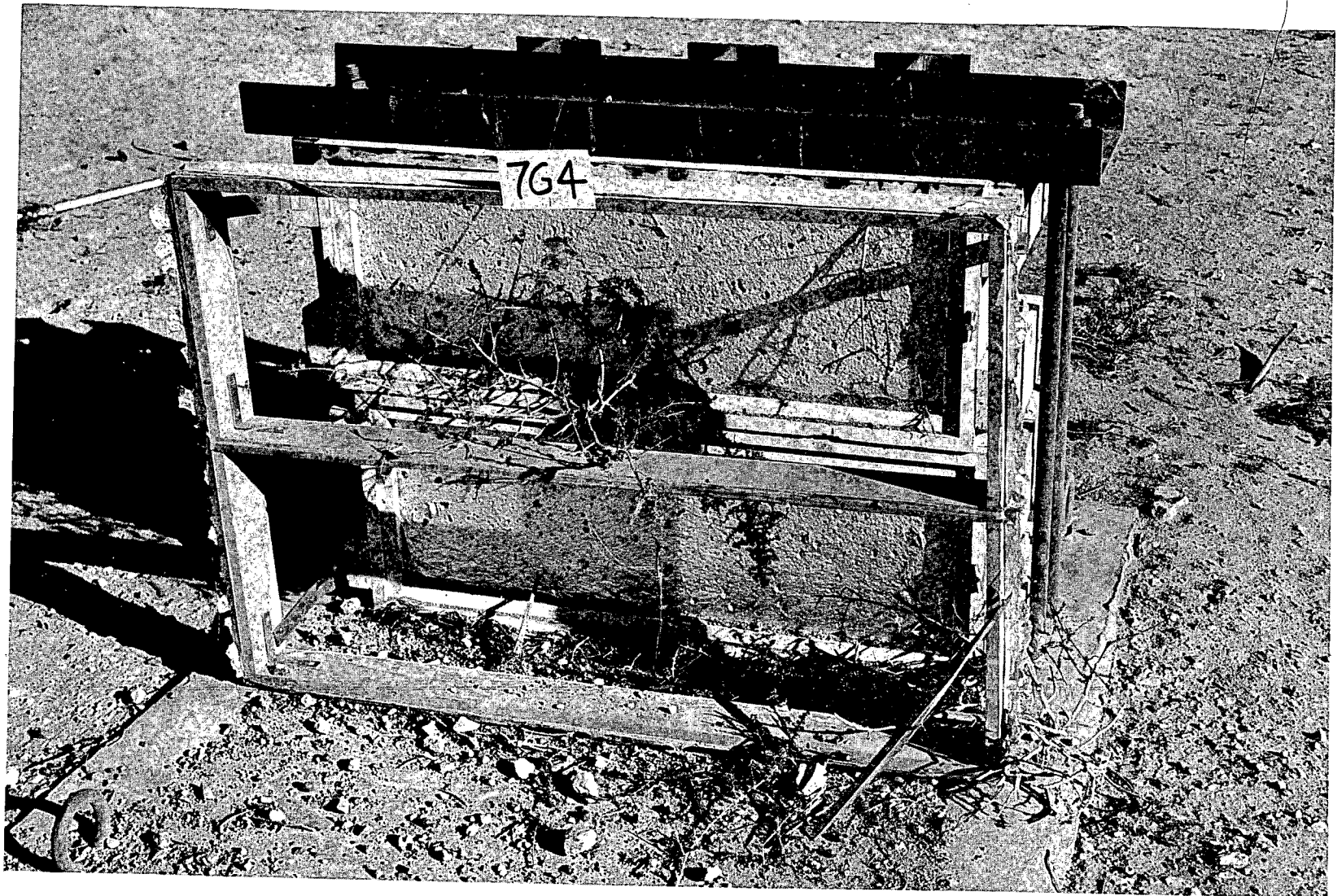
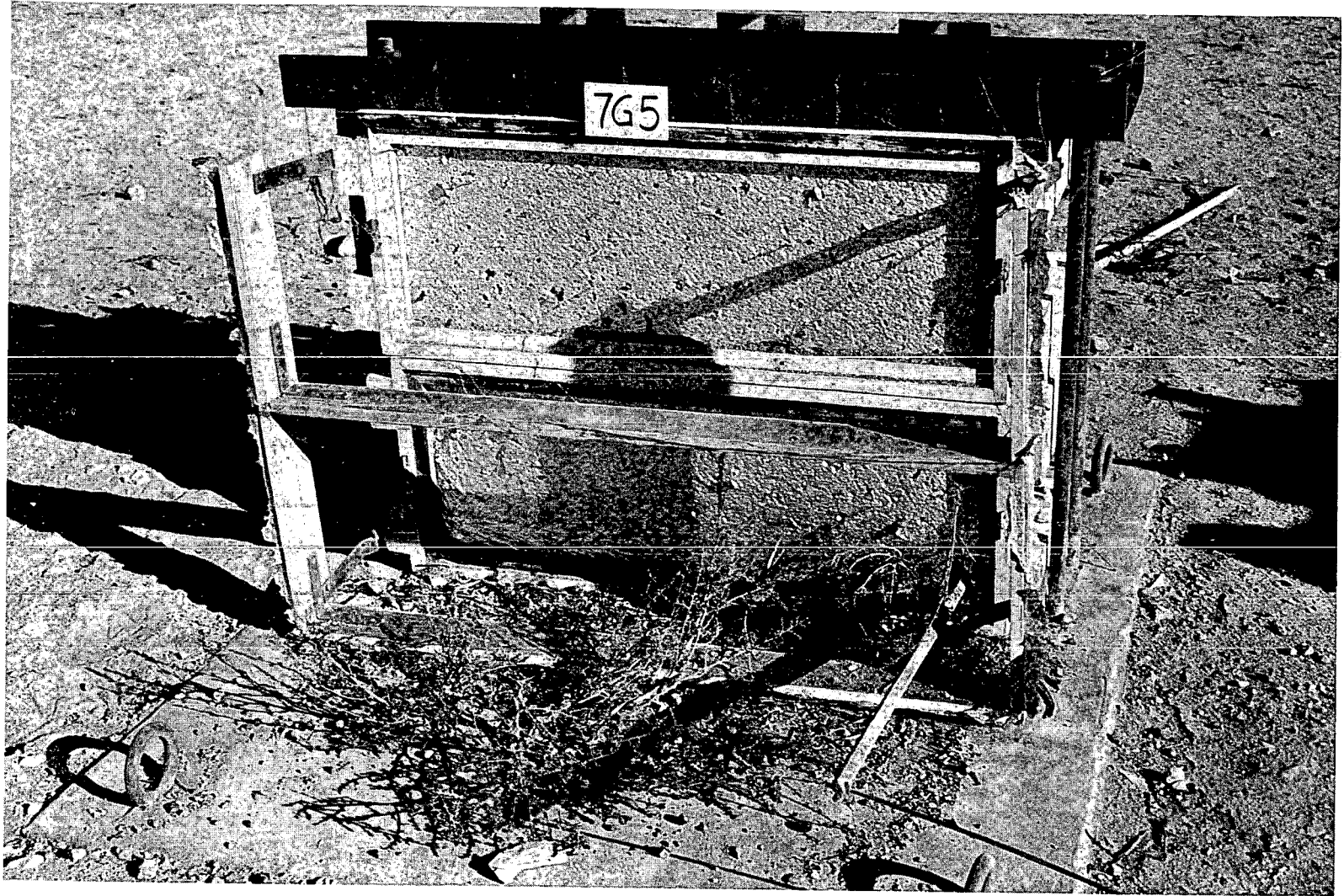


Fig. 6.85— Installation 7G4, postshot, showing frame that held aluminum foil for extra protection. These traps caught spheres and natural stones.



441

Fig. 6.86— Installation 7G5, postshot, showing remains of frame that held aluminum foil for extra thermal protection. These traps caught spheres and natural stones.

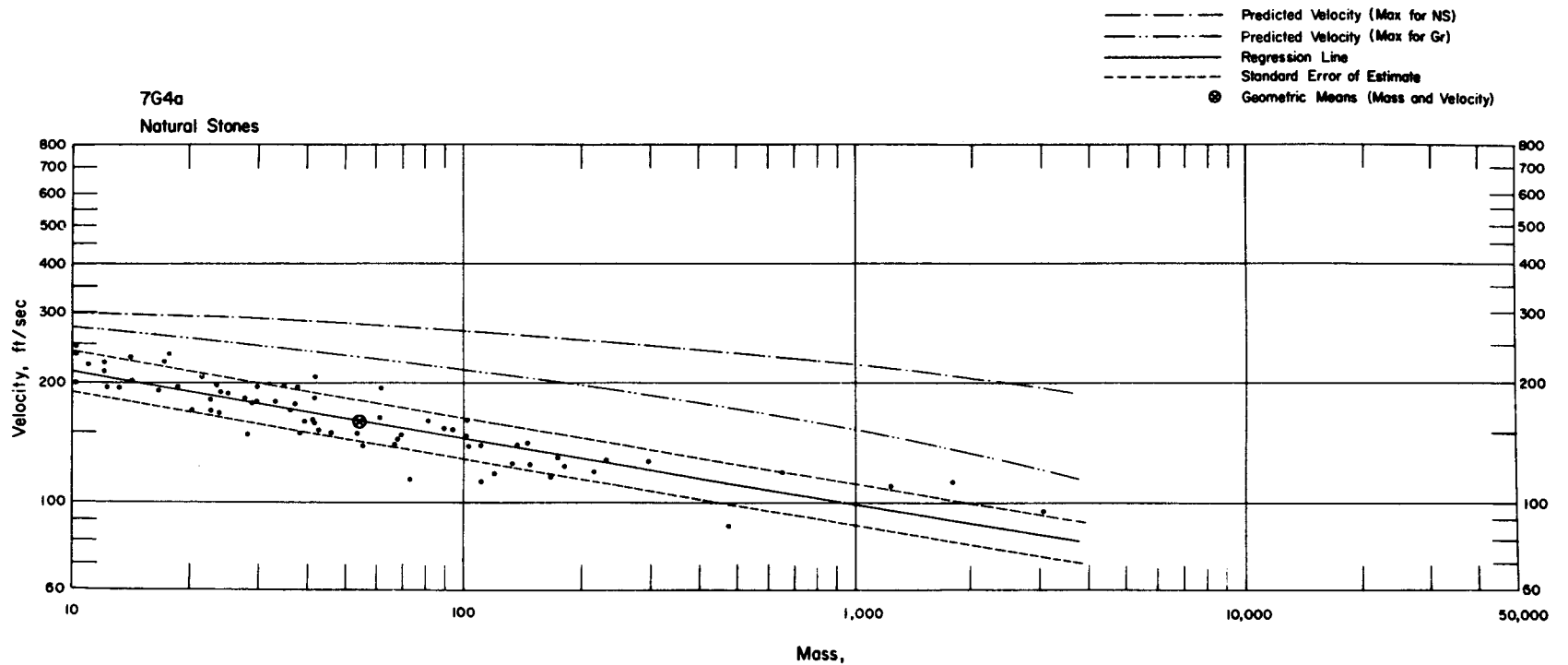


Fig. 6.87— Analysis of natural-stone missiles from trap 7G4a: $n = 73$; $\log v = 2.5126 - 0.1730 \log m$; $E_{GV} = 1.11$; $M_{50} = 53.1 \text{ mg}$; $V_{50} = 164 \text{ ft/sec}$.

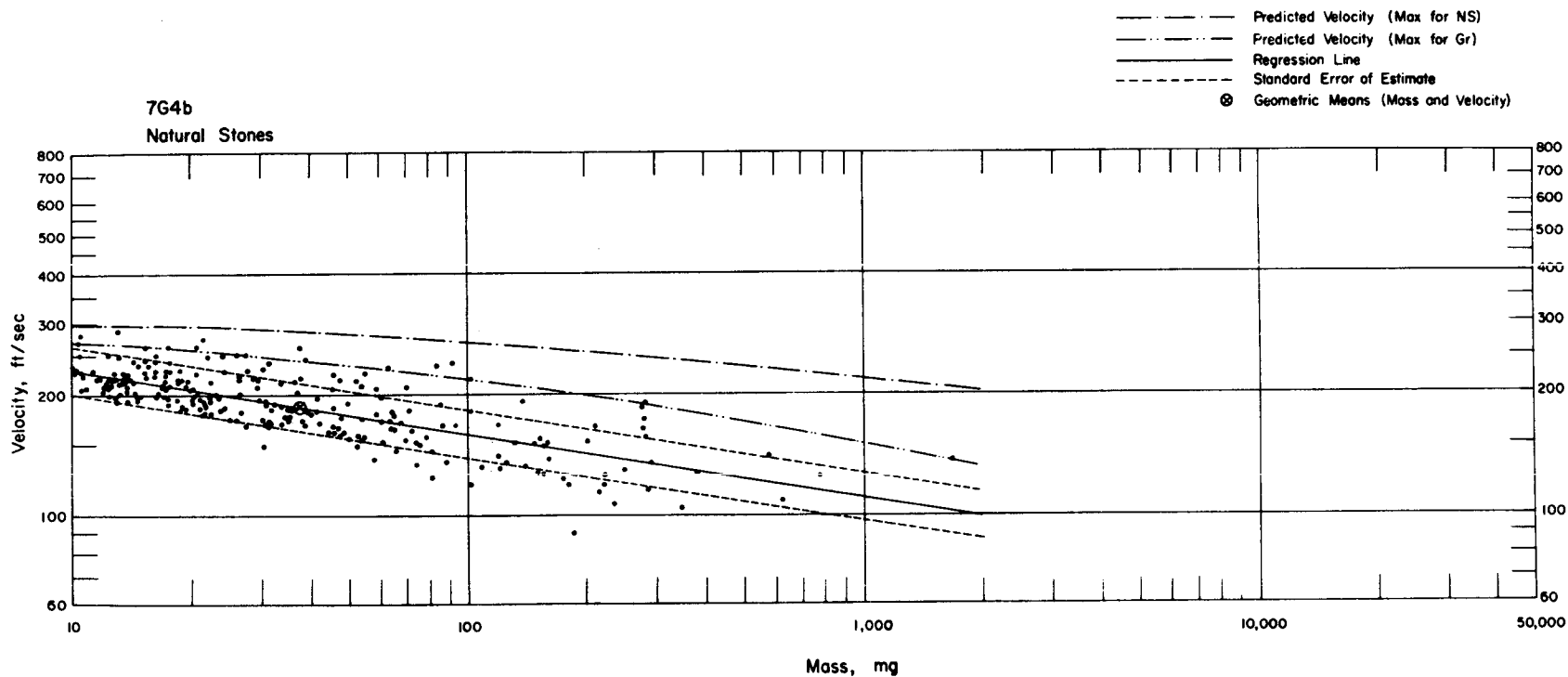


Fig. 6.88—Analysis of natural-stone missiles from trap 7G4b: $n = 244$; $\log v = 2.5393 - 0.1660 \log m$; $E_{GV} = 1.14$; $M_{50} = 36.9$ mg; $V_{50} = 190$ ft/sec.

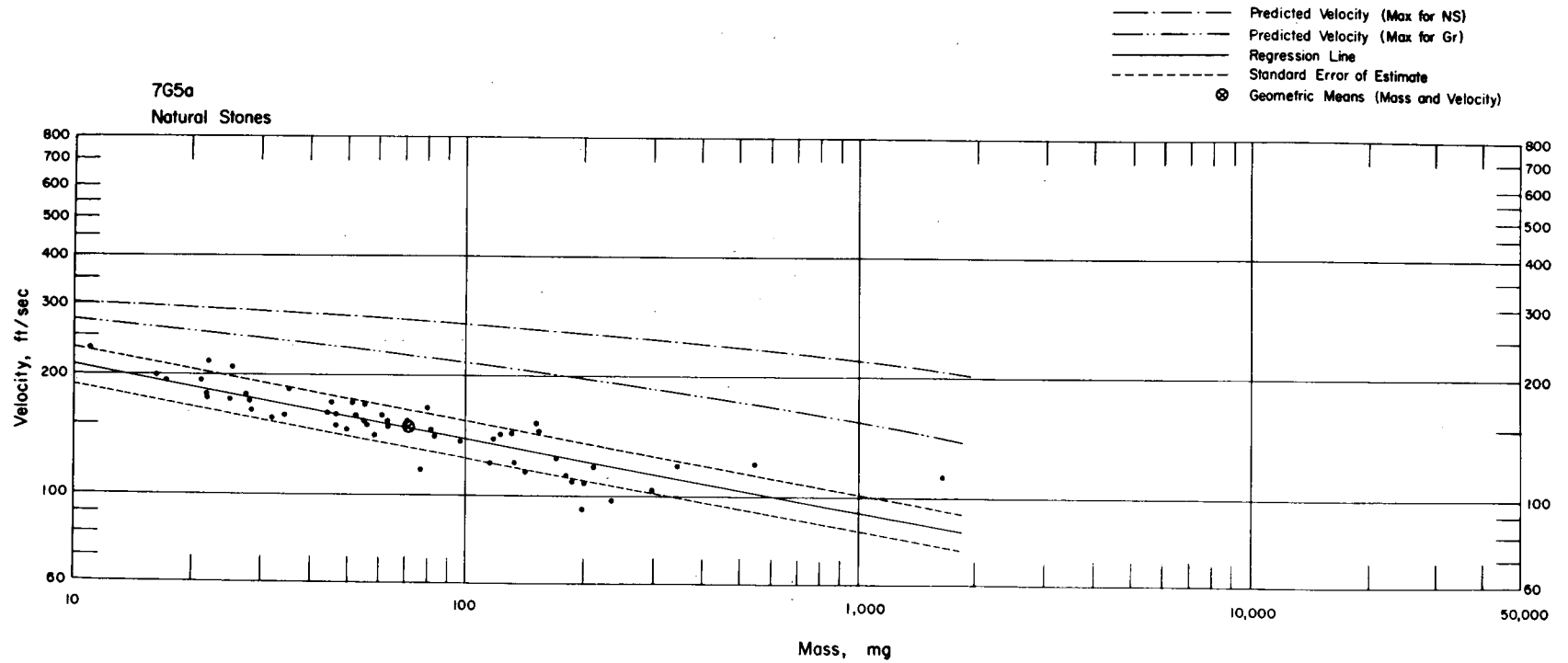


Fig. 6.89—Analysis of natural-stone missiles from trap 7G5a: $n = 54$; $\log v = 2.5215 - 0.1893 \log m$; $E_{gv} = 1.11$; $M_{50} = 7.1$ mg; $V_{50} = 148$ ft/sec.

445

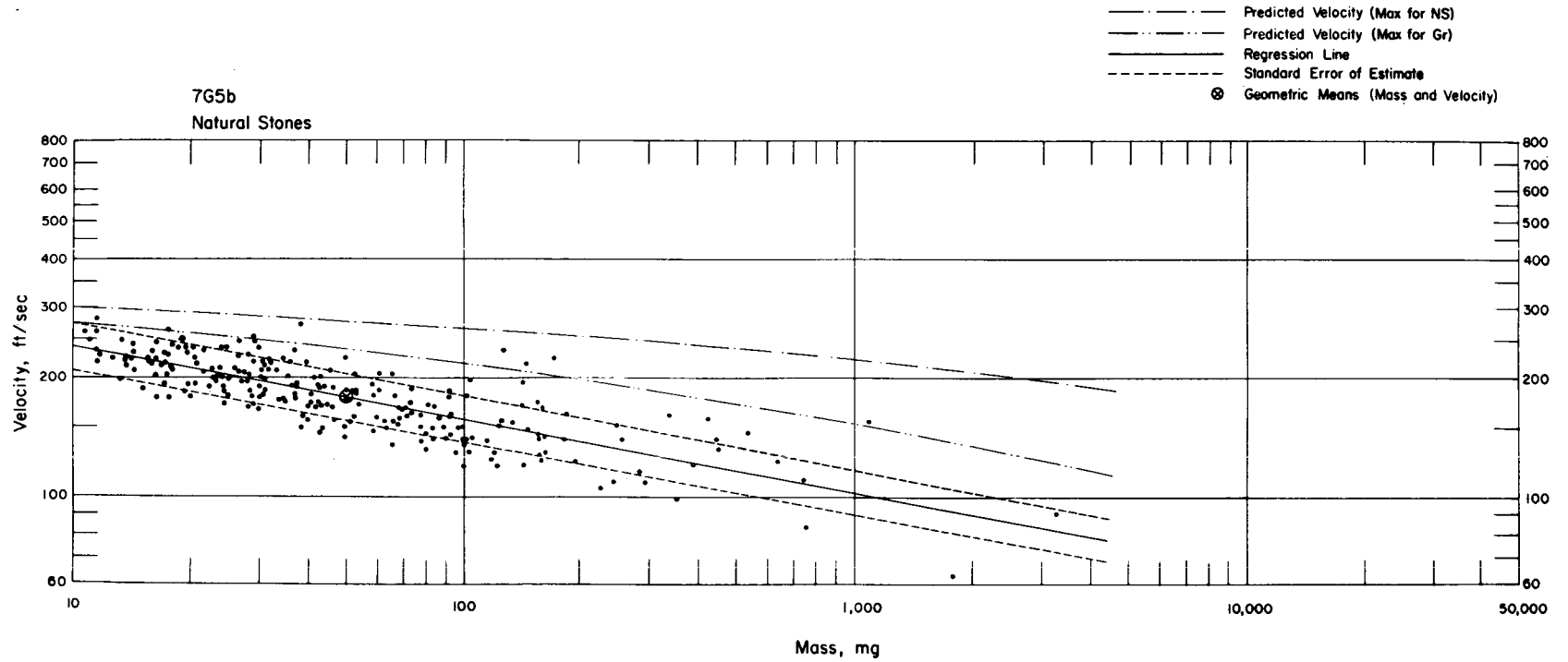


Fig. 6.90—Analysis of natural-stone missiles from trap 7G5b: $n = 236$; $\log v = 2.5609 - 0.1826 \log m$; $E_{GV} = 1.14$; $M_{50} = 49.8$ mg; $V_{50} = 178$ ft/sec.

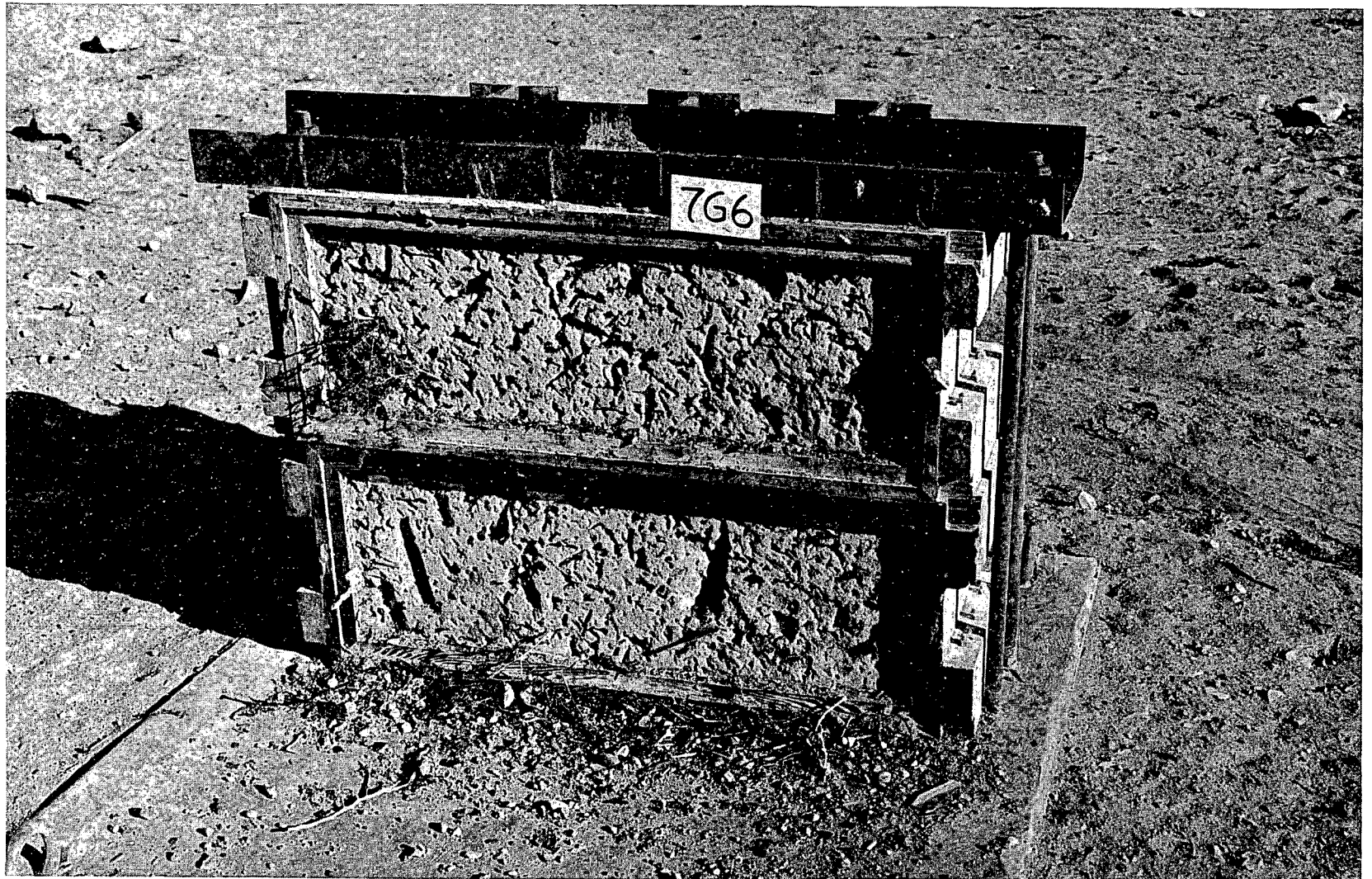


Fig. 6.91—Traps 7G6a and b, postshot, placed 21.2 ft behind window installation.

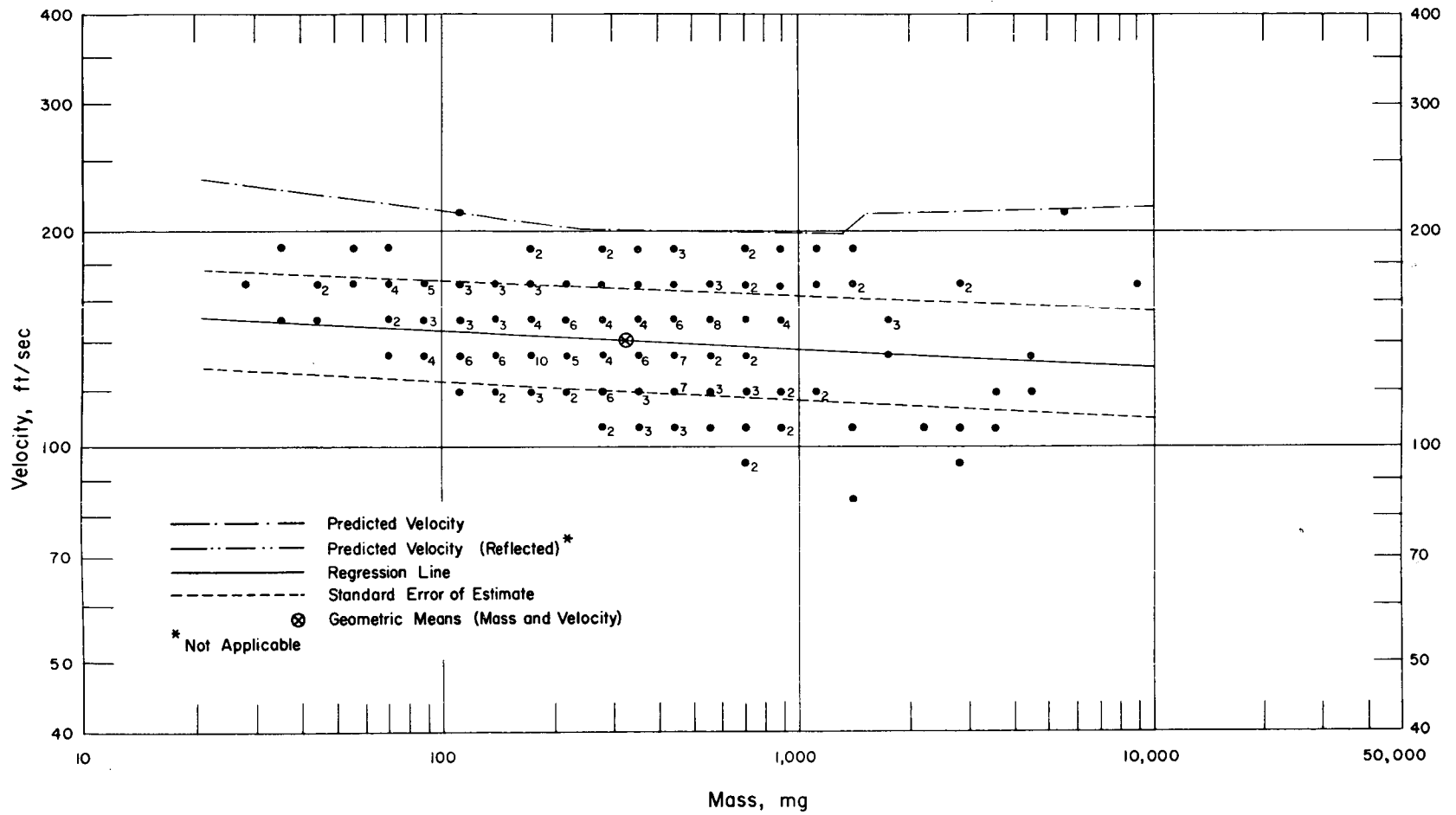


Fig. 6.92—Analysis of window-glass missiles from trap 7G6a: $d = 21.2$ ft; $n = 221$; $\log v = 2.2117 - 0.0248 \log m$; $E_{gv} = 1.19$; $M_{50} = 323$ mg; $V_{50} = 141$ ft/sec. The analysis of window glass impacting flat at trap 7G6a is presented in Fig. 6.94.

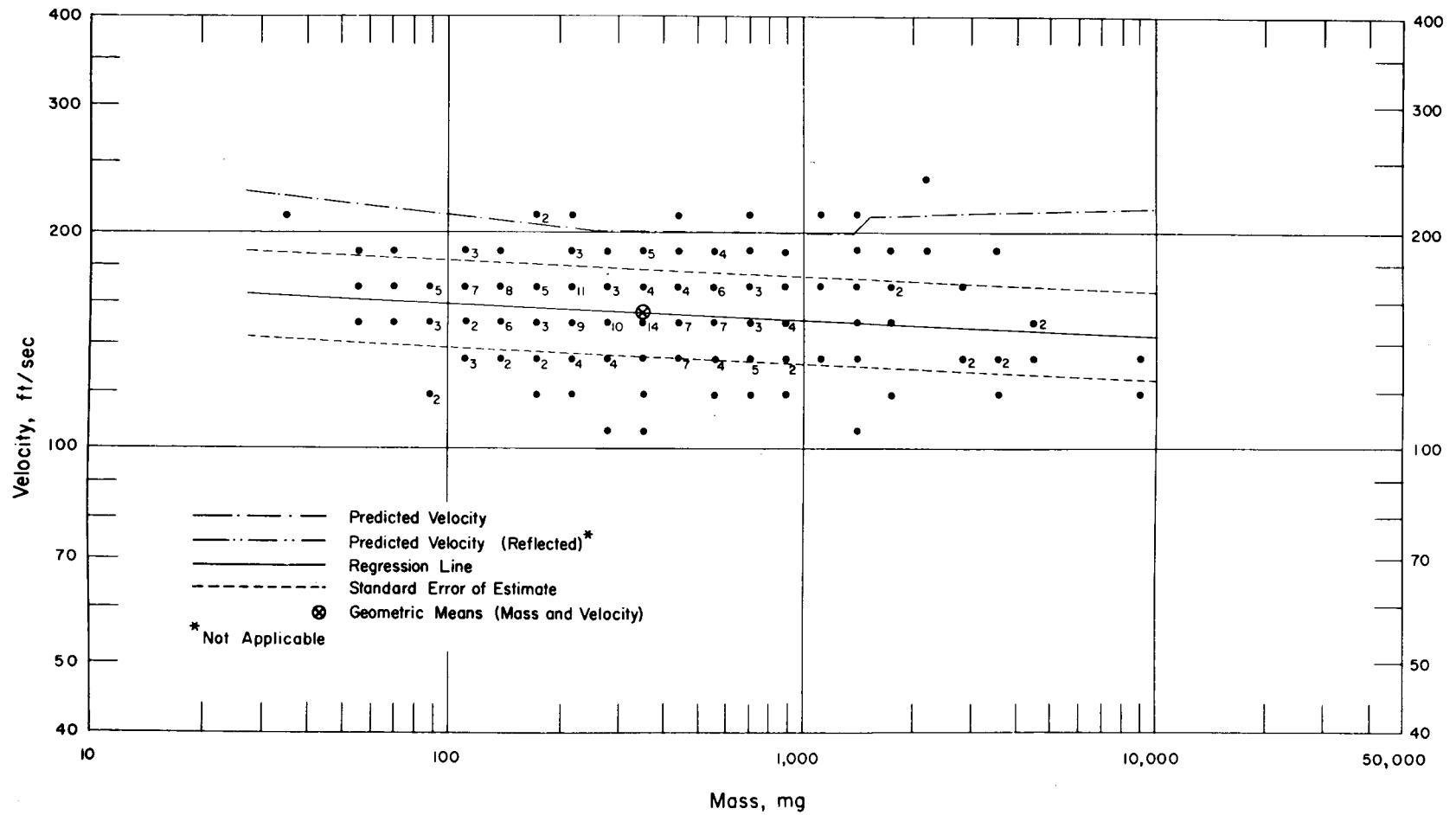


Fig. 6.93—Analysis of window-glass missiles from trap 7G6b: $d = 21.2$ ft; $n = 229$; $\log v = 2.2502 - 0.0234 \log m$; $E_{gv} = 1.15$; $M_{50} = 355$ mg; $V_{50} = 155$ ft/sec. The analysis of window glass impacting flat at trap 7G6b is presented in Fig. 6.94.

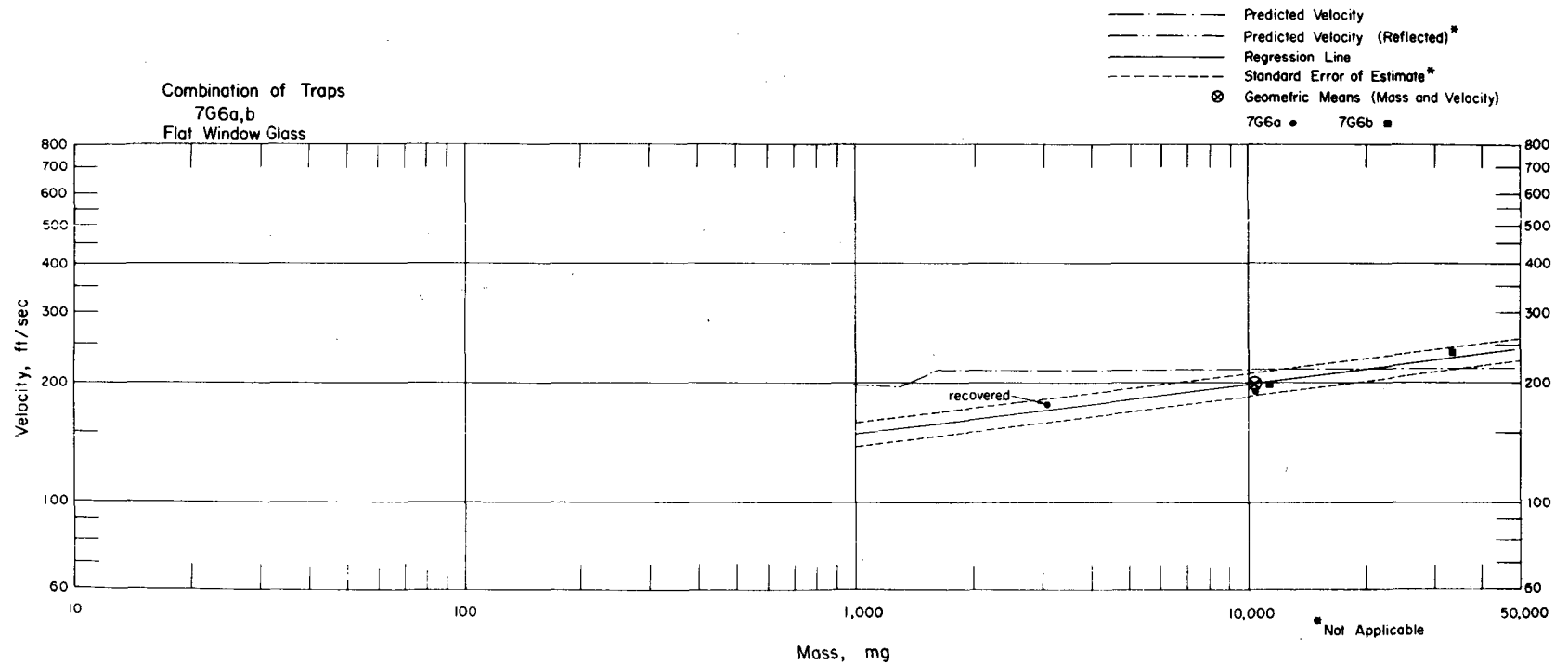


Fig. 6.94—Analysis of window-glass missiles that arrived flat at traps 7G6a and 7G6b (two from 7G6a and two from 7G6b). Masses of unrecovered missiles were determined from area of depression in absorber made by the glass fragment: $d = 21.2$ ft; $n = 4$; $\log v = 1.7958 + 0.1253 \log m$; $E_{gv} = 1.04$; $M_{50} = 10,387$ mg; $V_{50} = 199$ ft/sec.

450

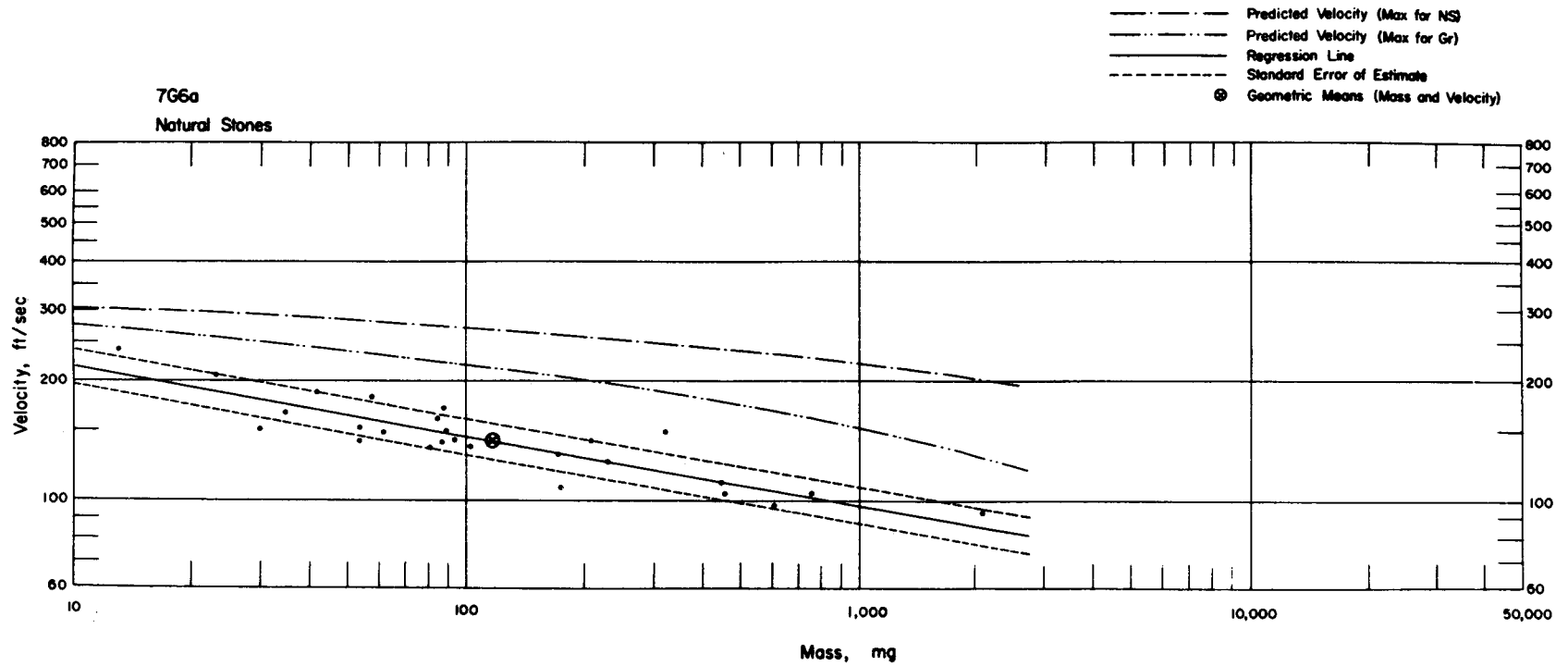


Fig. 6.95—Analysis of natural-stone missiles from trap 7G6a: $n = 26$; $\log v = 2.5112 - 0.1729 \log m$; $E_{gv} = 1.11$; $M_{50} = 116$ mg; $V_{50} = 143$ ft/sec.

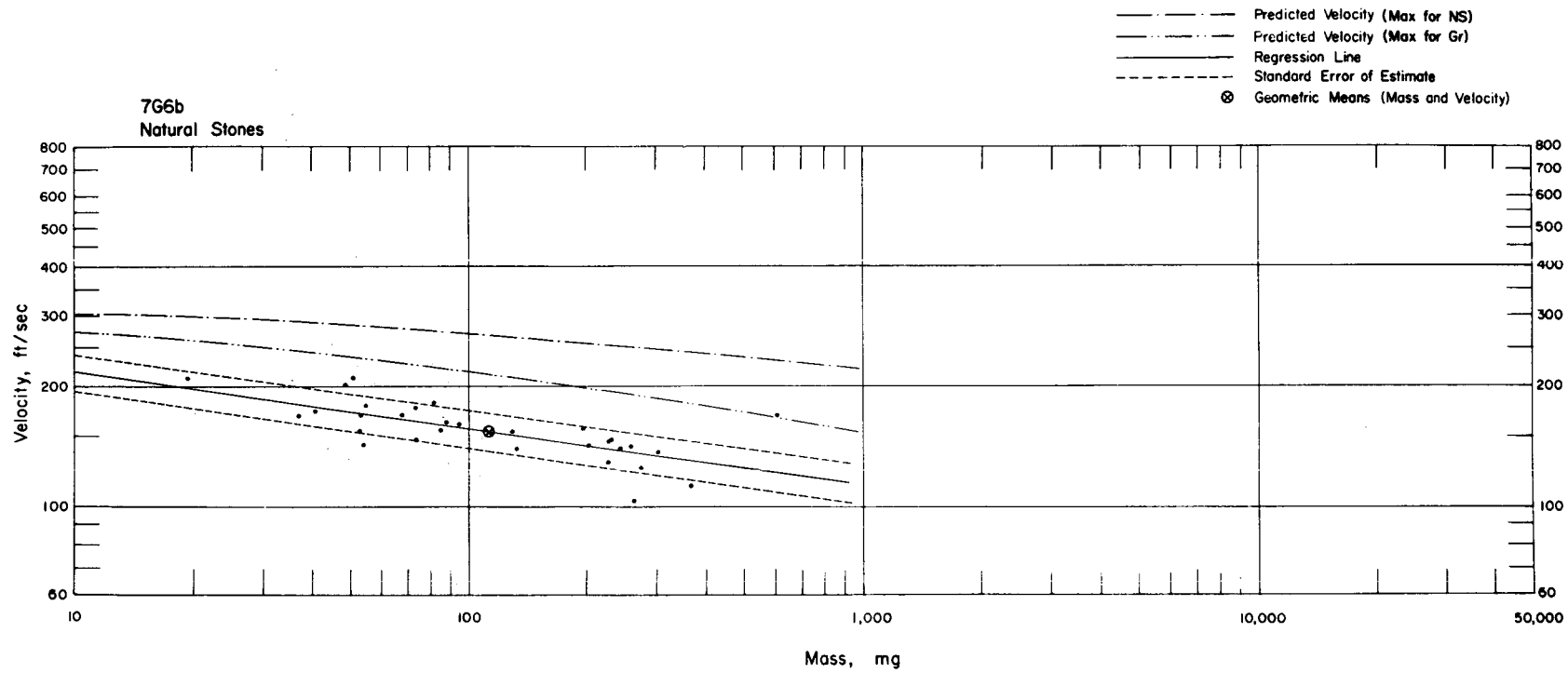


Fig. 6.96—Analysis of natural-stone missiles from trap 7G6b: $n = 30$; $\log v = 2.4875 - 0.1441 \log m$; $E_{gv} = 1.12$; $M_{50} = 112$ mg; $V_{50} = 156$ ft/sec.

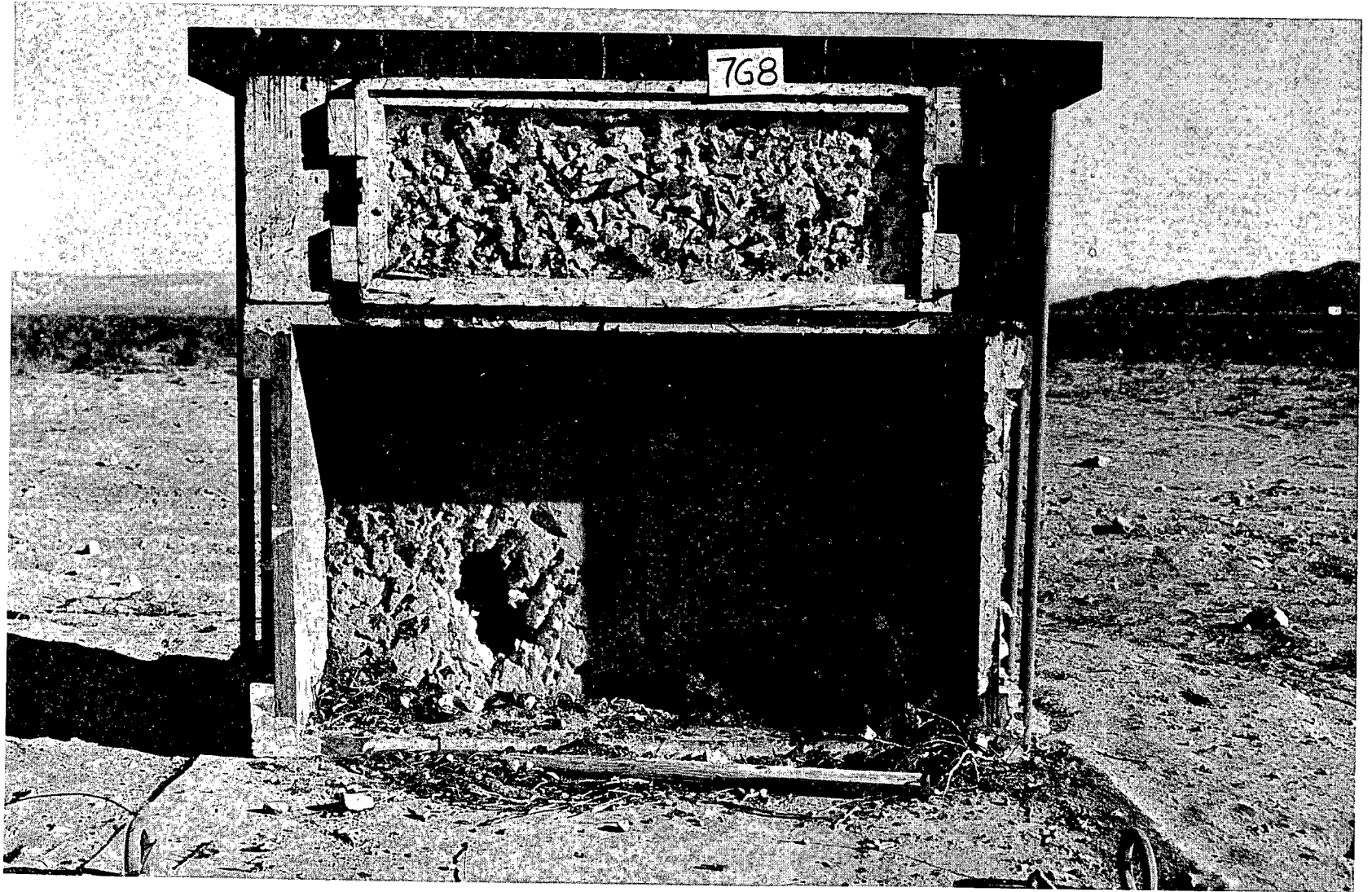


Fig. 6.97—Trap 7G8b, postshot, above dog installation (Project 33.4) and 11.2 ft behind window.

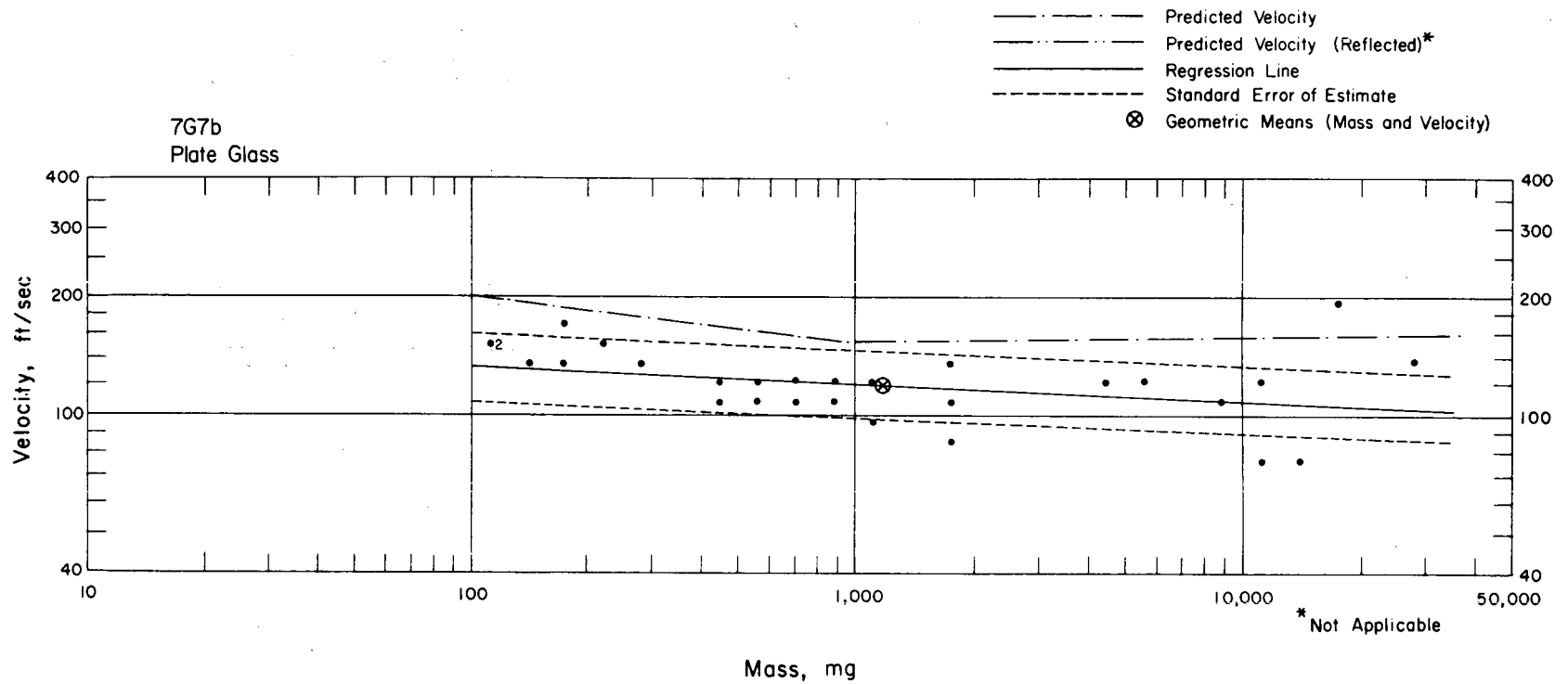


Fig. 6.98—Analysis of plate-glass missiles from trap 7G7b: $d = 11.2$ ft; $n = 28$; $\log v = 2.2144 - 0.0459 \log m$; $E_{gv} = 1.22$; $M_{50} = 1189$ mg; $V_{50} = 118$ ft/sec. The analysis of plate glass impacting flat at trap 7G7b is presented in Fig. 6.99.

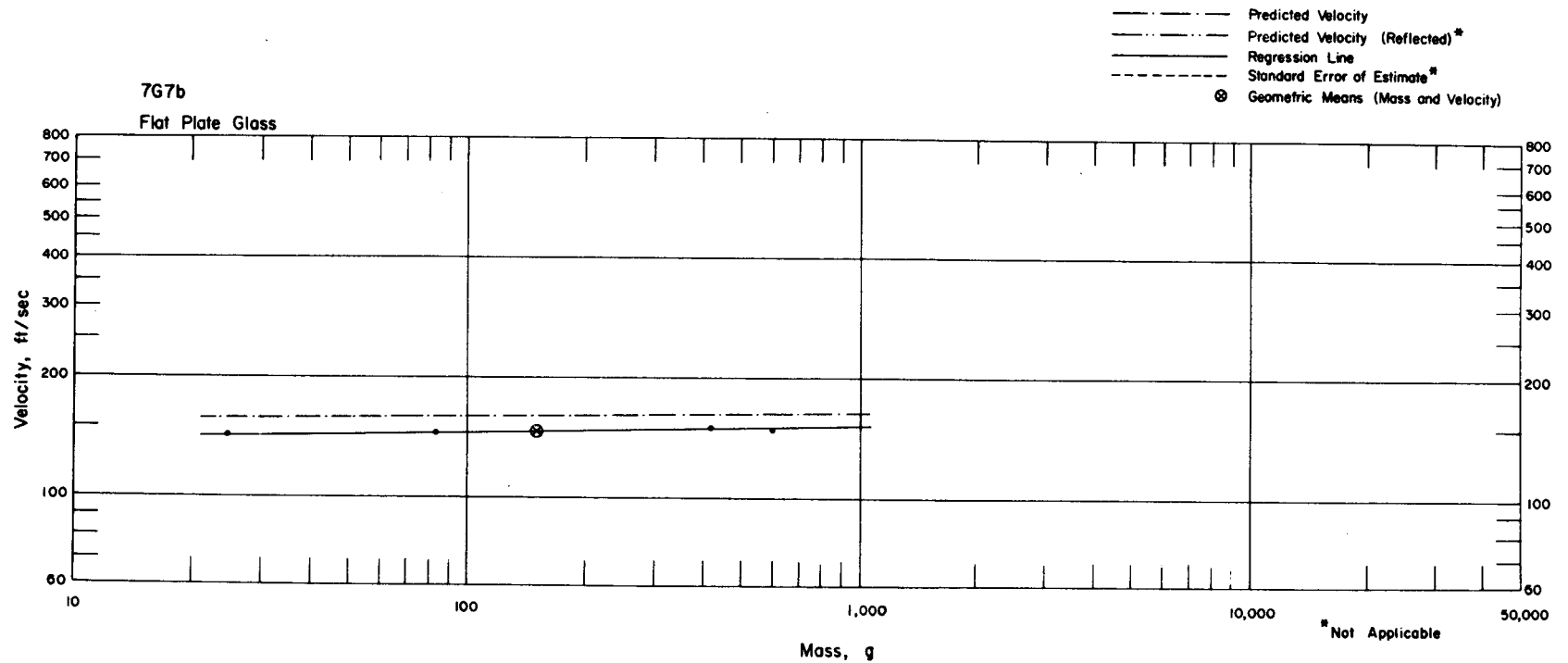


Fig. 6.99—Analysis of plate-glass missiles that arrived flat at trap 7G7b: $d = 11.2$ ft; $n = 4$; $\log v = 2.0829 + 0.0161 \log m$ (mg); $E_{gv} = 1.004$; $M_{50} = 151,000$ mg; $V_{50} = 147$ ft/sec. Since $E_{gv} = 1.004$, the standard-error-of-estimate lines fall almost upon the regression line and cannot be shown. These missiles were not recovered, but their masses were determined from areas of impression left in absorber.

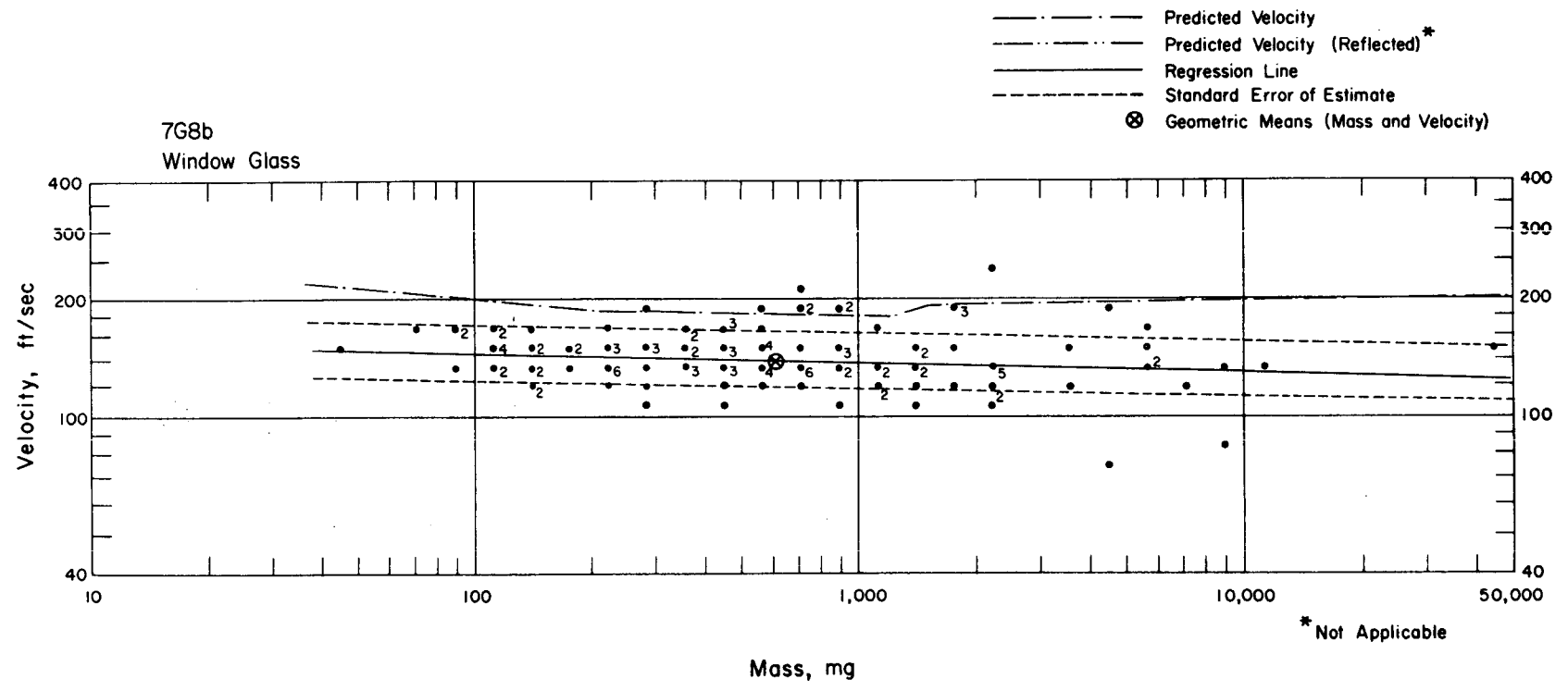


Fig. 6.100—Analysis of window-glass missiles from trap 7G8b: $d = 11.2$ ft; $n = 127$; $\log v = 2.2133 - 0.0220 \log m$; $E_{gV} = 1.18$; $M_{50} = 604$ mg; $V_{50} = 142$ ft/sec.

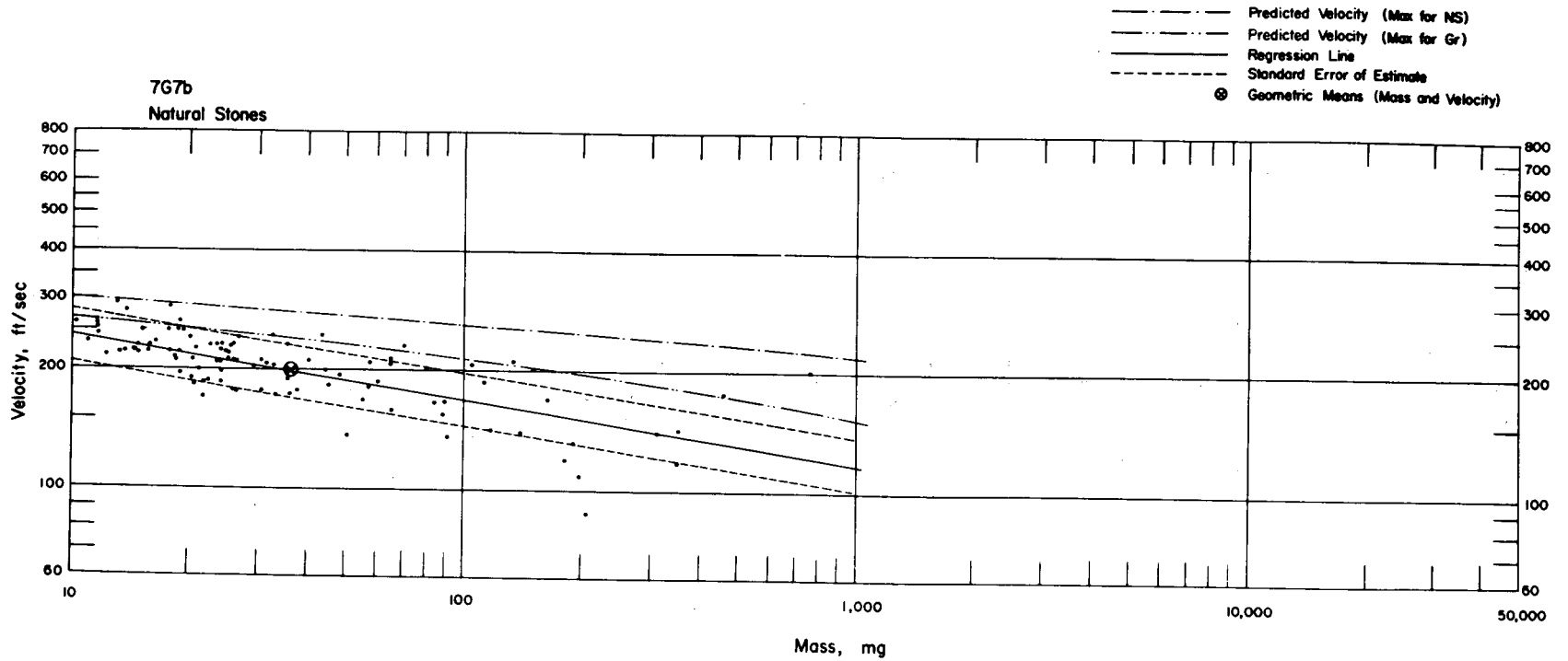


Fig. 6.101—Analysis of natural-stone missiles from trap 7G7b: $n = 101$; $\log v = 2.5475 - 0.1608 \log m$; $E_{gv} = 1.16$; $M_{50} = 36.3$ mg; $V_{50} = 198$ ft/sec.

457

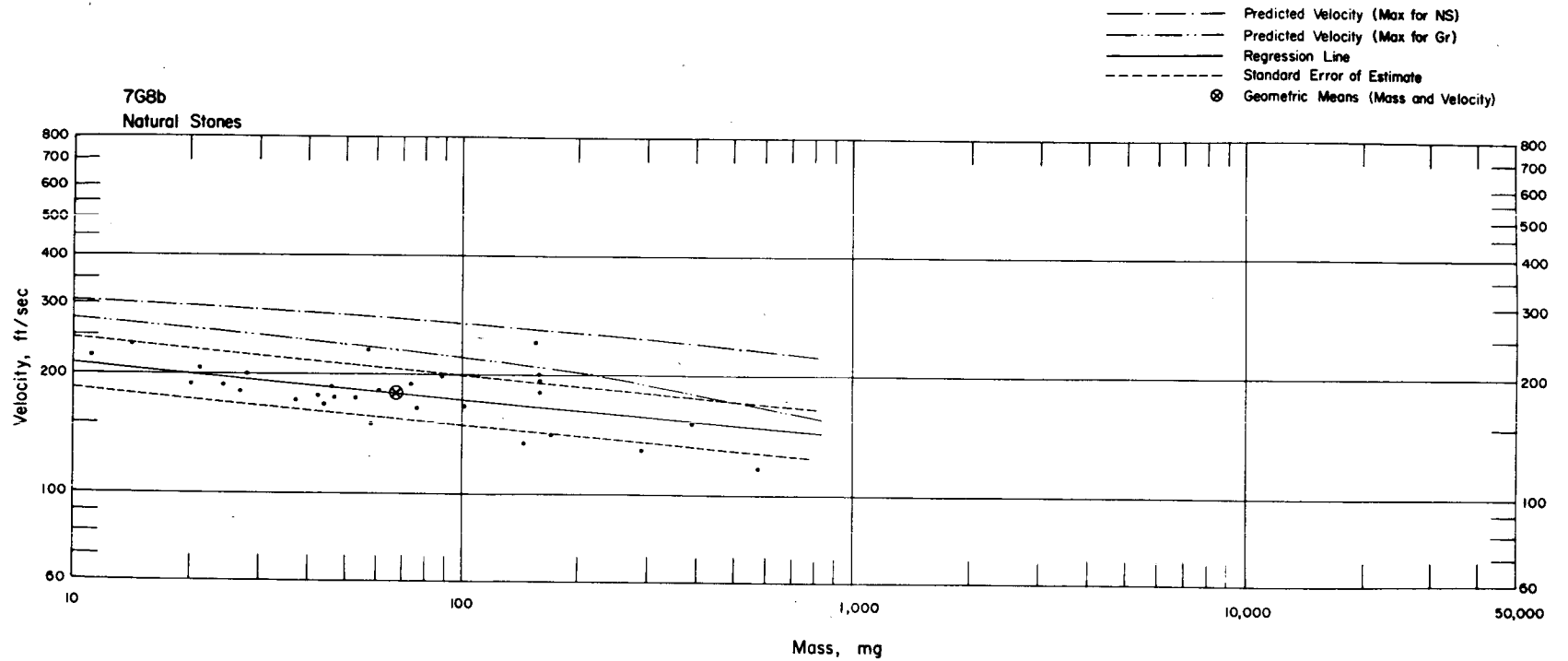


Fig. 6.102—Analysis of natural-stone missiles from trap 7G8b: $n = 29$; $\log v = 2.4335 - 0.0954 \log m$; $E_{gv} = 1.16$; $M_{50} = 67.2$ mg; $V_{50} = 182$ ft/sec.

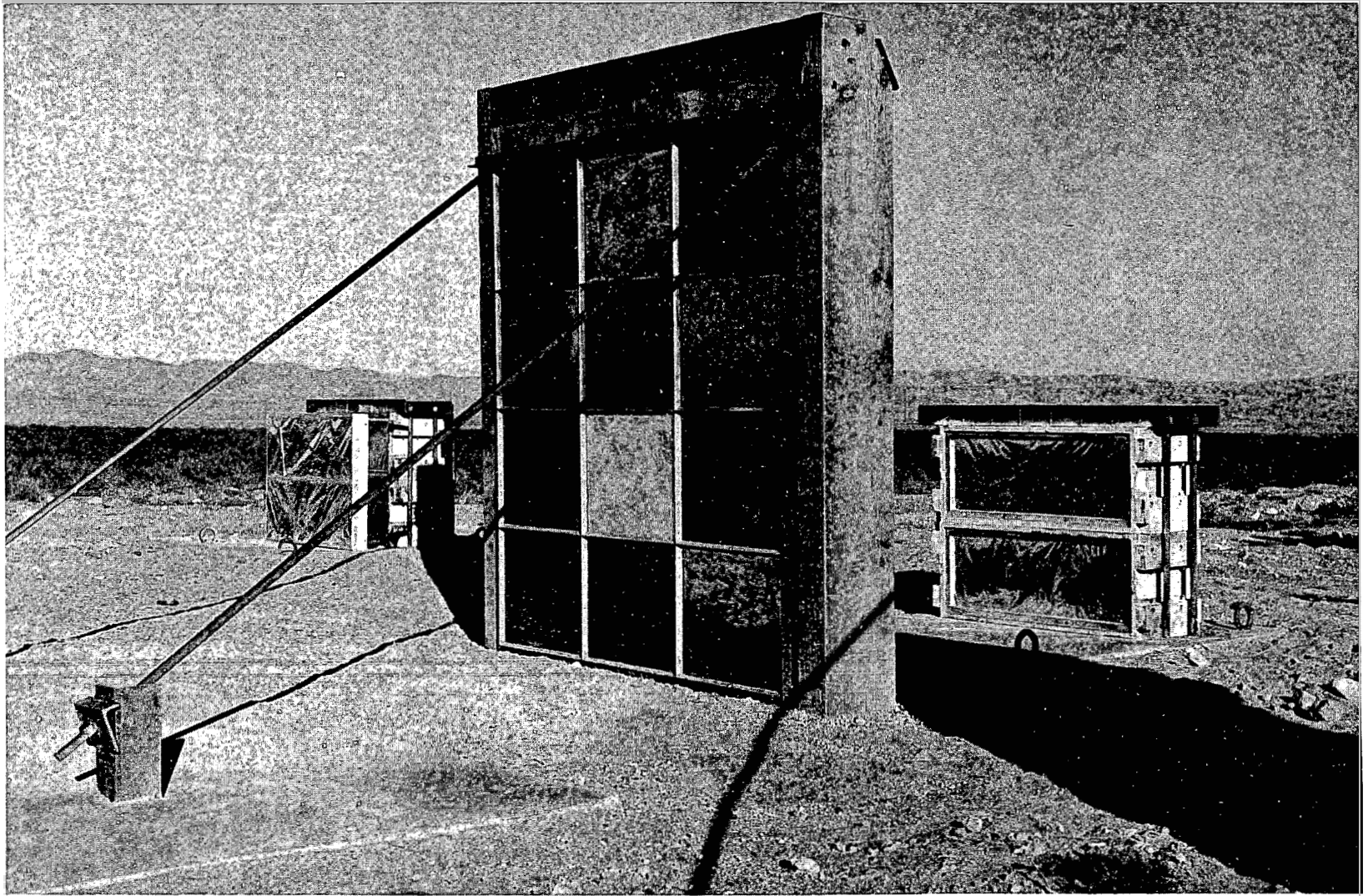
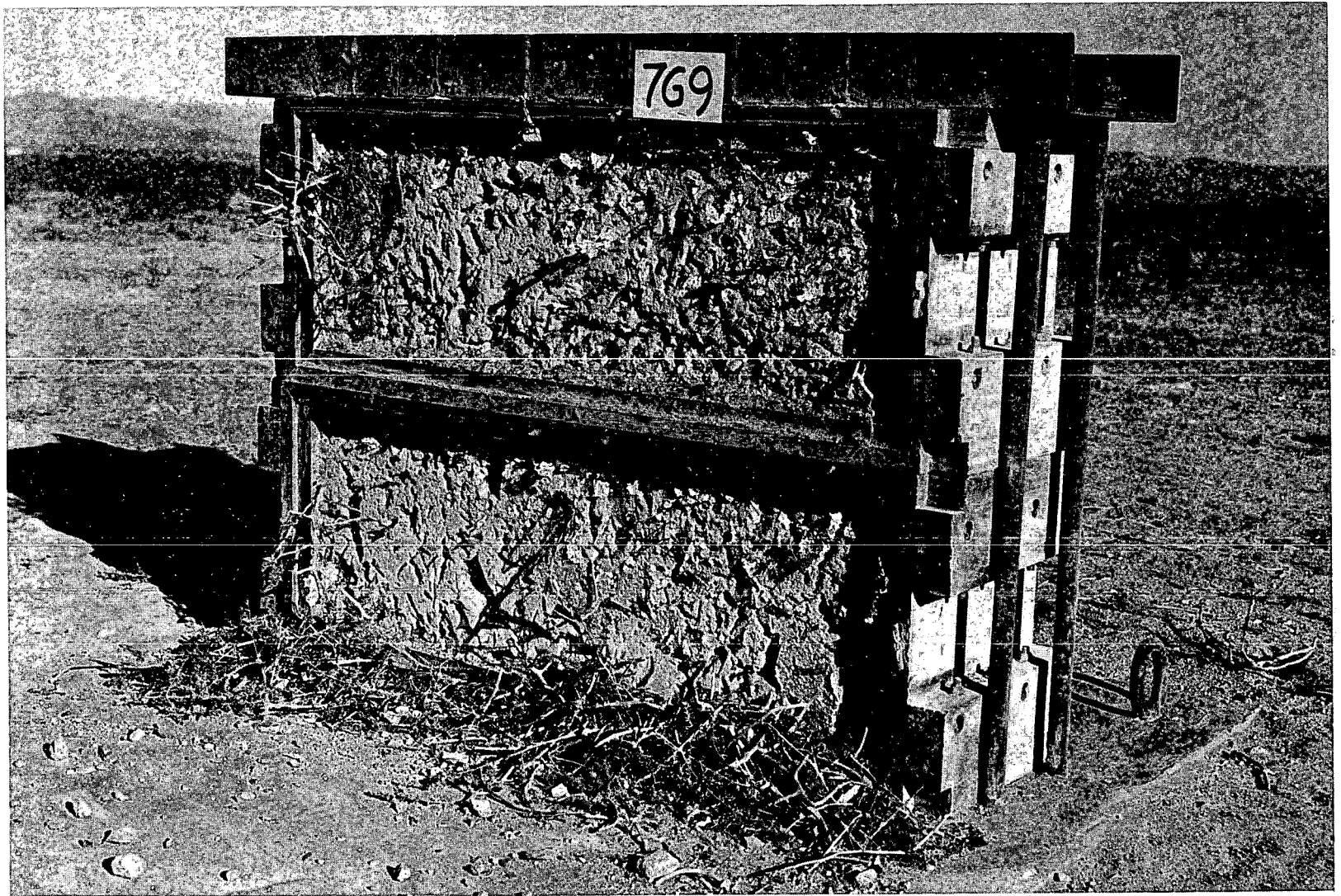


Fig. 6.103—Installation 7G9, preshot. Window is 6.2 ft from traps



459

Fig. 6.104—Installation 769 traps, postshot, placed 6.2 ft behind window.

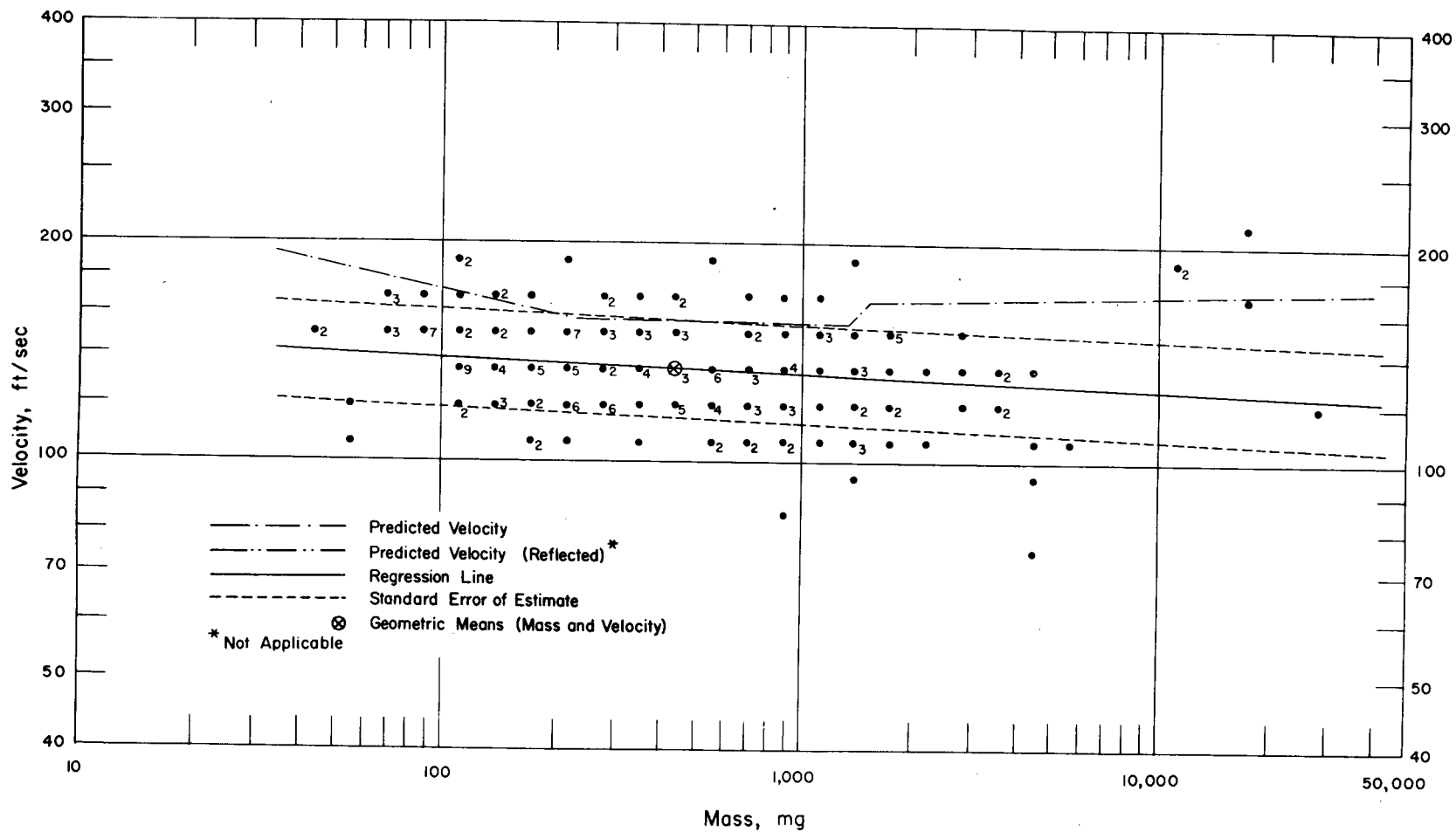


Fig. 6.105—Analysis of window-glass missiles from trap 7G9a: $d = 6.2$ ft; $n = 192$; $\log v = 2.1827 - 0.0211 \log m$; $E_{gv} = 1.17$; $M_{50} = 442$ mg; $V_{50} = 134$ ft/sec. The analysis of window glass impacting flat at trap 7G9a is presented in Fig. 6.107.

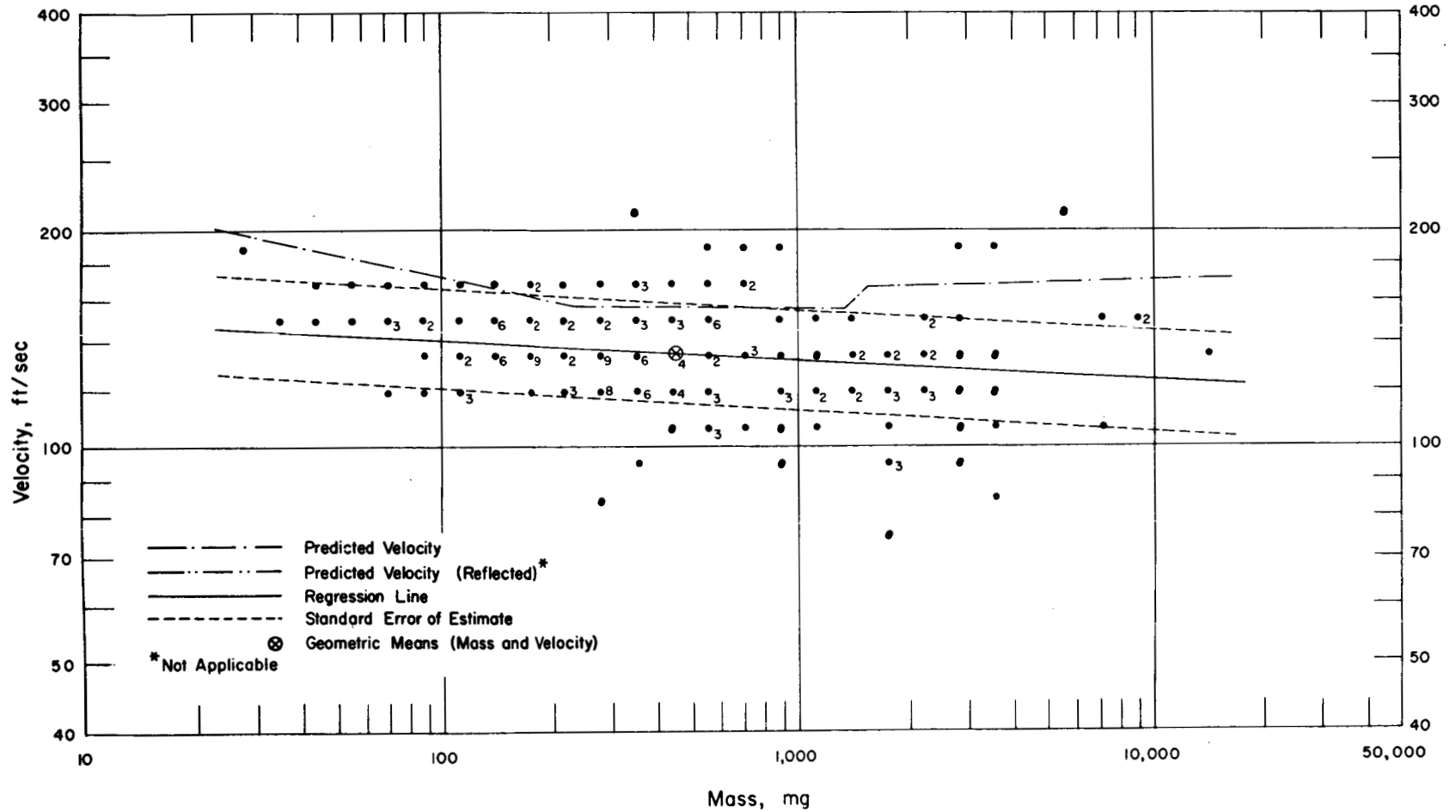


Fig. 6.106—Analysis of window-glass missiles from trap 7G9b: $d = 6.2$ ft; $n = 193$; $\log v = 2.2084 - 0.0304 \log m$; $E_{gv} = 1.18$; $M_{50} = 454$ mg; $V_{50} = 134$ ft/sec. The analysis of window glass impacting flat at trap 7G9b is presented in Fig. 6.107.

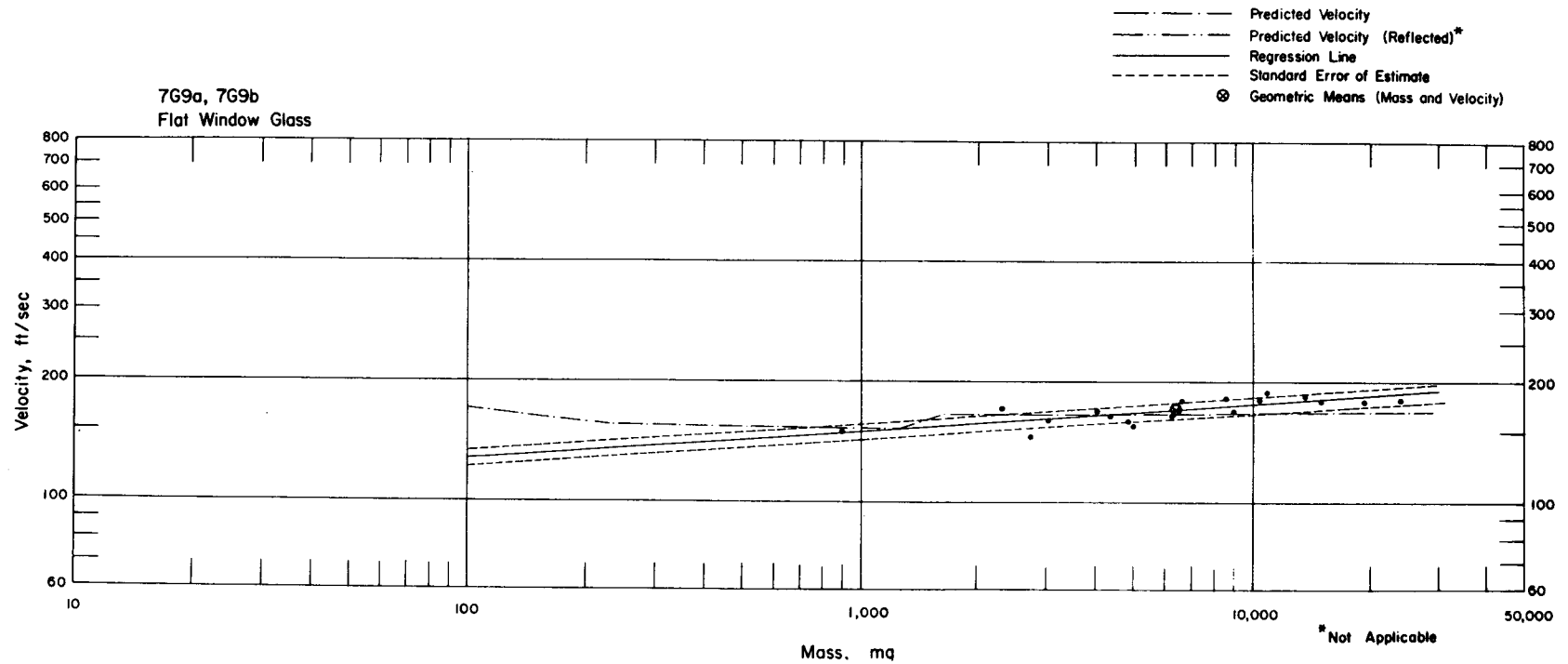


Fig. 6.107—Analysis of window-glass missiles that arrived flat at traps 7G9a and 7G9b (11 from 7G9a and 7 from 7G9b): $d = 6.2$ ft; $n = 18$; $\log v = 1.9735 + 0.0675 \log m$; $E_{gv} = 1.05$; $M_{50} = 6223$ mg; $V_{50} = 170$ ft/sec.

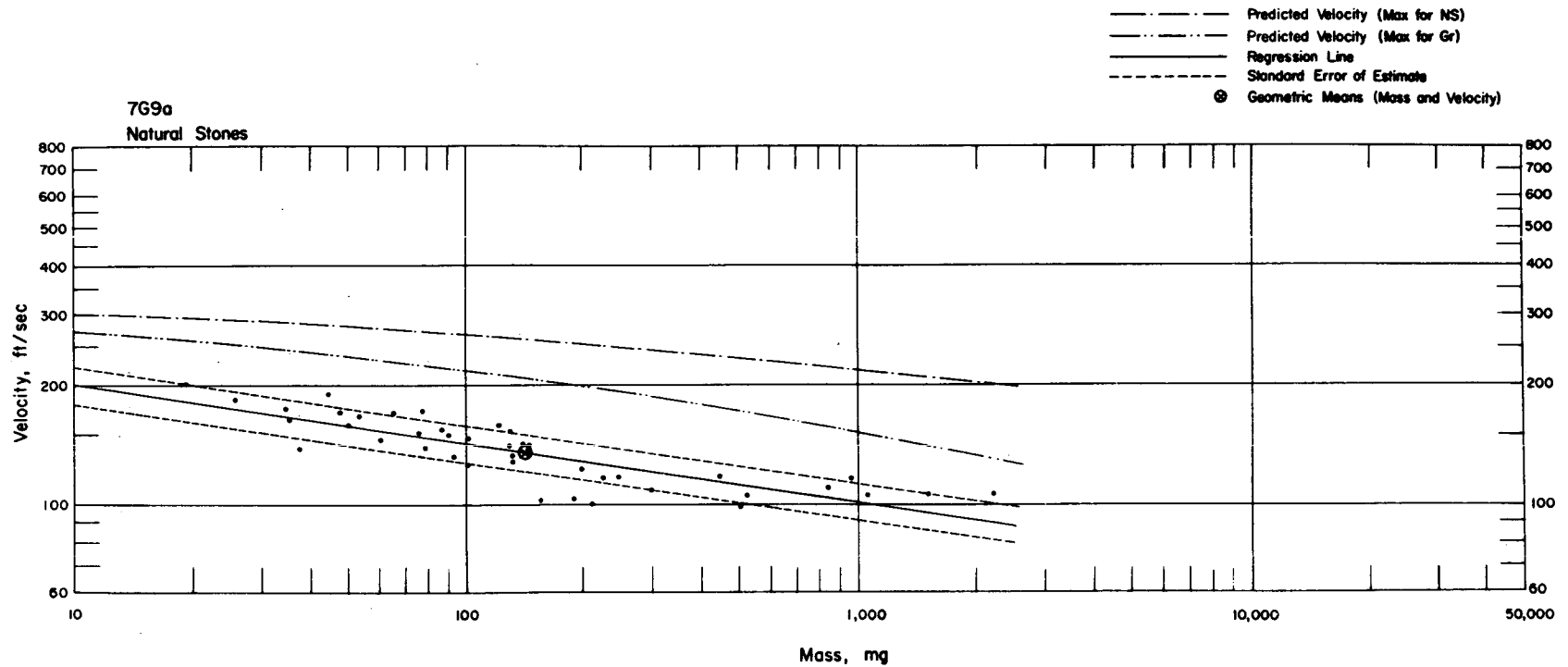


Fig. 6.108— Analysis of natural-stone missiles from trap 7G9a: $n = 42$; $\log v = 2.4539 - 0.1479 \log m$; $E_{GV} = 1.12$; $M_{50} = 140$ mg; $V_{50} = 137$ ft/sec.

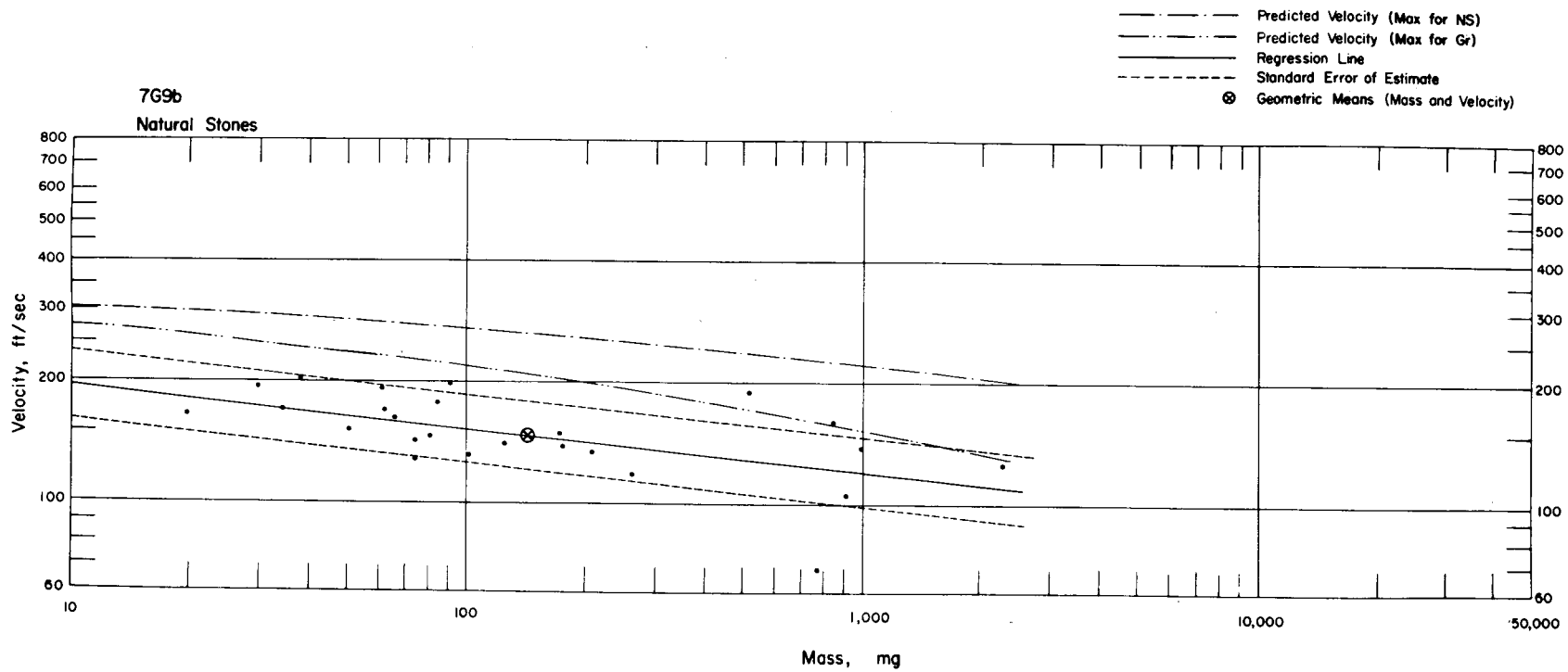


Fig. 6.109—Analysis of natural-stone missiles from trap 7G9b: $n = 25$; $\log v = 2.4198 - 0.1138 \log m$; $E_{gV} = 1.22$; $M_{50} = 141$ mg; $V_{50} = 150$ ft/sec.

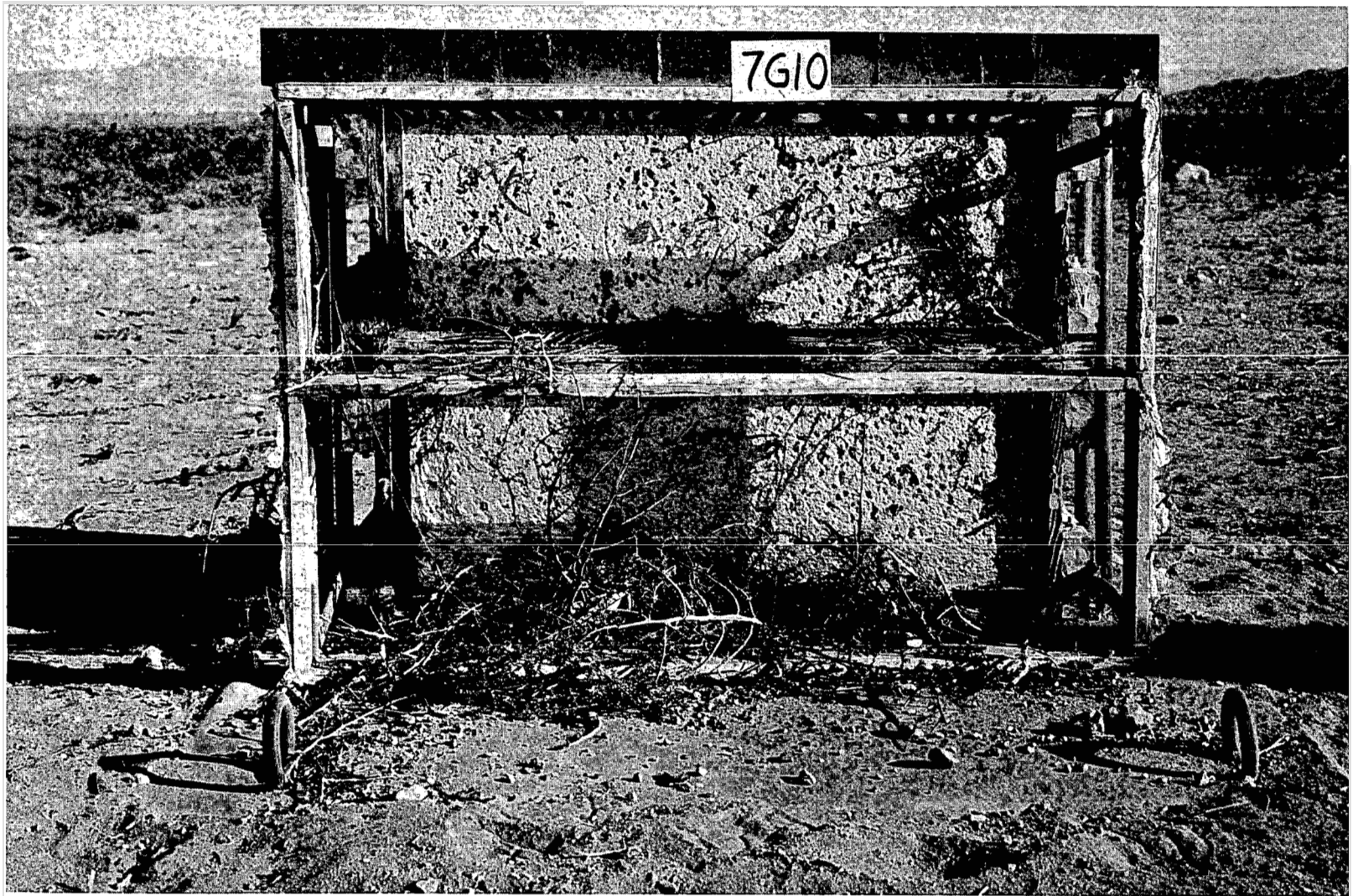


Fig. 6.110—Installation 7G10 traps, postshot. These traps caught marked gravel and natural stone:

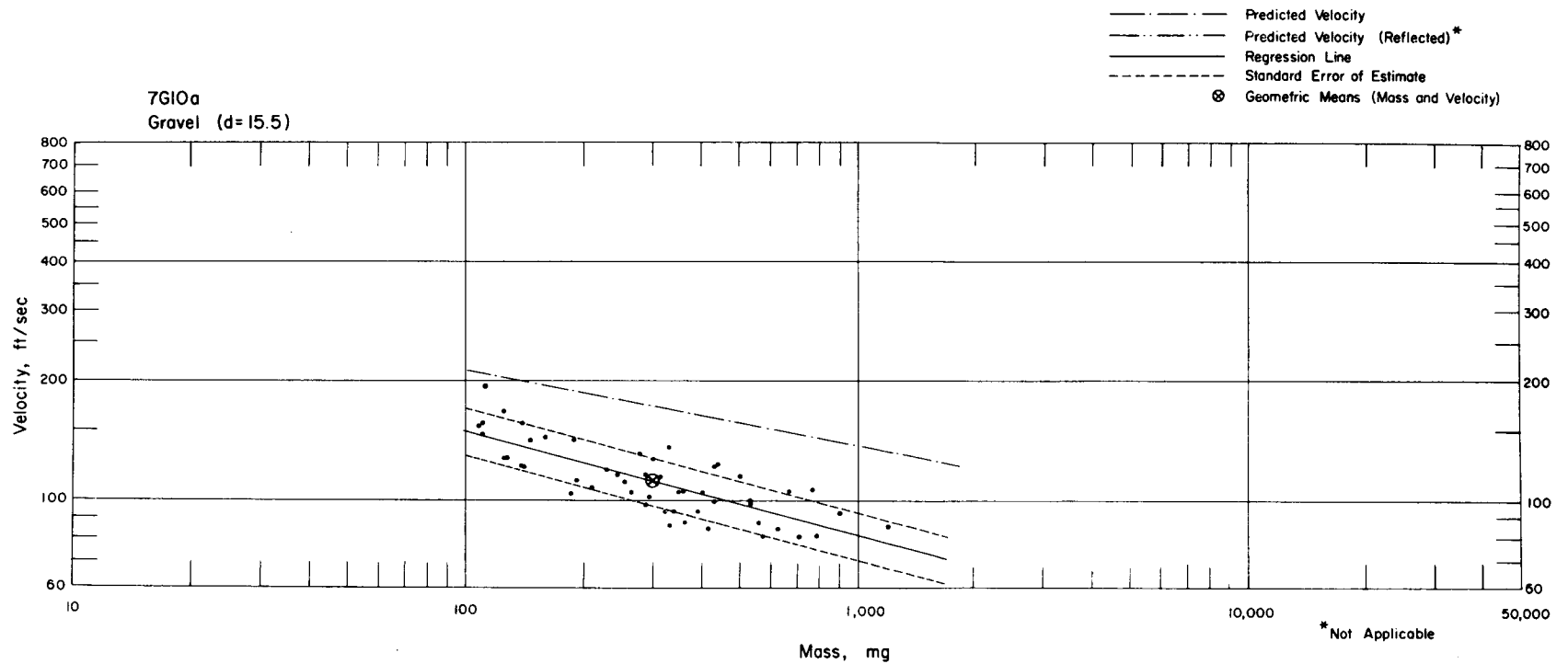


Fig. 6.111—Analysis of gravel missiles from trap 7G10a: $d = 15.5$ ft; $n = 51$; $\log v = 2.7053 - 0.2634 \log m$; $E_{gV} = 1.14$; $M_{50} = 302$ mg; $V_{50} = 113$ ft/sec.

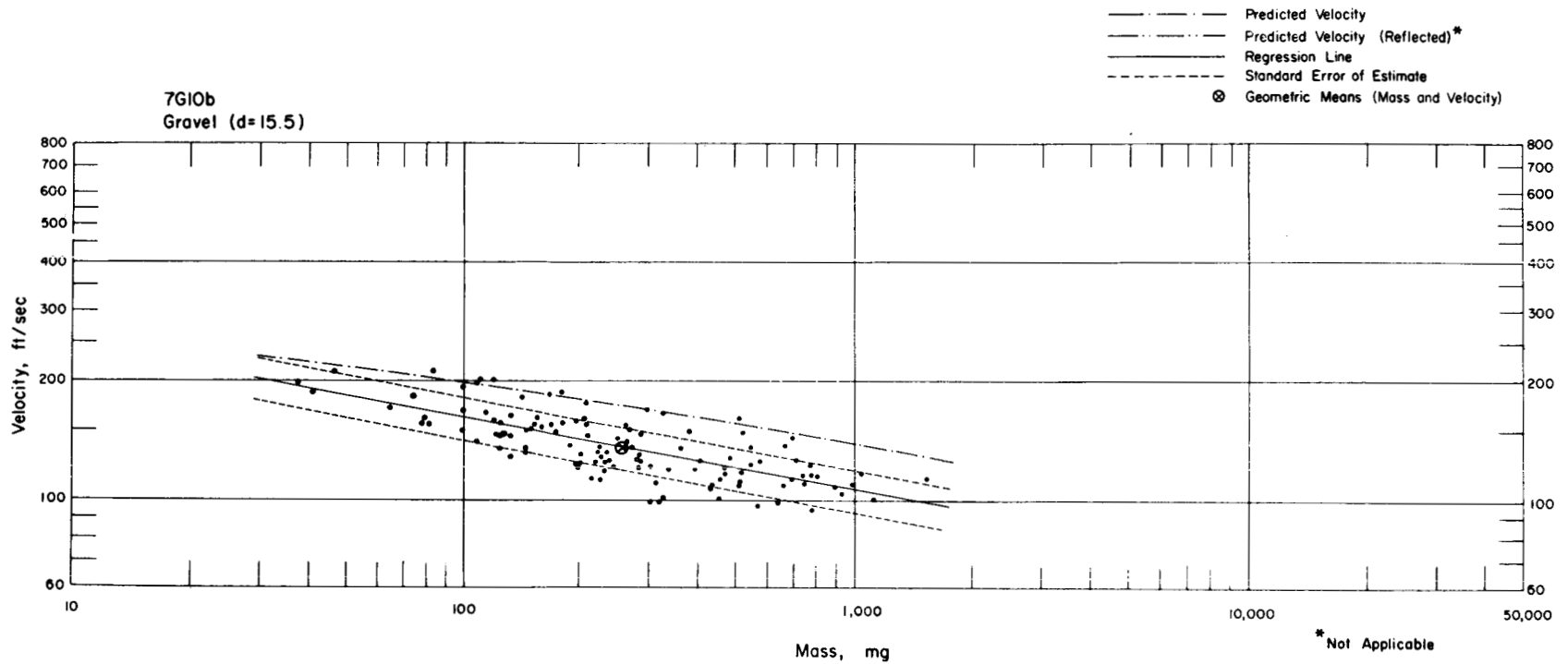


Fig. 6.112—Analysis of gravel missiles from trap 7G10b: $d = 15.5$ ft; $n = 117$; $\log v = 2.5716 - 0.1828 \log m$; $E_{gv} = 1.13$; $M_{50} = 255$ mg; $V_{50} = 135$ ft/sec.

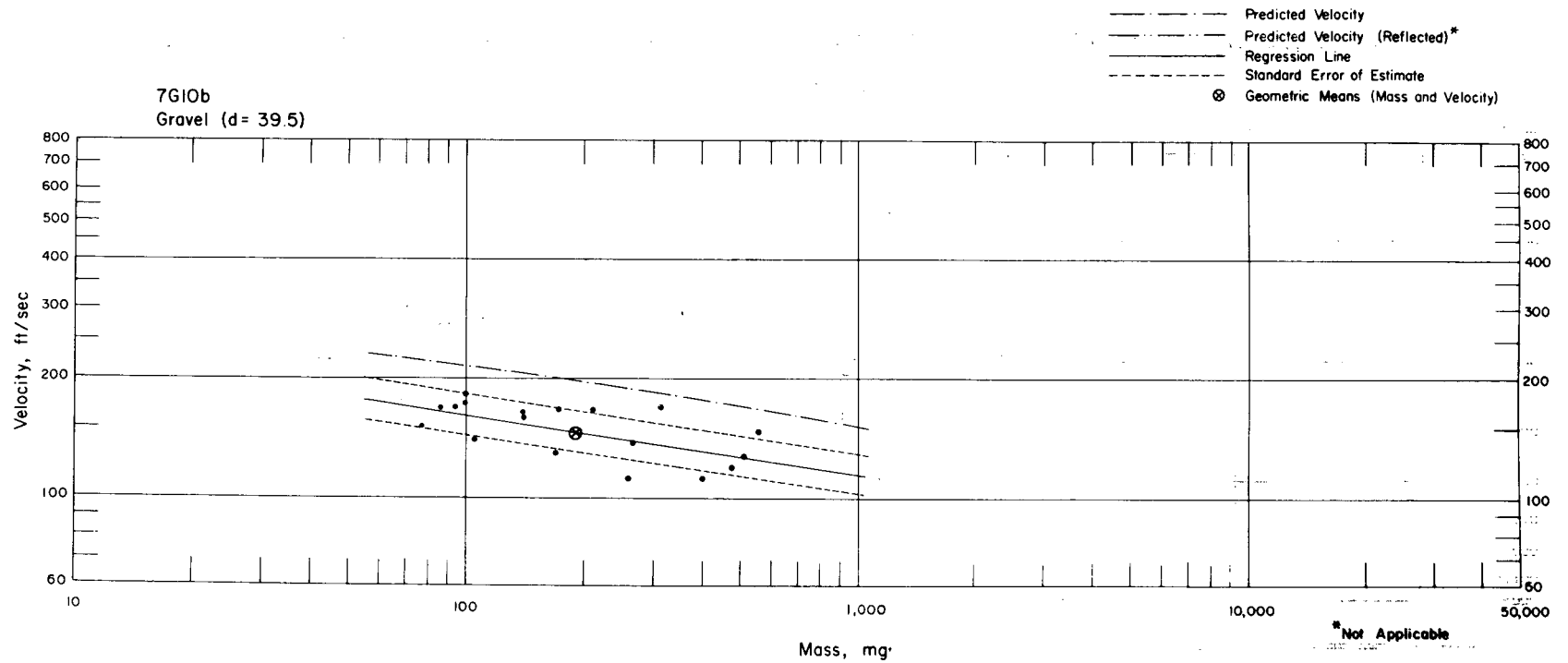


Fig. 6.113—Analysis of gravel missiles from trap 7G10b: $d = 39.5$ ft; $n = 18$; $\log v = 2.5056 - 0.1462 \log m$; $E_{gv} = 1.14$; $M_{50} = 190$ mg; $V_{50} = 149$ ft/sec.

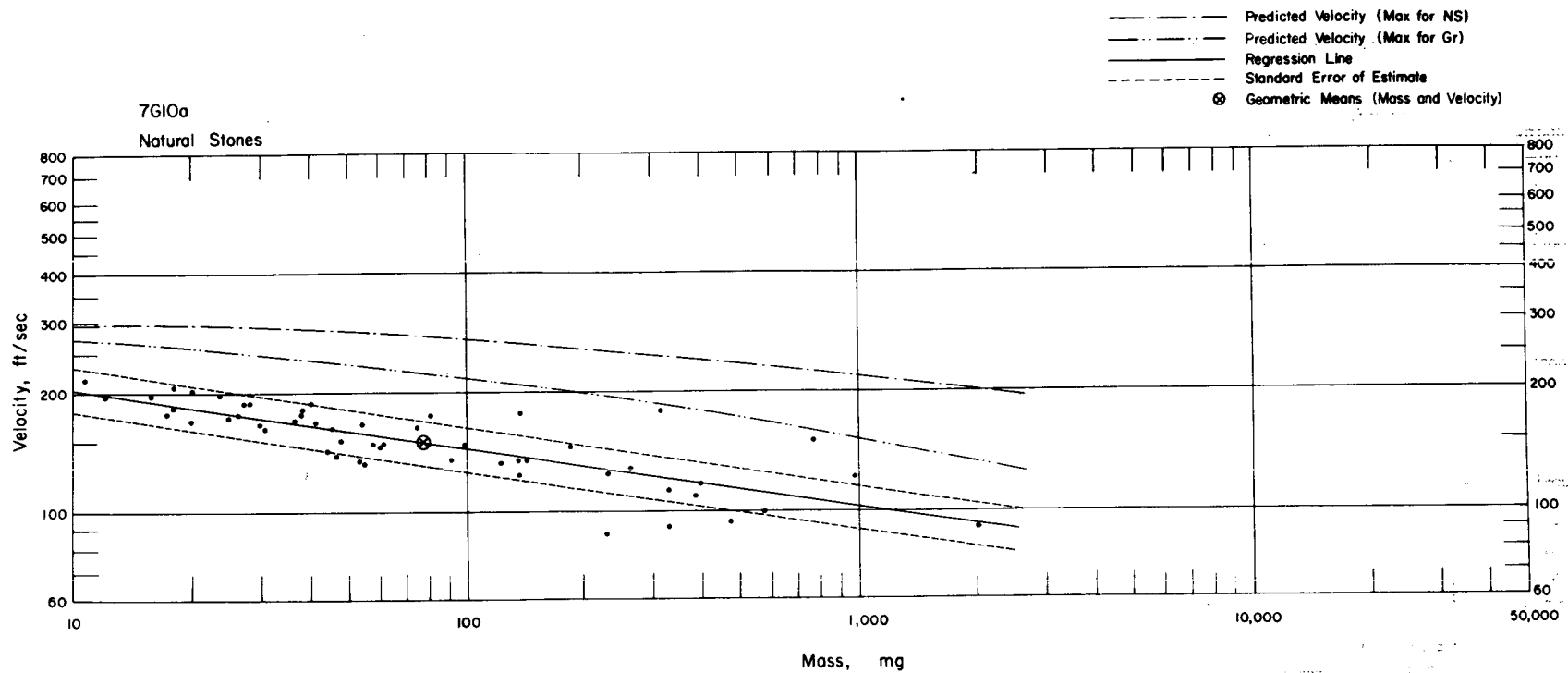


Fig. 6.114—Analysis of natural-stone missiles from trap 7G10a: $n = 51$; $\log v = 2.4807 - 0.1590 \log m$; $E_{gv} = 1.14$; $M_{50} = 73.3$ mg; $V_{50} = 153$ ft./sec.

470

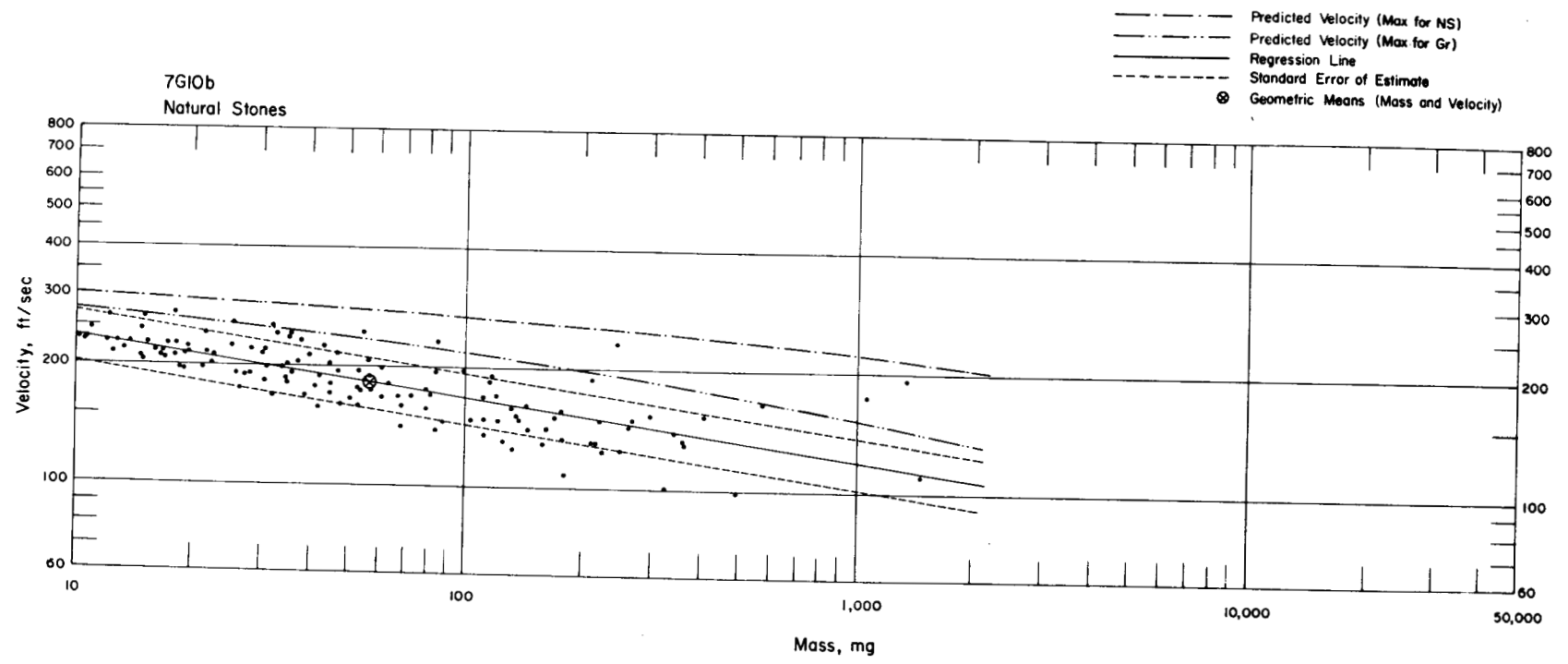


Fig. 6.115—Analysis of natural-stone missiles from trap 7G10b: $n = 133$; $\log v = 2.5913 - 0.1471 \log m$; $E_{gv} = 1.16$; $M_{50} = 56.6$ mg; $V_{50} = 183$ ft/sec.

Chapter 7

DISCUSSION AND SUMMARY

7.1 MISSILE STATIONS AND BLAST-WAVE PARAMETERS

Missile studies were made in open areas at 20 different ranges from GZ, in 8 shelters at 5 ranges, and in 2 houses at the same range. These stations were located on three shots. The code names and estimated yields for these shots were Priscilla, 38 kt; Smoky, 44.5 kt; and Galileo, 11 kt.

Attempts were made to measure overpressure and dynamic pressure as functions of time at most of the stations located in open areas. Measured overpressure impulse and duration were used to compute the equivalent ideal, or classical, blast-wave parameters in each instance (see Chap. 3). Maximum overpressures of the equivalent ideal waves are plotted in Fig. 7.1 as a function of range from GZ (small circles). Measured maximum overpressures vs. range are plotted as small triangles on the same charts. The points shown on the Priscilla chart for the ideal wave display an approximate linear relation (note the regression equations recorded on each chart). Because of distorted wave forms, the maximum overpressure measured for each of the three precursor stations for shot Priscilla (10P, 15P, and 20P) is lower than computed for an ideal wave with the same impulse and duration. Initial overshoot of the mechanical gauges resulted in the maximum overpressures measured at the nonprecursor stations (6P and 8P) being higher than those for the ideal wave.

Because of the irregular nature of the terrain, the data for shot Smoky, shown in the center chart of Fig. 7.1, display greater variability than those for Priscilla. Another factor that could have contributed to the variability in the blast data is that the Smoky stations were located in three general directions from GZ, viz., south, north, and northeast. Examination of the measured overpressure vs. time records presented in Chap. 5 reveals that the wave shapes recorded at all stations except the most distant one (9S) were distorted, particularly in the first portion of the wave. As a result, the measured values of maximum overpressure are generally lower than those computed for the ideal wave. The dales on the northeast blast line were shallow in comparison to the dale of the north line (see profile charts in Figs. 5.4 and 5.77). Figure 7.1 reveals that, with respect to the mean values defined by the regression line, the ideal-wave overpressures associated with the shallow dales are high but that the overpressure for the deeper dale (5S) is low. It is of interest to note that the maximum ideal-wave overpressures for the four stations on the relatively flat south line are near the regression-line values even though one of these stations (4S) was inside the precursor region.

Overpressure records were obtained at only two of the three ranges where stations were located on shot Galileo (see top chart in Fig. 7.1). Neither of these records shows any indication of precursor effects (see Figs. 6.3 and 6.55). Evidence of this is that the maximum overpressures measured are higher than for the ideal waves.

Blast-wave parameters associated with the ideal wave (equivalent in impulse and duration to the measured wave) were used to compute theoretical or predicted velocities for missiles caught at each of the stations designated by code number in Fig. 7.1. The computational procedure (discussed in Chap. 3) was based on material previously reported.^{1,2}

7.2 SUMMARY OF TRAPS AND MISSILES

The number of various sizes of traps used on each shot is listed in Table 7.1. The traps labeled "small" and "medium" consisted of absorbing material placed in suitable box-like housing; the areas of absorber exposed to the blast wave were 2.745 and 3.516 sq ft, respectively (see Chap. 2). The "large" traps consisted of 2-in. layers of plastic absorber cemented

Table 7.1 — SUMMARY OF TRAPS

Shot	No. of traps				Total missile-collecting area, sq ft
	Small	Medium	Large	Total	
Priscilla	88	0	4	92	367.6
Smoky	27	0	0	27	74.4
Galileo	19	22	2	43	229.0
Total	134	22	6	162	671.0

to the walls of structures, the missile-collecting area in each case depending upon the surface available. In the three shots 162 traps, having a total exposed area for the collection of missiles of 671 sq ft, were used. Only 9 of the 162 traps were made unusable by thermal, pressure, or missile effects, and 12 others underwent the blast experience without trapping any missiles. Seven of the latter group were inside closed shelters on shot Priscilla.

Table 7.2 — SUMMARY OF OBJECTS PLACED IN FRONT OF TRAPS

Shot	Area of glass, sq ft			Gr,* cu ft	MD,* pieces	Large steel spheres	Other spheres
	WGH*	WG*	PG*				
Priscilla	0	426.7†	106.7	10.5	5775	270	66,468
Smoky	0	0	0	0	4400	405	0
Galileo	108.8	160.0	53.3	2.9	0	450	28,742
Total	108.8	586.7†	160.0	13.4	10175	1125	95,210

*See list of symbols.

†Does not include about 2000 sq ft of glass used in the pig-pen studies. See Secs. 4.3, 4.5, 4.7, and 4.8.

Table 7.3 — NUMBER OF MISSILES FOR WHICH VELOCITIES WERE DETERMINED

Shot	WGH*	WG*	PG*	NS*	Gr*	MD*	Large steel spheres	Other spheres	Total
Smoky				2876		2	5		2883
Galileo	2523	1057	39	2966	697		11	233	7526
Total	2523	4785	127	7598	1496	34	28	933	17524

*See list of symbols.

Various objects and missile-producing material placed preshot in front of the traps are listed by shot in Table 7.2. If the same material were placed at more than one distance from a trap, the missiles placed at each location were painted a different color for later identification. The "large steel spheres" listed in the table were $\frac{7}{16}$, $\frac{1}{2}$, and $\frac{9}{16}$ in. in diameter.

Trapped missiles for which velocities were determined are listed in Table 7.3 by missile type for each shot. It is interesting to note that 52 per cent of the trapped missiles was stone

(natural stone and gravel) and 42 per cent was glass fragments (window glass—both in open areas and in houses—and plate glass). In addition to the missiles trapped (listed in Table 7.3), total displacements were measured for 145 large stones, 8 concrete blocks, and 8 bricks in shot Priscilla and for 1527 fragments from a concrete-block wall in shot Galileo.

7.3 GLASS FRAGMENTS FROM WINDOWS

It was found that ordinary windows in houses produced large numbers of fragment missiles in comparison with isolated windows mounted in open areas. As a crude indicator of this effect, 23 missiles per square foot of glass area were caught in the two Galileo houses, whereas only 6.6 fragments per square foot of glass were trapped in the open-area installations on the same shot.

The fragments trapped in houses, and to a lesser extent those in open areas at the lower pressures, had impact velocities higher than could be explained theoretically using the parameters of the incident blast wave. The highest velocities measured could be explained, however, by arbitrarily assuming that the blast wave accelerating the missiles had a maximum overpressure equal to the reflected value (normal incidence) of the free-field maximum overpressure (see Secs. 3.5 and 6.2.3). The fortuitousness of this computational procedure is apparent when the rather complicated phenomenon of missile production in houses is considered. First, the blast wave is reflected from windows as well as from the walls that contain the windows. Then, assuming that the windows fail but that the walls do not, the large volume of the house is filled with air streaming through relatively small window areas. Since the air flow through a window is divergent upon entering the house, the initially high air velocities rapidly decrease with distance.

It was observed that the steel window frames used in houses and in open areas were usually slightly bent in the direction of the blast wave. One frame in a house was actually blown free of its mount (see Fig. 6.22). It is doubtful that the frames would have been bent if they had not contained glass. Thus one might suppose that defractive loading contributed not only to fragmentation of the glass but also to the acquisition of an initial velocity by the window panes before fragmentation was complete (see discussion of this subject in Sec. 4.16.3). The latter effect would be more pronounced for situations where the duration of the defractive loading was greatest or where the time required for fragmentation was longest. Thus the velocities obtained for fragments from windows in open areas were higher than expected for stations where the blast waves were relatively weak but were more consistent with the predicted velocities where the blast waves were stronger.

In comparing the glass-fragment data obtained at all stations, a correspondence was noted between the geometric mean mass of the fragments caught in a trap and the geometric mean velocity. The samples containing the smaller fragments generally were the ones with the higher mean velocities. The variation of acceleration coefficient between small and large glass fragments is not large enough to explain the effect noted. An explanation is quite simple, however, if it is assumed that a relatively strong blast wave not only accelerates the fragments to higher velocities but also fragments the window glass into smaller pieces. Thus the fragments caught in the houses had smaller masses than those caught at the same range in open areas, but the reverse was true of their velocities.

It is significant that none of the fragments caught in houses impacted with the flat surface against the absorber but that 0.5 per cent of the window-glass fragments and 12.6 per cent of the plate-glass fragments caught in open areas impacted in this manner. Several factors could influence the rotation of a fragment during its travel from the window to the trap. One is missile size*—larger fragments have higher moments of inertia and therefore greater resistance to forces tending to cause rotation. Another phenomenon inducing rotation is turbulence of the wind, which is likely to be more pronounced inside houses than in open areas. Still another, but more subtle, phenomenon is the mechanism of breakage of window glass. Results obtained

*The largest fragments were plate glass. The window-glass fragments in open areas tended to be larger than those in houses.

from another study³ for low (marginal) blast pressures indicate that fragments from the center of the pane break free before those from the perimeter and therefore acquire correspondingly higher velocities. This sequence of events would not only result in an initial torque tending to cause rotation of many of the fragments but would also help explain the rather large variation in velocities measured in individual samples.

7.4 NATURAL STONES AND GRAVEL

In spite of irregularities in size and shape inherent in stones, those trapped in this series of experiments furnished the best experimental evidence with which to test the validity of the theoretical model for the prediction of missile velocities (see Chap. 3). The superiority of the data for stones over those for spheres resulted from the greater abundance and general reliability of the stone data. Data for gravel that was marked for identification and placed at certain distances in front of the traps could be compared directly with theory. Since the distance of translation of the natural stones was unknown, only the maximum velocities measured could be compared with the predicted maximum velocities.

In general the data obtained for stones were consistent with theory, based on a blast wave of the ideal form, except for stations where the wave was markedly altered by precursor or hill-and-dale effects. Velocities measured for stones in the precursor region were generally higher than predicted. Both hill and dale stations at the shorter ranges yielded natural stones with velocities above the predicted values.* This was also true of a hill station at a relatively large range (Sec. 5.2.6). At the greater ranges one station placed in a long flat dale (Sec. 5.2.7) yielded stone missiles with velocities that were consistent with theory, but other velocity measurements made in more pronounced dales (Secs. 5.2.5 and 5.4) were appreciably lower than those predicted.

Because of the abundance of the stone data and the interest in translational-velocity estimates for man, the theory and aerodynamic measurements documented in Refs. 1 and 2 were used to determine the theoretical relation between the maximum velocities measured for stone and those which would have been measured for an object with an acceleration coefficient equal to that for man. Empirically determined stone velocities are used to estimate the maximum velocity for man. Thus, to some extent, at least, the variations existing between the translational effects of atypical blast waves and those predicted from theory are taken into account. The theoretical ratios of the maximum velocities of man weighing 70, 100, and 165 lb to the maximum velocities for 100-mg stones are plotted in Fig. 7.2 for each station placed in open areas. These plots indicate that the ratio of the velocity of man to that of stone increases with overpressure as well as with yield.

The following is an example of the utilization of the information in Fig. 7.2 to estimate the velocity of a man† weighing 165 lb: For station 4S (shot Smoky) the appropriate velocity ratio read on the chart is about 0.22. From Figs. 5.67, 5.68, and 5.69, it is found that 100-mg stones at this station had maximum velocities between 400 and 500 ft/sec. Thus the maximum velocity for a 165-lb man is estimated to be between 88 and 110 ft/sec. It is appropriate to note that the maximum velocity for this size man predicted for this blast situation, but assuming an ideal-wave form, is only 66 ft/sec.

7.5 SPHERES

Sphere studies were made at most of the stations located in open areas and in a shelter with open entryway (see Sec. 4.13). Since the spheres used had approximately the same acceleration coefficients as man, the data obtained in the shelter has a special significance. The

*Because of the translational power of the blast wave at these ranges, stone missiles originating from a hill location may have been caught by a trap placed in the downwind dale.

†The field data for spheres were also used to estimate the velocity of man. See the following section.

shelter was located 900 ft from the GZ of a 700-ft air burst with a yield of about 38 kt (shot Priscilla). Velocities measured varied from 45 to 159 ft/sec.

Data for man-equivalent spheres were also obtained at three stations in open areas. At station 7G, located in the near-ideal blast region where the maximum overpressure was 8.4 psi, velocities were obtained for 11 steel spheres with diameters of $\frac{7}{16}$, $\frac{1}{2}$, and $\frac{9}{16}$ in. (see Secs. 6.4.4 and 6.5.3 and Table 6.2). These spheres have acceleration coefficients about the same as those of a 70-, 100-, and 165-lb man, respectively, for random orientations with respect to the wind. The averages of the measured velocities for the three sphere samples ranged from 32 to 44 ft/sec, and the deviations from the predicted velocities¹ vary from 0 to 12.7 per cent.

Two $\frac{1}{2}$ -in. steel spheres were caught at station 10P, which was located in the precursor region on shot Priscilla (see Sec. 4.10.4 and Table 4.6). The average velocity for these spheres was 198 ft/sec, 143 per cent greater than the value predicted (81 ft/sec), based on an ideal-wave form.¹ Although this deviation seems excessively high, it is about the same as those for a few of the higher velocity stones caught in the same trap (see Figs. 4.123 and 4.124.)

Data were also obtained for five $\frac{7}{16}$ -in. steel spheres at station 4S, which was located in the precursor region on shot Smoky (see Sec. 5.3.1 and Table 5.2). The average of the measured velocities for these spheres was 75 ft/sec, about 4 per cent less than the value predicted on the basis of an ideal blast wave. Natural stones caught at the same installation had measured velocities as much as 100 per cent greater than those predicted. Thus the sphere data from station 4S is not consistent with the stone data at the same station or with the sphere data from station 10P. The reason for this inconsistency is not known. However, one might speculate that the spheres at station 4S were dislodged from their mount by the earth shock prior to the arrival of the blast wave (see Figs. 5.2 and 5.62). The spheres at station 10P were suspended from a wire frame in aluminum-foil bags and thus would have been more difficult to dislodge.

The sphere velocities of the smaller spheres measured at the stations located in open areas where the blast wave was near ideal were generally in agreement with the predicted velocities provided the sample sizes were sufficiently large to make a valid comparison.* An exception to the above was encountered at some of the Priscilla stations where it was indicated that the velocity determinations were erroneous due to softening of the surface of the absorber by thermal effects. Installations on later shots were given additional thermal protection where appropriate.

7.6 MILITARY DEBRIS

Velocities were evaluated for only 34 pieces of military debris or fragments of steel. These missiles represent about 0.33 per cent of the total number of pieces of debris placed in front of traps in open areas on shots Priscilla and Smoky. The largest samples were obtained at the precursor stations 10P and 15P on shot Priscilla (see Figs. 4.118 and 4.131). The military-debris data obtained at these stations were similar to that obtained for gravel in that deviations of the measured from the predicted velocities were about the same for both types of missiles at each of the stations. The velocity and mass ranges for the military debris were 110 to 373 ft/sec and 4.495 to 289 g at station 10P and 195 to 301 ft/sec and 9.042 to 86 g at station 15P.

7.7 SPALLATION MISSILES

Missile traps were placed in seven underground shelters with closed entryways at ranges from 860 to 1360 ft from GZ on shot Priscilla (see Sec. 4.14). The purpose of the investigation was to measure the velocity of pieces of concrete which might spall from the shelter walls due

*Although the spheres of a particular type were relatively uniform in size and weight, the measured velocities for a given blast situation varied considerably.

to underground shock effects. No missiles were caught in any of the shelters, and postshot examination of the walls indicated that appreciable spallation had not occurred.

7.8 LARGE STONES, CONCRETE BLOCKS, AND BRICKS

Total displacement, rather than velocity, was measured for 145 large stones, 8 concrete blocks, and 8 bricks placed on shot Priscilla and for 1528 fragments from a concrete wall on shot Galileo.

Groups of stones and masses varying from 0.15 to 20 kg were placed at seven ranges from GZ on shot Priscilla (see Sec. 4.15). Two concrete blocks and two bricks were also included with each group of stones. The displacement of the stones placed outside the precursor region varied from 0 to 54 ft, the smaller stones tending to travel farther than the larger ones. For the stones that were inside the precursor region, the minimum displacement measured was 235 ft and the maximum, 1814 ft. There was no significant relation between stone mass and distance of travel.

A 40-ft concrete-block wall was built 2750 ft from GZ on shot Galileo (see Sec. 6.5.2). A broad side of the wall was oriented toward GZ. The blast wave at this location was near ideal in form and had a peak overpressure of about 8.4 psi. One block was found as far as 403 ft from the original position of the wall; the geometric mean, or median, distance of travel for whole blocks and multiple blocks joined with mortar was 38 ft. Final positions were measured for a total of 1528 wall fragments that weighed more than 0.1 lb.

REFERENCES

1. I. G. Bowen, R. W. Albright, E. R. Fletcher, and C. S. White, A Model Designed to Predict the Motion of Objects Translated by Classical Blast Waves, USAEC Report CEX-58.9, June 29, 1961.
2. E. R. Fletcher, R. W. Albright, V. C. Goldizen, and I. G. Bowen, Determination of Aerodynamic-drag Parameters of Small Irregular Objects by Means of Drop Tests, USAEC Report CEX-59.14, October 1961.
3. E. R. Fletcher, R. V. Taborelli, I. G. Bowen, and C. S. White, Window Glass Breakage and Translational Effects Due to Sonic Boom, USAEC Report CEX-60.4 (in preparation).

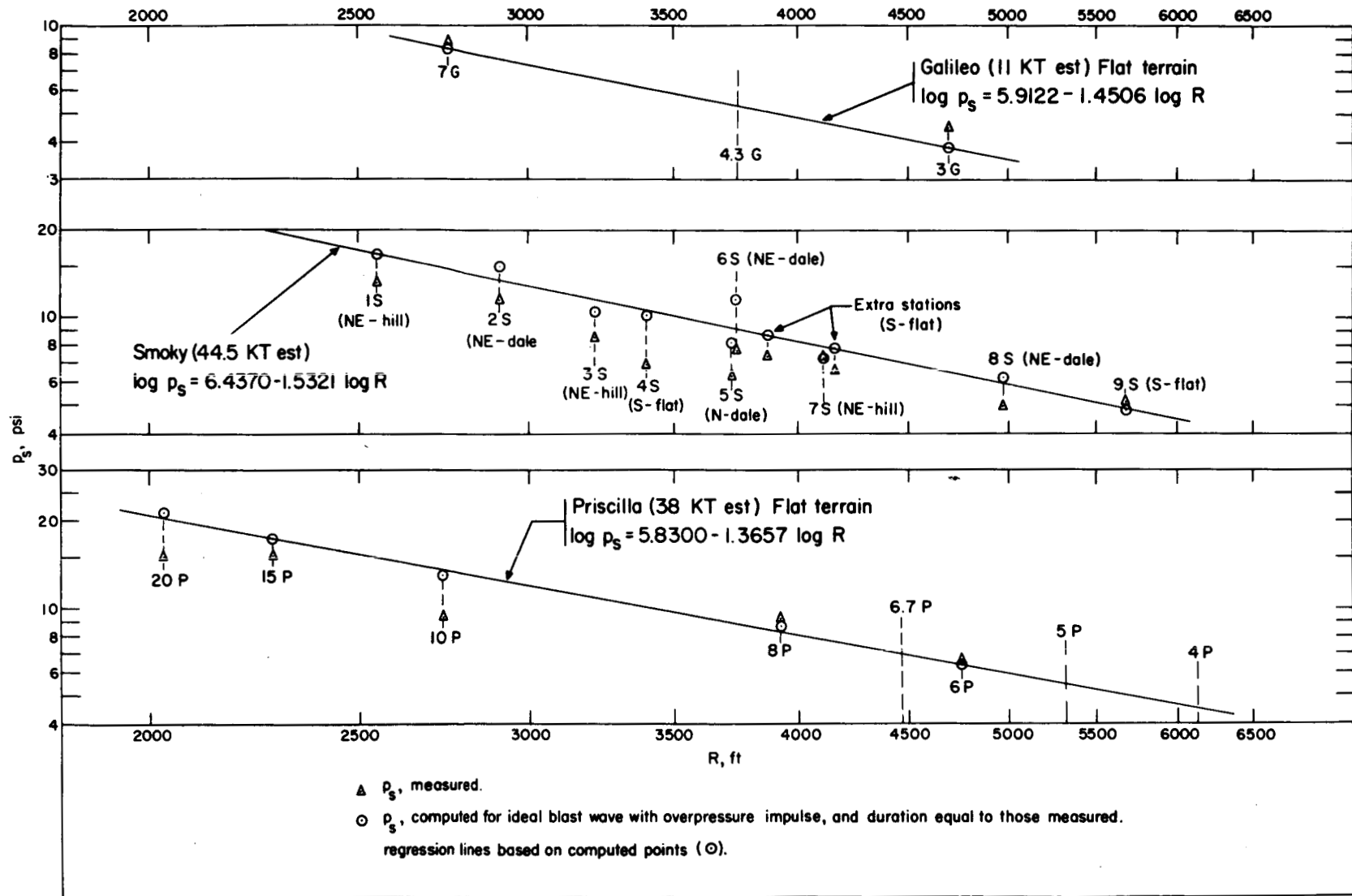


Fig. 7.1—Overpressure vs. range plots for missile stations on shots Priscilla, Smoky, and Galileo.

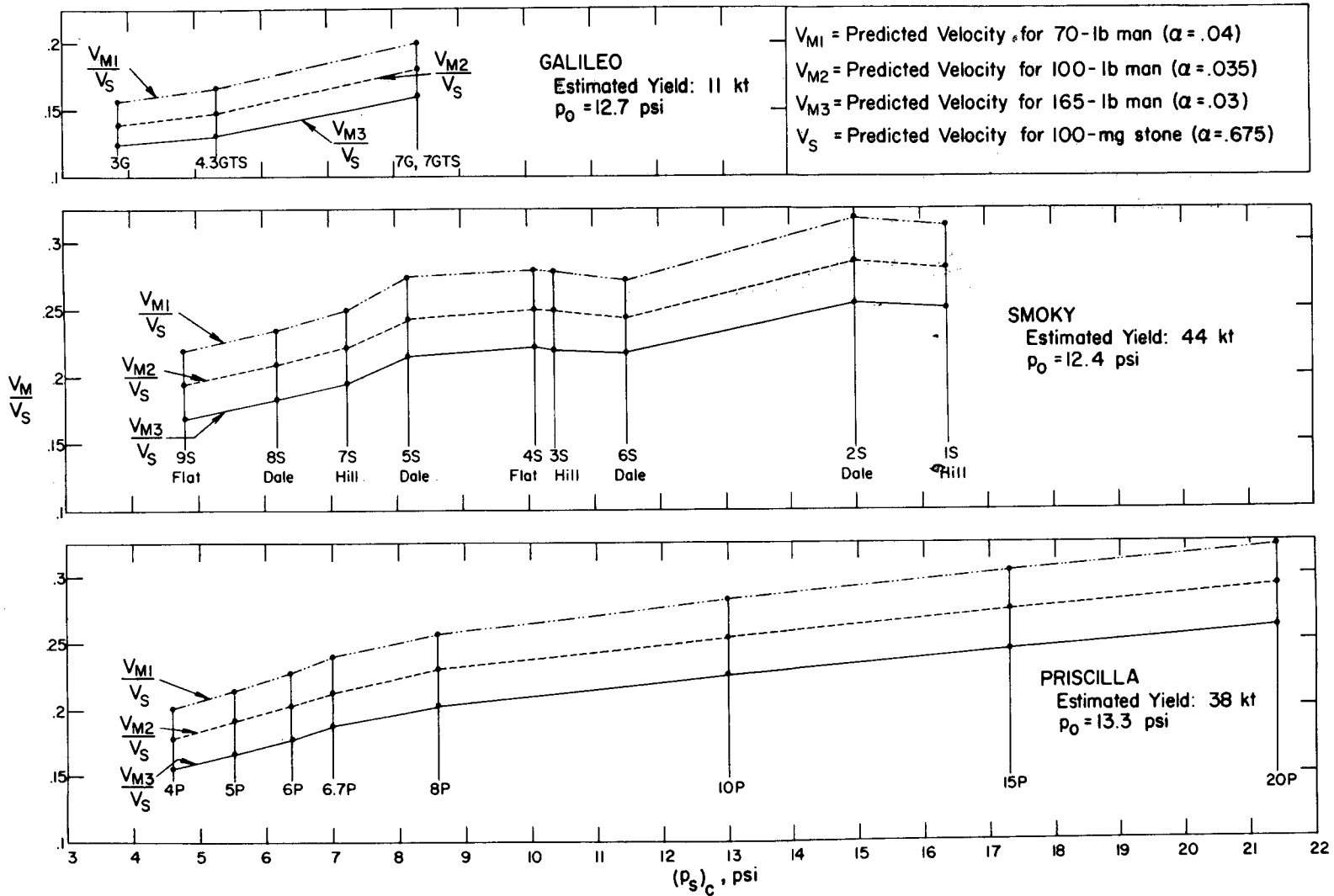


Fig. 7.2—Theoretical relations between maximum velocities of man and stone computed for each of the missile stations in open areas.

Appendix

RELATION BETWEEN THE MEAN, THE GEOMETRIC MEAN, AND THE GEOMETRIC STANDARD DEVIATION FOR A LOG-NORMAL DISTRIBUTION*

The density function of a normally distributed variable u can be stated as

$$p(u) = \{\exp [-(u - \bar{u})^2 / (2 S_u^2)]\} / (S_u \sqrt{2\pi}) \quad (\text{A.1})$$

where \bar{u} is the mean value of u and S_u is the standard deviation of u . Now, if $u = \log x$, the distribution is log normal in the variable x . To find \bar{x} , the mean or expectation value of x , multiply x ($x = 10^u$) by the probability function, Eq. A.1, and integrate from $-\infty$ to $+\infty$.

$$\begin{aligned} \bar{x} &= E(x) = E(10^u) = \int_{-\infty}^{+\infty} [10^u / (S_u \sqrt{2\pi})] [\exp [-(u - \bar{u})^2 / (2 S_u^2)]] du \\ &= \int_{-\infty}^{+\infty} [1 / (S_u \sqrt{2\pi})] \exp \{-[(u - \bar{u})^2 / (2 S_u^2)] + u \ln 10\} du \end{aligned} \quad (\text{A.2})$$

The next step involves rearrangement of the exponent to attain the same basic form of the exponent in Eq. A.1.

$$\begin{aligned} \bar{x} &= \exp \{\bar{u} \ln 10 + [(S_u^2 \ln^2 10) / 2]\} \cdot \\ & [1 / (S_u \sqrt{2\pi})] \int_{-\infty}^{+\infty} \exp \{-[u - (\bar{u} + S_u^2 \ln 10)]^2 / (2 S_u^2)\} du \end{aligned} \quad (\text{A.3})$$

The integrand is a normal probability distribution in u , the quantity $(\bar{u} + S_u^2 \ln 10)$ being the mean value. Except for the exponent outside the integrand (which does not contain the variable u), the form is now the same as Eq. A.1. Integration of the normal probability function from $-\infty$ to $+\infty$ gives a value of 1; i.e., the probability is 1.0 that all values of u are between $-\infty$ and $+\infty$. Thus Eq. A.3 reduces to

$$\begin{aligned} \bar{x} &= \exp \{\bar{u} \ln 10 + [(S_u^2 \ln^2 10) / 2]\} \\ &= 10^{\bar{u}} \exp [(S_u \ln 10)^2 / 2] \end{aligned} \quad (\text{A.4})$$

*Log is used to designate logarithms to the base 10, and ln, to the base e.

Since $u = \log x$, $\bar{u} = \overline{\log x}$. By definition of the geometric mean (x_{50}), $\log x_{50} = \overline{\log x}$. Thus $10^{\bar{u}} = 10^{\overline{\log x}} = 10^{\log x_{50}} = x_{50}$. Thus Eq. A.4 can be written

$$\bar{x}/x_{50} = \exp [(S_u \ln 10)^2/2] \quad (\text{A.5})$$

As defined above, S_u is the standard deviation in u . Since $u = \log x$, the standard deviation in u is also the standard deviation in $\log x$, or $S_u = S_{\log x}$. By definition the standard deviation in $\log x$ is the logarithm of the geometric standard deviation in x , $S_{\log x} = \log S_{gx}$. Thus $S_u = \log S_{gx}$. By using the latter relation in Eq. A.5 and the fact that $\log S_{gx} \ln 10 = \ln S_{gx}$, the following is obtained:

$$\bar{x}/x_{50} = \exp [(\log S_{gx} \ln 10)^2/2] = \exp [(\ln S_{gx})^2/2] \quad (\text{A.6})$$

The relation expressed by Eq. A.6 was used in the interpretation of mass and velocity samples obtained in the field study (see Sec. 2.6 and Fig. 2.12).